# The stratigraphy, sedimentology, and age
of the Late Palaeozoic Mesosaurus Inland Sea,
SW-Gondwana

New implications from studies on sediments and altered pyroclastic layers of the Dwyka and Ecca Group (lower Karoo Supergroup) in southern Namibia

vorgelegt von

Mario Werner

Würzburg 2006

Eingereicht am: 28 July 2006

1. Gutachter: Prof. Dr. Volker Lorenz

2. Gutachter: Assoc. Prof. Dr. Tobias Payenberg

1. Prüfer: Prof. Dr. Volker Lorenz

2. Prüfer: Prof. Dr. Franz Fürsich

**Tag der Prüfung (öffentlicher Vortrag und Disputation):** 31 January 2007

Doktorurkunde ausgehändigt am: _____

Werner, M. (2006): The stratigraphy, sedimentology, and age of the Late Palaeozoic Mesosaurus Inland Sea, SW-Gondwana: new implications from studies on sediments and altered pyroclastic layers of the Dwyka and Ecca Group (lower Karoo Supergroup) in southern Namibia. Dr. rer. nat. thesis, University of Würzburg, 428 pp., 167 figs., 1 table.

If we, citizens, do not support our artists, then we sacrifice our imagination on the altar of crude reality and we end up believing in nothing and having worthless dreams.

Yann Martel (in Life of Pi)
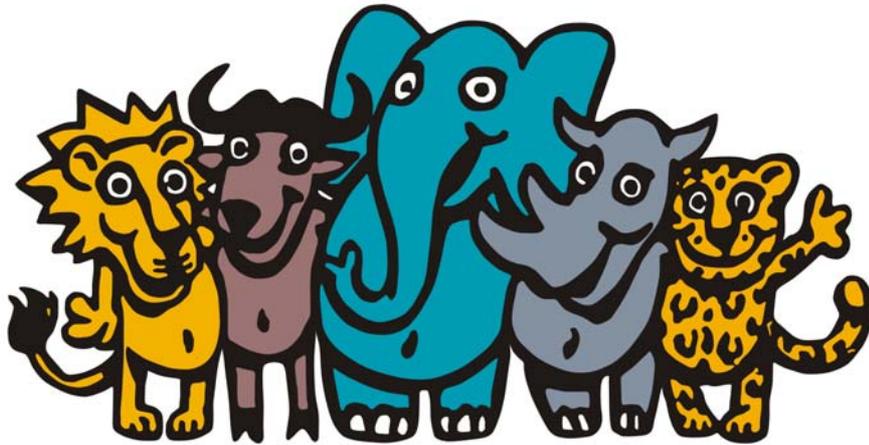
Why explore? It is as well as those who ask such a question that there are others who feel the answer and never need to ask.

Wozu sollte man ein Land erforschen? Für diejenigen, die solche Fragen stellen, ist es nur gut, dass es andere gibt, die die Antwort im Gespür haben und gar nicht erst fragen müssen.

Sir Wally Herbert

TABLE OF CONTENTS

Acknowledgements

Sir Geoffrey Tucker is thanked for his unconditional affection, his ever wagging tail, and for entertaining and making us laugh all day long. In the same way I also want to thank our 'Tiere', especially Bärchen & Weihnachtsbär, for keeping our spirits high.

Finally I want to thank Carmen for her love, patience and continuous and invaluable support. Without her all this would not have been possible. What can I say more? She is the best wife, friend, soul-, flat-, and fieldmate one could ever imagine. And, as all of you can see, she is the most beautiful scale in the world !!!!

And again in my native language (long live Franconia):

A SUBBER-DANGESCHÖÖN ANS LIEBE CARMELE,
AN MEIN VADDER UND MEI MUDDER,
AN ALLE SCHEFFS UND KUMBELS,
UND WER HALD NOCH SO ALLES MIDKHOLFN HADD.
OHNE EUCH WÄRSCH NIX MID'N DOGDER WORN !!!

Abstract

The Mesosaurus Inland Sea covered, in the Late Palaeozoic, vast areas (~5 Mio km^2) of the SW-Gondwanan continental interior. Major depocentres are represented by the Karoo basins of SW-Africa as well as the Paraná and Sauce Grande basins in South America. In Antarctica deposits of this inland sea can be found in the Ellsworth and Transantarctic Mountains. All these areas were interconnected prior to the break-up of Gondwana and the subsequent opening of the South Atlantic Ocean.

The basin areas, which were flooded by the Mesosaurus Inland Sea, evolved under the influence of various tectonic regimes. During the Late Palaeozoic oceanic crust of the Panthalassan Ocean was subducted beneath the southern continental margin of Gondwana, which was accompanied by the formation of a magmatic arc as well as accretion and mountain building processes. As a result of these subduction and orogenic processes an extensive retroarc foreland system developed along the southern convergent margin of Gondwana, including the Main Karoo Basin and the Sauce Grande Basin. Northeast of the Main Karoo Basin the tectonic regimes were dominated by extensional to transtensional stresses leading to the formation of the southeast African Karoo rift basins in which sedimentation took place mainly under terrestrial conditions. Karoo-aged basins located more towards the continental interiour of SW-Gondwana (Congo, Angola, and Paraná Basin) are commonly referred to as sag basins. Recent analysis of synsedimentary faulting, depositional style, facies architecture, and palaeocurrents of Karoo-aged sediments in the Paraná Basin and the Namibian part of the Kalahari-Karoo Basin strongly indicate the existence of a large intracontinental rift system. During the Late Palaeozoic, transgression of the Mesosaurus Inland Sea followed the axis of this rift system, which in the north runs approximately parallel to the elongation of the Paraná Basin and in the south along a region that was to become the continental margins of southwestern Africa and southeastern South America after opening of the South Atlantic Ocean.

In Namibia and South Africa deposits of the Mesosaurus Inland Sea are preserved in the successions of the glacial Dwyka Group and the postglacial Ecca Group (Karoo Supergroup). These deposits comprise the major part of a 60-70 Ma depositional supercycle and are the main focus of this study. The large-scale transgressive part of this supercycle started in the Late Carboniferous with continental glacial deposits followed by marine glacial and postglacial inland sea deposits. During the Early Permian the Mesosaurus Inland Sea reached its greatest extent, which was accompanied by widespread deposition of C$_{org}$-rich sediments and localized precipitation of evaporites. The large scale regressive part is recorded by successions ranging from deep water offshore pelites and turbidite sandstones to shallow water shoreface and delta sandstones, deposited in a brackish environment. Shallow water inland sea sediments are in turn overlain by fluvio-lacustrine deposits, which are assigned to the Beaufort Group and form the upper part (post-inland sea phase) of the supercycle. This successive change in the depositional environment from marine to brackish to freshwater is also reflected in the fossil record. During Dwyka times a marine association of the Gondwana faunal province was able to colonize parts of the Mesosaurus Inland Sea. Later, during lower Ecca times the connection to the Panthalassan Ocean became insufficient to retain normal marine conditions, leading to strong faunal endemism in an isolated and brackish inland sea environment. The most well-known and widespread representatives of this endemic fauna are mesosaurid vertebrates and megadesmid bivalves. In contrast, the fluvio-lacustrine deposits of the Beaufort Group are world-renowned for numerous findings of terrestrial vertebrates.

In southern Namibia the main Dwyka and Ecca Group outcrops are located between Mariental and Keetmanshoop as well as between Aussenkjer and Karasburg. These areas form the present-day erosional western margin of the Kalahari-Karoo Basin, which extends from Namibia eastward into Botswana, South Africa and Zimbabwe, with the largest part of the Karoo deposits covered by Cenozoic Kalahari sediments. The Mariental-Keetmanshoop Karoo outcrop area received detrital sediment input mainly from the north (Windhoek Highlands and Ghanzi Ridge), whereas the provenance area of detrital sediments of the Aussenkjer-Karasburg area was situated to the south (Cargonian Highlands?). A sequence stratigraphic framework was developed for the southern Namibian Dwyka and Ecca deposits in order to improve the understanding of the development of the Mesosaurus Inland Sea in terms of depositional environments as well as short-term and long-term sea-level changes. This also refined the correlation of the southern Namibian inland sea successions with those of other regions, e.g. the Main Karoo Basin in South Africa and the Paraná Basin in Brazil. Furthermore, this sequence stratigraphic analysis enabled, for the first time, a proper and detailed correlation of argillaceous successions deposited in the distal parts of the basin with time-equivalent sandy and coal-bearing successions deposited at the basin margin.

Numerous altered tuffs occur as thin, light-coloured interlayers within argillaceous sediments of the Dwyka and Ecca Group of southern Namibia. The highest frequency of tuff layers is encountered in the lower part of the Dwyka Group and in the Collingham Formation of the Ecca Group. The macroscopical appearance of the tuff layers in the field depends largely on their mineralogical composition. The vast majority of the altered tuffs within the Dwyka and Ecca Group are represented by soft and crumbly to hard and indurated, clay-mineral-rich, bentonitic layers. Another, much rarer type occurs in the Whitehill Formation and is represented by very hard, chert-like tuff layers, which are rich in plagioclase (mostly albitic). Furthermore, white tuff layers within the Gai-As Formation of the Huab area are rich in potassium feldspar and have a porcelain-like appearance.

In the field the altered tuffs occur as laterally continuous laminae or thin layers with thicknesses ranging mainly from 1 mm to 2 cm. The basal contact of the tuffs is commonly plane and sharp, whereas the upper contact can either be sharp or gradational. All investigated tuff layers represent fine-grained, altered pyroclastic rocks. The diagenetically modified matrix is mainly crypto- to micro-crystalline and the grain size of primary pyroclastic crystal components ranges from fine to coarse ash. Normal grading can be frequently observed in thin sections. Crystal-rich basal parts of the tuffs often have a poorly sorted appearance, whereas the upper parts are always very well sorted. The majority of the tuffs appear at first sight massive. However, polished specimen show, in some tuffs, plane lamination or bedding with two or more subunits forming a tuff layer. Some display a weakly developed, discontinuous, and wavy lamination. Only in very rare cases have structures reminiscent of sedimentary micro-cross lamination been observed. Bioturbation, however, is a common feature of the tuff layers. The sedimentary textures and structures of the tuffs indicate that they have been deposited mainly as distal ash-fall layers by suspension settling in water. Some may have also been deposited or modified under the influence of weak bottom currents.

The primary, pyroclastic macro-components of the tuffs are mainly represented by crystals of quartz, plagioclase, and biotite. In some thin sections pseudomorphs after pyroxene or hornblende have been observed. Almost all of these crystals display either highly angular (often splintery) or euhedral shapes, whereas rounded crystals are more or less absent. Euhedral zircon and apatite crystals, despite being accessory components, have been observed in fair amounts in almost every tuff. Vitric or formerly vitric macro-components are very rare. In some tuffs dark lens- and schlieren-like, flattened clasts, which behave isotropic under crossed polars, possibly represent altered remnants of originally vitiric pyroclasts. In contrast, samples of the Gai-As Tuffs from the NW-Namibian Huab area contain large concentrations of very well-preserved former glass shards, now mainly replaced by barite. They show mainly platy and arcuate forms but also tricuspate and Y-shaped bubble-wall shards are common.

The matrix of the majority of the investigated tuffs is predominantly composed of clay minerals. However, the matrix of the tuff layers originally consisted most probably of fine vitric ash particles. Soon after deposition the volcanic ash was diagenetically altered to smectitic clay minerals. At a later stage smectite was progressively replaced by illite under prograde conditions. Nowadays the matrix of the bentonitic tuffs is strongly illite-dominated and only in the softer tuff layers a minor smectite content can be detected. Within some of the softer bentonites large booklets and vermicules reminiscent of kaolinite can be found. In thin sections their bright interference colours under crossed polars however rule out a kaolinitic composition. It is suspected that these booklets and vermicules originally represented early diagenetically formed crystal aggregates of kaolinite, which were replaced by illite at a later stage. The illitization of the tuffs may have been initiated already during burial of the deposits. However, the main thermal overprinting occurred most probably during the Jurassic when thick dolerite sills and dykes intruded the strata. This intrusion of hot basaltic magma caused, in many tuffs, a strong contact-metamorphic overprinting, which is documented by the widespread growth of cordierite porphyroblasts. The latter cause the intensive greenish speckling of many tuff layers (chlorite-rich, pinitized cordierite). The progressive illitization is geochemically reflected by increasing potassium and alumina as well as decreasing silica, sodium, and calcium contents of the tuffs. Furthermore, this process is also responsible for the increasing induration of the tuffs. Major element geochemistry shows that the softer bentonitic tuffs have low potassium contents, whereas the stronger indurated samples are high in potassium. The genesis of the plagioclase-rich tuffs, which are mutually associated with bentonitic tuffs within the Whitehill Formation, is not fully understood. The original presence of evaporites within this formation however may have in some way been responsible for the later albitization of a few of the tuff layers. Similarly, the potassium feldspathization of the Gai-As tuffs has been attributed to deposition in an alkaline lacustrine environment.

Both the primary macrocrystic components (qz, pla, bio, ± px/hbl?, ± K-fsp?, zr, ap) as well as the trace and rare earth element geochemistry of the altered tuffs indicate that their source magmas were mainly of intermediate, rhyodacitic-dacitic composition. Only some samples of the Ganigobis Tuffs from the Dwyka Group have a more andesitic-basaltic affinity. The abundance of splintery quartz and feldspar crystal fragments within the tuffs hints at a highly explosive plinian or phreatoplinian eruption style of the source volcanoes, which were most probably located within a subduction-related volcanic arc region along the southern margin of Gondwana. The presence of euhedral magmatic zicons of Lower-Middle Ordovician (Fammatinian) ages (~480-460 Ma) within two tuffs from the basal part of the Ecca Group in southern Namibia and in the western Cape Province of South Africa support a distal origin for the majority of the tuffs found in southern Africa and central-eastern South America within Late Palaeozoic successions. Possible source regions in SW-Gondwana, where Ordovician and Late Palaeozoic magmatic rocks are mutually associated, are the southwestern part of South America and the Antarctic Peninsula. A more proximal (but largely unknown) source area for some Dwyka tuffs, however, cannot be ruled out and is even very likely for Upper Permian to Lower Triassic pyroclastics in the Beaufort Group.

New single zircon U-Pb SHRIMP datings of selected volcanic ash layers, combined with earlier SHRIMP ages, provide a much more reliable age control of the sedimentary succession of the Dwyka and Ecca Groups and refine earlier, often ambiguous age constraints mainly derived from biostratigraphic data. U-Pb SHRIMP ages for tuff layers from the glaciogenic Dwyka Group in southern Namibia and southwestern South Africa range from 302.0 ± 3.0 to 297.1 ± 1.8 Ma (Gzehlian-Asselian). The basal part of the early post-glacial Prince Albert Formation is dated at around 290 Ma (Sakmarian) and deglaciation appears to be largely synchronous for the southwestern part of the Karoo Basin. SHRIMP ages for tuff layers from the upper part of the Prince Albert Formation, the Whitehill Formation, and the middle part of the Collingham Formation indicate that the Mesosaurus Sea reached its greatest extent at around 280 Ma (Artinskian). Radiometric ages for tuff layers in the fluvio-lacustrine Gai-As (~265 Ma) and Teekloof Formations (~261 Ma) show that the Mesosaurus/Ecca Inland Sea existed until the Middle-Late Permian, documenting an enormous life span of about 40-50 million years for this Late Palaeozoic inland sea.

Kurzfassung

Während des Spätpaläozoikums waren riesige Areale (~5 Mio km^2) Südwest-Gondwanas vom sogenannten Mesosaurus Inlandmeer bedeckt. Die Karoo Becken Südwest-Afrikas sowie das Paraná und das Sauce Grande Becken Südamerikas stellen dabei die Hauptablagerungsgebiete dieses Inlandmeeres dar. Weitere Ablagerungen finden sich auch im Ellsworth und im Transantarktischen Gebirge der Antarktis. Alle diese Gebiete waren vor dem Auseinanderbrechen Gondwanas und der darauf folgenden Öffnung des Südatantiks miteinander verbunden.

Die vom Mesosaurus Inlandmeer überfluteten Beckenbereiche bildeten sich in unterschiedlichen tektonischen Regimes. Während des Spätpaläozoikums wurde ozeanische Kruste des Panthalassischen Ozeans unter den südlichen Kontinentalrand Gondwanas subduziert, was mit der Bildung eines magmatischen Bogenkomplexes einherging und von Akkretions- und Gebirgsbildungsprozessen begleitet wurde. Im Zuge dieser Subduktions- und Deformationsprozesse bildeten sich entlang des südlichen, konvergenten Kontinentalrandes Gondwanas ausgedehnte Vorlandbeckensysteme im Rückraum des magmatischen Bogenkomplexes. Zu diesen Vorlandbecken gehören unter anderen das Haupt-Karoo Becken und das Sauce Grande Becken. Nordöstlich des Haupt-Karoo Beckens war die Tektonik hauptsächlich durch extensionale und transtensionale Spannungszustände gekennzeichnet. Dies führte zur Bildung der südostafrikanischen Riftbecken, in denen im Spätpaläozoikum hauptsächlich terrestrische Sedimente zur Ablagerung kamen. Karoo-zeitliche Becken, die sich mehr im Zentralbereich Südwest-Gondwanas befanden, wie z.B. das Kongo, Angola und Paraná Becken, werden gewöhnlich als intrakontinentale Sackungsbecken bezeichnet. Neueste Studien synsedimentärer Störungsaktivität in Karoo-zeitlichen Sedimenten sowie deren Ablagerungsbedingungen, Faziesarchitektur und Paläoströmungsrichtungen im Paraná Becken und im namibianischen Teil des Kalahari-Karoo Beckens lieferten überzeugende Hinweise auf die Existenz einer intrakontinentalen Riftzone. Die Transgression des Mesosaurus Inlandmeeres erfolgte entlang der Achse dieser Riftzone, die im Norden in etwa der Längsachse des Paraná Beckens folgte. Im Süden verlief die Riftachse entlang eines Bereiches, aus dem später, nach Öffnung des Südatlantiks, die Kontinentalränder Südwest-Afrikas und Südost-Südamerikas hervorgingen.

In Namibia und Südafrika sind die Ablagerungen des Mesosaurus Inlandmeeres in den Sedimentabfolgen der glazialen Dwyka Gruppe und der postglazialen Ecca Gruppe überliefert, welche den älteren Teil der Karoo Supergruppe bilden. Diese Sedimente umfassen den größten Teil eines etwa 60-70 Ma langen Ablagerungs-Großzyklus. Ihnen gilt das Hauptaugenmerk dieser Untersuchungen. Der transgressive Teil dieses Großzyklus begann im späten Karbon mit der Ablagerung von kontinentalen Glazialsedimenten, auf die marine Glazial- und Post-Glazialablagerungen des Mesosaurus Inlandmeeres folgten. Während des frühen Perms erreichte dieses Inlandmeer seine größte Ausdehnung, was mit der weit verbreiteten Ablagerung von C$_{org}$-reichen Sedimenten und der lokalen Abscheidung von Evaporiten einherging. Der regressive Teil ist durch Sedimentabfolgen gekennzeichnet, die von Tiefsee-Peliten und Turbiditen zu Küsten- und Delta-Sandsteinen reichen, welche in einem brackischem Milieu abgelagert wurden. Auf die Flachwasser-Sedimente dieses Inlandmeeres folgen fluvial-lakustrine Ablagerungen, die in die Beaufort Gruppe gestellt werden und die den oberen Teil (Post-Inlandmeer-Phase) des Ablagerungs-Großzyklus bilden. Diese Wechsel in den Ablagerungsmilieus von Salzwasser über Brackwasser zu Süßwasser spiegeln sich auch in den Fossilienfunden wider. Zur Zeit der Dwyka konnten marine Vertreter der Gondwana-Faunenprovinz Teile des Mesosaurus Inlandmeeres besiedeln. Später, während der frühen Ecca-Zeit, konnten die marine Bedingungen aufgrund der stark eingeschränkten Verbindung zum Panthalassischen Ozean nicht aufrecht erhalten werden, was schließlich zu einem ausgeprägten Faunen-Endemismus in einem nahezu abgeschnittenen Brackwasser-Inlandmeer führte. Die bekanntesten und am weitesten verbreiteten Vertreter dieser endemischen Fauna sind mesosauride Wirbeltiere und megadesmide Muscheln. Die fluvial-lakustrinen Ablagerungen der Beaufort Gruppe sind dagegen für die zahlreichen Funde festländischer Wirbeltiere weltberühmt.

In Südnamibia befinden sich die Hauptaufschlußgebiete der Dwyka und Ecca Gruppe zwischen Mariental und Keetmanshoop sowie zwischen Aussenkjer und Karasburg. Diese Gebiete stellen heute den westlichen Erosionsrand des Kalahari-Karoo Beckens dar, welches sich von Namibia ostwärts nach Botswana, Südafrika und Zimbabwe erstreckt, wobei jedoch der größte Teil der Karoo-Sedimente durch känozoische Kalahari-Ablagerungen überdeckt ist. Der detritische Sedimenteintrag in das Mariental-Keetmanshoop Karoo-Aufschlußgebiet erfolgte hauptsächlich von Norden (vom Windhoek Hochland und vom Ghanzi Rücken), wohingegen das Liefergebiet detritischer Sedimente des Aussenkjer-Karasburg Gebietes im Süden lag (Cargonisches Hochland?). Für die südnamibianischen Dwyka und Ecca Ablagerungen wurde ein sequenz-stratigraphischer Rahmen erstellt, um

die Entwicklung des Mesosaurus Inlandmeeres hinsichtlich der Ablagerungsmilieus sowie hoch- und niederfrequenter Meeresspiegelschwankungen besser zu verstehen. Darüber hinaus diente dies zur Verfeinerung der Korrelation der südnamibianischen Inlandmeer-Abfolgen mit denen des Haupt-Karoo Beckens in Südafrika und des Paraná Beckens in Brasilien. Desweiteren ermöglichte diese sequenz-stratigraphische Analyse zum ersten mal die exakte und detaillierte Korrelation von distalen tonigen Beckensedimenten mit proximalen sandigen und kohleführenden Ablagerungen des Beckenrandes.

In den tonigen Sedimenten der Dwyka und Ecca Gruppe treten im südlichen Namibia zahlreiche alterierte Tuffe als geringmächtige, helle Zwischenlagen auf. Die höchste Anzahl von Tuffen findet sich im unteren Teil der Dwyka und in der Collingham Formation der Ecca Gruppe. Das makro-skopische Erscheinungsbild der Tuffe im Gelände hängt größtenteils von deren mineralogischen Zusammensetzung ab. Die überwiegende Anzahl der alterierten Tuffe bilden tonmineralreiche, bentonitische Lagen innerhalb der Dwyka und Ecca Gruppe. Sie können sowohl weich und bröckelig als auch stärker verfestigt und härter ausgebildet sein. Ein anderer, viel selteneren Typ tritt in der Whitehill Formation auf, welcher durch sehr harte, chertartige Tufflagen gekennzeichnet ist, die reich an Plagioklas (hauptsächlich Albit) sind. Desweiteren treten in der Gai-As Formation des Huab Gebietes porzellanartige, weiße Tufflagen auf, die reich an Kalifeldspat sind.

Im Gelände treten die Tuffe als horizontbeständige Laminae oder Lagen auf, deren Mächtigkeiten hauptsächlich zwischen 1 mm und 2 cm liegen. Der Basiskontakt der Tuffe ist gewöhnlich eben und scharf begrenzt, wohingegen der Topbereich sowohl scharf als auch graduell zum Nebengestein ausgebildet sein kann. Alle untersuchten Tuffe stellen feinkörnige, alterierte pyroklastische Gesteine dar. Die diagenetisch veränderte Matrix der Tuffe ist hauptsächlich krypto- bis mikrokristallin und die Korngröße primärer pyroklastischer Kristallkomponenten liegt im Bereich feiner bis grober Asche. In Dünnschliffen kann man häufig normale Gradierung beobachten. Die häufig kristallreichen Basal-bereiche der Tuffe erscheinen meist schlecht sortiert, wohingegen die oberen Bereiche immer sehr gut sortiert sind. Die Mehrheit der Tuffe erscheint makroskopisch zunächst massig. Polierte Hand-stücke lassen jedoch erkennen, daß manche Tuffe horizontalgeschichtet oder laminiert sind, wobei eine Tufflage aus zwei oder mehr Untereinheiten aufgebaut sein kann. Einige wenige lassen auch eine undeutlich entwickelte, nicht durchgängige, wellige Lamination erkennen. Nur in sehr seltenen Fällen konnten Strukturen beobachtet werden, die an sedimentäre Mikroschrägschichtung erinnern. Bioturbation ist ein häufiges Merkmal der Tuffe. Die Sedimentgefüge der Tuffe lassen darauf schliessen, daß diese hauptsächlich subaquatische Suspensionsablagerungen distalen Aschenfalls darstellen. Einige wenige können auch unter dem Einfluss schwacher Bodenströmungen ab- oder umgelagert worden sein.

Quarz-, Plagioklas- und Biotitkristalle bilden den Hauptteil der primären, pyroklastischen Makro-komponenten der Tuffe. In einigen Dünnschliffen konnten auch Pseudomorphosen nach Pyroxen oder Hornblende beobachtet werden. Fast alle diese Kristalle zeigen entweder stark eckige (oft splittrige) oder nahezu idiomorphe Formen, wohingegen gerundete Kristalle mehr oder weniger nicht vor-kommen. Idiomorphe Zirkon- und Apatitkristalle konnten als akzessorische Komponenten in nahezu jedem Tuff in recht hoher Anzahl beobachtet werden. Glasige oder ehemals glasige Makrokompo-nenten sind dagegen sehr rar. In einigen Tuffen wurden dunkle, linsen- und schlierenartige, geplättete Klasten beobachtet, die sich unter gekreuzten Polarisatoren isotrop verhalten. Dabei kann es sich möglicherweise um alterierte Relikte von ehemals glasigen Pyroklasten handeln. Die Proben der Gai-As Tuffe aus der NW-namibianischen Huab Region enthalten dagegen eine große Anzahl an gut erhaltenen Glasscherbenrelikte, die hauptsächlich durch Baryt ersetzt sind. Diese zeigen haupt-sächlich plattige und bogenartige Formen, aber auch sternförmig-dreizackige und ypsilonförmige Scherben von Blasenwandungen sind anzutreffen.

Die Matrix der meisten untersuchten Tuffe ist überwiegend aus Tonmineralen aufgebaut. Ursprünglich setzte sich die Matrix der Tuffe jedoch höchstwahrscheinlich aus feinkörnigen, glasigen Aschen-partikeln zusammen. Schon bald nach Ablagerung der vulkanischen Asche wurde diese diagenetisch zu smektitischen Tonmineralen umgewandelt. Zu einem späteren Zeitpunkt wurde dann Smektit zunehmend von Illit unter höhergradigen Bedingungen verdrängt. Heute ist die Matrix der bentonitischen Tuffe stark Illit-dominiert und nur in den weicheren Tufflagen lassen sich noch geringe Smektitgehalte nachweisen. In den weicheren Bentoniten finden sich auch große buch- und wurm-artige Kristalle, die stark an Kaolinit erinnern. In Dünnschliffen zeigen diese Kristalle unter gekreuzten Polarisatoren jedoch bunte Interferenzfarben und schliessen damit eine kaolinitische Zusammen-setzung aus. Es wird daher vermutet, daß es sich bei diesen buch- und wurmartigen Kristallen um frühdiagenetisch gebildete Kristallaggregate von Kaolinit handelt, die dann später illitisiert wurden. Die Illitisierung der Tuffe mag schon früh während der Versenkung der Ablagerungen begonnen haben,

aber die thermische Hauptüberprägung fand höchstwahrscheinlich im Zuge der jurassischen Dolerit-intrusionen statt, die als Gänge und Lagergänge in die Schichten eindrangen. Diese Intrusion von heissem basaltischem Magma verursachte in vielen Tuffen eine starke kontakt-metamorphe Über-prägung, die durch das weitverbreitete Auftreten von Cordierit-Porphyroblasten dokumentiert ist. Letztere sind für die intensive grüne Sprenkelung vieler Tuffe verantwortlich (chloritreiche, pinitisierte Cordierite). Die progressive Illitisierung spiegelt sich geochemisch durch ansteigende Kalium- und Aluminiumgehalte sowie durch abnehmende Silizium-, Natrium- und Calciumgehalte in den Tuffen wider. Desweiteren ist dieser Vorgang auch für eine zunehmende Verfestigung der Tuffe verant-wortlich. Die Hauptelement-Geochemie der Tuffe zeigt, daß die weicheren, bentonitischen Tuffe niedrigere Kaliumgehalte aufweisen, wohingegen die stärker verfestigten an Kalium angereichert sind. Die Bildung der plagioklasreichen Tuffe, die in der Whitehill Formation in engem räumlichen Zusammenhang mit den bentonitischen Tuffen stehen, ist noch nicht völlig verstanden. Das ursprüngliche Vorhandensein von Evaporiten in dieser Formation lässt jedoch einen Zusammenhang mit der späteren Albitisierung einiger weniger Tufflagen vermuten. In ähnlicher Weise wird auch die Kalifeldspatisierung der Gai-As Tuffe mit der Ablagerung in einem alkalischen Seemilieu in Ver-bindung gebracht.

Sowohl die primär-pyroklastischen Makrokristallkomponenten (Qz, Pla, Bio, ± Px/Hbl?, ± K-Fsp?, Zr, Ap) als auch die Spuren- und Seltene-Erden-Element-Geochemie der alterierten Tuffe weisen darauf hin, daß ihre Ursprungsmagmen von intermediärer, rhyhodazitischer-dazitischer Zusammensetzung waren. Einige wenige Proben der Ganigobis Tuffe aus der Dwyka Gruppe habe auch eine stärker andesitisch-basaltische Affinität. Das zahlreiche Auftreten von splittrigen Quarz- und Feldspat-Kristallfragmenten in den Tuffen weist auf einen hochexplosiven, plinianischen oder phreato-plinianischen Eruptionsstil der Vulkane hin, die höchstwahrscheinlich in einer subduktionsbeinflussten vulkanischen Bogenregion am Südrand Gondwanas gelegen waren. Das Auftreten idiomorpher, magmatischer Zirkone mit unter- bis mittelordovizischen (fammatinischen) Altern (~480-460 Ma) in zwei Tuffen aus dem Basalbereich der Ecca Gruppe in Südnamibia und der westlichen Kapregion Südafrikas unterstützt die Vermutung, daß die Mehrheit der spätpaläozoischen Tuffe im südlichen Afrika und im zentral-östlichen Südamerika distalen Ursprungs sind. Mögliche Herkunftsgebiete in SW-Gondwana, wo ordovizische und spätpaläozoische Magmatite in engem räumlichen Zusammen-hang stehen, sind der südwestliche Teil Südamerikas und die Antarktische Halbinsel. Ein mehr proximales, aber weitgehend unbekanntes Herkunftsgebiet kann für einige wenige Dwyka Tuffe nicht ausgeschlossen werden, und ist sogar sehr wahrscheinlich für die oberpermischen-untertriassischen Pyroklastika der Beaufort Gruppe.

Neue U-Pb Einzelzirkon SHRIMP-Datierungen von ausgesuchten vulkanischen Aschenlagen, in Kombination mit früheren SHRIMP-Daten, ermöglichen nun eine viel verlässlichere Alterskontrolle der Sedimentabfolge der Dwyka und Ecca Gruppe. Weiterhin können damit nun frühere, oft wider-sprüchliche Altersangaben, die hauptsächlich aus biostratigraphischen Daten abgeleitet wurden, ver-feinert werden. U-Pb SHRIMP-Alter für Tufflagen aus der glazialgeprägten Dwyka Gruppe aus Süd-namibia und SW-Südafrika reichen von 302.0 ± 3.0 to 297.1 ± 1.8 Ma (Gzehlian-Asselian). Der Basalbereich der früh-postglazialen Prince Albert Formation ist auf etwa 290 Ma (Sakmarian) datiert und der Gletscherrückzug erscheint zumindest für den südwestlichen Teil des Karoo Beckens mehr oder weniger gleichzeitig abgelaufen zu sein. SHRIMP-Alter von Tufflagen im oberen Bereich der Prince Albert Formation, innerhalb der Whitehill Formation und im mittleren Teil der Collingham Formation belegen, daß das Mesosaurus Inlandmeer seine größte Ausdehnung vor etwa 280 Ma (Artinskian) erreichte. Radiometrische Alter für Tufflagen in der fluvial-lakustrinen Gai-As Formation (~265 Ma) und der Teekloof Formation (~261 Ma) zeigen, daß das Mesosaurus/Ecca Inlandmeer etwa bis zum mittleren bis späten Perm existierte. Dies dokumentiert die enorm lange Lebensdauer dieses spätpaläozoischen Inlandmeeres von ca. 40-50 Ma.

Chapter 1 – Introduction

1.1 Objectives of the study

The main focuses of this study are the Carboniferous-Permian Karoo deposits of southern Namibia, which are represented by the Dwyka and Ecca Groups. The majority of these deposits form a part of those sediments, which were laid down in a large inland sea underlain by continental crust. This inland sea, which is in this study referred to as the Mesosaurus Inland Sea, covered in the Late Palaeozoic vast areas (~5 Mio km^2) of the SW-Gondwanan continental interior. Major depocentres of the Mesosaurus Inland Sea are represented by the Kalahari-Karoo Basin (Namibia, Botswana), the Main Karoo Basin (South Africa & Falkland Islands), the Paraná Basin (Brazil, Paraguay and Uruguay) and the Sauce Grande Basin (central-eastern Argentina). In addition, deposits of the Mesosaurus Inland Sea can also be found in the Ellsworth and Transantarctic Mountains of Antarctica. These South American and southern African basins as well as the mentioned areas in Antarctica were originally interconnected prior to the break-up of Gondwana and the formation of the South Atlantic Ocean.

The Dwyka Group comprises all sediments of glacial origin, which were deposited during the Late Palaeozoic Ice Age in South Africa and Namibia. In southern Namibia only the basal part of the Dwyka Group sediments are of glacio-terrestrial origin, whereas the majority was deposited in an inland sea under glacio-marine conditions. The subsequent, post-glacial inland sea deposits of southern Africa are placed into the Ecca Group. Fluvio-lacustrine sediments succeeding the inland sea deposits of the Ecca Group are represented by the Beaufort Group in South Africa.

In southern Namibia the glacial deposits of the Dwyka Group and the basal sandy deposits of the Ecca Group were lately studied by Grill (1997), Stollhofen (1999), Bangert (2000), and Geiger (2000). This study extends these investigations to the younger deposits of the Ecca Group in order to provide an updated and comprehensive picture of the lithostratigraphy and the sedimentological development of the Mesosaurus Inland Sea in its southern Namibian region. Additionally, an updated and extended sequence stratigraphic framework is errected for the successions of the southern Namibian Dwyka and Ecca Groups. In combination with other stratigraphic methods this enables, for the first time, a proper correlation of argillaceous successions deposited in the distal parts of the basin with time-equivalent sandy and coal-bearing successions deposited at the basin margin. Furthermore, this sequence stratigraphic interpretation also improves the understanding of the development of the Mesosaurus Inland Sea in terms of short-term and long-term sea-level changes, which also refines the correla-

tion of the southern Namibian inland sea succession with those of other regions, e.g. that of the Main Karoo Basin in South Africa and that of the Paraná Basin in Brazil.

Another main focus of this study is the thorough investigation and description of the altered pyroclastic layers, which are intercalated as thin ash-fall tuffs in the argillaceous inland sea deposits of the Dwyka and Ecca Groups. The tuff layers of the southern Namibian Dwyka Group were already studied in detail by Bangert (2000) and Geiger (2000). Therefore, the Dwyka tuffs are only shortly reviewed and some alternative interpretations concerning the observed mineralogy are presented. The newly discovered tuff layers within Ecca Group deposits are presented in greater detail. Comprehensive petrographic descriptions supported by XRD measurements provide detailed information about their mineralogy reflecting both primary compositions and secondary alteration processes. Major, trace and REE element compositions of the tuff layers have been determined in order to gain information about their present-day mineralogical composition, the orginal geochemical character of the source magma as well as its possible tectonic setting, and the influence of secondary processes. For comparison purposes also a tuff layer from the younger (Upper Permian), fluvio-lacustrine Gai-As Formation of the NW-Namibian Huab area is described. The Gai-As Tuff was deposited in an alkaline lake environment, which succeeded the inland sea environment of the Ecca Group deposits in this area after a depositional hiatus of 10-15 Ma.

From selected tuff layers of the Ecca Group euhedral zircons of suspected magmatic origin were separated in order to obtain single zircon U-Pb radiometric ages for the tuff layers using the SHRIMP method. Apart from the calculated ages, the U and Th isotope measurements also provide interesting hints about the zircon sources and possible provenance areas. An important aspect of these new tuff datings is that they provide new age constraints for the Late Palaeozoic succession of southern Namibia. In addition, due to the highly reliable corre-lation of the southern Namibian Late Palaeozoic Dwyka and Ecca successions with those of the western part of the South African Main Karoo Basin and those of the Brazilian Paraná Basin these newly obtained radiometric ages are also valid and transferable to these other depocentres of the Mesosaurus Inland Sea. Furthermore, these ages also provide a new calibration tool for biostratigraphic data and the early deformational history of the Cape Fold Belt.

1.2 Study area

The study area lies in southern Namibia, where Late Palaeozoic sediments of the Dwyka and Ecca Groups (Karoo Supergroup) form the western outcrop margin of the Kalahari-Karoo Basin (Fig. 1.1). Towards the east these sediments are covered by Cenozoic Kalahari sediments but continue in subcrop far into Botswana and even up to Zimbabwe. The Namibian part of the Kalahari-Karoo Basin is also known as the northerly Aranos Basin and the southerly Karasburg Basin. In southern Namibia the main Karoo outcrops are situated between Mariental and Keetmanshoop as well as between Aussenkjer and Karasburg (Fig. 1.1). For the eastern part of the Aranos Basin the data of more than sixty coal exploration wells are available. Fieldwork for this study concentrated mainly on the areas between Tses and Keetmanshoop as well as between Aussenkjer and Noordoewer (Fig. 1.1).
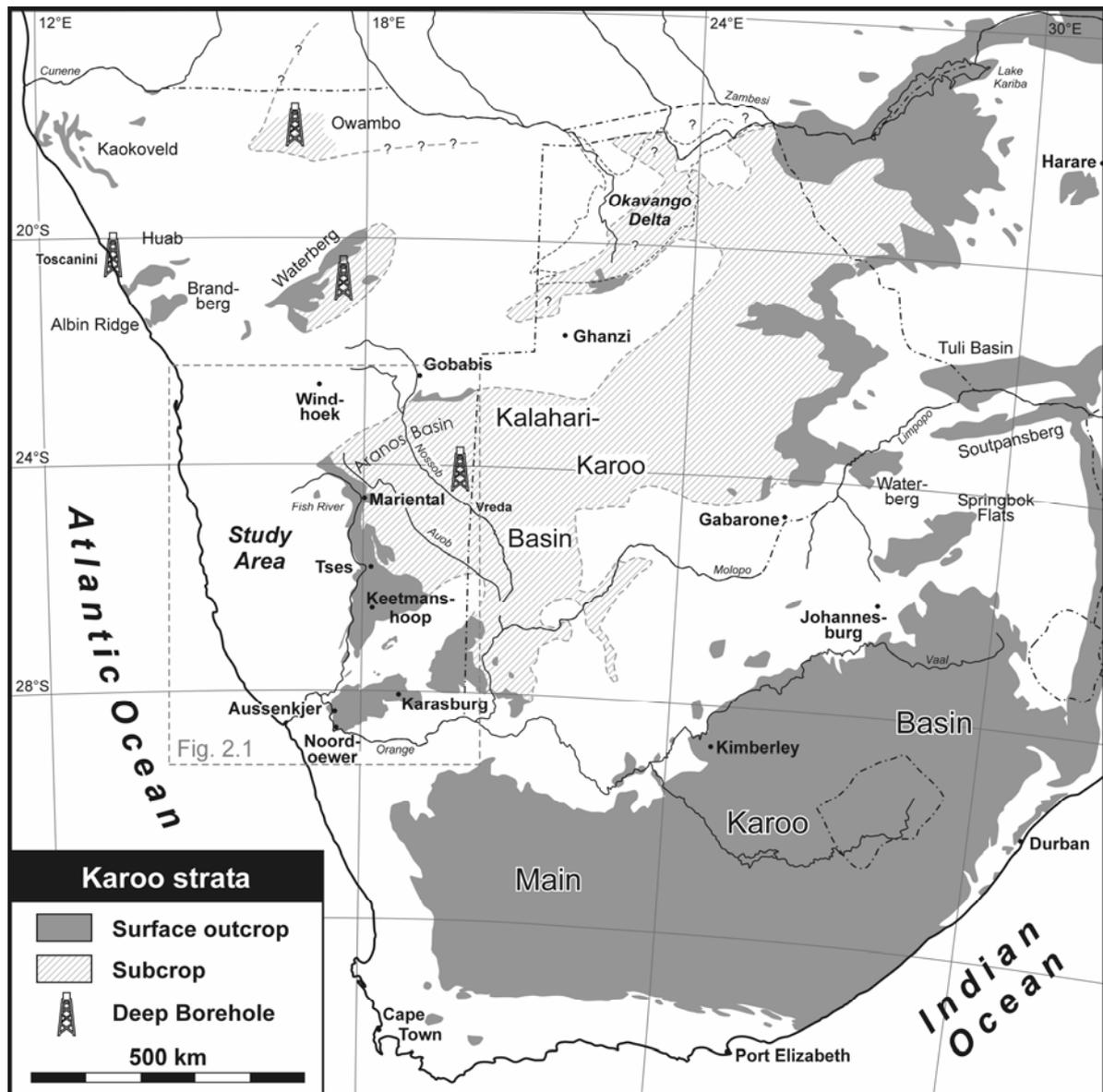
Fig. 1.1: Location map showing the study area in southern Africa. Within southern Africa the study area is located in southern Namibia and forms the western outcrop margin of the Kalahari-Karoo Basin. This map was compiled from numerous sources.

Towards the north the Dwyka and Ecca Group deposits of the Kalahari-Karoo Basin are separated from the northerly Karoo outcrop areas (Huab, Waterberg, Kaokoveld, Owambo, and Okavango area) by basement outcrops of the Windhoek Highlands and the Ghanzi Ridge (Fig. 1.6). This basement high existed in a similar form already during the Late Palaeozoic. However, during periods of high sea level some Ecca Group sediments may have transgressed certain parts of this highland to connect for example the Kalahari-Karoo Basin with the northerly Waterberg Basin. In the south, Karoo outcrops between Keetmanshoop and Karasburg are today separated by the Karasburg Ridge (Fig. 1.6), a mountain range consisting of basement outcrops (Karas Mountains). During deposition of the Dwyka and Ecca Groups this basement high formed most probably a largely submergent swell with some smaller areas possibly forming emergent islands. The Kalahari-Karoo Basin is also separated today from the Main Karoo Basin of South Africa by basement outcrops. During deposition of the Dwyka Group this area acted as a glaciated basement high, which is known as the so-called Cargonian Highlands (Visser, 1983a) (Fig. 1.6). During deposition of the lower Ecca Group the western part of this highland was probably largely flooded by the transgressing Mesosaurus Inland Sea. Originally the sediments of the Dwyka and Ecca Groups of southern Namibia continued farther to the west and were connected with the Paraná and Sauce Grande Basins of eastern South America, with the Uruguay Shield between forming a large island (Visser & Praekelt, 1998). During the break-up of Gondwana and the formation of the South Atlantic Ocean the continental margin of southwestern Africa was uplifted causing erosion of the Karoo deposits in southwestern Namibia.

1.3 The Mesosaurus Inland Sea

1.3.1 Palaeogeography

During the Late Palaeozoic the Mesosaurus Inland Sea covered vast areas (~5 Mio km^2) of the SW-Gondwanan continental interior. The Mesosaurus Inland Sea is is named after the small swimming vertebrate *Mesosaurus,* which inhabited for a short time in the early Permian this inland sea. Today it can be found both in South America and southern Africa and its distribution on the two continents was one of the major arguments for the supporters of the hypothesis of continental drift in the first half of the 20th century (e.g. du Toit, 1937). Deposits of this inland sea can be found in present-day South America and southern Africa as well as in parts of Antarctica. Palaeogeographic maps, which show the position and extent of the Mesosaurus Inland Sea, all vary to a certain degree. This results mainly from the uncertainties about the marginal areas of this inland sea, which are not very well constrained. The palaeogeographic maps for the Permian compiled by Ziegler et al. (1997) give a frist good impression of the position of the Mesosaurus Inland Sea. Fig. 1.2-A & B represent two

time slices, which according to Ziegler et al. (1997) show the palaeogeography during the Artinskian (~260 Ma; late Early Permian) and the Kazanian (~253 Ma; early Late Permian). According to newer geochronological data and the recently published Geologic Time Scale 2004 (Gradstein et al., 2005) Fig. 1.2-A reflects more the situation during deposition of the uppermost Dwyka Group and lowermost Ecca Group around 290 Ma (Sakmarian), whereas Fig. 1.2-B reflects more or less the situation during deposition of the lower to middle Ecca Group between 280 and 270 Ma (Artinskian-Kungurian).
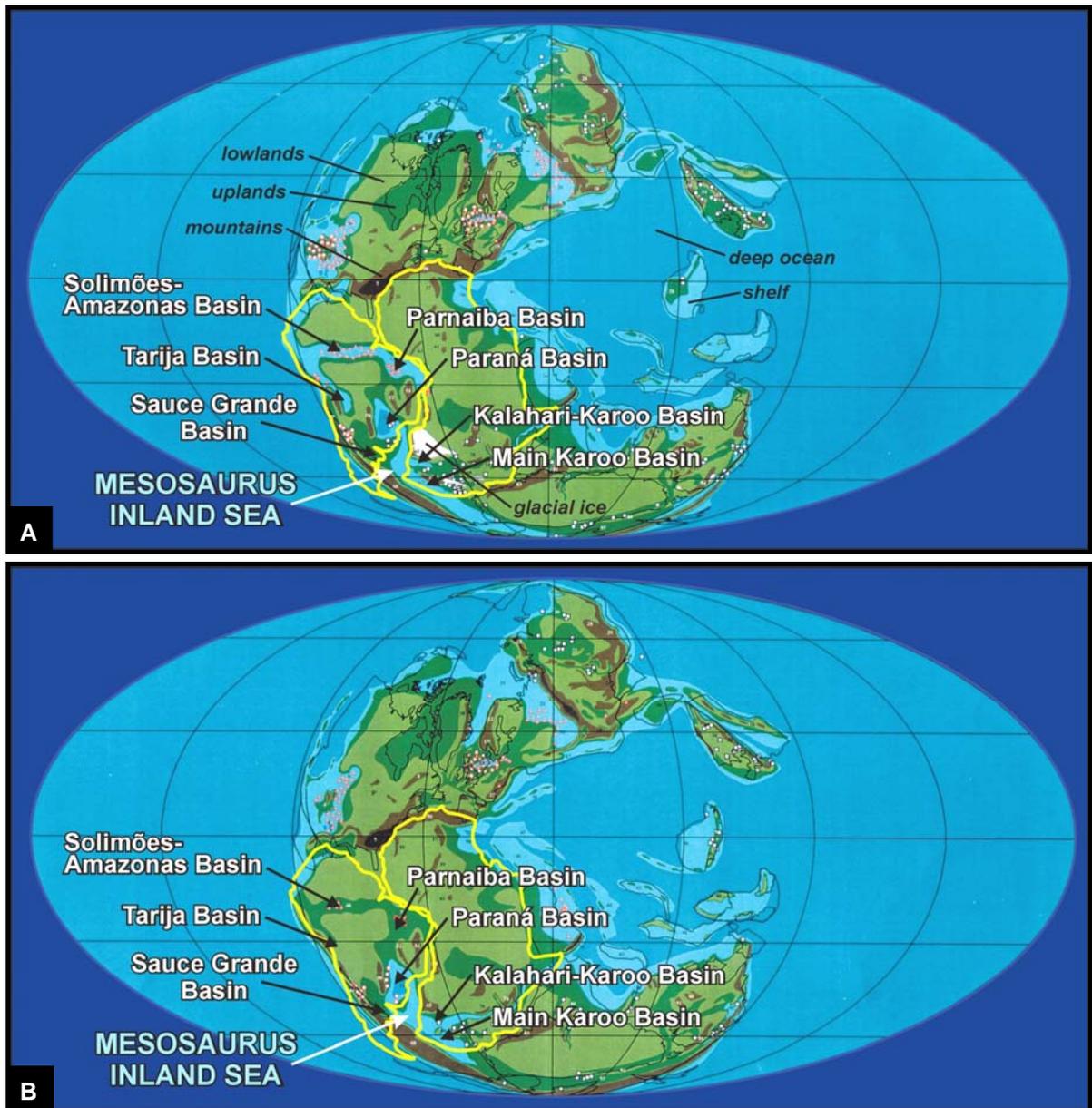
Fig. 1.2: Palaeogeographic maps for the Permian from Ziegler et al. (1997) showing the position and extent of the Mesosaurus Inland Sea as well as major depocentres within or in the vicinity of this inland sea. For a better orientation the present-day outlines of Africa and South America are highlighted. **(A)** Map showing the palaeogeographic situation during deposition of the uppermost Dwyka Group and the lowermost Ecca Group in the Sakmarian at around 290 Ma (originally the 'Artinskian' map). **(B)** Map showing the palaeogeographic situation during deposition of the lower to middle Ecca Group in the Artinskian-Kungurian between 280 and 270 Ma (originally the 'Kazanian' map). Small white squares indicate coal deposits and red triangles and circles indicate evaporites and aeolian sand dunes.

The main depositional areas of the Mesosaurus Inland Sea are represented in South America by the Paraná Basin of Brazil, Paraguay and Uruguay as well as the Sauce Grande Basin of central-eastern Argentina. In the 'Artinskian' map of Ziegler et al. (1997) a continental environment is shown by mistake for the Sauce Grande Basin, however, this area contains *Eurydesma*-bearing glaciomarine deposits and the post-glacial development mirrors that of the southern part of the Main Karoo Basin (Harrington, 1955; López-Gamundí & Rosello, 1998). Several authors suggested that the Paraná Basin area of the Mesosaurus Inland Sea was possibly connected to the north with the Parnaiba Basin and possibly even with the Solimões-Amazonas Basin during maximum sea level highstand in the Early Permian (Oelofsen & Araújo, 1983; Williams, 1995; Stollhofen, 1999). In southern Africa deposits of the Mesosaurus Inland Sea are mainly preserved in the Kalahari-Karoo Basin of Namibia and Botswana as well as in the Main Karoo Basin of South Africa (Visser & Praekelt, 1996 & 1998; Visser, 1997; Faure & Cole, 1999; Stollhofen, 1999). In addition, the Falkland-Malvinas Islands, which were positioned close to the SE coast of South Africa during the Late Palaeozoic, formed a small part of this depositional area. Towards the east deposits of this inland sea can be found in the Ellsworth and Transantarctic Mountains of Antarctica (Miller & Collinson, 1994; Veevers, 2000 & 2001). The Mesosaurus Inland Sea was possibly connected during its early stages to the south with the Panthalassan Ocean, with a connection located somewhere between Patagonia and the Antarctic Peninsula (Visser & Praekelt, 1996 & 1998) or between Thurston Island and Mary Bird Land (Miller & Collinson, 1994).

More detailed palaeogeographic reconstructions for the Mesosaurus Inland Sea, compiled by Visser & Praekelt (1998) and by Faure & Cole (1999), are shown in Fig. 1.3 & 1.4. Both reconstructions again show the Paraná Basin (including the Chaco-Paraná Basin as its southwestern appendix), the Sauce Grande Basin, the Kalahari-Karoo Basin, and the Main Karoo Basin as the major depocentres of the Mesosaurus Inland Sea with the Uruguay Shield representing a large island within the sea. Differences in its distribution mainly arise due to uncertainties in the marginal areas. It is still very uncertain how far the Mesosaurus Sea transgressed eastward into the Kalahari-Karoo Basin. In the maps of Visser & Praekelt (1998) the southeastward extension of the Mesosaurus Inland Sea into the present-day Transantarctic Mountains area is well displayed. Note that the palaeo-south pole is positioned in the maps of Faure & Cole (1999) east of the Gamburtsev Mountains of Antarctica, whereas Visser & Praekelt (1998) placed the palaeo-south pole south of Antarctica resulting in different palaeo-latitudes and palaeo-north directions.
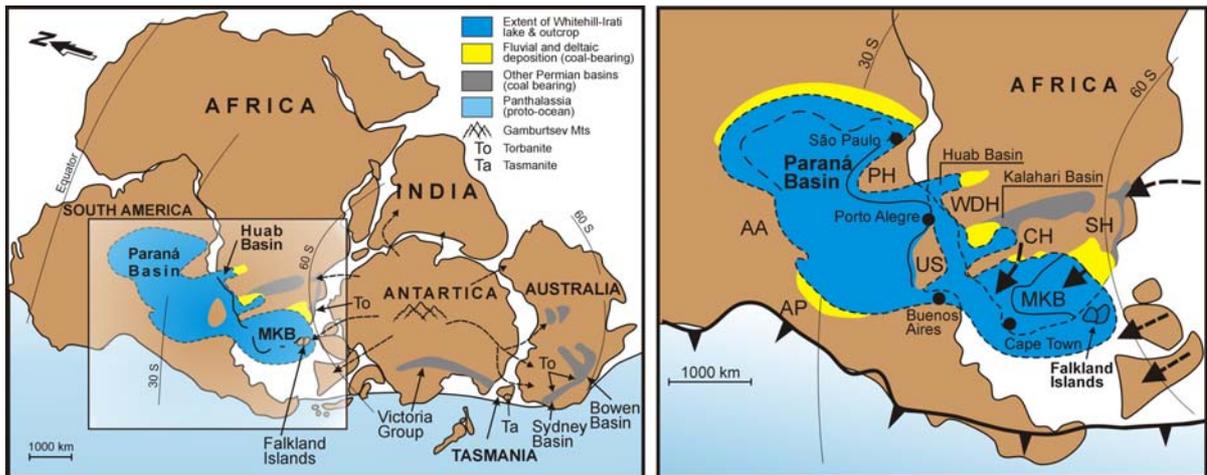
Fig. 1.3: Palaeogeographic maps showing the position of the Mesosaurus Inland Sea within SW-Gondwana during the Early Permian. These maps were originally compiled by Faure & Cole (1999) and redrawn (and kindly provided) by K. Scheffler. Symbols for palaeo-high terraines: AA = Asunción Arch; AP = Pampean Arch; US = Uruguay Shield; PH = Ponta Grossa High; WDH = Windhoek Highlands; CH = Cargonian Highlands; SH = Swaziland High. MKB = Main Karoo Basin.
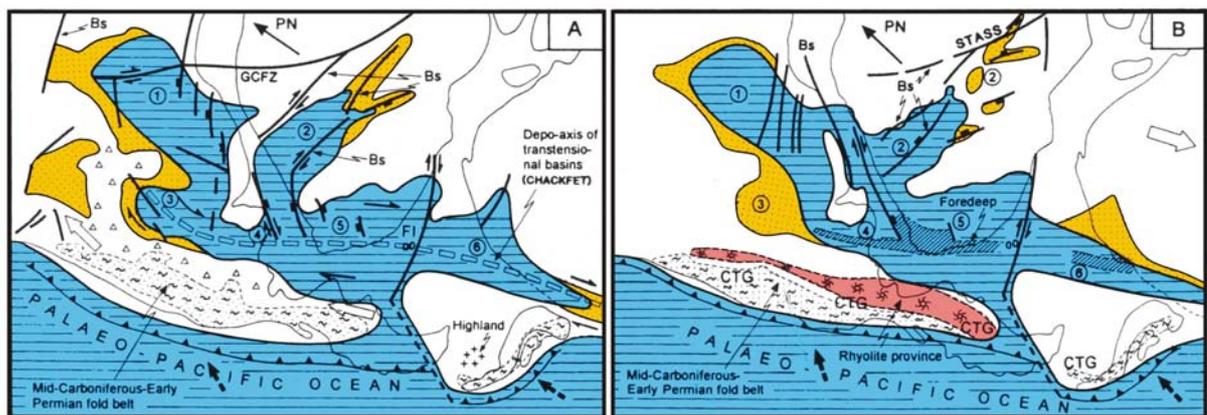
Fig. 1.4: Palaeogeographic maps of Visser & Praekelt (1998) showing the distribution and extent of the Mesosaurus Inland Sea during **(A)** the latest Carboniferous to earliest Permian and **(B)** during the Early Permian. Marine areas are coloured in blue and the areas marginal to the inland sea with terrestrial depositional conditions are coloured in yellow. In the right map the position of a part of the volcanic arc, which fringed the southern margin of Gondwana, is coloured in red. Newer data show that this arc was already existent in an incipient state during the Late Carboniferous. Furthermore, this arc was most probably continuous to east and reached into the area of the West-Antarctic terraines. This subduction-related magmatic arc represents the source area for most of the numerous tuff layers that can be found in the deposits of the Mesosaurus Inland Sea.

The palaeogeographic reconstruction shown in Fig. 1.5 advocates the possible northward extension of the Mesosaurus Inland Sea via a connecion of the Paraná Basin with the Parnaiba Basin and even parts of the Solimões-Amazonas Basin resulting in an elongate, probably rift-related seaway (Stollhofen, 1999; Stollhofen et al. 2000a).
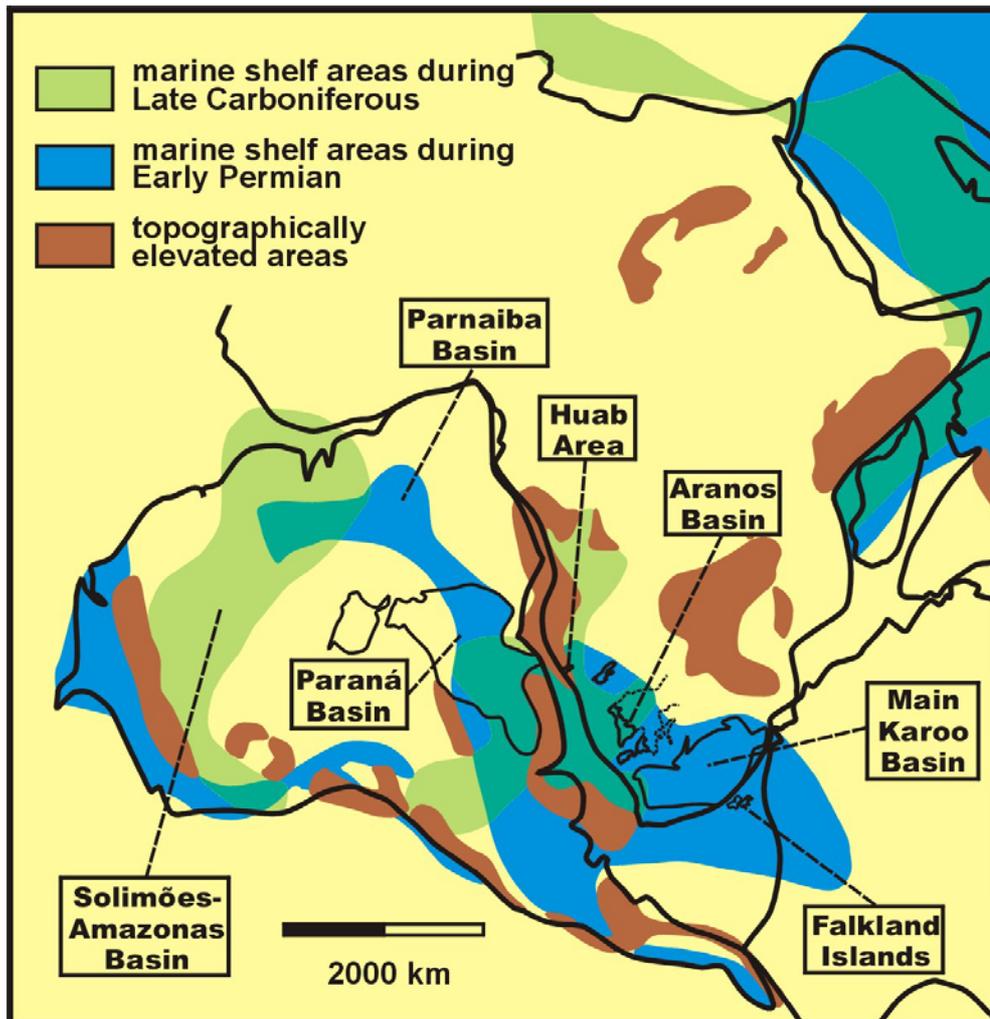
Fig. 1.5: Distribution of marine shelf areas during the Late Carboniferous (glacial) and the Early Permian (post-glacial). This palaeogeographic reconstruction advocates the possible northward extension of the Mesosaurus Inland Sea via a connection of the Paraná Basin with the Parnaiba Basin in northern Brazil resulting in an elongate, probably rift-related seaway. This map is slightly modified after Stollhofen et al. (2000a).

For the present-day southern African region the possible extent of the Mesosaurus Inland Sea during maximum transgression in the Early Permian is shown in Fig. 1.6. The western part of the Kalahari-Karoo Basin was most probably completely flooded during transgressive periods by this inland sea as indicated by glauconite occurrences in coal-bearing strata in the southwest Botswanan Ncojane area (Smith, 1984). It is however not known if and how far the sea could advance into the eastern parts of the Kalahari-Karoo Basin, which were character-ized by extensive, low lying coal swamps during the Early Permian. Similarily, the glauconite occurrences in coal strata in the northwestern part of the South African Main Karoo Basin suggest that during transgressions the sea could reach the area of the Witbank Coal Fields east of Johannesburg (Stanistreet et al., 1980). At the present-day southern and south-western margin of the Main Karoo Basin the development of the Cape Fold Belt was only in its incipient stage during deposition of the Ecca Group and probably became emergent not
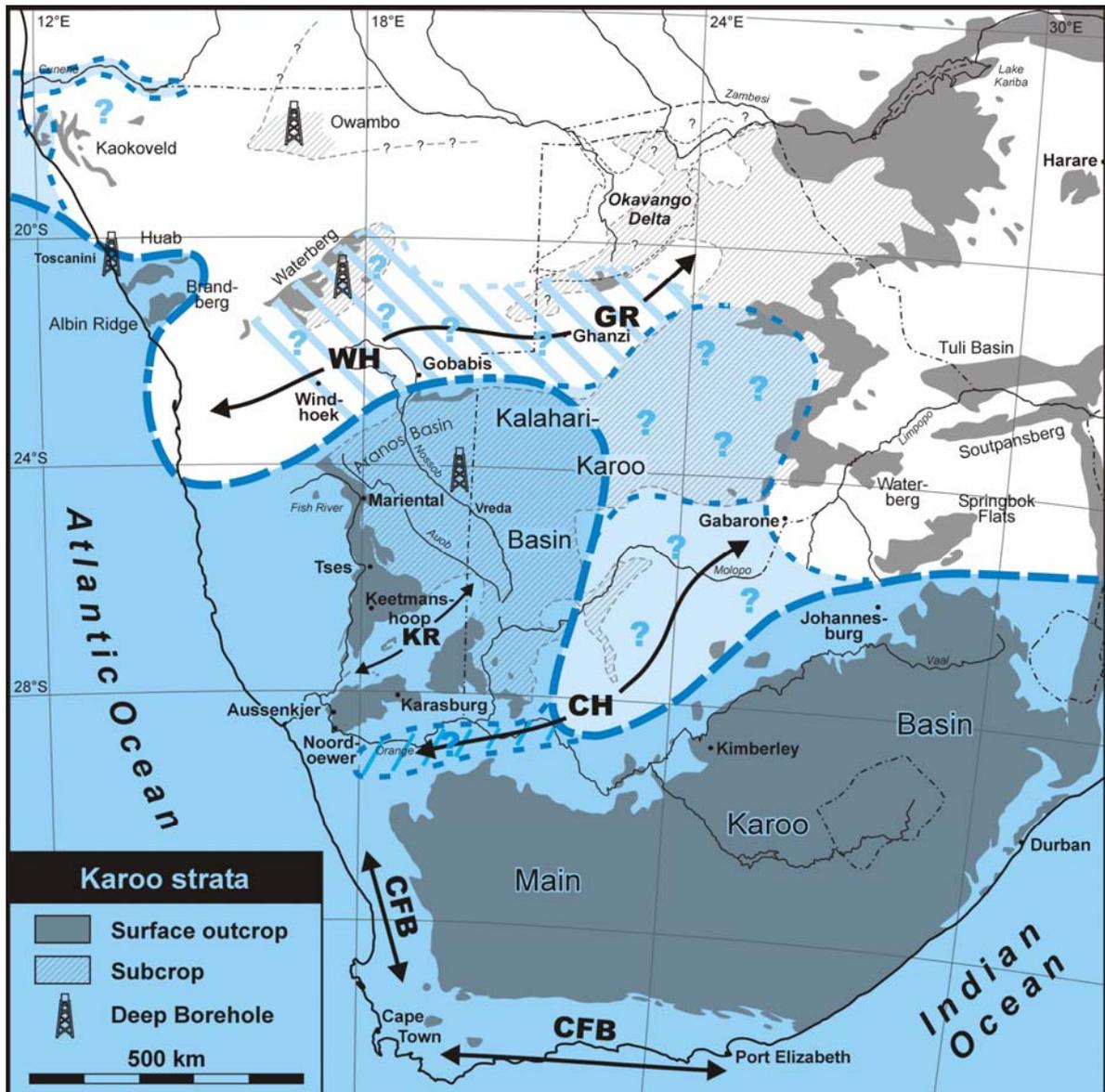
Fig. 1.6: Distribution and extent of the Mesosaurus Inland Sea in southern Africa during the time of maximum transgressions in the Early Permian (lower Ecca Group). The darker blue part represents areas, which were with reasonable certainty covered at least temporarily by the Mesosaurus Inland Sea. The situation for the light blue coloured areas is much less certain but transgression of the Mesosaurus Inland Sea into these regions seems plausible (see text for discussion). Symbols for palaeo-high areas (submergent swells and emergent lands): WH = Windhoek Highlands; GR = Ghanzi Ridge; KR = Karasburg Ridge; CH = Cargonian Highlands; CFB = Cape Fold Belt.

before the Upper Permian. Great uncertainties exist for the area, which today separates the Kalahari-Karoo and the Main Karoo Basins. This area, which is today underlain by Precambrian basement rocks, represented during deposition of the Dwyka Group a glaciated highland, for which Visser (1983a) created the name 'Cargonian Highlands'. At least some parts of these ancient highlands were flooded by the sea indicated by overstepping, transgressive, post-glacial Ecca Group sediments, which were later removed by uplift-induced erosion. During the regressive phase of the Ecca Group deposition abundant plant material in tempestitic sediments of the higher Ecca strata in the Aussenkjer-Noordoewer area of

southernmost Namibia, however requires the vicinity of a vegetated land area, probably in the area of the Cargonian Highlands. The small Karasburg Ridge to the north formed probably largely a submarine swell during deposition of the Ecca Group and it is not known if parts of it were emergent. Another palaeo-highland was postulated for the Windhoek-Ghanzi area (Windhoek Highlands-Ghanzi Ridge), deduced from thinning, coarsening and shallowing trends at the northern margin of the Kalahari-Karoo Basin. Isolated remnants of sandy and shaly sediments of supposed Early Permian age on the northern slope of the Ghanzi Ridge (Lake Ngami area and the Namibian-Botswanan borderland northeast of Gobabis; Hegenberger, 1985) as well as glauconite reports from the coal-bearing Tevrede Formation in the Waterberg subsurface area (Gunthorpe, 1987) imply that these regions were possibly temporarily transgressed by the sea and also represented marginal parts of the Mesosaurus Inland Sea in the Early Permian. Further to the northwest, *Mesosaurus* remains are known from the Huab-Brandberg area, which is considered as a small eastern appendix of the Paraná Basin. In the far northwest of Namibia the Cunene and Engo Valleys may have been flooded in a fjord-like manner by the Mesosaurus Inland Sea during the Late Palaeozoic.

1.3.2. Stratigraphic overview

It is beyond the scope of this thesis to extensively review the stratigraphy of all areas, which were once covered by the Mesosaurus Inland Sea. However, quite reliable correlations between some of the depocentres or basins have already been achieved and are refined by data presented in this thesis. Consequently, the geochronological data, which are obtained from tuff layers in southern Namibia and which are presented in this thesis, can also be transferred to neighbouring areas. Therefore, an overview of the lithostratigraphic subdivision of Late Palaeozoic successions from some major and minor depositional areas of the ancient Mesosaurus Inland Sea as well as their large-scale correlation is illustrated in Fig. 1.7. In all the mentioned regions sedimentation started with the deposition of glacial rocks. In Namibia and South Africa these glacial deposits are assigned to the Dwyka Group and in Brazil to the Itararé Group. The subsequent post-glacial, mainly subaqueously deposited inland sea sediments of Namibia and South Africa are represented by the Ecca Group, whereas the post-inland sea sediments deposited in terrestrial environments (fluvial, lacustrine) are placed into the Beaufort Group (incl. the Gai-As & Doros Formations in NW Namibia). In Brazil the post-glacial inland sea phase is represented by sediments of the Guatá and Passa Dois Groups, with the Rio do Rasto Formation on top of the Passa Dois Group already representing a correlative of the continental lower Beaufort Group. Within the Early Permian successions the Irati-Huab-Whitehill-Black Rock stratigraphic units are considered as a largely chronostratigraphic zone (Oelofsen, 1987).

PARANÁ BASIN (Brazil)	HUAB AREA (NW-Namibia)	W-KALAHARI-KAROO BASIN (S-Namibia)	MAIN KAROO BASIN (N-Cape/RSA)	MAIN KAROO BASIN -Tanqua- (W-Cape/RSA)	MAIN KAROO BASIN -Laingsburg- (W-Cape/RSA)	MAIN KAROO BASIN -South. Subb.- (E-Cape/RSA)	FALKLAND/ MALVINAS ISLANDS
Rio do Rasto Formation	Gai-As & Doros Formation ★	BEAUFORT GROUP: Amibberg Fm.	BEAUFORT GROUP: Waterford Fm.	BEAUFORT GROUP: Waterford Fm.	BEAUFORT GROUP: Waterford Fm.	BEAUFORT GROUP: Waterford Fm.	Bay of Harbours Fm.: Egg Harbour Mb.
PASSA DOIS GROUP: Teresina Fm.	(hiatus)	Aussenkjer Fm.	Tierberg Fm.	Kookfontein Fm. / Skoorsteenberg Fm.	Fort Brown Fm.	Fort Brown Fm.	Praltos Mb. / Saladero Mb.
Sierra Alta Fm.	Huab Fm.	Colling-ham Fm. ★★	ECCA GROUP	Tierberg Fm.	Laingsburg Fm.	Ripon Fm.	Brenton Loch Fm.: Cantera Mb. / Terras Motas Mb.
Irati Fm.	Tsarabis Fm.	Whitehill Fm. ★★	Whitehill Fm.	Collingham Fm.	Vischkuil Fm.	Collingham Fm.	Shepards Brook Mb.
GUATÁ GROUP: Palermo Fm.	Verbrandeberg Fm.	Prince Albert Fm. ★★	Prince Albert Fm.	Whitehill Fm.	Collingham Fm.	Whitehill Fm.	Port Sussex Fm.: Black Rock Mb.
Rio Bonito Fm.		★★		Prince Albert Fm.	Whitehill Fm.	Prince Albert Fm.	Hells Kitchen Mb.
ITARARÉ GROUP	DWYKA GROUP	DWYKA GROUP ★★	DWYKA GROUP	DWYKA GROUP	Prince Albert Fm.	DWYKA GROUP	Fitzroy Tillite Formation
					DWYKA GROUP		

Fig. 1.7: Lithostratigraphic overview of Late Palaeozoic successions from some selected depositional areas covered by the ancient Mesosaurus Inland Sea. White striped parts represent hiatal intervals. Red stars indicate stratigraphic intervals from which tuff layers are described in this thesis. The light coloured interval of the Irati-Huab-Whitehill-Black Rock stratigraphic units is considered as a largely chronostratigraphic zone (Oelofsen, 1987).

1.3.3 Tectonics

The basin areas, which were transgressed by the Mesosaurus Inland Sea in the Late Palaeozoic, evolved under the influence of several distinct tectonic regimes, which have been recently reviewed by Catuneanu et al. (2005). During this time oceanic crust of the Panthalassan Ocean was subducted beneath the southern continental margin of Gondwana, which was accompanied by the formation of a magmatic arc as well as accretion and mountain building processes. As a result of these subduction and orogenic processes an extensive retroarc foreland system developed along the southern convergent margin of Gondwana, which included in SW-Gondwana the Sauce Grande Basin, the Main Karoo Basin of South Africa and certain regions of Antarctica (Ellsworth and Transantarctic Mountains area). Accomodation in the retroarc foreland basins was created by flexural tectonics due to supracrustal loading as well as dynamic subsidence caused by the drag force of viscous mantle corner flow coupled to the subducting plate (Pysklywec & Mitrovica, 1999). Recent studies on the Karoo basins of South Africa by Catuneanu (2004a & b) showed that the foreland system was partitioned into foredeep, forebulge and back-bulge flexural provinces. During deposition of the Dwyka Group marine conditions prevailed only in the southern part of the Main Karoo Basin and were mainly confined to the foredeep area (Catuneanu, 2004a). With the successive northward migration of the foredeep basin axis and additional generation of accomodation by dynamic subsidence almost the entire Main Karoo Basin was flooded during deposition of the Ecca Group by the Mesosaurus Inland Sea and sedimentation took place also on the forebulge area.

To the northeast of the Main Karoo Basin, the tectonic regimes were dominated by extensional to transtensional stresses that propagated southwestwards into the super-continent from the divergent Tethyan margin of Gondwana (Wopfner, 2002). These tectonic forces led to the formation of several southeast African Karoo rift basins (e.g. Ruhuhu and Luangwa Basins), whose Late Palaeozoic sedimentary fills are of terrestrial origin. Towards the west, the Congo Basin, the Karoo Basin of Angola and also the Paraná Basin are often referred to as sag basins, the accomodation mechanisms of which are rather enigmatic. The Paraná Basin formed a major depositional area in the northwest of the Mesosaurus Inland Sea, whereas the Congolese and Angolan basins were during the Early Permian most probably characterized by terrestrial depositional conditions.

The study area in southern Namibia, representing the western part of the Kalahari-Karoo Basin, lies approximately in the middle of the aforementioned basins, which are characterized by different tectonic regimes (foreland, rift and sag basins). It is not clear if and to what extent accomodation in the southern Namibian Kalahari-Karoo Basin was controlled

by flexural tectonics (as a back-bulge province to the Main Karoo Basin) or by extensional rift tectonics related to Tethyian spreading processes (as a distal extension of the East African Karoo rift basins). More recently Stollhofen (1999) and Stollhofen et al. (2000b) presented a rift model for the generation of accomodation in the regions of the Paraná Basin and the Namibian Karoo basins. Analysis of synsedimentary faulting, depositional style, facies architecture, and palaeocurrents of Karoo-aged sediments in these regions indicates the existence of an intracontinental rift system, whose origin reaches back to the Late Palaeozoic and finally led to the opening of the South Atlantic Ocean in the Cretaceous. The axis of this rift system follows in the north approximately the elongation of the Paraná Basin and runs southward along a region that was to become the continental margins of southwestern Africa and southeastern South America after opening of the South Atlantic Ocean. Study of the Namibian Karoo sediments led to the recognition of a tectonic zonation of this area. From west to east a central rift valley depression is followed by an adjacent rift shoulder that underwent pronounced thermal uplift, a rotational block faulted zone floored by major down-to-the-west detachments, and farther inland the relativly stable cratonic continental interior (Stollhofen, 1999).

During deposition of the Dwyka and Itararé Groups in the Upper Carboniferous and the Earliest Permian converging palaeo-ice flow directions in southwestern Gondwana (westerly in central South America and easterly in eastern South America and southern Africa) suggest already the existence of an embryonic, linear rift valley depression extending deeply into Gondwana, from southern Africa through the Brazilian interior of South America (Stollhofen et al., 2000a). Marine incursions (e.g. *Eurydesma* transgression) flooded this depression from the south forming precursor or incipient stages of the Mesosaurus Inland Sea. Maximum flooding of this rifted region took place in the early Permian, during deposition of the lower Ecca Group, when the Mesosaurus Inland Sea reached its maximum extent. During intermittent regressions delta complexes advanced in the Aranos Basin of southern Namibia to the south, parallel to the rift axis. Contemporaneous with maximum flooding of the SW Gondwanan continental interior tectonic barriers formed along the active Panthalassan margin of Gondwana. These barriers restricted the interchange of the water between the Panthalassan Ocean and the Mesosaurus Inland Sea resulting in a widespread black shale event (Irati-Whitehill Formations).

1.3.4 Sedimentary development

The origin of the Mesosaurus Inland Sea goes back to the Upper Carboniferous when marine water of the Panthalassian Ocean first flooded parts of the SW Gondwanan continental interior from the south. This early period was strongly influenced by glacial climatic conditions as indicated by subaqueously deposited diamictites and dropstone-bearing shales of the Dwyka and Itararé Groups. During glacial intervals the inland sea was probably covered to a large extent by floating ice sheets or drifting icebergs but larger parts may have also been ice-free during inter-glacials. Fossil finds (e.g. the bivalve *Eurydesma*) in southern Namibia (Kalahari-Karoo Basin) and central-eastern Argentina (Sauce Grande Basin) show that a marine fauna was able to colonize parts of this early inland sea. With the melting of the ice in the final phase of the Late Palaeozoic Ice Age sea level rose and the Mesosaurus Sea fully established as a vast inland sea. The post-glacial inland sea deposits are represented in SW Africa by the Ecca Group. Some regions experienced a regressive phase at the end of the Late Palaeozoic Ice Age due to iso-static crustal rebound (uplift) of formerly glaciated areas. This led to the progradation of deltaic sandstone complexes into basinal areas. During the early post-glacial time (early Lower Permian) the central-southern part of the Mesosaurus Inland Sea was characterized by the wide-spread deposition of argillaceous sediments, whereas towards the northerly continental interior and in marginal areas arenaceous deposits are more common. The large-scale transgressive development probaly culminated in the Artinskian with the Mesosaurus Inland Sea reaching its maximum extent during deposition of the lower Ecca and Passa Dois Groups. This time was also characterized by the onset of widespread deposition of C_{org}-rich sediments such as black shales and limestones as well as coal (Whitehill-Irati-Vryheid Formations). It is believed that the magmatic arc complex at the Panthalassan margin of Gondwana may have acted as a barrier or sill, which restricted the interchange of water with the open ocean (Collinson et al., 1992). The restricted circulation led to a stratified water body with an oxygenated upper layer and an anoxic lower layer. The fossil record for this period is dominated by a highly endemic fauna consisting of free swimming organisms (e.g. *Mesosaurus*), whereas benthic lifeforms or their signs of activity (bioturbation) are largely absent. Dolomitic limestones, gypsum and anhydrite occurrences as well as pseudomorphs after evaporite minerals indicate hypersaline conditions. After this black shale event a large-scale regressive development led to the gradual shallowing and infilling of the Mesosaurus Inland Sea during the early Upper Permian. Thick shaly offshore successions are finally overlain by nearshore and coastal sand deposits. The transition from deltaic (Ecca Group) to continental fluvio-lacustrine (Beaufort Group) deposits is quite gradual and diachronous (Rubidge et al., 2000; Rubidge, 2005). The southern parts of the Mesosaurus (Ecca) Inland Sea were strongly affected in Mid-Permian times by deformation that lead to the deposition of turbiditic deep water sandstone complexes in foredeep areas (López-Gamundí & Rosello, 1998; Johnson et al., 2001).

Chapter 2 – Stratigraphy and sedimentology of the Dwyka and Ecca Groups in southern Namibia

2.1 Principal outcrop and subcrop areas of Dwyka and Ecca rocks in southern Namibia

In southern Namibia Dwyka and Ecca sediments are exposed in two main outcrop areas, namely the northerly Mariental-Keetmanshoop area and the southerly Noordoewer-Karasburg area. The Mariental-Keetmanshoop area forms the western outcrop margin of the so-called Kalahari-Karoo Basin (Martin, 1961) with Dwyka and Ecca rocks continuing east-ward into Botswana and South Africa, mainly in subcrop under Cenozoic Kalahari cover. The Namibian part has also been referred to as the Aranos Basin (Hegenberger, 1992). The Noordoewer-Karasburg Karoo outcrop belt is variably referred to as the Karasburg (Schreuder & Genis, 1975), Warmbad (Haughton & Frommurze, 1936), Nabas (de Villiers & Söhnge, 1959) or Orange River Basin (Frakes & Crowell, 1970).

The Mariental-Keetmanshoop outcrop area stretches over a distance of approximately 400 km from the small village of Schlip in the north to the southwestern tip of the Little Karas Mountains in the south (Fig. 2.1). In W-E direction the width of this outcrop area ranges in the northern part between 10 and 30 km but widens in its southern part around Keetmanshoop to about 150 km. Towards the east Dwkya and Ecca sediments are covered by Cenozoic Kalahari sediments but have been encountered in numerous coal and some hydrocarbon exploration boreholes in the Aranos area (Fig. 2.1) and in Botswana. From the topographic height data of the base of the Dwyka Group in the Mariental area and in the Vreda borehole it can be calculated that the Dwyka and Ecca strata is dipping in the Mariental-Keetmanshoop area with approximately 0.25-0.30° towards the east.

The southerly main outcrop area between Noordoewer and Karasburg forms a WSW-ENE oriented outcrop belt about 160 km long and 50-70 km wide. In its southwestern part both Dwyka and Ecca sediments are preserved, whereas in the northeastern part (east of about 18°20'E), in the vicinity of Karasburg, only Dwyka rocks can be found due to erosion of the overlying Ecca sediments (Fig. 2.1). Northeast of Karasburg Dwyka deposits are also known but outcrop conditions become progressively poorer due to increasing cover by Cenozoic Kalahari sediments. The southwestern part of the Noordoewer-Karasburg outcrop area represents a large-scale saucer- or bowl-shaped tectonic structure with the Amibberg Massif in its centre. This large-scale tectonic structure is warped and deformed by several anti- and synclines as well as monoclines and fractured by faults. This structure probably originated due to the intrusion of several extensive dolerite sheets in the Jurassic and due to later uplift

of the surrounding basement rocks. The steep contact to the crystalline basement in the northwest near Aussenkjer, for example, is characterized by a steep dipping thrust fault (Schreuder & Genis, 1975). One minor outcrop lies in the vicinity of Gobabis at the northwestern margin of the Kalahari-Karoo Basin and another between the Little and the Great Karas Mountains (Fig. 2.1). Fieldwork for this study concentrated on smaller regions within the two main outcrop areas. Within the Mariental-Keetmanshoop outcrop area fieldwork was focused on the southern part between Ganigobis and Keetmanshoop and within the Noordoewer-Karasburg outcrop area fieldwork was focused on the area between Aussenkjer and Noordoewer including the Amibberg Massif (Fig. 2.1).

The Dwyka and Ecca strata in the above mentioned two main Karoo outcrop areas (Fig. 2.2) were first studied on a broad scale by Range (1908, 1912, 1920, 1928), Versfeld (1914), Wagner (1915), du Toit (1916, 1921), Haughton & Frommurze (1927, 1936), and Krenkel (1939). Later more detailed studies in the Mariental-Keetmanshoop area concentrated mainly on the glacigenic Dwyka Group (Martin, 1953, 1981a; Martin & Wilczweski, 1970; Stratten, 1977; Visser, 1983a & b). In Brandt et al. (1961) an early overview about the then knowledge of the Dwyka and Ecca rocks in all Karoo outcrop areas of Namibia can be found. Heath (1972) mapped and investigated the Dwyka and Ecca succession between Mariental and Asab, however, his study was mostly based on aerial photographs and rather broad-scaled field sections (Grill, 1997). More recent studies by Grill (1997), Stollhofen et al. (2000a), and Bangert (2000) were focused on the glacigenic Dwyka Group and the sandstone complexes in the lower Ecca Group in the northern part of the Mariental-Keetmanshoop outcrop area. The geology of the Dwyka and Ecca strata in the southern part of this outcrop area around Keetmanshoop and in the nearby Karas Mountains remained until today largely unexplored. In the Aranos area five major companies sunk more than 60 exploration boreholes between 1981 and 1983 (Hegenberger, 1992). The cored coal-bearing Ecca Group deposits were studied by Kingsley (1985, 1990) and McDaid (1985). First general ideas of the lithology and distribution of Karoo rocks in the Noordoewer-Karasburg outcrop area were given by Range (1912), Versfeld (1914), Wagner (1915) and du Toit (1921). After the early more detailed studies by Haughton & Frommurze (1927, 1936) the Dwyka and Ecca deposits were comprehensively mapped in this area and briefly described by Schreuder and Genis (1975). Frakes & Crowell (1970) and Martin (1981b) shortly summarized the Dwyka geology of this area. Since then this Karoo outcrop region remained scientifically more or less a 'forgotten' area, except minor studies by Anderson (1975) and Visser (1983a & b) on the basal part of the Dwyka Group. The discovery of bentonitic ash-fall tuff layers in the Dwyka exposures along the Orange River west of Noordoewer resulted in a very detailed study mainly on the Dwyka Group within a small restricted area opposite of Zwartbas (Geiger, 1999, 2000).
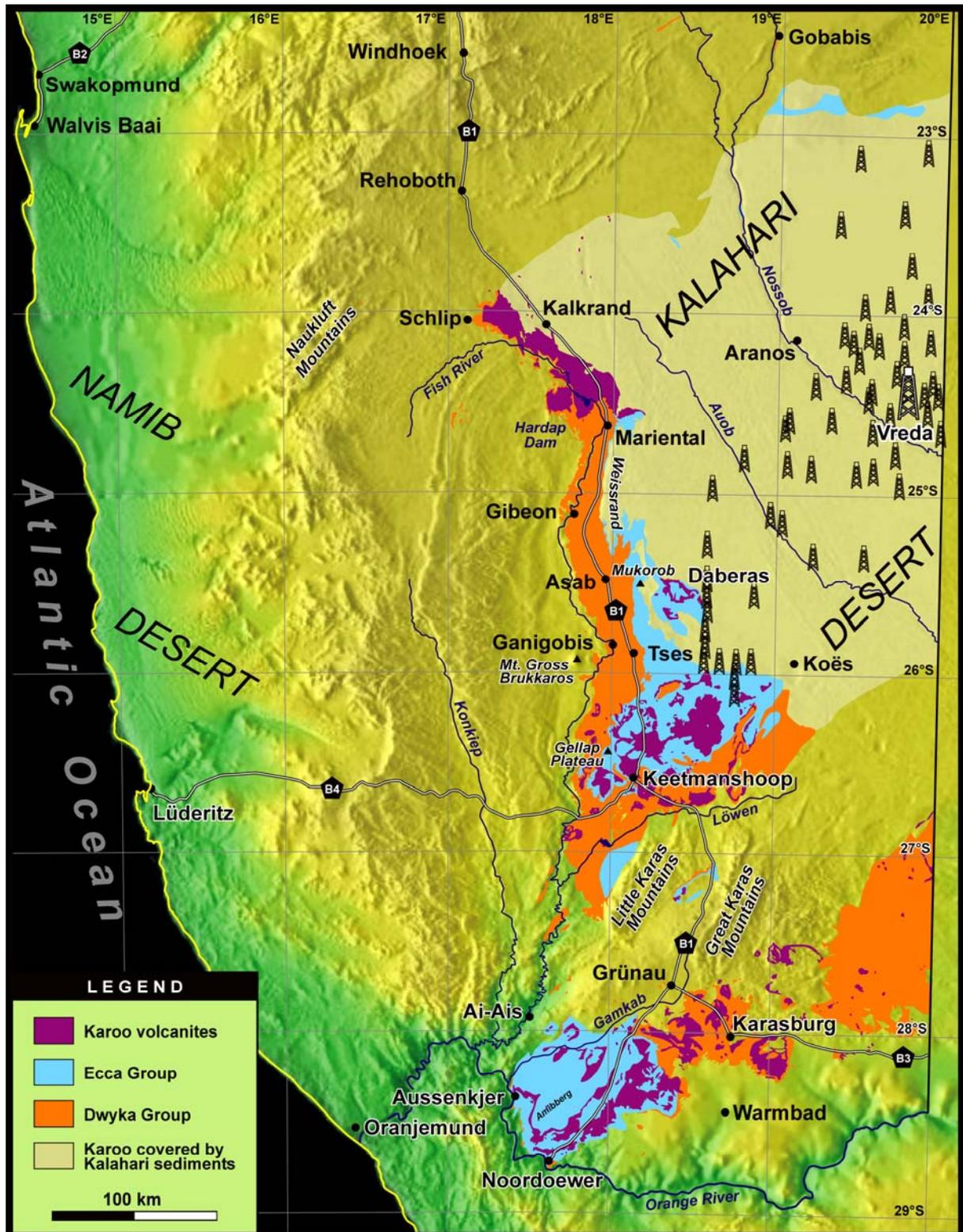
Fig. 2.1: Distribution of Dwyka and Ecca Group sediments in southern Namibia superimposed on a digital elevation model provided by the US National Geophysical Data Center on the internet (URL: ftp://ftp.ngdc.noaa.gov/GLOBE_DEM/pictures/AFRICAcolshade.jpg).
The geology is adopted from Miller & Schalk (1980). Note that in the Aussenkjer-Noordoewer outcrop area only tillitic rocks have been assigned to the Dwyka Group, whereas all glacigenic mudrocks have been incorporated into the overlying Ecca Group. So far, the Dwyka-Ecca boundary has not yet been mapped properly in this area (except a small area 7 km northwest of Noordoewer; cf. Geiger, 1999). Boreholes sites are from Kingsley (1985).

	Mariental-Keetmanshoop	Noordoewer-Karasburg
Late Perm. · **Ecca Group**		**Amibberg Fm.**
		Aussenkjer Fm.
(270) Ma ↑ **Permian**	(Neu Loore Fm.?) (Vreda Fm.?)	Inaub Sandstone Bed
		Polisiewater Chert Bed **Collingham Fm.**
280 Ma	**Whitehill Fm.** Goris Limestone Beds ⟨ Rietmond Sh. Mb. ⟩	**Whitehill Fm.**
	Prince Albert Fm. — Auob Sst. Mb. — Mukorob Sh. Mb. — Nossob Sst. Mb.	Uhabis Mb. **Prince Albert Fm.** Owl Gorge Mb.
290 Ma — **Early** — **Dwyka Group**	**Tses Boulder-Mudstones** (incl. Hardap Shales)	**bluish-grey weathering glacial facies** (mainly dropstone-bearing shales, incl. the Hippo and Goats Cliff Diamictites)
300 Ma **Late Carbonif.**	**Ganigobis Shales** **Gibeon Tillite**	**red weathering glacial facies** (tillites, sandstones, shales)

Fig. 2.2: Stratigraphic subdivision of the Dwyka and Ecca Groups in the two principal outcrop areas in southern Namibia (modified after Martin & Wilczewski, 1970; SACS, 1980; Haughton & Frommurze, 1936; Geiger, 1999; Stollhofen, 1999; and supplemented by own suggestions for stratigraphic unit names). Note that the Vreda and Neu Loore Formations, unconformably overlying Whitehill-equivalent sediments, are only known from the Aranos Karoo subsurface area. Although their age is unknown these two formations probably belong also to the lower Ecca Group of Early Permian age.

2.2 Dwyka Group

The Dwyka Group comprises all sediments, which were deposited during the Late Carboniferous to Early Permian glaciation in Namibia and South Africa. The boundary to the overlying Ecca Group is defined as the transition from glacigenic to post-glacial sediments. In southern Namibia the base of the Dwyka Group is characterized by a pronounced basal unconformity with Late Carboniferous deposits overlying Palaeoproterozoic to Early Palaeozoic metamorphic, igneous and sedimentary rocks. The top of the Dwyka Group is nowadays drawn at the stratigraphic level at which the last dropstones occur. In southern Namibia this stratigraphic level corresponds approximately with the position of the Nossob Sandstone Member, which is commonly regarded as the basal unit of the Prince Albert Formation and hence the Ecca Group (Fig. 2.2).

In the study area between Ganigobis and Keetmanshoop the glacigenic succession of the Dwyka Group overlies mainly Neoproterozoic to Early Palaeozoic sediments of the Nama Group. At the base the Dwyka Group contains continental subglacial and proglacial deposits, otherwise, mud-rich marine deposits make up its major part (Martin, 1953; Frakes & Crowell, 1970; Martin & Wilczewski, 1970; Heath, 1972; McLachlan & Anderson, 1973; Grill, 1997; Stollhofen et al., 2000a). According to the early studies of Martin & Wilczewski (1970) and Martin (1973) it seems possible to subdivide the Dwyka Group in the central part of the Mariental-Keetmanshoop area lithostratigraphically roughly into three larger subunits, namely the Gibeon Tillite, the Ganigobis Shale, and the Tses Boulder-Mudstone Members (Martin & Wilczewski, 1970) (Fig. 2.3).

At the base of the Dwyka Group the so-called Gibeon Tillite is dominated by tillites and diamictites with minor sandstone and shale interbeds. These rocks represent mainly glacio-terrestrial rocks including subglacial groundmoraine (tillites) and esker (sandstones) deposits, proglacial glaciofluvial conglomerates and sandstones as well as glaciolacustrine mudrocks (Martin, 1953; Heath, 1972; Grill, 1997; Stollhofen et al., 2000a). This basal part attains a maximum thickness of about 30 m. Higher up in the succession the coarse glacio-terrestrial rocks grade into more mud-rich diamictic rocks, which were laid down sub-aqueously as tunnel mouth, debris flow and debris rain-out deposits in a proximal, proglacial marine environment (Grill, 1997, Stollhofen et al., 2000a).

This basal subunit is followed by a succession of dark coloured, partly carbonaceous shales, which contain only very low amounts of dropstones or are largely dropstone-free and represent mainly distal debris rain-out (from drifting and melting ice floes) and offshore suspension fall-out deposits (Grill, 1997; Stollhofen et al., 2000a). This shale succession is

referred to as the Ganigobis Shale Member (Martin & Wilczewski, 1970). The lower part of this shale succession is characterized by the presence of numerous phosphatic concretions, which often contain abundant tiny, spherical radiolarian remains and well-preserved parts of palaeoniscoid fishes. The upper part contains a horizon, in which small calcareous algal mounds and columnar build-ups (up to 4 m high) occur frequently (Fig. 2.3 & 2.5-A/B). Associated with this limestone zone is a marine fauna containing crinoids, ostracodes, nuculid bivalves, gastropods, sponges and the single find of a conularia as well as cyano-phycean and dasycladacean algae (Schroeder, 1908; Range, 1912; Martin, 1953; Dickins, 1961; Grill, 1997; Bangert et al., 2000). Furthermore, up to 10 cm long, dark brown, blade-like and rhomb-shaped glendonite crystals have been found in this stratigraphic level (cf. McLachlan et al., 2001) (Fig. 2.5-C/D). Interbedded within this stratigraphic interval in the lower part of the Dwyka Group are also the so-called Ganigobis Tuffs (Grill, 1997; Bangert et al., 1999; Bangert, 2000; Stollhofen et al., 2000a), which are briefly described in Chapter 3.4.1. At the type locality the Ganigobis Shale Member shows a thickness of approximately 50-60 m (Martin, 1973). Towards the north (Gibeon to Mariental) and south (Tses to Keet-manshoop) the fine-grained facies of the Ganigobis Shale Member loses its distinct litho-logical character and grades into more coarser or dropstone-richer glacial rocks (Grill, 1997; Stollhofen et al., 2000a).

The following upper part of the Dwyka Group, called the Tses Boulder-Mudstones, is characterized by dropstone-rich mudrocks to dropstone-poor shales, which represent mainly proximal to distal debris rain-out deposits (Stollhofen et al., 2000a) and contain in certain levels abundant large carbonate concretions. These concretions contain the foraminiferas mentioned by Martin & Wilczewski (1970) and also the orthocerid cephalopod mentioned by du Toit (1915). Intercalated within the shaly succession are also diamictic horizons and several more or less continuous and prominent, often intensively slumped and deformed turbiditic sandstone layers (Fig. 2.5-E/F). Associated with this sandstone layers in the upper part of the Dwyka Group are the famous findings of transported and disarticulated *Eurydesma* shells, bryozoans, gastropods, and a starfish remain (Dickins, 1961; Lane & Frakes, 1970; Martin & Wilczewski; 1970; Wass, 1970, 1972; Grill, 1997). Furthermore, also a rich trace fossil fauna can be observed in association with these turbiditic sandstones (Fig. 2.5-G/H). One of these sandstones (here informally called 'Tses Sandstone' (Fig. 2.3); also mapped by and shown in Martin, 1953) forms a small but conspicuous ledge or plateau directly east and north above the village of Tses lying stratigraphically c. 40-50 m below the Nossob Sandstone.

This upper part of the Dwyka Group reaches a thickness of up to 150 m in the Mariental-Keetmanshoop outcrop area. A dropstone-poor shale packet within the Tses Boulder-Mudstone Member was designated by Stollhofen et al. (2000a) the so-called Hardap Shale Member (SACS, 1980; Martin, 1981a). The *Eurydesma*-bearing sandstones within shales south of the Hardap Dam may also be positioned within this stratigraphic interval. However, it must be noted that in older publications the Hardap Shales and the Ganigobis Shales have been considered as largely synonymous and as stratigraphically equivalent (Martin, 1953; Heath, 1972; Martin, 1981a; Grill, 1997). Stollhofen (1999) and Stollhofen et al. (2000a) were the first who recognized that these fossil-bearing shaly successions actually belong to different stratigraphic intervals. Own investigations are supporting this view. The *Eurydesma*-bearing turbiditic sandstone interval in the upper part of the Dwyka Group, cropping out at the western margin of the Gellap Plateau, is most probably also correlatable with the *Eurydesma*-bearing turbidite sandstones at Hardap near Mariental and does not represent an equivalent of the stratigraphically lower Ganigobis Shales. It furthermore appears that *Eurydesma* is only found as allochthoneous specimens within sandy turbidite beds (cf. Martin, 1973; McLachlan & Anderson, 1975) in the stratigraphically higher parts of the Dwyka Group but not within the lower stratigraphic interval of the Ganigobis Shales. Apart from southern Namibia *Eurydesma* was also found within the SW Gondwanan region in the Sauce Grande Basin of eastern Argentina (Harrington, 1955). The goniatite, which was found at a locality near Schlip within one of the radiolarian-bearing phosphatic concretions, belongs to the genus *Eoasianites*, subgenus *Glaphyrites* (Martin et al., 1970). From the descriptions of Martin et al. (1970) it can be speculated that the stratigraphic interval, in which the goniatite was found, probably correlates with the Ganigobis Shales rather than the stratigraphically higher Tses Boulder-Mudstones - Hardap Shales. *Eoasianites (Glaphyrites)* was also found in phosphatic concretions of the Dwyka-equivalent Itataré strata of the Paraná Basin in Uruguay (Closs, 1967, 1969).

Heath (1972) subdivided the Dwyka Group in the northern part of the Mariental-Keetmanshoop area into seven members. The resulting geological map, however, shows more the distribution of certain Dwyka lithofacies rather than a succession of lithostratigraphic units and correlation with the threefold subdivision suggested by Martin & Wilczewski (1970) is highly problematic. In adaptation to the concepts of Theron & Blignault (1975) and Visser (1997b), who recognized several deglaciation cycles in the Dwyka successions in South Africa, Stollhofen et al. (2000a) also subdivided the Dwyka Group in the Mariental-Keetmanshoop outcrop area into four deglaciation cycles (DS I-IV). DS I attains a thickness of only 8 m at the Ganigobis locality, where a coarse lodgement tillite is overlain by glaciolacustrine varved siltstones and fine sandstones (Fig. 2.3). DS II forms an upward-fining unit with

massive tillites and fluvioglacial outwash conglomerates in the lower part, followed by subaqueous proglacial tunnel mouth and debris rain-out diamictites, which grade into dropstone-bearing mudrocks and intercalated sandy turbidites. This succession comprising DS I and the lower part of DS II is comparable to the Gibeon Tillite Member of Martin & Wilczewski (1970). The upper part of DS II is finally represented by the largely dropstone-free, carbonaceous Ganigobis Shales (Fig. 2.3), which host also a marine fauna and numerous thin ash-fall tuff layers (Ganigobis Tuffs). DS III and IV, which largely comprise the Tses Boulder-Mudstones, are mainly composed of dropstone-rich sandy mudrocks with inter-calated diamictite and sandstone horizons, and represent approximately the upper half of the Dwyka Group in the Mariental-Keetmanshoop outcrop area (Fig. 2.3). A dropstone-poor to -free shale unit within the Tses Boulder-Mudstones has been designated the Hardap Shale Member, which forms the top of DS III (Stollhofen et al., 2000a). Prominent turbiditic sand-stones in the lower part of DS IV yielded the famous *Eurydesma* findings.

Bangert et al. (1999, 2000) and Bangert (2000) claimed that outcrops in the Ganigobis-Tses area expose only DS I to III implying that DS IV is missing and that consequently the Nossob Sandstone overlies in this region the Dwyka deposits with a major unconformity possibly associated with a several million years long hiatus. However, the reported absence of DS IV may originate from the misinterpretation of the Tses Sandstone as the Nossob Sandstone. Furthermore, the apparent 'transgression' of the Nossob Sandstone over different Dwyka subunits reported by Heath (1972) and Grote (1984) is actually the result of changing Dwyka lithofacies along the Mariental-Keetmanshoop outcrop belt and does not indicate the erosion of 'missing' Dwyka units prior to the deposition of the Nossob Sandstone.

From the thickness distribution of the Dwyka Group in the Mariental-Keetmanshoop outcrop area two major trends are recognizable, (1) a N-S thickening trend and (2) a W-E thickening trend.
(1) From Mariental in the north, where the whole Dwyka Group attains a thickness of about 105 m (Heath, 1972; Schalk & Germs, 1980), its thickness increases in a southerly direction to about 215 m in the Gibeon area (Martin, 1981a) and to a maximum thickness in the order of about 250 m in the Asab-Tses area (Martin, 1953; Martin & Wilczewski, 1970; Visser, 1983a). Associated with this thickness increase in a southerly direction is also a trend from proximal towards more distal deposits. The basal tillite thins in a southerly direction and in the southern part of the Mariental-Keetmanshoop area continental glacial deposits are largely absent (Grill, 1997). Furthermore, turbiditic sandstones also show an overall decrease in frequency and thickness in a southerly direction and the marine glacial and proglacial deposits undergo a similar southward fining trend with a change from dominantly clast-poor

massive diamictites to dropstone-bearing mudstones (Grill, 1997). This indicates a general southward deepening of the water body in which the Dwyka deposits were laid down.
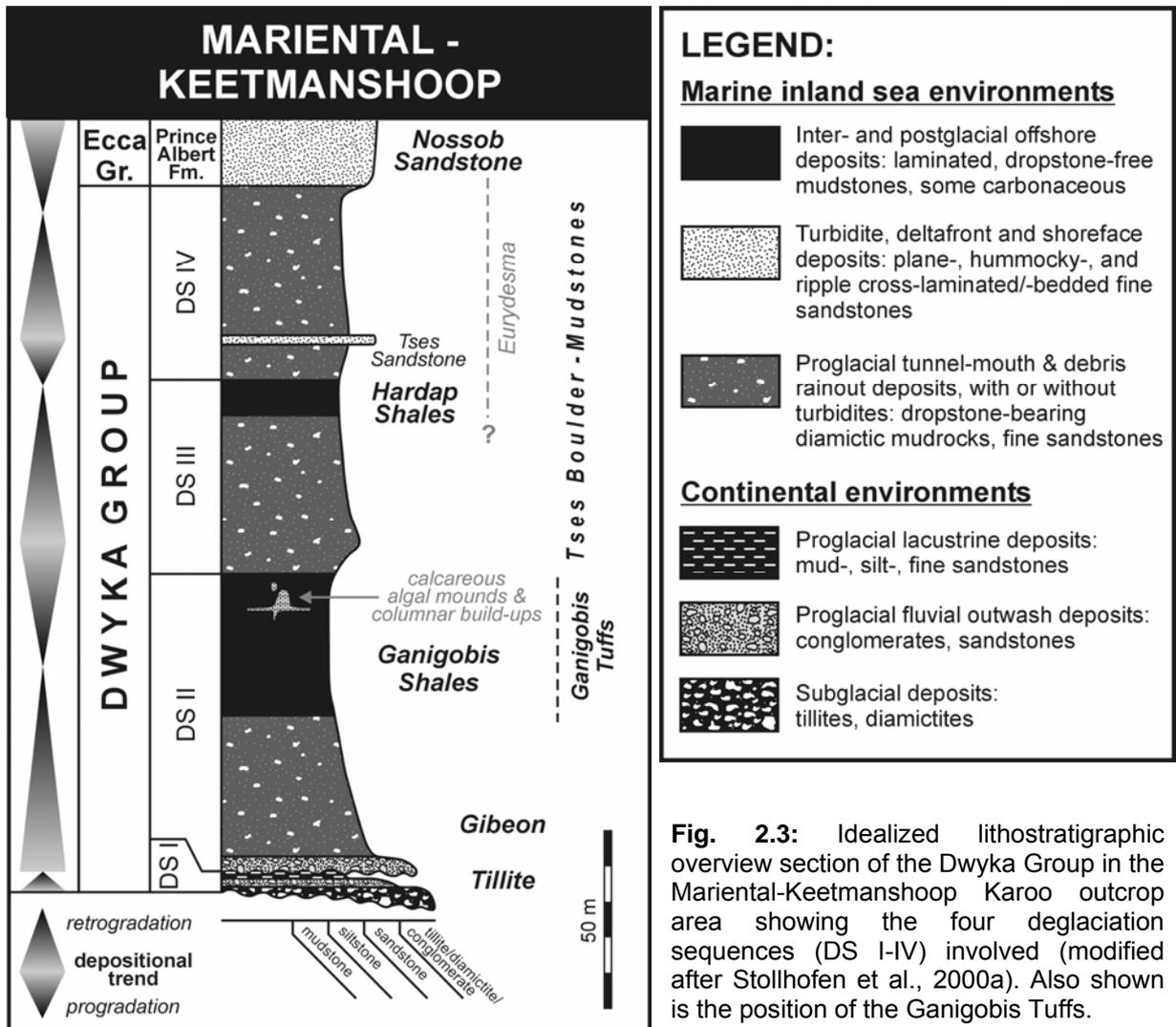
Fig. 2.3: Idealized lithostratigraphic overview section of the Dwyka Group in the Mariental-Keetmanshoop Karoo outcrop area showing the four deglaciation sequences (DS I-IV) involved (modified after Stollhofen et al., 2000a). Also shown is the position of the Ganigobis Tuffs.

The same N-S trend is also reflected by the borehole data from the Aranos area. In the ACP 21 borehole, one of the northernmost boreholes between Gobabis and Aranos (Fig. 2.1), the Dwyka Group only shows a thickness of 75 m (Hegenberger, 1985), whereas in the Vreda borehole 150 km to the south a Dwyka thickness of about 440 m was recorded (Wilson, 1964).

(2) From Mariental in the west towards the Vreda borehole in the east the Dwyka Group significantly thickens from 105 m to c. 440 m. With the lower part of the Dwyka Group (basal tillite, max. 30 m between Mariental and Asab; Heath, 1972) thickening in an eastward direction (lower 200 m of the Dwyka deposits in the Vreda core is dominated by a coarse, tillite-like rock; Wilson, 1964) more proximal conditions seem to prevail in the east and more distal conditions in the west.

In summary it can be concluded that the N-S trending thickness increase and grain size decrease between Mariental and Keetmanshoop reflects deposition in a southward deepening marine basin. Furthermore, the northward thinning of Dwyka sediments combined with a more proximal, coarse-grained facies in the northern part indicates that the Windhoek area and the easterly lying Ghanzi Ridge area (Fig. 1.6) represented, during Dwyka deposition, an emergent palaeohigh (Windhoek Highlands), forming the NW boundary of the so-called Kalahari-Karoo Basin (Hegenberger, 1985) and separating it from the northerly lying Karoo outcrop and subcrop areas (Waterberg, Huab, Ovambo, Kaoko areas) (Fig. 1.6). The Dwyka thickness decrease in a westward direction could reflect a more proximal depositional environment for the Vreda section in the east compared to a more distal (deeper?) depositional environment for the Mariental section in the west (Martin & Wilczewski, 1970; Visser, 1983a). Alternatively, Stollhofen et al. (2000a) suspected from this westward thinning trend the existence of the palaeohigh of a palaeorift shoulder in the west of the outcrop belt.

Glacial striations, palaeocurrent measurements in sandstones and till fabric measurements in the Mariental-Keetmanshoop area resulted in two main directions. One direction indicates flow towards S to SSW, the other towards WSW-SW (du Toit, 1916, 1921; Wagner, 1915; Frakes & Crowell, 1970; Martin & Wilczweski, 1970; Heath, 1972; Stratten, 1977; Schalk & Germs, 1980; Visser, 1983a; Genis & Schalk, 1984). These different directions were interpreted to originate from two different ice centres. The so-called Namaland Ice Lobe flowed from the Windhoek Highlands southward, whereas the WSW-SW directed ice flow is attributed to the Botswana Lobe/Transvaal Ice Sheet/Cargonian Highlands (Fig. 1.6) positioned in the present-day continental interior of southern Africa (Frakes & Crowell, 1970; Stratten, 1977; Visser, 1993a, 1997a).

Palaeocurrent measurements of the basal pro- and subglacial sandstones and conglomerates as well as turbidites in the lower half of the Dwyka Group are widely consistent with those of the N-S directed ice-flow and imply that the basin floor, in which the Dwyka sediments were deposited in the Mariental-Keetmanshoop area, was sloping towards the south to southwest (Martin & Wilczewski, 1970; Heath, 1972; Grill, 1997). A dominantly westerly to southwesterly ice flow direction for the southern Namibian part of the Kalahari-Karoo Basin during Dwyka deposition, propagated by Visser (1983a, 1987b, 1993a & b, 1997a & b), was apparently partly based on till fabric measurements by Heath (1972) and Stratten (1977) on diamictic mudrocks overlying the Ganigobis Shales in the Mariental-Keetmanshoop area. However, such till fabric measurements can be ambiguous, difficult to comprehend, and hence should be treated with great care. On the other hand, the lower Dwyka deposits contain for example in this area apparently non-deformed aphyric,

porphyritic or amygdaloidal mafic to felsic volcanic clasts. Especially the amygdaloidal basaltic lava clasts show a striking similarity to the Neoarchean (~2.6 Ga) Ventersdorp lavas, and no pre-Dwyka Group volcanics of this type are know from Namibia. SHRIMP U-Pb dating of zircons extracted from a porphyritic rhyolite clast yielded a Paleoproterozoic age of about 2050 Ma (Bangert, 2000). Such felsic volcanics of this age are known from the Orange River Group in southernmost Namibia but are also very common in the Bushveld Complex. The main outcrop areas of the Ventersdorp lavas and the Bushveld volcanics are both found in northern and northeastern South Africa and it seems indeed highly likely that clasts of these volcanics have been transported by a general westward ice flow from South Africa to Botswana and Namibia.

The palaeogeographical situation in the Keetmanshoop and Karas Mountains area is considerably less clear. Thickness reports for the Dwyka Group in the Keetmanshoop area raise no uniform picture. Martin (1981a) shows a Dwyka thickness of 170 m for the Gellap area west of Keetmanshoop, whereas Grill (1997) reports 250 m apparently for the same area (Snyfontein section). Genis & Schalk (1984) report of a mean thickness in the Keetmanshoop region of about 200 m, but also mention that a 330 m thick Dwyka succession was intersected in a borehole on Gellap Ost 3.

Schreuder & Genis (1977) gave no information about the entire Dwyka thickness within the Karas Mountains area. From own observations a first carefull estimate on the Dwyka thickness can be done. South of the Dassiefonteinrivier at the western steep flank of the Great Karas Mountains the base of the Nossob Sandstone lies at about 1260-1270 m asl., whereas the base of the Dwyka Group lies at the eastern margin of the Little Karas Mountains at Aningoas at about 1120-1140 m resulting in a Dwyka thickness of about 120-150 m, a horizontal layering and no faulting assumed. However, Schreuder & Genis (1977) placed an inferred reverse fault between the two mentioned outcrop localities, which would actually result in an overestimation of the Dwyka thickness. Nevertheless, the thickness of the Dwyka Group in the Karas Mountains area seems to be more or less reduced compared to the Keetmanshoop area. The Dwyka lithofacies of the Karas Mountains area is quite comparable to the Keetmanshoop area, dominantly composed of dropstone-bearing mudrocks with phosphatic concretions in the lower part and several intensively slumped and deformed turbidite sandstone layers in the upper part (Fig. 2.5-E). Since the Nossob Sandstone shows on Dassiefontein 87 a higher thickness (~8 m) compared to the Gellap area (2.5 m) and a facies that indicates a higher energetic, shallower depositional environment it can be concluded that the reduced Dwyka thickness in the Karas Mountains area indicates the existence of a sub-

marine swell in this region during deposition of the Dwyka Group (and the basal Ecca Group), which was already suggested by Martin & Wilczweski (1970).

The Noordoewer-Karasburg Karoo outcrop area is today separated from the Mariental-Keetmanshoop area by the Karas Mountains. The great faults delimiting the horst structures show both pre- and post-Karoo displacements. As a result of the pre-Karoo movements a swell may have existed at the site of the Karas Mountains during Dwyka deposition but there are sufficient outliers of Dwyka beds to prove that this swell did not protrude above sea level (Martin & Wilczewski, 1970). This was notoriosly disregarded by J.N.J. Visser, who continuously showed in his palaeogeographic reconstructions a subglacial mountain range in this area, as a northern outlier of the Cargonian Highlands dividing and separating the Mariental-Keetmanshoop and the Noordoewer-Karasburg outcrop areas (Visser, 1983a & b, 1987a & b; 1989, 1990, 1991a & b, 1992a & b, 1993a & b, 1994, 1995, 1996, 1997a). Visser's palaeogeographic and palaeotopographic reconstructions for the Dwyka Group in the southern part of Namibia was apparently strongly guided by the present-day morphology of the region, which is, however, largely the product of Mesozoic and Cenozoic crustal movements

In the Noordoewer-Karasburg Karoo outcrop area the Dwyka Group overlies unconformably a large variety of age-different lithostratigraphic units. The oldest are represented by the Palaeo- to Mesoproterozoic metamorphic rocks of the Orange River Group, the Vioolsdrif Intrusive Suite and the Namaqualand Metamorphic Complex. Furthermore, it overlies also granites of the older Neoproterozoic part of the Richtersveld-Bremen Complex, Neoproterozoic to Early Palaeozoic low-grade to non-metamorphic sediments of the Gariep Complex and the Nama Group.

The floor of the depositional basin, in which the Dwyka rocks have been laid down, had a considerable relief with scarps and valleys up to 30 m deep (Schreuder & Genis, 1975; Martin, 1981b; Visser, 1983a). Consequently, the basal-lower part of the Dwyka Group shows remarkable facies changes over relatively short distances. At a famous and spectacular outcrop 6 km northwest of Noordoewer, opposite the small South African settlement of Zwartbas, tillitic and diamictic, strongly calcareous Dwyka deposits rest in small hollows or are plastered as a thin veneer on partly near-vertical, polished, grooved and striated faces of pre-Dwyka rocks (Numees Tillite of Gariep Complex?) (Fig. 2.5-L/M) on the northern shores of the Orange River ('Fossil bend' locality of Geiger, 1999; see also Fig. 3.6). Close to this outcrop, just below the Felix Unite Provenance Camp, fissures and joints within a breccia-like, glaciotectonized Nama Group limestone are filled with diamictic material

overlain by diamictites, dropstone-bearing shales and intercalated beds of boulder-mud-stones (Fig. 2.5-N). The cliffs along the cut bank of the Orange River also expose at this locality beautifully the numerous yellowish bentonite horizons (the so-called Zwartbas Tuffs, briefly described in Chapter 3.4.1) intercalated in dark dropstone-bearing shales.

Since the early studies by Haughton & Frommurze (1927, 1936) two distinct Dwyka facies have been distinguished in the Noordoewer-Karasburg area. Firstly, a red weathering, in places buff coloured facies, which consits of sandy mudstones, turbiditic sandstones, and siliceous shales with lenticular layers of boulder beds and calcareous concretionary masses. The sandstones are frequently ripple-marked and intensively traversed by invertebrate tracks (Anderson, 1975) (Fig. 2.5-I/K). Secondly, a dark bluish-grey facies, which is mainly composed of dropstone-bearing shales and intercalated layers of boulder-mudstones. This facies contains also small and large spherical, ellipsoidal or amoeboidal phosphatic and calcareous concretions, which often contain fossil remains (Fig. 2.5-O to S) (e.g. palaeo-niscoid fishes, bivalves, gastropods, foraminifera, radiolaria, wood, spiral coprolites, etc.; Martin & Wilczewski, 1970; McLachlan & Anderson, 1973; Geiger, 1999). Higher up in the succession also thin bands and lenticles of a dark bluish-grey phosphatic rock occur (Fig. 2.5-T). The spatial distribution of the two facies shows that the reddish to buff weathering glacial deposits were laid down earlier and are in places overlain by the bluish-grey facies. These two facies were interpreted to originate from two different ice sheets, in correspondence with the situation in the Mariental-Keetmanshoop area. The reddish facies was deposited by the generally southward flowing Namaland Ice, whereas the bluish-grey facies was deposited by the WSW-ward flowing Griqualand/Transvaal Ice (du Toit, 1921; Haughton & Frommurze, 1927, 1936; Schreuder & Genis, 1975).

Since the Nossob Sandstone at the Dwyka-Ecca boundary is not present in the Noordoewer-Karasburg area the boundary between the glacigenic Dwyka Group and the postglacial Prince Albert Shales is not sharp and not distinct. Due to this lithologically quite incon-spicuous transition only the boundary between tillitic-diamictic and shaly rocks within the Dwyka Group was mapped in the past and hence the glacigenic shales of the Dwyka and the postglacial shales of the Prince Albert Formation are shown as one single unit on published geological maps. Consequently, the entire thickness of the Dwyka Group is largely unknown. Only within a small restricted area opposite Zwartbas on Namibian ground Geiger (1999) has mapped for the first time properly the Dwyka-Ecca boundary. A few metres below the last occurrences of dropstones Geiger (1999) recognized within shales a quite conspicuos 10-15 m thick marker band. This succession contains conspicuous white weathering, slightly coarser-grained shale horizons, which show low-angle micro-cross lamination and are inter-

bedded in dark coloured shales. This marker zone was called 'White Horizon' by Geiger (1999) and is here informally referred to as the Owl Gorge Member. As in the Mariental-Keetmanshoop area the last dropstones occur also in shales a few metres above the Nossob Sandstone, the Owl Gorge Member can certainly be considered as a correlative of the latter. Thin mud-clast/pebble layers (tempestites?) (Fig. 2.5-V/W) in the upper part of the Dwyka shales below the Owl Gorge Member can be compared with the turbidite sandstones in the upper part of the Dwyka Group in the Mariental-Keetmanshoop area and be seen as similar high-energy depositional events. Within the small mapped area opposite of Zwartbas the Dwyka Group shows a total thickness of about 145 m. Only at the base tillitic and diamictic material is present, whereas the major part of this Dwyka succession consists of shales containing variable amounts of dropstones. Intercalated within these shales is in the lower third a conspicuous, unstratified ~1 m thick layer of a dropstone-rich mudstone ('Hippo Diamictite') and in the upper third a similar but slumped, deformed and only patchily distributed horizon ('Goats Cliff Diamictite', Fig. 2.5-U) (Geiger, 1999). Both diamictites occur within shales that are largely free of dropstones. Especially the Hippo Diamictite was considered by Geiger (1999) as a so-called 'Heinrich layer' (Heinrich, 1988) representing a phase of increased terrigenous input in reference to an increased deglaciation activity with intensively calving glaciers. Consequently, in order to define deglaciation boundaries within this succession, those shales that contain more abundant dropstones are considered as the lower part of such sequences, whereas the more or less dropstone-free units, which also contain the Hippo and Goats Cliff Diamictite, are considered as the upper part of the deglaciation sequences (Fig. 2.4). At the base of the Dwyka Group the reddish-buff weathering glacial facies may represent deglaciation sequence DS-I.
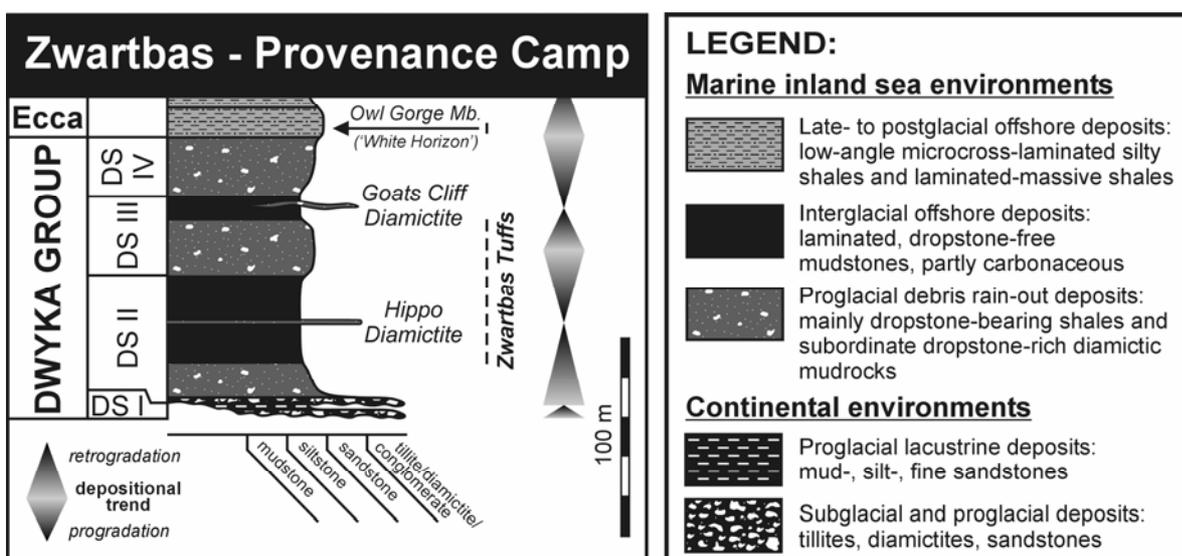
Fig. 2.4: Idealized lithostratigraphic overview section of the Dwyka Group opposite of Zwartbas in the vicinity of the Felix Unite Provenance Camp (see also Fig. 3.6) showing the possible four deglaciation sequences (DS I-IV) involved (modified after Geiger, 1999, 2000). Also shown is the position of the Zwartbas Tuffs.

Correlatives of the Dwyka Group deposits in southern Namibia can also be found in South Africa, Botswana and NW-Namibia, where the term 'Dwyka Group' is also applied (Johnson et al., 1997). In eastern South America the Itararé Group of the Paraná Basin and the Sauce Grande Formation of the Sauce Grande Basin are also correlatives of the Dwyka Group (López-Gamundí et al., 1994). On the Falkland Islands the Fitzroy Tillite Formation (former Lafonian Diamictite) comprises the Late Palaeozoic glacial deposits (Trewin et al., 2002) and in Antarctica the Whiteout Conglomerate (Ellsworth Mountains), the Gale Mudstone (Pensacola Mountains), the Pagoda – Scott Glacier – Buckeye Formations (Transantarctic Mountains), and the Darwin and Metschel Tillites (Victoria Land) can be considered as Dwyka correlatives (Collinson et al., 1994).
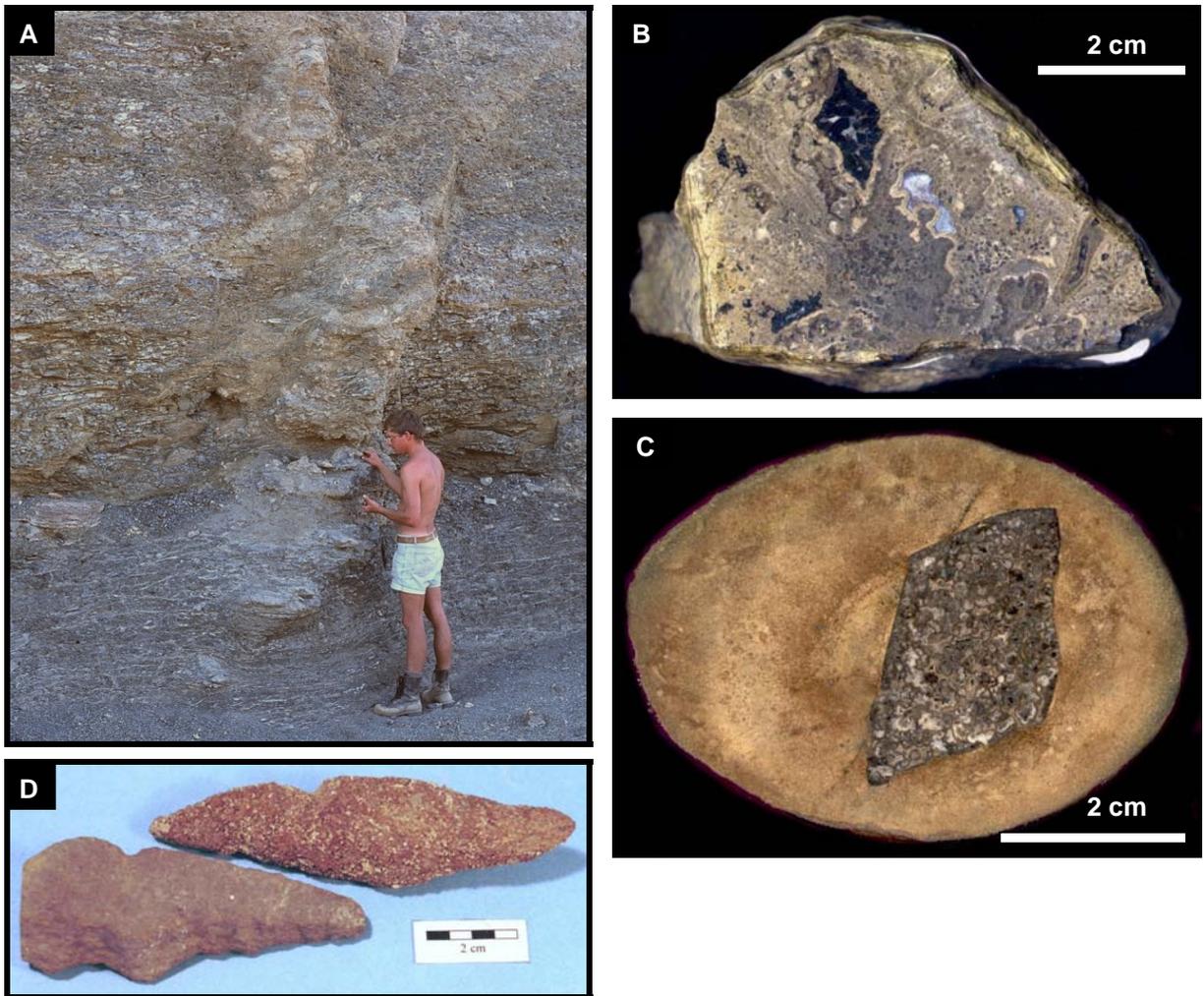
Fig. 2.5: Dwyka Group in southern Namibia: **(A)** Columnar, calcareous build-up in Ganigobis Shales (photo H. Stollhofen). **(B)** Polished hand specimen of algal mound limestone in Ganigobis Shales. **(C)** & **(D)** Rhomb-shaped glendonite crystals (pseudomorphs after ikaite) from the Ganigobis Shales (in (C) enclosed in phosphatic nodule). Locality for (A) to (D) between Asab and Tses along Brukkaros Rivier.
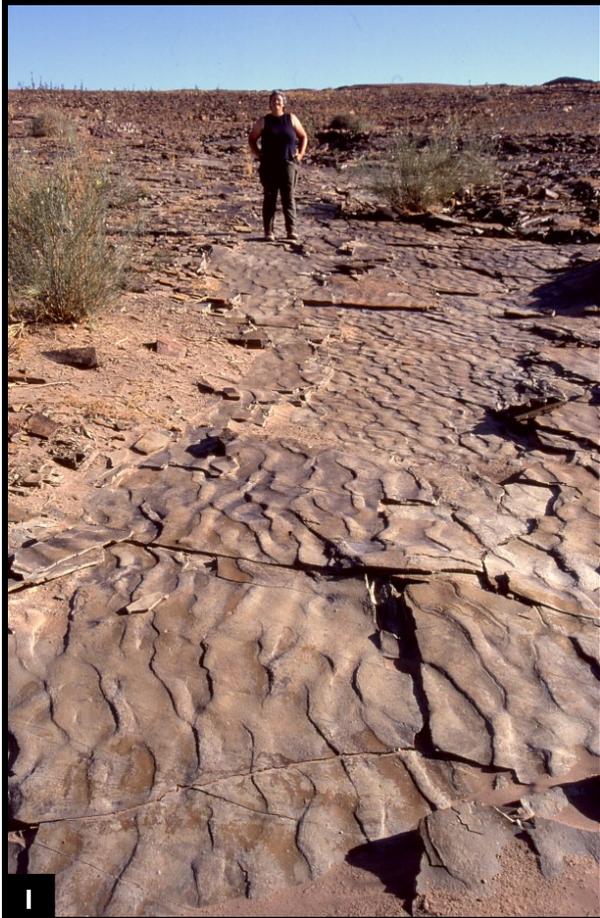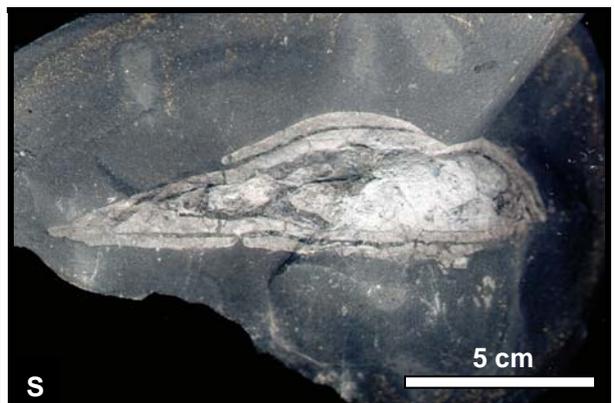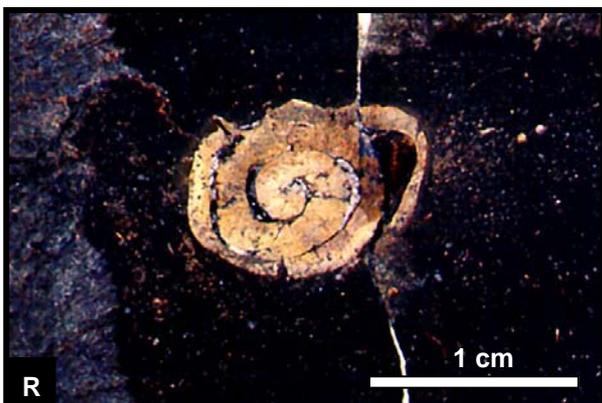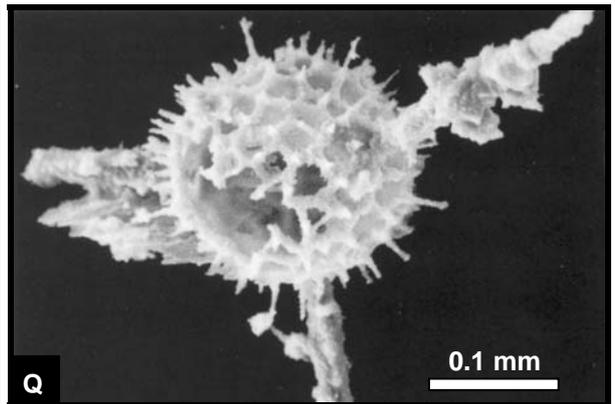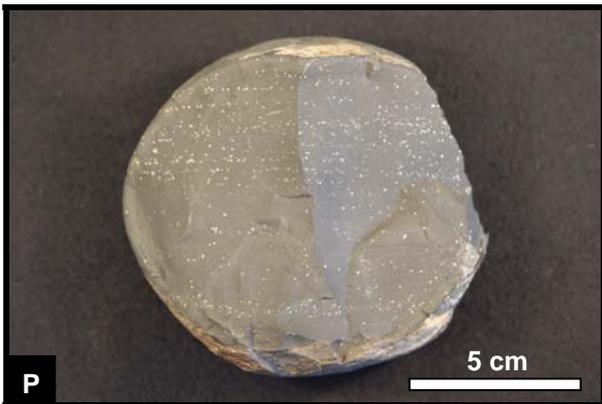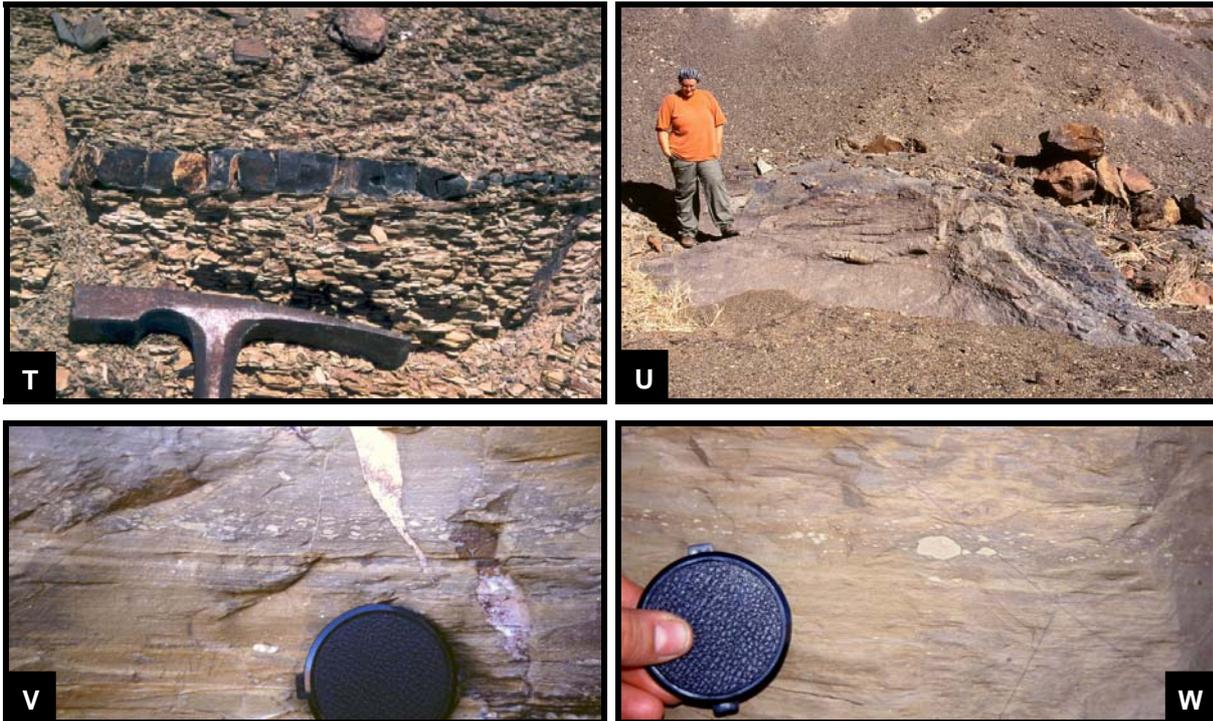
Fig. 2.5 (prev. pages and this page): Dwyka Group in southern Namibia (cont.): **(E) & (F)** Slumped turbiditic sandstones from the upper part of the Dwyka Group. Localities are Dassiefontein/Karas Mountains (E) and Hardap Dam (F). **(G) & (H)** *Rhizocorallium* (G) and *Rosselia* (H) within turbiditic sandstones of the upper part of the Dwyka Group exposed south of the Hardap Dam. **(I) & (K)** Ripple-marked fine sandstone and intensively traversed (*Umfolozia*) upper surface of a siltstone from the red-buff weathering glacial Dwyka facies in the Noordoewer-Karasburg area. Locality for (I) is Klipneus near Aussenjker and for (K) outcrops east of Noordoewer. **(L)** Polished and striated near-vertical face of a pre-Dwyka (Gariep?) rock. **(M)** Patch of a highly calcareous, yellowish weathering Dwyka tillite plastered on the uneven surface of a pre-Dwyka (Gariep?) rock. Locality for (L) and (M) is Fossil Bend at the Orange River (see Fig. 3.6). **(N)** Brecciated, glaciotectonized Nama Group limestone (left) overlain by bluish-grey weathering, grooved Dwyka diamictites (right). **(O)** Large amoeboid calcareous/phosphatic concretion within shales of the lower part of the Dwyka Group. Localities for (N) and (O) are in the vicinity of the Jet Cliff at the Orange River (see Fig. 3.6). **(P)** Spherical phosphate concretion with layers of calcified radiolarian remains within shales of the lower part of the Dwyka Group exposed in the vicinity of the Felix Unite Provenance Camp (see Fig. 3.6). **(Q)** Radiolarian skeleton extracted from a diagenetic nodule of the Dwyka Group. Foto by Ian McLachlan, illustrated in MacRae (1999). **(R)** Cross section along short axis of a spiral coprolite. **(S)** Cross section along long axis of a spiral coprolite. **(T)** Bluish-black phosphate lenticle in shales from the middle part of the Dwyka Group (Centipede Gorge; see Fig. 3.6). **(U)** Deformed and slumped Goats Cliff Diamictite within shales of the upper part of the Dwyka Group (Centipede Gorge). **(V) & (W)** Layers with abundant angular clay clasts and roundish clay pebbles within shales of the uppermost part of the Dwyka Group maybe representing tempestites. Localitiy is Hare Valley-Owl Gorge (see Fig. 3.6).

2.3 Ecca Group

The Ecca Group comprises those sediments, which have been deposited in the Karoo basins of southern Africa subsequent to the melting of the Dwyka ice. The biggest part of the post-glacial sediments was deposited subaqueously in a large inland sea under marine, evaporitic, brackish or freshwater conditions. Hence the Ecca Group is mostly represented by basinal shales with minor intercalations of sandstones. However, at the basin margins both terrestrial and inland sea sediments can be found, often forming stronger sand-dominated successions. The boundary between the Ecca Group and the overlying Beaufort Group is marked by a shift from subaqueously deposited inland sea sediments to continental, fluvio-lacustrine sediments (SACS, 1980; Rubidge et al., 2000; Rubidge, 2005). Within the studied Karoo outcrop areas in southern Namibia the Ecca Group is also dominated by basinal shales but towards the east borehole data show that the Ecca succession contains beneath the Kalahari cover a markedly increased sand content. In southern Namibia the Ecca Group is, in adaption to the South African stratigraphy, subdivided into the Prince Albert, Whitehill, Collingham, Aussenkjer and Amibberg Formation (Fig. 2.2). The latter three formations can only be found in the southwestern part of the Noordoewer-Karasburg outcrop area, whereas in the Mariental-Keetmanshoop outcrop area only the lower two formations are preserved. Succeeding deposits of the Beaufort Group are not preserved in the southern Namibian Karoo outcrop areas but are known from the NW Namibian Hub area in form of the Gai-As and Doros Formations (Stollhofen et al., 2000b).

2.3.1 Prince Albert Formation

Both in the Mariental-Keetmanshoop and in the Noordoewer-Karasburg Karoo outcrop area basinal shales largely dominate this basal formation of the Ecca Group. However, in the northern part of the Mariental-Keetmanshoop area both the base and the top of this formation are characterized by the presence of a sandy succession, namely the Nossob and the Auob Sandstone. The shale-dominated succession sandwiched between these sandstones has been designated the Mukorob Shales (SACS, 1980). Within the Mariental-Keetmanshoop area both sandstones thin towards the south but only the Auob Sandstone completely peters out between Asab and Tses. Therefore, in the vicinity of Keetmanshoop the Prince Albert Formation is commonly not subdivided into members although the Nossob Sandstone is still recognizable, even within the Karas Mountains according to own observations. In the Mariental-Keetmanshoop area bentonitic tuff layers within shales of the Prince Albert Formation have been discovered by this author between Tses and Keetmanshoop (Itzawisis Tuffs) (Fig. 3.1 & 3.2). Sandy to silty shales overlying the Auob Sandstone in the northern part of the Mariental-Keetmanshoop area are designated Rietmond Shales and were assigned in the past to the Prince Albert Formation. However, newer observations by

this author strongly indicate that these shales actually represent lateral equivalents of the lower part of the Whitehill Formation (Werner et al., 2002). Further to the east the stratigraphic interval of the Prince Albert Formation has been penetrated by numerous boreholes in the Aranos area in the search for coal deposits. Thin tuff layers (Vreda Tuffs) have been reported by Grill (1997) and Stollhofen et al. (2000a) from the Vreda core in shales just beneath the base of the Auob Sandstone (Fig. 3.1 & 3.2). In the Noordoewer-Karasburg area the Prince Albert Formation does not contain sandstone intercalations but similar to the situation further north both the basal and the top part of the Prince Albert Shales contain more coarser grained silty material deposited under somewhat higher energetic conditions due to regressions. The basal unit of the Prince Albert Formation outcropping in the vicinity of Noordoewer was first named 'White Horizon' by Geiger (1999) but is here referred to as the Owl Gorge Member. It can be considered as a correlative of the Nossob Sandstone Member. The uppermost coarser grained part of the Prince Albert Shales in the Noordoewer-Karasburg outcrop area, which can be correlated with the Auob Sandstone, is here informally named the Uhabis Member. Tuff layers have been discovered in this area within the Owl Gorge Member near Noordoewer (Owl Gorge Tuffs), within greenish-grey shales of the middle to upper part of Prince Albert Formation in roadcuts of the B1 highway near farm Korabib (Korabib Tuffs), and in the uppermost part of the Prince Albert Shales south of Uhabis (Uhabis River Tuff) (Fig. 3.1 & 3.2).

The sandstone complexes of the Prince Albert Formation in southern Namibia were first briefly described by Range (1912, 1928) as mica-rich sandstones, which contain in places plant fossils and thin coaly lenses. Martin (1953) was the first who produced a geological map showing the outcrop distribution and extent of the Nossob and Auob sandstones in the area between Mariental and Tses. Due to the coal occurrences associated with the Auob Sandstone a more detailed description of the lower part of the Ecca Group was undertaken by H. Martin in the Interim Report of the SWA Coal Commission (Brandt et al., 1961). Initial drilling operations (Silurian borehole, Gibeon District, drilled in 1951) had shown that the Auob Sandstone is directly overlain in the Aranos area by a coal seam. Heath (1972) and Grote (1984) further investigated the Prince Albert Formation in the Mariental-Keetmanshoop area in some detail. The most recent and most detailed work on the outcropping part of the Prince Albert Formation was undertaken by Grill (1997) with a focus on the Nossob and Auob Sandstones. Most information about the coal-bearing Prince Albert Formation in subcrop under Kalahari cover in the Aranos area can be gathered from Kingsley (1985), McDaid (1985) and Hegenberger (1992). In the Noordoewer-Karasburg area descriptions of the Prince Albert Formation can be found in Haughton & Frommurze (1936), Schreuder & Genis (1975), and Geiger (1999).

2.3.1.1 Nossob Sandstone Member and Owl Gorge Member

The Nossob Sandstone is commonly regarded as the basal unit of the post-glacial Prince Albert Formation. However, it should be noted that the last dropstones occur in many places in southern Namibia actually a few metres above this sandstone. From Mariental southward the Nossob Sandstone is well exposed along the prominent N-S trending Weissrand escarpment east of the B1 highway almost up to the area of Asab (Fig. 2.1). Further to the south good outcrops of the Nossob Sandstone can be found along an escarpment running from Tses northward approximately half way to the Mukorob. A third region with excellent outcrop conditions lies west and southwest of Keetmanshoop in the vicinity of the Gellap Plateau (Fig. 2.6-A). Genis & Schalk (1984) wrongly wrote that around Keetmanshoop the Dwyka-Ecca boundary lies within shales due to the absence of the Nossob Sandstone and hence must be drawn just above the uppermost pebbly zone within shales. These authors apparently were not aware that the prominent, escarpment-forming sandstone layer in the west and southwest of Keetmanshoop, at the western margin of the Gellap Plateau, actually represents the southern expression of the Nossob Sandstone. Poor outcrops of this sandstone were even discovered by the author northeast of Keetmanshoop (farm Goris) at the position of the mapped Dwyka-Ecca boundary. Furthermore, the Nossob Sandstone has been identified by this author in the outcrops between the Little and Great Karas Mountains (Fig. 2.6-B). The c. 8 m thick sandstone cropping out on Dassiefontein 87 at the western steep flank of the Great Karas Mountains and positioned by Schreuder & Genis (1977) within the Prince Albert Formation represents actually also the Nossob Sandstone and the underlying succession of grey and green shales with interbeds of calcareous, slumped sandstones belongs to the the upper part of the Dwyka Group as evidenced by numerous dropstones.

From north to south the Nossob Sandstone undergoes a considerable thickness and facies change. In the vicinity of Mariental the Nossob Sandstone attains a maximum thickness of about 20-25 m (Heath, 1972; Martin, 1981a; Grill, 1997) and thins southward to about 10-15 m, e.g. in the Asab area. South of Asab the thickness can vary somewhat but is distinctly reduced (<1(?) to ~10 m). From the western margin of the Gellap Plateau (2.5 m at Tsaraxa-aibes; own measurement) the Nossob Sandstone appears to thicken again in a south-westerly direction (15 m, 10 km south of Snyfontein; Grill, 1997) (Fig. 2.6-A). From these areas west of Keetmanshoop the Nossob Sandstone actually seems to thin and lose its character in satellite images in an easterly direction. However, on Dassiefontein in the Karas Mountains area, southeast of Keetmanshoop, the Nossob Sandstone clearly reappears (Fig. 2.6-B).

In the northern part of the study area the proximal facies of the Nossob Sandstone is mainly that of a southward prograding fluvially-dominated delta complex, whereas in the south the more distal facies of the Nossob Sandstone shows characteristics of depositional environments such as storm wave-dominated shorelines and basin floor turbidites (Grill, 1997; and own observations).

In the northern area between Mariental and Asab thin siltstone and fine sandstone layers with ripple cross-lamination (distal turidites) are increasingly intercalated in dark dropstone-bearing shales of the uppermost part of the Dwyka Group. Directly underneath the Nossob Sandstone greenish-grey siltstones and fine sandstones, showing plane and climbing ripple cross-lamination as well as in places convolute bedding and local scouring, more and more replace the dark coloured shales of the upper part of the Dwyka Group. This facies is followed by stacked fining-upward sandstone units (proximal high-density turbidites/liquified flows) (Grill, 1997). At the base of such units fine- to medium-grained, ripple cross-laminated sandstone overlies a pelitic shale layer with a sharp but non-erosional contact. The basal part often shows intensive soft sediment deformation (convolute bedding and ball-and-pillow structures) and the middle part is characterized by dish-and-pillar structures indicating water-escape (Fig. 2.7-A to C). On top of such units often symmetrical wave ripples are preserved. At some outcrops unspecific thick sandstone beds overlying the Dwyka Shales with a sharp and often erosional contact can also represent the basal part of the Nossob Sandstone. In places the Nossob Sandstone has a conglomeratic base (Grote, 1984; Grill, 1997), which in some cases contains *Eurydesma* shells. At the top of the Nossob Sandstone medium- to coarse-grained, feldspathic, trough and ripple cross-bedded sandstones with a sharp erosional base, frequently overlain by a gravelly lag, can be found in some outcrops within the northern facies type area (Fig. 2.7-D). These sandstones represent distributary channel fills (Grill, 1997).

East of Mariental the Nossob Sandstone is also known from many boreholes in the Aranos area (Hegenberger, 1985, 1992; Kingsley, 1985; McDaid, 1985; Grill, 1997). Its thickness varies from somewhat more than 20 m to about 40 m. The facies is mainly that of a coarsening-upward, prograding deltaic succession with prodelta to mouth bar to delta plain distributary channel depositional environments.
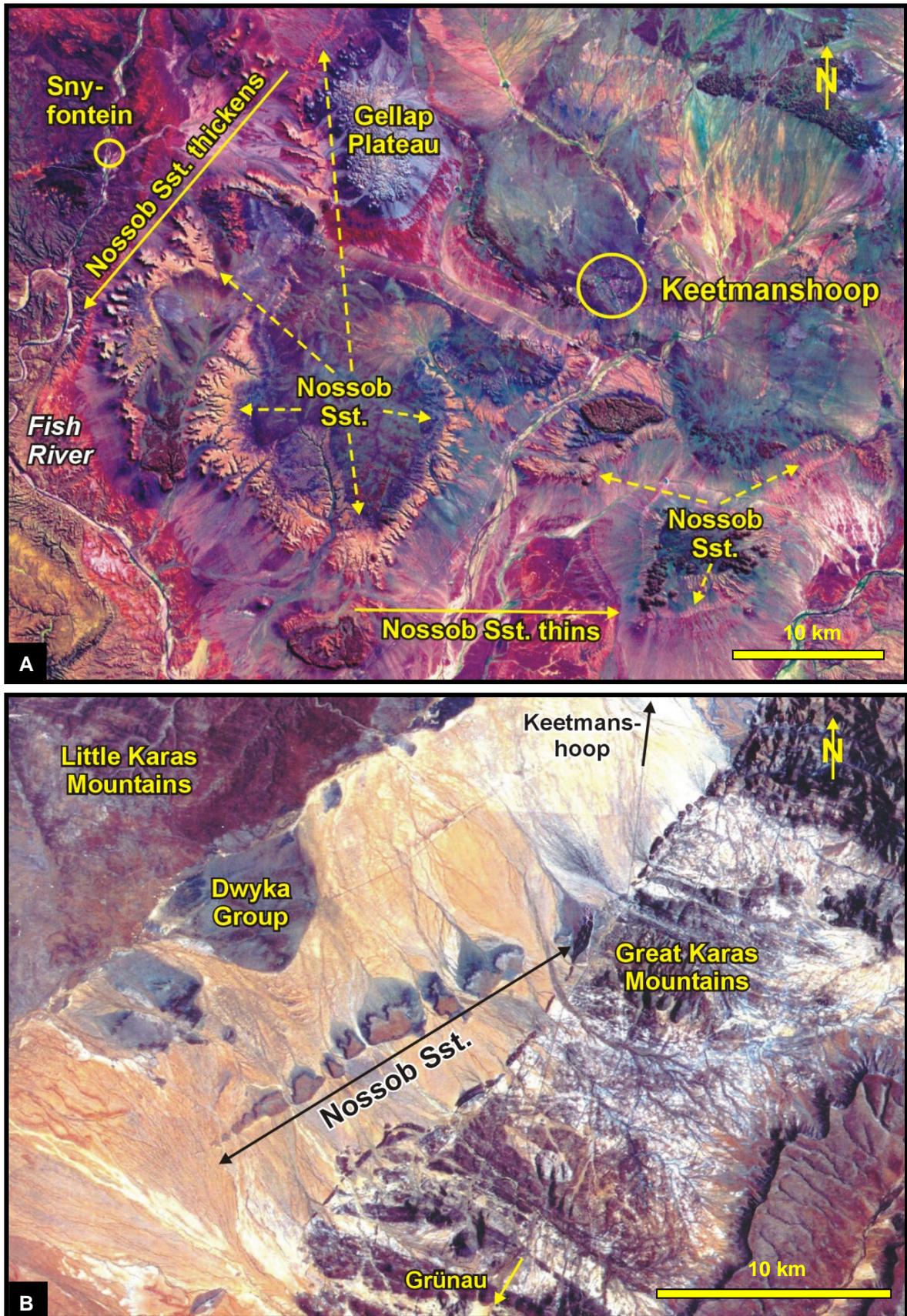
Fig. 2.6: Nossob Sandstone: **(A)** Outcrops of the Nossob Sandstone in the western and southern vicinity of Keetmanshoop. **(B)** Trail of mesa-like outcrops of the Nossob Sandstone between the Little and Great Karas Mountains. Both pictures are Landsat TM-5 scenes. Data processing by C. Krapf.

In the region south of Asab the more distal expression of the Nossob Sandstone can be quite heterogeneous in facies and thickness. From Asab to Tses the Nossob Sandstone consists mainly of distal and proximal turbidites but no distributary channel or liquified flow facies occurs indicating a southward deepening of the basin and a more distal depositional environment. In the area between Tses and the Gellap Plateau the Nossob Sandstone has so far not been followed and studied. East of Snyfontein, near Tsaraxa-aibes at the western margin of the Gellap Plateau an only 2.5 m thick, upward-fining Nossob Sandstone was observed by the author. It has a channel-shaped, erosional, conglomeratic base, which is followed by massive and plane-laminated sandstone grading into ripple cross-laminated and convolute bedded sandstone. Diagenetic carbonate concretions mark the top of the Nossob Sandstone. At this locality the Nossob Sandstone has more the characteristics of a turbiditic basin floor fan. Further to the southwest the Nossob Sandstone thickens again. Grill (1997) described from a locality 10 km south of Snyfontein a 15 m thick coarsening- and shallowing-upward succession with proximal turbidite sandstones at the base, overlying Dwyka shales with a sharp but non-erosional contact, followed by plane-laminated, hummocky cross-stratified and wave rippled sandstones of a lower to upper shoreface environment. Further to the east, towards Keetmanshoop, aerial and satellite images show that the Nossob Sandstone loses its distinct character and seems to pinch out in this direction (Fig. 2.6-A).

Further to the southeast, on Dassiefontein at the western flank of the Great Karas Mountains the Nossob Sandstone shows a coarsening and shallowing-upward succession with a thickness of about 8 m. At this locality the uppermost part of the Dwyka Group consists of laminated and convolute bedded siltstones and very fine sandstones with coarser sandlenses and reworked dropstones. The actual base of the Nossob Sandstone is characterized by erosional channels (Fig. 2.7-E), which are filled with greenish-grey, mud-rich, very fine-grained, massive sandstone, in places also showing a pebbly coarse sand-stone base. One of these channels has a depth of 1.2 m and a width of 22 m. This basal zone is followed by thin (10-20 cm), stacked fining-upward sandstone cycles of wavy laminated to climbing ripple cross-laminated very fine- to fine-grained sandstones (Fig. 2.7-F). Then follows a zone, which is characterized by thicker (30-60 cm), stacked fining-upward cycles composed of massive fine-grained sandstones with an erosional base grading into climbing ripple cross-laminated sandstones. A thick packet of massive to laminated fine-grained sandstones characterizes the overlying upper 3.5 m of the Nossob Sandstone. Some parts seem to consist of amalgamated low amplitude-high wavelength channels filled with laminated fine-grained sandstones. This part of the sandstone also shows spectacular soft sediment deformation structures (convolute bedding) due to dewatering and is strongly carbonate-cemented, giving the sandstone a dark brown colour (Fig. 2.7-G). This locality is

the southernmost outcrop of the Nossob Sandstone. The thickness and the sedimentary structures indicate high-energy sedimentation, high sedimentation rates and strong sand input implying the proximity of a source area. However, no hummocky cross-stratification has been observed, which could point to storm-wave activity. The sedimentary facies actually resembles more the northern facies type of the Nossob Sandstone, however, without distributary channels on top of it. The sandy succession on Dassiefontein probably reflects deposition in a prodelta to deltafront environment. The palaeogeographic situation in the Karas Mountains area during deposition of the Nossob Sandstone is not yet fully understood but it seems that this area formed a shoal within the basin and there may have even existed emergent islands.

The nature of the basal contact of the Nossob Sandstone to the underlying Dwyka Shales is assessed variably. Martin (1981a) stated that the contact is conformable in the Keetmans-hoop area but becomes slightly disconformable northwards. Heath (1972) and Grote (1984) as well as Schalk & Germs (1980) described the contact in the area between Mariental and Tses as unconformable. Visser (1983b) even showed a major unconformity at the base of the Nossob Sandstone. Also Bangert (2000) and Bangert et al. (2000) show in their interpretations of N-S cross-sections that the Nossob Sandstone overlies unconformably various deglaciation sequences of the Dwyka Group, which actually would imply a major erosional unconformity. In the Aranos area the base of the Nossob Sandstone is characterized by a basal scour, which is recognizable throughout the whole area (Kingsley, 1985). In contrast, Stollhofen (1999) and Stollhofen et al. (2000a) interpreted the Dwyka deglaciation sequence boundaries within the same sections of this N-S cross-section differently and show a more or less conformable contact to the Nossob Sandstone. Also Grill (1997) wrote that the Nossob Sandstone rest conformably on top of the Dwyka Group. Furthermore, Smith (1984) reported that in adjacent areas in Botswana the Nossob-equivalent Ncojane Sandstone overlies conformably glacigenic shales. Based on the available literature and own observations in southern Namibia it seems that despite the sometimes sharp and erosional base of the Nossob Sandstone it has not been convincingly proven that there exists really a major hiatus or unconformity between the Dwyka Group and the Nossob Sandstone in the Mariental-Keetmanshoop area. The fact that the Nossob Sandstone overlies different Dwyka sediments or sedimentary successions is not necessarily indicative of a hiatus or the erosion of now 'missing' Dwyka units but seems rather related to facies changes of the Dwyka deposits along the N-S trending outcrop belt. Also the Nossob Sandstone and the overlying deposits of the Prince Albert and Whitehill Formations undergo considerable facies changes from N to S.

In the Noordoewer-Karasburg outcrop area no sandstones occur at the base of the Prince Albert Formation. However, in the Karoo outcrops north of the Orange River near Noordoewer a conspicuous marker zone with several white weathering, slightly coarser grained shale horizons within dark greenish-grey shales can be found at the Dwyka-Ecca boundary. This stratigraphic interval was first discovered by Geiger (1999), who decribed it as the so-called 'White Horizon', but is here referred to as the Owl Gorge Member. So far it has been traced from opposite of Zwartbas in an eastward direction to an area northeast of Noordoewer. In the latter area it was originally misinterpreted by Schreuder and Genis (1975) as outcrops of the also white weathering Whitehill Formation overlying conformably the Prince Albert Formation. Neither the Dwyka-Ecca boundary nor the full areal extent of the Owl Gorge Member has yet been mapped throughout the entire Noordoewer-Karasburg area. However, it appears that in the west (Aussenkjer) and in the north (Ai-Ais) of this area the Owl Gorge Member loses its distinctive white weathering character indicating a source area in the south to southeast.

The Owl Gorge Member consists in the Owl Gorge type locality of three white weathering horizons named W-I to W-III (Fig. 2.7-H) and attains a thickness of 12.5 m. Intercalated in this shale succession are thin diagenetic layers and lenses of bluish-grey to black, highly phosphatic shale impregnations (Fig. 2.7-M/N) and light coloured, diagenetic carbonate concretions and layers. For example, the dark brownish weathering shales between W-I and W-II are divided by a conspicuous, lateral continuous, diagenetic carbonate layer into two parts of approximately equal thickness (Fig. 2.7-H/K). The white weathering horizons show a relatively sharp base and a more transitional, sometimes banded top (Fig. 2.7-K/L). Each of these horizons is interpreted as a fining-upward parasequence. The uppermost horizon (W-III) is the least conspicuous of the three and shows a light olive-grey weathering colour. Hence the succession from W-I to W-III is interpreted to represent a large-scale (3rd order) fining-upward, retrogradational succession. Parallel lamination and very low angle micro cross-lamination (Fig. 2.7-I) can bee seen within the white weathering horizons, which are interpreted as very distal turbidite deposits within the laminated to massive bownish weathering shales, which most probably have largely a suspension fall-out origin. The Owl Gorge Member can certainly be considered as a correlative of the Nossob Sandstone, both deposited during a time of lowered sea level at the Dwyka-Ecca boundary. However, the Owl Gorge Member is not the distal equivalent of the Nossob Sandstone. Palaeocurrent measurements by Heath (1972) and Grill (1997) within the Nossob Sandstone in the areas between Mariental and Keetmanshoop consistently show dominantly southwesterly to southeasterly directions indicating a northerly source area (Windhoek Highlands). In contrast, the pinching out of the Owl Gorge Member towards the west and north indicates a southern to southeastern source area (Cargonian Highlands).
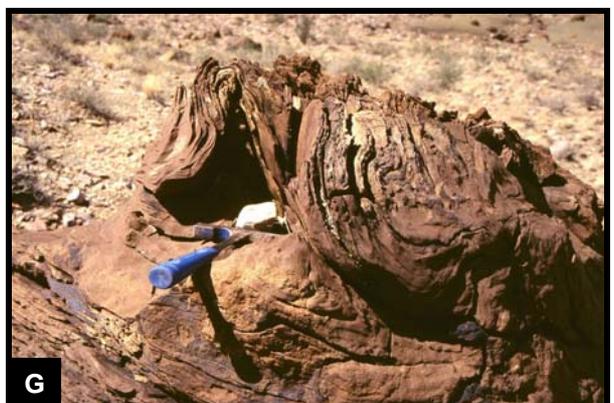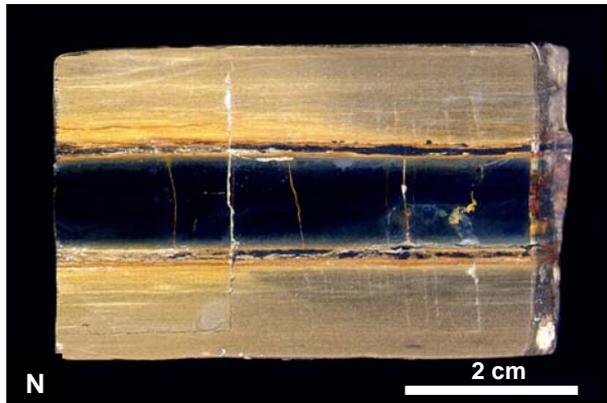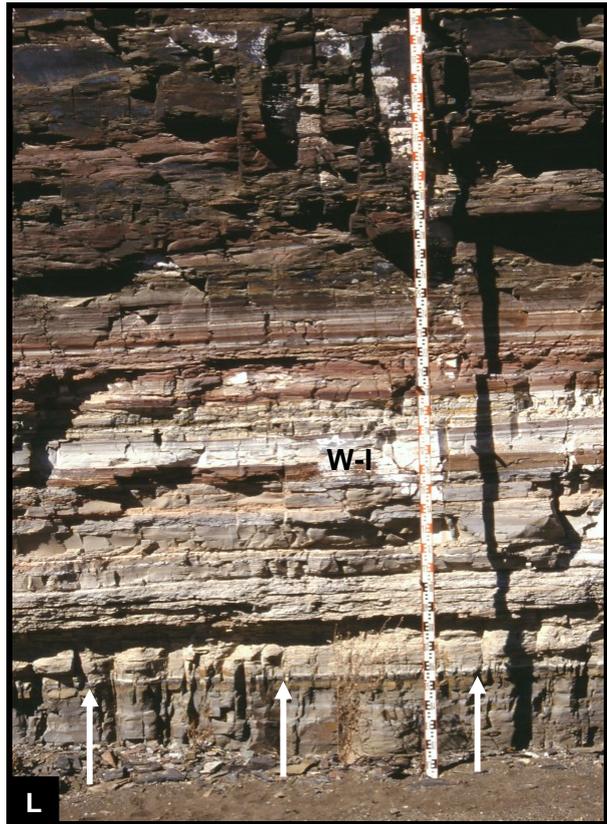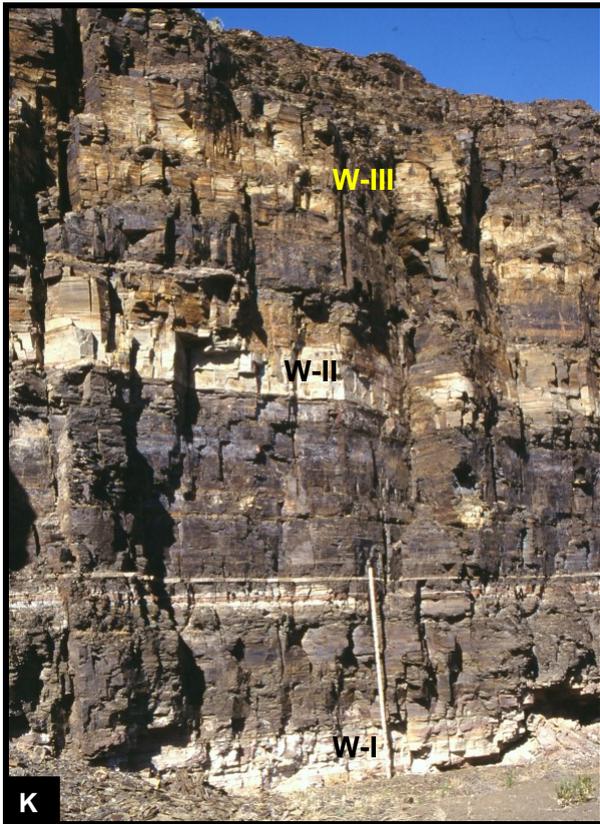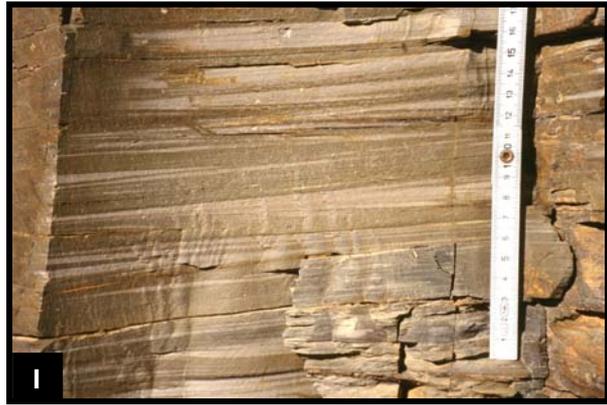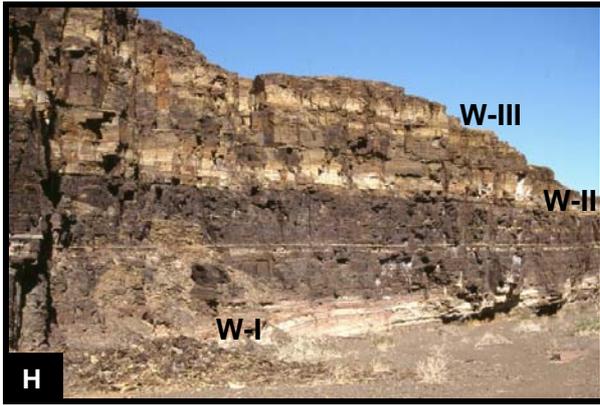
Fig. 2.7 (prev. pages): Nossob Sandstone and Owl Gorge Member: **(A)** Convolute bedding. **(B)** Load casts. **(C)** Dish-and-pillar structures. **(D)** Trough cross-bedded distributary delta plain channel sandstone on top of the Nossob Sandstone. Locality for (A) to (D) is farm Orab south of Mariental. **(E)** Erosional channel at the base of the Nossob Sandstone, filled with massive, muddy, very fine-grained sandstone, emplaced within flaser-bedded and ripple cross-laminated fine sandstones and siltstones, and overlying dark grey, deformed (slumping, ball-and-pillow structures) siltstones and fine sandstones of the uppermost Dwyka Group. **(F)** Wavy laminated and climbing ripple cross-laminated fine sandstone of the middle part of the Nossob Sandstone. **(G)** Strongly deformed and convolute bedded, carbonate cemented, brown coloured, and fine-grained sandstone in the upper portion of the Nossob Sandstone. Locality for (E) to (G) is Dassiefontein on the western flank of the Great Karas Mountains (see also Fig. 2.6-B). **(H)** Overview over the three white weathering horizons in the Owl Gorge. Note the thin, light coloured and lateral continuous diagenetic carbonate layer in the middle of the dark coloured shale succession between W-I and W-II (see also Fig. 2.7-K). **(I)** Very low angle micro cross-lamination within one of the white weathering horizons of the Owl Gorge Member. **(K)** W-II displays a very sharp base and a transitional top in this picture. Scale is 4 m. **(L)** Sharp base of W-I is directly underlain by a dark and thin layer of strongly phosphate-impregnated shale (arrows). The top of W-I is quite transitional and shows white-brown-red colour banding. **(M) & (N)** Bluish-grey to black, highly phosphatic shale impregnations within the Owl Gorge Member. Locality for (H) to (L) is the Owl Gorge (see also Fig. 3.6).

2.3.1.2 Prince Albert Shales, Mukorob Shale Member and Uhabis Member

The fine-grained, argillaceous succession sandwiched between the Nossob and the Auob sandstones is called the Mukorob Shales (SACS, 1980). There is actually no defined southern boundary for the Mukorob Shales but south of Tses, where the Auob Sandstone completely peters out, the argillaceous succession is commonly just simply called the Prince Albert Shales. Due to the mud-rich nature of the soft Mukorob Shales they do not show a great resistance against weathering and hence good outcrops are very rare. Only at few localities are a few metres well exposed above the Nossob Sandstone but the best outcrops can be found beneath the Auob Sandstone. However, there is no continuous outcrop existing from base to top. Towards the east the Mukorob Shale Member was penetrated by a number of coal exploration boreholes in the Aranos area and several cores are available containing the whole succession from the Nossob to the Auob Sandstone. Thin tuff layers have been identified within the uppermost Mukorob Shales by Grill (1997) and Stollhofen et al. (2000a) from the Vreda core just beneath the base of the Auob Sandstone (Fig. 3.1). In outcrops in the northern part of the Mariental-Keetmanshoop area the Mukorob Shales consist mainly of dark grey to slightly greenish clay- and siltstones with intercalations of fine sandstones, the latter being found especially at the base and at the top. The whole succession becomes towards the east coarser grained and sandier, whereas towards the south it becomes finer grained and more clay-rich. Heath (1972) reported a thickness of about 60-90 m for the Mukorob Shales in the area between Mariental and Asab.

Grill (1997) described from one locality that distributary channels of the Nossob Sandstone are overlain by a succession of intercalated sand- and siltstones deposited by proximal and

distal turbidites, which indicate a rapid deepening of the depositional environment. This basal succession shows an overall fining-upward, retrogradational trend. In contrast, the uppermost part of the Mukorob Shales shows an overall coarsening-upward, progradational trend with shales containing more and more silt- and fine sandstone interlayers of distal to proximal turbidite origin, conformably overlain by lower to upper shoreface deposits of the Auob Sandstone.

In the Aranos area the lower portion of the Mukorob Shale Member consists of dark grey to greenish shales, which are silty in places. In the upper portion a thin limestone marker band between the lower shale and the upper more sandy zone is regionally persistent in this area. Above this limestone the Mukorob sediments become progressively coarser grained and pass upwards into interstratified shale, siltstone and sandstone. This coarsening-upward succession reflects transition from offshore shelf to prodelta deposition. The lower shale unit attains a maximum thickness of 63 m and averages about 50 m. The upper coarsening-upward succession is about 40 m thick (Kingsley, 1985; McDaid, 1985). A coarsening-upward succession at the top of the Mukorob Shales was also described by Grill (1997) from the Mukorob locality, where offshore mudrocks grade into interbedded shales, siltstones and sandstones of a distal turbidite/transitional shoreface environment. A few hundreds of metres south of this locality a dark brown, strongly indurated, massive, highly ferruginous and phosphatic shale layer is interbedded in the softer and fissile bluish-grey Mukorob Shales, approximately at the base of the coarsening-upward succession towards the Auob Sand-stone (Fig. 2.8-A). This layer could represent a maximum flooding surface below the Auob Sandstone and is most probably a correlative of the above mentioned limestone marker band in the Aranos area. This is further supported by the possible occurrence of glauconite in a green, very fine-grained sandstone just underneath the limestone marker band (borehole ACP 24; Kingsley, 1985). In thin sections the hard phosphatic shale contains numerous opaque, hematitic-phosphatic diagenetic spherules (~120 µm) dispersed in a clay-rich matrix. Furthermore, this phosphatic shale also contains tiny (~20-30 µm) microspherules, which may again represent radiolarian remains (Fig. 2.8-B), indicating marine conditions, together with the possible glauconite occurrence.

South of Tses the Mukorob Shales grade laterally into the Prince Albert Shales. They consist mainly of olive-green to greyish silty shales, which often have a slightly cherty appearance. The Itzawisis Tuffs south of Tses are for example interbedded in such shales. Due to the numerous dolerite intrusions the shales often have a spotted appearance as a result of contact-metamorphic cordierite growth and its subsequent downbreak to chloritic pinite. Not very much is known about the Prince Albert Shale succession in the Keetmanshoop area. An

interesting observation is that northeast of Keetmanshoop the Prince Albert Shales attain a thickness of about 50 m, whereas towards the northwest at the Gellap Plateau they attain a thickness of about 100 m. The same is also valid for the overlying Whitehill Shales and it is suggested that this thickness distribution might be controlled by synsedimentary fault activity. At the western margin of the Gellap Plateau the Nossob Sandstone is overlain by greenish-grey shales, which contain in the lowermost 15-20 m still dropstones and slumped turbiditic sandstone layers. Above this zone follows a quite monotonous shale succession, which in places contains chert-like, phosphatic shale horizons. On weathered surfaces of these hard shales abundant microspherules are weathered out (radiolarian remains?). At many visited localities in the Keetmanshoop area the boundary between the Prince Albert and the overlying Whitehill Shales is very transitional and extremely difficult to define. There, no coarsening-upward trend at the top of the Prince Albert Formation has been observed.

In the Noordoewer-Karasburg area the Prince Albert Formation also consists of a very monotonous bluish- to greenish-grey shale succession apart from the Owl Gorge Member at its base. Where the basal Owl Gorge Member is not present the boundary to the Dwyka Group is, apart from the last occurrence of dropstones, characterized by a marked decrease in the abundance of carbonate concretions. Most of the shales have a somewhat silty appearance. Occasionally up to 10 cm big phosphatic nodules can be found within the shales (Fig. 2.8-C). Furthermore, in some parts of the shale succession bioturbation is quite conspicuous (Fig. 2.8-D). The Korabib Tuffs are intercalated in the upper part of the Prince Albert Shales. The uppermost part of the Prince Albert Formation is characterized in the Noordoewer-Karasburg area by a slight but distinct and often morphologically well-expressed coarsening-upward trend. The fissile shales grade in the uppermost 10-15 m into harder and slabbier weathering shales, which form steep, cliff-like exposures below the overlying Whitehill Formation (Fig. 2.8-E). Polished surfaces of these coarser shales show a flasery interlayering of clay, fine and coarse silt (Fig. 2.8-F). This coarsening-upward succession, here informally called the Uhabis Member, can be compared to that at the top of the Mukorob Shales in the northern part of the Mariental-Keetmanshoop and the Aranos area, which finally leads to the deposition of the Auob Sandstone. However, the Auob Sandstone has a northerly source area, whereas the uppermost coarser part of the Prince Albert Shales in the vicinity of Aussenkjer and Noordoewer has most probably a southerly source area. The Uhabis River Tuff close to the base of the upward-coarsening succession in the Noordoewer-Karasburg area might therefore be equivalent to one of the tuff layers (Vreda Tuffs) at the base of the Auob Sandstone in the Vreda core.
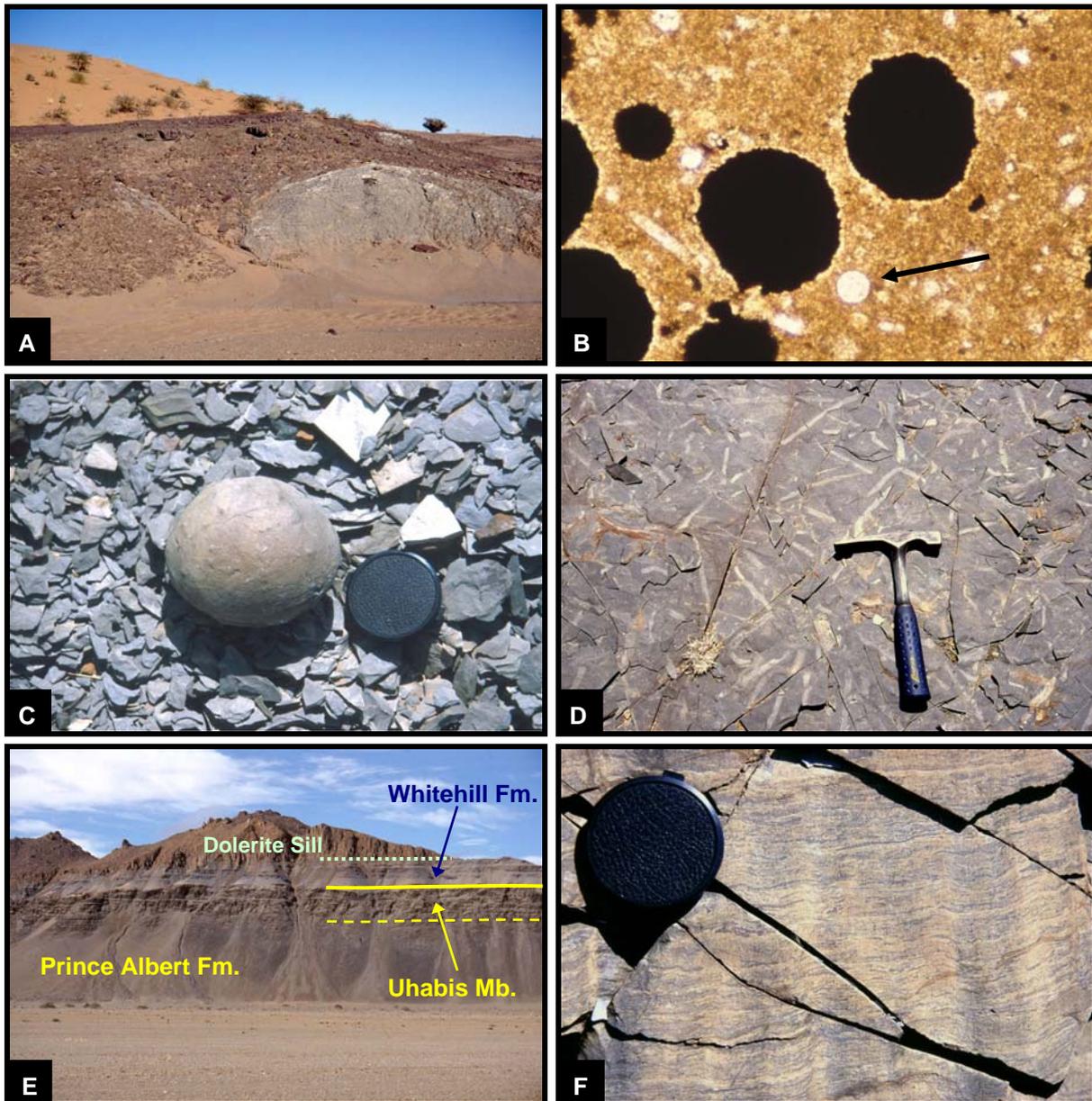
Fig. 2.8: Mukorob and Prince Albert Shales: **(A)** Indurated, red-brown, highly ferruginous and phosphatic shale horizon interbedded in soft and fissile, bluish-grey shales of the Mukorob Member, probably representing the maximum flooding zone below the Auob Sandstone. Locality is south of the Mukorob. **(B)** Thin section image of the indurated shale containing opaque, hematitic-phosphatic diagenetic spherules (~120 μm) and small, light coloured microspherules (~25 μm) (arrow) of possibly radiolarian origin. Plane-polarized light. **(C)** Diagenetic phosphate nodule in bluish-grey shales of the Prince Albert Formation near Aussenkjer. **(D)** Bioturbation in dark grey shales of the Prince Albert Formation near Noordoewer. **(E)** The lower two third of the outcrop represents the upper part of the Prince Albert Formation, which shows at its top a cliff-forming coarsening-upward succession here informally called the Uhabis Member. This coarser uppermost part of the Prince Albert Formation can be compared to the situation in the northern part of the Mariental-Keetmanshoop area, where the Auob Sandstone overlies the Mukorob Shales. This is followed by the bluish-grey weathering band of the Whitehill Formation, which is intruded by a dolerite sill, the latter forming the brownish rock on top of the outcrop. Locality is the Uhabis River north of Noordoewer. **(F)** Polished surface of the coarser shales at the top part of the Prince Albert Formation (Uhabis Member) with flasery interlayering of clay (dark stringers), fine and coarse silt (light stringers). Locality is north of the Owl Gorge near Noord-oewer.

2.3.1.3 Auob Sandstone Member

The Auob Sandstone is well exposed only in two areas within the Mariental-Keetmanshoop region. The northern outcrop locality lies about 10 km east of Mariental, whereas the southern outcrops are found east of the Asab-Tses area, from the former Mukorob National Monument c. 15-20 km to the south until the Auob Sandstone completely peters out.

Early descriptions by H. Martin can be found in Brandt et al. (1961), followed by investigations on the outcropping part of the Auob Sandstone by Heath (1972) and Grote (1984). Extensive descriptions of the Auob Sandstone from the Aranos subsurface area can be found in Kingsley (1985) and McDaid (1985). A brief and comprehensive overview is provided by Hegenberger (1992). The most recent and most extensive descriptions of the Auob Sandstone outcrops in southern Namibia were undertaken by Grill (1997).

The Auob Sandstone overlies the Mukorob Shales conformably. The upper, coarsening-upward portion of the Mukorob Shales, with successively more and thicker turbiditic sand-stone interlayers within shales, grades rapidly into an almost entirely sandstone-dominated stratigraphic interval representing the Auob Sandstone Member. At the outcrops in the vicinity of the Mukorob the boundary between the Mukorob Shales and the Auob Sandstone is characterized by a conspicuous colour change from bluish-grey shales to ochreous sandstones (Fig. 2.9-A).

The outcropping part of the 'Mukorob Shale-Auob Sandstone-Rietmond Shale' succession records a large scale (3rd order) progradational, coarsening- and shallowing-upward development from offshore shales with interbedded turbiditic sandstones to lower and upper shoreface sandstones, followed by a large scale (3rd order) retrogradational, fining and deepening-upward phase with delta plain deposits, comprising arkosic distributary channel sandstones as well as carbonaceous interdistributary and reddish floodplain fines, overlain by offshore shales with thin interbedded turbiditic sandstone layers. The outcropping facies succession of the Auob Sandstone was compared by Grill (1997) with a prograding storm wave-dominated shoreface environment with the feeding delta system locally preserved in the form of distributary channels and other delta plain deposits.

The lower shoreface facies association is built up by plane- to ripple cross-laminated sand-stones and interbedded silt-/sandstones, whereas the upper shoreface facies association is characterized by fining-upward packets of medium- to coarse-grained plane-laminated sand-stones grading into fine- to medium-grained hummocky cross-stratified sandstones (Fig. 2.9-B). Along the escarpment south of the Mukorob large-scale foresets or clinoforms, dipping

towards the south (direction of progradation of the shoreface system), are well exposed in the upper part of the shoreface facies association (Grill, 1997). The shoreface sandstones are often moderately to very intensively bioturbated (Fig. 2.9-C). In the upper part of the Auob Sandstone large lenticular bodies of medium- to coarse-grained, arkosic, trough cross-bedded sandstones can be observed (Fig. 2.9-D). These sandstone bodies have an erosional base and frequently a glavelly lag is present at the base. Grill (1997) interpreted these sandstones as delta plain distributary channel fills. Also in the upper part of the Auob Sandstone a facies association with interlayered dark carbonaceous mudstones and ripple cross-laminated sandstones is quite common, which were laid down in an interdistributary bay environment (Grill, 1997). Finally, on top of some of the distributary channel sandstones reddish sandy siltstones and lenticular fine-grained sandstones can locally be found probably representing floodplain fines and local crevasse splays (Grill, 1997).

Palaeocurrent measurements by Heath (1972) and Grill (1997) consistently show southerly transport directions similar to the situation for the Nossob Sandstone. The thickness of the Auob Sandstone east of Mariental in the northern part of its outcrop area is given by Brandt et al. (1961) and Heath (1972) as about 60 m, whereas Grill (1997) reported only 14 m. Along the N-S trending outcrop belt the Auob Sandstone shows a thickness of 40-45 m at the Mukorob National Monument site but rapidly thins and completely peters out in a southerly direction.
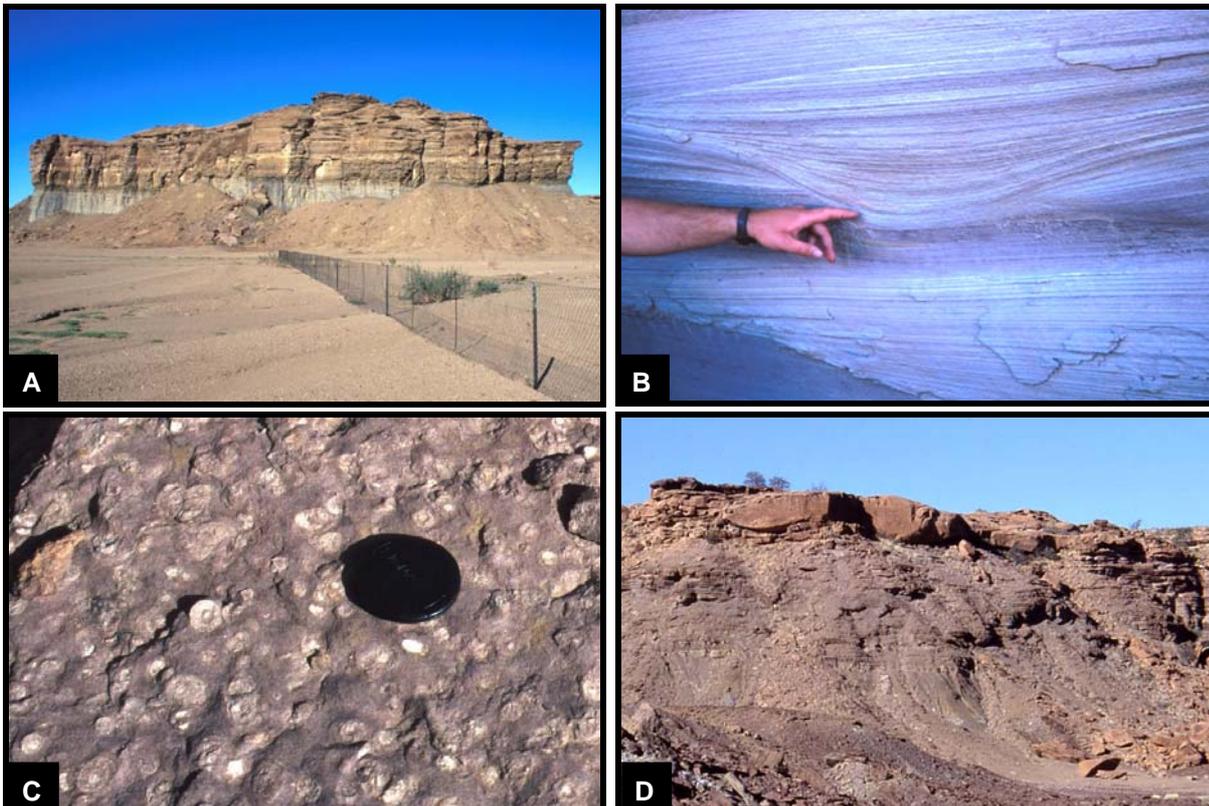
Fig. 2.9 (prev. page): Auob Sandstone: **(A)** At the Mukorob National Monument outcrop locality the boundary between the Mukorob Shales and the Auob Sandstone is characterized by a relatively sharp colour change from bluish-grey shales to ochreous sandstones. **(B)** The upper shoreface facies of the Auob Sandstone is characterized by amalgamated plane laminated to hummocky cross-stratified sandstone units, in places displaying trough-like features ('swales'). **(C)** The Auob shoreface sandstones are quite intensively bioturbated, here with vertical, concentrically laminated burrows assigned to the ichnogenus *Siphonichnus*. **(D)** Large lenticular sandstone bodies with erosive and gravelly bases are commonly found in the upper part of the Auob Sandstone exposures just south of the Mukorob and are interpreted as delta plain distributary channels (Grill, 1997).

In the Aranos Karoo subsurface area the Mukorob Shales are overlain by a succession of sandstone and sandstone-shale units with minor black shale and coal. The stratigraphic subdivision of the post-glacial Ecca Group deposits, penetrated by numerous coal exploration boreholes, differs from that of the outcrop area between Mariental and Keet-manshoop. In the Aranos area generally only the coarse-grained, trough cross-bedded arkosic channel sandstones with an erosional base, which are lateral equivalents of the distributary channel sandstones at the top of the outcropping Auob Sandstone, have been considered by McDaid (1985) as the basal part of the Auob Member, whereas the underlying subaqueously deposited upper shoreface/beach sand deposits are variably placed either at the top of the Mukorob Member or at the base of the Auob Member (McDaid, 1985; Kinglsey, 1985). The arkosic sandstones are overlain by a lower coal zone, also called the Impala Coal Seam (Kingsley, 1985), followed by a sandstone succession and a second, upper coal zone. The lower coal zone and the overlying sandstone succession were also considered as a part of the Auob Member by McDaid (1985). The upper coal zone is correlated with the Whitehill Formation, exposed in the southern part of the Mariental-Keetmanshoop outcrop area (McDaid, 1985). The upper coal zone is overlain with a pronounced erosional unconformity by coarse-grained sandstones. In some places erosion has completely removed the upper coal zone and even cut into the underlying sandstones. The sandstones above the upper coal zone have been designated the Vreda Formation (McDaid, 1985). Grill (1997) has incorporated the entire sandstone succession above the Mukorob Shales as well as the two coal zones into the Auob Member. Own investigation have now shown that there are strong indications that the two coal zones and the interbedded sandstone succession are probably lateral equivalents (proximal basin margin facies) of the black shale-bearing Whitehill Formation (distal basin centre facies). The same is also suggested for the Rietmond Shales (intermediate proximal-distal facies), overlying the Auob Sandstone (*sensu stricto*) in the northern part of the Mariental-Keetmanshoop outcrop area, and probably representing a lateral equivalent of the lower part of the Whitehill Formation (Werner et al., 2002). Therefore, in the following paragraph only the lower part of the subsurface Auob Member will be briefly described, whereas the coal-bearing zone and the Rietmond Shales will be treated in the following chapter as a correlative part of the Whitehill Formation.

Kingsley (1985) described the sandy part below the Impala Coal Seam as a progradational succession from prodelta to distributary mouth deposits. On these follow coarse-grained, arkosic cross-bedded sandstones representing fluvial or delta plain distributary channel fills in the northern part of the Aranos area, whereas in the southern part beach sands predominate. This facies change occurs in an area between the Nossob and the Auob River. A WNW-ESE-trending sand facies cut-off towards the south can be drawn west of Koës, which connects westward with the Auob Sandstone pinch-out between the Mukorob and Tses (Fig. 2.10).
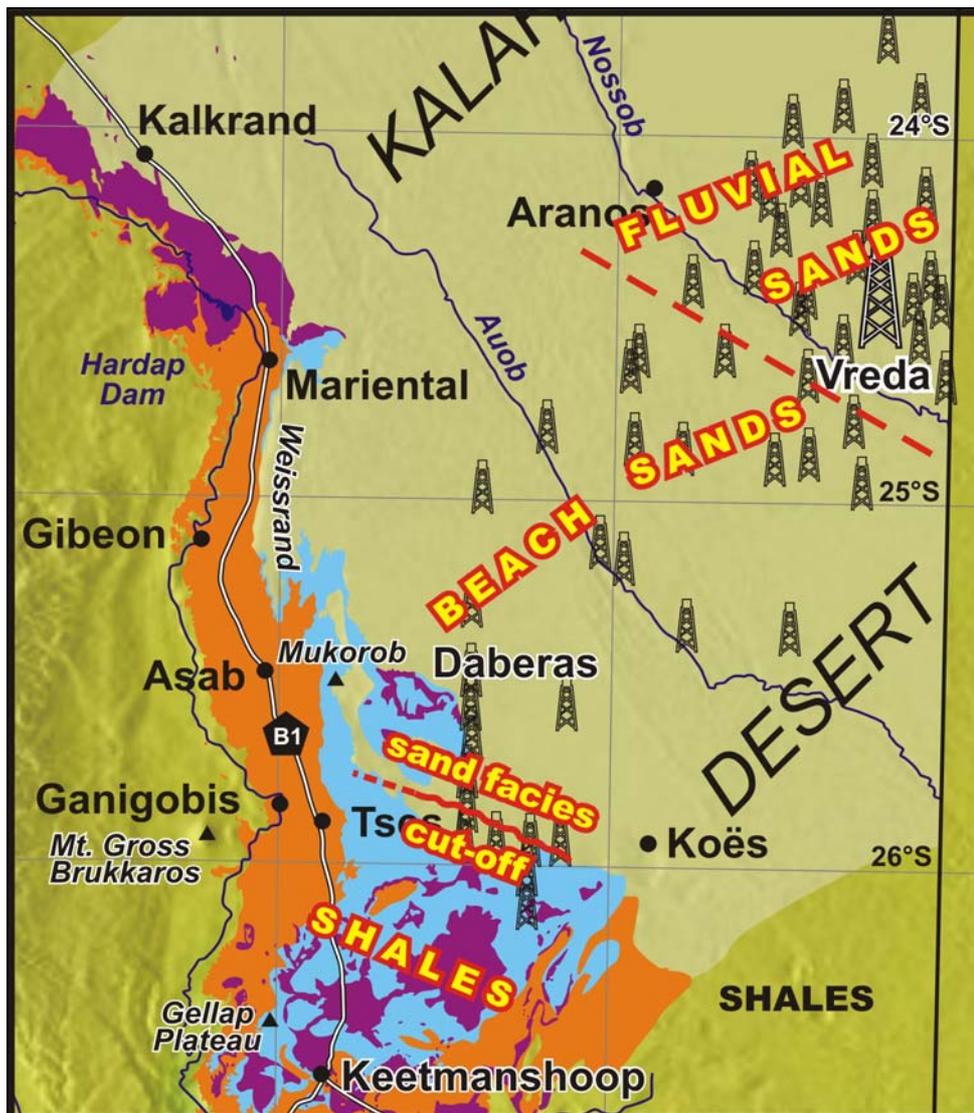
Fig. 2.10: Part of the map of Fig. 2.1, which shows the regional distribution of various facies developments of the upper part of the Auob Sandstone (i.e. the upper part of the sandstone succession directly underneath the Impala Coal Seam and correlative black shales) after Kingsley (1985). Note that the fluvial sand facies also contains delta plain distributary channels and that the beach sand facies probably also contains upper shoreface sand deposits. The petering out of the Auob Sandstone in outcrops between the Mukorob and Tses can be connected with the sand facies cut-off line in the eastsoutheasterly adjacent subsurface area.

2.3.1.4 Deposits tentatively assigned to the Prince Albert Formation and other correlatives

At the northern margin of the Kalahari-Karoo Basin, southeast of Gobabis (Fig. 2.1) on the southern side of the Ghanzi Ridge, Hegenberger & Seeger (1980) described occurrences of yellowish to brownish shales, siltstones and sandstones, passing downward into dark-grey to black carbonaceous shales below Kalahari cover and tentatively correlated them with the Prince Albert Formation. The succession attains a thickness of at least 200 m. Furthermore, the former presence of Ecca deposits on the Windhoek Highland-Ghanzi Ridge area (Fig. 1.6) is indicated by several isolated remnants of sandy to shaly sediments which are also attributed to the Prince Albert Formation, occuring on the northwestern slope of the Ghanzi Ridge (Hegenberger, 1985). Also on the northern side of the Ghanzi Ridge Ecca-equivalent mudrocks are known from Botswana south of Lake Ngami (Smith, 1984). Based on the knowledge of these occurrences it can be speculated that during deposition of the lower Ecca Group the Windhoek Highlands-Ghanzi Ridge area was maybe at least partly submerged and covered by sediments during lower Ecca deposition. The depositional environments are not known very well (marine/lacustrine/floodplain?) but there is a possibility that the Kalahari-Karoo Basin was connected with the Waterberg Basin in central northern Namibia, where also deposits of supposed lower Ecca age are know in form of the Tevrede Formation. This formation contains carbonaceous and coaly shales locally associated with glauconite (Gunthorphe, 1987). This association of coal-bearing sequences and local glauconite occurrences within the lower part of the Ecca Group is also known from the Ncojane area in western Botswana (Smith, 1984), from the Witbank, Highveld, Orange Free State and KwaZulu-Natal coal fields in the eastern part of the South African Main Karoo Basin (Barton et al., 2004) as well as from coal fields in the Paraná Basin in Brazil (Ketzer et al., 2003). These approximately age-equivalent (lower Ecca Group) glauconite occurrences may indicate that the mentioned areas were at least temporarely connected and flooded by the Ecca or Mesosaurus Inland Sea during the Lower Permian.

Apart from southern Namibia the Prince Albert Formation can also be found in the western part of the South African Main Karoo Basin. In the eastern parts of the latter basin the Pietermaritzburg Formation and the lower part of the Vryheid Formation are most probably age-equivalent to the Prince Albert Shales in the west (Johnson et al., 1997). In NW-Namibia the argillaceous and coal-bearing Verbrandeberg Formation as well as the arenaceous Tsarabis Formation correlates with the Prince Albert Formation in southern Namibia (Holzförster et al., 2000). In the Paraná Basin of Brazil the coal-bearing Rio Bonito Formation and the following Palermo Formation are also largely age-equivalent to the Prince Albert Formation (Stollhofen, 1999). Equivalent to the Prince Albert Formation are also the Hells

Kitchen Member of the Port Sussex Formation on the Falkland/Malvinas Islands (Trewin et al., 2002) as well as the lower parts of the Polarstar Formation in the Ellsworth Mountains (Antarctica).

2.3.1.5 Sequence-stratigraphic subdivision of the Prince Albert Formation

In the northern part of the Mariental-Keetmanshoop area the erosional bases of the channel sandstones in the upper portion of the Nossob and Auob Sandstones are interpreted as 3rd order sequence boundaries with erosional unconformities at their base (Fig. 2.11). Consequently, the channel fills can be considered as the subsequent low stand systems tracts. Southward the erosional unconformities grade into correlative conformities separating progradational 'prodelta/lower shoreface to deltafront/upper shoreface' highstand systems tracts from retrogradational 'proximal to distal turbidite/offshore' transgressive systems tracts. In the Gellap area the Nossob Sandstone is represented by a thin, fining-upward basin floor turbidite sandstone with an erosional base. This turbidite base is correlated with those of delta plain distributary channels in the north and hence can be considered as the expression of a sequence boundary in an offshore, deeper water environment. Further to the south, in the Noordoewer area, a sequence boundary characterized by a correlative conformity can be placed at the base of the Owl Gorge Member. This unit consists of three recognizable fining-upward parasequences, which form the basal part of a retrogradational transgressive systems tract. A shallowing trend in the preceeding highstand systems tract can be deduced from the intercalation of shale pebble beds (tempestites) in the uppermost portion of the Dwyka Shales (Fig. 2.11). Apart from the sequence boundaries associated with the Nossob and Auob Sandstones a third sequence boundary within the Prince Albert Formation is inferred from comparison with correlative deposits (Rio Bonito-Palermo Formations) in southern Brazil (Paraná Basin). The Nossob/Owl Gorge sequence boundary correlates with one placed at the base of the Rio Bonito Formation and the Auob sequence boundary with one placed at the top of the Palermo Formation (Holz et al., 2002). However, these authors could also demonstrate the presence of another sequence boundary between the other two. Due to the more distal position of the Prince Albert deposits in southern Namibia compared to the Rio Bonito-Palermo deposits in Brazil this additional sequence boundary has not yet been observed in the outcrop areas of the Prince Albert Formation in southern Namibia. However, a slight coarsening-upward shale succession within the middle part of the Mukorob Shales has been observed by Kingsley (1985) in some boreholes within the Aranos area probably indicating the position of this additional sequence boundary (Fig. 2.11). Furthermore, also Visser (1992b, 1993b) indicated a regressive event in the middle part of the Prince Albert Formation in the western part of the Great Karoo Basin of South Africa. A correlative conformity to the erosional unconformity in the upper part of the Auob Sandstone

has been found in the Aussenkjer-Noordoewer area. This sequence boundary can be placed between the progradational, coarsening-upward succession (Uhabis Member) at the top of the Prince Albert Formation and the retrogradational, fining-upward succession at the base of the overlying Whitehill Formation (Fig. 2.8-E). The position of a maximum flooding surface below the Auob Sandstone is most probably marked by the limestone marker band found in the Aranos subsurface area and the correlative ferruginous/phosphatic shale horizon cropping out below the Auob Sandstone south of the Mukorob (Fig. 2.8-A/B & Fig. 2.11).
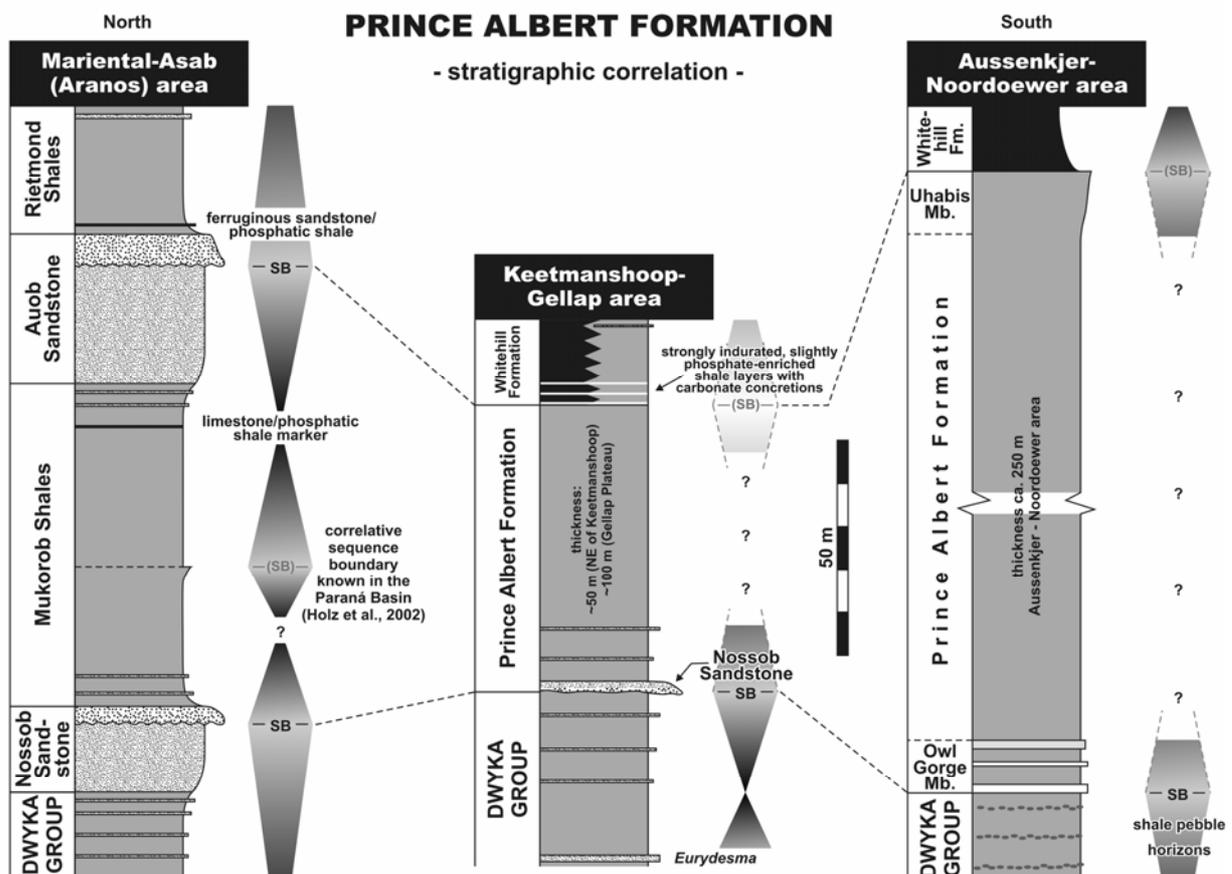
Fig. 2.11: Correlation and sequential (3rd order) framework of the Prince Albert Formation from more proximal localities in the north to more distal localities in the south. Sequence boundaries have been placed at the channel bottoms in the upper part of the Nossob and Auob Sandstones. These erosional unconformities grade basin-ward into correlative conformities. In the distal environments the position of sequence boundaries can be deduced from the change of a progradational to a retrogradational depositional trend.

2.3.2 Whitehill Formation and lateral correlatives (e.g. Rietmond Shale Member)

The Whitehill Formation, formerly known as the 'White Band' in the uppermost part of the former 'Upper Dwyka Shales', was originally defined in South Africa entirely on a lithological basis as a white-weathering, fine-grained, black carbonaceous shale unit, distinguished from adjacent units by its conspicuous white weathering colour in outcrop (Cole & Basson, 1991). The Whitehill Fomation is well known for its *Mesosaurus* findings, forming an important part of a fauna, which is endemic to the Paraná Basin and the western parts of the Kalahari-Karoo Basin and the South African Main Karoo Basin. In southern Namibia the facies of the Whitehill Formation in the Aussenkjer-Noordoewer Karoo outcrop area is very similar to that described above consisting almost entirely of white weathering, black carbonaceous shales. In the vicinity of Keetmanshoop and further north the onset of black shale deposition was in some areas distinctly retarded in time or even did not take place at all, which causes a change of the black shale facies to a greenish-grey silty shale facies. Since only successions of black carbonaceous shales were considered indicative of the Whitehill Formation, correlative and age-equivalent deposits in southern Namibia, which were primarily not carbonaceous or were pervasively bleached by secondary processes, were strictly excluded by most earlier researchers from the Whitehill Formation and placed stratigraphically into the underlying Prince Albert Formation, even if *Mesosaurus* remains were present (e.g. the Gellap Plateau area). The latter led to the unsatisfactory situation that lithostratigraphic boundaries (Prince Albert-Whitehill Formation) were crossed by biostratigraphic horizons (*Mesosaurus* zone). Furthermore, with this situation of facies changes in mind, the validity of interpretations drawn from Whitehill Formation isopach maps had to be brought into serious question, because they are based on comparison of sediment packets deposited during unequal periods of time. To resolve this problem a multi-stratigraphic approach was under-taken to trace time-equivalent, isochronous (more or less) upper and lower boundaries of the Whitehill Formation as well as chronostratigraphic marker horizons or zones within the formation from south to north in southern Namibia (Werner et al., 2002). This approach aimed at understanding the complex lateral facies changes, which have taken place during the time of deposition of the Whitehill Formation. By intensive fieldwork and logging of lower Ecca Group sections as well as the study of the subsurface borehole data it can be demonstrated that for the Whitehill Formation at least six different facies successions characteristic for individual regions can be distinguished in southern Namibia. They are named here the (1) Aussenkjer-Noordoewer, (2) Goris, (3) Panorama, (4) Gellap, (5) Mukorob-Daberas, and (6) Aranos Whitehill facies successions and will be described from south to north in the following paragraph. A correlation scheme of the individual successions is shown in Fig. 2.23.

2.3.2.1 Facies successions of the Whitehill Formation and equivalent deposits in southern Namibia

Aussenkjer-Noordoewer Whitehill facies succession

In this area in the southwest of the Noordoewer-Karasburg outcrop area the thickness of the Whitehill Formation was measured at several localities to be around 40-45 m, which is in accordance with data of Schreuder & Genis (1975) (45 m at Aussenkjer) but does not confirm the lower thickness of c. 20 m given by Oelofsen (1987). Within this area the Whitehill Formation is almost entirely composed of black shales and in outcrops it can be roughly divided into three subzones. The lower and upper part of the formation shows a light, white to bluish-grey weathering colour, whereas the middle part is formed by a dark, olive-green to brownish weathering horizon (Fig. 2.12-A). In this respect this facies of the Whitehill Formation is very similar to that of parts in adjacent South Africa (cf. Martin, 1981b). Between Aussenkjer and Noordoewer the coarsening-upward succession of greenish-grey silty shales of the uppermost Prince Albert Formation (Uhabis Member) is conformably overlain by white weathering, fissile silty shales forming the base of the Whitehill Formation. Bioturbation has been observed in some places. These shales grade into rhythmically banded shales (Fig. 2.12-B) with oscillating dark grey and light-weathering thin beds (0.5-1 cm), which commonly split into paper-thin laminae. These banded shales grade and fine upward into deep black, laminated and fissile claystones. These claystones in turn grade and coarsen upward into dark olive-green to brownish weathering black shales with a slightly silty and micaceous appearance forming the conspicuous dark weathering middle part of the Whitehill Formation. Burrows can be observed commonly in this part. This middle part is transitionally overlain by bluish-grey weathering, carbonaceous black claystones (Fig. 2.12-C). Despite their very fine lamination they commonly disintegrate to irregular-shaped to somewhat slabby or blocky pieces and only the uppermost 2-3 metres show a well-developed fissility. Small slump folds as well as flat clay pebbles have been observed in some places. At a few localities a somewhat harder, slightly cherty shale bed of 10-20 cm thickness has been observed in the uppermost 5 metres of the formation. *Mesosaurus* remains were found approximately in the upper 10 metres of the Whitehill Formation, whereas arthropods (*Notocaris* and maybe other species) are restricted to the uppermost 1-2 metres of fissile shales. Fish remains have been found from below the middle part up to the uppermost part of the formation. Some sporadic findings of plant fragments also originate from the upper part. The uppermost fissile shales are topped by a horizon with abundant burrows, which is taken as the top of the Whitehill Formation. This horizon is followed conformably by greenish to brownish weathering, black, cherty mudrocks of the Collingham Formation (Fig. 2.12-D). Visser (1992b, 1993a & b, 1994) incorporated these cherty shales into the Whitehill Formation but due to the occurrence of

bioturbation and thin volcanic ash laminae they are here considered as the basal part of the Collingham Formation. No phosphatic concretions have been observed within the Whitehill Formation but a geochemical profile across the Whitehill succession shows that the transgressive events at the base and in the middle part of the formation are associated with elevated phosphate contents in the shales (Fig. 2.13). This phosphate enrichment is probably a result of condensation associated with low sedimentation rates during transgression. In contrast, the increased phosphate content in the Collingham Fomation is most probably related to the substantial input of volanic ash.

A major dolerite sill, continuous throughout the whole Aussenkjer-Noordoewer area, showing an estimated thickness in the order of about 100 m and forming the rugged Tandjieskoppe Mountains, has intruded the uppermost part of the Whitehill Formation in the Lower Jurassic. Commonly the uppermost metres of the Whitehill Formation are therefore found above this sill. At several localities also minor dolerite sills intruded as thinner, decimetre to several metres thick sheets into lower stratigraphic levels of the Whitehill Formation (Fig. 2.12-A). The dolerite intrusions caused local deformation and folding of the Whitehill Shales (Fig. 2.12-E). Contact-metamorphic and hydrothermal imprint on the Whitehill Shales resulted in the growth of andalusite (chiastolite) porphyroblasts (Fig. 3.31) and intensive veining with porcelain-white alunite, an alkali aluminium sulfate (Fig. 2.12-F), which most probably causes also the whitish coating on the carbonaceous shales. Directly at the lower contact of the dolerite sill to the Whitehill Shales the latter show signs of anatexis resulting in a schlieren-like textured, migmatic rock due to separation of an aluminium-rich phase from a graphite-rich phase (Fig. 2.12-G). Melted portions of the shales intruded at numerous localities the solidified but still hot dolerite sill as felsic dykes (Fig. 2.12-H). In one case such a dyke re-intruded Whitehill Shales overlying the dolerite sill in form of a breccia-like, fragment-rich sill. These felsic dykes, originating from partial melting of Prince Albert and Whitehill Shales due to dolerite intrusions, were originally interpreted as rhyolite dykes by Schreuder & Genis (1975).
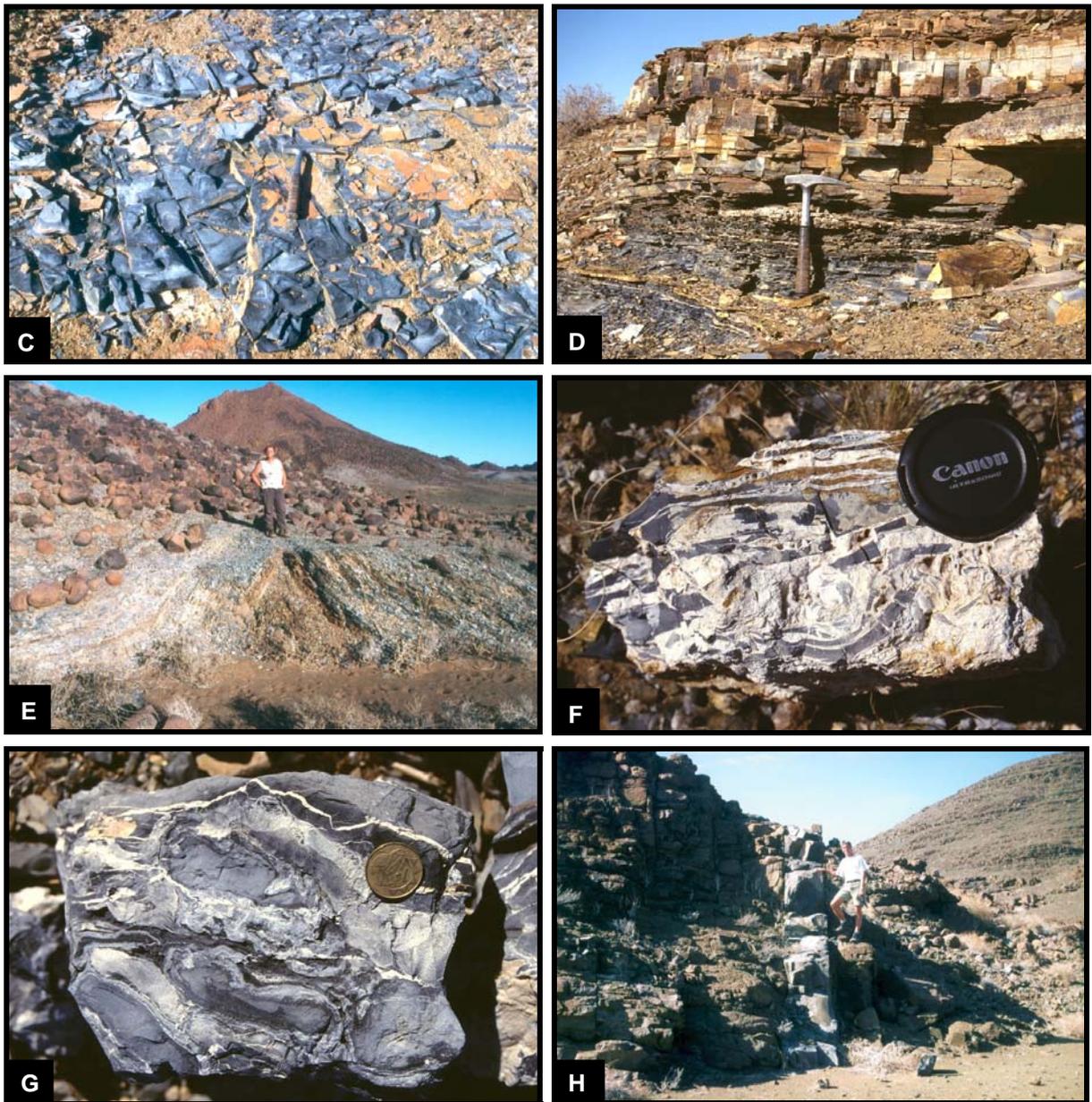
Fig. 2.12 (prev. and this page): Whitehill Formation in the Aussenkjer-Noordoewer area: **(A)** Outcrop showing the threefold subdivision of the Whitehill Formation in this area. White weathering black shales are separated by a dark greenish to brown weathering middle part. A dolerite sill represented by the brownish rocks intruded both the base and the top of the formation at the shown locality. **(B)** Rhythmically banded shales in the lower part of the formation. **(C)** Conspicuously bluish-grey weathering shales of the upper part of the formation. **(D)** This picture shows the boundary (hammer head) between the fissile black shales in the uppermost part of the Whitehill Formation and the overlying blocky weathering cherty shales at the base of the Collingham Formation. **(E)** Due to dolerite intrusions the Whitehill Shales are locally folded. **(F)** Dolerite intrusions and associated hydrothermal alteration caused brecciation and intensive veining of the black Whitehill Shales with porcelain-white alunite. **(G)** Directly at the lower contact surface to a dolerite sill the Whitehill Shales show signs of anatexis resulting in a migmatic rock that shows separation of an aluminium-rich phase from a graphite-rich phase. **(H)** Melted portions of the Whitehill Shales intruded the overlying, already solidified but still hot dolerite sill forming a felsic dyke.
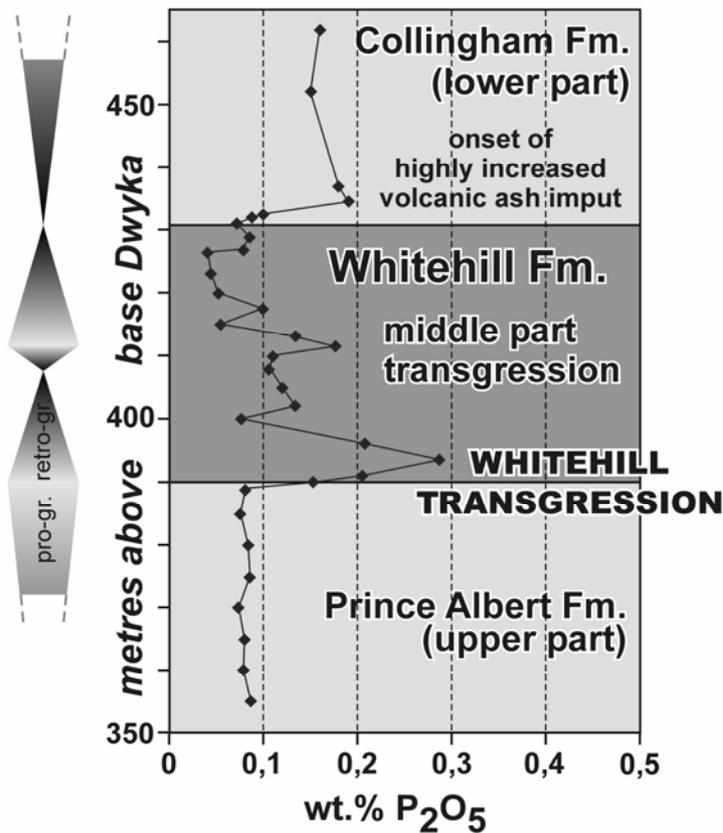
Fig. 2.13: Geochemical profile over the Whitehill Formation in the Aussenkjer - Noordoewer area including the upper part of the underlying Prince Albert Formation and the lower part of the overlying Collingham Formation. The transgressive events at the base and in the middle part of the Whitehill Formation are characterized by elevated phosphate contents in the shales. The higher phosphate contents in the Collingham Shales are attributed to the substantial admixture of volcanic ashes. The column at the left shows the depositional trends (retro- and progradational) within this stratigraphic interval.

Goris and Panorama Whitehill facies successions

Both the so-called Goris and Panorama Whitehill facies successions can be found in the northeastern vicinity of Keetmanshoop (for localities see Fig. 2.16 & 3.35). The Goris facies succession is named after farm Goris 148 east of the Quivertree Forest Restcamp and Giants Playground, whereas the Panorama facies succession is named after the Panorama Restcamp on farm Spitzkoppe Ost 159 north of the C17 regional road. In both facies successions a stratigraphic interval with dolomitic limestone layers in the upper half of the Whitehill Formation has been observed in all visited outcrops of this formation except those in the Aussenkjer-Noordoewer area. This limestone horizon represents the most important and mappable marker horizon within the Whitehill Formation in the southern part of the Mariental-Keetmanshoop outcrop area and is informally designated here the Goris Limestone Beds (Fig. 2.2).

The **Goris Whitehill facies succession** consists almost entirely of black carbonaceous shales, however, weathering and hydrothermal alteration decoloured the rocks to various degrees. Hence surface samples can show black, grey, beige, off-white, greenish, brownish and bluish hues. Outcrops of this facies succession can be subdivided into five main weathering colour zones (from base to top): (1) lower dark zone, (2) bright band, (3) middle

dark zone, (4) upper light zone, and (5) upper dark zone (Fig. 2.14-A/B, 2.23 & 3.42). The whole facies succession attains a total thickness of about 55-65 m. This contrasts markedly with earlier thickness reports for the Whitehill Formation from the Keetmanshoop area. Genis & Schalk (1984) as well as Oelofsen (1987) reported only about 20 m for the Whitehill Formation, whereas Barnard (1962) reported a thickness of 30-45 m for the area between Tses and Keetmanshoop. Obviously these authors only considered the upper half or third of the carbonaceous shale succession as a part of the Whitehill Formation due to their lighter weathering colours. In this study all carbonaceous shales above the greenish-grey shales of the Prince Albert Formation are assigned to the Whitehill Formation regardless of their weathering colour. However, it is admitted that the boundary to the underlying Prince Albert Formation is difficult to draw in the field. The lower dark zone of the Goris facies succession has generally a dark-grey to brownish weathering colour. Surface samples can be vari-coloured, dark fissile shales, which sometimes weather to a light colour. Digging, however, always yielded carbonaceous shales from this zone. Some parts appear silicified and break to flaggy or slabby fragments showing a well-developed lamination. Carbonate concretions are present in this lower zone. To delimit this lower dark zone of carbonaceous shales from the underlying dark olive-green to greenish-grey shales of the Prince Albert Formation close inspection of outcrops is necessary. However, the transition zone between these shale types is marked by several thin (~10-30 cm) but conspicuous, hard, brownish-ferruginous, and bioturbated shale horizons with intervening carbonate concretions (Fig. 2.14-C). Geo-chemical analyses of these shales revealed slightly increased phosphate contents (up to 0.6 wt.% P_2O_5) and are interpreted as condensed horizons at the base of a transgressive succession. Therefore, this zone of hard shale horizons is considerd as a usefull indicator for the Prince Albert-Whitehill Formation boundary in the Keetmanshoop area. Unlike in the Aussenkjer-Noordoewer area, no distinctive grain-size variations have been observed at this formation boundary in the vicinity of Keetmanshoop. The lower dark zone is followed by a white weathering horizon (bright band) of about 2-5 m thickness. This zone is composed of pervasively bleached shales, which show only grey, irregular distributed, cloudy relicts of carbonaceous matter. This bright band is in turn followed by the middle dark zone, which is composed of fissile black shales that have a slightly micaceous appearance. Brownish 'snuff-box' carbonate concretions are quite common (Fig. 2.14-D). The middle dark zone is overlain by the upper light zone composed of whitish weathering fissile shales. In many outcrops a more or less continuous, dark grey diagenetic carbonate horizon composed of coarse crystalline, columnar calcite can be found at the boundary (Fig. 2.14-E). In some places the basal part of the upper light zone has a distinct greenish weathering colour. In the middle to upper part of the upper light zone slightly coarser grained shales form a more or less well-developed cliff horizon (Fig. 2.14-F), in which the first *Mesosaurus* remains (bones) occur. At

the base of these cliffs or slightly below several layers of 5-20 cm thick, black dolomitic limestones of sedimentary origin occur throughout the whole studied area (Fig. 2.14-G & 3.43). They form a mappable horizon and have been named here informally the Goris Limestone Beds. These limestones also occur in the Panorama, Gellap, and Daberas Whitehill facies successions and they represent the only limestones of sedimentary origin within the whole Ecca Group in southern Namibia. Just below these limestones two thin tuff layers have been discovered on farm Eisenstein (Eisenstein Tuffs) (Fig. 3.44/45). The white weathering shales of the upper light zone grade upward into the upper dark zone (Fig. 2.14-H), in which finely laminated, deep black and strongly carbonaceous shales weather to a striking bluish-grey colour. Near the top of this zone at some places a circa 10 cm thick, somewhat harder and slightly cherty shale bed occurs (similar to the situation in the Aussenkjer-Noordoewer facies succession). Fish remains are frequently found within this upper dark zone and again arthropods (e.g. *Notocaris*) mark the uppermost 2-3 metres of the Whitehill Formation. Directly at the top small burrows have been observed in cherty shales at several outcrops. The top of the Whitehill Formation is in the whole Keetmanshoop area always overlain by a dolerite sill. At the contact the Whitehill Shales are transformed into a shiny, cherty hornfels, which is often coated by reddish-brown weathering products.
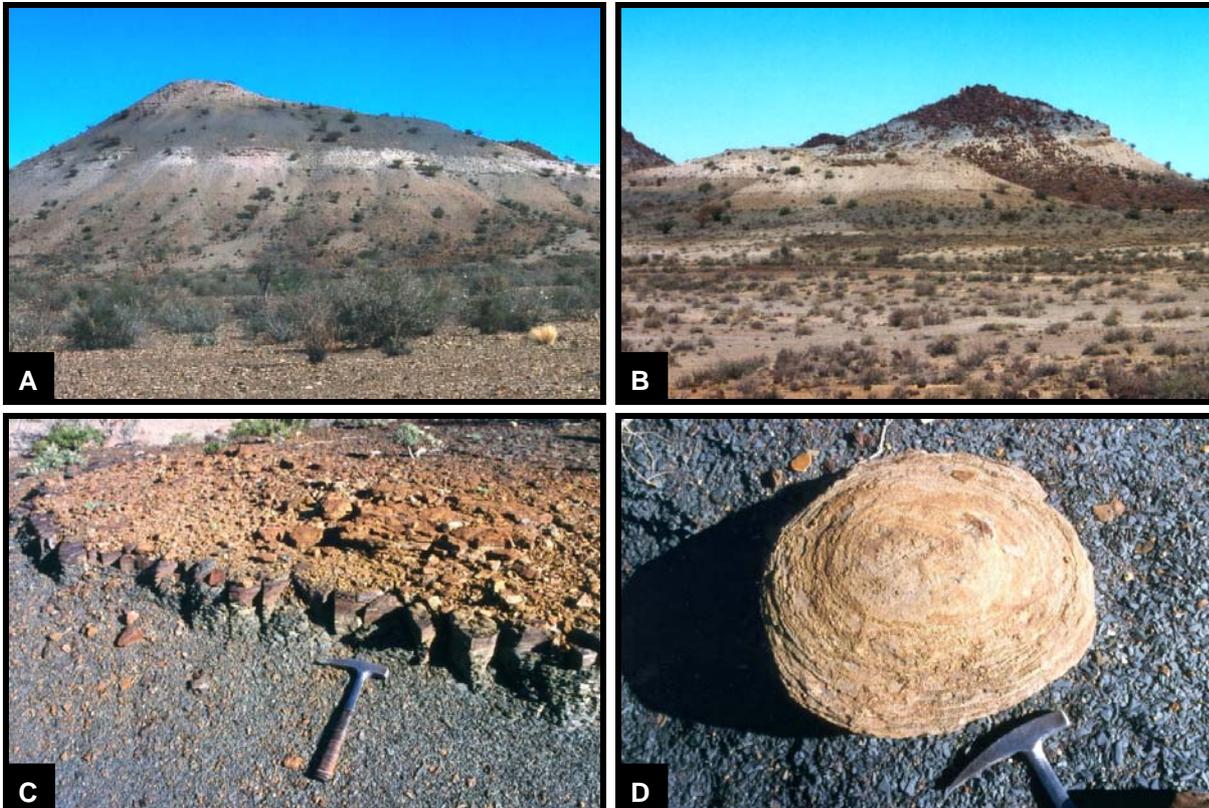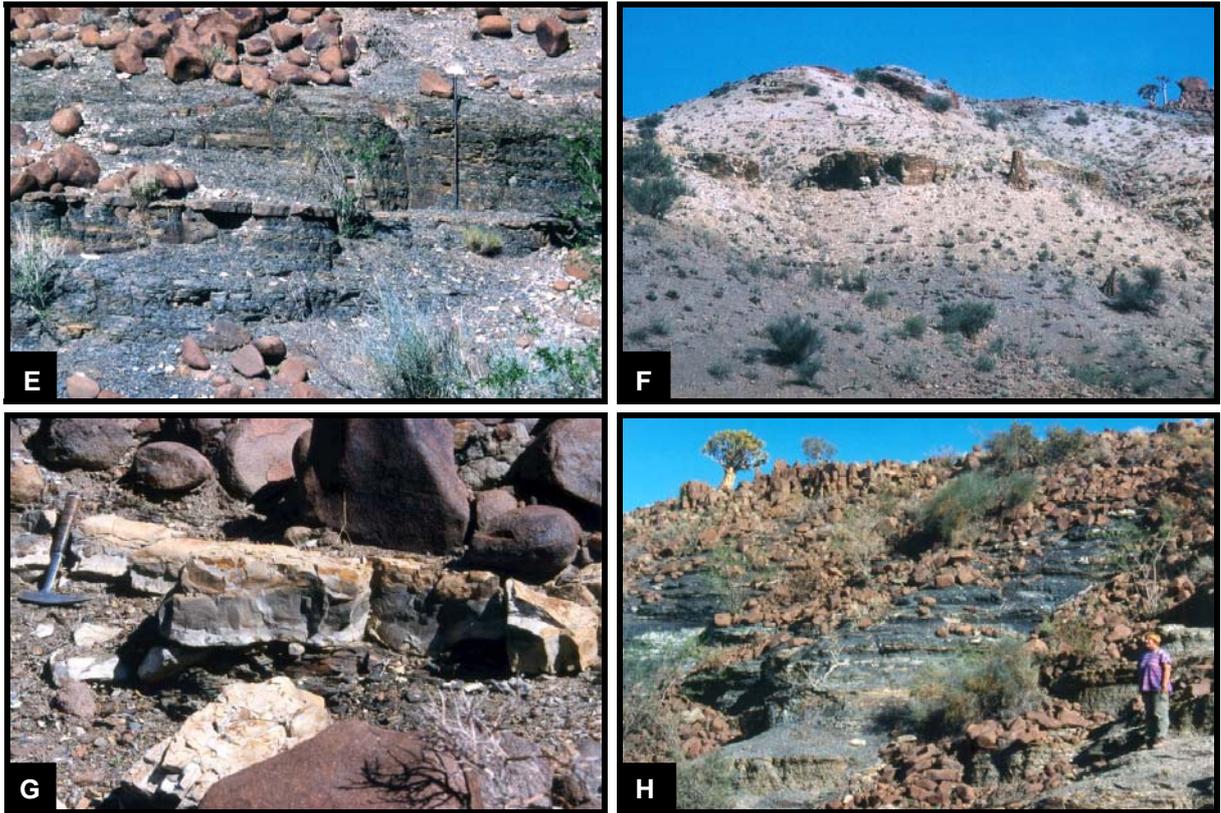
Fig. 2.14 (prev. and this page): Goris Whitehill facies successsion: **(A)** The lower half of the hill is build up by the lower dark zone of the Whitehill Formation, followed by the conspicuous bright band marker. The latter is overlain by the middle dark zone and on top of the hill parts of the upper light zone can be seen. **(B)** The bright band is outcropping in the plain in front of the hill. The foot of the hill is formed by the middle dark zone, on which the upper light zone follows. Between the latter two a greenish zone can be recognized at this outcrop. In the upper part of the upper light zone cliffs are developed, in which the first occurrences of *Mesosaurus* remains can be found. The upper dark zone is represented by striking bluish-grey weathering shales, which are overlain (intruded) by a brownish weathering dolerite sill. **(C)** Indurated, ferruginous shale bed topped by ochreous diagenetic carbonate. Such hard shale beds occur at the Prince Albert-Whitehill Formation boundary and are interpreted as condensed horizons at the base of a transgressive succession. **(D)** 'Snuff-box' carbonate concretions within shales of the middle dark zone. **(E)** Lateral continous diagenetic carbonate layer between the middle dark zone (below) and the greenish shale base (above) of the upper light zone. **(F)** Cliff-like exposures of slightly coarser grained regressive shales within the upper light zone, representing the stratigraphically lowest level in which *Mesosaurus* bones occur. **(G)** A dolomitic limestone layer exposed below the cliffs of the upper light zone. This zone of dolomitic limestones forms a mappable unit in the whole southern part of the Mariental-Keetmanshoop outcrop area and is here informally referred to as the Goris Limestone Beds. **(H)** Transition of the upper light zone into the upper dark zone. All shown outcrops are in the southwestern corner of the Goris farmground (Fig. 3.35).

The ***Panorama Whitehill facies succession*** can be subdivided into two major subunits according to their weathering colour in outcrops. The lower and thicker part consists mainly of bluish- to greenish-grey shales and mudrocks, which grade upward into more light brownish, buff weathering, slightly coarser grained siltstones. The top of this lower part is marked morphologically in outcrops by a small but conspicuous cliff (Fig. 2.15-A/B). This zone is conformably overlain by white weathering shales which grade upward into dark carbonaceous, bluish-grey weathering shales. From a lithological point of view only the upper part of the Panorama facies succession consists of the Whitehill-characteristic carbonaceous shales, however, the presence of a dolomitic limestone zone (Goris Limestone Beds) in the lower part of the succession indicates that the greenish-grey mudrocks below the white weathering shales in the Panorama facies succession are correlatives of carbonaceous shales in the Goris facies succession. A big problem is that the lower greenish-grey shales of the Panorama Whitehill facies succession are virtually indistinguishable from the underlying shales of the Prince Albert Formation. However, small creeks incised into the pediment in front of the hills north of the C17 gravel road on farm Spitzkoppe Ost expose here and there ferruginous and calcareous horizons, which are very similar to those found at the base of the Goris Whitehill facies succession (Fig. 2.15-C). With these ferruginous horizons considered as marking the Prince Albert-Whitehill Formation boundary the total preserved thickness of the Panorama Whitehill facies succession is in the order of about 50-60 m, however, with only the uppermost 5-10 m consisting of light-weathering carbonaceous shales. Interbedded within the bluish- to greenish-grey silty shales of the lower part of the Panorama facies succession are thin (1-5 cm), discontinuous layers of light coloured cherty rocks. Further-more, also greyish to ochreous calcareous concretions occur in places. Within some of the laminated cherty rocks crystal impressions are well preserved. These euhedral crystals grew probably within the muddy substrate in a very early diagenetic phase but were later leached out after solidification of the clayey host matrix. It is believed that these casts represent crystal impressions of evaporite minerals. Two types have been observed. One type of casts was caused by a mineral with an elongate crystal from and with a rhombic cross section. Most conspicuous is the stripening along the long axis of the crystal (Fig. 2.15-E/F). The origin of these crystals is unknown. The other type is represented by casts of thin tabular crystals, which show in plane view a slightly barrel-shaped form (Fig. 2.15-G/H) and which could have been platy gypsum crystals. Halite impressions and pseudomorphs were described from the basal part of the Whitehill Formation in South Africa by van der Westhuizen et al. (1981). In Brazil anhydrite deposits are known from the basal part of the Whitehill-equivalent Irati Formation (de Castro, 1994) and Hachiro (2000) reported of further evaporite deposits in the upper part of the Irati Formation. These evaporite occurrences indicate that at least the lower water layer within the Mesosaurus Inland Sea showed during

certain times and in certain areas an increased salinity. Furthermore, the chemistry of organic extracts of the Whitehill-equivalent Irati Formation shales also show characteristic features indicating a hypersaline depositional environment (Mello et al., 1993). However, large parts of the greenish-grey shales of the Panorama facies succession are quite intensively bioturbated causing often a more massive and crumbly rather than fissile appearance of the mudrocks. Less bioturbated shales show abundant simple burrows, which were in the past sometimes interpreted as algal remains (Fig. 2.15-D). These bioturbation features show that this part of the Panorama facies succession was sufficiently oxygenated to support a benthic infauna and strongly increased salinities were probably more local and temporary phenomena. The uppermost 10 m of the lower part of the Panorama facies succession have been studied in more detail due to the occurrence of a tuffaceous zone exposed at some localities below the cliffs. Between the top of the cliffs and the tuffaceous zone lies also the zone of dolomitic limestones (Goris Limestone Beds). The base of the tuffaceous zone is marked by a prominent and more or less lateral continuous carbonate concretion horizon (Fig. 2.15-I), which is most probably correlatable with the diagenetic carbonate horizon shown in Fig. 2.14-E at the boundary between the middle dark and upper light zone in the Goris facies succession. Above this concretion layer follows a circa 6 m thick interval, in which several thin bentonitic layers (Panorama Tuffs) are interbedded in greenish-grey, bioturbated, crumbly shales. Also the very conspicuous albitic Khabus-Panorama Tuff 1 is found here (Fig. 2.15-K, 3.39 & 3.40; see also Chapter 3.4.2.2). About two metres above the tuffaceous zone follows an up to 1.5 m thick zone, in which thin (1-15 cm) limestones layers are interbedded in platy weathering non-bioturbated shales of the cliff zone (Fig. 2.15-L & Fig. 3.39). The cliff zone itself is formed by a coarsening-upward succession of thinly bedded, platy to flaggy, laminated silty shales of distal turbidite origin (Fig. 2.15-M). They are in turn overlain by whitish weathering, fissile to papery shales, which grade into bluish-grey weathering, very fine-grained, laminated, black carbonaceous claystones. So far no *Mesosaurus* or arthropod fossil remains have been found in outcrops of the Panorama facies succession. Without the findings of arthropod remains (e.g. *Notocaris*) it is not clear if the uppermost part of the Whitehill Formation is preserved below the dolerite sill, which tops all Whitehill Formation outcrops of the Panorama facies succession. At least the bioturbated horizon at the very top of the Whitehill Formation in the Aussenkjer-Noordoewer and Goris facies successions seems to be missing.
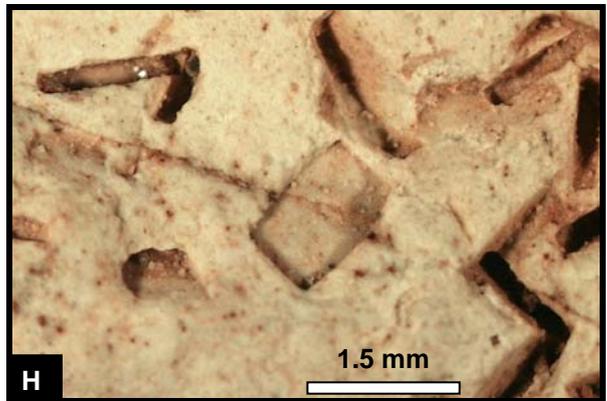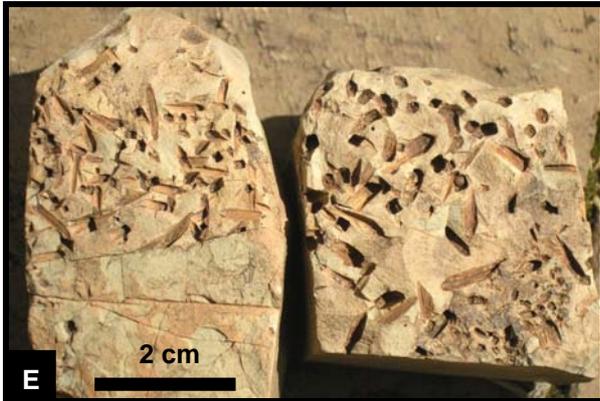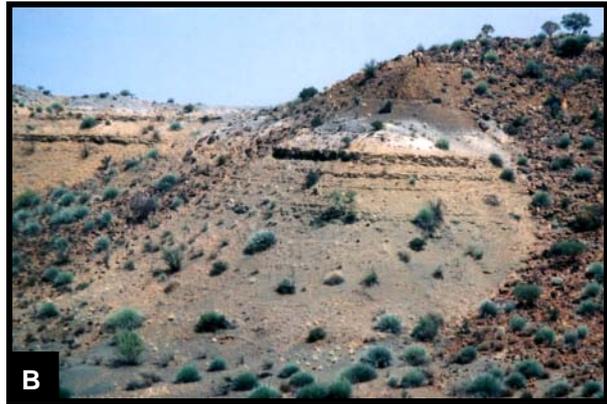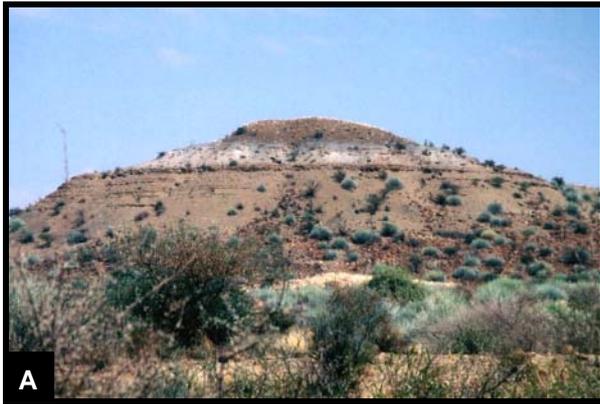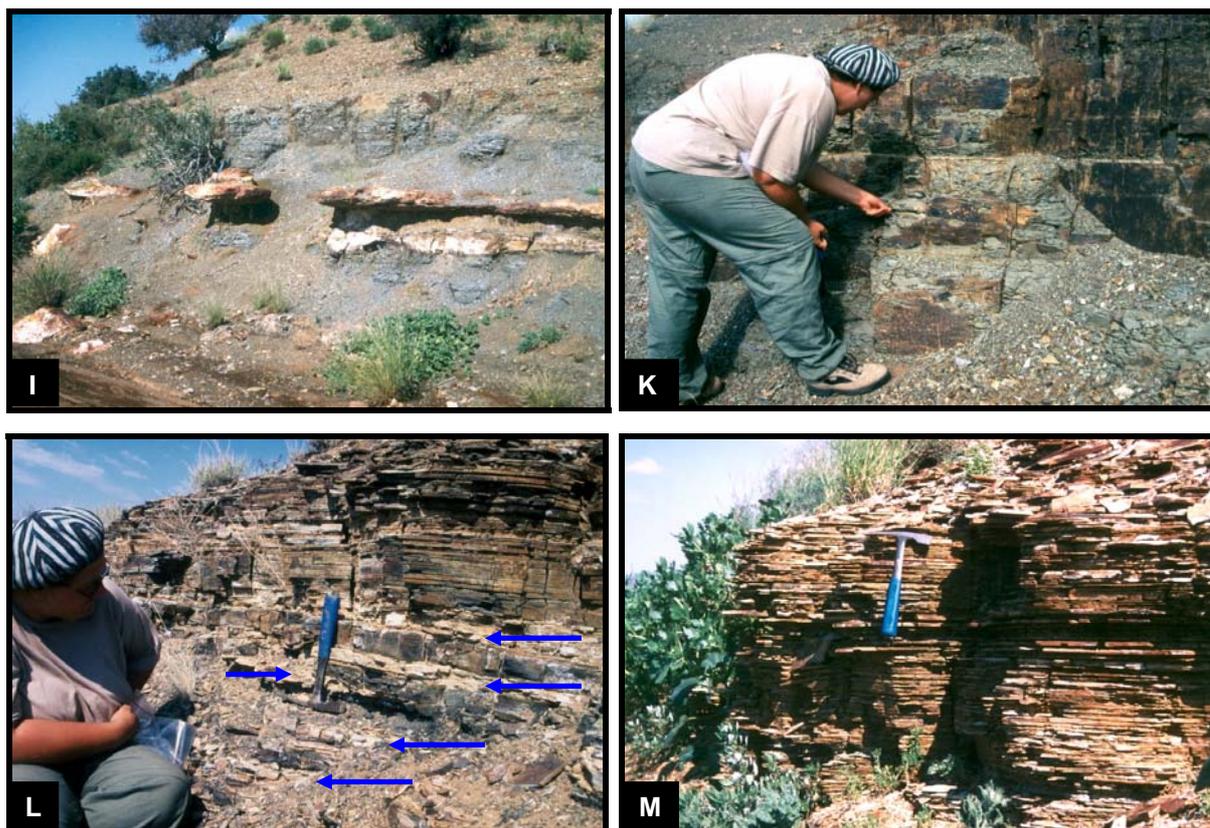
Fig. 2.15 (prev. and this page): Panorama Whitehill facies successsion: **(A) & (B)** Outcrops of the Panorama Whitehill facies succession on farm Spitzkoppe Ost north of the C17 gravel road. Only the uppermost part consists of white to bluish-grey weathering carbonaceous shales, whereas the lower part is mainly formed by bluish- to greenish-grey, bioturbated mudrocks. The boundary between these two zones is characterized by a circa 3-4 m thick coarsening-upward succession, which forms a small prominent cliff. **(C)** Ferruginous and calcareous shale layers may indicate, in accordance with the situation at the base of the Goris Whitehill facies succession, also the base of the Panorama Whitehill facies succession. **(D)** Bioturbation in shales of the lower part of the Panorama facies succession. **(E) to (H)** Crystal impressions of supposed evaporite minerals in cherty rocks from the lower part of the Panorama facies succession. **(I)** Prominent carbonate concretion horizon at the base of the tuffaceous zone. **(K)** The so-called Panorama Tuff 1 forms the conspicuous light coloured layer within bluish-greenish-grey, bioturbated shales. **(L)** Several thin dolomitic limestone layers (arrows) (Goris Limestone Beds) are interbedded in silty shales at the base of the cliffs. **(M)** Thinly bedded, platy to flaggy, laminated silty shales of distal turbidite origin forming the top of the coarsening-upward succession. They are conformably overlain by whitish to bluish-grey weathering carbonaceous shales.

It has been realized that the Goris and Panorama Whitehill facies successions are mutually associated in the region northeast of Keetmanshoop but the full areal extent and the boundaries between these two facies successions have not been mapped yet. However, in certain spectral channel combinations of satellite data the two Whitehill facies successions can be distinguished on the basis of their spectral properties and a reasonable prediction of the distribution of the two facies successions can be done. For example, in the Google-Earth satellite image of the Keetmanshoop region outcrops of the Goris facies succession show steel-grey-bluish colours, whereas outcrops of the Panorama facies succession show more

greenish-blue-cyan colours (Fig. 2.16). From the lithofacies of the Goris and Panorama facies successions it became clear that the Goris facies succession has been deposited in a deeper water, lower energy environment with more or less continuous anoxic conditions at the sea bottom. Hence the Goris facies succession is almost entirely composed of black carbonaceous shales which at or near the present-day surface have been bleached to various degrees. Furthermore, this facies succession almost completely lacks bioturbation or other signs of benthic life activity confirming anoxic bottom conditions. In contrast, the Panorama facies succession was deposited in a shallower water, higher energy environment, which was sufficiently oxygenated to support a benthic fauna or infaunal organisms during a considerable time of Whitehill deposition. Only the upper and younger part is characterized by non-bioturbated, black carbonaceous shales indicative of anoxic conditions. The relation between these two Whitehill facies successions, mutually associated within one region, is still not fully understood. From the studies of outcrops and satellite images it appears that the lateral transition from one facies succession into the other seems to be relatively abrupt although no outcrop has been found so far where this can be seen and investigated in detail. However, at one locality it seems that close to the boundary to the Panorama facies the Goris facies contains redeposited material, which originated from the Panorama facies. The C17 gravel road separates on farm Spitzkoppe Ost outcrops of the Panorama facies succession north of the road from those of the Goris facies succession south of the road (Fig. 2.16). As illustrated in Fig. 2.15-L the dolomitic limestones in the Panorama facies succession north of the road are represented by relatively thin and light coloured layers, which are faintly laminated or appear massive. South of the road (near the soldiers graves) the dolomitic limestone layers are generally thicker and contain a large number of predominantly light coloured, laminated intraformational limestone clasts, which show soft-sediment deformation features and float in a microsparitic, dark grey to black carbonaceous limestone (Fig. 2.17-A/B). These intraformational limestone soft clasts within the Goris facies probably originated as slumps sourced from the Panorama facies. From these observations a palaeogeographical picture evolves, in which the area northeast of Keetmanshoop seems to have been segmented during deposition of the Whitehill Formation into local 'highs' and 'lows'. It is believed that this palaeotopographic segmentation of the sea bottom was caused by syn-sedimentary tectonic activity and that the boundaries between the Goris and Panorama facies successions actually are represented by faults or fault zones, which were active during deposition of the Whitehill Formation (Fig. 2.18). Syndepositional tectonics have been evidenced for the Mariental-Keetmanshoop area during deposition of the lower Dwyka Group, respectively the Ganigobis Shales, by Stollhofen et al. (2000a) and for younger rocks of the Karoo Supergroup in other regions of SW-Gondwana by Stollhofen (1999), Holzförster et al. (2000), Stollhofen et al. (2000b), Wanke et al. (2000), and Werner & Stollhofen (2004).
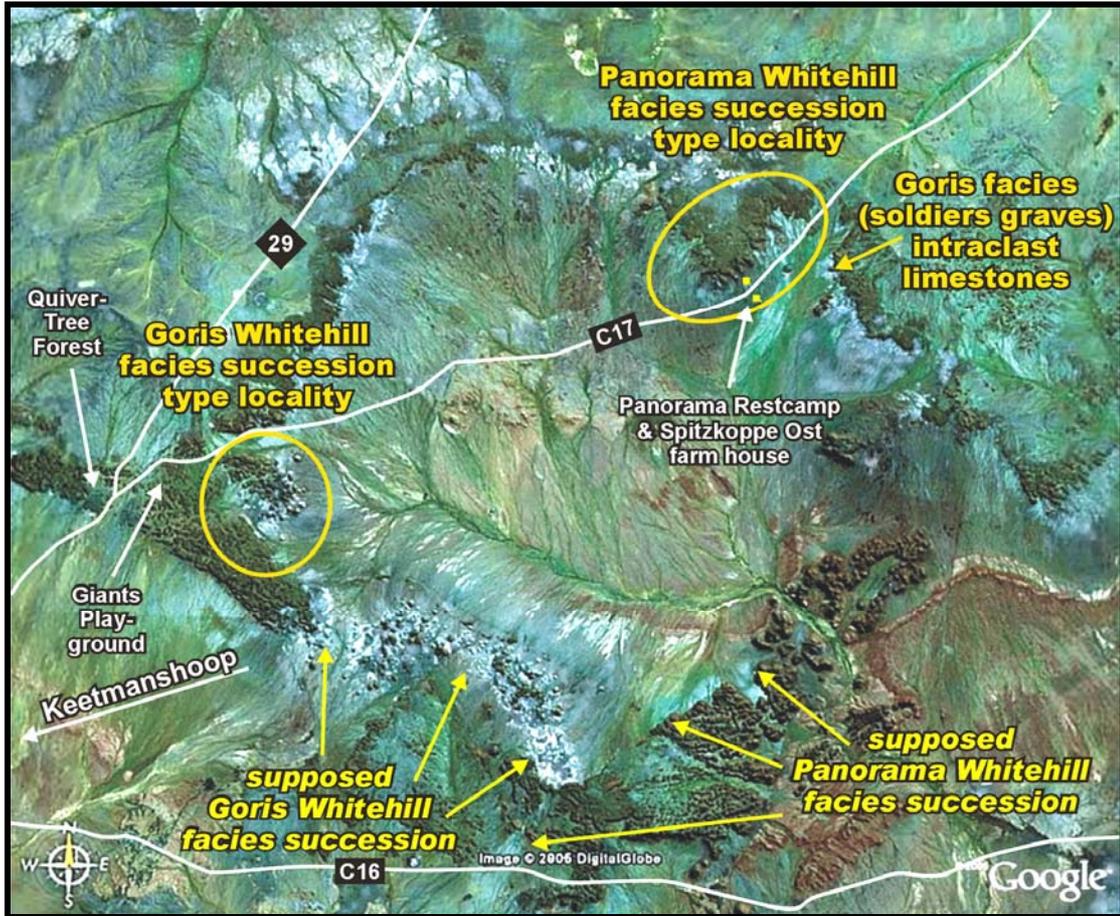
Fig. 2.16: Google-Earth satellite image of the region northeast of Keetmanshoop showing the type localities of the Goris and Panorama Whitehill facies successions. The distribution of the two facies successions can be predicted from the differential spectral response of the outcropping rocks of the two Whitehill facies succession resulting in a different colour. In this satellite image (data processiong by Google-Earth) the Goris facies succession shows steel-grey-bluish colours, whereas more greenish-blue-cyan colours characterize the Panorama facies succession. It is suggested that synsedimentary active faults or fault zones separated the two facies successions.
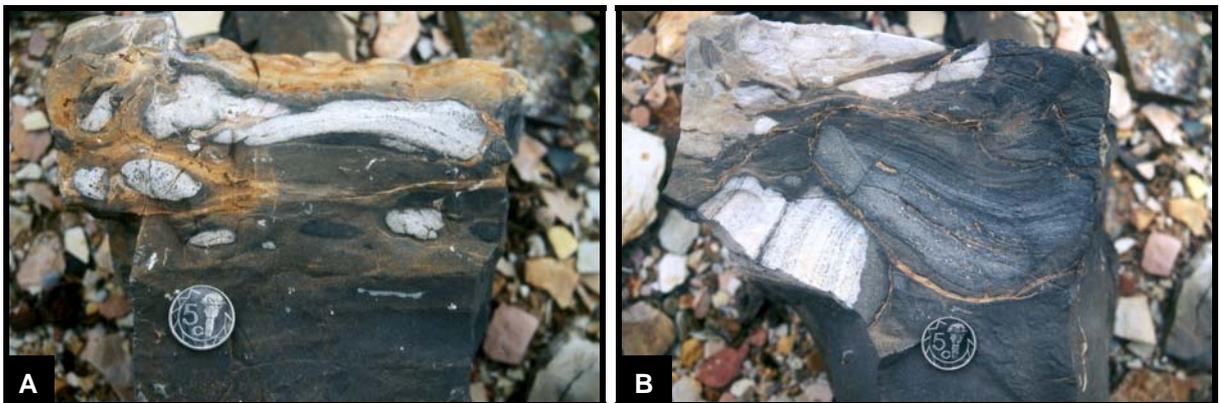
2.17: (A) & (B) Light coloured, laminated limestone intraclasts floating within a massive, dark grey, carbonaceous limestone. The outcrop lies within the Goris facies succession at the soldiers grave locality but it is believed that the intraclasts are derived (as slumps) from the nearby Panorama facies succession (see Fig. 2.16).
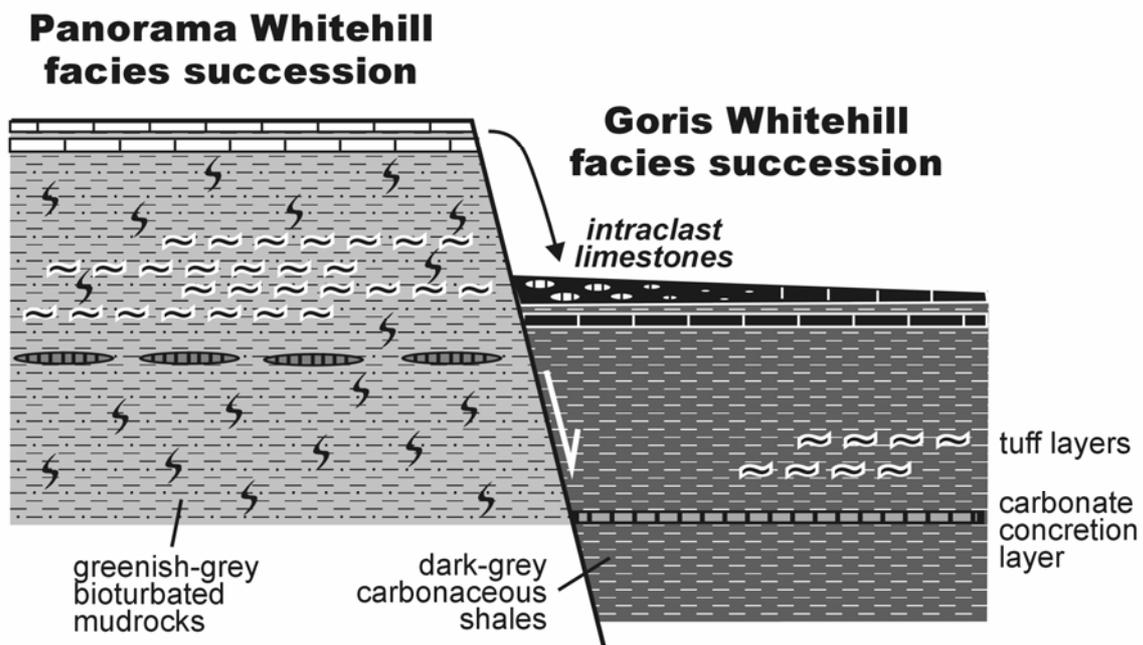
Fig. 2.18: Depositional model for the Panorama-Goris Whitehill facies succession relationship deduced from observations on farm Spitzkoppe Ost and other nearby outcrops. Due to syn-sedimentary tectonic activity the area was probably topographically segmented into 'highs' (Panorama facies) and 'lows' (Goris facies). It is believed that the intraclasts within the limestones (Goris Limestone Beds) at the soldiers graves locality (Fig. 2.16 & 2.17-A/B) were derived from the Panorama facies via slumping from an inferred fault scarp.

The type locality of the *Gellap Whitehill facies succession* is the Gellap Plateau (or Gellap Hills) about 25 km eastnortheast of Keetmanshoop (Fig. 2.6). For this area Martin (1953) stated that the 'White Band', meaning a succession of white weathering black carbonaceous shales, is not developed in the Gellap Mountains. Therefore, the geology of the Gellap Plateau area was later shown in the Geological Map of Bethanien (Schulze-Hulbe, 1979) and in the Geological Map of Namibia (Miller & Schalk, 1980) as a part of the Prince Albert Formation despite the presence of *Mesosaurus* remains. In a later publication Martin (1981a) reported a 195 m thick succession of greenish-grey siltstones, shales and claystones, which he then assigned to the Prince Albert and Whitehill Formations. From the uppermost part of the succession he also reported casts of *Mesosaurus* skeletons. Own measurements con-firmed the c. 200 m thickness for the shaly succession between the top of the Nossob Sand-stone, cropping out on the western margin of the Gellap Plateau, and the highest preserved stratigraphic level on top of the Gellap Plateau. Approximately in the middle of the shale succession a zone with brown, indurated, chert-like, bioturbated shale horizons with large intercalated carbonate concretions has been detected. These hard shale layers with a thick-ness of 30-40 cm are intercalated in dark bluish-greenish-grey fissile shales (Fig. 2.19-A) and

form on the eastern side of the Gellap Plateau in its foot region a number of conspicuous small plateaus or mesa-like outcrops due to their erosional resistance (Fig. 2.19-B). A sample of these hard shale layers revealed elevated phosphate contents and again these layers are interpreted as condensed horizons at the base of a transgressive succession, marking the base of the Whitehill Formation. Consequently, the thicknesses of the Prince Albert and Whitehill Formations are both in the order of about 100 m, with the Whitehill Formation up to c. 110 m and the Prince Albert Formation probably between 80 and 100 m. This is about twice as much compared to the outcrops directly northeast of Keetmanshoop (Goris-Panorama area), where the Prince Albert Formation is circa 40-50 m and the Whitehill Formation circa 55-65 m thick. Probably synsedimentary tectonics may have been responsible for the thickness and facies contrasts in two neighbouring regions. In the Gellap area the lower two third of the Whitehill Formation are mainly composed of bluish-greenish-grey, fissile to somewhat platy, silty shales. Intercalated in the lower third are thin (~5 cm), light-weathering, cherty layers (Fig. 2.19-C), which are in places associated with dark grey carbonate concretions and ferruginous crusts. Circa 15 m above the base of the Whitehill Formation a 10 cm thick turbiditic sandstone layer occurs, which consists of a coarse sand base fining-upward into very fine sand and silt. On top of this sandstone layer plant debris can be found (Fig. 2.19-D). The flasery to lenticular-bedded sandstone shows mainly a buff weathering colour but in places it appears carbonaceous (Fig. 2.19-D). At about 70 m above the base of the Whitehill Formation occurs a colour change from bluish-greenish-grey shales to light brownish, buff weathering shales and in some places this colour boundary is also marked morphologically by a small (~1 m) edge (Fig. 2.19-E/F). At one locality, where the shales of this small edge form the top of a hill, numerous burrows have been observed (Fig. 2.19-G/H). These burrows are often somewhat concentrated in bands within which they form an irregular network, resembling that of *Megagrapton aequale* (Seilacher, 1977). Approximately 8 m above the colour change and the associated small edge follows a morphologically very pronounced cliff zone of 2-4 m thickness (Fig. 2.19-E/F/I). The cliffs are composed of somewhat coarser grained, slightly siltier shales forming the top of a coarsening-upward succession, which is equivalent to that in the middle to upper part of the other Whitehill facies successions. Circa 5 m below the base of the cliff the dolomitic limestone layers of the Goris Limestone Beds can also be found within this Whitehill facies succession (Fig. 2.19-F). Above the cliff zone follows a 20-30 m thick upward-fining shale succession, in which numerous *Mesosaurus* remains have been observed by the author. The uppermost part of this succession, which forms the top of the Gellap Plateau, is composed of white weathering, partly bleached, bluish-grey, finely laminated, carbonaceous shales (Fig. 2.19-K). These shales are very hard and splintery. It is not clear if a dolerite sill originally

covered the present-day top of the Gellap Plateau. However, the chert- or hornfels-like appearance of the uppermost shales seems to affirm this possibility.
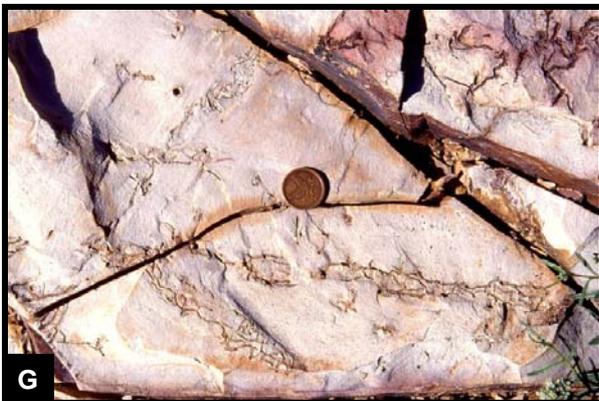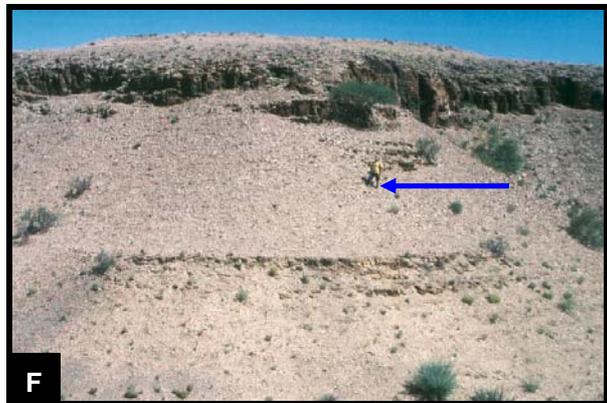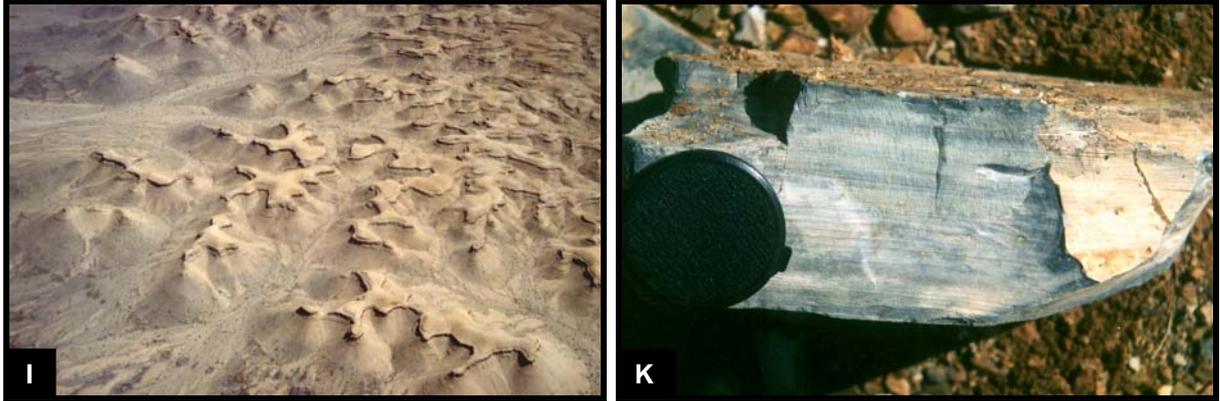
Fig. 2.19 (prev. and this page): Gellap Whitehill facies successsion: **(A)** Indurated, chert-like, bioturbated shale layer with large intercalated carbonate concretion, interpreted as condensed horizon and forming the base of the Whitehill Formation in the Gellap area. **(B)** These indurated shale layers form small mesa-like outcrops in the eastern foot region of the Gellap Plateau. **(C)** Thin light coloured chert layer intercalated in bluish-greenish-grey fissile shales. **(D)** Turbiditic sandstone layer circa 15 m above the base of the Whitehill Formation. The sandstone shows a flasery to lenticular bedding and on top of the layer plant fragments can be found. **(E)** Approximately 70 m above the base of the Whitehill Formation occurs a colour change from bluish-greenish-grey shales to light-brown, buff weathering shales. At this boundary often a small edge within the shale succession is developed (arrow). The top of a coarsening-upward shale succession is marked by a morphologically very pronounced cliff, which is in turn overlain by a fining-upward shale succession. **(F)** Between the colour change and the cliff zone outcrop also thin dolomitic limestone layers of the Goris Limestone Beds (arrow: author is standing on a limestone layer). **(G) & (H)** Burrows forming irregular networks are often arranged in band-like trails. Some of these networks resemble that of *Megagrapton aequale*. **(I)** The cliff-forming coarsening-upward shale succession in the upper part of the Whitehill Formation as seen from the air. **(K)** Bluish-grey weathering, finely laminated, carbonaceous shales from the top of the Gellap Plateau.

The ***Mukorob-Daberas Whitehill facies succession*** is represented by the outcropping silt-stone-sandstone succession overlying the Auob Sandstone at the Mukorob National Monument site in the west and the easterly following, stratigraphically higher outcrops along the gravel road 619/620 on farm Daberas Pforte, Dorn-Daberas, Gross Daberas, and Daberas Ost. Since there is no continuous outcrop the section shown in Fig. 2.23 is compiled from data of Grill (1997) for the Mukorob area and from own observations in the Daberas area. The lowermost part of the Mukorob-Daberas Whitehill facies succession is exposed in the Mukorob area above the Auob Sandstone and the upper part is exposed in several small outcrops in the Daberas area to the east. The lower part of the succession, conformably overlying the Auob Sandstone at the Mukorob locality, has been assigned by Grill (1997) to the Rietmond Shale Member.

In the northern part of the Mariental-Keetmanshoop Karoo outcrop area, where the type locality (farm Rietmond) of the Rietmond Shale Member is situated, the Rietmond Shales consist according to Heath (1972) of light grey to pinkish shales with a few sandstone

interbeds. H. Martin (in Brandt et al., 1961) already recognized that the fine-grained buff, brown and pink micaceous sandstones and arenaceous shales of the Rietmond Member in the north pass southward gradually into a facies of carbonaceous shales outcropping near Daberas and Keetmanshoop. Also Grote (1984) noticed that the Rietmond Shales grade southward, in the area between Asab and Tses, into bluish-grey to greenish, in places bioturated shales with interbeds of siltstones and fine-grained sandstones. Werner et al. (2002) have shown in a multistratigraphic correlation approach that the Rietmond Shales can be correlated with the lower part of the Whitehill Formation (Fig. 2.23). More recently, also R.McG. Miller confirmed in a personal communication to P. Kukla (2004) that the Rietmond Shales are a northerly equivalent of the Whitehill Formation cropping out further to the south.

The offshore silt- and mudstones of the Rietmond Shales, which conformably overly the Auob Sandstone (here considered as the top unit of the Prince Albert Formation) at the Mukorob locality, indicate a rapid deepening (sea level rise) of the depositional environment (Grill, 1997) after deposition of the deltaic sands and muds in the upper part of the Auob Sandstone Member. Within the lowermost stratigraphic interval above the Auob Sandstone Grill (1997) described a thin horizon consisting of bioturbated, ferruginous and calcareous sandstones interbedded with thin grey carbonate layers (Fig. 2.20). Grill (1997) wrote that this interval records condensation during rapid flooding associated with low sedimentation rates and may therefore be interpreted as a marine condensed horizon. A reevaluation of a sample from this specific horizon has now shown that the supposed carbonate layers are actually highly phosphatic shales with ~30 wt% P_2O_5, corresponding to ~70 wt% fluor-apatite in the sample. This phosphatic horizon near the base of the lower Whitehill-equivalent Rietmond Shales can be compared with the slightly phosphate-enriched, indurated and bioturbated shale layers at the base of the Whitehill Formation in the Goris, Panorama and Gellap area as well as with the phosphate enrichment in the carbonaceous shales at the base of the Whitehill Formation in the Aussenkjer-Noordoewer area (Fig. 2.13). All these phosphate-enriched layers demarcate the onset of a pronounced transgression during depo-sition of the early Whitehill Formation and equivalent sediments. The thickness of the Riet-mond Shales was repeatedly estimated to be in the order of about 80 m in the region east of Asab (Heath, 1972; Hegenberger, 1992; R.McG. Miller, pers. comm. to P. Kukla, 2004).

Within the transgressive shale succession a circa 3 m thick, fine-grained sandstone, positioned approximately 20 m above the Auob Sandstone, has been reported by Grill (1997). It is very tempting to correlate this sandstone with the thin turbidititc sandstone layer occuring approximately 15 m above the base of the Whitehill Formation in the Gellap area (Fig. 2.23). However, it must be noted that no turbiditic sandstone or siltstone layers have

been discovered in a comparable stratigraphic interval in the nearby Goris and Panorama Whitehill facies successions. Hence the turbidite sandstones in the basal part of the Mukorob-Daberas and Gellap succession could also be unrelated.

Fig. 2.20: Polished hand specimen of the phosphatic horizon discovered in and sampled from the lowermost part of the Rietmond Shales in the vicinity of the Mukorob National Monument site by Grill (1997). There, the Rietmond Shales conformably overlie the Auob Sandstone. Towards the south, the Rietmond Shales grade into carbonaceous shales of the Whitehill Formation.

The reddish-brown layers represent ferruginous sandstones, which are in places intensively bioturbated (top right: *Siphonichnus*?). The fine-grained greyish layers were originally described as carbonates (Grill, 1997), however, new geochemical analyses performed within this study have shown that these layers contain phosphate contents of about 30 wt% P_2O_5 corresponding to about 70 wt% fluor-apatite. The volumetrically measured CO_2 content of 2.7-4.3 wt% in these phosphatic layers is probably related to carbonate incorporated within the apatite-francolite structure.

This phosphatic horizon was interpreted by Grill (1997) as a condensed interval in the basal part of the Rietmond Shales related to rapid sea level rise (transgression) after deposition of the Auob Sandstone.

From the Daberas area H. Martin (in Brandt et al., 1961) reported black, pyrite-rich, highly carbonaceous shales, which have been encountered in a number of boreholes. Furthermore, he reported of *Mesosaurus* findings in surface outcrops. Barnard (1962), studying the alunite economic potential of the Daberas area, mentioned black carbonaceous shales and a black limestone band. During a visit of the Daberas area a very small outcrop of a light bluish-grey weathering, black limestone interbedded in dark grey shales was discovered next to the gravel road 619/620 at S 25° 34.531' E 18° 22.414' (Fig. 2.21-A). There is no doubt that this outcrop exposes the Goris Limestones of the Whitehill Formation. Within this outcrop some parts of the limestone have a homogeneous and massive appearance, whereas others are

almost entirely composed of limestone pebbles (intraclasts) (Fig. 2.21-B) hinting at reworking. Within one sample of these limestones H. Stollhofen has discovered calcite pseudomorphs after gypsum. These pseudomorphs show a normal grain size distribution within the limestone with a maximum crystal size of about 600 μm in the basal part (Fig. 2.21-C). Some of the crystals have the shape of an arrow head, which is quite characteristic for Montmartre twins of gypsum (Fig. 2.21-D). Dolomite pseudomorphs after primary gypsum crystals in limestones and gypsum lenticles were also reported from the South African part of the Whitehill Formation by McLachlan & Anderson (1977) and Cole & McLachlan (1991). Further to the east at the N-S trending farm fence between Dorn Daberas and Gross Daberas exploration trenches and a small hill expose sediments of the Whitehill Formation above the limestone horizon. At the foot of the hill intensively bioturbated bluish-grey and ferruginous shales crop out. Within this stratigraphic interval also brownish permineralized wood fragments have been found. The bluish-grey, bioturbated shales grade and coarsen upward into creamy to buff weathering laminated siltstones forming a more resistant horizon (top of coarsening-upward succession). The overlying finer shales have a light grey weathering colour.
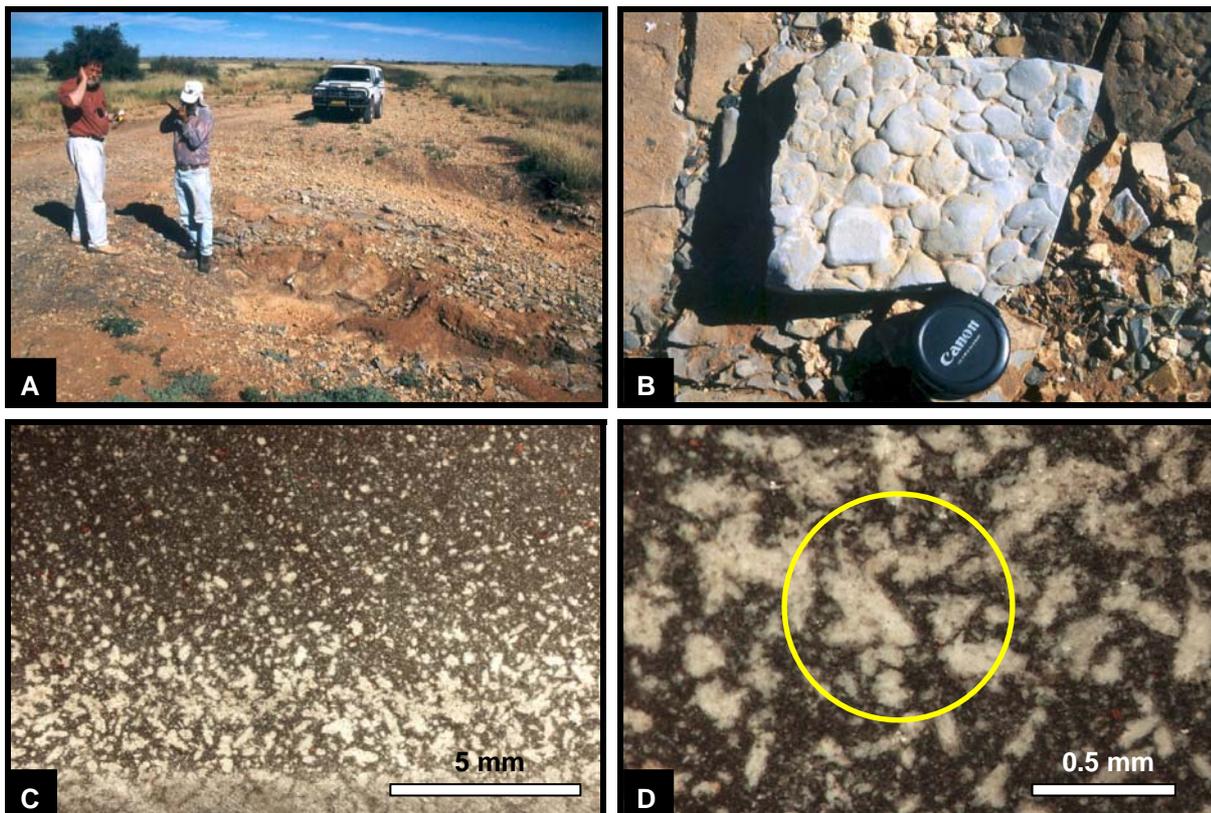
Fig. 2.21: Goris Limestone in outcrops at the Daberas area (Mukorob-Daberas Whitehill facies succession). **(A)** 'Pothole' outcrop of a limestone layer within dark grey shales next to the gravel road 619/620 (Mukorob to Leybank). **(B)** Part of the limestone consists almost entirely of limestone pebbles (intraclasts). **(C)** Polished hand specimen of the limestone with white calcite pseudomorphs after gypsum. **(D)** 'Arrow head'-shaped crystals (encircled) probably representing pseudomorphs after Montmartre twins of gypsum.

In the Aranos area the stratigraphic interval of the Prince Albert and Whitehill Formations have been penetrated by numerous coal exploration boreholes (Fig. 2.1). The correlative part of the outcropping Auob Sandstone is overlain in the Aranos subsurface area by a sedimentary succession consisting in upward direction of a basal lower coal zone, a lower arenaceous zone, an upper coal zone, and an upper arenaceous zone (Fig. 2.23). Kingsley (1985) named the lower coal zone the Impala Coal Seam. McDaid (1985) incorporated the lower coal zone and the subsequent lower arenaceous zone into the Auob Sandstone Member and correlated only the upper coal zone with the Whitehill Formation. According to McDaid (1985) the lower channel sandstones of the Auob Sandstone plus the lower coal zone and the following lower arenaceous zone have a cumulative thickness of 60-102 m, with the lower Auob channel sandstones alone attaining 10-30 m. The upper coal zone lies 40-70 m above the lower coal zone (Impala coal seam) and attains a thickness of up to 32 m.

The base of the upper arenaceous zone represents a major erosional unconformity cutting in places deeply into the upper coal zone or in some cases completely removing it. Consequently, McDaid (1985) separated this upper arenaceous zone from the underlying succession and designated it the Vreda Formation. The Vreda Formation consists mainly of fine- to coarse-grained micaceous to feldspathic fluvial sandstones intercalated with minor siltstones and black shales (McDaid, 1985). The age of the Vreda Formation is unknown, but as it was considered by Grill (1997) as a part of the Auob Sandstone it might be of Early Permian age.

Both coal zones, marking swamp periods, grade towards the southwest into carbonaceous shales recording the deposition of black, C_{org}-rich muds in a shallow sea (Kingsley, 1990). Therefore, as Fig. 2.23 illustrates, the entire succession from the base of the lower coal zone to the top of the upper coal zone is now correlated in this study with the Whitehill Formation (**Aranos Whitehill facies succession**) and consequently the lower part of this Whitehill-equivalent succession correlates with the Rietmond Shales elsewhere. R.McG. Miller (pers. comm. to P. Kukla, 2004) recently noticed that the Rietmond Shales are in some subsurface areas unconformably overlain by the so-called Neu Loore Formation, which consists of orange deltaic sandstones. However, no mention was made whether the Neu Loore Formation sandstones correlate with the Vreda Formation sandstones or not.

The economically interesting Impala Coal Seam of the lower coal zone is actually only developed in an area north of the Nossob River, whereas south of it this coal facies changes into a facies consisting of black and grey shales as well as sandstones (Kingsley, 1985; McDaid, 1985) (Fig. 2.22-A). The Impala Coal Seam was deposited mainly behind beach barriers on the lower delta plain in an area east of Aranos and northeast of the Nossob River. Towards the southwest of this river the delta plain environments change to shallow open marine and shelf environments (Kingsley, 1985). Due to the torbanitic nature of the lower coal zone in the Vreda borehole, drilled by Artnell Exploration Company in 1963, Engen Ldt. decided to drill a new borehole directly next to the old Vreda drilling site in 1989 in order to gain some fresh core material. The new drilling revealed that at the Vreda site the lower coal seam (2.86 m thick) could be differentiated into a lower oil shale zone (1.44 m) and an upper torbanite zone (1.42 m). The torbanite is characterized by relatively high tar yields and alginite contents, whereas the oil shale can be distinguished from carbonaceous shale by the relatively high tar yields and a high vitrinite content. The difference was attributed to a change in the depositional environment from a distal or marginal peat swamp to an open lacustrine environment. The high proportion of vitrinite and visible minerals in the oil shale zone indicate an influx of clastics and terrestrial organic material that is common in a distal or marginal swamp. The high alginite content in the torbanite zone and the reduced vitrinite content are indicative of a more open lacustrine environment favourable for algal organisms. The significant visible mineral and vitrinite contents, however, indicate that this environment was still being contaminated by the influx of clastic and terrestrial organic material (Winter, 1990). These results and interpretations of parts of the lower coal zone in the Aranos area are also in accordance with the here suggested correlation of this zone with the Whitehill Formation elsewhere. The results of studies on the organic matter in shales of the Whitehill Formation by Faure & Cole (1999) suggested a manifestation of an enormously expansive microbial bloom event during deposition of the Whitehill Formation and equivalent deposits.

In the early 1990's the Euro Namibian Investment Company (1992) made a proposal for the erection of a mine in the Miltonsrus area east of Aranos. There, an area of approximately 110 km^3 was identified, which is underlain by coal of the lower zone with a thickness of greater than or equal to 1.5 m (average ~2.2 m). However, the project never came to life.

The roof of the lower coal zone generally consists of fine- to medium-grained, very bio-turbated sandstones (McDaid, 1985). These were interpreted as shoreface sandstones (Fig. 2.23), deposited during a transgression, and several limestone beds and small fining-upward sandstone-siltstone units were interpreted as intertidal deposits (Kingsley, 1985). In upward direction follows an arenaceous succession, which shows very rapid and complex lateral facies changes. Fining-upward units of fine-grained micaceous sandstones, siltstones and shales were interpreted as crevasse splay deposits on a delta plain. Intercalated within these deposits occur (isolated?) distributary channel and mouth bar sandstones. Kingsley (1985) noticed an overall coarsening-upward and thickening-upward nature of this upper part of the lower arenaceous succession and interpreted it as a progradational succession. Locally evaporites precipitated in the lower part of this succession as shown by siderite, limestone and gypsum beds (Kingsley, 1985). Towards the southwest again a major facies change from channel and crevasse splay to prodelta and shelf deposits can be recognized approximately in the vicinity of the Auob River (Fig. 2.22-B).

Delta plain sedimentation was then again replaced by a second event of widespread swampy conditions recorded in the upper coal zone, which consists of coal-bearing carbonaceous shale bands interbedded with grey shales and sandstones. In the southern part of the coal exploration area in some boreholes the upper coal-bearing zone is represented by whitish weathered, laminated, black carbonaceous, and pyritic shales and in one borehole this zone is represented by a black, highly carbonaceous, well laminated limestone (Kingsley, 1985; McDaid, 1985).

Major scouring, followed by deposition of coarse-grained, plane- and cross-bedded arkosic channel sandstones (Vreda Formation), defines the beginning of widespread fluvial activity (Kingsley, 1985). Channel incision eroded in many places the entire upper coal unit or parts of it. The fluvial channels are filled with gritty, coarse- to fine-grained sandstones, arranged in fining-upward units. In some places typical overbank deposits overlie these sandstones as a result of channel abandonment (Kingsley, 1985).
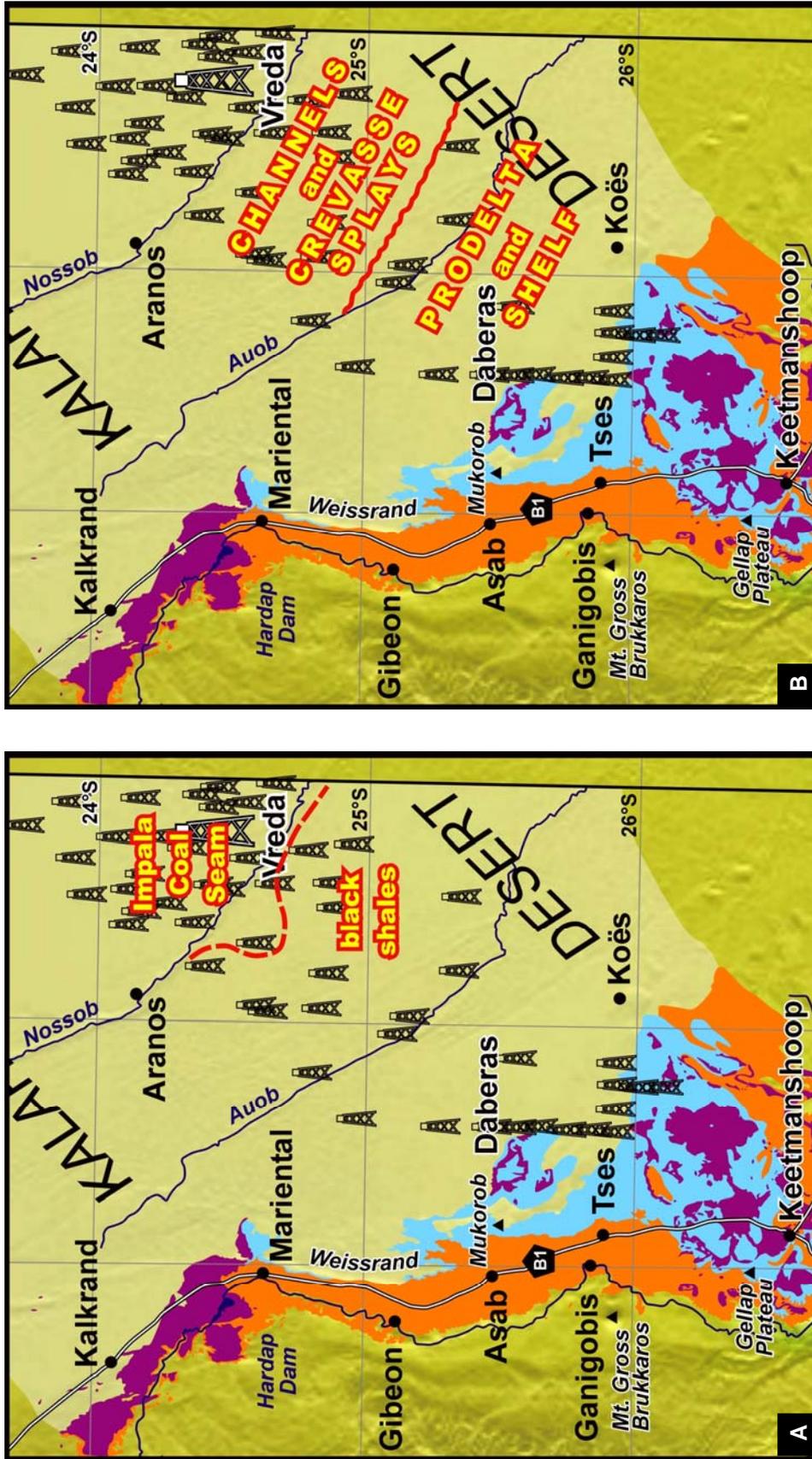
Fig. 2.22: (A) Part of the map of Fig. 2.1, which shows the regional distribution of the coal and black shale facies of the lower coal zone (Impala Coal Seam) in the Aranos Karoo subsurface area. **(B)** Same map showing the regional distribution of the two principal depositional environments for the lower arenaceous succession between the lower and the upper coal zone in the Aranos Karoo subsurface area. Facies boundaries after Kingsley (1985).

2.3.2.2 Correlatives of the Whitehill Formation outside southern Namibia

In the western part of the Main Karoo Basin of South Africa the Whitehill Formation is very similar to that of the Aussenkjer-Noordoewer area in southernmost Namibia. Towards the northeastern part of the Main Karoo Basin the Whitehill Formation loses its typical lithological character as the more distal and deeper water black shale facies grades laterally into a shallower water, less- or non-carbonaceous, siltier and sandier facies. In the Boshof-Hertzogville area, for example, Cole & McLachlan (1991) reported of hummocky-like ripple cross-lamination within the marginal facies of the Whitehill Formation. A NW-SE trending line between Kimberly and East London represents the eastern limit of the Whitehill Formation in the Main Karoo Basin of South Africa (Anderson & McLachlan, 1979). Further to the northeast the upper part of the coal-bearing Vryheid Formation is commonly correlated with the Whitehill Formation (e.g. Visser 1992b; Johnson et al., 1997). Kingsley (1985) suggested that the Impala Coal Seam, forming the basal part of the Whitehill-equivalent coal-bearing succession in the Aranos area in Namibia, might correlate with the No. 2 Coal Seam in the Transvaal and the upper coal zone of the Aranos area with the No. 4 Coal Seam. However, the correlation of the basinal black shale facies of the Whitehill Formation with the marginal coal-bearing facies of the Vryheid Formation is still a matter of debate. On the Falkland/Malvinas Islands, which were positioned during the Permian close to the south-eastern coast of South Africa, the Black Rock Member of the Port Sussex Formation can almost certainly be considered as an equivalent of the Whitehill Formation although palae-ontological evidence is still missing (Trewin et al., 2002). Time-equivalent deposits have probably also been laid down in the Antarctic region, however, direct correlatives of the Whitehill Formation have not been identified yet.

In northwestern Namibia the findings of disarticulated and transported *Mesosaurus* bones in the upper part of the Huab Formation proves its time-equivalence with the Whitehill Formation. The Huab Formation consists in the western part of the Huab area mainly of offshore pelites. Towards the east follows a stromatolite barrier belt with oolite-rich flat limestone pebble conglomerates deposited in channels between stromatolite bioherms. In the marginal eastern part pedogenetically modified, calcareous pelitic deposits prevail (Horsthemke et al., 1990; Horsthemke, 1992; Ledendecker, 1992; Holzförster et al., 2000; Wanke, 2000; Holzförster, 2002). The Huab area in northwestern Namibia can be considered as a small part of the eastern basin margin of the Paraná Basin and links the Late Palaeozoic deposits of southwestern Africa with those of eastern South America.

In the Paraná Basin of Brazil the Whitehill-equivalent and also *Mesosaurus*-bearing succession is called the Irati Formation, which is mainly composed of black carbonaceous

shales and limestones (de Castro, 1994; Milani & Zalan, 1999; Milani & Filho, 2000). In adjacent Uruguay the Mangrullo Formation and in Paraguay the uppermost part of Tubarão Formation correlates with the Irati Formation in Brazil (Oelofsen & Araújo, 1983). López-Gamundí et al. (1995) correlated the Tacuary Formation in Paraguay with the Whitehill and Irati Formations. Outside what is normally considered as the Paraná Basin, mesosaurid remains were also recovered from the pisolithic and oolithic limestones that outcrop in the upper Araguaia River area, on the border of Goiás and Mato Grosso in Brazil. These sediments were in turn correlated with similar sediments of the Pedra do Fogo Formation in the Parnaíba and Tocantins Basins of Piauí, Maranhão and Bahia (Oelofsen & Araújo, 1983). The Pedra do Fogo Formation is composed mainly of siltstones, shales and limestones, which have been deposited in lagoonal to fluvail environments, with locally some aeolian and marine influence (Schobbenhaus et al., 1984). Due to the occurrences of evaporites in the Whitehill, Irati and Pedra do Fogo Formations Oelofsen & Araújo (1983) proposed an extension of the Whitehill-Irati Inland Sea across the central Brazilian Shield up to northern Brazil. Furthermore, one could speculate if the Early Permian(?) carbonate and evaporite units of the Carauari Formation (Solimões Basin) and the Itaituba and Nova Olinda Formations (Amazonas Basin) (Milani & Filho, 2000) in northwestern Brazil could be related to the Pedra do Fogo, the Irati, and consequently also the Whitehill Formation, indicating a trans-SW Gondwanan connection. In this context it should also be investigated in the future if there might have existed a connection between the above mentioned carbonaceous-calcareous-evaporitic deposits and the Permian Copacabana/Vitiacuas limestones of the Tarija Basin in Bolivia (França et al., 1995).

In the Chaco-Paraná Basin, a southwestern extension of the Paraná Basin, the Chacabuco Formation, composed of locally bituminous siltstones and shales as well as lenticular beds of limestone (Milani & Filho, 2000), may also represent a correlative of the Irati, respectively the Whitehill Formation. Correlation of the Whitehill Formation with sediments of the northern Argentinian Sauce Grande Basin, which was connected in the Permian to the northwest with the Chaco-Paraná Basin and to the east with the South African Main Karoo Basin, appears still confusing. Although López-Gamundí & Rosello (1998) correlated the Whitehill Formation with the lower part of the Tunas Formation, their [2]nd order sequence stratigraphic interpretation of the Dwyka-Ecca Group and the Pillahuinco Group successions seems to favour rather a correlation of the Whitehill Formation with the Piedra Azul Formation.

2.3.2.3 A multi-stratigraphic correlation approach for the Whitehill Formation and its various facies successions in southern Namibia

The combination of various stratigraphic methods (litho-, bio-, tephro-, chemo-, and sequence stratigraphy) resulted in the recognition of several different Whitehill facies successions in southern Namibia and made their correlation with one another possible (Fig. 2.23). Altogether the Whitehill Formation comprises two transgressive phases and an intercalated regressive episode.

From outcrops in southernmost Namibia (Aussenkjer-Noordoewer area) it became evident that the boundary between the Prince Albert and the Whitehill Formation represents the turning point from a progradational to a retrogradational succession. In this area the uppermost part of the Prince Albert Formation is characterized by a coarsening-upward succession of shales (Uhabis Member), which is also well expressed in the steepening morphology. However, due to the distal basinal position of this area no erosional unconformity associated with subaerial exposure and incision has developed and the sequence boundary is characterized by a correlative conformity. A corresponding coarsening-upward trend as seen in the Uhabis Member can be found further north in southern Namibia in form of the change from offshore to lower and upper shoreface deposition recorded in the Mukorob Shales - Auob Sandstone transition. In places, where erosive fluvial or distributary delta plain channels form the top of the Auob Sandstone (predominantly in the northern part of the Mariental-Keetmanshoop outcrop area and the Aranos subcrop area) a sequence boundary can be drawn at the base of such incised channels. Consequently, the channel fills are considered here as a low stand systems tract (Fig. 2.23). In the vicinity of Keetmanshoop no obvious grain size trends have yet been observed at the Prince Albert-Whitehill Formation boundary. This could be explained by the central position of the Keetmanshoop area. The Aussenkjer-Noordoewer area south of it received detrital input during deposition of the Ecca Group mainly from a southern to southeastern source (Cargonian Highland), whereas the Mariental-Keetmanshoop area received detrital input mainly from the north to northeast (Windhoek Highlands – Ghanzi Ridge). However, it should be noted that these northerly and southerly highlands were most probably partly or even widely submerged during early Ecca times.
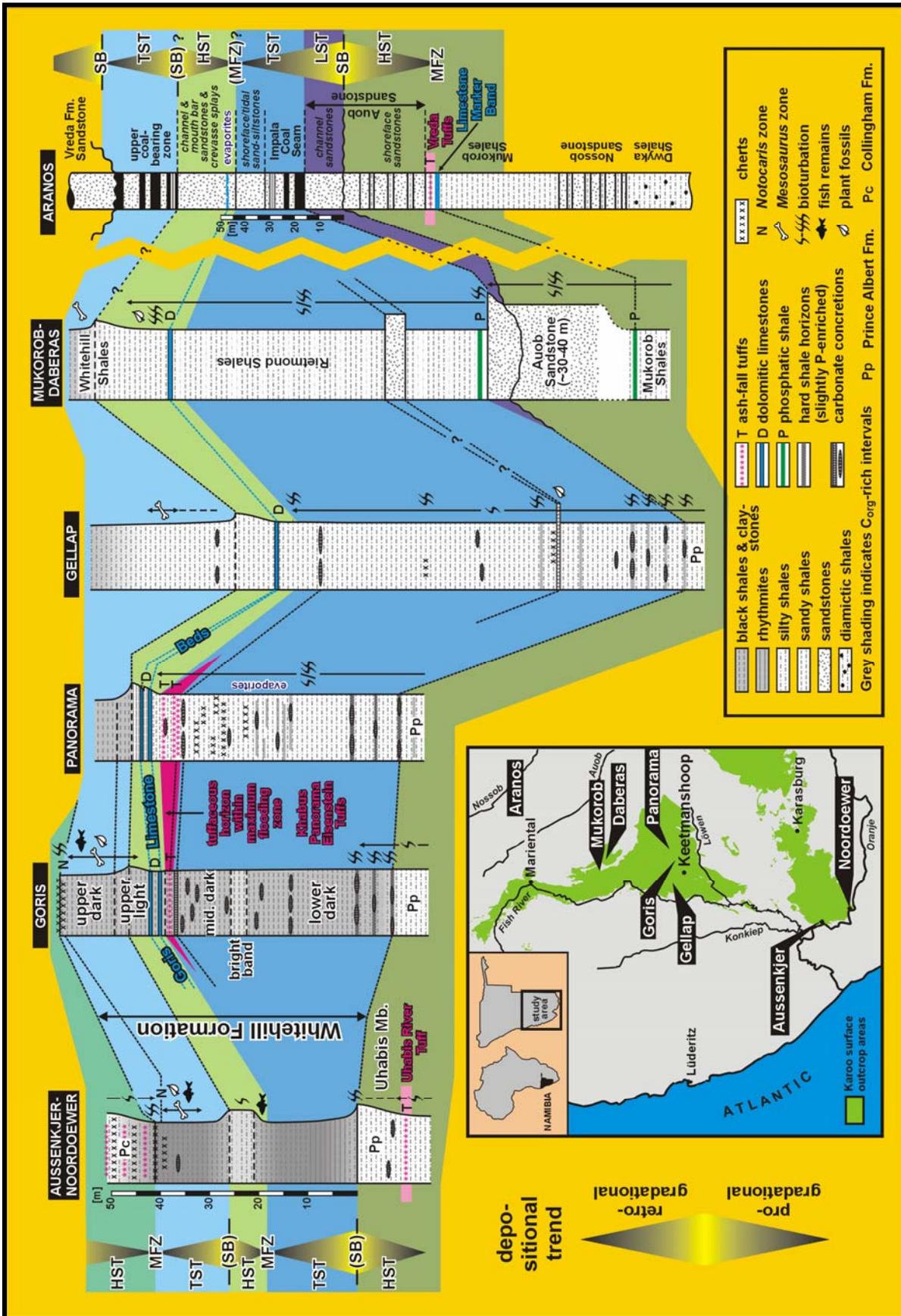
Fig. 2.23: Correlation scheme and sequence stratigraphic framework for the studied Whitehill facies sequences in southern Namibia (modified after Werner et al., 2002).

The base of the Whitehill Formation is characterized in the Aussenkjer-Noordoewer area by a retrogradational succession (transgressive systems tract) reflected by the transition of rhythmically bedded to finely laminated carbonaceous shales. Geochemical data revealed that the early part of this transgression is accompanied by elevated phosphate contents within these shales (Fig. 2.13). Further north in the Keetmanshoop area a conspicuous zone of hard, intensively bioturbated, slightly phosphate-enriched shale horizons with intervening ferruginous carbonate concretions probably reflects the same flooding event and, therefore, represents the basal part of the Whitehill Formation for the Goris, Panorama, and Gellap facies successions. Although the phosphate enrichment is only small (0.3-0.6 wt% P_2O_5) it is nevertheless significant. In the study area non-carbonaceous shales showed an average P_2O_5 content of less than 0.1 wt% and carbonaceous shales between 0.1 and 0.15 wt%. This basal zone of phosphate enrichment can be correlated with the zone of alternating ferruginous sandstone and highly phosphatic shale layers (Fig. 2.20) in the lowermost part of the Rietmond Shales in the vicinity of the Mukorob locality, showing that the Rietmond Shales are a correlative of the lower part of the Whitehill Formation.

This lower transgressive part of the Whitehill Formation is represented in the Aussenkjer-Noordoewer and in the Goris facies successions by non-bioturbated laminated carbonaceous shales, whereas in the Panorama and Gellap successions mainly bioturbated greenish-bluish-grey silty shales constitute this part. In the Mukorob-Daberas facies succession this part is dominated by greyish silty to sandy shales. In the Aranos Karoo subcrop area a base level rise is documented in the onset of widespread swampy conditions leading to the deposition of carbonaceous shales and coal (Impala Coal Seam). Transgression of the sea deposited over the coaly interval sandy shoreface and silty-sandy tidal sediments (Fig. 2.23).

Higher up in the Whitehill succession a subsequent regressive event is clearly documented in the Aussenkjer-Noordoewer area by a brownish weathering silty shale zone sandwiched between the whitish weathering shales. In the Keetmanshoop area this regressive event can be recognized by a subtle coarsening-upward shale succession. This coarsening trend is morphologically well expressed by a widespread cliff zone in the Goris, Panorama, Gellap, and Mukorob-Daberas facies successions. At the base of this progradational coarsening-upward succession an interval with dolomitic limestones forms an important and mappable marker zone (Fig. 2.23). In the corresponding part in the Aranos area evaporite layers in the lower part of a coarsening-upward succession overlying the transgressive shoreface and tidal deposits can certainly be correlated with the dolomitic limestone zone (Goris Limestone Beds) elsewhere.

A few metres below this coarsening-upward succession in the middle to upper part of the Whitehill Formation a zone with bentonitic and feldspathic tuff layers have been discovered in the Goris and Panorama facies successions (Fig. 2.23). At the base of this tuff-bearing zone a conspicuous and lateral continuous carbonate concretion horizon or layer can be found. This carbonate concretion layer and the overlying tuff zone are probably positioned within a maximum flooding zone separating the lower transgressive systems tract of the Whitehill Formation from a highstand systems tract, which is characterized either by a coarsening-upward shale succession in the outcropping part of the Whitehill Formation (cliff zone) or by a coarsening-upward succession of distal to proximal splay to distributary channel and mouth bar sandstones in the Aranos subcrop area. Interestingly, the appearance of mesosaurids and their colonization of the Mesosaurus Inland Sea in South America and southern Africa seem to be linked with this regressive phase. Mesosaurids are believed to have evolved in the northern part of the Paraná Basin, where they appear lowest down in the stratigraphy. The presence in this area of an unspecialised, plesiomorphic species (*Brazilosaurus sanpauloensis*), which shows none of the special adaptations for aquatic life of the other mesosaurus species (*Mesosaurus tenuidens* and *Stereosternum tumidum*), is taken as further proof of this assumption (Oelofsen, 1987). The lowermost occurrences of *Mesosaurus* bones in southern Namibia have been discovered within the coarsening-upward shale succession in the upper third of the Goris Whitehill facies succession (Fig. 2.24-A to D).
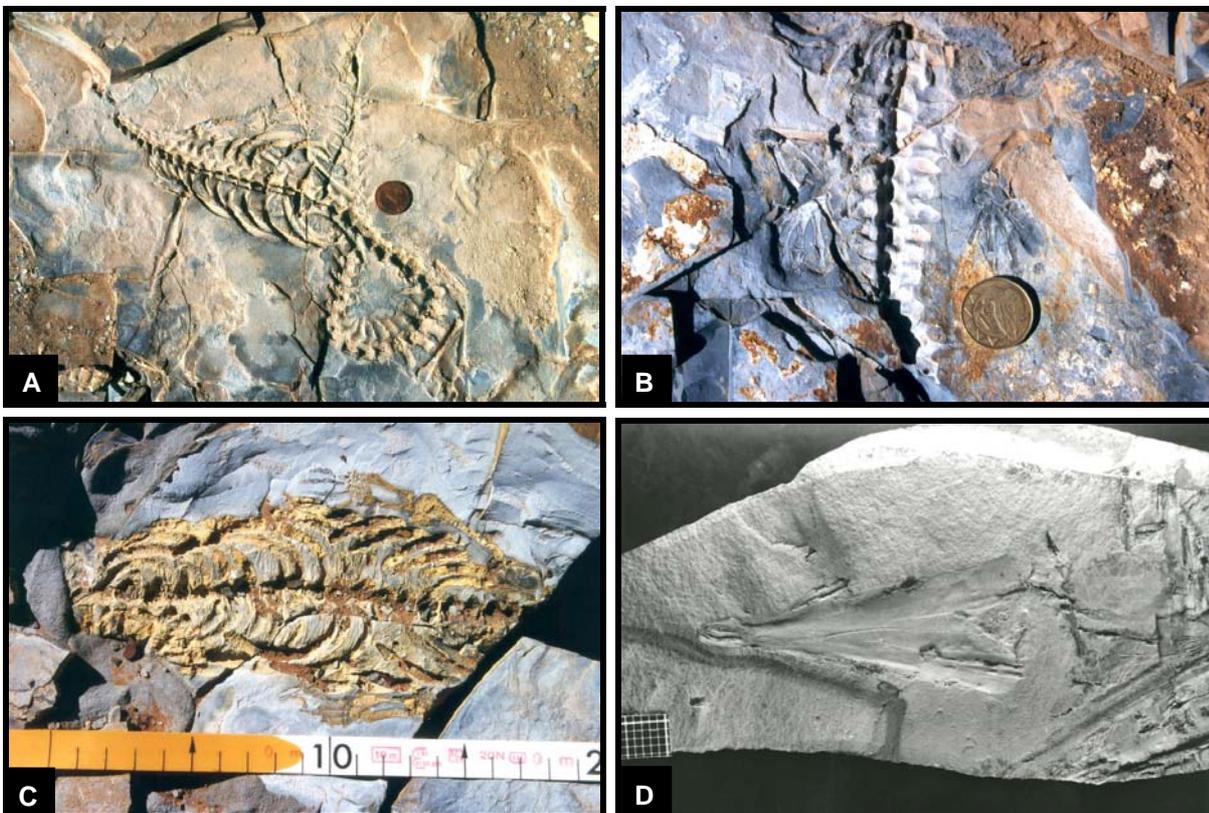
Fig. 2.24 (prev. page): *Mesosaurus* specimens from the Whitehill Formation: **(A) & (B)** Goris facies succession. Locality: Farm Goris. **(C)** Goris facies succession. Locality: Farm Spitzkoppe Ost. **(D)** Jaw bones of *Mesosaurus*. Locality: Keetmanshoop Townlands.

The coarsening-upward succession is in turn followed by a fining-upward succession with white weathering shales grading into bluish-grey weathering, finely laminated claystones in the Aussenkjer-Noordoewer, Goris, Panorama, Gellap, and Mukorob-Daberas Whitehill facies successions. In the Aranos area this upper transgressive succession is once again marked by the deposition of carbonaceous shales and thin coal seams recording the development of a second swamp period. Black carbonaceous shales characterize this higher part of the Whitehill Formation in all facies successions. Due to the widespread anoxic conditions at the sea bottom combined with very low energy depositional enviroments fossils are generally very well preserved in this zone. Apart from mesosaurids also fish remains and plant fossils can be found quite frequently (Fig. 2.25-A to D). The uppermost part of the Whitehill Formation is characterized by the occurrence of arthropod remains among which the crustacean *Notocaris tapscotti* is best known (Fig. 2.26-A to D). The boundary between the uppermost fissile black shales of the Whitehill Formation and the overlying black cherty shales of the Collingham Formation is only exposed and preserved in the Aussenkjer-Noordoewer area. The entire Collingham Formation comprises one coarsening-upward succession (highstand systems tract) overlying the upper transgressive systems tract of the Whitehill Formation (Fig. 2.23).
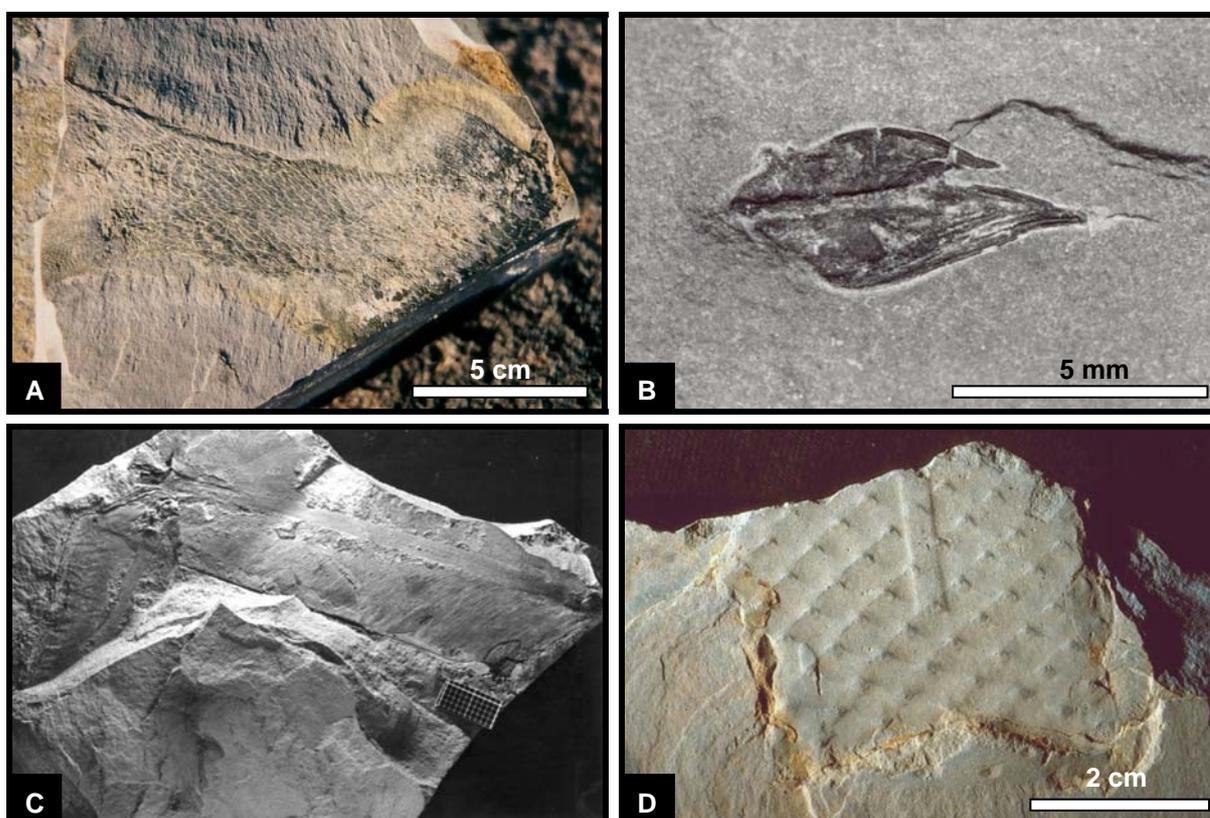
Fig. 2.25 (prev. page): Fish and plant fossils from the Whitehill Fromation: **(A)** Part of a palaeoniscoid fish with the tail in the left and a dorsal fin in the upper right corner of the picture. Locality: Farm Goris. **(B)** Single scale of a palaeoniscoid fish. Locality: Farm Goris. **(C)** Large *Glossopteris* leave. Locality: Farm Goris. **(D)** Lycopd fragment (*Lycopodiopsis*?; pers. comm. R. Rohn, 2004). Locality: Aussenkjer.
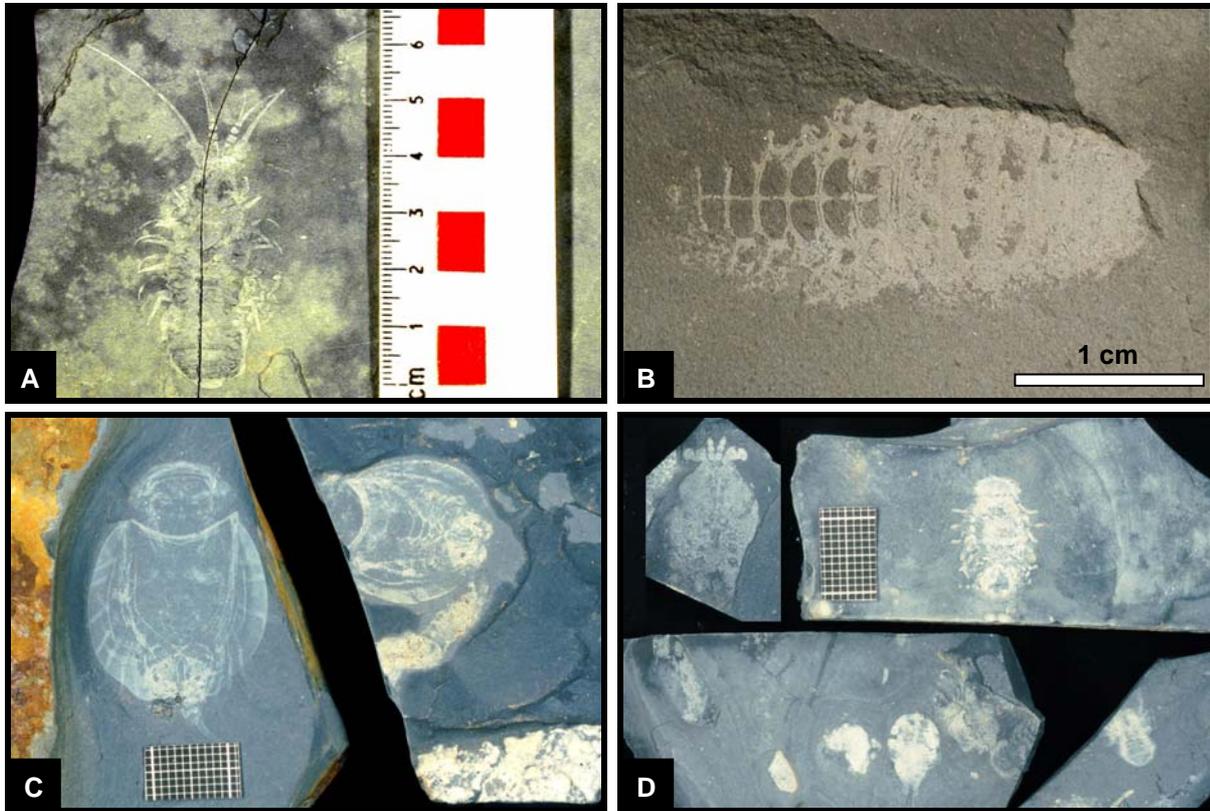
Fig. 2.26: (A) to (D): Arthropod remains found in the Whitehill Formation showing a large morphological variability. The specimen shown in (B) represents the most frequently found preservation form of the crustacean *Notocaris tapscotti*. It is not clear if the other shown forms also represent this crustacean in various states of preservation or if other species are present. Localities: (A) & (B): Farm Goris, (C) & (D): Aussenkjer.

As shown above the deposits of the Whitehill Formation - and lateral correlatives - record two transgressive phases separated by a regressive episode. Only in the northern part of the Mariental-Keetmanshoop outcrop area and the Aranos subcrop area a sequence boundary associated with an erosional unconformity underlies the Whitehill Formation, with erosive channel sandstones in the upper part of the Auob Sandstone Member probably representing a low stand systems tract. Southward this erosional unconformity passes into a correlative conformity. Also the contact between the high stand systems tract and the upper transgressive systems tract within the Whitehill Formation is conformable, possibly throughout the whole studied area, and hence can only be recognized by the change from a progradational to a retrogradational depositional trend. These transgressive-regressive phases illustrated for the Prince Albert and Whitehill Formations form 3rd order sequences,

with each cycle representing a time period of about 3 to 5 Ma (see also Chapter 5 – Geochronology). It has been realized earlier that the whole succession of the Dwyka and Ecca Groups, as well as their correlatives in South America, forms the major part of a 2nd order transgressive-regressive sequence. Some authors believe that the Whitehill and Irati Formations represent the maximun flooding zone within this 2nd order transgressive-regressive sequence, e.g. Zalan et al. (1991), Grill (1997), López-Gamundí & Rosello (1998), Stollhofen (1999). Other researchers favoured more the shales in the upper part of the underlying Prince Albert and Palermo Formations to represent the maximum flooding stage, e.g. Visser (1993b) and Milani & Filho (2000). Nevertheless, the carbonaceous shales of the Whitehill Formation were deposited during 3rd order transgressive events, associated with algal blooms, within the period of a 2nd order sea-level highstand (Visser, 1992b, 1993a, b). Having this in mind, the deposition of the Whitehill black shales is somewhat reminiscent of the so-called 'oceanic anoxic events' (OAEs) describing widespread horizons of black shales in the Cretaceous oceans. They signify periods of poor circulation and oxygen deficiency and are thought to result from increased organic productivity associated with transgressive events that produced widespread shallow seas (Bellanca et al., 1999; Tucker, 2001), a situation that is quite comparable to the Mesosaurus Inland Sea. However, these OAEs occurred at a time of global equable (warm) climate, when there was little dense, cold water produced at the poles for ventilation of ocean basins. In contrast, the restricted circulation in the Mesosaurus Inland Sea is believed to have been caused by the near cut-off of this inland sea from the world ocean by a magmatic arc complex along the active southern margin of Gondwana, which might have acted as a barrier or sill to restrict the interchange of water with the Panthalassan Ocean (Collinson et al., 1992).

2.3.3 Collingham Formation

In the Aussenkjer-Noordoewer area the Whitehill Formation is conformably overlain by an approximately 75 m thick succession of mainly olive green to grey, buff weathering shales, which contain abundant intercalations of thin tuff layers (Ufo Valleys-Rhyofontein Tuffs; see Chapter 3.4.2.3, Fig.3.50). Formerly the several hundreds of metres thick shale succession, overlying conformably the Whitehill Formation in the Aussenkjer-Noordoewer area, was named Aussenkjer Formation (SACS, 1980; Miller, 1992). Some very brief lithological descriptions of the Aussenkjer Formation can be found in Haughton & Frommurze (1927 & 1936) as well as in Schreuder & Genis (1975) but none of these authors recognized the numerous pyroclastic layers in the basal part of this post-Whitehill Formation shale succession. Fieldwork within the scope of this study has shown that the basal 75 m of the succession can undoubtedly be correlated with the Collingham Formation, which was known so far only from outcrops in the southern Cape Region of South Africa. There, it is represented by a rhythmically-bedded succession of alternating thin tabular beds of hard, grey, olive green and brownish siliceous mudrocks and very thin beds of softer yellowish bentonitic tuffs (SACS, 1980; Viljoen, 1992a & 1994; Johnson et al., 1997). The most distinctive mutual character of the Collingham Formation in South Africa and its counterpart in southern Namibia is the richness in bentonitic tuff layers intercalated in basinal shales. Due to the striking similarity of the South African and Namibian successions it seems justified to transfer the term Collingham Formation to the southern Namibian outcrops. Furthermore it is suggested to restrict the term Aussenkjer Formation to the argillaceous deposits, which conformably overlie the Collingham-equivalent part of the Ecca Group in the Aussenkjer-Noordoewer area.

In the Aussenkjer-Noordoewer area the uppermost carbonaceous fissile shales of the Whitehill Formation, which commonly contain a distinct arthropod fauna (*Notocaris* zone), are conformably overlain by dark grey to black, whitish or brownish weathering cherty mudrocks. The blocky weathering of these cherty rocks contrasts markedly with the fissility of the uppermost Whitehill Shales (Fig. 2.12-D & 2.27-A). Furthermore, the base of the Collingham Formation is also characterized by the appearance of very thin, light coloured tuff laminae and by the reappearance of bioturbation. The dark coloured cherty shales commonly can be found in the lowermost 10-15 m of the Collingham Formation but gradually pass upward into predominantly olive green, greenish-brown to buff weathering shales demonstrating the transition from dysoxic to better oxygenated conditions at the sea bottom. The following major part of the Collingham Formation is composed of greenish-grey to brownish basinal shales, which contain numerous intercalations of light-weathering tuff layers (Fig. 2.27-B & 3.51). The highest frequency of tuff layers with a thickness >1 cm is found within the middle

part of the formation (Fig. 3.50). In contrast to South Africa, where tuff beds constitute between 5 and 30% of the Collingham Formation thickness (Viljoen, 1992a, 1994), in Namibia the tuffs make up only about 1% of the whole thickness. Many of both the shale beds and the tuff layers do not form exactly tabular units but show slightly undulating bounding surfaces what is expressed in an inconspicuous lateral thickening or thinning of individual beds. This undulation is of a very low amplitude (<1 cm to few centimetres) and high wavelength (generelly several metres) nature. Probably the fine-grained muds and volcanish ashes were not exclusively deposited by pure suspension settling. Some of the layers were to some degree also deposited by low-density turbidites, tempestites, contourites, or from nepheloid clouds. At two stratigraphic levels quite conspicuous stellate and triradiate syneresis cracks (cf. Leeder, 1982; Viljoen, 1994) have been discovered (Fig. 2.27-C). Commonly, such syneresis cracks are attributed to salinity fluctuations. The occurrence of such syneresis cracks within the Ecca Group is largely restricted to the Collingham Formation (Viljoen, 1994; and this study) and therefore this formation most probably represents a period, in which the salinity of the basin waters of the Mesosaurus Inland Sea episodically, but finally gradually, changed from normal to brackish. It is believed that these salinity changes were caused by inflows of freshwater plumes or currents into the basin (cf. Viljoen, 1994). Bioturbation is fairly abundant in the Collingham Shales. Observed traces include simple burrows, branching burrows forming irregular networks, winding and looping burrows, paired sinusoidal grooves made by fishes (*Undichna*; see Fig. 3.52-A), and distinctly segmented traces reminiscent of *Scalarituba* (Fig. 2.27-D & 3.52-C). A similar ichnocoenosis was also reported by Kingsley (1981) and Viljoen (1992a) for the South African part of the Collingham Formation. Both the shales and tuffs have in the study area an intensively speckled appearance (Fig. 3.53) caused by countless tiny greenish spots, which represent pinitized cordierite porphyroblasts that grew contact-metamorphically due to Jurassic dolerite intrusions.

In the upper part of the Collingham Formation an upward-coarsening trend can be observed with the shales becoming siltier. Isolated occurrences of hummocky cross-stratification and mud pebble layers were observed within the uppermost 10 m of very hard, cherty, and blocky weathering mudrocks. The mud pebbles weather to a light colour and contrast well with the surrounding greyish cherty mudrock. The form of individual mud pebbles ranges from pancake- to shard-like indicating that they were during deposition cohesive and of semi-solidified consistency. Within thicker layers a clear reverse grain-size grading is visile (Fig. 2.27-E). Together with the hummocky cross-stratification in this stratigraphic interval these mud pebble layers can be interpreted as tempestites. The upper, coarser-grained part of the Collingham Formation is also characterized by numerous, yellowish-brownish, ellipsoidal

carbonate concretions, which can reach a diameter of almost one metre (Fig. 2.27-F & G). Towards the top of the Collingham Formation the mudrocks become successively chertier. This chertification also affects the numerous carbonate concretions (Fig. 2.27-H) and must therefore be of a later diagentic origin. It is suggested that this chertification is associated with contact-metamorphic and hydrothermal-metasomatic processes caused by Jurassic dolerite intrusions. The mineralogical changes within the argillaceous sediments and the early diagenetic carbonate concretions have not been studied in detail. However, one has to be carefull to ascribe this chertification merely to silicification of the rocks. The microscopic study of a 'siliceous' concretion within a tuff layer of the Collingham Formation revealed that it consists of a complex assemblage of calc-silicate minerals (see also Chapter 3.4.2.3, Fig. 3.58). Furthermore, the so-called Matjiesfontein Chert, a marker layer in the lower part of the South African Collingham Formation, which is not present in the Namibian part of the the formation, actually consists mainly of secondary albite (Knütter, 1994).

The top of the Collingham Formation is formed by a very conspicuous, very hard, white to orange weathering chert bed, which covers in a number of outcrops the greenish-brown shales of the Collingham Formation in a lid-like fashion (Fig. 2.27-I) or forms a conspicuous white band within olive green to dark grey shales (Fig. 2.27-K). In wide parts of the Aussenkjer-Noordoewer area it forms a mappable unit, which is also very well visible on aerial photographs or satellite images (Fig. 2.28). In this study this unit at the top of the Collingham Formation is informally called Polisiewater Chert Bed. The Polisiewater Chert is composed of extremely chertified mudrocks and its thickness is in the order of a few decimetres to somewhat more than a metre. In many outcrops the Polisiewater Chert shows a millimetre to centimetre thick lamination or bedding giving the rock a banded appearance, however, in some places the Polisiewater Chert is composed mainly of shred-like mud clasts forming a mud pebble breccia. This mud pebble breccia is somewhat similar to the mud pebble layer shown in Fig. 2.27-E but is generally coarser-grained (average mud clast is in the order of 1 cm) and the mud clasts are more angular. Slumping structures and hummocky cross-lamination were also observed in the Polisiewater Chert. In places large amounts of plant debris are common on upper surfaces as well as large tree trunks composed of black permineralized wood (Fig. 2.27-L to O). The long axes of leaves and trees show an unpronounced NW-SE preferential orientation (Fig. 2.29). It is suggested that this layer was formed by a severe storm that also had a devastating effect on a nearby vegetated and wooded land mass transporting and dispersing large amounts of plant and wood debris into the sea. The chertification of the rock, however, is probably much younger and caused by hydrothermal-metasomatic processes due to dolerite intrusions. The Polisiewater Chert is best developed and thickest in the west, south and east of the Amibberg Massif but loses its

character and peters out northeast of Aussenkjer and northeast of the Gemsbokberg (Fig. 2.28). Only in two small anticlines north of the gravel road 316 to Ai-Ais and north of the Amibberg Massif it reappears. Its thickness generally decreases towards the north but completely peters out only towards the northwest and northeast. Therefore, the Polisiewater Chert forms a N-S oriented, northward thinning, fan-, lobe- or tongue-shaped sedimentary body. Consequently a southerly source area can be supposed, what is in accordance with the observations from the Owl Gorge and Uhabis Members, which seem to be only present in the southern part of the Aussenkjer-Noordoewer area. Furthermore, in the following chapters it will be shown that also sandstone layers and packages above the Polisiewater Chert thin or peter out towards the north. The abundance of plant debris and tree trunks indicates that the southerly source area (parts of the Cargonian Highlands?) must have been emergent and vegetated.

The Collingham Formation represents an overall coarsening- and shallowing-upward succession with black, carbonaceous cherty shales at the base, overlain by silty-muddy basin shales, and tempestites in the uppermost part. In sequence-stratigraphic terms the Collingham Formation forms the progradational highstand systems tract, which overlies the upper transgressive systems tract of the Whitehill Formation underneath.
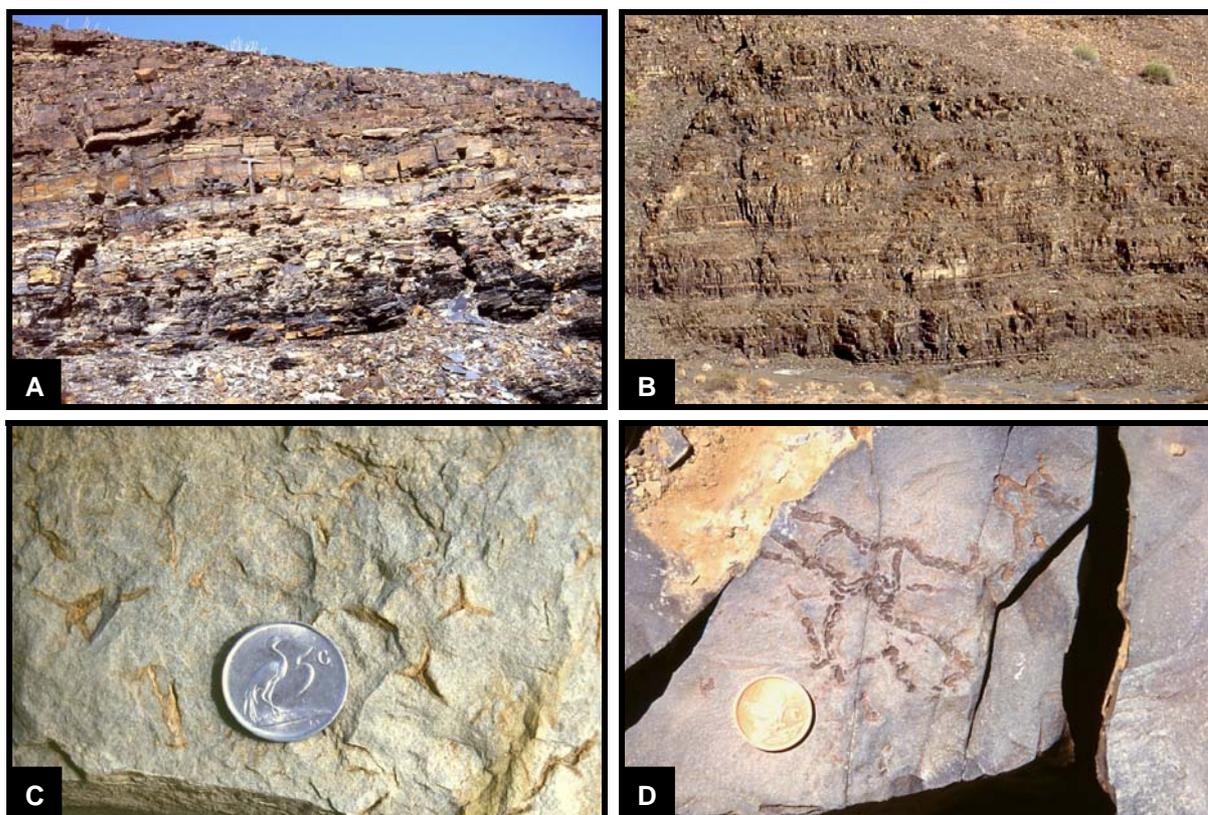
Fig. 2.27: Collingham Formation: **(A)** Approximately in the middle of the photo just below the hammer runs the boundary between the uppermost, fissile black shales of the Whitehill Formation and the basal, blocky weathering black cherts of the Collingham Formation. **(B)** Outcrop of the middle part of the Collingham Formation with olive brown weathering shales and intercalations of light-weathering tuff layers. **(C)** Triradiate syneresis cracks indicating salinity fluctuations. **(D)** Segmented trace fossil (*Scalarituba*?) in basal grey shales of the Collingham Formation.
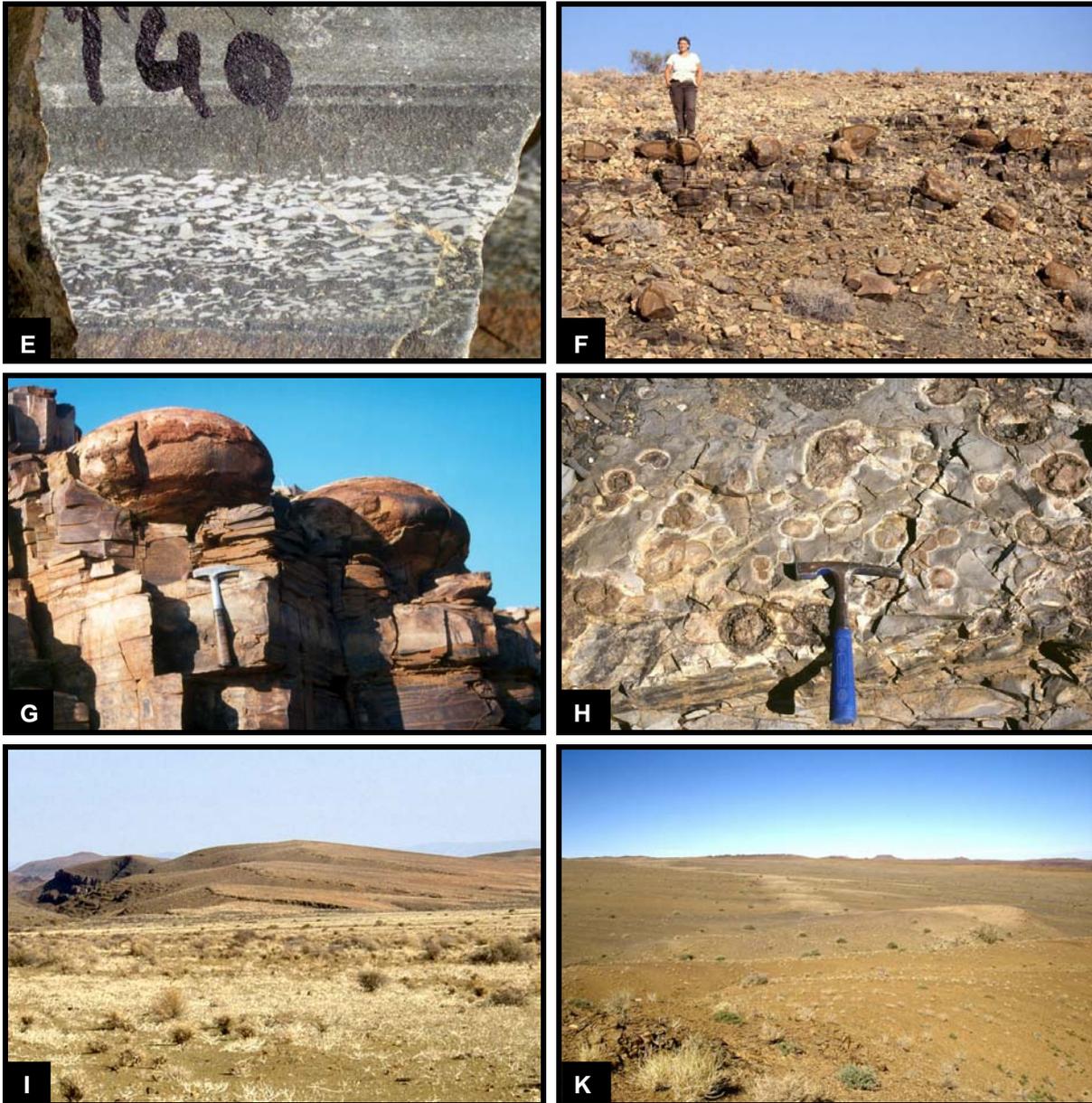
Fig. 2.27: Collingham Formation (cont.): **(E)** Mud pebble layer in the upper part of the Collingham Formation showing inverse grading. Such layers, which can laterally be associated with hummocky cross-stratification, are interpreted as tempestites. **(F) & (G)** Large carbonate concretions in the upper, coarsening-upward part of the Collingham Formation. **(H)** In the uppermost part of the Collingham Formation chertification affects both argillaceous deposits as well as carbonate concretions, the latter probably transformed into calc-silicate nodules (note the white coloured reaction rim around the concretions). This chertification is probably related to hydrothermal-metasomatic processes caused by thick and widespread dolerite sill intrusions of Jurassic age. **(I)** The orange weathering Polisiewater Chert forms the top of the Collingham Formation covering olive green to brownish weathering shales in a lid-like fashion. **(K)** In the marginal areas, where the thickness of the Polisiewater Chert decreases, it forms a whitish weathering band within greenish-brown basinal shales. The Polisiewater Chert forms in the Aussenkjer-Noordoewer area a northward thinning, fan-, lobe- or tongue-shaped sedimentary body and is interpreted as a tempestite caused by a severe storm event.
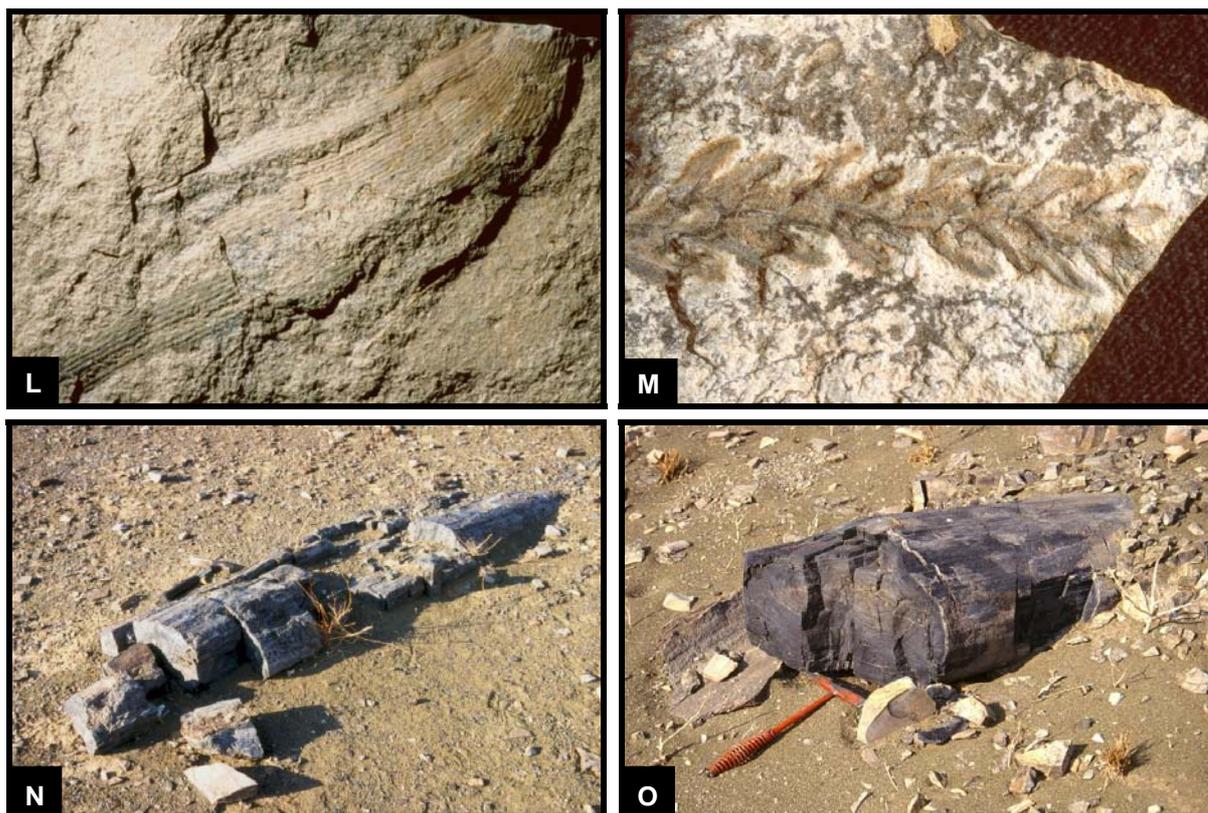
Fig. 2.27: Collingham Formation (cont.): Plant fossils within the Polisiewater Chert: **(L)** Segmented trunk of the sphenopsid plant *Paracalamites* (R. Rohn, pers. comm., 2004). The length of the shown part is approximately 10 cm. **(M)** Conifer branch probably representing *Pagiophyllum* (M. Bamford, pers. comm., 2004). The shown length of the branch is approximately 5 cm. **(N) & (O)** Gymnosperm tree trunks consisting of black permineralized wood and showing well developed growth rings.

Deposits of the Collingham Formation in southern Namibia and in the southern Cape Region of South Africa correlate with the lowermost part of the Tierberg Formation in the northern part of the South African Main Karoo Basin, with the lower part of the Volksrust Formation in Natal, and with the Grootegeluk Formation in the Ellisras Basin (Waterberg Coalfield) (Viljoen, 1994). On the Falkland/Malvinas Islands the Shepards Brook Member of the Port Sussex Formation, consisting of a ~140 m thick succession of shales, turbiditic fine sandstones, and more than 70 K-bentonite beds, is essentially similar to the Collingham Formation (Trewin et al., 2002). In the Paraná Basin of Brazil the Sierra Alta Formation correlates with the Collingham Formation. Although the Sierra Alta Formatiom contains tuff layers, it seems not to be exceptional rich in them (Coutinho et al., 1991)
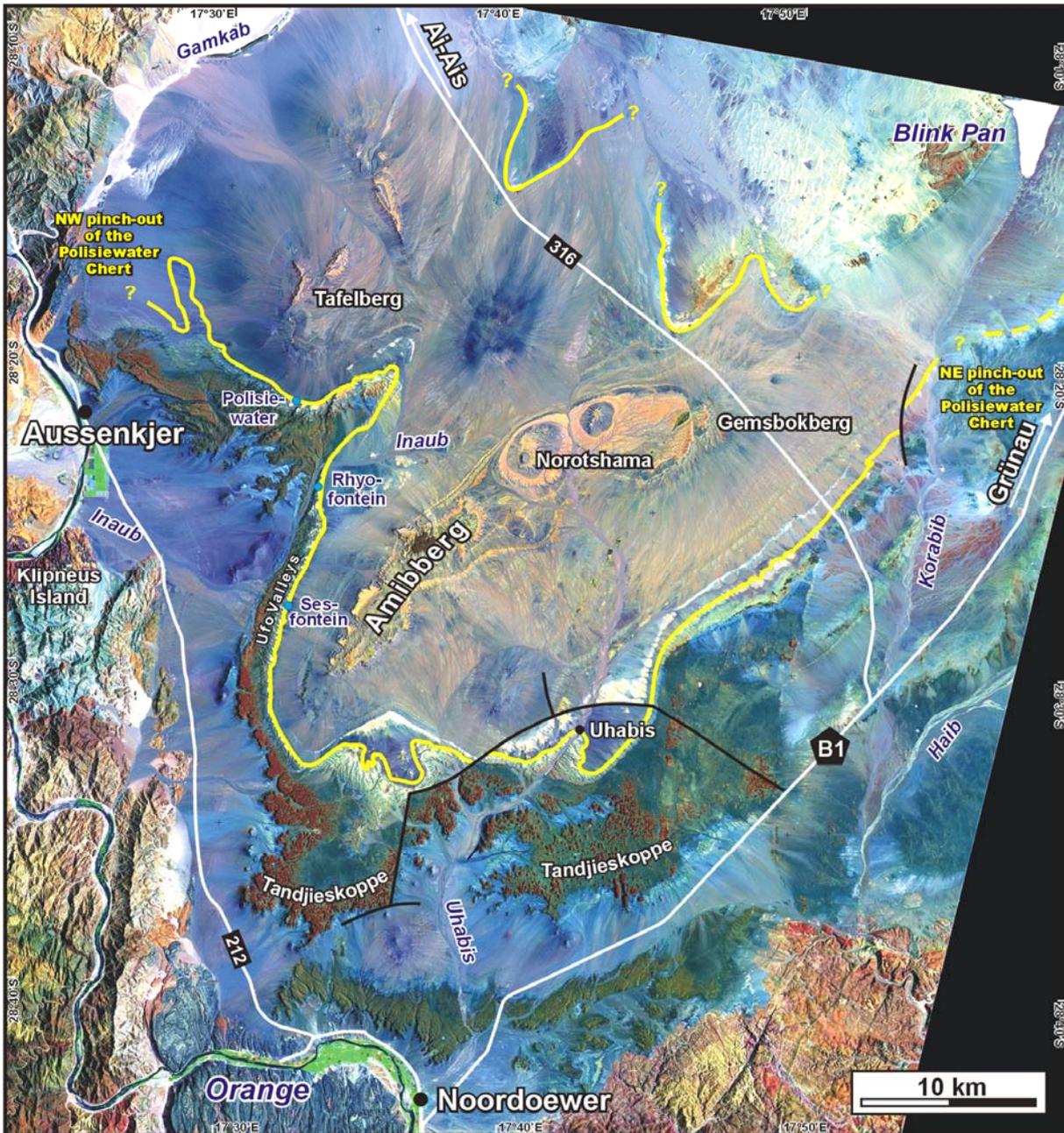
Fig. 2.28: The yellow line superimposed on the satellite image represents the boundary between the Polisiewater Chert (top of the Collingham Formation) and the Aussenkjer Formation. The Polisiewater Chert is best developed in the west, south and east of the Amibberg Massif and pinches out northeast of Aussenkjer and northeast of the Gemsbokberg. North of the gravel road 316 it reappears in two small anticlines. From the outcrops of the Polisiewater Chert it is supposed that it forms a N-S oriented, northward thinning, fan-, lobe- or tongue-shaped sedimentary body of tempestitic/turbiditic origin. Abundant plant debris and tree trunks (composed of permineralized wood) within the Polisiewater Chert have been found northwest of the Polisiewater spring.

n=38
largest petal: 4.00 Values
largest petal: 10 % of all values
Strike Direction: 10° classes

n=32
largest petal: 6.00 Values
largest petal: 18 % of all values
Strike Direction: 10° classes
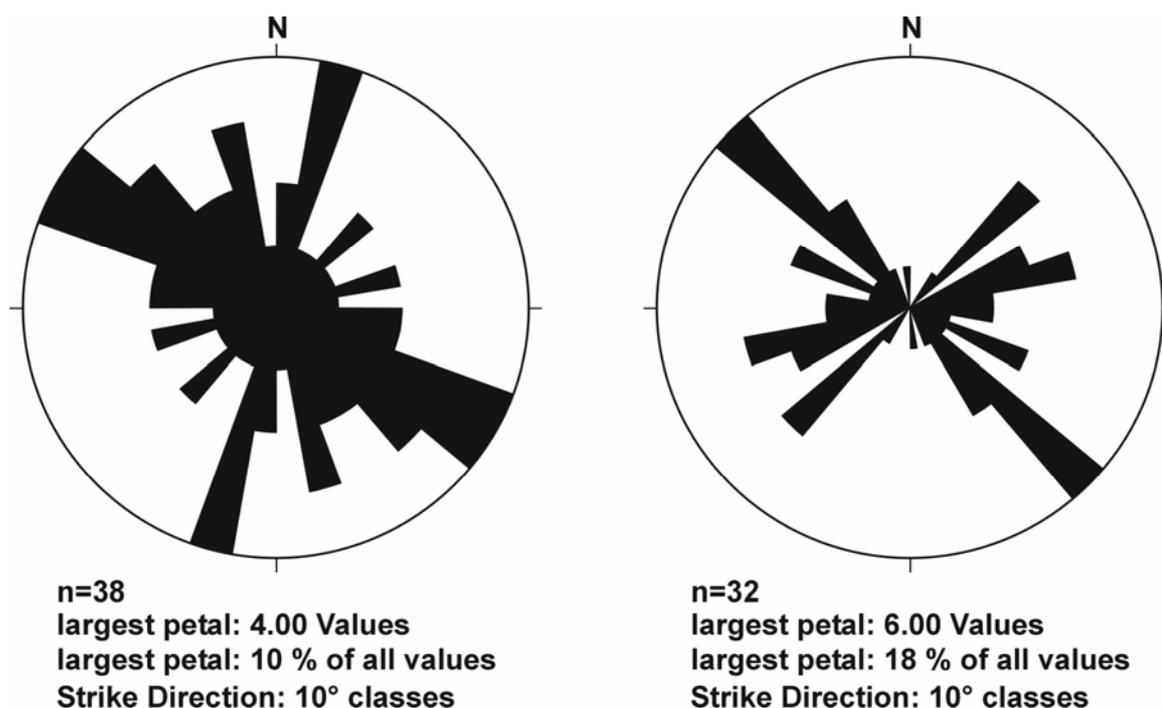
Fig. 2.29: Orientation of the long axis of tree trunks (left) and leaves (right) in the Polisiewater Chert showing a rather unpronounced NW-SE preferential orientation. Measurements were undertaken in outcrops northwest of the Polisiewater spring (Fig. 2.28).

2.3.4 Aussenkjer Formation

Originally the Aussenkjer Formation represented the greenish shale succession between the black shales of the Whitehill Formation and the sandstone-shale succession of the Amibberg Formation in the Aussenkjer-Noordoewer area (Schreuder & Genis, 1975; SACS, 1980; Miller, 1992). As described in the previous chapter the basal part of the original Aussenkjer Formation can undoubtedly be correlated with the Collingham Formation and is therefore excluded here from the Aussenkjer Formation. The newly defined Aussenkjer Formation overlies conformably the Collingham Formation, whose top is characterized by the Polisie-water Chert Bed. Only in the northwestern and northeastern part of the Aussenkjer-Noord-oewer area, where the Polisiewater Chert peters out, the demarcation of the two formations may be difficult due to a similar major lithology represented by olive green basinal shales. However, in outcrops above the Ufo Valleys, west of the Amibberg, the Polisiewater Chert is overlain first by a circa 20-30 m thick succession of fissile black shales, which gradually turn upward into more greenish shales (Fig. 2.30 & Fig. 2.31). This black shale interval may indicate the basal part of the Aussenkjer Formation in areas where the Polisiewater Chert is absent.
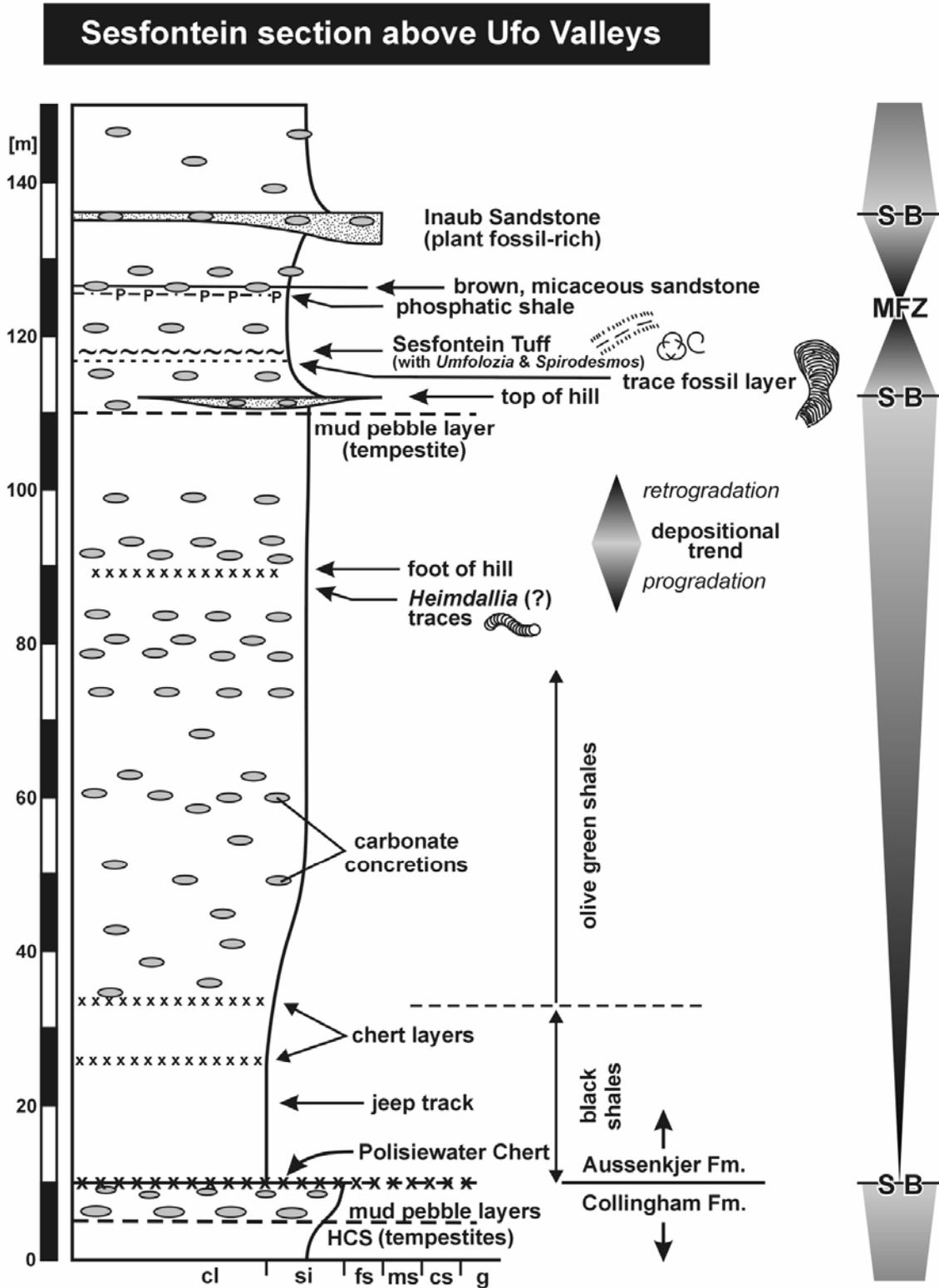
Fig. 2.30: Stratigraphic section and sequence-stratigraphic interpretation of the lower part of the Aussenkjer Formation measured from the Sesfontein locality upwards, i.e. towards SE (see also Fig. 2.32).
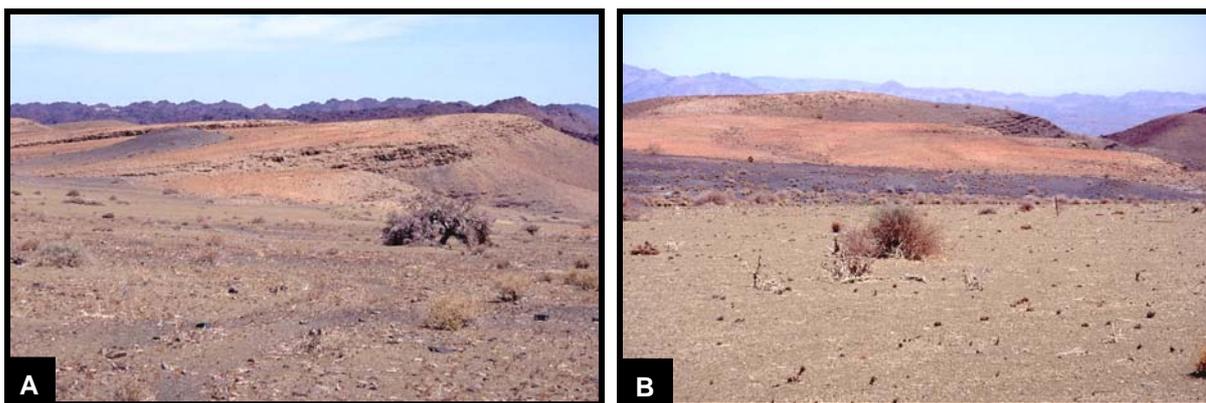
Fig. 2.31: **(A)** Photo showing from right to left the coarsening-upward succession in the uppermost part of the Collingham Formation, which is topped by the orange-brown weathering Polisiewater Chert. The basal part of the overlying Aussenkjer Formation is represented by black shales (small hillock in the left), which grade upward into olive green shales (foreground). **(B)** Same succession as in (A). In the middle background olive green shales of the uppermost Collingham Formation are overlain by the orange-brown Polisiewater Chert. The latter is conformably overlain first by black shales (forming the base of the Aussenkjer Formation), which are in turn overlain by olive green shales representing the dominant lithology of the Aussenkjer Formation. Locality: above the Ufo Valleys west of the Amibberg Massif.

The sediments of the Aussenkjer Formation were first briefly mentioned by Haughton & Frommurze (1927 & 1936). Later, Schreuder & Genis (1975) briefly described these sediments as a monotonous shale succession with intercalated limestone bands as well as carbonate and phosphate concretions. They reported a maximum thickness of 620 m for the whole shale succession (original Aussenkjer Formation including the circa 75 m thick Collingham Formation) on Farm Aussenkjer. Own investigations suggest that this value is too high and that the thickness of the Aussenkjer Formation (excluding the Collingham Formation) is rather in the order of about 400 m.

Due to the argillaceous nature of the Aussenkjer Formation its sediments form the extensive pediment surfaces around the Amibberg Massif and further to the northwest around the Tafelberg Mountains up to the Gamkab Rivier (Fig. 2.28). A closer look at the sediments of the Aussenkjer Formation revealed that this shale succession is not as monotonous as described earlier. It contains a number of thin but quite conspicuous interlayers, of which the so-called Inaub Sandstone, positioned about 125 m above the base of the Aussenkjer Formation, can be traced almost throughout the entire Aussenkjer-Noordoewer area. Within the scope of this study at one locality the lower part of the Aussenkjer Formation was logged in detail. It comprises the circa 125 m thick succession from the base of the Aussenkjer Formation to the Inaub Sandstone Bed (Fig. 2.30). The section was logged from the Sesfontein spring above the Ufo Valleys upward in a southeasterly direction (Fig. 2.32).
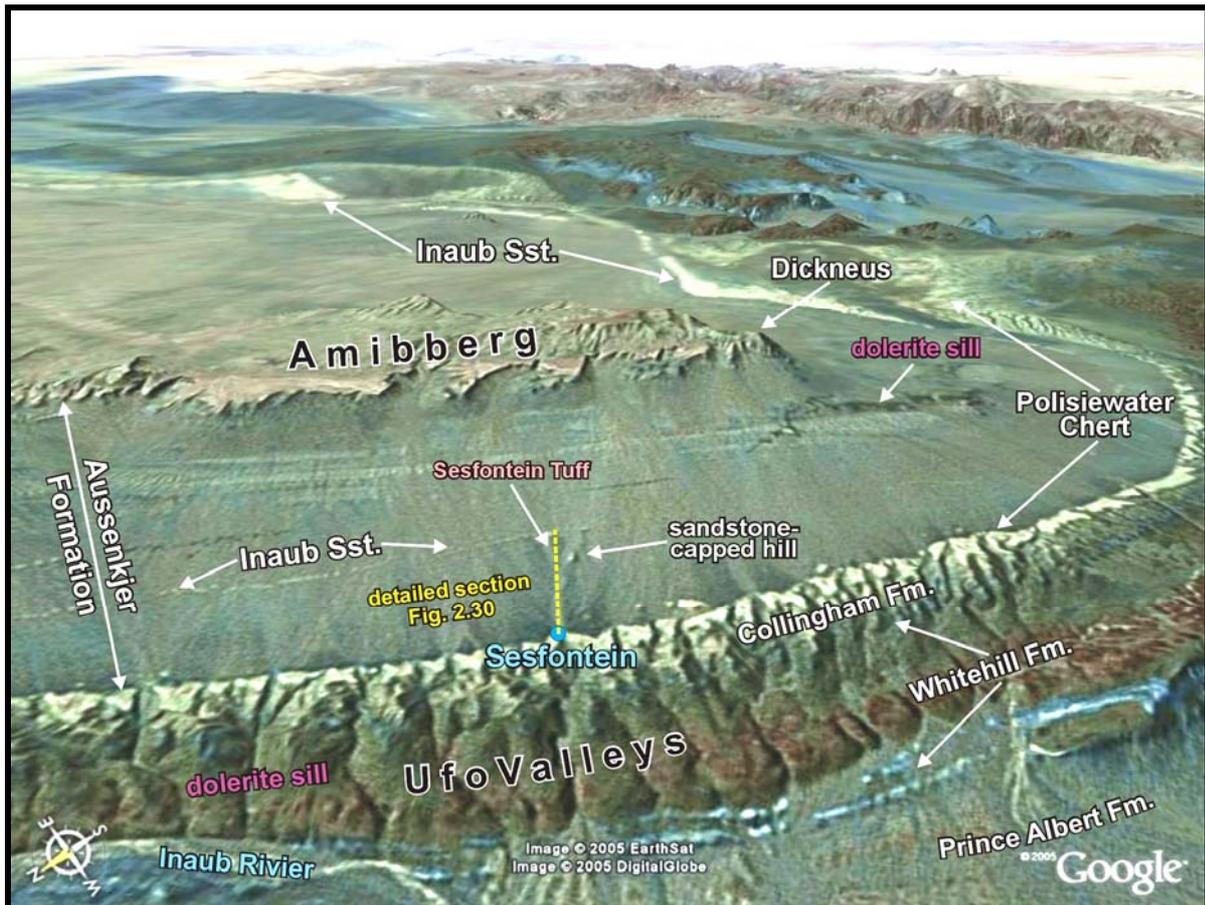
Fig. 2.32: Google-Earth satellite image showing the area where a detailed section of the lower 125 m of the Aussenkjer Formation was logged. The section, which is shown in Fig. 2.30, comprises the stratigraphic interval from the Polisiewater Chert at the top of the Collingham Formation to the Inaub Sandstone 125 m above the base of the Aussenkjer Formation. Several conspicuous layers (e.g. the Sesfontein Tuff) occur between these units and are described in the text. At least the Inaub Sandstone can be traced on aerial photos and satellite images almost throughout the whole Aussenkjer-Noordoewer area (Fig. 2.37). The lateral extent of the other marker layers has not yet been mapped in the field. See also Fig. 3.49 for a geological map of this region.

The measured section starts at Sesfontein with fissile black shales, which overlie conformably the Polisiewater Chert. These basal black shales attain a thickness of about 20-30 m and grade upward into olive green silty shales. Bioturbation can be observed in several stratigraphic levels. Intercalated in the black shales are several white chert layers with thicknesses ranging from less than 1 cm up to 15 cm. Carbonate concretions are quite rare within the black shales but become very abundant in the overlying greenish shales. Approximately 100 m above the base of the Aussenkjer Formation occurs a mud pebble layer (Fig. 2.30). The lower part of this layer consists of cm-sized greenish pebbles and is clast supported. In the outcrop one can see how the undisturbed underlying greenish shale gradually disintegrates in upward direction into these pebbles, which probably were ripped off from the cohesive muddy underground by traction currents and may not have been

transported over long distances. The texture is more or less massive and a subtle normal grading can be observed. This part of the mud pebble layer shows a brownish to blackish weathering colour (Fig. 2.33-A). The upper part of this mud pebble layer weathers to a lighter brown colour and is composed of several stacked, normal graded, upward-fining and upward-thinning pebble beds giving the rock a plane-bedded appearance (Fig. 2.33-B). The individual pebbles weather to a creamy colour. The bedding indicates that the pebbles in this upper part were transported by strong currents. The gradual disintegration of the shale, the transition from a massive to a plane-bedded part, and the overall fining-upward trend suggests that this layer was produced by a storm and is therefore interpreted as a tempestite. The upper pebble beds grade upward into a fine-grained sandstone, which appears strongly silicified and forms the inclined top of a small hill (sandstone-capped hill in Fig. 2.32). Some carbonate concretions can be found within the sandstone. The pebble beds can be traced laterally at least over a few hundreds of metres, however, the overlying sandstone forms an extremely localized phenomenon. Its extent reaches only a few tens of metres along strike and rapidly pinches out laterally. Such a sandstone-capped hill was not only observed at the Sesfontein locality but also further northwest in the Tafelberg area, where such a very localized sandstone occurrence forms another small hill, supposedly in the same stratigraphic level (Fig. 2.33-C). The thickness of the tempestite succession from the base of the mud pebble layer to the top of the overlying silicified sandstone reaches a maximum thickness of about 2-3 m at the Sesfontein locality.

Just at the foot of the sandstone-capped hill above Sesfontein a very conspicuous trace fossil occurs in the greenish shales underlying the tempestite layer (Fig. 2.30). This trace fossil is composed of vertical but laterally migrating cylindrical tubes producing in plan view the appearance of a meniscate-like burrow. The individual tubes show diametres of about 1 cm. The migration path can be straight or slightly curved but also spiral segments have been observed (Fig. 2.34). Very similar trace fossils were described from Lower Permian marine siliciclastic deposits (Snapper Point Formation) from the southern Sydney Basin in Australia. Carey (1978) doubtfully referred this trace fossil to *Zoophycus*. Here it is suggested that it might belong to the ichnogenus *Heimdallia* (cf. Buckman, 1996).

Fig. 2.33: (A) Tempestitic mud pebble layer approximately 100 m above the base of the Aussenkjer Formation. Greenish shales gradually disintegrate into cm-sized pebbles forming a massive unit (dark weathering unit and two specimens in the foreground). The upper, light brownish weathering part of this layer consists of several stacked, upward-fining and upward-thinning pebble beds giving this part a plane-bedded appearance. **(B)** Normal graded, upward-thinning and upward-fining mud pebble beds in the upper part of the tempestite layer. **(C)** The mud pebble layer is overlain in places by a spatially very restricted sandstone, which forms the top of small hills at this stratigraphic level. A small sandstone-capped hillock (right margin of photo) raises from the pediment in front of the Tafelberg Mountains (see also Fig. 2.37).
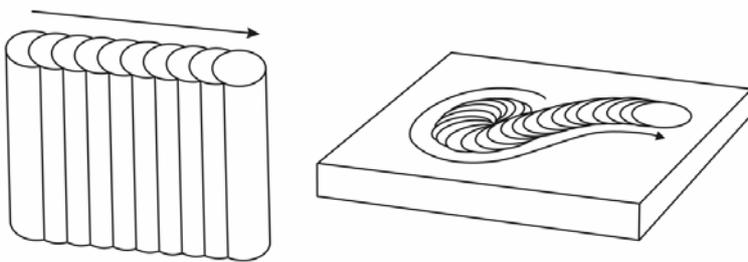
Fig. 2.34: Conspicuous trace fossil occuring in the greenish shales at the foot of the sandstone-capped hill above Sesfontein. In plan view it looks like a meniscate burrow similar to *Scoyenia*, however, 3D-cross sections revealed that it actually consists of laterally migrating, vertical tubes (left). Some specimens also contain spiral segments (right). This trace may belong to the ichnogenus *Heimdallia*.

Above the mud pebble layer and the locally associated sandstone the shales of the Aussenkjer Formation appear to become finer-grained, less silty and display darker colours. Some of the dark layers form resistant horizons composed of blocky weathering and chert-like rocks, which may be phosphatic. At approximately 107 m above the base of the Aussenkjer Formation spectacular trace fossils have been discovered within lithologically inconspicuous greenish shales (Fig. 2.30, Fig. 2.35-A/B & Fig. 3.60-C/D). These trace fossils resemble at first sight helminthoid grazing traces with their closely spaced meander trails. Commonly they possess a 'head' with a concentric grazing pattern giving the trace often the form of a mushroom with a closed head. The segmentation of the meandering trails could represent pellets and might indicate also some relation to *Scalarituba/Neonereites/Nereites*. The same trace fossil was also discovered by Wickens (1996) in shales of the Tierberg Formation in the southwestern part of the South African Main Karoo Basin. The Tierberg Formation can be considered as a correlative of the Aussenkjer Formation.

5-10 cm above this trace fossil layer a thin (1 mm), very micaceous layer with carbonate concretions can be found. After some more 60-70 cm of shales follows the Sesfontein Tuff (Fig. 2.30), which is characterized by a conspicuous greyish-white outcrop surface, formed by a thin tuff lamina within dark olive grey to brownish shales. This surface is also intensively traversed by trace fossils of mainly two types. One type represents arthropod trackways of the ichnospecies *Umfolozia sinuosa* (Savage, 1971; Anderson, 1981) (Fig. 2.35-C & Fig. 3.60-A), the other type forms arcuate to spiral, epichnial grooves (Fig. 2.35-D & Fig. 3.60-B), which are very similar to traces described from the Vryheid Formation (Ecca Group) of KwaZulu-Natal (South Africa) by Mason et al. (1983). These authors assigned these spiral traces to the ichnogenus *Spirodesmos*, however, the South African as well as the Namibian spiral traces differ from the type specimen *Spirodesmos archimedeus* (Hückreide, 1952) in having fewer coils in each spiral (up to a maximum of two).

About 115 m above the base of the Aussenkjer Formation at Sesfontein occurs a quite conspicuous, several centimetre thick, brownish weathering, very micaceous, carbonate-cemented, fine-grained sandstone layer, which shows hummocky cross-stratification (Fig. 2.30 & Fig. 2.36-A/B). The sandstone is underlain by a 20-30 cm thick hard shale band. The uppermost 5 cm of this shale band are composed of a very hard, blackish-greenish, whitish weathering, intensively bioturbated cherty shale (Fig. 2.36-A). A XRF analysis revealed that this hard shale is markedly phosphate-enriched and contains about 6 wt.% P_2O_5.
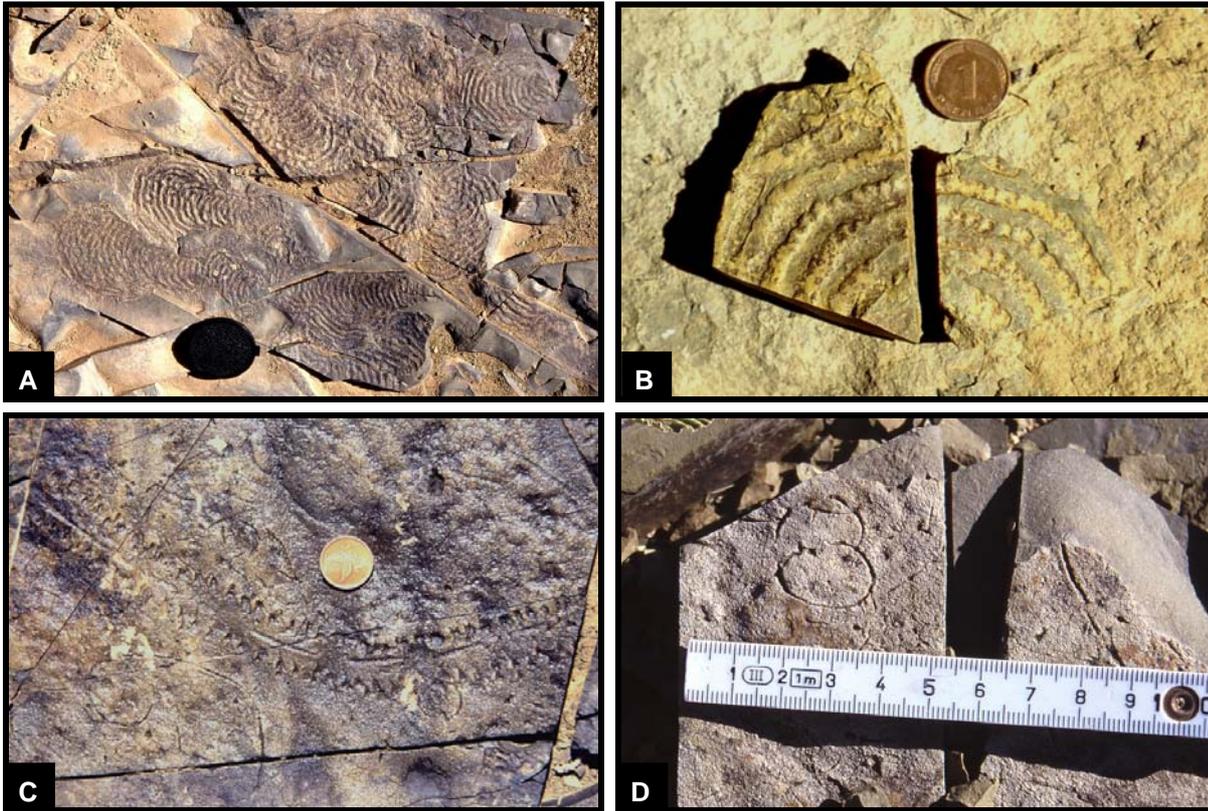
Fig. 2.35: (A) Helminthoid trace fossil with closely spaced meandering trails. The 'head' region often shows a concentric grazing pattern. **(B)** Fragment of the helminthoid trace fossil showing that the epichnial ridges (left) are composed of spherical pellets indicating a relation to *Scalarituba-/NeonereitesNereites*. To the right is the corresponding hypichnial cast. **(C)** Biserial trail consisting of transverse impressions of arthropod appendices belonging to the ichnospecies *Umfolozia sinuosa*. Upper surface of the Sesfontein Tuff. **(D)** Arcuate to spiral furrows within the Sesfontein Tuff possibly representing the ichnogenus *Spirodesmos*.
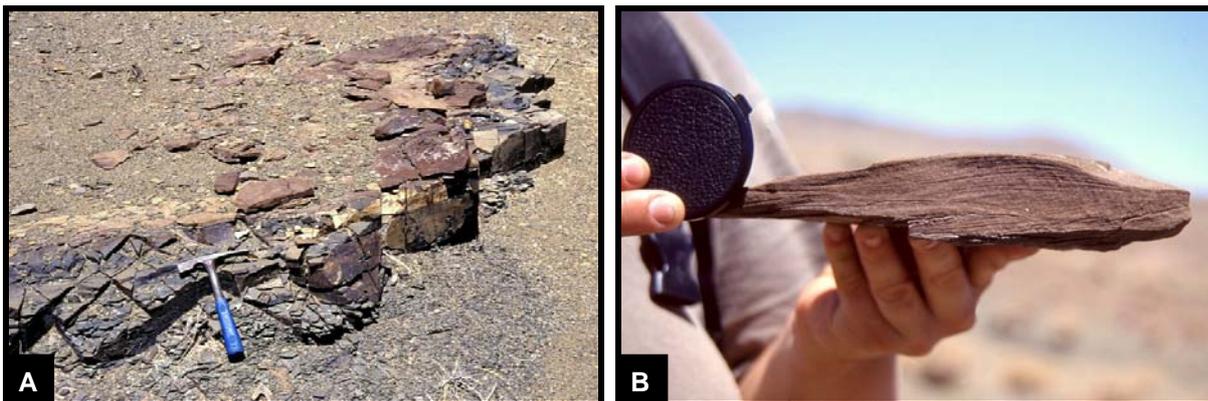
Fig. 2.36: (A) Brownish weathering, very micaceous, carbonate-cemented, fine-grained sandstone layer cropping out circa 115 m above the base of the Aussenkjer Formation at Sesfontein. The sandstone is underlain by a 20-30 cm thick hard shale band. The uppermost 5 cm of this shale band are composed of a very hard, blackish-greenish, whitish weathering, intensively bioturbated cherty shale, which contains about 6 wt.% P_2O_5. **(B)** Hummocky cross-stratification within the brownish weathering sandstone.

In the Sesfontein section occurs about 125 m above the base of the Aussenkjer Formation a sandstone layer, which can be traced laterally over long distances. This sandstone is here informally designated the Inaub Sandstone Bed (Fig. 2.30). Similar to the Polisiewater Chert the Inaub Sandstone is best developed in the southern part of the Aussenkjer-Noordoewer area, where it forms in aerial photos and satellite images a prominent and continuous unit, but thins in a northerly direction. Again its outcrop trace is lost in the northwest in the Tafelberg Mountains area and in the northeast between the Gemsbokberg and the Blink Pan, but reappears in two anticlines north of the gravel road 316 to Ai-Ais (Fig. 2.37).

Fig. 2.37: The yellow line superimposed on the satellite image represents the outcrop trace of the Inaub Sandstone, which occurs about 125 m above the base of the Aussenkjer Formation. Similar to the Polisiewater Chert the Inaub Sandstone is best developed in the south and thins towards the north. It may pinch out in the northwest and northeast but reappears north of the gravel road 316 in two small anticlines. It probably represents a fan-, lobe- or tongue-shaped basin floor tempestite with a southerly source area. Red stars indicate visited localities of the Inaub Sandstone, to which is referred to in the text.

In the field the Inaub Sandstone has been studied at three localities, namely east of the Sesfontain spring above the sandstone-capped hill, south of the Amibberg, and in the northwestern small anticline north of the gravel road to Ai-Ais (Fig. 2.37). In all visited outcrops the Inaub Sandstone is represented by a greenish-grey to yellowish-brown, well-sorted, fine-grained sandstone, which can be in parts quite micaceous. Carbonate concretions are quite common within this sandstone and in the outcrops south of the Amibberg they can attain diameters of well over one metre. The thickness of the Inaub Sandstone can vary considerably. Within the Sesfontein section the Inaub Sandstone is normally about 30-40 cm thick but can locally swell to one metre (Fig. 2.38-A). At the Ai-Ais locality a thickness of about 1.5-2 m has been recorded. In contrast, south of the Amibberg, where the Inaub Sandstone forms a roof-shaped outcrop in plan view (Fig. 2.37), its thickness increases up to about 8-10 m. Furthermore, at the Sesfontein and the Ai-Ais road localities the Inaub Sandstone represents a single layer, whereas south of the Amibberg it forms a succession of several, upward-thickening sandstone layers (Fig. 2.38-B).
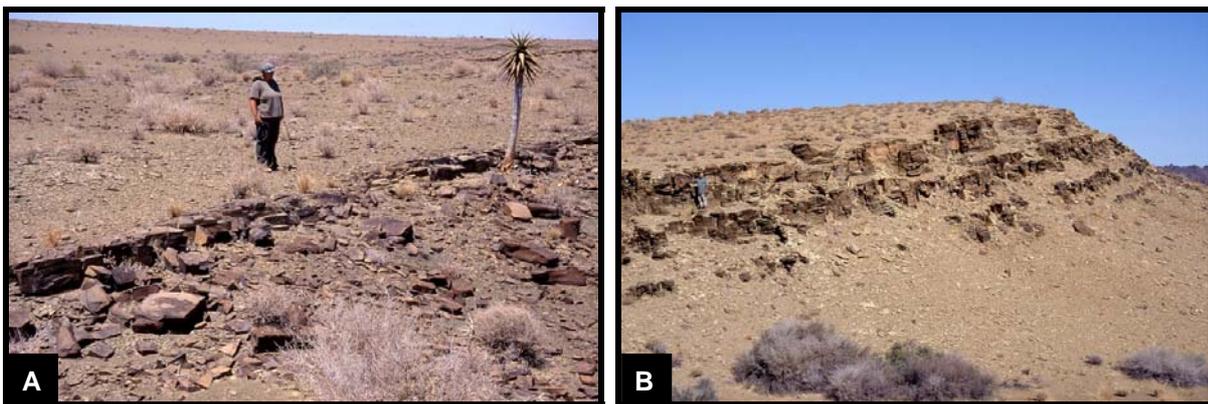
Fig. 2.38: **(A)** The Inaub Sandstone at the top of the Sesfontein section showing a thickness of only 30-40 cm. **(B)** South of the Amibberg the Inaub Sandstone attains a thickness of up to about 10 m and is composed of a succession of several, upward-thickening sandstone units (author is standing at the left margin of the photo on the base of the uppermost sandstone unit next to a large carbonate concretion).

Plane lamination or plane bedding as well as hummocky cross-stratification are the dominant sedimentary structures within the Inaub Sandstone. At the Ai-Ais road locality one can see that the base of the Inaub Sandstone is not very sharp. Greenish, silty shales are overlain by plane-laminated, fine-grained sandstones (Fig. 2.39-A), which grade upward into wavy-laminated sandstones (Fig. 2.39-B). The wave legth of these sedimentary structures is increasing in upward direction. In this lower part the sandstone appears relatively mud-rich and in places the sandstone becomes a coarse-grained appearance due to numerous sand-sized mud grains. Towards the top the mud content in the sandstone is decreasing markedly. The upper part of the sandstone is characterized by hummocky cross-stratification, which is

especially well visible in brownish carbonate concretions (Fig. 2.39-C). This succession indicates that from base to top the individual subunits of the Inaub Sandstone were deposited under successively higher energetic conditions. This is also reflected in the upward-thickening of individual sandstone layers at the Inaub Sandstone locality south of the Amibberg (Fig. 2.38-B). Locally, at the base of the Inaub Sandstone the greenish shales are turned into black shales due to a strong phosphate impregnation (Fig. 2.39-D). One sample of these black phosphatic shales yielded a phosphate content of 16.7 wt.% P_2O_5.
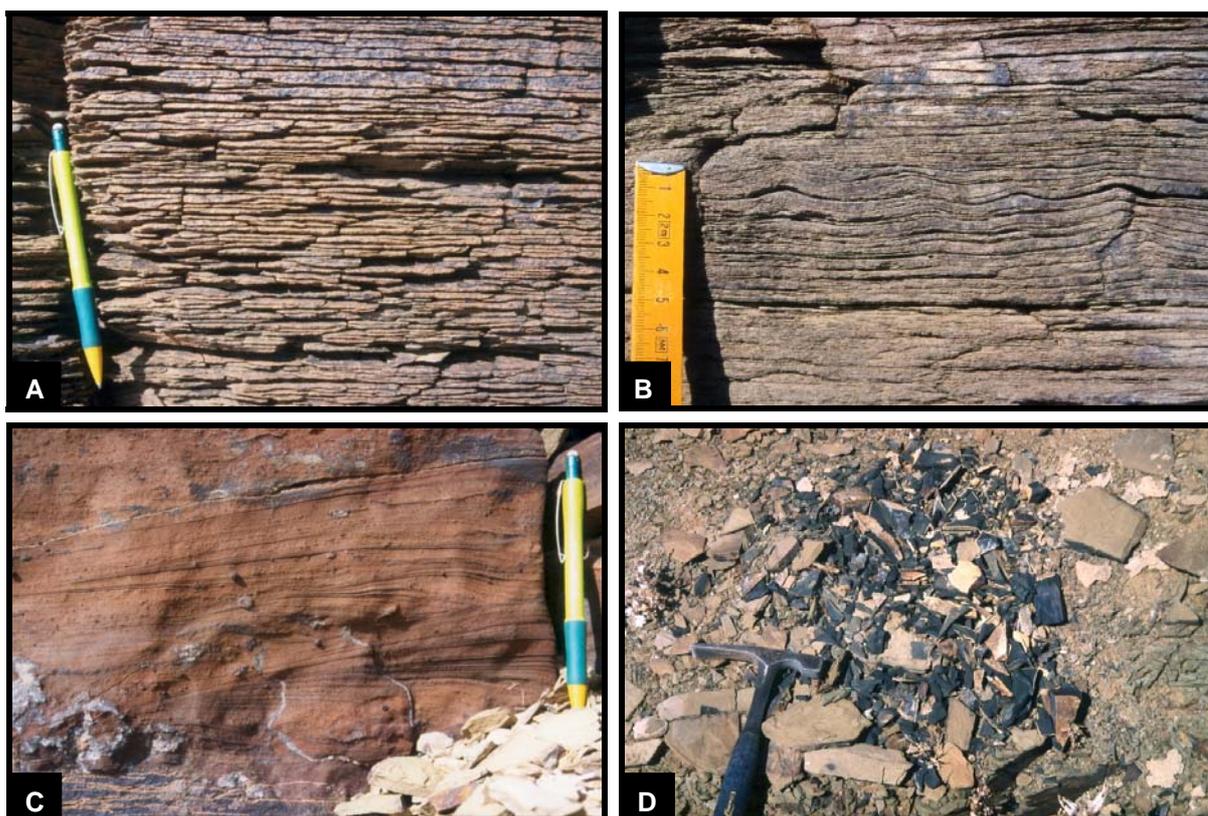
Fig. 2.39: The Inaub Sandstone at the Ai-Ais road locality: **(A)** The lower part of the sandstone is characterized by plane lamination. **(B)** In the middle part wavy lamination is present. **(C)** In the upper part hummocky cross-stratification dominates, which is well visible in brownish carbonate concretions. **(D)** Black phosphatic shale lens at the base of the Inaub Sandstone.

Locally, the Inaub Sandstone is very rich in plant debris and black permineralized wood fragments. However, here and there leaves and other parts of plants are exceptionally well preserved (Fig. 2.40-A to H). The measurement of the long axis of plant fragments shows a slightly preferred NW-SE orientation (Fig. 2.41) similar to the plant fragment orientation in the Polisiewater Chert (Fig. 2.29). The sedimentary structures, the vertical succession and the abundance of plant fragments suggest that the Inaub Sandstone is mainly of a tempestitic origin. The thickness distribution indicates that it forms a northward thinning, fan-, lobe- or tongue-shaped sedimentary body with a southerly source area, very similar to the Polisie-water Chert.
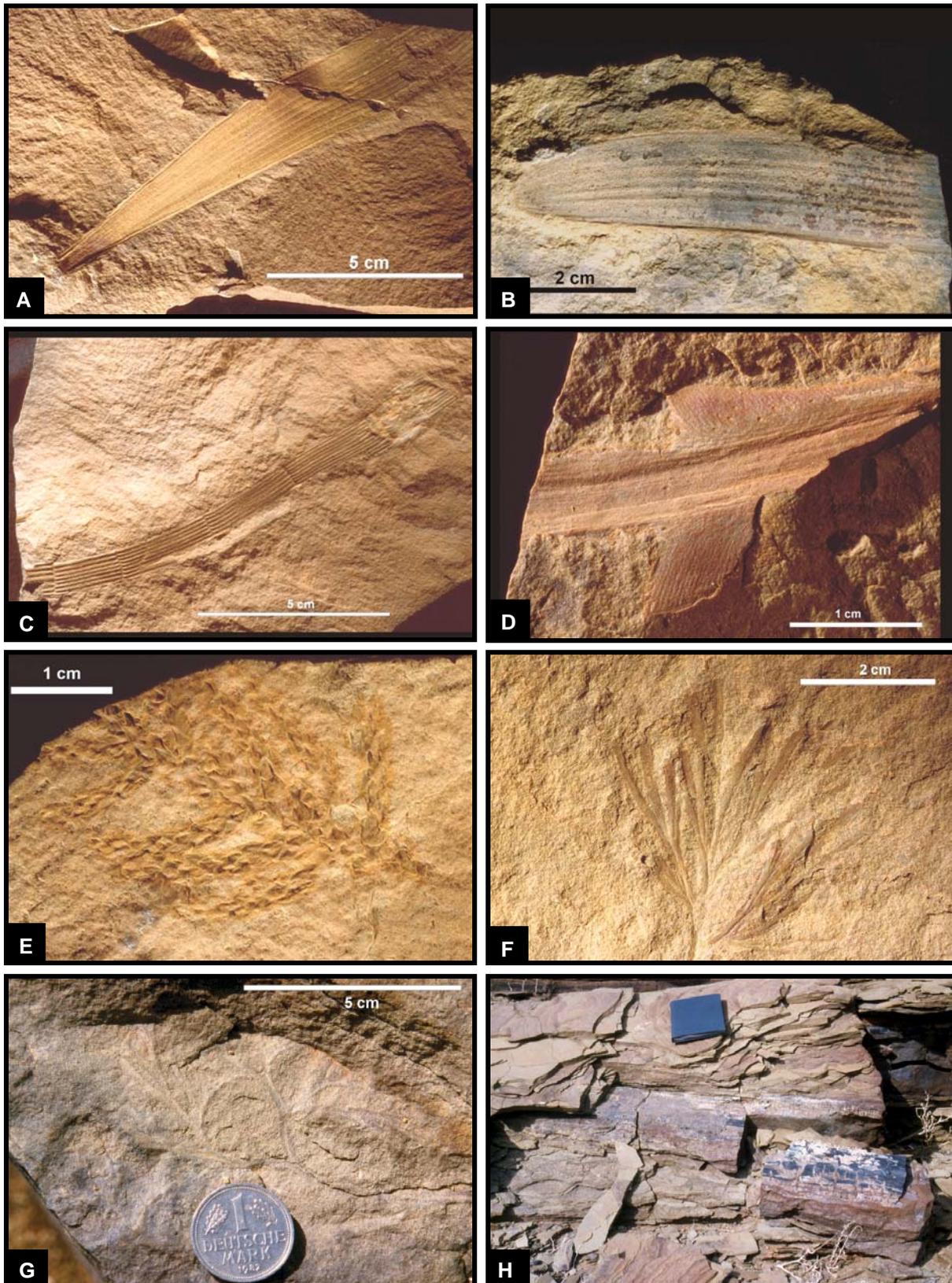
Fig. 2.40: Plant fossils from the Inaub Sandstone Bed: **(A) & (B)** Leaves of a cordaitean tree (*Noeggerathiopsis*). **(C)** Segmented trunk of the sphenopsid plant *Paracalamites*. **(D)** Fragment of a *Glossopteris* leave. **(E)** Undetermined conifer branch. **(F)** Dichotomising leavy twig of undetermined affinity. **(G)** Another dichotomising leavy twig. **(H)** Black permineralized wood.
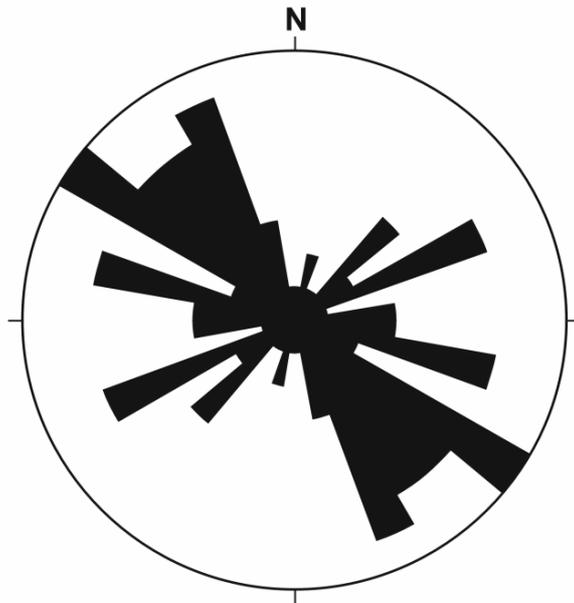
n=63
largest petal: 8.00 Values
largest petal: 12 % of all values
Strike Direction: 10° classes

Fig. 2.41: Measurements of the long axis of plant fragments in the Inaub Sandstone at the Ai-Ais road locality. The rose diagram shows that the plants are preferentially oriented in NW-SE direction, however other orientations are also quite common.

In satellite images it can be seen that above the Inaub Sandstone two or three more sandy layers, which are less pronounced, follow in an upward-thinning and possibly upward-fining fashion. The following shale succession is not very well exposed and has not been studied in detail. Only below a thin dolerite sill below the Dickneus, which is the southernmost peak of the Amibberg Mountains (Fig. 2.32), outcrops provide a good insight into the lithological nature of the middle part of the Aussenkjer Formation. There, thin, 5-10 cm thick, silty-sandy, micaceous, and slightly carbonate-cemented shale bands, probably representing very distal turbidites, are rhythmically interbedded in muddy shales (Fig. 2.42-A). Above the thin dolerite sill the greenish shales of the upper part of the Aussenkjer Formation contain numerous yellowish-brownish carbonate concretions (Fig. 2.42-B), which exhibit sedimentary structures excellently due to weathering. Sedimentary structures that are very common are plane to wavy lamination, starved ripples and ripple cross-lamination (Fig. 2.42-C to E) as well as bioturbation features. The uppermost part of the Aussenkjer Formation is composed of stacked, low-order coarsening-upward cycles in which bluish-grey silty shales grade upward into greenish-grey, bioturbated, plane-laminated siltstones and ripple cross-bedded fine-grained sandstones of distal turbidite origin (Fig. 2.42-F). From one locality below the Dickneus the dip direction of ripple forsets have been measured. The rose diagram in Fig. 2.43 shows that current directions towards the NW prevail, which is in accordance with the predominantly NW-SE orientation of plant fragments in the Polisiewater Chert and the Inaub Sandstone.
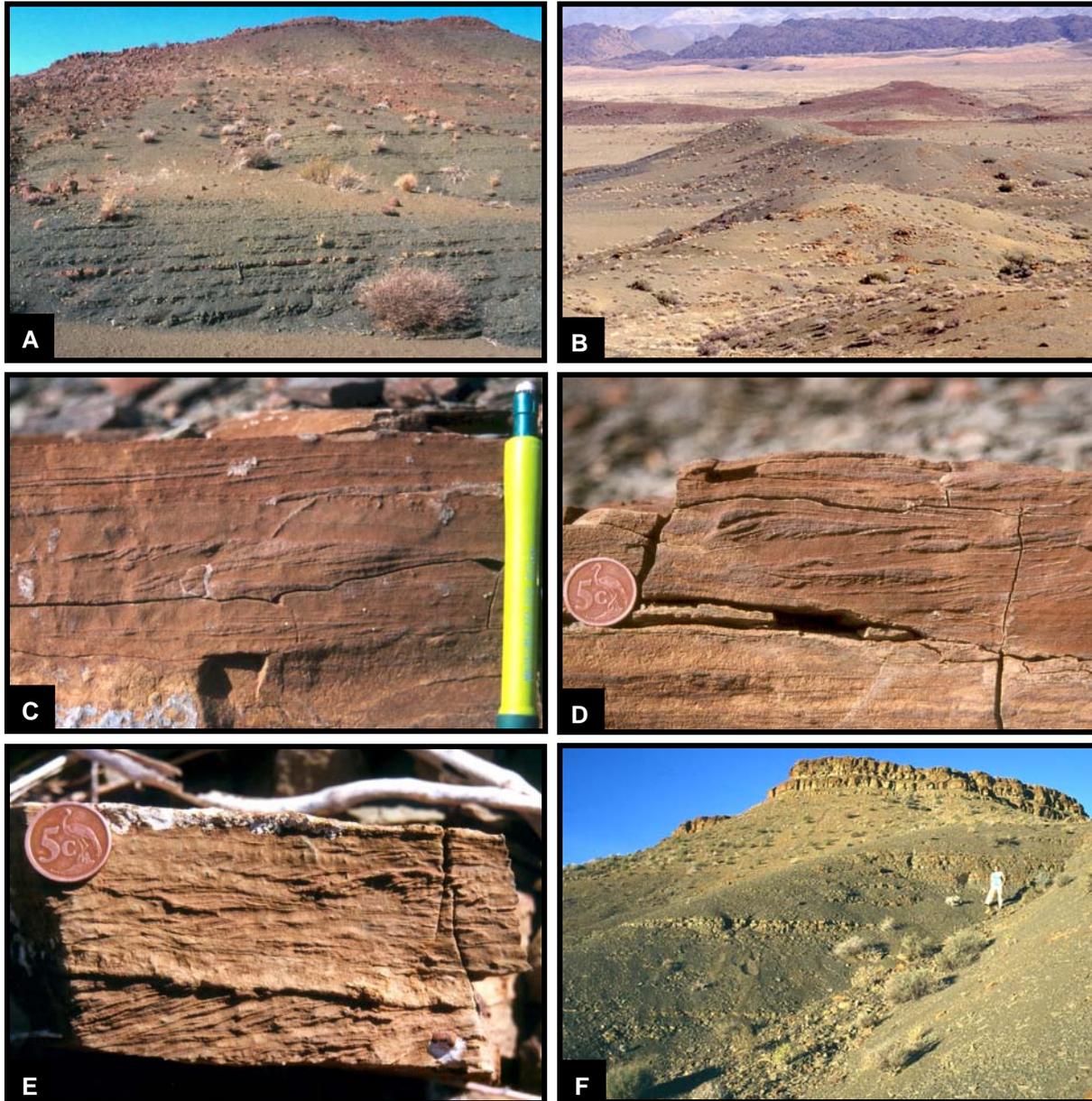
Fig. 2.42: Higher part of the Aussenkjer Formation: **(A)** Silty-sandy, micaceous, and slightly carbonate-cemented shale bands, probably representing very distal turbidites, are rhythmically interbedded in muddy shales. Outcrop below a dolerite sill west of the Dickneus (Fig. 2.32). **(B)** Above a dolerite sill greenish shales of the upper part of the Aussenkjer Formation contain numerous yellowish-brownish carbonate concretions exhibiting sedimentary structures. **(C) & (D)** Starved sand ripples within carbonate-cemented mudrocks. **(E)** Flaser bedding, plane lamination and ripple cross-lamination in carbonate-cemented silt-/sandstone. **(F)** Stacked, low-order coarsening-upward cycles in which bluish-grey silty shales grade upward into greenish-grey, bioturbated, plane-laminated siltstones and ripple cross-bedded, fine-grained sandstones of distal turbidite origin. Picture shows the upper-most part of the Aussenkjer Formation below the basal part of the Amibberg Formation represented by the sandstone cliffs in the background.
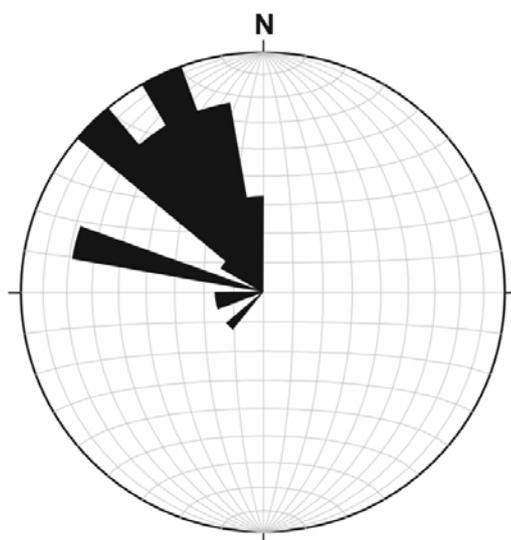
n=28
largest petal: 5.00 Values
largest petal: 17 % of all values
Dip Direction: 10° classes

Fig. 2.43: Dip directions of ripple foresets from sandstones in the uppermost part of the Aussenkjer Formation below the Dickneus. The data indicate prevailing south-easterly current directions, which is in accordance with the predominantly NW-SE orientation of plant fragments in the Polisie-water Chert and the Inaub Sandstone.

Approximately 20 m below the base of the Amibberg Formation, defined by the base of the first major sandstone succession of the Amibberg (AMB-Sst.1), a very conspicuous shale layer occurs below the Dickneus Peak at the southern tip of the Amibberg Massif. This shale layer lies on the top of the first conspicuous coarsening-upward parasequence below the first sandstone complex of the Amibberg Formation, which itself forms another coarsening-upward parasequence but composed of more proximal deposits (Fig. 2.44-A/B). The mentioned shale layer is composed of mixed muddy, silty, and sandy material and is stronger indurated than the over- and underlying shales. Pre-existing sedimentary structures have almost been completely obliterated due to extreme bioturbation. On the upper surface mainly two types of trace fossils are well preserved. One type represents ribbon-like, flattened, endostratal traces with three lobes on the upper surface (Fig. 2.45-A/B). These traces can be ascribed to the ichnogenus *Curvolithus* (cf. Buatois et al., 1998). The other type is a trace fossil, which consists of a row of meniscate bends and which has been found also in South Africa in stratigraphically equivalent upper Ecca Group deposits (Anderson, 1974; Wickens, 1984 & 1996; Rubidge et al., 2000). Anderson (1974) first briefly mentioned this curious trace fossil and compared (not interpreted!) it to *Plagiogmus*. Since then this trace fossil was in later publications repeatedly - but wrongly - ascribed to *Plagiogmus*. A comparison with descriptions of *Plagiogmus* from Cambrian rocks revealed that the Namibian and South African '*Plagiogmus*' must be a different trace fossil (M. Schlirf, pers. comm., 2001). For practical purposes this enigmatic trace fossil is here informally called '*Pseudo-Plagiogmus*'. On top of the mentioned shale layer *Pseudo-Plagiogmus* is morphologically quite variable (Fig. 2.45-C to F). Two further specimens from the Tierberg Formation in South Africa, found in the vicinity of Kimberley, are illustrated in Fig. 2.45-G/H. Most forms actually consist of a

row of bended knobs or contain lobated rows, which appear to be covered by scratch marks resembling at first glance clusters of small *Rusophycus* (Fig. 2.46). However, these traces are undoubtedly positive epireliefs. Initially this trace fossil was interpreted to be probably the result of the activities of an infaunal organism, with arthropods to be very likely the possible producers (Schlirf & Werner, 2001). However, polished specimens of the *Pseudo-Plagiogmus*-bearing shale have shown that this trace fossil is underlain by a succession of laminated sediment forming a box-like (in cross-section) or rail-like (in three dimensions) feature within an otherwise completely bioturbated shale (Fig. 2.45-E/F). The laminated part contains internal disconformities indicating phases of non-deposition and erosion. Only the uppermost 1-5 mm represent a bioturbated and reworked zone directly underlying the superficial part of *Pseudo-Plagiogmus* with its bended or lobated rows. Fault-like micro-structures and displacements within the laminated part show that the laminated sediment must have been a cohesive and coherent substrate. A possible explanation of this structure could be that the laminated part actually represents a microbialite- or stromatolite-like structure produced by algal growth and algal binding of sediment (M. Schlirf, pers. comm., 2002). The uppermost reworked part probably could be a result of grazing activity of an invertebrate epifaunal organism. However, it is admitted that the genesis of this enigmatic structure is still not well understood. For example, it is quite puzzling, why the laminated part is preserved within a completely bioturbated sediment. The almost complete bioturbation and the position of this layer at the boundary between two coarsening-upward parasequences indicate that the top of this layer represents a flooding surface characterized by low sedimentation rates, starvation and condensation. In this context it can be speculated if the present-day recognizable strong induration of this shale layer could reflect early diagenetic cementation of siliciclastic sediment resulting in a firmground-like substrate.
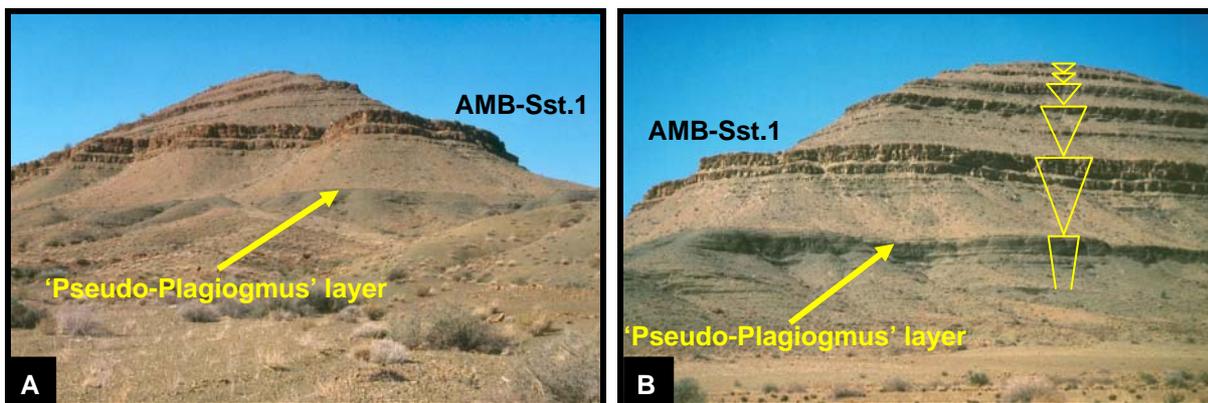
Fig. 2.44: (A) & (B) Flooding surface on top of a coarsening-upward parasequence below the first sandstone complex of the Amibberg Formation, which forms itself the top of a coarsening-upward parasequence. This flooding surface is composed of an almost completely bioturbated silty-sandy shale layer, which is covered by two types of trace fossils illustrated in Fig 2.45 (*Curvolithus* & *Pseudo-Plagiogmus*). The shown mountain is the Dickneus at the southern tip of the Amibberg Massif. Coarsening-upward parasequences are indicated by triangles.
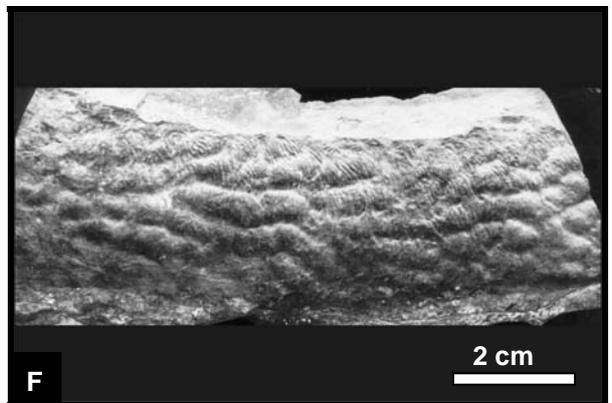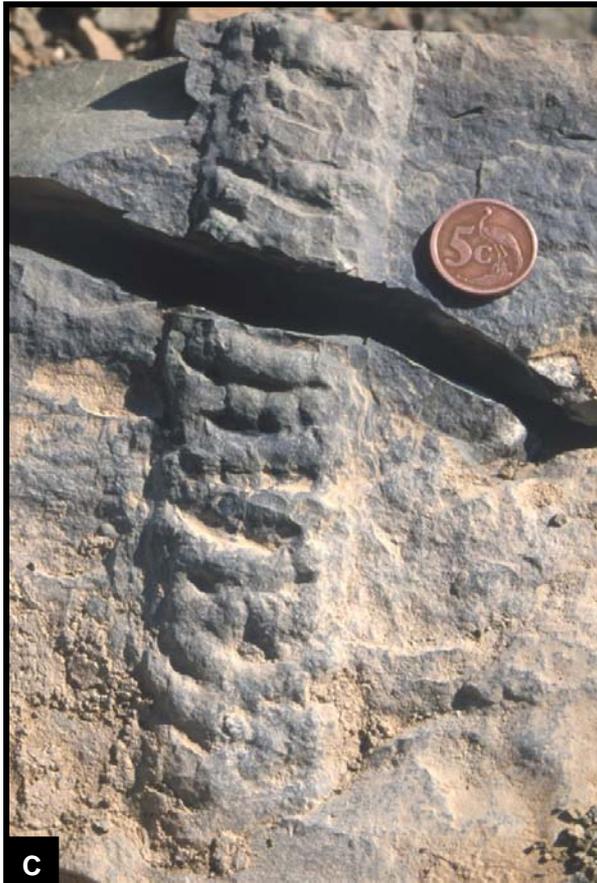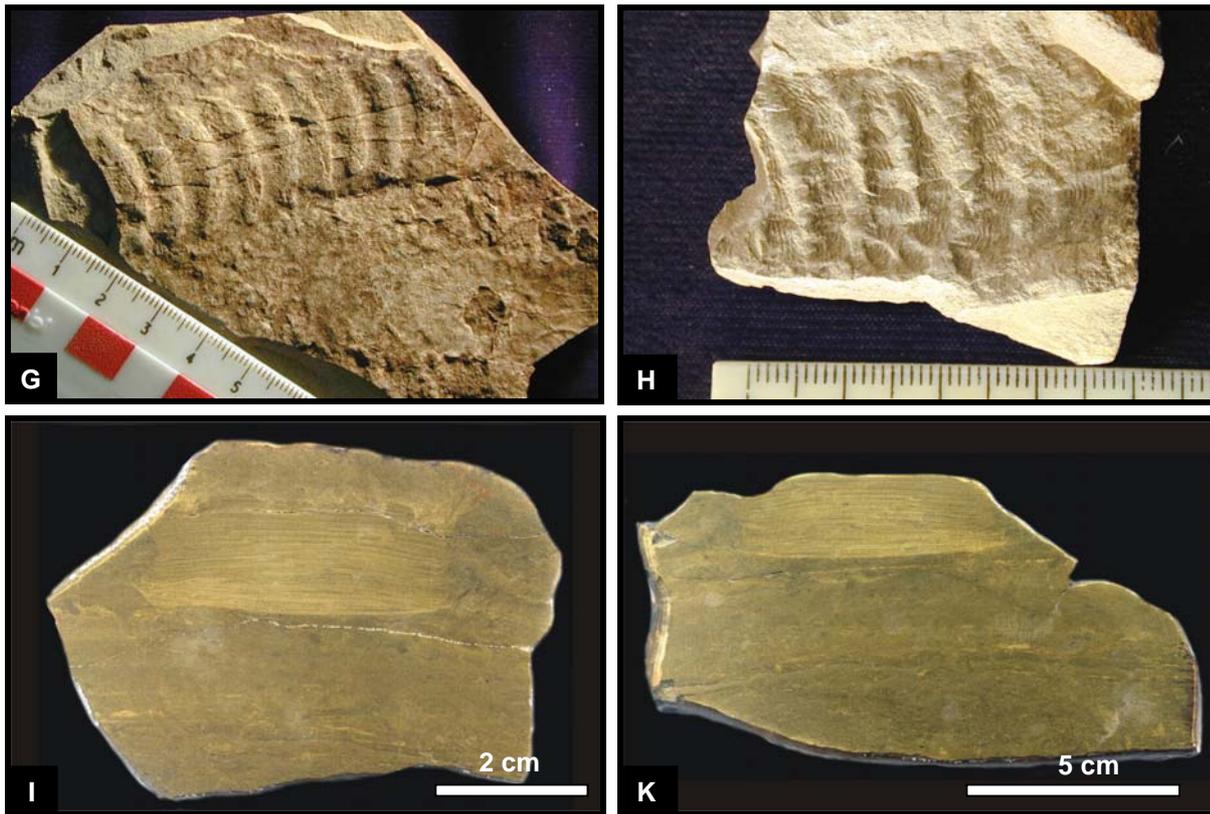
Fig. 2.45 (prev. and this page): (A) & (B) Ribbon-like, flattened, threelobate trace fossil probably representing the ichnogenus *Curvolithus*. Flooding surface in the uppermost part of the Aussenkjer Formation. **(C) to (F)** Several morphological variants of '*Pseudo-Plagiogmus*' found together with *Curvolithus* on a flooding surface between two coarsening-upward parasequences (transition area Aussenkjer-Amibberg Formation). **(G) & (H)** Two '*Pseudo-Plagiogmus*' specimens from the Aussenkjer-equivalent Tierberg Formation in South Africa. **(I) & (K)** Polished vertical cuts through '*Pseudo-Plagiogmus*' and the underlying shale. The polished sections show that the trace fossil is underlain by a box-shaped area, which is characterized by laminated sediment that is surrounded by a completely bioturbated shale. Only the upper part of the laminated area shows signs of reworking and bioturation (I).
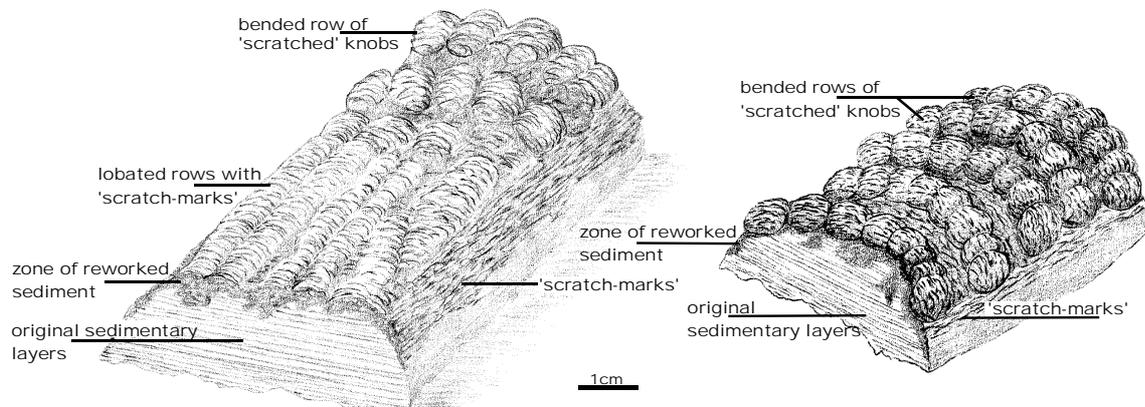
Fig. 2.46: Two morphological variants of the curious trace fossil, which is here referred to as '*Pseudo-Plagiogmus*'. It occurs in the Aussenkjer and Amibberg Formations (Upper Ecca Group) in southern Namibia, but was also found in Upper Ecca Group deposits in South Africa. Drawing by M. Schlirf (Schlirf & Werner, 2001).

The sequence-stratigraphic subdivision of the Aussenkjer Formation is shown in Fig. 2.30 and Fig. 2.47. Above the Polisiewater Chert transgressive black shales coarsen upward into olive green shales documenting a regressive development. These olive green shales are topped by a tempestitic mud pebble layer and locally fine-grained sandstone. Above these deposits the shales appear to become finer-grained and darker coloured indicating a transgressive phase. Consequently, a sequence boundary can be inferred on top of the tempestite layers. The helminthoid trace fossil layer and *Spirodesmos* within the Sesfontein Tuff above the tempestitic mud pebble layer indicate deep water conditions. The phosphatic shale above the Sesfontein Tuff could represent a possible candidate for the maximum flooding zone. The following part up to the Inaub Sandstone represents a progradational succession with a very thin tempestitic sandstone bed at the base and the Inaub Sandstone at the top. The latter itself is build up by several thickening-upward parasequences in the south and a shallowing-upward succession in the north. From satellite

Fig. 2.47: Sequence-stratigraphic subdivision of the Aussenkjer Formation in the area southwest of the Amibberg Massif.

images it is inferred that above the Inaub Sandstone several thinner and less conspicuous tempestite or turbidite beds follow in an upward-thinning fashion indicating a retrogradational trend. Consequently, another sequence boundary can be positioned at the stratigraphic level of the Inaub Sandstone. The retrogradational succession above the Inaub Sandstone, representing the middle part of the Aussenkjer Formation, is overlain by a progradational, coarsening- and shallowing-upward succession forming the upper part of the Aussenkjer Formation. The latter represents a succession of silty shales with intercalated sandstone lenses (starved ripples), grading into interbedded shales, siltstones, and parallel laminated

and ripple cross-bedded, fine-grained sandstones arranged in low-order coarsening-upward parasequences. The *Curvolithus/Pseudo-Plagiogmus* shale layer forms the top of the conspicuous, shaly coarsening-upward parasequence below the basal Amibberg sandstone packet (AMB-Sst. 1). The latter represents itself a coarsening-upward parasequence, however with more proximal deposits (shoreface sandstones) and a sequence boundary at the top. The top of the *Curvolithus/Pseudo-Plagiogmus* shale layer represents a flooding surface.

The Aussenkjer Formation of southern Namibia can be correlated with the dominantly argillaceous Tierberg Formation in the northwestern part of the South African Main Karoo Basin. Southward, the Tierberg-equivalent stratigraphic interval is subdivided into several argillaceous and arenaceous formations. Towards the east the major part of the Volksrust Formation is most probably a correlative of the Aussenkjer, respectively the Tierberg Formation (Johnson et al., 1997). On the Falkland/Malvinas Islands the Brenton Loch Formation is most probably partly a correlative of the Aussenkjer Formation, however, its lithology resembles more that of the southern Ecca facies of the South African Main Karoo Basin (basin floor turbidites) (Trewin et al., 2002). In the Brazilian Paraná Basin the lower part of the Teresina Formation can be considered largely equivalent to the Aussenkjer Formation.

2.3.5 Amibberg Formation

The Amibberg Formation consists both of sandstone- and shale-dominated intervals. Three major sandstone packages or complexes within the preserved succession form morphologically very conspicuous elements like mountain tops, sandstone cliffs and plateaus. Two major shale and mudrock successions with intercalated sandstone horizons are sandwiched between the three major sandstone complexes. The contact to the underlying Aussenkjer Formation is conformable and the boundary between the two formations was laid at the base of the first major sandstone complex. The sediments of the Amibberg Formation form in the Aussenkjer-Noordoewer area the NE-SW trending Amibberg Massif with the Dickneus Peak at its southwestern tip (Fig. 2.44-A/B). The Norotshama Peak and the Gemsbokberg form the northeastern extension of the Amibberg Massif (Fig. 2.48-A). Further outcrops of the Amibberg Formation can be found at the Tafelberg Mountains in the northwest of the Amibberg-Norotshama-Gemsbokberg mountain range. On top of the Hoenderknoppe some relictic sandstone patches of the basal Amibberg Formation may be preserved. Fig. 2.49-A to D shows the outcrops of the Amibberg Formation in the northern part of the Amibberg, at the Norotshama Peak, at the Tafelberg, and at the unnamed mountain north of the Tafelberg and south of the Ai-Ais gravel road (Fig. 2.48-A).

The arenaceous and argillaceous sediments of the Amibberg Formation were first briefly mentioned by Haughton & Frommurze (1927 & 1936) and later mapped as well as briefly described by Schreuder & Genis (1975). The term 'Amibberg Formation' was formally introduced by SACS (1980). The provisional Geological Map of Oranjemund (Becker & Schreiber, 1999) shows the distribution of the sandstones of the Amibberg Formation based on hand-coloured draft maps in the scale 1:50000 by C.P. Schreuder, G. Genis, and G.J. Beukes. Fig. 2.48-B shows a considerably improved map of the distribution of the three major sandstone complexes of the Amibberg Formation (mapped by the author of this thesis). The first, basal sandstone complex (AMB-Sst. 1) is best developed in the southern portion of the Amibberg, where it forms conspicuous cliffs and plateaus. Towards the northeast this basal sandstone complex loses its lithological and morphological character and peters out northeast of the Gemsbokberg. The second sandstone complex (AMB-Sst. 2) forms a small plateau at the southwestern end of the Amibberg and a circular plateau around dolerite intrusions in the northeastern part of the Amibberg. Furthermore, it forms another circular plateau around the Norotshama Peak. These outcrops continue towards the northeast forming a large inclined surface with the top of the Gemsbokberg at the northeastern end (Fig. 2.48-A/B). Within the Amibberg-Norotshama-Gemsbokberg mountain range the highest preserved stratigraphic level forms the top of the Norotshama Peak (basal succession above AMB-Sst. 3). The thickness of the preserved part of the Amibberg Formation, deduced from two compiled sections measured with a Jacob staff, sums up to about 250 m. The first section was measured in the southern part of the Amibberg including the Dickneus Peak and comprises the stratigraphic interval from the base of the first to the top of the second sandstone complex (Fig. 2.50-A). The second section was measured at the Norotshama Peak and comprises the succession from the top of the second sandstone complex to the top of the mountain, partly fringed and partly capped by the third sandstone complex (Fig. 2.50-B). So far, the Amibberg-Norotshama-Gemsbokberg succession has not yet been correlated with those of the Tafelberg region in the northwest. The shale-out of the basal sandstone complex (AMB-Sst. 1) in a northeasterly direction towards the Gemsbokberg resembles the pinch-out of the underlying Polisiewater Chert and Inaub Sandstone towards the northwest and the northeast. If the sedimentary body of the AMB-Sst. 1 complex shows the same geometry it can be speculated that the Tafelberg region lies in the area of a supposed northwestern shale-out of the basal Amibberg Formation sandstone complex. Consequently, the AMB-Sst. 1 complex could be missing or inconspicuous and for the succession of the Amibberg Formation a reduced thickness could be expected in the Tafelberg region. However, this has to be verified by future logging and mapping.

Fig. 2.48: (A) Satellite image of the Aussenkjer-Noordoewer area with the Amibberg-Norotshama-Gemsbokberg area representing the main outcrop area of the Amibberg Formation. Smaller outcrops of the Amibberg Formation can be seen towards the northwest in the Tafelberg Mountains area. The sandstones of the Aussenkjer Formation display in this image light orange-brown colours, whereas shales show bluish colours. The dark, brown to greenish coloured areas represent dolerite sills. The western part and the southeastern part of the shown area is composed of crystalline basement rocks. **(B)** Enlarged image of the central area shown in (A). Mapped on this satellite image are the outcrops of the three major sandstone complexes of the Amibberg Formation in the Amibberg-Norotshama-Gemsbokberg mountain range. Sandwiched between these major sandstone complexes are two successions of shaly mudrocks and intercalated sandstone horizons. The highest stratigraphic level (shales and sandstones c. 20 m above AMB-SSt. 3) is preserved at the Norotshama Peak. Sandstone complex AMB-SSt. 1 shows a shale-out towards the northeast in the Gemsbokberg area. A shale-out towards the northwest in direction of the Tafelberg Mountains is also suspected, however, correlation of the Amibberg Formation sequence of the Amibberg-Norotshama-Gemsbokberg area with that of the Tafelberg area has not yet been achieved to verify this assumption.
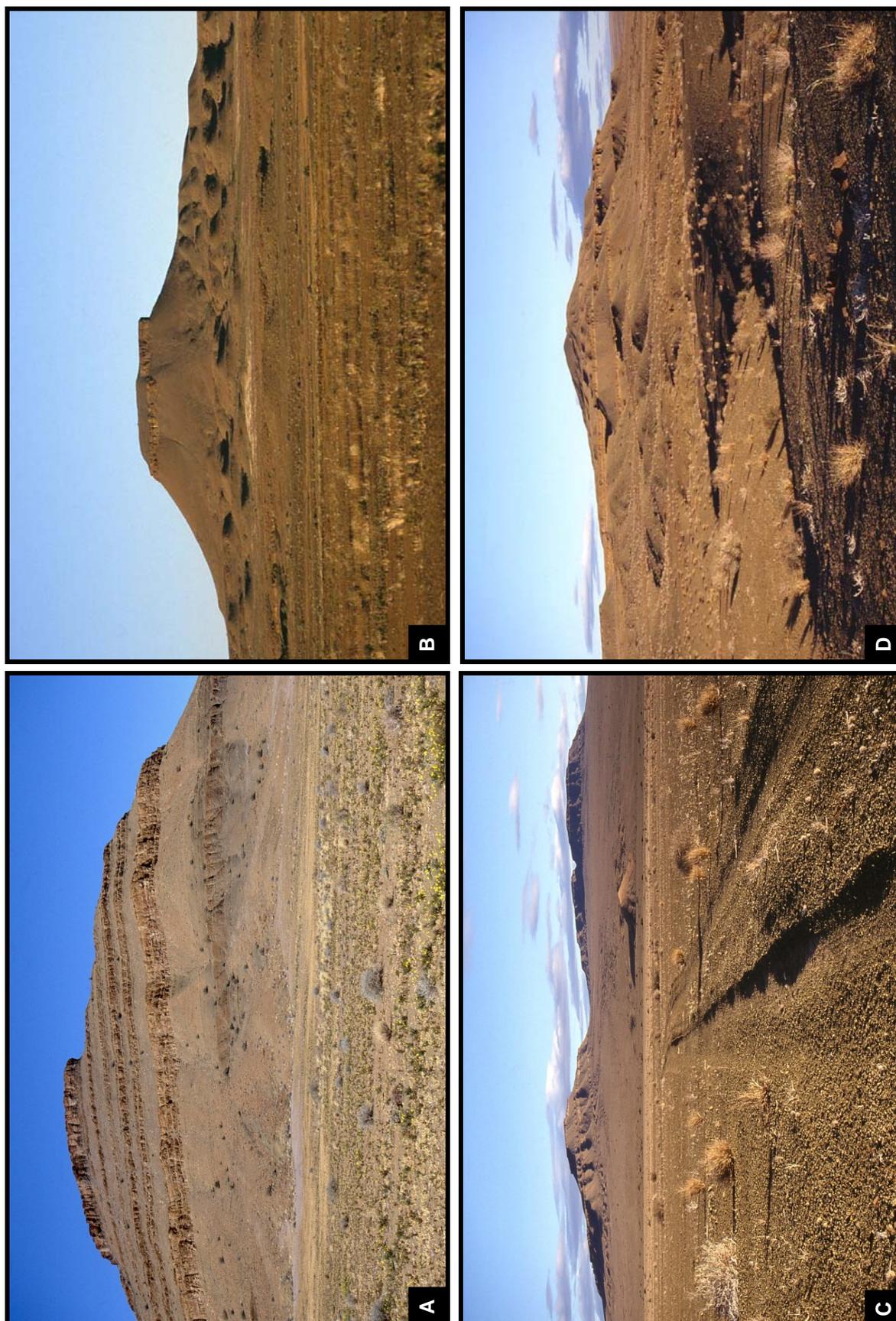
Fig. 2.49: Principal outcrop areas of the Amibberg Formation consisting of intercalated shale and sandstone successions: **(A)** Northern part of the Amibberg. View towards SE. **(B)** Norotshama Peak. View towards NE. **(C)** Tafelberg Mountains. View towards E. **(D)** Unnamed mountain north of the Tafelberg Mountains and south of the Ai-Ais gravel road. View towards ENE.
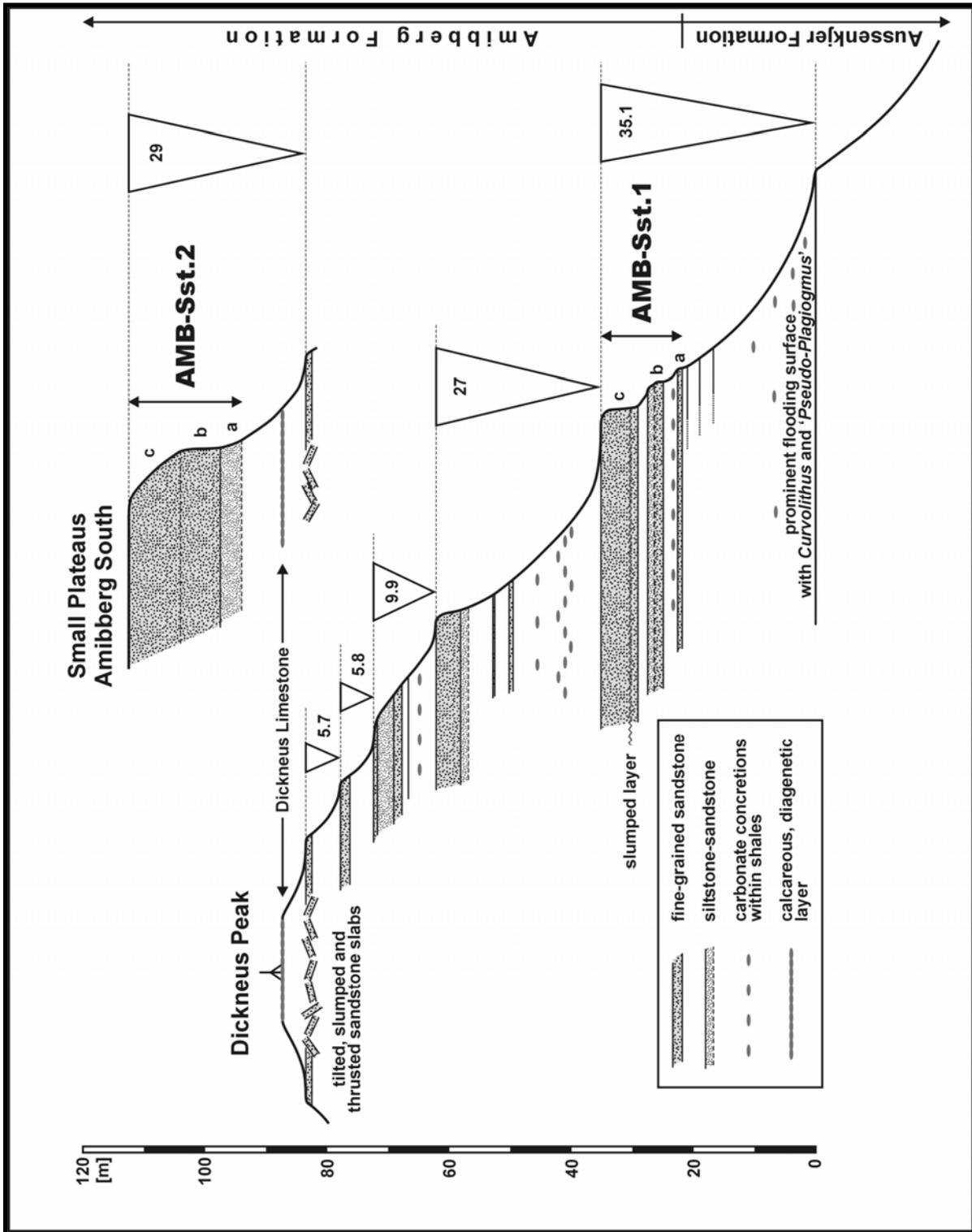
Fig. 2.50: (A) Section of the lower part of the Amibberg Formation measured at the southern end of the Amibberg (Dickneus section). The base of the first thicker sandstone layer (80-90 cm) above the prominent flooding surface with *Curvolithus* and *Pseudo-Plagiogmus* was arbitrarily taken as the base of the Amibberg Formation. The so-called Dickneus Limestone forms the most important marker layer, which can be traced laterally at least up to the Norotshama. Triangles indicate coarsening- and shallowing-upward cycles or parasequences and the number within or next to the triangles indicates the thickness of them. Fig. 2.44-A/B shows the Dickneus Peak seen from the SW and the SE. Fig. 2.51-A shows the sandstone-shale successions of the Amibberg Formation at the southwestern flank of the Dickneus corresponding to the Dickneus section above.
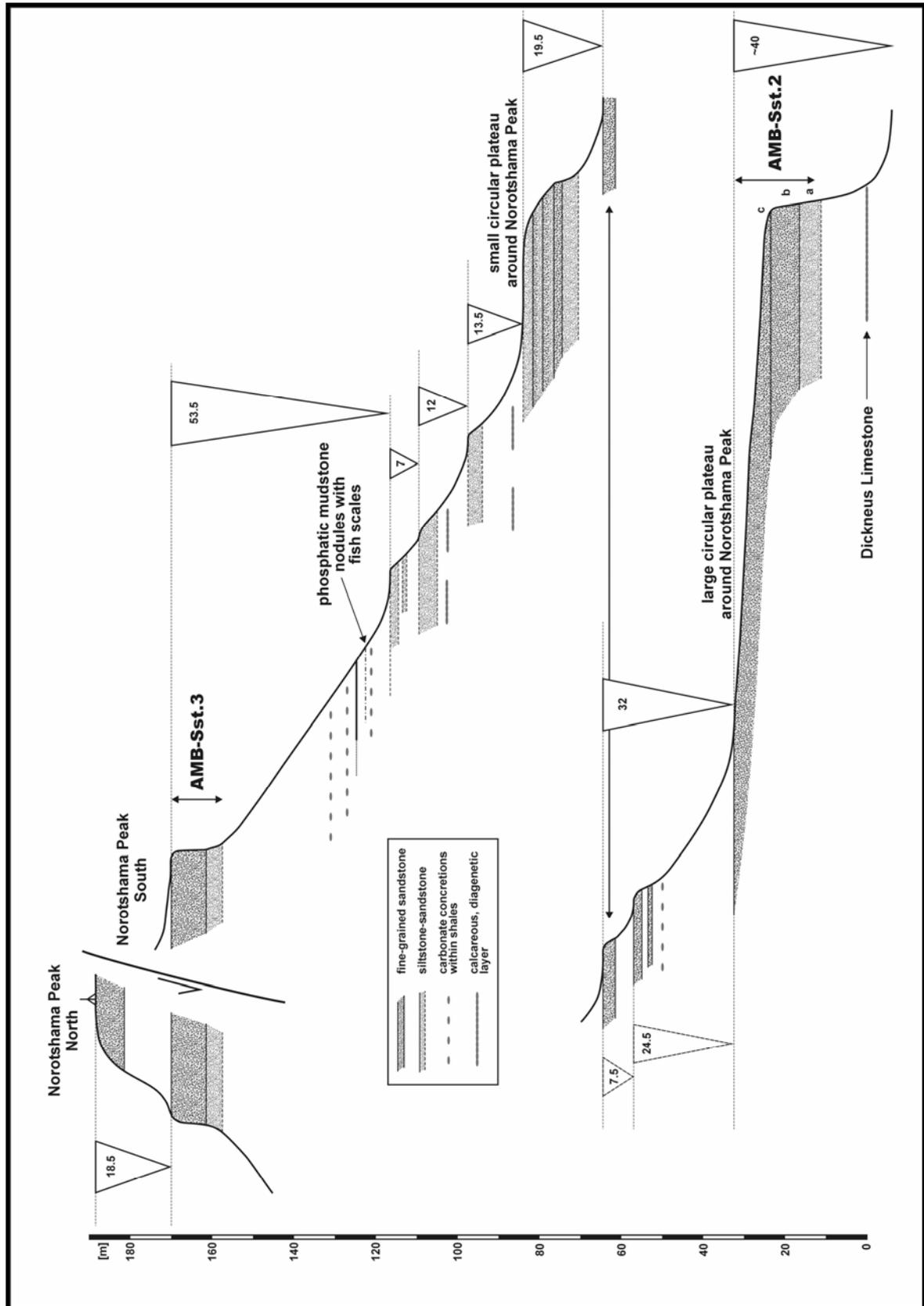
Fig. 2.50: (B) Section of the upper part of the Amibberg Formation measured at the Norotshama Peak (Norotshama section). Triangles indicate coarsening- and shallowing-upward cycles or parasequences and the number within or next to the triangles indicates the thickness of them. This section is linked with the Dickneus section (Fig. 2.49-A) via the Dickneus Limestone. The highest preserved stratigraphic interval forms the northern part of the Norotshama Peak, which is separated from the southern part by a normal fault (see also Fig. 2.60-A).

Within the Dickneus section the lower part of the Amibberg Formation is composed of a number of coarsening-upward parasequences with shales at the base and sandstones at the top (Fig. 2.50-A & 2.51-A). Calcareous concretions occur mainly within the lower to middle shaly part of these parasequences but are also common at their sandy top. Below the Dickneus Peak the lowermost parasequence above the *Pseudo-Plagiogmus* layer shows the highest total thickness as well as the thickest and most prominent sandstone packet at its top, here called AMB-Sst. 1 (Fig. 2.51-A). In upward direction, towards the top of the Dickneus Peak, these parasequences as well as the capping sandstone layers become successively thinner (Fig. 2.50-A). Above the prominent flooding surface with *Curvolithus* and *Pseudo-Plagiogmus* greenish-grey shales grade upward into sandy siltstones, which contain thin (1-15 cm) interbeds of fine-grained sandstones. The following AMB-Sst. 1 complex is composed of three reddish-brown weathering, upward-thickening sandstone layers (AMB-Sst. 1-a, -b, and -c), which are separated by two greenish-grey interlayered mudstone-sandstone intervals (Fig. 2.51-B/C). In the Dickneus section AMB-Sst. 1a has a thickness of 75 cm, AMB-Sst. 1b a thickness of 2.55 m, and AMB-Sst. 1c a thickness of 6.05 m.
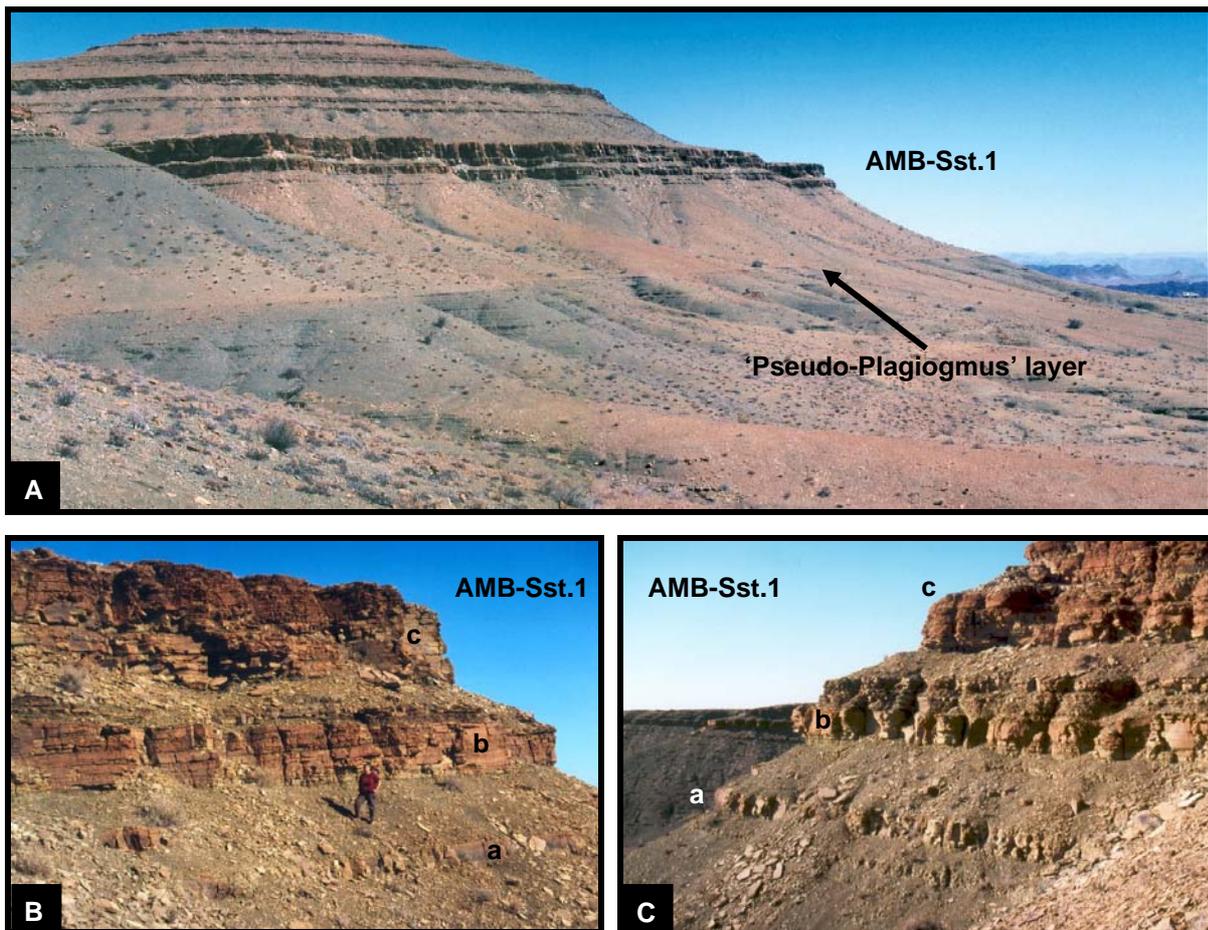
Fig. 2.51: (A) The western flank of the Dickneus Peak at the southwestern end of the Amibberg. In the lower third of the photo the prominent flooding surface with *Curvolithus* and *Pseudo-Plagiogmus* can be seen. The overlying coarsening-upward parasequence is topped by the AMB-Sst. 1, which forms the most prominent sandstone complex below the Dickneus Peak. **(B) & (C)** AMB-Sst. 1 itself is composed of three thickening-upward sandstone layers, which are separated by two greenish-grey interlayered mudstone-sandstone intervals.

The finer grained interlayers between the sandstone layers of AMB-Sst. 1 are composed of alternating mudstones and fine-grained sandstone layers and lenses. Bioturbation within these deposits is commonly very intensive. The mudstones show flaser and lenticular bedding or can be massive due to bioturbation, whereas the sandstones show plane lamination, climbing ripple and hummocky cross-lamination (Fig. 2.52-A to D). In places, successions of fining-upward units can be seen, which are characterized by light coloured, sharp-based, plane laminated to hummocky cross-laminated sandstones that grade into dark coloured, intensively bioturbated mudstones with thin intercalations of sandstone layers or lenses (Fig. 2.52-B). The sand-mud-mixture, the sedimentary structures and the intensive bioturbation indicate that these sediments were deposited most probably in a lower shore-face environment. The hummocky cross-laminated sandstones represent tempestites and indicate deposition above storm wave base.
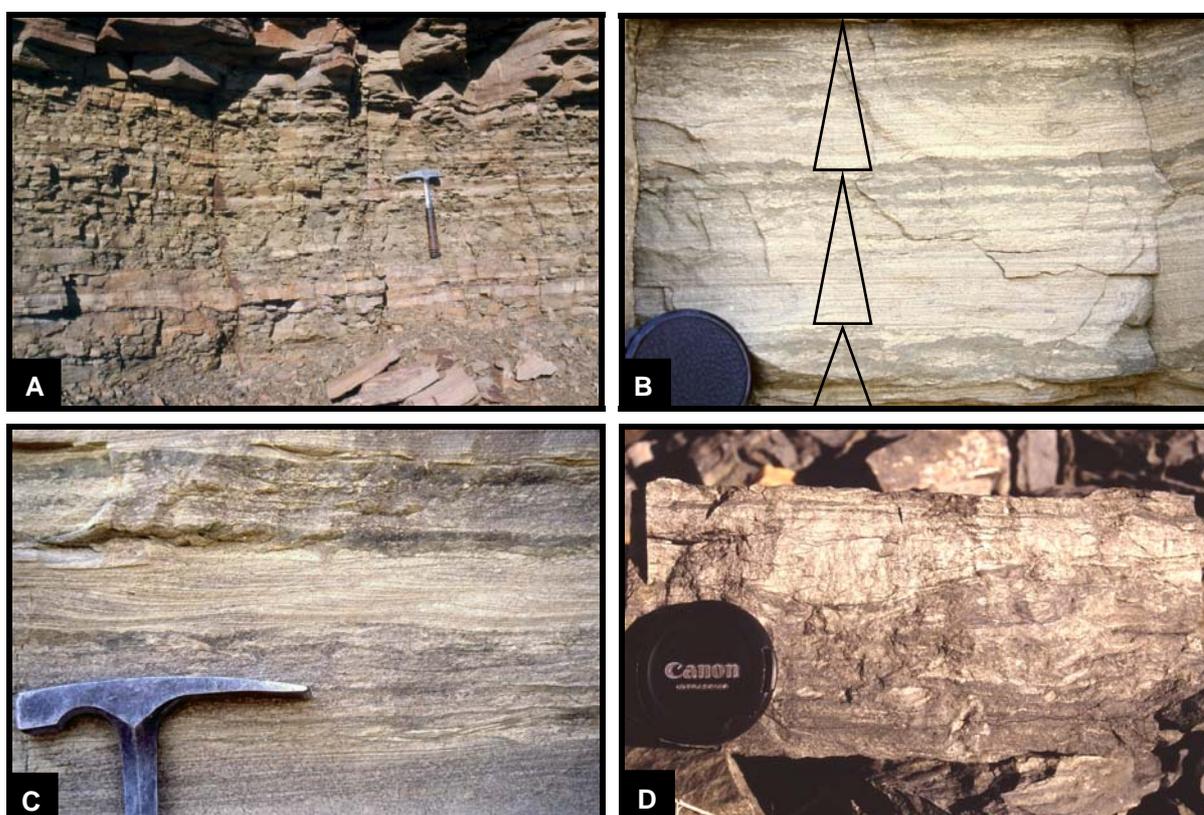
Fig. 2.52: Lower shoreface deposits of the Amibberg Formation: **(A)** Alternating mudstones and fine-grained sandstones layers. **(B)** Succession of fining-upward units with light coloured, sharp-based, plane laminated to hummocky cross-laminated sandstones of tempestitic origin grading into dark coloured, intensively bioturbated mudstones with thin intercalations of sandstone layers or lenses. **(C)** Climbing ripple cross-laminated sandstone layer within flaser-bedded and plane laminated sandstones and sandy siltstones. **(D)** Intensive bioturbation causes in places an intimate mixture of sandy and muddy substrate.

The sandstones of AMB-Sst. 1 are mainly fine-grained to transitionally fine- to medium-grained. The first sandstone layer (AMB-Sst. 1a) appears at first sight massive and completely bioturbated, however, here and there some relicts of parallel lamination and ripple cross-lamination can be detected. AMB-Sst. 1b consists of two subunits (Fig. 2.53-A). The lower part is composed of plane to wavy parallel laminated sandstones, which grade upward into low angle, hummocky cross-stratified sandstones (Fig. 2.53-B). The basal contact to the underlying mudstones-sandstones is quite variable. At some places the contact can be somewhat gradual (Fig. 2.52-A), whereas at other places the contact is quite sharp (Fig. 2.53-B). Within the lower part of AMB-Sst. 1b also stacked and alternating layers of plane laminated, ripple cross-bedded, and hummocky cross-stratified sandstones can be observed (Fig. 2.53-C). The upper part of AMB-Sst. 1b is characterized by alternating mudstones and thin, wave ripple-topped sandstone layers (Fig. 2.53-D). The whole succession of AMB-Sst. 1b represents a fining-upward succession of plane laminated and hummocky cross-stratified tempestitic sandstones of upper shoreface origin grading into alternating mudstones and wave-rippled sandstones of a middle shoreface origin.
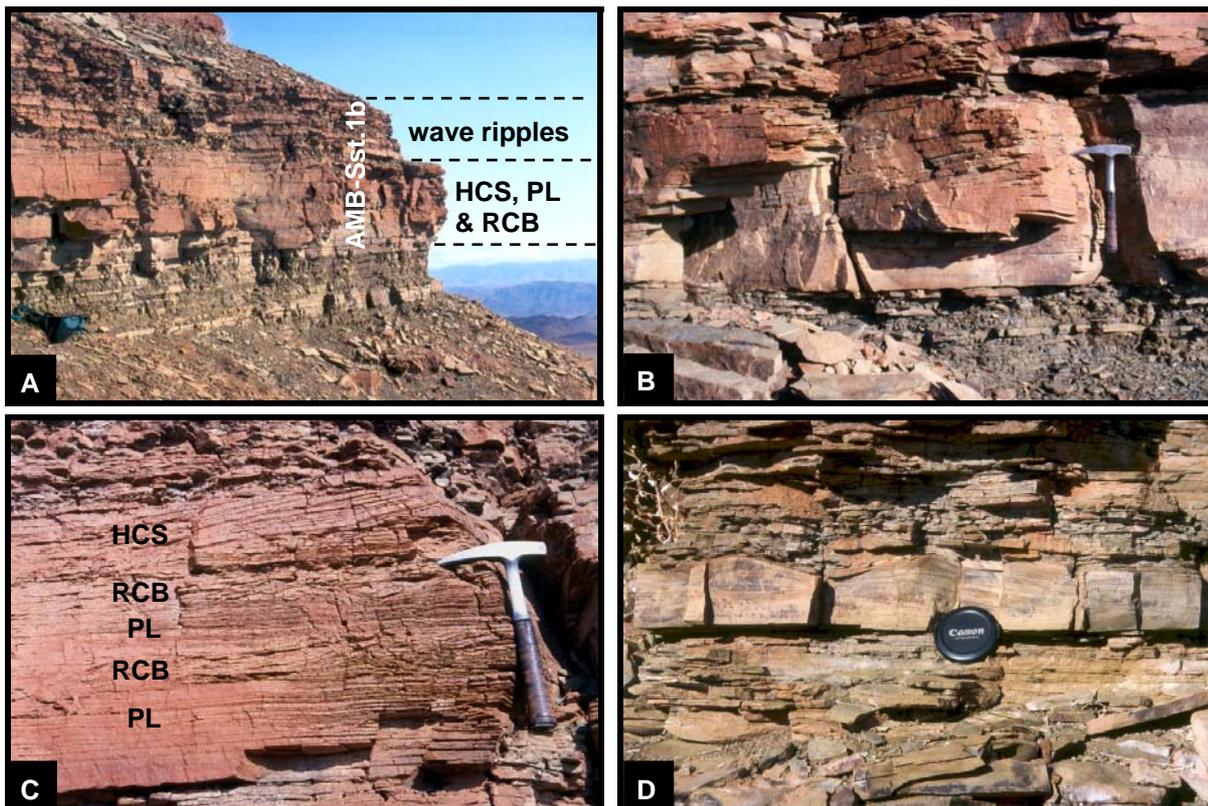
Fig. 2.53: Middle and upper shoreface deposits of the Amibberg Formation: **(A)** AMB-Sst. 1b is composed in its lower half of hummocky cross-stratified (HCS), plane laminated (PL), and ripple cross-bedded (RCB) sandstones of upper shoreface origin. The upper half is characterized by alternating mudstones and wave-rippled sandstone layers of a middle shoreface origin. **(B)** Low angle hummocky cross-stratified sandstone of upper shoreface origin in the lower half of AMB-Sst. 1b. **(C)** Stacked units of plane laminated (PL), ripple cross-bedded (RCB), and hummocky cross-stratified (HCS) sandstones of upper shoreface origin at the top of the lower half of AMB-Sst. 1b. **(D)** Wave-rippled sandstone layer within mudstones in the upper half of AMB-Sst. 1b (middle shoreface).

AMB-Sst. 1c represents a circa 6 m thick sandstone succession, which consists mainly of amalgamated tempestite layers characterized by plane lamination and hummocky cross-stratification. Thin ripple cross-bedded sandstone units also occur in places within the tempestite succession. Less frequently are thin intercalations of wave-rippled sandstone layers within sandy mudstones. Distributed throughout the tempestite sandstones are mud pebble layer or lenses. In the lower third of AMB-Sst. 1c a conspicuous slumped sandstone layer occurs (Fig. 2.54-A/B). Deformation structures due to dewatering can be observed in the uppermost part of AMB-Sst. 1c. Such dewatering structures are also very common in the thinner sandstone horizons above AMB-Sst. 1 (Fig. 2.54-C/D). Furthermore, these fine-grained sandstones display mainly sedimentary structures such as plane lamination, hummocky cross-stratification as well as climbing and wave ripple cross-lamination (Fig. 2.54-E/F). These sandstones also represent storm layers, which are interbedded in mudstones of offshore to lower shoreface origin.
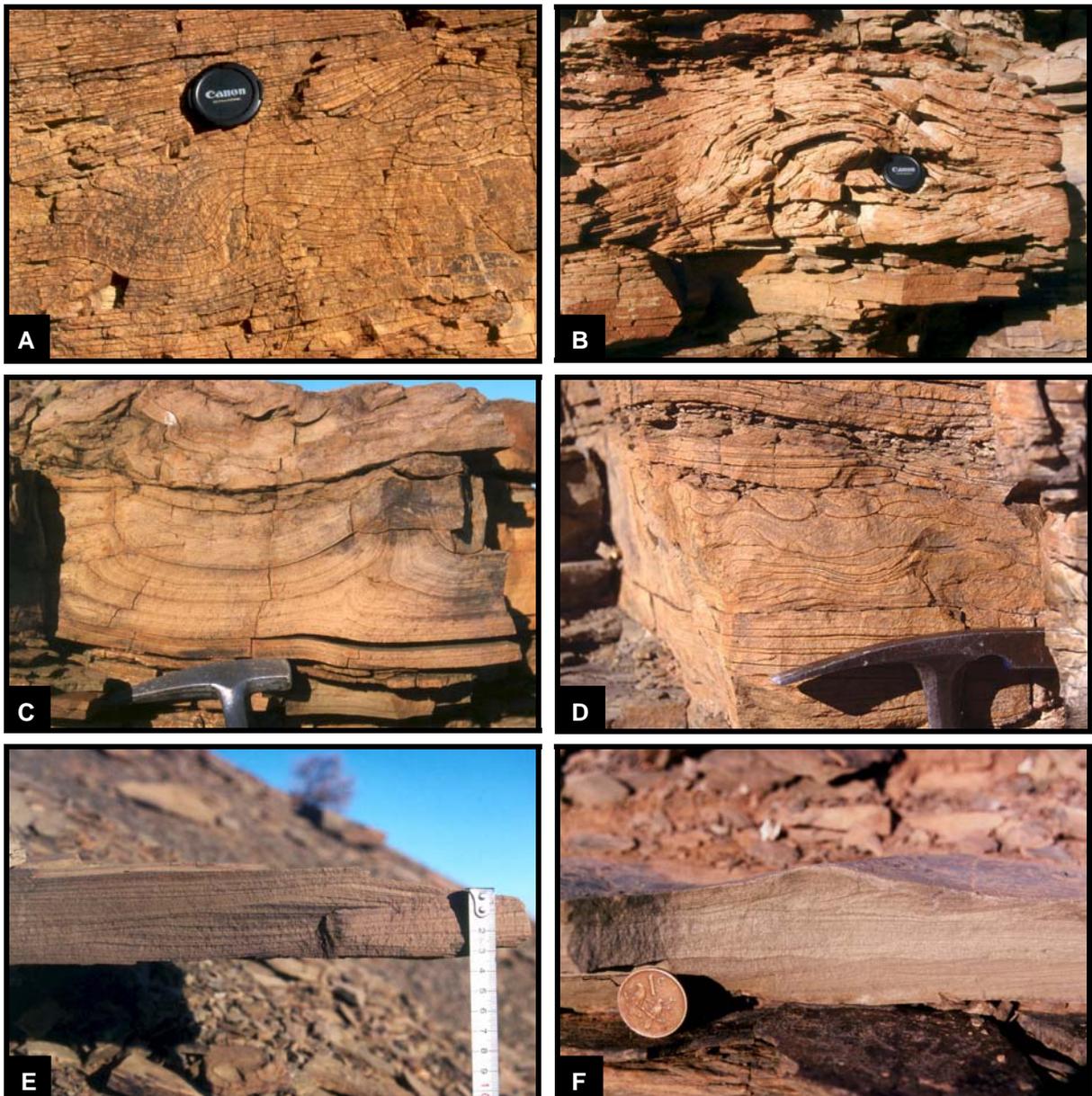
Fig. 2.54 (prev. page): (A) & (B) Conspicuous, slumped sandstone layer in the lower part of AMB-Sst. 1c. **(C) & (D)** Synsedimentary deformation structures due to dewatering are very common in the thinner storm sandstone layers between AMB-Sst. 1 and 2. **(E)** Climbing ripple cross-lamination and **(F)** wave ripple cross-lamination in storm sandstone layers.

About 4.5 m below the top of the Dickneus a circa 1 m thick sandstone layer is disrupted into metre-sized slabs, which are tilted, deformed and even thrusted on top of each other due to slumping and sliding (Fig. 2.50-A and 2.55-A/B). This layer froms a quite conspicuous marker horizon that can be followed from Dickneus Peak northward at least up to the dolerite intrusions in the middle of the Amibberg Massif (Fig. 2.48). It can be speculated that possibly an earthquake has triggered and caused this intensive disruption and disintegration of this sandstone layer. The dip of 25 tilted sandstone slabs around the Dickneus has been measured, however, no obvious systematics in the tilt direction can be seen (Fig. 2.56).
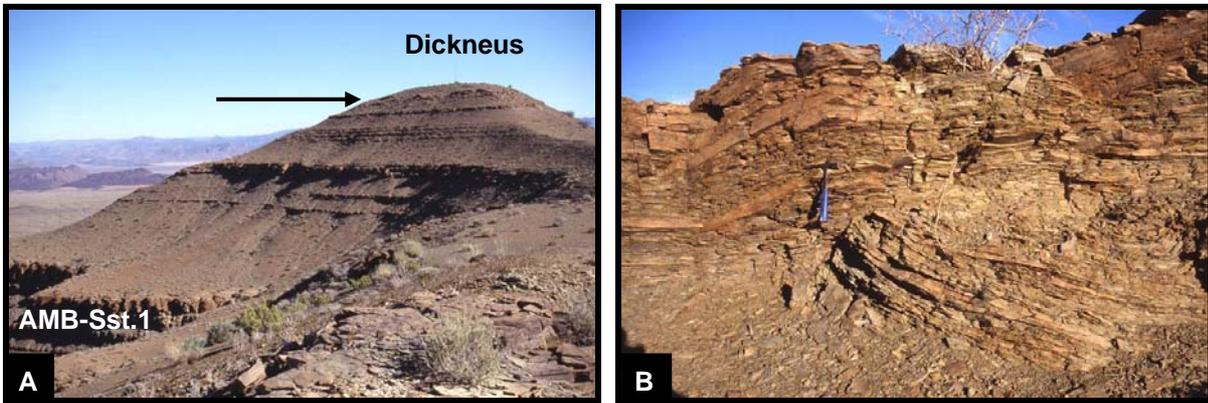
Fig. 2.55: (A) About 4.5 m below the top of the Dickneus a circa 1 m thick sandstone layer (indicated by the arrow) is completely disintegrated into metre-sized slabs, which are tilted and deformed due to slumping. **(B)** Within this layer tilted sandstone slabs are in places thrusted on top of each other.
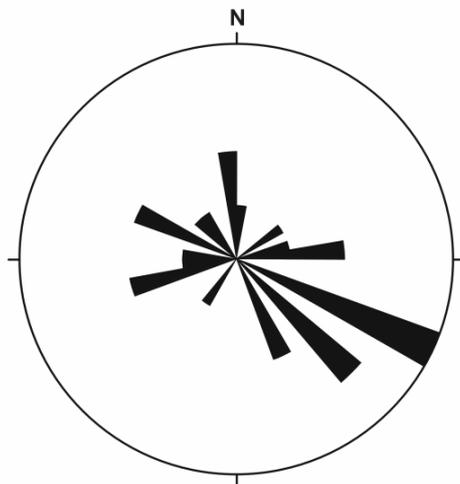
n = 25
largest petal 4.00 values
largest petal 16% of all values
Dip Direction: 10° classes

Fig. 2.56: Rose diagram showing the dip directions of 25 tilted sandstone slabs from the slumped layer circa 4.5 m below the Dickneus Peak.

The small plateau-like top of the Dickneus Peak is formed by a very hard and resistant, highly calcareous diagenetic layer, which is here informally called 'Dickneus Limestone' (Fig. 2.57-A). It weathers yellowish-brown but the fresh rock is almost black. This calcareous layer has a thickness of about 10 cm and forms a more or less continuous bed, which has been traced from the Dickneus Peak in a northward direction all along the Amibberg Massif up to the foot region of the Norotshama Peak. It represents a very important marker layer, which allows the linking of the Dickneus section with the Norotshama section (Fig. 2.50-A/B). The Dickneus Limestone is actually a mixed siliciclastic-calcareous rock, which is composed according to XRF and CO_2-volumetrical analyses of about 30 wt.% SiO_2, 6.5 wt.% Al_2O_3, 30 wt.% CaO, and 24 wt.% CO_2. The highest preserved stratigraphic level in the southern part of the Amibberg Massif is represented by the second prominent sandstone complex (AMB-Sst. 2) of the Amibberg Formation, which forms some small plateaus in the southern part of the Amibberg Massif (Fig. 2.48-B). The plateau edges of AMB-Sst. 2 form very steep and prominent sandstone cliffs (Fig. 2.57-B/C), which can easily be reached from the Dickneus Peak via a connecting ridge (about half a kilometre walking distance). The Dickneus Limestone is well exposed at the foot of these sandstone cliffs, where it is interbedded in offshore mudstones (Fig. 2.57-D), and can be used to extend the Dickneus section up to the top of AMB-Sst. 2. This sandstone complex can be subdivided into three subunits (Fig. 2.50-A). AMB-Sst. 2a is composed of ripple cross-bedded and hummocky cross-laminated, fine-grained sandstone layers, which are interstratified in sandy mudstones. The lithofacies of this basal part reflects deposition in a lower shoreface environment. The following AMB-Sst. 2b forms the near-vertical cliffs and is composed of stacked sandstone layers, which exhibit mainly hummocky cross-stratification and plane lamination. These sandstones represent amalgamated tempestites deposited in an upper shoreface environment. In the upper part of the AMB-Sst. 2 a morphological knickpoint can be recognized in the sandstone cliffs, at which the steepness of the profile decreases (Fig. 2.57-B/C). In this upper part (AMB-Sst. 2c) the mud content of the sandstones increases slightly and apart from hummocky cross-stratification also ripple cross-bedding is present in places. It is suggested that these sandstones were also deposited in an upper shoreface environment but probably under somewhat lower energy conditions in possibly slightly deeper water than the amalgamated tempestites of the middle part of AMB-Sst. 2.
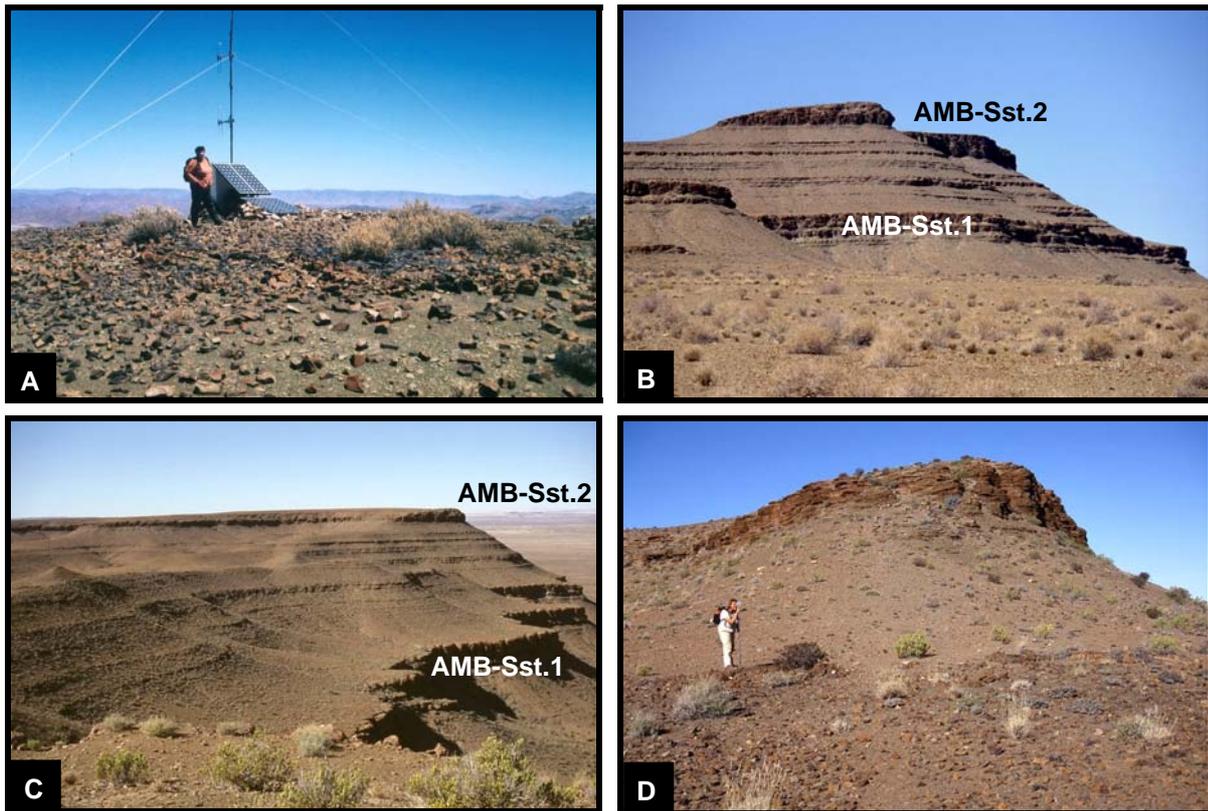
Fig. 2.57: (A) Plateau at the top of the Dickneus Peak partly covered by blocky pieces of the so-called Dickneus Limestone, which is a yellowish-brown weathering, mixed siliciclastic-calcareous diagenetic rock. It forms an important marker layer, which has been traced northward up to the foot region of the Norotshama Peak. **(B)** The southern part of the Amibberg Massif with the first two prominent sandstone complexes of the Amibberg Formation seen from a pediment surface in the south. **(C)** Plateau in the southern part of the Amibberg Massif underlain by the AMB-Sst. 2 complex as seen from the Dickneus. From the Dickneus this plateau is accessible via a connecting ridge seen in the middle right part of the photo. **(D)** Person is standing on top of the Dickneus Limestone, which is interbedded in offshore mudstones. The latter are overlain by a coarsening-upward succession composed of interstratified, bioturbated siltstones-sandstones of lower shoreface origin (olive green outcrops below the sandstone cliff) and fine-grained, plane laminated, ripple cross-bedded, wave-rippled and hummocky cross-stratified, amalgamated tempestitic sandstones of upper shoreface origin (brownish sandstone cliff).

The Norotshama section, illustrated in Fig. 2.50-B, comprises the stratigraphic interval from the Dickneus Limestone exposed in the foot region of the Norotshama below AMB-Sst. 2 to the top of the Norotshama preserving a stratigraphic interval about 20 above AMB-Sst. 3. Sandwiched between these prominent sandstone complexes is a series of coarsening-upward cycles (Fig. 2.58-A), the thickness of which decreases in upward direction, similar to the geological situation at the Dickneus. In the southwestern foot region of the Norotshama the sediments of the coarsening-upward succession from the Dickneus Limestone to the sandstones of AMB-Sst. 2 are excellently exposed (Fig. 2.58-B). The Dickneus Limestone forms a light-weathering, 10-20 cm thick, laterally discontinuous layer, which is embedded in dark grey offshore mudstones. The latter grade in upward direction into grey mudstones and

siltstones with interbedded fine-grained sandstone ripples, lenses and thin layers, representing deposits of a transitional offshore to lower shoreface environment. These sediments are followed by olive green siltstones and fine-grained sandstones, which show plane lamination, ripple and hummocky cross-lamination as sedimentary structures and are interpreted as lower shoreface deposits, forming the basal part of AMB-Sst. 2. These deposits in turn grade upward into brownish weathering sandstones, which are plane laminated, ripple cross-bedded and hummocky cross-stratified. This circa 6 m thick sandstone packet is composed of amalgamated tempestite layers, deposited in an upper shoreface environment, and forms the middle part of AMB-Sst. 2. The upper part of AMB-Sst. 2 is not very well exposed and forms the large lower circular plateau surrounding the Norotshama (Fig. 2.48). As already described in the Dickneus section the sandstones of the upper part of this second prominent sandstone complex of the Amibberg Formation are slightly more mud-rich and wave-rippled sandstones are more common.
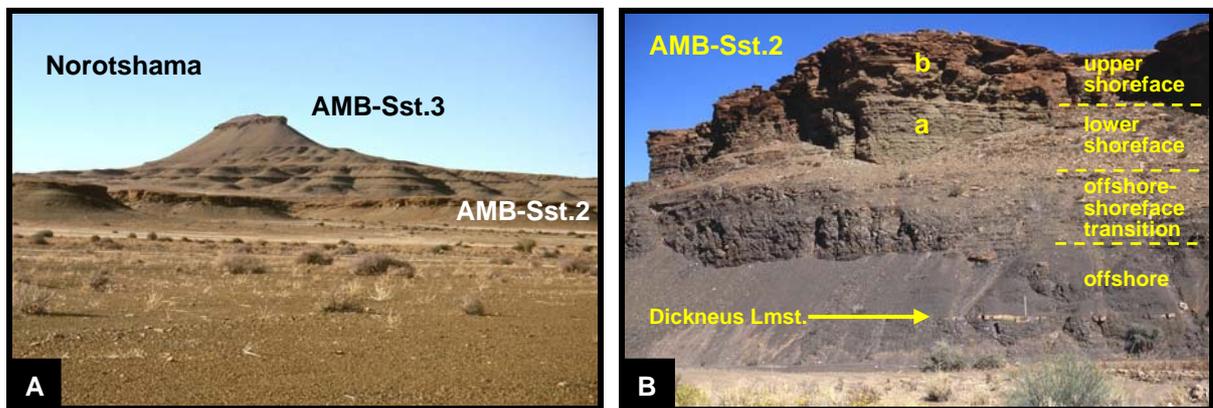
Fig. 2.58: (A) At the Norotshama Peak AMB-Sst. 2 and 3 form two prominent sandstone complexes, which enclose a number of sandstone-topped, coarsening-upward cycles. The latter become in upward direction finer grained and thinner. **(B)** Transition from offhore shales, with the Dickneus Limestone marker intercalated, to upper shoreface sandstones of AMB-Sst. 2 exposed in the south-western foot region of the Norotshama.

Above AMB-Sst. 2 follows a shaly succession, in which three sandstone horizons of 1-3 m thickness are intercalated forming less conspicuous ledges within the succession (Fig. 2.59-A). About 50 m above the lower large circular plateau underlain by AMB-Sst. 2 another smaller circular plateau around the Norotshama is underlain by a circa 12 m thick siltstone-sandstone complex (Fig. 2.59-B). Up to this level the described sandstone layers contain thicker lower zones, which are dominated by ripple cross-bedding (lower shoreface) and thinner upper zones, which are dominated by hummocky cross-bedding (upper shoreface). In some cases the latter are again overlain by a zone of ripple cross-bedded or wave-rippled sandstones, which grade upward into silty mudstones. The coarsening-upward cycles in the following 22.5 m contain at their tops only siltstones and fine-grained muddy sandstones, which are mainly ripple cross-bedded, whereas hummocky cross-laminated layers are much

less frequently observed (Fig. 2.59-C). This indicates deepening of the basin with time so that only lower shoreface deposits on top of the coarsening-upward cycles above the second smaller circular plateau around the Norotshama were laid down. Above the top of the last coarsening-upward cycle circa 115 m above the Dickneus Limestone or circa 32.5 m above the higher second smaller plateau follows a 40 m thick shale interval, which is overlain by the cliff-forming sandstones of AMB-Sst. 3 (Fig. 2.59-D). The basal 10-15 m of this shale interval are characterized by dark coloured, very fine-grained shales. Within this basal zone B. Rubidge discovered a horizon of nodular weathering mudstones, which frequently contain white weathering fish scales (Fig. 2.60-A). XRF analysis of one of these nodules revealed that they are highly phosphatic (21.4 wt.% P_2O_5). Furthermore, within this specific horizon also pieces of very hard and massive mudstones occur, in which light and dark coloured fine-grained sediment is intimately mixed due to strong bioturbation (Fig. 2.60-B). One sample of these mudstones contained a phosphate content of 1.2 wt.% P_2O_5. This phosphate-enriched stratigraphic zone can be found in the 2-3 metres of fine shales below a thin, circa 50 cm thick sandstone, which forms a thin ledge within dark grey shales above the last coarsening-upward cycle with only lower shoreface deposits on top (see Fig. 2.50-B & 2.59-D).
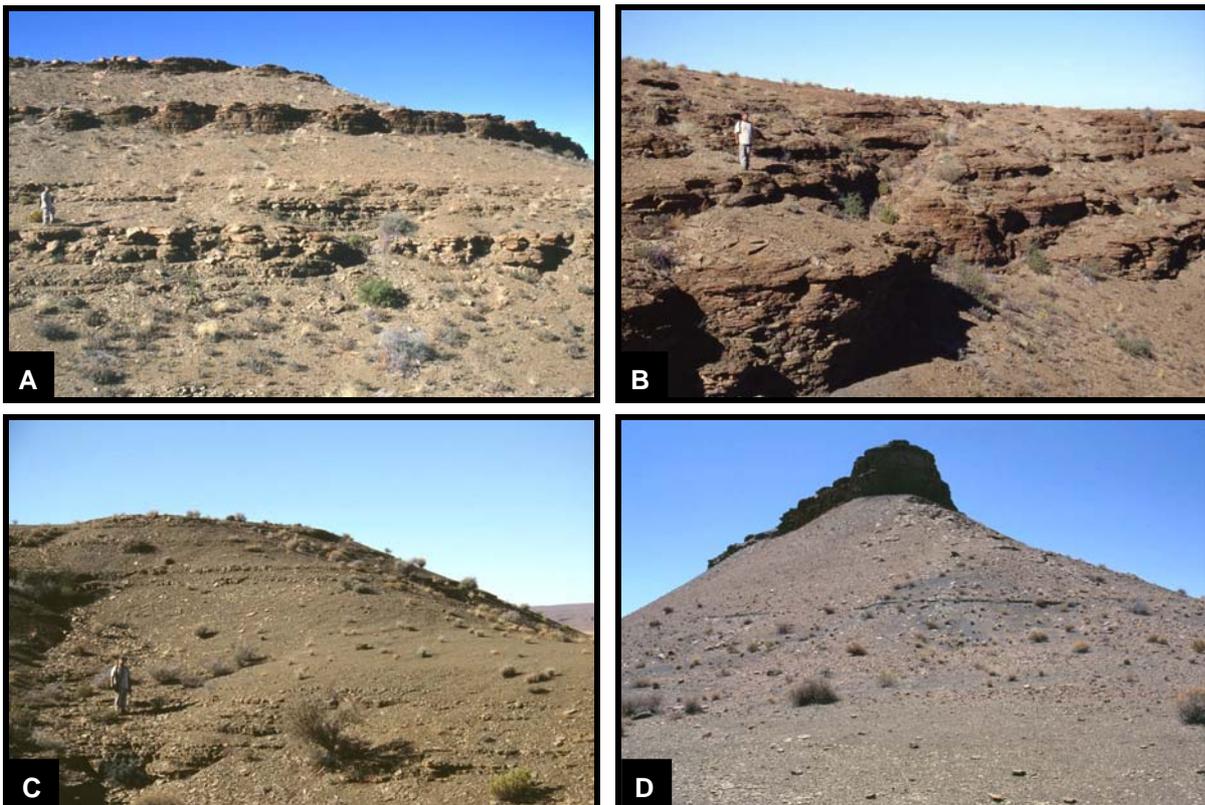
Fig. 2.59: (A) The lowermost three coarsening-upward cycles with upper shoreface sandstones at the top above AMB-Sst. 2 at the Norotshama. **(B)** Thick sandstone complex underlying a smaller circular plateau around the Norotshama circa 50 m above the large circular plateau underlain by AMB-Sst. 2. **(C)** Higher part of the succession of coarsening-upward cycles at the Norotshama with morphologically less prominent lower shoreface sandstones on top. **(D)** View from the uppermost small sandstone plateau towards the top of the Norotshama. The sandstone cliffs are built up by AMB-Sst. 3. Below the small sandstone layer within dark shales in the middle of the photo occurs the zone with phosphatic and fish scale-bearing nodules (Fig. 2.60-A/B).
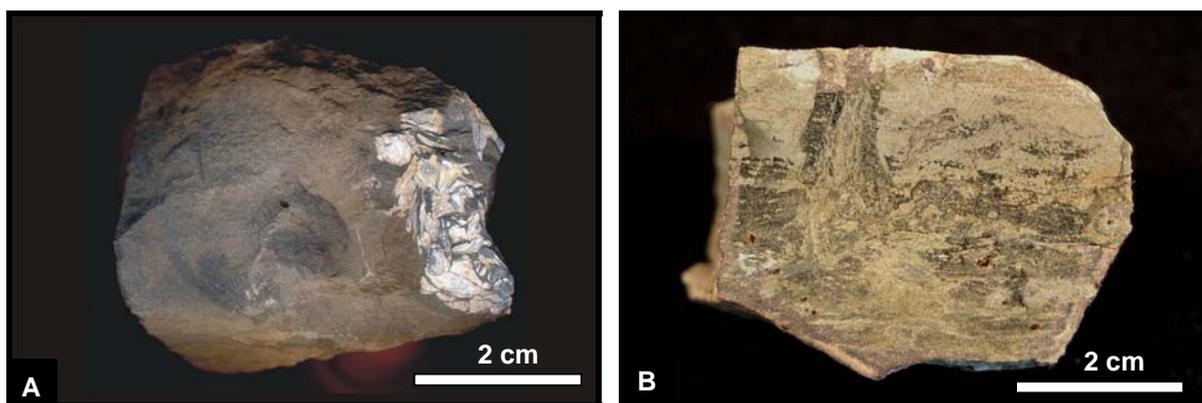
Fig. 2.60: (A) Phosphatic mudstone nodule (21.4 wt.% P_2O_5) with white weathering fish scales found in very fine-grained shales at the base of the 40 m thick shale succession in the upper part of the Norotshama. **(B)** Polished section of a hard mudstone from the same stratigraphic interval, in which also the phosphatic nodules have been found. The mudstone is intensively bioturbated and shows a slightly enriched phosphate content (1.2 wt.% P_2O_5).

The ~40 m thick shale succession, which forms the upper part of the Norotshama, is overlain in turn by a 10-15 m thick sandstone succession, representing the third prominent sandstone complex of the Amibberg Formation (AMB-Sst. 3). This sandstone complex forms the top of the southern part of the Norotshama Peak. Due to a normal fault the sandstone is downthrown about 10 m in the north and therefore fringes the northern part of the top of Norotshama Peak (Fig. 2.61-A). Similar to AMB-Sst. 1 and 2 this third sandstone complex is also composed of a coarsening-upward succession from lower shoreface siltstones-sandstones to amalgamated fine-grained upper shoreface sandstones (Fig. 2.61-B). Within the upper shoreface sandstones hummocky cross-stratification is very common (Fig. 2.61-C). However, in the upper part of AMB-Sst. 3 also thin (~30-40 cm) layers of parallel laminated, very 'clean' and mature, quartzitic, non-bioturbated sandstones are intercalated in the hummocky cross-stratified and ripple cross-bedded sandstones. The position of two of these sandstone layers is indicated in Fig. 2.61-B by arrows and Fig. 2.61-D shows a close-up of them. It is suggested that these layers possibly could represent beach sandstones. Above AMB-Sst. 3 follows on the northern side of the fault another coarsening-upward cycle with offshore shales in the lower part and mainly plane laminated, ripple cross-bedded, and wave-rippled sandstones, which show dewatering deformation structures, in the upper part. Mud pebble layers are also quite abundant.
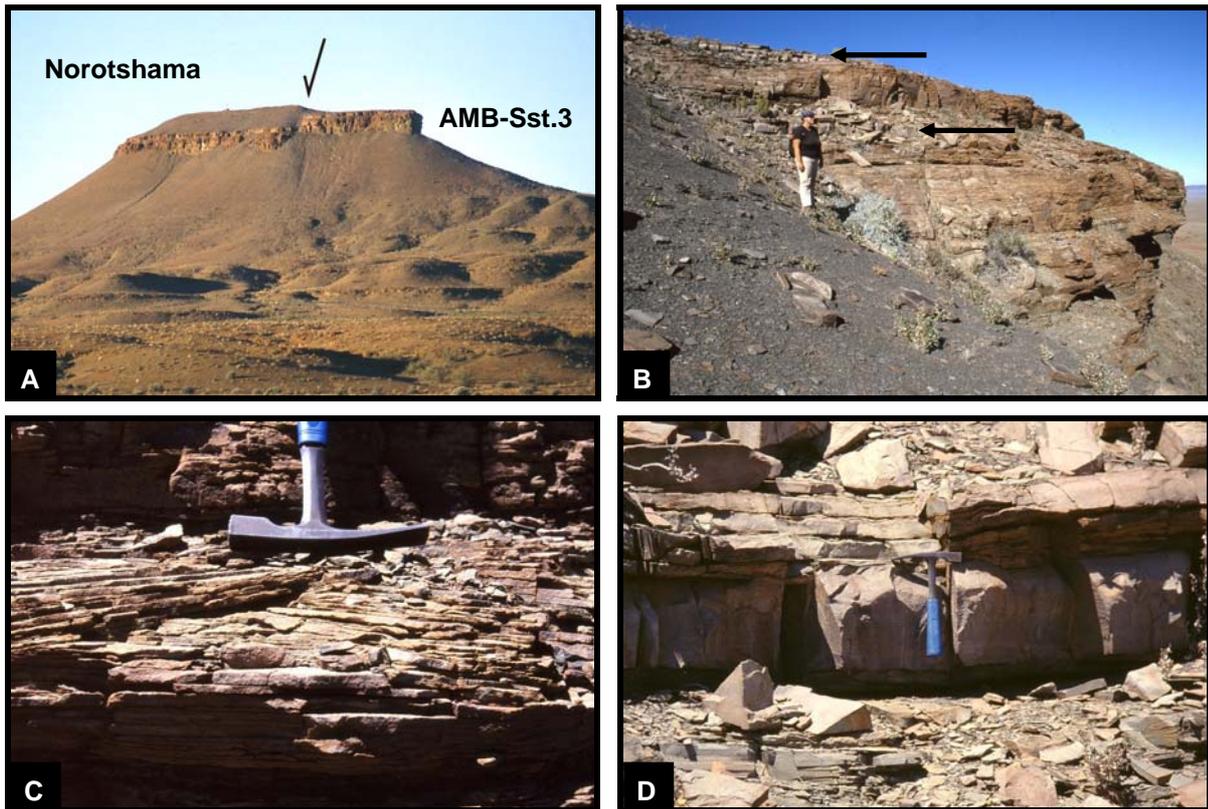
Fig. 2.60: (A) Due to a normal fault the sediments in the northern part of the Norotshama are downthrown about 10 m. **(B)** Top region of the Norotshama with upper shoreface sandstones of AMB-Sst. 3 in the background (foot wall) and dark grey offshore shales in the foreground (hanging wall). The trace of the normal fault runs in the photo from the upper left to the lower right. Arrows indicate the position of specific sandstone layers in the upper portion of AMB-Sst. 3 illustrated in (D). **(C)** Hummocky cross-stratification in tempestitic upper shoreface sandstones of AMB-Sst. 3. **(D)** In the upper portion of AMB-Sst. 3 30-40 cm thick, parallel laminated layers composed of 'clean' and mature sandstone occur (middle part of photo). These layers could possibly represent beach sandstones.

The fossil record of the Amibberg Formation appears at first sight rather poor. However, abundant trace fossils and bioturbation document that life was rich and diverse at and below the sea bottom of the Mesosaurus or Ecca Inland Sea during this time. Besides fish scales in phosphatic nodules (Fig. 2.60-A) only one indeterminable bone fragment (Fig. 2.61) and one bivalve (Fig. 2.62-A/B) was found. The bivalve is embedded in fine-grained sandstone and preserved as an internal mold. It is composed of two articulated valves, which are strongly inflated. Only the dorsal-anterior part can be seen and the size is dorsal to ventral about 3.5 cm and laterally about 3 cm. The surface sculpture shows faint, evenly spaced concentric growth lamellae. The form of the visible part of the bivalve closely resembles a megadesmid specimen with its relatively enrolled umbo, a deep lunule, and the strongly convex (inflated) valves. A comparison of this bivalve with those found in correlative strata in the Main Karoo Basin of South Africa (Waterford Formation - Cooper & Kensley, 1984; Volksrust Formation - Cairncross et al., 2005) and the Paraná Basin in South America (Passa Dois Group -

Runnegar & Newell, 1971) shows similarities with *Plesiocyprinella carinata* and *Casterella gratiosa*. In all these strata megadesmid bivalves are the dominant elements. This specific bivalve fauna is extraordinary in that sense that the Upper Ecca-Passa Dois strata contains bivalve genera and species that are not known from any other part of the world outside the Karoo and Paraná Basins. They apparently evolved in isolation and are thus endemic to the the Mesosaurus Inland Sea. However, Runnegar & Newell (1971) wrote that this bivalve fauna retains affinities with the marine Permian of Australia. Based on their studies on an unusual family of bivalves from the marine Permian of Australia these authors suggested that many of the endemic bivalve genera of the Paraná (and the Karoo) Basin are derived from somewhat dissimilar marine forms commonly found in late Carboniferous and Permian sediments of southern continents. Although the bivalve fauna of the Upper Ecca-Passa Dois strata clearly is different from any other known fauna, its closest similarity is to the Permian marine faunas from Australia, New Zealand, India, and South America. In this context the abundance of megadesmid genera is of particular interest as it suggests a close link between the faunas of the Paraná-Karoo Basin and the Permian marine faunas of Australia and New Zealand. For example *Plesiocyprinella*, *Casterella*, and *Ferrazia* are clearly related to the Australian genera *Megadesmus* and *Astartila* (Runnegar & Newell, 1971). In an environmental model for the Paraná Basin Runnegar & Newell (1971) compared the conditions to that of the Caspian Sea, which contained molluscan faunas that were dominated by brackish-water endemic genera and species (until foreign species were introduced by man). These exceedingly diverse endemic bivalve faunas apparently developed in situ during the Pliocene and apparently derived from species of the common Mediterranean cockle, *Cerastoderma*. Therefore it can be concluded that sedimentation within the later phase of the Mesosaurus Inland Sea occurred most probably mainly within a brackish water body, which showed complex salinity gradients, as well as temperature and oxygen stratification. After the early, glacially influenced inland sea phase, during which a marine association of the Gondwana faunal province was able to colonize parts of the Mesosaurus Inland Sea, the connection to the Panthalassan Ocean became during the later phase insufficient to retain normal marine conditions, leading to strong faunal endemism in an isolated and brackish inland sea environment.

Fig. 2.61: Bone fragment of unknown affinity found by H. Stollhofen in the sandstone talus above AMB-Sst. 1 at the Dickneus locality.

Fig. 2.62-A & B: Internal mold of a bivalve of megadesmid appearance. Comparison with bivalves from correlative strata in South America and South Africa shows similarities with *Plesiocyprinella carinata* and *Casterella gratiosa*. The shown specimen was found by C. Krapf in the talus below AMB-Sst. 1 at the Dickneus locality.

Bioturbation in the sediments of the Amibberg Formation is generelly quite abundant but varies depending on the sediment type. Generally the mixed muddy-sandy lower shoreface deposits seem to show the highest bioturbation intensity (e.g. Fig. 2.52-D). But also certain horizons in the offshore shales and mudstones can be quite intensively bioturbated. Especially prominent flooding zones like the *Curvolithos/Pseudo-Plagiogmus* layer below AMB-Sst. 1 (Fig. 2.45-A/B) and the phosphatic nodule-bearing mudstones at the base of the shale succession below AMB-Sst. 3 (2.60-B) appear almost completely bioturbated probably as a result of low sedimentation rates and condensation. Within the upper shoreface sandstones bioturbation in the upper part of individual tempestite layers can be so intense that original sedimentary structures are almost completely obliterated and often in these parts the sandstones become a conspicuous crumbly and friable appearance (Fig. 2.63-A). Bioturbation features in the lower part of individual tempestite cycles are generally scarce except characteristic escape traces due to high sedimentation rates (Fig. 2.63-B).
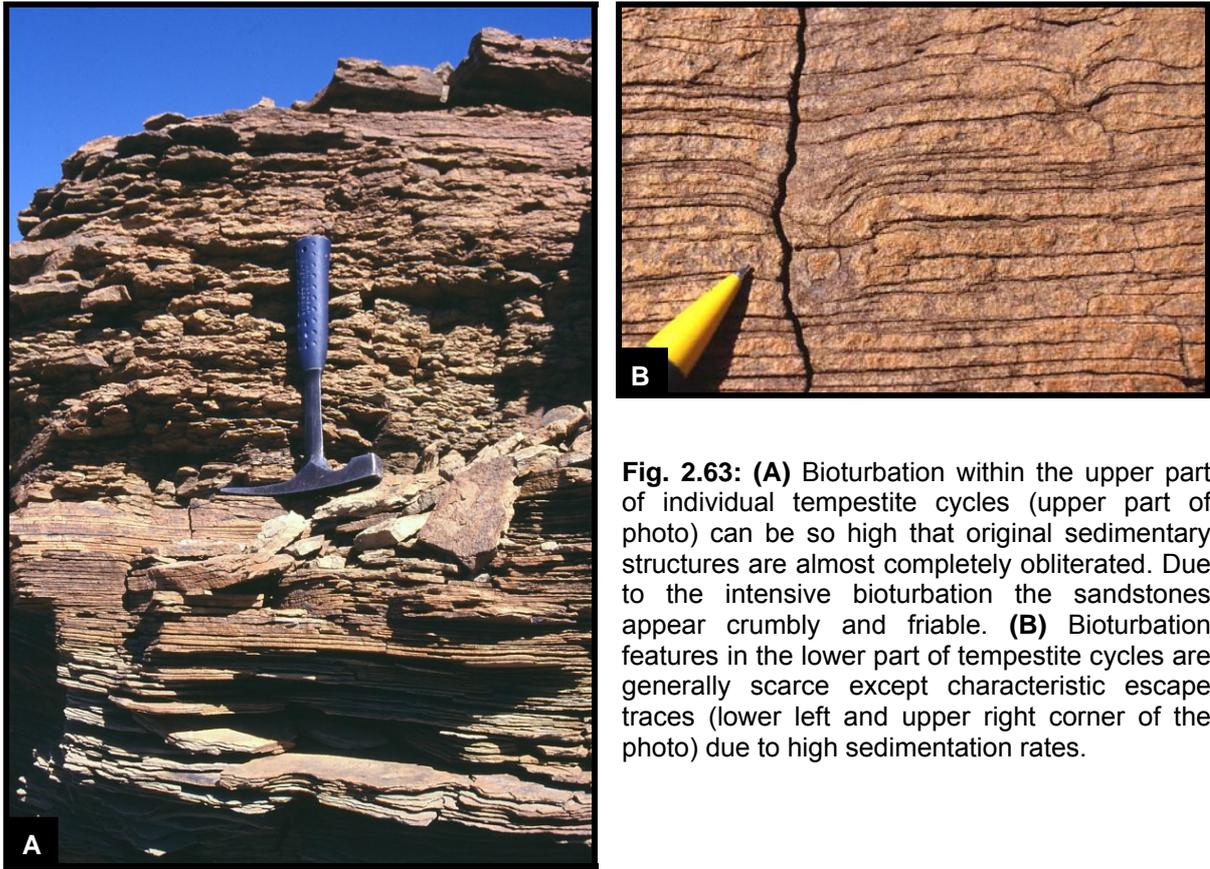
Fig. 2.63: (A) Bioturbation within the upper part of individual tempestite cycles (upper part of photo) can be so high that original sedimentary structures are almost completely obliterated. Due to the intensive bioturbation the sandstones appear crumbly and friable. **(B)** Bioturbation features in the lower part of tempestite cycles are generally scarce except characteristic escape traces (lower left and upper right corner of the photo) due to high sedimentation rates.

Specific trace fossils, which have been found within the Amibberg Formation include *Skolithos*, *Planolites*, *Palaeophycus*(?), *Helminthopsis*, *Cochlichnus*, *Gordia*, *Taenidium*, *Teichichnus*, *Phycodes*(?), *Halopoa*, and *Pseudo-Plagiogmus*. Vertical, concentrically laminated traces could represent *Siphonichnus* and looped trails of 'needle stitches' were compared by Anderson (1974) with *Hormosiroidea*. Furthemore, some traces could represent phyllopod trackways (Uchman, pers. comm., 2002). There are certainly much more trace fossils to be found and identified, and a proper future investigation of the ichnofauna of the Amibberg Sandstones is strongly suggested. Fig. 2.64-A to M illustrate most of the above mentioned traces.
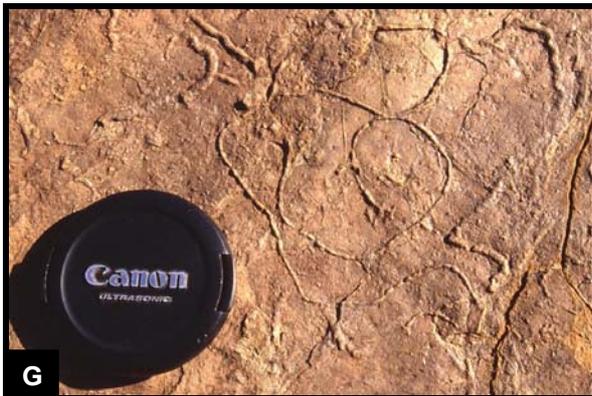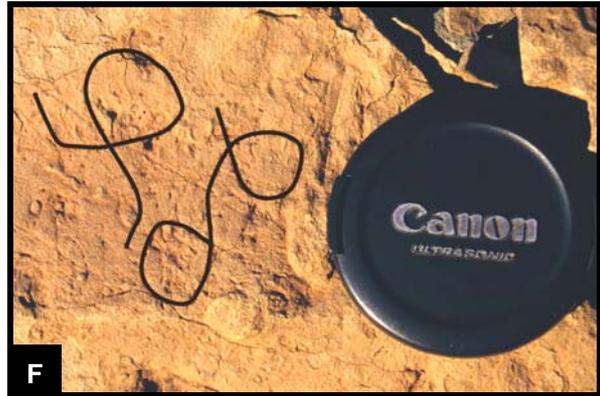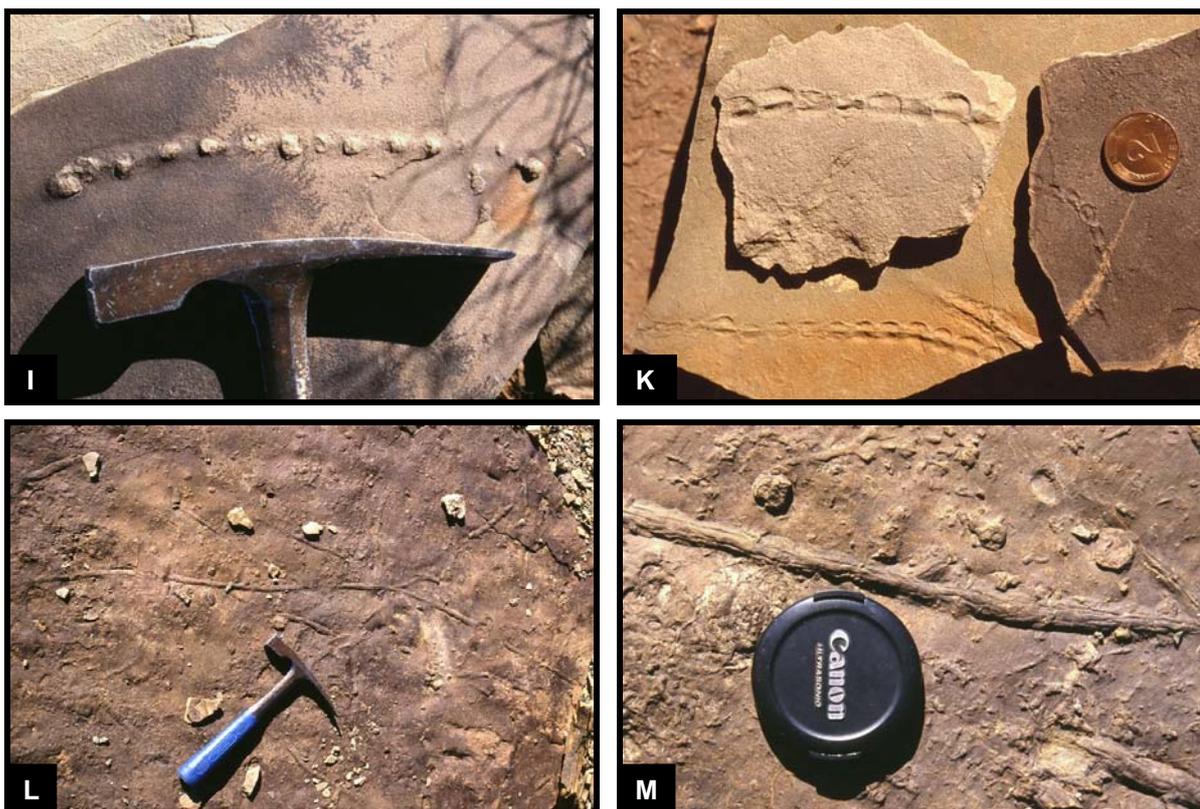
Fig. 2.64 (prev. and this page): Trace fossils: (A) Thin vertical burrows: *Skolithos*. **(B)** Winding cylindrical burrows: *Planolites*. **(C)** Possibly lined cylindrical burrow: *Palaeophycus*(?). **(D)** Meandering horizontal traces: *Helminthopsis*. **(E)** Looped trail of 'needle stitches': were compared by Anderson (1974) with *Hormosiroidea*. **(F)** Black line drawn on the looped trail of 'needle stitches' of (E). **(G)** Looped trail of a 'beaded string' possibly representing *Gordia*. **(H)** Meniscate backfilled trace: *Taenidium*. **(I)** Upward branching burrows from central horizontal tube: *Phycodes*(?). **(K)** Trails of impressions possibly made by a phyllopod (Uchman, pers. comm., 2002). **(L) & (M)** Tubular circular burrow with external striations and massive (not meniscate backfill) internal structure: *Halopoa* (note: can easily be confused with *Scoyenia*, who contains meniscate backfills).

In summary, the prominent sandstones of the Amibberg Formation show mainly hummocky cross-stratification, ripple cross-bedding, and plane lamination. Wave-rippled surfaces are quite abundant and mud pebbles are commonly distributed throughout the sandstone layers. No planar or trough cross-bedding has been observed. These sedimentary features indicate that the sandstones of the Amibberg Formation were largely laid down during storms and therefore classify as tempestites, deposited in lower to upper shoreface environments. The shale-out of AMB-Sst. 1 towards the northeast and the dip directions of current ripple foresets below AMB-Sst. 1 point to a southerly source area. Together with the information from lower stratigraphic units, e.g. the thinning and pinch-out of the Polisiewater Chert and the Inaub Sandstone towards northely directions, indicates that a wave-dominated shoreline of the Mesosaurus or Ecca Inland Sea must have been present in the south of the Aussenkjer-Noordoewer Karoo outcrop area. Also the plant-debris, wood fragments and tree

trunks proof that an emergent and vegetated land must have existed in the vicinity of this region. It can only be speculated that this proposed land may represent re-emerged parts of the so-called Cargonian Highlands, which probably formed during Dwyka glaciation an ice-covered dividing range between Namibia and Botswana on the northern side and South Africa on the southern side, and which was probably largely submergent (at least its western part) during lower Ecca times (cf. Veevers et al., 1994). The strike direction of wave ripple crests measured throughout the Amibberg Formation in the southern and middle part of the Amibberg Massif as well as at the Norotshama shows a dominant NNE-SSW orientation (Fig. 2.65). This is very similar to measurements in the Carnarvon Formation in the northwestern part of the South African Main Karoo Basin. The Carnarvon Formation is nowadays incorporated into the Waterford Formation, which is a correlative of the Amibberg Formation. Similarily to the latter the Carnarvon Formation consists also mainly of shales and plane laminated, ripple cross-bedded as well as hummocky cross-stratified sandstones and attains also a thickness of about 250 m (Rust et al., 1991). The strike of wave ripple crests in the Carnarvon Formation is mainly NNW-SSE oriented, which was interpreted by Rust et al. (1991) to reflect the existence of a parallel oriented shoreline of the Ecca Inland Sea west of the present-day western margin of Karoo outcrops in South Africa. However, the wave ripple crest orientation is also perpendicular to the supposed main wind direction during the Permian in this region (mainly westerly winds). Consequently, the NNE-SSW orientation of wave ripple crests in the Amibberg Formation might rather reflect the main wind direction during time of sand deposition rather than the orientation of a nearby shoreline.
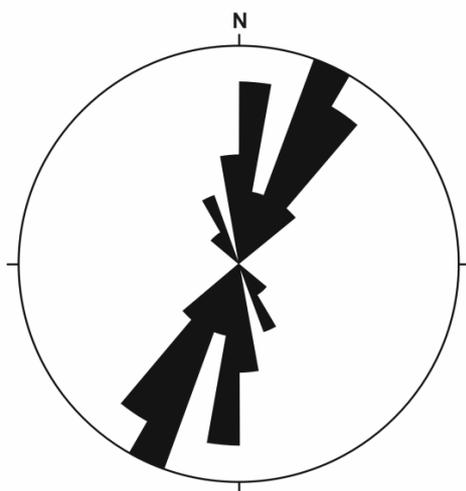
n = 27
largest petal: 6.00 values
largest petal: 22% of all values
Strike Direction: 10° classes

Fig. 2.65: Rose diagram showing the strike direction of wave ripple crests measured throughout the Amibberg Formation from localities in the southern and middle part of the Amibberg Massif as well as from the Norotshama. The dominating NNE-SSW orientation is interpreted to reflect a dominantly westerly main palaeo-wind direction in the depositional area (in the Permian).

The cyclicity of the deposition of the Amibberg Formation is well expressed by the stacked coarsening- and shallowing-upward successions, which are separated by flooding surfaces. These coarsening-upward cycles consist in most cases of basal offshore mudstones, which grade upward into silty mudstones and alternating siltstones-sandstones. Plane laminated, ripple cross-bedded and hummocky cross-stratified, fine-grained upper shoreface sandstones form the top of most of these cycles. The form and composition of these individual cycles is in accordance with the definition of parasequences *sensu* van Wagoner et al. (1988). The thicknesses of the parasequences constituting the Amibberg Formation range between somewhat more than 5 m up to more than 50 m (Fig. 2.50-A & B).

Within the Amibberg Formation the stacking pattern of parasequences and their lithofacies development indicates also a higher-order cyclicity. Applying sequence stratigraphic principles (see Catuneanu et al. (2005) for a recent overview and references therein) successions of parasequences can be combined to form depositional sequences. Three sequence boundaries and two maximum flooding surfaces can be indentified within the sedimentary succession of the Amibberg Formation (Fig. 2.66). The prominent sandstone complexes AMB-Sst. 1, 2, and 3 contain the most proximal lithofacies in the Amibberg Formation and indicate the positions of sequence boundaries. In contrast, the Dickneus Limestone (between AMB-Sst. 1 & 2) and the shale horizon with phosphatic mudstone nodules (between AMB-Sst. 2 & 3), which are interbedded in very fine-grained shales, most probably represent the most distal facies and therefore indicate the position of maximum flooding surfaces (Fig. 2.66).

The transgressive systems tracts (TST) of the depositional sequences are characterized by a conspicuous retrogradational parasequence stacking pattern, in which the thickness of subsequent coarsening-upward parasequences continuously decreases in upward direction (Fig. 2.50-A/B) and in which the sediments at the top of each of these parasequences indicate a successively more distal depositional environment. The latter is also reflected by the upward decreasing sand to mud ratio of the sandstones at the top of each parasequence. The higstand systems tracts (HST), representing the regressive part of each sequence, are characterized in the Amibberg Formation by a single coarsening-upward parasequence respectively, topped either by AMB-Sst. 2 or 3. The parasequence that is topped by AMB-Sst. 1 is underlain by a coarsening-upward parasequence of more distal origin (topped by the Pseudo-Plagiogmus layer in the uppermost part of the Aussenkjer Formation), which might still belong to the HST below the sequence boundary at the top of AMB-Sst. 1 (Fig. 2.66).
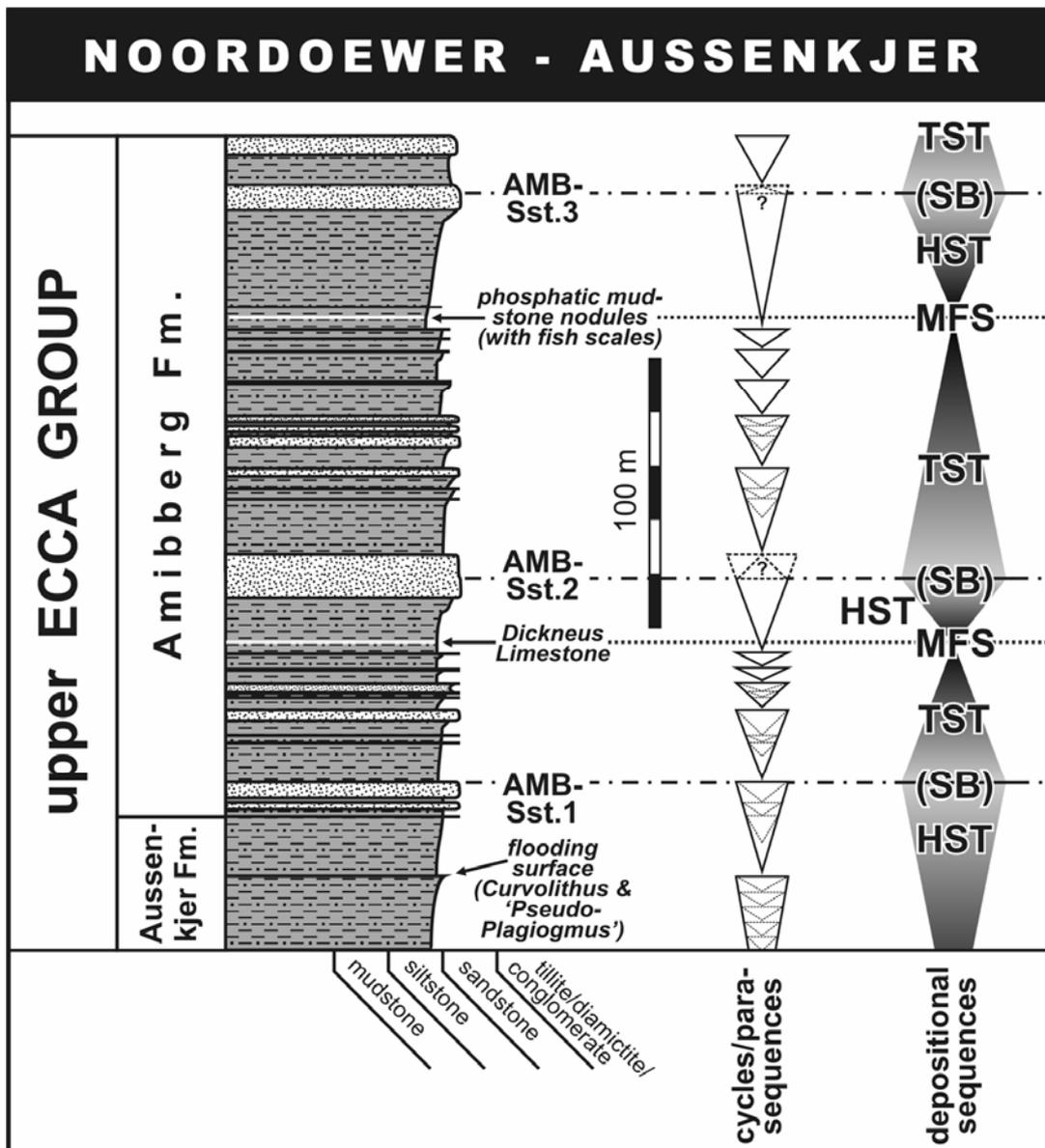
Fig. 2.66: Stratigraphic overview of the Amibberg Formation and the sequential framework of the offshore to upper shoreface deposits. The repetitive stacking pattern of coarsening- and shallowing upward cycles reveals the presence of higher-order depositional sequences. Maximum flooding surfaces (MFS) within the succession are characterized by calcareous or phosphate-enriched intervals. The positioning of sequence boundaries (SB) is somewhat problematic due to the absence of subaerial unconformities. However, sequence boundaries are inferred at the top of the most proximal deposits within each prominent sandstone complex (AMB-Sst. 1 to 3). In the apparent absence of lowstand deposits these maximum regression surfaces probably merge with correlative conformities (see text for explanation). The transgressive systems tracts (TST) are characterized by successions of coarsening-upward parasequences, which show in upward direction successively lower thicknesses and more distal deposits.

The exact placement of sequence boundaries within the Amibberg Formation is somewhat problematic due to the absence of subaerial unconformities. At first sight it appears justified to place the correlative conformities at the top of the three prominent sandstone complexes as they represent the most sand-prone interval within each depositional sequence. AMB-Sst.

1 is composed of three major thickening-upward sandstone layers or packets which are separated by shale intervals. A sequence boundary is placed at the top of the uppermost sandstone packet, which probably contains the most proximal facies and represents a time of maximum regression. In contrast, AMB-Sst. 2 forms a stronger amalgamated sandstone package without prominent shale interlayers. Numerous wave ripple surfaces and thin shale horizons in its uppermost part (AMB-Sst. 2c) indicate a somewhat lower energy and possibly deeper depositional environment compared to that for the amalgamted hummocky cross-stratified sandstones in the middle part (AMB-Sst. 2b). Consequently, the middle part is considered to reflect the most proximal deposits and the time of maximum regression. Therefore, the position of the sequence boundary is inferred in the upper third of AMB-Sst. 2 (Fig. 2.66). In the case of AMB-Sst. 3 the situation is similar with the uppermost part containing thin shale interlayers. However, this part hosts also sandstone horizons of suspected beach origin, the latter possibly representing the most proximal facies. As a preliminary solution a sequence boundary is placed in the upper third of this sandstone complex.

This concept of placing sequence boundaries at the top of the most regressive deposits, respectively at the maximum regressive surface, is not in full accordance with existing sequence stratigraphic models. The maximum regressive surface actually forms the base of the transgressive systems tract (TST), whereas the correlative conformity forms the base of a lowstand systems tract (LST) (Catuneanu et al., 2005). However, in the apparent absence of lowstand deposits these two key surfaces obviously merge to a single surface.

The above mentioned depositional sequences could be described as 3rd order sequences according to their suspected duration (in the range of 1 to 5 Ma). Is in the succession of the Amibberg Formation also the higher-(second)-order regressive trend from the Whitehill Formation upward observable? There is actually no general thickening or coarsening trend visible from ASB-Sst. 1 to 3. However, AMB-Sst. 2 shows a much higher degree of amalgamation than AMB-Sst. 1, which contains shaly intervals. Furthermore, the plane laminated, 'clean', quartzitic sandstone layers within AMB-Sst. 3 may represent beach deposits and therefore may indicate the most proximal facies within the whole Amibberg Formation. Furthermore, the shale-out of AMB-Sst. 1 indicates that the higher sandstone complexes AMB-Sst. 2 and 3 prograded farther to the north into the basin than AMB-Sst. 1. Therefore, an overall, large scale regressive trend can indeed be inferred for the Amibberg Formation.

Chapter 3 – Altered volcanic ash-fall tuff layers

3.1 Previous records

Karoo-aged altered volcanic ash layers were actually first described from Southern Africa as cherts in the Upper Permian Beaufort Group by Blignaut et al. (1948), Haughton et al. (1953), Rossouw & de Villiers (1953), and Rossouw et al. (1964), however, at this time their volcanic nature was not recognized. Blignaut et al. (1948), for example, interpreted the 'cherts' as siliceous precipitates within a swampy environment. Thin bentonitic layers within rocks of the Lower Permian Ecca Group were then recognized as altered ash-fall tuffs in the Main Karoo Basin of South Africa by consultants for SOEKOR in the mid to late 1960's (Bourdon et al. 1966; Robertson Research, 1967, 1968; Venter, 1969) and subsequent descriptions of tuff layers were provided by Elliot & Watts (1974), Lock & Johnson (1974), Martini (1974), Lock & Wilson (1975), and McLachlan & Anderson (1977). On these early records of altered volcanic ash beds followed more detailed investigations by Wickens (1984, 1996), Viljoen (1987, 1990, 1992a, 1994, 1995), McLachlan & Jonker (1990), Knütter (1994), Veevers et al. (1994), and Knütter (1994), as well as Knütter et al. (1995). The majority of these tuff beds are intercalated in fine-grained argillaceous sediments of the Permian Ecca Group, deposited subaqueously in a marine-brackish inland sea. Records of tuff occurrences within glacigenic deposits of the Late Carboniferous Dwyka Group in South Africa were comparatively sparse. Volcanic ash layers within fluvio-lacustrine deposits of the Upper Permian to Lower Triassic Beaufort Group were studied by Ho-Tun (1979), Keyser & Zawada (1988), and Karpeta (1996). In addition to those occurring in the Main Karoo Basin, altered tuffaceous beds have also been identified in the Grootegeluk Formation of the Waterberg Coalfield, Ellisras Basin (Spears et al., 1988; Faure et al., 1996b). Furthermore, bentonites and tonsteins also occur in many other South-Gondwanan basins in equivalent age and stratigraphical positions compared to those from the Main Karoo Basin in South Africa. From South America altered tuff beds are known from the Paraná Basin in Brazil (Coutinho et al., 1991; López-Gamundí, 1996; Maynard et al., 1996; Formoso et al., 1997; López-Gamundí & Rosello, 1998; Matos et al., 2000, 2001; Calarge et al., 2003a/b), from the Sauce Grande and Paganzo basins in Argentina (Iñíguez et al., 1988; López-Gamundí et al., 1990, 1995; López-Gamundí, 1996; López-Gamundí & Rosello, 1998; Net et al., 2002), from northern Chile (Breitkreuz, 1991), and from the Falkland/Malvinas Islands (Trewin et al., 2002). In Antarctica, Karoo-aged tuff layers were found in the Polarstar Formation in the Ellsworth Mountains (Collinson et al., 1992) and in the Buckley Formation in the Transantarctic Mountains (Barrett, 1969). Tonsteins are also described from the Australian Bowen and Sydney Basin within Permian coal measures (Kisch, 1966; Diessel, 1985; Jones et al., 1987; Kramer et al., 2001; Creech, 2002).

In central-southern Namibia H. Stollhofen initially discovered bentonitic tuff layers in 1994 in glacigenic mudrocks of the Dwyka Group in the vicinity of Ganigobis. First descriptions of these ashfall tuff layers were given by Grill (1997) and a detailed and comprehensive investigation followed by B. Bangert (Bangert et al., 1999; Bangert, 2000; Bangert et al., 2000). Similar, but generally thicker and better preserved tuff beds were discovered in 1998 by V. Lorenz in the Dwyka Group of southernmost Namibia, in cut banks of the Orange River on the opposite side of Zwartbas, c. 6 km northwest of Noordoewer. They were studied to greater detail by M. Geiger (Geiger, 1999, 2000; Bangert et al., 2000). In addition, a few tuff layers were also recognized in a core of the Vreda borehole near the Botswanan border in rocks of the lower Ecca Group (Grill, 1997; Stollhofen et al., 2000a).

In northwestern Namibia Karoo-aged tuff layers were already described earlier by Horsthemke et al. (1990) and Horsthemke (1992). They interpreted thin, light coloured, zeolitic and feldspathic layers within red continental beds of the Gai-As Formation (Beaufort Group equivalent) in the Huab area as altered pyroclastic rocks. These tuff layers were later resampled and radiometrically dated by Holzförster (2000, 2002) and Wanke (2000) (see also Stollhofen et al., 2000b; Wanke et al., 2000).

During the fieldwork for this study a number of new tuff horizons were discovered at several localities in southern Namibia within argillaceous deposits of the lower part of the Ecca Group. They form the main focus of the descriptions within this thesis, but for completeness and comparison, tuffs from the Dwyka and Beaufort Groups are reviewed and the descriptions are supplemented by new observations.

3.2 Nomenclature and classification

Many of the altered tuff layers occurring in the lower Karoo Supergroup of Namibia and South Africa were described in the past as bentonites because of their deposition in a large marine to brackish water body (Ecca Sea or Mesosaurus Sea).

The term 'bentonite' has been applied worldwide very often in descriptions of altered tuff layers. Bentonite was originally used for deposits of smectite-dominated clays derived from tephra deposits by alteration (Benton Group in Montana: Ross & Shannon, 1926). This definition is based on the predominating clay mineral species and not on a precursor mineral. However, the term 'bentonite' has for many decades been used to describe widespread, clay-altered ash layers that are commonly, but not necessarily, dominated by smectite (Fisher & Schmincke, 1984). Bohor & Triplehorn (1993) restrict the term 'bentonite' to altered volcanic ash layers found in marine depositional environments, usually smectitic in compo-

sition, whereas 'tonsteins' are found in non-marine environments commonly associated with coal formation, and usually kaolinitic in composition.

Since most of the Namibian and South African altered tuff layers of the Dwyka and Ecca Groups are dominated by illite-rich instead of smectite-rich clayey matrices, these illitic, potassium-rich tuff layers often have been referred to as K-bentonites (e.g. Viljoen, 1990, 1995). Some altered tuff layers in the Dwyka Group of southern Namibia contain well developed crystal booklets and vermicules, implying a kaolinite origin (Bangert et al., 1999; Bangert, 2000). Most of these booklets and vermicules however show in thin sections bright interference colours under crossed polars, indicating a transformation of kaolinite to illite by later stage diagenetic processes. These tuffs certainly resemble kaolinitic tonsteins but were definitely deposited subaqueously as volcanic ash fall in a marine to brackish water body and therefore should also be designated as bentonites. True kaolinitic tonsteins however occur in the Permian coal measures of the Ecca Group in South Africa, e.g. in the Grootegeluk Formation of the Waterberg Coalfield (Ellisras Basin) (Spears et al., 1988; Faure et al., 1996). Some volcanic ash layers of the Karoo Supergroup appear silicified and form very hard rocks. XRD analyses show that their matrices can be silica-, feldspar-, or zeolite-rich. To distinguish them from the softer, clay mineral-rich bentonites and tonsteins they are here referred to as 'cherts' or 'chert-like' rocks.

In this study bentonites, tonsteins, and 'cherts' are united under the general heading of tuffs (resp. altered tuffs), which are defined here as semi- to fully consolidated rocks of pyroclastic origin with a mean grain size <64 mm, regardless of the depositional process (fall-flow-surge), the depositional environment (marine-continental), the mineralogical composition (crystals-glass-lithics-matrix minerals), and the degree of alteration.

The term 'tuffaceous' is used in this study for layers that proved in thin sections to be mixtures of detrital-siliciclastic and pyroclastic components. Such mixtures can be generated either primarily by low volume fall-out of volcanic ash settling simultaneously with detrital background sedimentation of suspended muds or secondarily by reworking and mixture of basinal muds and interlayered volcanic ash beds. In the first case these tuffaceous layers commonly do not display sharp upper and lower sedimentary boundaries. However, due to their volcanogenic components these tuffaceous layers can behave during diagenesis quite different compared to the enclosing detrital mudrocks and may develop a very distinct and contrasting secondary mineralogy. This can also affect their macroscopic appearance in such a way that they form lithologically conspicuous horizons.

3.3 Regional distribution and stratigraphic position of altered tuff layers in southern Namibia

All localities, from where Karoo-aged tuff beds were described earlier or have been discovered newly in southern Namibia, are indicated on the map in Fig. 3.1. So far, tuff beds are mainly known from two Karoo outcrop areas within this region: (1) the area between Asab and Keetmanshoop, representing the southern part of the Mariental-Keetmanshoop Karoo outcrop area (as the western part of the so-called 'Kalahari Karoo Basin' or 'Aranos Basin'), and (2) the area in the vicinity of Noordoewer and Aussenkjer at the Orange River, representing the southwestern part of the Aussenkjer-Karasburg Karoo outcrop area (also known as the so-called 'Karasburg Basin', 'Nabas Basin', 'Orange River Basin' or 'Warmbad Basin'). In addition, the position of the Vreda well near the Botswanan border is marked, from where tuff layers have been reported in cores (Grill, 1997; Stollhofen et al., 2000a).

The tuff layers, which have been discovered up to now in southern Namibia, are mainly known from single outcrop locations and have not been traced or mapped on a broader, region- or basin-wide scale so far. This is largely due to the lack of detailed mapping of the Karoo deposits in this area at a smaller scale since the discovery of the tuff layers. However, it is difficult to follow the tuff layers in the field in most cases, because excellent outcrop conditions must be available to discover and trace the thin pyroclastic marker horizons. Therefore, most tuffs have been discovered in road cuts, river cut banks and gorges, or in steep cliff sections below dolerite sills. Some other tuff beds are only known from cores, e.g. the tuffs from the Vreda borehole. However, through very detailed and focused field work Bangert (2000) was able to trace a characteristic succession of tuff beds in the Ganigobis Shales laterally over a distance of at least 25 km from outcrop to outcrop. In other cases a correlation of individual tuff levels over longer distances may be achieved by comparing detailed stratigraphic sections, which contain the tuff beds. Other lithological marker beds (e.g. calcareous or phosphatic horizons), fossil zones and sedimentological trends can play an important role in correlating widely separated localities.

The stratigraphic distribution of the tuff beds in the two mentioned outcrop areas is shown in Fig. 3.2. In the area between Asab and Keetmanshoop the oldest tuff beds of the Karoo occur in the so-called Ganigobis Shale Member of the glacigenic Dwyka Group (Bangert, 2000 and references therein). No other tuff layers have been recognized in higher strati-graphic levels of the Dwyka Group so far in this area. Within the post-glacial Ecca Group several tuff beds have been newly discovered in two stratigraphic levels. In the vicinity of the small village of Itzawisis, tuff layers are exposed in several road cuts along the B1 highway within shales of the Prince Albert Formation. A tuffaceous zone within the Whitehill Formation

has been recognized at several localities (Khabus, Panorama, Eisenstein). This tuff zone lies a few metres below the limestone/dolomite marker layers at the base of the regressive succession, which forms the top of the lower part of the Whitehill Formation. The tuff layers of the Vreda core occur in the uppermost part of the Mukorob Shale Member below the Auob Sandstone and their position is projected into the stratigraphic column for the Tses-Keetmanshoop area.

In the vicinity of Noordoewer numerous tuff layers can be found in Dwyka mudrocks exposed along cut banks of the Orange River. Opposite the small settlement of Zwartbas, on the Namibian side of the river, the tuff-bearing succession within the Dwyka Group is about 70 m thick and partly correlates with the tuff succession at Ganigobis. The next younger tuffs have been discovered at the base of the Prince Albert Formation within the white weathering Owl Gorge Member ('White Horizon' of Geiger, 1999), a distal equivalent of the Nossob Sandstone Member. Tuff beds, which are exposed in a road cut of the B1 highway c. 30 km northeast of Noordoewer (farm area Korabib), are positioned approximately in the middle to upper third of the Prince Albert Formation. East of the Uhabis River at the southeastern margin of the Tandijeskoppe Mountains, a single tuff layer was detected about 10 m below the Prince Albert – Whitehill Formation contact. This so-called Uhabis River Tuff probably correlates with the Vreda Tuffs due to their similar stratigraphic position. Within the Whitehill Formation no tuff layers could be found in the Orange River area despite the knowledge of their existence and stratigraphic position in the Keetmanshoop area. Within the overlying Collingham Formation tuff layers are most abundant and can easily identified. At two localities, the Ufo Valleys and Rhyofontein, these tuffs were logged and sampled in detail. The following, several hundreds of metres thick Aussenkjer Formation, a correlative of the Tierberg Formation in the northern Cape Province/RSA, was not investigated in great detail. Only the lower 130 m were logged but no prominent tuff horizon could be detected with certainty. Only a conspicuous whitish weathering lamina, only c. 1 mm thick, intensively traversed by arthropod tracks and other trace fossils, interspersed in dark greenish shales, was recognized east of the Ufo Valleys about 110 m stratigraphically above the top of the Collingham Formation. Due to its resemblance to the thin basal tuffs of the Collingham Formation it is interpreted as a possible tuff layer ('Sesfontein Tuff').
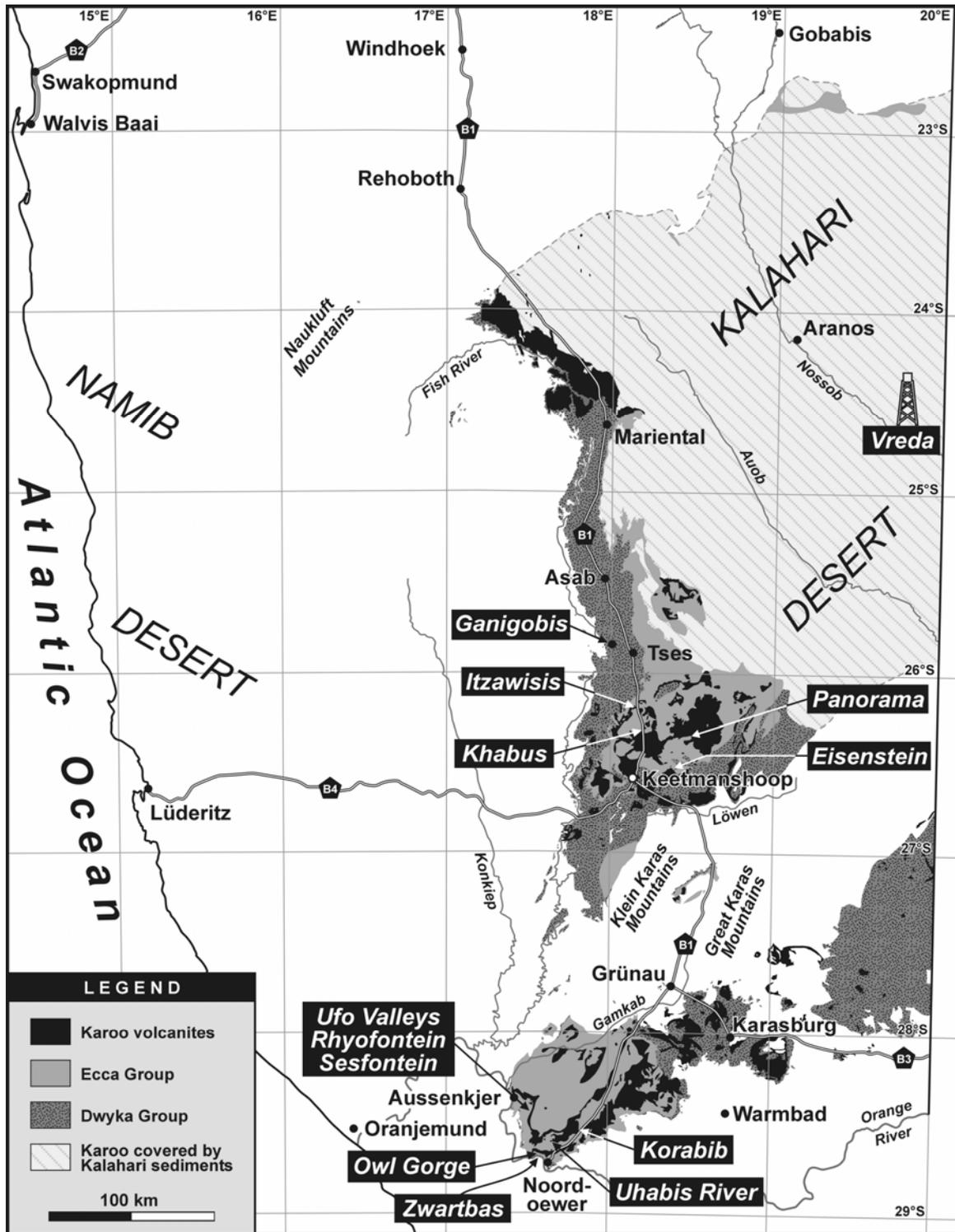
Fig. 3.1: Simplified geological map of the Karoo outcrop areas in southern Namibia showing the locations of the described tuffs. The geology is compiled after Miller & Schalk (1980).
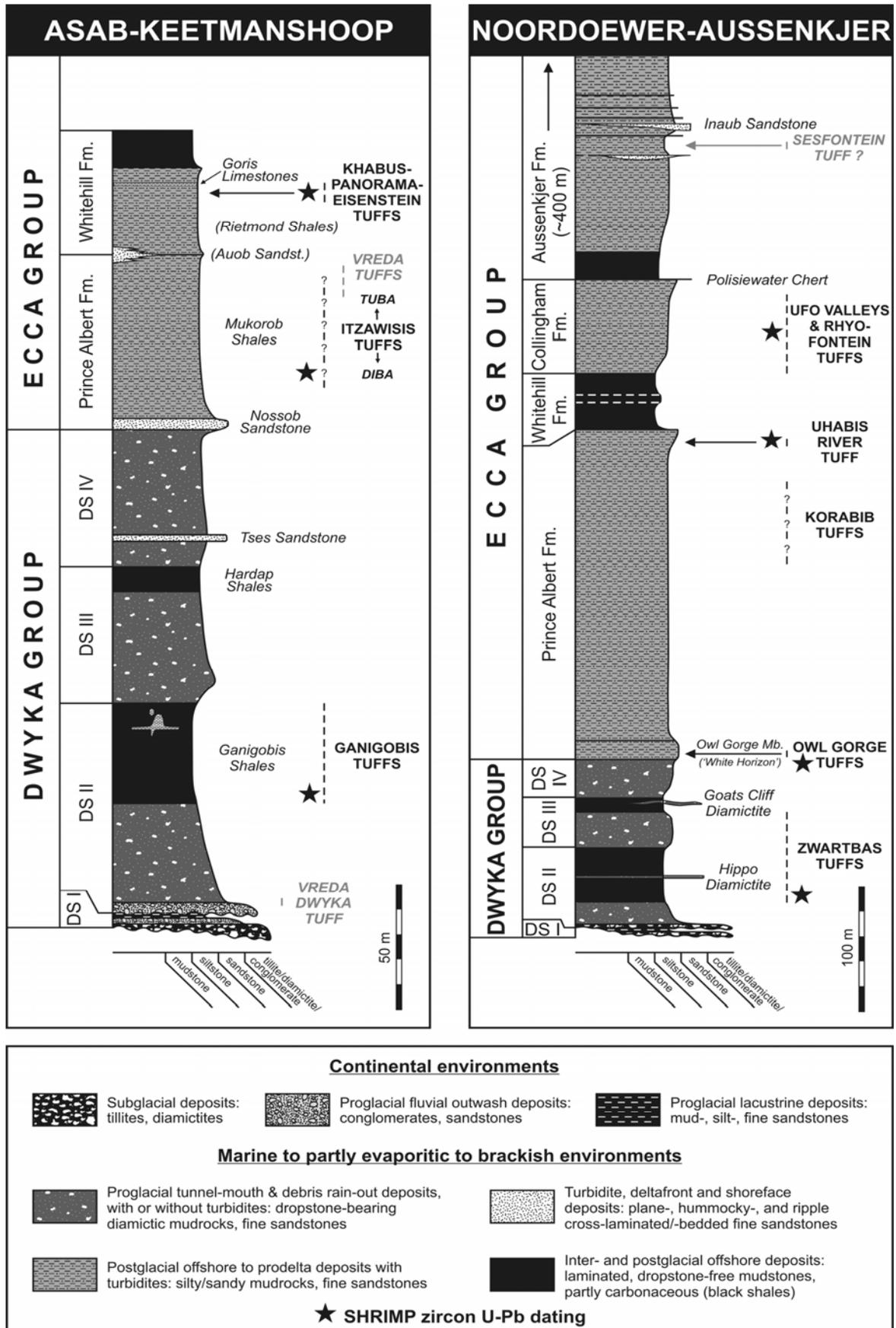
Fig. 3.2: Idealized sections for the two studied Karoo outcrop areas in southern Namibia showing the stratigraphic position of the described tuff beds. Compiled after Martin, 1953; Heath, 1972; Schreuder & Genis, 1975; Genis, 1982; Grill, 1997; Bangert et al., 2000; Geiger, 2000; Stollhofen et al., 2000a; supplemented and modified according to this authors measurements and interpretations.

3.4 Outcrop descriptions and petrography of the tuff layers

3.4.1 Tuff beds in the Dwyka Group

The Ganigobis Tuffs

The type area of the Ganigobis Tuffs lies in the vicinity of the small village of Ganigobis, about 12 km northwest of Tses (Fig. 3.1), where they are mainly exposed in eroded river-banks of the Fish River and its tributaries (Tses, Ganigobes and Asab Rivers). They were initially discovered by H. Stollhofen in 1994 and first described by Grill (1997). Bangert (2000) has investigated them in great detail in a following dissertation project. Within the Ganigobis Shale Member 21 fine-grained ash-fall tuff horizons were detected, which are bundled into eight groups (Fig. 3.3). The whole tuff-bearing interval has a thickness of about 35-40 m. The Ganigobis Shale Member consists essentially of dropstone-free mudstones, which form the upper portion of the second deglaciation sequence (DS II) of the Dwyka Group (Stollhofen et al., 2000a). Therefore, the Ganigobis Tuffs, together with the Zwartbas Tuffs, represent the earliest evidence of volcanism synchronous with Karoo deposition in southern Africa.

In the outcrops the bentonitic tuff layers form thin, very soft and crumbly, conspicuous light yellow to orange-brown weathering layers, which contrast markedly in colour with the dark grey to black mudstones. Limonite staining causes the ochreous colour of the tuffs. The thickness of the tuff layers ranges from less than 1 mm to about 2.5 cm, the majority of which can be traced laterally over tens of kilometres in the type area. Thicker, normally graded tuff beds commonly show sharp planar basal contacts and wavy, blurred upper parts. Together with the remarkable lateral continuity, despite their limited thickness, these character-istics suggest a derivation of the tuffs by ash fallout in a relatively distal setting with respect to its source (Stollhofen et al., 2000a).

The primary volcanic ash is almost completely altered (devitrified) to a mixture of micro- to cryptocrystalline clay minerals and minor amounts of microcrystalline quartz. The main clay minerals are illite and mixed layered illite-
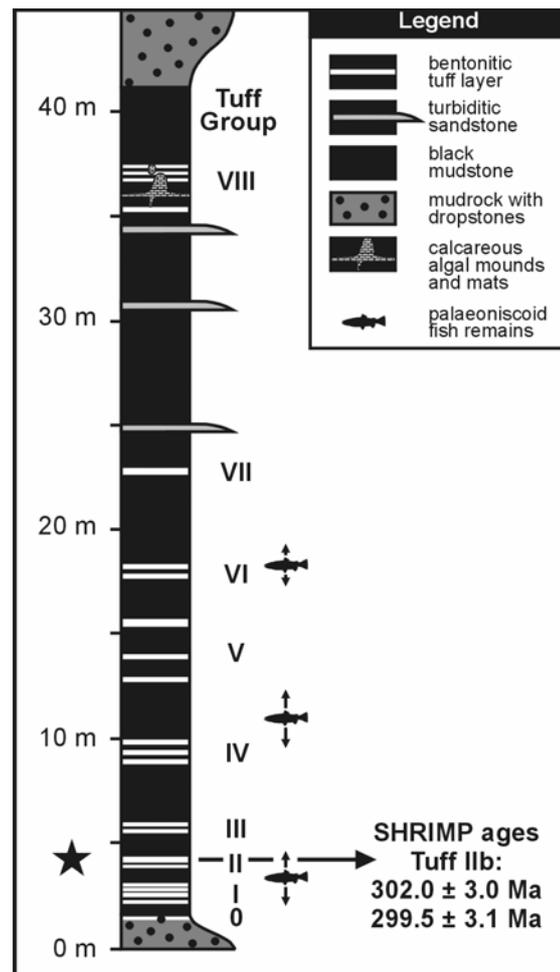
Fig. 3.3: Detailed tephrostratigraphy of the Ganigobis Shale Member (after Bangert et al., 2000).

smectite (IS-ML). The percentage of smectite within the IS-ML has been determined to vary between 20-30%. Also minor amounts of chlorite and kaolinite were identified (Bangert, 2000). The smectitic portion of the clay minerals gives the tuffs a somewhat soapy feeling, especially when the tuffs get into contact with water and rapidly swell. The matrix of the tuffs generally amounts to about 80-95% of the total rock volume. Crystals and crystal fragments of quartz, biotite, zircon and apatite, as well as a few possible relicts of volcanic glass have been identified as juvenile components in the tuffs (Bangert, 2000; Stollhofen et al., 2000a). Volcanically derived quartz is the most common juvenile mineral present in the analysed tuff beds and can reach in some cases up to 30% of the total rock volume. Quartz splinters with a length of 20-120 µm display angular to cuspate or thorn-shaped forms indicating an explosive pyroclastic origin. They are in some cases aligned parallel to the bedding of the tuff bed. One euhedral quartz crystal shows an almost hexagonal outline, what Bangert (2000) has interpreted as beta-quartz morphology indicative of high temperature volcanic quartz. Subhedral crystals of plagioclase have an average diameter of about 100 µm (Bangert et al., 1999). Biotite occurs in thin sections of almost all tuffs as euhedral to anhedral flakes, which often represent the largest phenocrysts with sizes reaching up to 240 µm. Biotite is normally not fresh and usually bleached displaying light brown to greenish-yellow colours in thin sections. They are often altered to pseudomorphs reminiscent of kaolinite booklets. Juvenile, magmatic zircons are mostly euhedral with elongated prismatic to needle-like forms and reach sizes of 30-260 µm. Some zircons show dark globular or tube-like inclusions of volcanic glass. Colourless, euhedral apatite crystals with a crystal size of 15-280 µm are also a common juvenile component within the tuffs. They frequently contain brownish melt inclusions as well as clear fluid inclusions. Other probable juvenile minerals that have been observed in heavy mineral separates are monazite and sphene. In addition to these juvenile minerals, Bangert (2000) also reports relict structures of volcanic glass. These represent decomposed ash grains or aggregates up to 220 µm in size that are completely recrystallized to fine-grained quartz or kaolinite. Some of them may represent former pumice clasts. A single y-shaped bubble wall shard was also observed in one of the tuff beds in thin section. According to thin section analyses kaolinite is reported to be one of the major secondary components within the tuffs (Bangert, 2000). Diagenetic aggregates of straight-sided kaolinite vermicules, 40-200 µm in diameter, can form up to 30% of the total rock volume (Stollhofen et al., 2000a). Apart from these large kaolinite vermicules and booklets also fibrous stacks of kaolinite (40-230 µm) and very fine-grained kaolinite aggregates dispersed in the matrix are reported (Bangert, 2000). Further frequently observed secondary minerals are barite, fibrous gypsum, blocky calcite, zeolite and hematite/goethite.

Contrary to the reported abundance of kaolinite, XRD analyses of the Ganigobis Tuffs revealed that kaolinite appears only in minor amounts, while illite is always the dominant clay mineral (Bangert, 2000). A re-examination of the Ganigobis Tuffs thin sections revealed that in many thin sections the 'kaolinite' booklets and vermicules show under crossed polars bright interference colours (see Fig. 3.4). This observation is not in accordance with the optical characteristics of kaolinite, whose low birefringence (0.0070) generates only first order shades of grey. As most of these crystal booklets and vermicules indeed have a striking similarity to typical kaolinite morphologies found in tonsteins, it is supposed that the majority of the reported crystal booklets and vermicules originally consisted of kaolinite but were transformed later under higher temperatures to illite (cf. Bohor & Triplehorn, 1993; Viljoen, 1994; Christidis, 1995; Knight et al., 2000). What still remains to be explained is the timing of the kaolinite growth. The depositional environment was surely saline during sedimentation of the tuffs, as indicated by the marine fauna in the Ganigobis Shales, which should lead to a smectitic alteration of the volcanic ash. However, organic matter in marine environments can also promote early diagenetic kaolinitization of volcanic ash (Bohor & Triplehorn, 1993; Tucker, 2001). Since the Ganigobis Shales are rich in organic matter (Grill, 1997; Bangert, 2000), this could explain an early diagenetic kaolinite growth in the Ganigobis Tuffs. At a later stage, transformation of smectite and kaolinite to illite was probably caused by burial diagenesis or, even more likely, by thermal overprinting due to very widespread Jurassic (dolerites) igneous activity. Finally, also a late stage, subrecent formation of kaolinite could have taken place due to surface weathering. Weathering of finely dissiminated pyrite in the enclosing shales by meteoric water produces sulfuric acid, which can cause mobilization and leaching of alkalies and lead to formation of kaolinite.
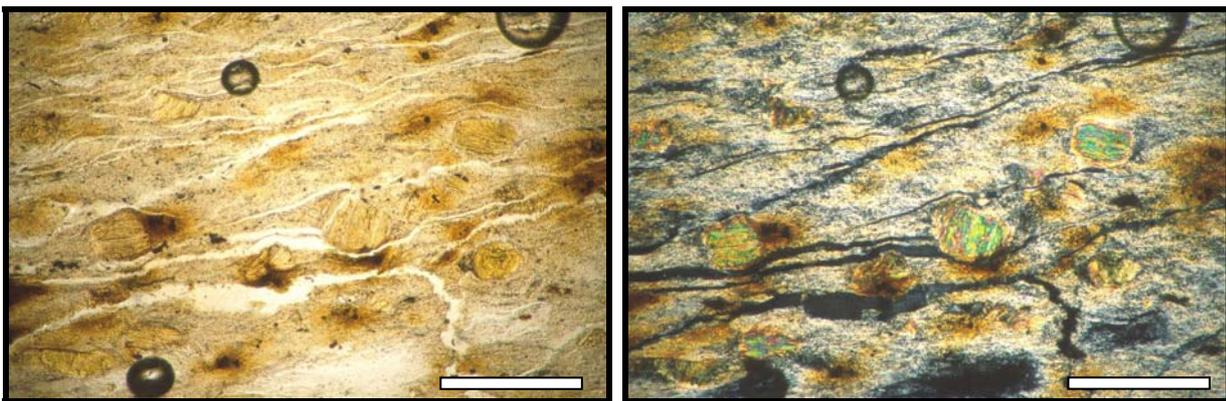
Fig. 3.4: (A/l.) The typical appearance of the Ganigobis Tuffs in thin sections with so-called 'kaolinite booklets' interspersed in a fine-grained argillaceous matrix (sample locality 23, Waterval, c. 10 km west of Tses, Bangert, 2000). **(B/r.)** Under crossed polars these booklets, however, display bright interference colours and therefore most probably represent illite pseudomorphs after kaolinite. Scale bar 200 µm.

The Zwartbas Tuffs

At the Orange River in southernmost Namibia altered tuff layers in the Dwyka Group were discovered in 1997 by V. Lorenz during a fieldtrip. These bentonites are excellently exposed along cliffs of the Orange River cut banks on Namibian territory, opposite of the small village of Zwartbas, located about 6 km northwest of Noordoewer on South African territory. The best outcrops are found in the vicinity of the Felix Unite Provenance Camp (Fig. 3.5 & 3.6) on the northern shore of the Orange River south of the gravel road D 212, which leads from Noordoewer to Aussenkjer and Rosh Pinah. The outcrops below this river-rafter camp were termed 'Fossil Bend' and 'Jet Cliff' by Geiger (2000), who investigated these tuff layers within the scope of a diploma project. Geiger (2000) logged altogether 65 distinct ash fall-derived volcanic tuff beds within the basal 95 m of the lower part of the Dwyka Group exposures on the Namibian side of the river opposite of Zwartbas (Fig. 3.7). Closely spaced tuff beds of the 65 tuff layers were bundled into 38 tuff groups. Tuff groups 36-38 were found higher up in the Dwyka succession north of the D 212 in the so-called Hare Valley and at the Goats Cliff locality (Fig. 3.6). The bentonites are interbedded in dark coloured, C_{org}-rich, marine dropstone-poor to dropstone-free shales of the Dwyka Group (Fig. 3.5-B). The total thickness of the tuffaceous interval is about 75 m. Commonly the tuffs display light yellowish to brownish colours and the thickness of the bentonites varies normally from less than 1 mm to a few millimetres, in few cases layers are up to 4 cm thick. A local thickening of tuff layers is ascribed to secondary gypsum growth. In some cases tuff beds pass laterally into con-cretionary carbonate horizons. Over shorter distances the tuff layers are laterally continuous, the wider lateral extent of the tuff layers was not studied. Upper and lower contacts of the tuff layers are generally sharp and planar. Some of the tuff layers are normally graded. The tuffs feel somewhat soapy or waxy and disintegrate easily when moistened.

Fig. 3.5: (A/l.) Along these cliffs at the northern (Namibian) side of the Orange River, below the Felix Unite Provenance Camp, the Zwartbas Tuffs are excellently exposed. The left, western part of the cliff represents the so-called 'Fossil Bend', whereas the right (eastern) part is named 'Jet Cliff' (see Fig. 3.6; Geiger, 2000). In the background shales of the Dwyka and lowermost Ecca Group are topped by a dolerite sheet. **(B/r.)** The typical field appearance of a light coloured bentonite layer within dropstone-bearing black shales of the basal Dwyka Group at the 'Fossil Bend'.
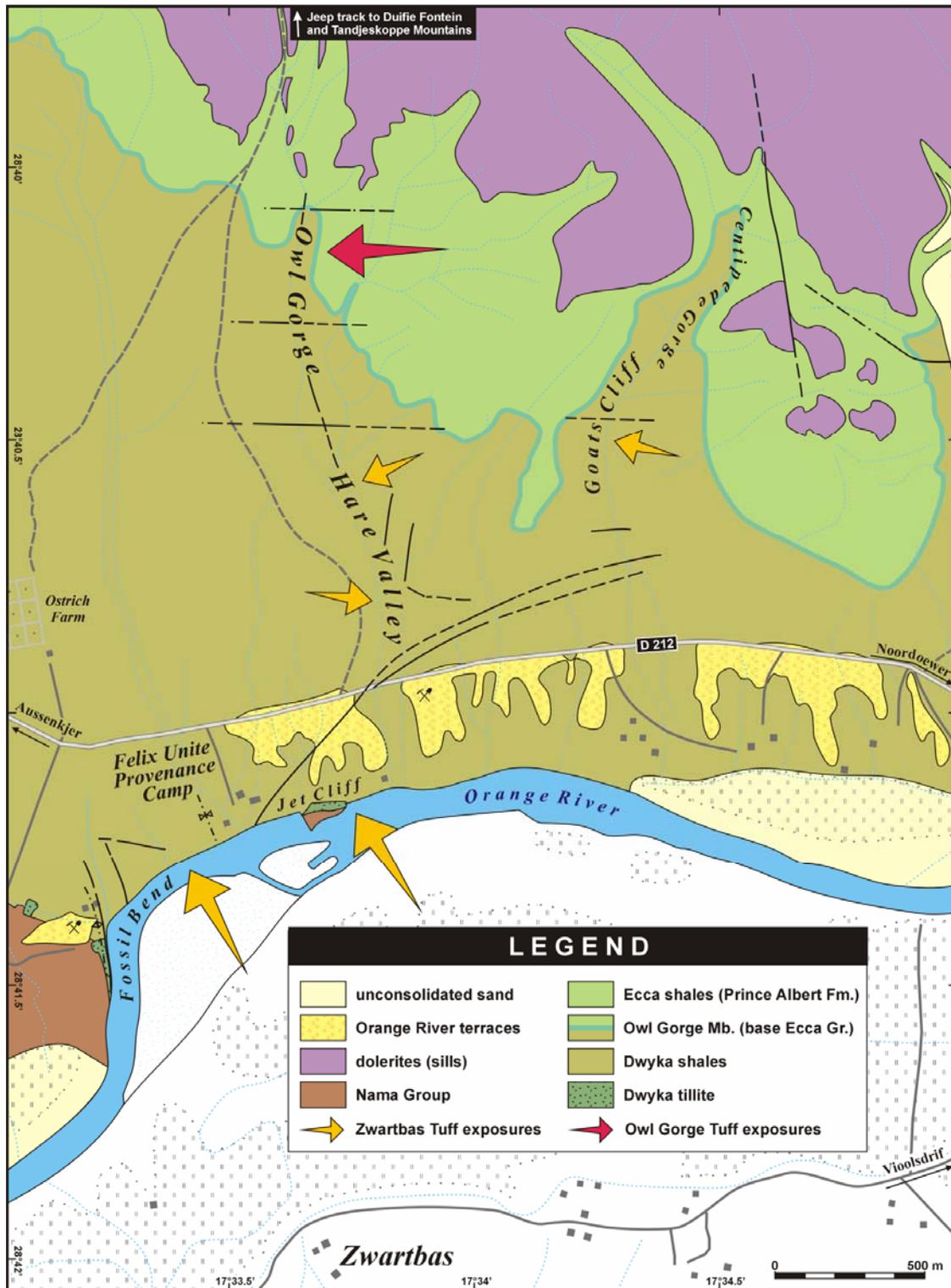
Fig. 3.6: Geological map of the Orange River area in the vicinity of the Felix Unite Provenance Camp, c. 6 km NW of Noordoewer, showing the outcrop localities of the Zwartbas and Owl Gorge Tuffs. The map is mainly adopted from Geiger (2000). However, the Dwyka-Ecca boundary is placed here alternatively along the whitish weathering horizon of the Owl Gorge Member, a distal equivalent of the Nossob Sandstone Member farther north.

The bentonites consist mainly of clay minerals formed by alteration of former volcanic ash. The clay mineral matrix is dominated by illite but also minor amounts of kaolinite, chlorite and smectite were detected by XRD measurements (Geiger, 2000). The largest and most abundant juvenile crystals within the matrix are clear, mono-crystalline quartz grains with a size of up to 100 μm. They are highly angular and often show splinter- and thorn-shaped forms. Quartz prob-ably constitutes about 1% of the total mode in thin sections. The presence of plagioclase crystals has been reported, too. Furthermore, a few circular, internal structureless ash aggre-gates, 60-100 μm in diameter, have been observed in thin section. Biotite occurs as flakes with a size of 100-150 μm and is in many cases either marginally altered to chlorite or almost completely replaced by kaolinite, forming con-spicuous 'kaolinite' booklets. As Geiger (2000) explicitly notes that these booklets display under crossed polars bright interference colours, it is interpreted that these 'kaolinite' booklets are replaced by illite. This phenomenon was already mentioned in the description of the Ganigobis Tuffs. Heavy mineral separates of the tuff layers mainly yielded juvenile zircons and apatites. They occur as euhedral, colourless elongate crystals with lengths of up to 200 μm. Both minerals frequently contain globular to tubular, dark brown glass or light coloured fluid inclusions. Apart from the 'kaolinite' booklets, gypsum, barite, pyrite and hematite/goethite are reported as secondary minerals.

Fig. 3.7: Detailed tephrostratigraphy of the Dwyka Group at Zwartbas. Note that an alternative model for the position of the deglaciation sequence (DS) boundaries is proposed here. Profile after Geiger (2000).
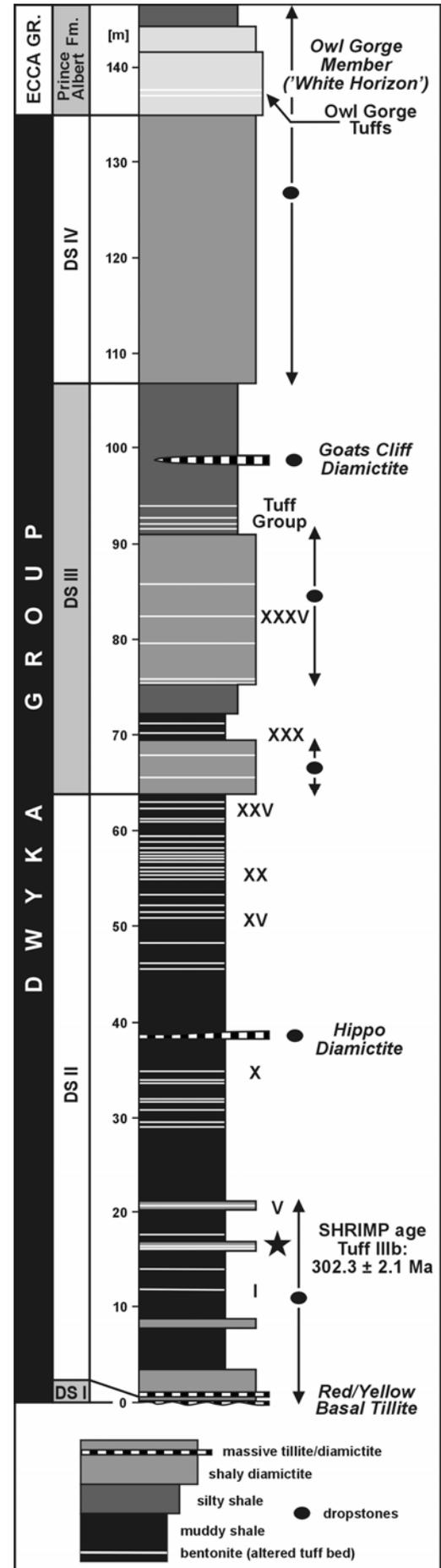
Other tuff recordings from the Dwyka Group and equivalent deposits

Bentonitic ash-fall tuff beds are also known from outcrops of the Dwyka Group in the southern part of the South African Main Karoo Basin (Western and Eastern Cape Provinces), namely at Willowmore and Klaarstroom, where they occur in the upper part of DS-III of the Dwyka Group (Viljoen, 1990; Veevers et al., 1994; Bangert, 2000). One tuff layer from the Klaarstroom locality was dated by Bangert et al. (1999) and yielded a SHRIMP age of 297 ± 1.8 Ma (Asselian after Gradstein et al., 2005) .

In addition, cores of SOEKOR wells in the southwestern part of the Karoo Basin also contain tuff beds in the Dwyka Group. Two XRD analyses on such Dwyka tuffs from the Main Karoo Basin showed illite, quartz and albite as the only determined components (Viljoen, 1995). High concentrations of ash beds occur in the upper parts of the Dwyka Group in the southern SOEKOR wells. Again, these tuff beds mainly originate from the uppermost part of DS-III, only in well OL 1/69 two thin tuff beds were detected in DS-II (Bangert, 2000). This is in marked contrast to the Namibian Dwyka tuff occurrences, which are mainly known from DS-II and where from the upper part of DS-III no tuff beds are recorded yet. The lowermost tephra beds were observed in the boreholes KL1/65 and QU1/65, where they occur in mudrock-rich units at 87 and 31 m, respectively, above the base of the Dwyka Group (Viljoen, 1998). According to log data of Bangert (2000) these lowermost Dwyka tuff beds lie within (KL1/65) or at the top (QU1/65) of DS-I and should therefore represent the oldest Karoo tuffs layers. Interestingly, a tuff bed in a similar stratigraphic position is known from the core of the Vreda well in Namibia. In the working documents of H. Grill it was listed that in the Vreda well 21.34 m above the base of the Dwyka Group a tuff layer occurs, corresponding to a position in the lowermost parts of DS-II. A thin section of this tuff displays large, illitized 'kaolinite booklets' dispersed in a fine-grained clay matrix, similar to the appearance of the Ganigobis Tuffs.

In the eastern part of the South African Karoo Basin, in KwaZulu-Natal, two multiple normal graded tuffaceous beds were identified in deposits of the Dwyka Group in an outcrop 2 km east of Nondweni. As the base of these tuffaceous deposits is mostly undulatory, it is suggested that they represent volcanic ash-fall material, which was reworked and redeposited by traction current activity in a proglacial marine environment (Bangert & von Brunn, 2001).

No tuff layers have so far been reported from the glacigenic Itararé Group, the equivalent of the Dwyka Group in the Brazilian Paraná Basin. Also no tuff occurrences in Dwyka-equivalent rocks are known from the Falkland/Malvinas Islands and Antarctica. However, igneous activity and pyroclastic rocks of Late Carboniferous age are known from the eastern South American Paganzo Basin and from northern Chile (López-Gamundí et al., 1990; Breitkreuz, 1991; López-Gamundí & Breitkreuz, 1997; Net et al., 2002). Especially the chert beds in the upper part of the Tupe Formation (Paganzo Basin), which are interpreted as altered pyroclastic ash fall deposits (Net, 1999) and which are found in the top part and above Stephanian transgression mudstones, might well be time-equivalent with the latest Carboniferous tuffs of the Dwyka Group in South Africa and Namibia.

3.4.2 Tuff beds in the Ecca Group

3.4.2.1 Prince Albert Formation

The Owl Gorge Tuffs

The Owl Gorge Member, a conspicuous marker zone with light-weathering shale intervals at the Dwyka-Ecca boundary in the Noordoewer area, contains a number of thin, mm- to cm-thick, light coloured, whitish to yellowish horizons, of which two of them have been positively identified as altered volcanic ash layers. These two bentonites are named OG-9 and OG-12. For the other light coloured, thin layers a pyroclastic origin is not substantiated, some of them may have a detrital siliciclastic origin, others might have formed entirely diagenetically. The OG-9 and OG-12 Tuffs have been discovered in the Owl Gorge (Fig. 3.6), the type locality of the Owl Gorge Member, and they can be traced laterally over the entire outcrop locality, which is about 250 m. The Owl Gorge can be reached via a jeep track that leaves the D 212 c. 450 m east of the entrance gate to the Felix Unite Provenance Camp in a northerly direction (towards the spring at Duifie Fontein and the western Tandjeskoppe Mountains). About 2.5 km north of the D 212 this track leads to the upper section of the Owl Gorge (Fig. 3.6). From this point one has to leave the car and walk downstream a few tens of metres to reach the stratigraphic level of the Owl Gorge Member. Alternatively, one can also follow the Hare Valley upstream from the D 212. The Hare Valley is accessible with a 4x4 vehicle up to an area quite close to the southern end of the Owl Gorge. The whole succession of the Owl Gorge Member is excellently exposed at the eastern gorge walls, where the two bentonite horizons are found between the first bleached shale horizon W-I and the second prominent carbonate concretion layer C-II (Fig. 3.8 & 3.9). Dark, brownish weathering shales enclose the two light coloured tuff layers.
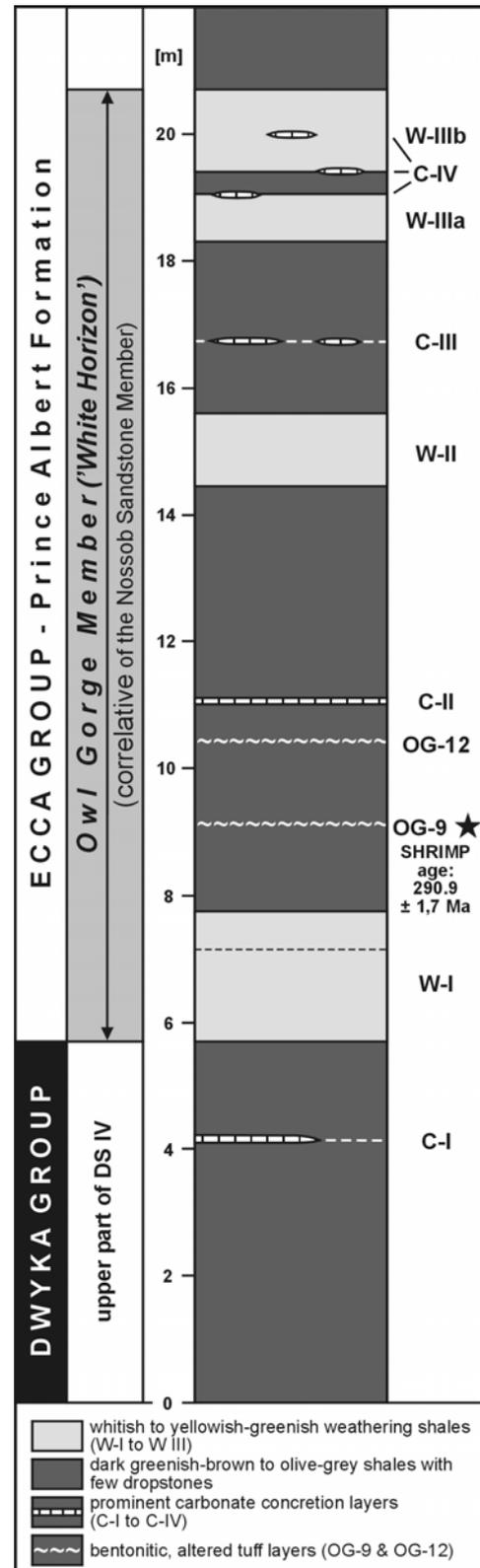
Fig. 3.8: Overview section of the Owl Gorge Member at its type locality showing the position of the OG-9 and OG-12 Tuffs.
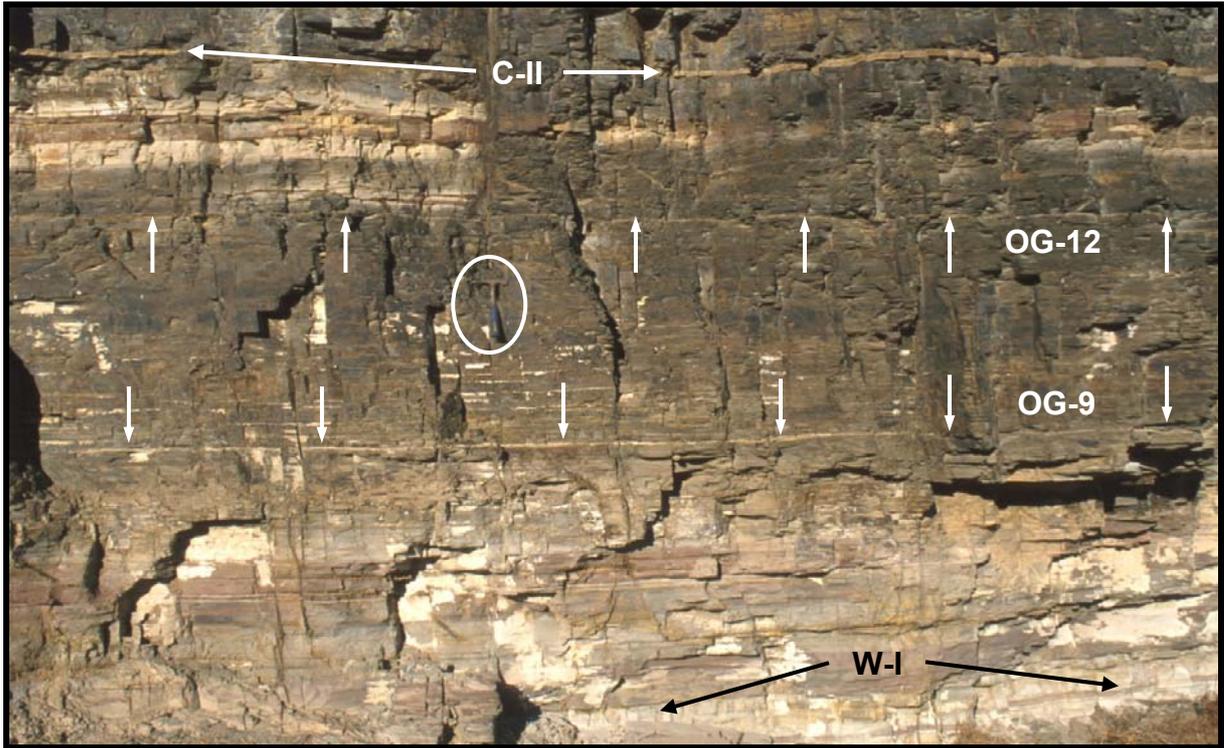
Fig. 3.9: Bentonitic tuff layers OG-9 and OG-12 between the upper part of the light-weathering shales of horizon W-I and carbonate concretion layer C-II exposed at the eastern walls of the Owl Gorge. Hammer (encircled) for scale. See also Fig. 3.8 for the position of the displayed stratigraphic interval of the Owl Gorge Member.

Tuff OG-9 has a light greenish-grey colour and attains a fairly constant thickness of 8-9.5 mm. This tuff forms a relatively resistant layer and can be broken off the outcrops as cm- to dm-sized slabs, which readily separate from the host rock. It does not swell or disintegrate when it is wet. An indistinct and discontinuous lamination can be observed in the upper part of the tuff. Already in macroscopical view the normal grading of the tuff layer is visible. The lower contact is sharp and non-erosive, the upper contact is sharp, too, and not gradational towards the overlying shale. At the top of the tuff layer a very fine-grained, whitish to light grey lamina developed, which apparently attained some cohesiveness before sedimentation of the overlying silty muds. During deposition of these silty muds sharp-contoured erosional structures were cut into the lamina at the top of the tuff and small, soft tuff particles were ripped off from the top lamina, now floating as sand-sized tuff grains in the overlying massive shale (see Fig. 3.10). During suspension settling of the fine-grained top of the tuff layer, volcanic ash was obviously not mixed with detrital mud. This implies that detrital muddy background sedimentation was either extremely low or ceased for a certain time during and also shortly after deposition of the volcanic ash. This obviously led to a slight stabilization or solidification of the top of the tuff. Since the overlying shale is clearly erosive it must have been deposited by a silty-muddy, distal turbidity current.
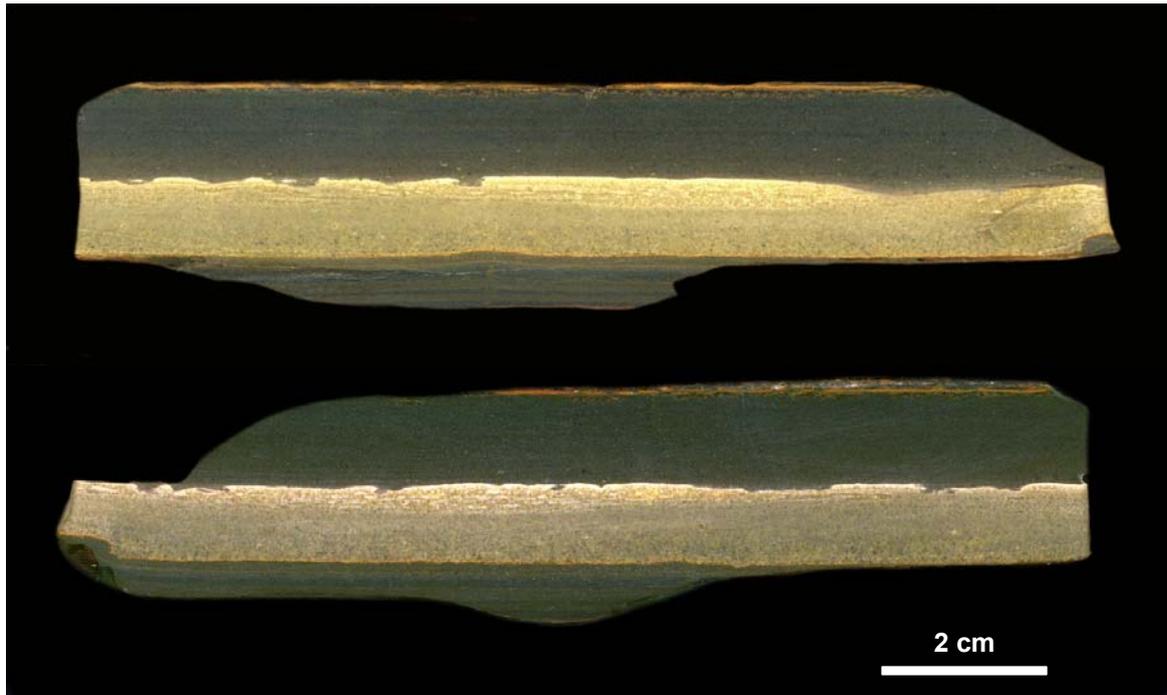
Fig. 3.10: Polished slabs of the OG-9 Tuff showing sharp-contoured erosional cuts in the fine-grained, obviously cohesive lamina at the top of the tuff. Note that the underlying shale is laminated, whereas the overlying shale is massive due to deposition as a distal turbidite.

Whole rock powder diffraction analyses reveal that the OG-9 Tuff is mainly composed of illite, quartz and plagioclase (albite). The presence of chlorite is indicated by reflections at ~6.2° and ~12.5° 2θ (CuKα), however, only as a trace component. Biotite, and its probable alteration products hydrobiotite, vermiculite or kaolinite, could not be identified in whole rock powder diffraction samples because its most prominent reflections overlap with those of illite, quartz and chlorite. In thin sections the normal grading of the tuff is clearly visible. The lower, coarser-grained part of the tuff is rich in crystal fragments, poorly sorted and matrix supported. It grades into the fine-grained, crystal fragment-poor/free, well sorted upper part of the tuff. Crystal fragments of quartz, feldspar, and biotite as well as pseudomorphs are dispersed in a fine-grained, recrystallized matrix (Fig. 3.11-A). Elongate quartz splinters and platy biotite flakes are often aligned parallel to the bedding and produce a planar structure, which, however, becomes apparent only in thin section. Subspherical, greenish-yellowish spots give the tuff a speckled appearance, especially in its upper part (Fig. 3.11-B).

Quartz is by far the most abundant crystal component of the coarser fraction of the tuff. The majority of the quartz grains is highly angular, often with extreme splinter- or thorn-shaped forms (Fig. 3.11-A), but more equidimensional quartz grains are also observed frequently. Very rare, in contrast, are quartz crystals with subspherical to roughly hexagonal outlines and partly regular crystal faces, probably representing beta-quartz (high temperature) para-morphs. Almost all quartz grains are monocrystalline with uniform extinction, only a few are

polycrystalline or show undulose extinction. Some quartz grains contain fluid or mineral inclusions. At the base of the tuff the mean grain size of quartz lies between 100 and 200 µm but some quartz splinters can reach lengths of more than 400 µm. Feldspar is quite frequently observed in thin sections. Plagioclase crystals and crystal fragments, easily identified by their polysynthetic twinning (Fig. 3.11-C), are mainly angular but also lath-shaped, euhedral to subhedral crystals can be observed. The average size of plagioclase is about 100 µm at the base of the tuff. Only a few possible K-feldspar grains with Carlsbad twinning have been observed (Fig. 3.11-C). The true amount of K-feldspar is difficult to ascertain because of its resemblance to quartz and plagioclase when unaltered or untwinned. However, since no K-feldspar was detected in the XRD diagrams with certainty, its content is probably very low. Alteration of feldspar is highly variable. Some grains are virtually free of alteration signs, others are almost completely altered (Fig. 3.11-D). All transitions from fresh to dusty-dirty to partly or entirely replaced grains are sometimes visible in one thin section. The alteration product of feldspar is mainly a greenish-yellowish, slightly pleochroitic phyllosilicate (sericite-chlorite mixture?). It occurs as thin lamellae between cleavage planes (Fig. 3.11-E) or as intergrown flakes replacing feldspar (Fig. 3.11-D). The occurrence of fresh to almost entirely altered feldspar (plagioclase) grains in thin sections was already mentioned in earlier studies on K-bentonites from the South African Karoo Basin (e.g. Elliot & Watts, 1974; Viljoen, 1995). Biotite is quite abundant in thin sections of the OG-9 Tuff. It forms mainly subhedral to anhedral flakes and crystal stacks, some of the flakes, however, are euhedral and display perfectly hexagonal crystal shapes (Fig. 3.11-F). In the basal part of the tuff the biotite flakes reach average lengths of 200-300 µm when cut parallel to the c-axis. The largest observed biotite flake has a length of approximately 600 µm. The biotite flakes are often aligned parallel to the bedding. Many biotite grains are bleached and exhibit pale greenish-yellowish colours in thin sections with a pleochroism from pale yellowish to darker greenish-yellowish hues. Some of the biotite grains, however, have retained their typical darker yellowish- to reddish-brown colour and are still strongly pleochroitic. Many of the only slightly altered biotite flakes show cross-forming isogyres in conoscopical view when cut perpendicular to the c-axis. The more strongly altered biotites resemble the alteration products of feldspar, showing similar optical properties (colour, pleochroism). The optical properties of these alteration products are not fully characteristic for chlorite, which is anyhow not very pronounced in the XRD diagrams. Some of the altered biotite stacks are strongly expanded and swollen with a pronounced disruption of the individual platelets, typical of biotite alteration (Bohor & Triplehorn, 1993) (Fig. 3.11-G). Under crossed polars these altered biotite stacks display bright interference colours. These observations point rather to an alteration of biotite to hydrobiotite, vermiculite or illite but not to pure kaolinite or chlorite (Tröger, 1969). Within some of the altered biotite stacks also

colourless lamellae or domains can be observed. These colourless lamellae or domains display under crossed polars clear and bright interference colours typical of illite or muscovite. Within a few biotite grains a network of tiny acicular alteration products, so-called sagenite (rutile needles), have been observed (Fig. 3.11-H). In addition to quartz, feldspar and biotite are pseudomorphs after an unknown precursor mineral which are abundant in thin sections. The size of these pseudomorphs lies in the size range of quartz and feldspar. These pseudomorphs are filled with interlocking flakes of a greenish-yellowish, slightly pleochroitic phyllosilicate (similar to the alteration products of feldspar and biotite) intergrown with quartz (Fig. 3.11-I/K). Often a dark, iron oxide-rich margin is developed around the pseudomorphs, which indicates a certain iron content in the original mineral. The precursor mineral was mainly subhedral to anhedral to somewhat rounded and obviously had a shortprismatic habitus. Some of the pseudomorphs still display remnants of prismatic crystal faces (Fig. 3.11-L). From relictic crystal outlines it is suggested that at least some of the pseudomorphs represent former pyroxenes and/or amphiboles. The dark-rimmed pseudo-morphs do not represent biotite pseudomorphs because altered biotite crystals are in the studied thin sections normally not surrounded by dark alteration products. Very similar pseudomorphs were described by McLachlan & Jonker (1990) from a deformed bed of an altered air-fall tuff from the northwestern part of the South African Karoo Basin. They inter-preted the replaced minerals as being originally pyroxene. With quartz, plagioclase and biotite as the dominant crystal fragments, a more intermediate, rhyodacitic-dacitic compo-sition of the igneous source rock is expected. From this point of view the original presence of pyroxene appears not too unlikely. In addition to these pseudomorphs, similar pyroclasts with a dirty, dark greenish-yellowish colour occur in thin sections. In contrast to the described pseudomorphs they show more roundish-elliptical to flattened, lens-like outlines and some contain inclusions of angular quartz or feldspar grains (Fig. 3.11-P/Q). Under crossed polars they appear almost isotropic. They are interpreted as altered remnants of originally vitric pyroclasts. Characteristic, y-shaped glass shards, however, have not been observed in any of the studied thin sections. Zircon, although an accessory phase, can be found in almost every thin section and forms mostly euhedral to subhedral grains with a size of 30-150 µm. Both longprismatic to acicular and equidimensional to stubby forms are observed. Some of the zircons show oscillatory growth zoning and some contain brownish globular inclusions (Fig. 3.11-N). Apatite forms another frequently observed accessory phase, which is mainly present as elongate, euhedral crystals with etched crystal surfaces and reaching lengths of up to 150 µm. Due to the strong basal cleavage most crystals are broken and consist of fragments, which are slightly displaced against each other (Fig. 3.11-O). Some crystals contain tubular inclusions. The finely recrystallized matrix of the tuff consists of tiny, inter-locking, and lath-shaped to acicular crystallites, which show under crossed polars mainly

grey first order interference colours (Fig. 3.11-E). In the lower, more coarse-grained part of the tuff the crystallites reach average sizes of 5 to 10 µm. These crystallites probably represent intergrown albite, quartz and illite. In a few thin sections small, dark-rimmed, perfectly round micro-spherules with a size of 20-40 µm can be observed within the matrix (Fig. 3.11-M). They are either filled with quartz or behave isotropically under crossed polars. Such micro-spherules have also been described by several authors from the underlying shales of the Dwyka Group (e.g. Bangert, 2000; Geiger, 2000) and have also been observed in phosphatic shales of the lower Ecca Group by the author (see Fig. 2.5-P). The question about their origin is not fully resolved but the most probable explanation is that they represent remains of radiolarians. Regardless of their organic or inorganic origin, they are considered to be a primary component of the tuff. Clearly of secondary origin are the numerous greenish-yellowish-brown spots (50-100 µm), which give the tuff a speckled appearance (Fig. 3.11-B). These subspherical to ovoid porphyroblasts enclose crystallites of the matrix and behave pseudoisotropically under crossed polars. It is suggested that they grew during a high temperature imprint caused by extensive dolerite intrusions of Jurassic age and that they originally were composed of poikiloblastic cordierite, which is now completely altered to pinite, a complex and variable mixture of mainly sericite and chlorite (Tröger, 1969; Ogiermann, 2002). Similar contact-metamorphic spots were also described for altered tuff layers from the northwestern part of the South African Karoo Basin and interpreted as vermiculite and/or chlorite porphyroblasts (McLachlan & Jonker, 1990). Another peculiar feature in thin sections are small vugs or vesicles (0.2-1.5 mm in diameter), which have roughly circular, polygonal or irregular outlines. They are filled with coarse-grained quartz (up to 500 µm) intergrown with small crystals of a flaky, greenish-yellowish, slightly pleochroitic phyllosilicate (Fig. 3.11-R/S). Under crossed polars only the paler parts of the crystals show anomalous bluish-grey interference colours, whereas the darker coloured, oxidized parts of the crystals show more yellowish to reddish-orange interference colours. These phyllo-silicates may be mainly composed of chlorite or oxidized chlorite. Within some of the vesicles also larger crystals with a lamellar structure can be observed. Most probably they also represent completely pinitized, multiple lamellar twinned cordierite crystals. Often the vesicles are surrounded and outlined by a greenish-yellowish to dark brown rim possibly composed of chlorite or a chlorite-bearing phyllosilicate mixture. Present within the vesicles are sometimes tiny (10-20 µm), euhedral to subhedral, deep orange-brown hematite and/or goethite platelets. The same minerals, filling the vesicles, are also observed in veins (Fig. 3.11-A). From observations in tuff OG-12 (see following description) it is suggested that the filled vesicles could have originally represented trapped air or biogenically or chemically generated gas bubbles.

Due to its key stratigraphic position very close to the Dwyka-Ecca boundary Tuff OG-9 was chosen for radiometric age dating. It has been dated by SHRIMP single zircon U-Pb isotopes analyses at 290.9 ± 1.7 Ma (Sakmarian), but contained also a slightly older zircon fraction with a weighted mean age of 298.7 ± 2.0 Ma (Early Asselian) and one zircon with an Early Ordovician age (~480 Ma) (see also Chapter 4; age stages after Gradstein et al., 2005).
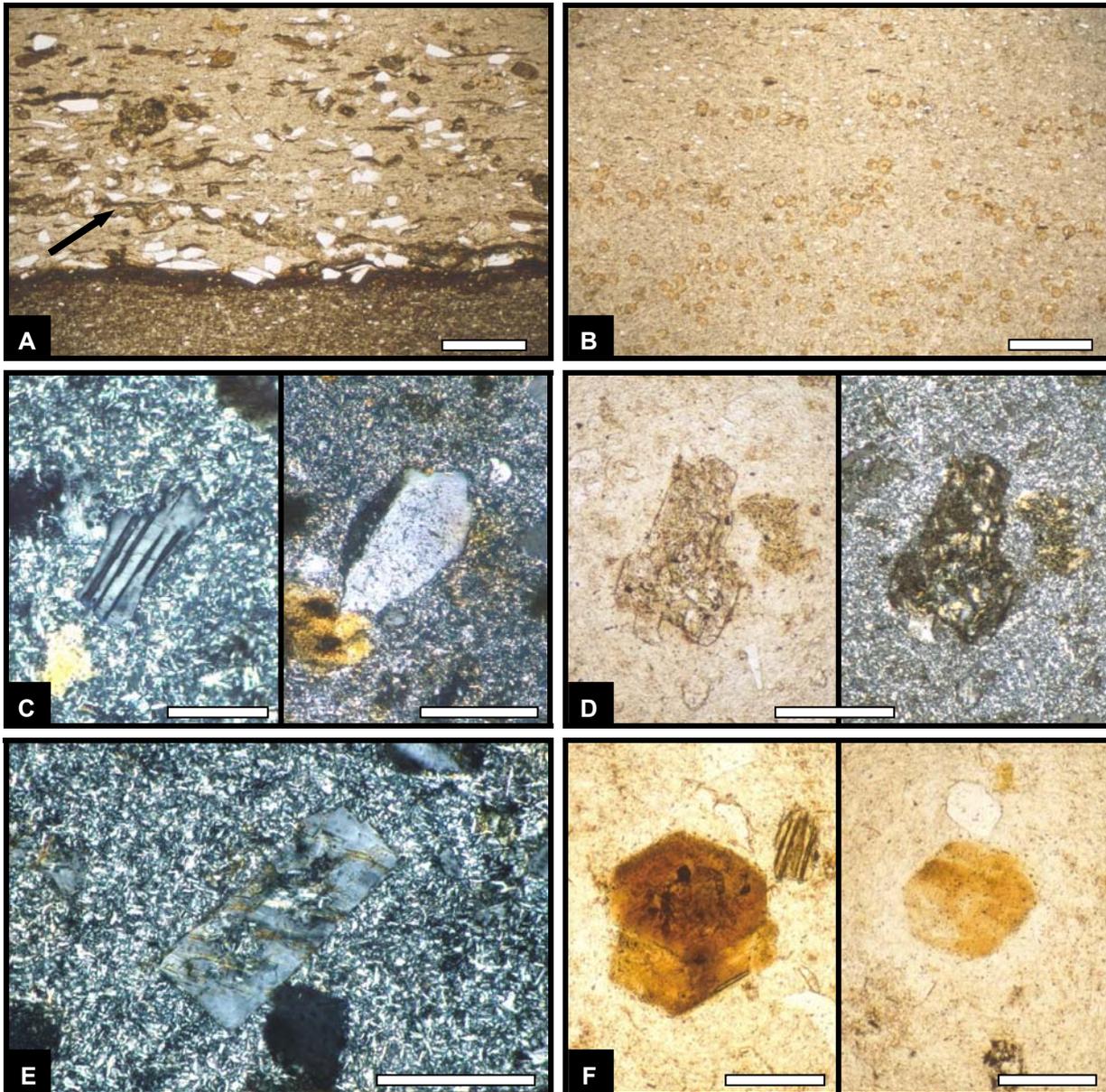
Fig. 3.11: Thin section photographs of tuff OG-9: **(A)** Crystal-rich, lower part of the tuff with light coloured quartz and feldspar grains as well as dark coloured biotite flakes and pseudomorphs interspersed in a light coloured matrix. The underlying dark greenish-brown rock is a silty shale. Arrow points to a vein cross-cutting the tuff. Plane-polarized light. Scale bar 500 μm. **(B)** Crystal-poor, upper part of the tuff with greenish-yellowish-brown, subspherical spots (interpreted as completely pinitized cordierite porphyroblasts) giving the tuff a speckled appearance. Plane-polarized light. Scale bar 500 μm. **(C)** Fresh to only slightly altered, angular plagioclase (left) and K(?)-feldspar (right) crystal. Crossed polars. Scale bar 50 μm (left) and 150 μm (right). **(D)** Highly altered feldspar grain partly replaced by greenish-yellowish phyllosilicates (sericite-chlorite mixture?). Plane-polarized light (left) and crossed polars (right). Scale bar 150 μm. **(E)** Euhedral feldspar grain with greenish-yellowish phyllosilicate lamellae between cleavage planes. Note the finely recrystallized tuff matrix composed of tiny, interlocking, acicular to lath-shaped crystallites. Crossed polars. Scale bar 100 μm. **(F)** Euhedral biotite flakes with perfectly hexagonal crystal shapes. Plane-polarized light. Scale bars 100 μm.
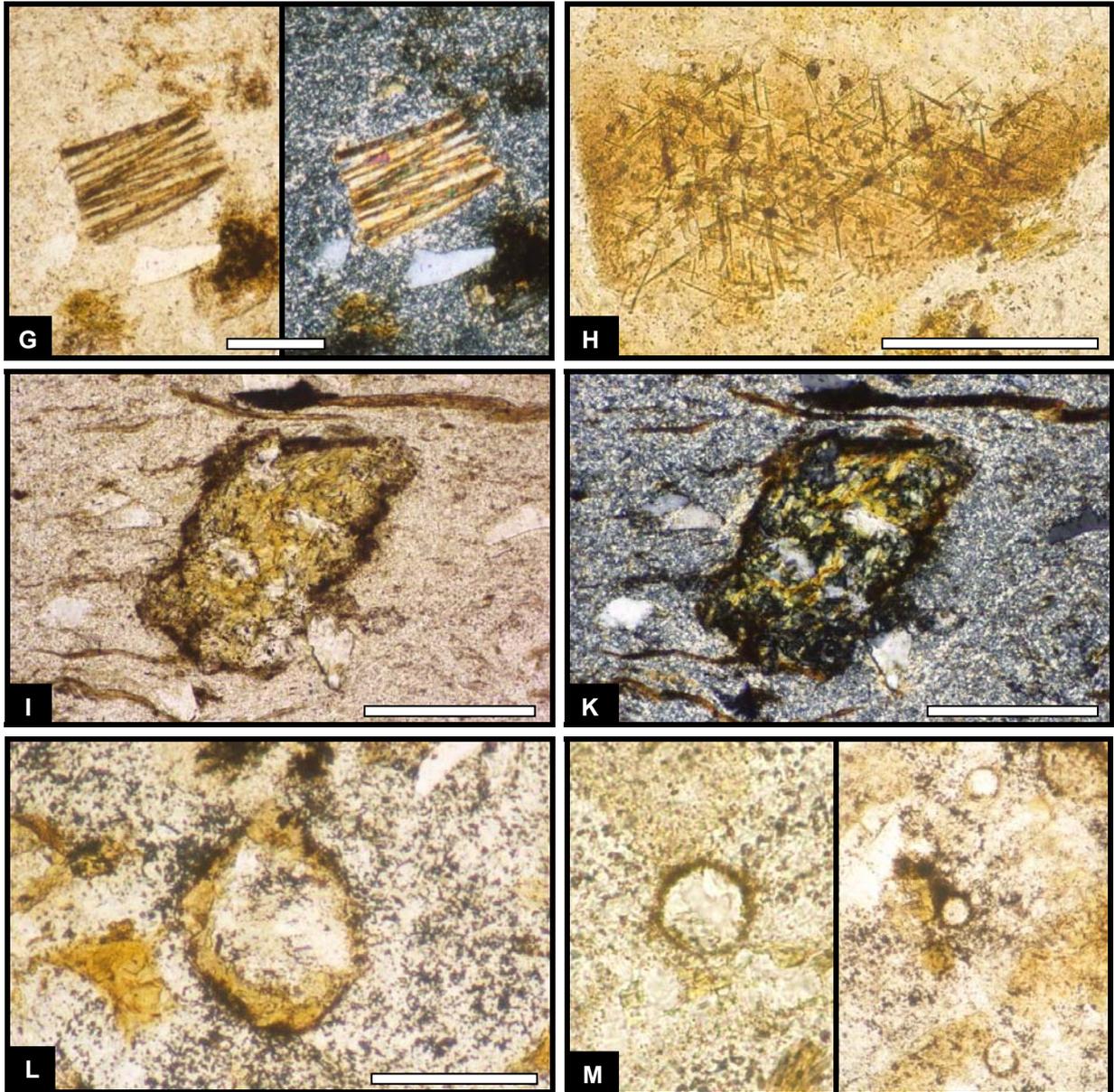
Fig. 3.11: Thin section photographs of tuff OG-9 (cont.): **(G)** Altered and expanded biotite stack with disrupted platelets. Plane-polarized light (left) and crossed polars (right). Scale bar 100 µm. **(H)** Network of acicular alteration products (rutile needles; so-called sagenite) in biotite. Plane-polarized light. Scale bar 100 µm. **(I) & (K)** Dark-rimmed pseudomorph after subhedral pyroxene(?) filled with quartz and greenish-yellowish phyllosilicates. Plane-polarized light left, crossed polars right. Scale bars 200 µm. **(L)** Dark-rimmed pseudomorph after almost euhedral pyroxene(?). Plane-polarized light. Scale bar 100 µm. **(M)** Dark-rimmed micro-spherules possibly representing radiolarian remains. Plane-polarized light. Size of the displayed micro-spherules is ~30 µm.
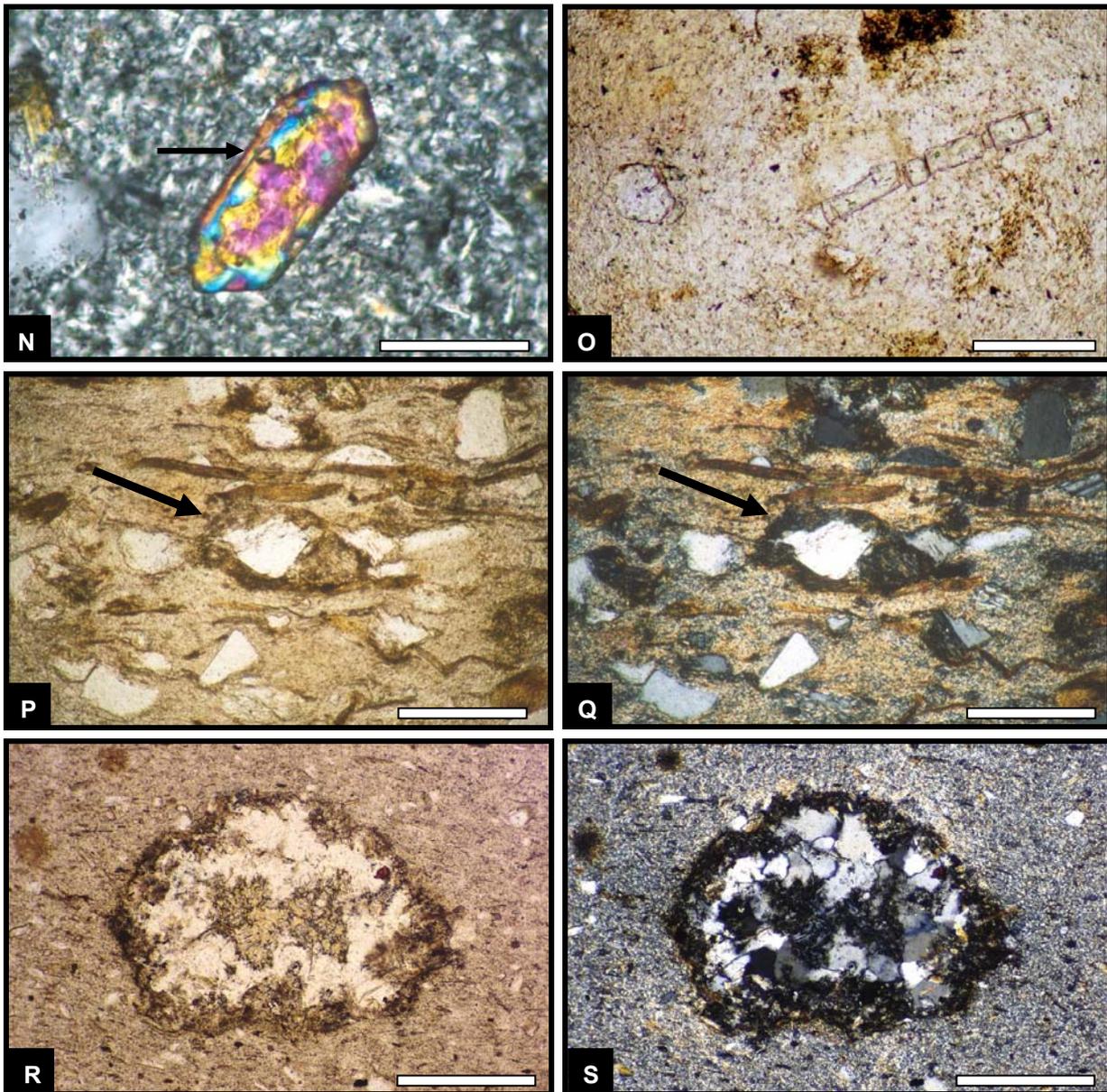
Fig. 3.11: Thin section photographs of tuff OG-9 (cont.): **(N)** Euhedral, shortprismatic to squat, juvenile zircon crystal with a small globular inclusion (arrow). Crossed polars. Scale bar 50 µm. **(O)** Euhedral to subhedral, juvenile apatite with etched crystal surfaces. Left crystal cut approximately perpendicular to the c-axis, right crystal parallel to it. Due to the strong basal cleavage the crystals are often broken and consist of fragments, which are slightly displaced against each other. Plane-polarized light. Scale bar 100 µm. **(P) & (Q)** Lens-like, dark brown coloured clast with quartz inclusion (arrow) probably representing an altered, originally vitiric pyroclast. The brownish substance mantling the quartz grain behaves under crossed polars (right image) almost isotropic. Plane-polarized light (left) and crossed polars (right). Scale bars 200 µm. **(R) & (S)** Vesicle filled with a mosaic of coarse-grained quartz intergrown with greenish-yellowish phyllosilicates (centre and rim of the vesicle). The latter exhibit under crossed polars often yellowish interference colours. Only in some cases dark, anomalous bluish-grey interference colours have been observed (chlorite or chlorite-bearing phyllosilicate mixture). Plane-polarized light (left) and crossed polars (right). Scale bars 300 µm.

Tuff OG-12, lying 1.2 m above tuff OG-9, has a thickness of about 7 mm. It has normally a light grey colour but due to streaky phosphate impregnations its colour changes in places to dark grey to black, especially in the upper part of the tuff (Fig. 3.12). Such phosphate impregnations are also very common in the shales of the Owl Gorge Member, in which thin, bluish-grey to black phosphatic bands are laterally fairly consistent. Apart from the portion that is indurated by phosphate, tuff OG-12 is a little bit softer than tuff OG-9 and weathers more easily but is still a firm rock. It also does not swell or disintegrate when it comes into contact with water. Due to the high abundance of dark coloured, filled vesicles tuff OG-12 is much more intensively spotted than tuff OG-9 (Fig. 3.13-A/B). Upper and lower contacts are, as far as is visible, sharp and plane. No sedimentary structures have been observed macro-scopically. Whole rock powder diffraction analyses reveal that also tuff OG-12 is mainly composed of illite, quartz and plagioclase. Chlorite peaks are clearly more pronounced in XRD than for tuff OG-9 and dark, phosphatic samples contain significant amounts of francolite, a carbonate hydroxyl fluorapatite. Thin sections show that tuff OG-12 is composed of a poorly sorted, crystal fragment-rich lower half and a well sorted, crystal fragment-poor/free upper half. The tuff is normally graded, the boundary between the upper and lower half is in thin sections quite distinct. The overall content in macrocrystals is in tuff OG-12 generally much lower than in tuff OG-9.
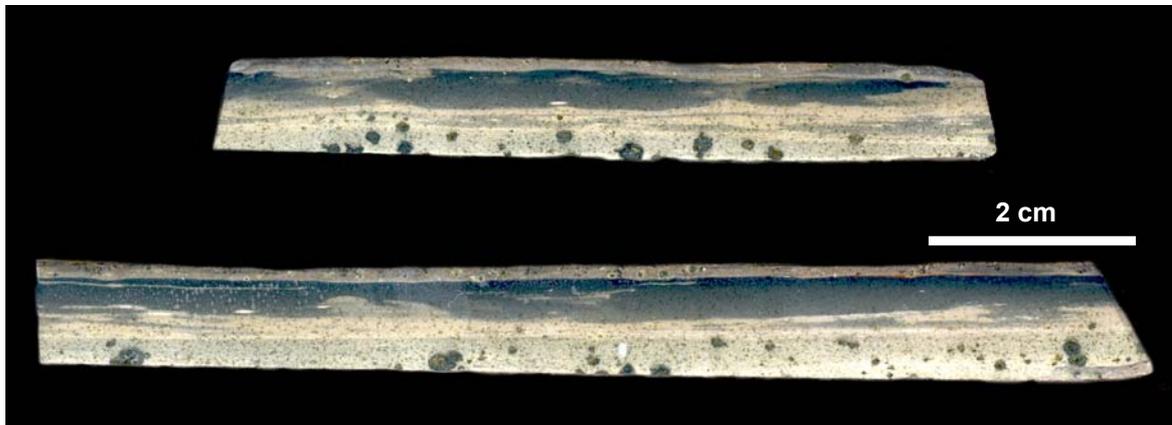
Fig. 3.12: Black, streaky phosphate impregnations in the upper half of Tuff OG-12. The black spots in the lower half of the tuff represent vesicle-like structures, which are filled with quartz and greenish-yellowish phyllosilicates (chlorite or chlorite-bearing, pinitic(?) phyllosilicate mixture).

Juvenile crystal components include (in decreasing abundance) biotite, quartz, apatite, and zircon. Feldspar has not been positively identified. Probably also juvenile components are dark coloured, elongate, schlieren-like clasts, perhaps representing flattened and altered, originally vitric pyroclasts (Fig. 3.13-C/D). Perfectly round microspherules, most probably representing radiolarian remains, are a minor biogenic component. Millimetre-sized vesicles, filled with quartz and chlorite, are abundant in the lower half of the tuff. Randomly distributed, small, greenish, spherical spots, probably composed of microcrystalline chlorite, are of contact-metamorphic origin. Together with the macroscopically dark coloured vesicles they

give the tuff a intensively spotted and speckled appearance (Fig. 3.13-B). Biotite, by far the most abundant juvenile crystal component, is mainly subhedral and the crystal flakes attain on average lenghts of 100-300 µm. Under plane-polarized light the strongly altered biotites (hydrobiotite or vermiculite?) show a pale greenish-yellowish colour and are still pleochroitic. Due to alteration individual crystal stacks often appear vertically expanded (Fig. 3.13-E/F). Compared to tuff OG-9, angular quartz crystals are much less common in tuff OG-12 and reach average sizes of only 50-120 µm. Fairly abundant are small, euhedral apatite crystals, which reach lengths of up to 100 µm when cut parallel to the c-axis. When cut perpendicular to the c-axis the diameter of the apatites is in the range of 20-40 µm. Only very few, tiny (<10 µm), subhedral zircons have been observed. Under the microscope, dark schlieren-like clasts form a very conspicuous component of tuff OG-12. These almost black, elongate, lens-like, flattened clasts are often warped, draped over or bent around crystals or contain mineral inclusions (Fig. 3.13-C to F). Their appearance is similar to so-called 'fiamme' in ignimbrites, representing flattened pumice due to welding. A vitric origin seems highly likely for the schlieren-like clasts, their flattening, however, is most probably of diagenetic origin (compaction). These clasts attain average lenghts of 50-200 µm, some can reach sizes over 300 µm. Together with the altered biotite flakes they give the tuff a microscopic planar structure. Like in tuff OG-9, perfectly round microspherules with a size of 25-30 µm have also been observed in the lower half of tuff OG-12. Although their origin is controversal, the inter-pretation as radiolarian remains is supported as McLachlan & Anderson (1973) reported of marine faunal elements from the lower Orange River region at the top of the glacial succession, which corresponds to the stratigraphic position of the Owl Gorge Member (a beautifully preserved radiolarian skeleton from Dwyka rocks is illustrated in MacRae, 1999). Subspherical, elliptical to irregularly shaped vesicles with sizes of 500-2500 µm are common in the lower half of the tuff. They are filled with coarse-grained quartz, intergrown with pale greenish-yellowish to brownish, slightly pleochroitic phyllosilicates. The flaky to needle-like crystallites are mainly arranged in a sheaf-like fashion. The greenish-yellowish parts of the phyllosilicates show under crossed polars dark anomalous bluish-grey interference colours hinting at chlorite (Fig. 3.13-G/H). In contrast, the more brownish parts exhibit light yellowish to intensive reddish-brown interference colours, probably representing an oxidised alteration product of chlorite or a chlorite-bearing phyllosilicate mixture (pinite?). In the stronger oxidized vesicles tiny platelets of goethite were observed (Fig. 3.13-I). Some vesicles contain crystals which are most probably completely pinitized, multiple lamellar twinned cordierite (Fig. 3.13-K). The vesicles are surrounded by a dark rim, which is probably formed by crypto- to microcrystalline, oxidized chlorite or a pinitic phyllosilicate mixture. In some cases it can be observed that biotite flakes and the schlieren-like clasts (former vitric pyroclasts) are wrapped around the vesicles indicating that maybe they had existed and were filled prior to

compaction of the tuff (Fig. 3.13-D). Since the vesicles do not contain any fine-grained matrix minerals, it is supposed that they represent originally trapped air or biogenically or chemically generated gas bubbles, which were filled at an early diagenetic stage with quartz and chlorite. Similar, vesicle-like structures filled with calcite were also described by McLachlan & Jonker (1990) from a feldspathic tuff within the Whitehill Formation in the northern part of the South African Karoo Basin. Subspherical to ovoid, greenish-brown spots are distributed randomly within the whole tuff, giving it a speckled appearance (Fig. 3.13-B). The size of these spots is typically in the range of about 50-100 µm. The spots grew within the tuff by enclosing the small matrix crystallites without replacing them and again they are interpreted as pinitized cordierite poikiloblasts, which formed due to Jurassic dolerite intrusions (cf. McLachlan & Jonker, 1990). Under crossed polars these spots appear pseudoisotropic due to the microcrystalline and non-oriented growth of pinite, a complex mixture of mainly sericite and chlorite. The fine-grained, recrystallized matrix of the tuff consists of a mixture of interlocking microlites probably consisting of quartz, albite and illite-dominated clay minerals. The recrystallization of the matrix may have taken place contemporaneously with the growth of the cordierite poikiloblasts.
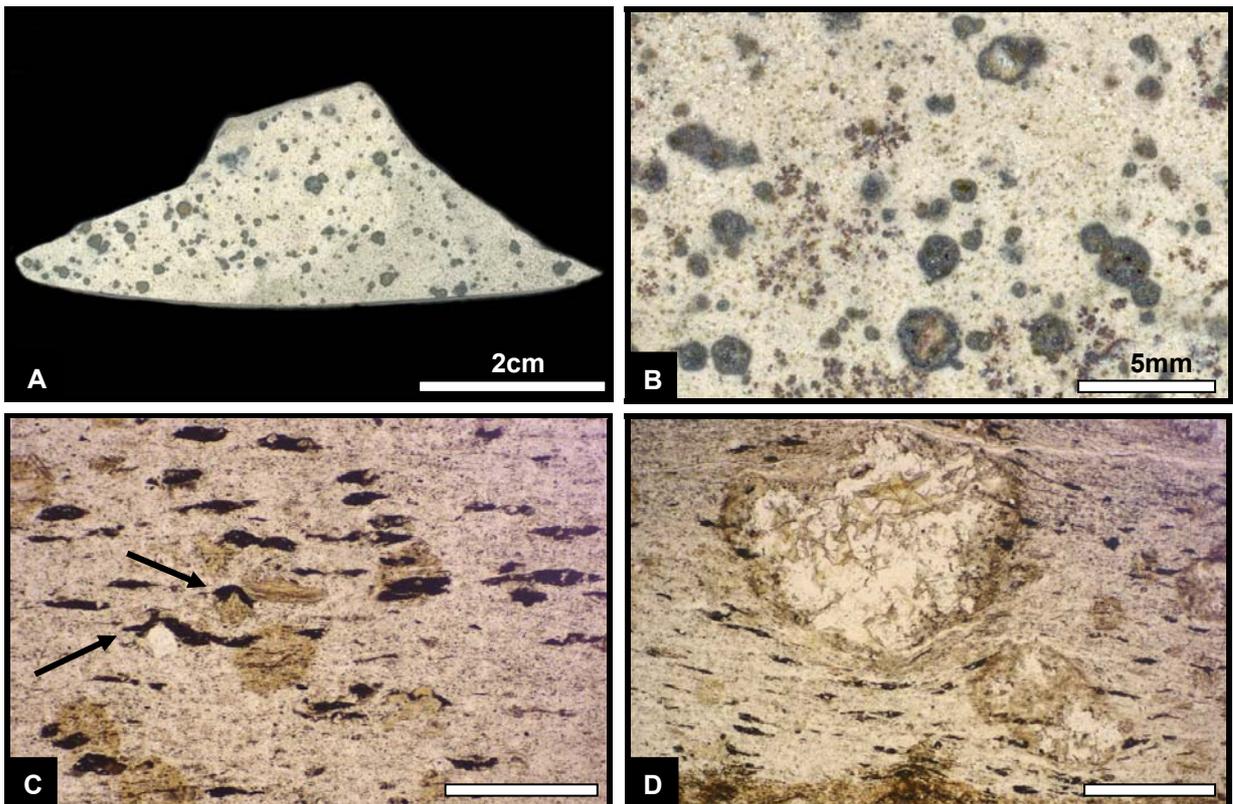
Fig. 3.13: Polished slab and thin section photographs of tuff OG-12: **(A) B**asal part of tuff OG-12 showing abundant dark coloured vesicles, filled mainly with quartz and possibly chlorite. **(B)** Same as (A) in detailed view. Apart from the large, dark coloured vesicles, the tuff matrix is speckled with tiny (50-100 µm), light coloured spots, composed of completely pinitized cordierite. **(C)** Dark coloured, elongate, fiamme-like clasts possibly representing flattened, originally vitric pyroclasts. Some of these clasts are draped over quartz crystals or other macrocrysts (arrows). Plane-polarized light. Scale bar 100 µm. **(D)** Biotite flakes and fiamme-like clasts are bent together with the tuff matrix around the

vesicles indicating that they might have existed and were filled prior to compaction. It is suggested that these vesicles originally represented trapped air bubbles. Plane-polarized light. Scale bar 500 µm.
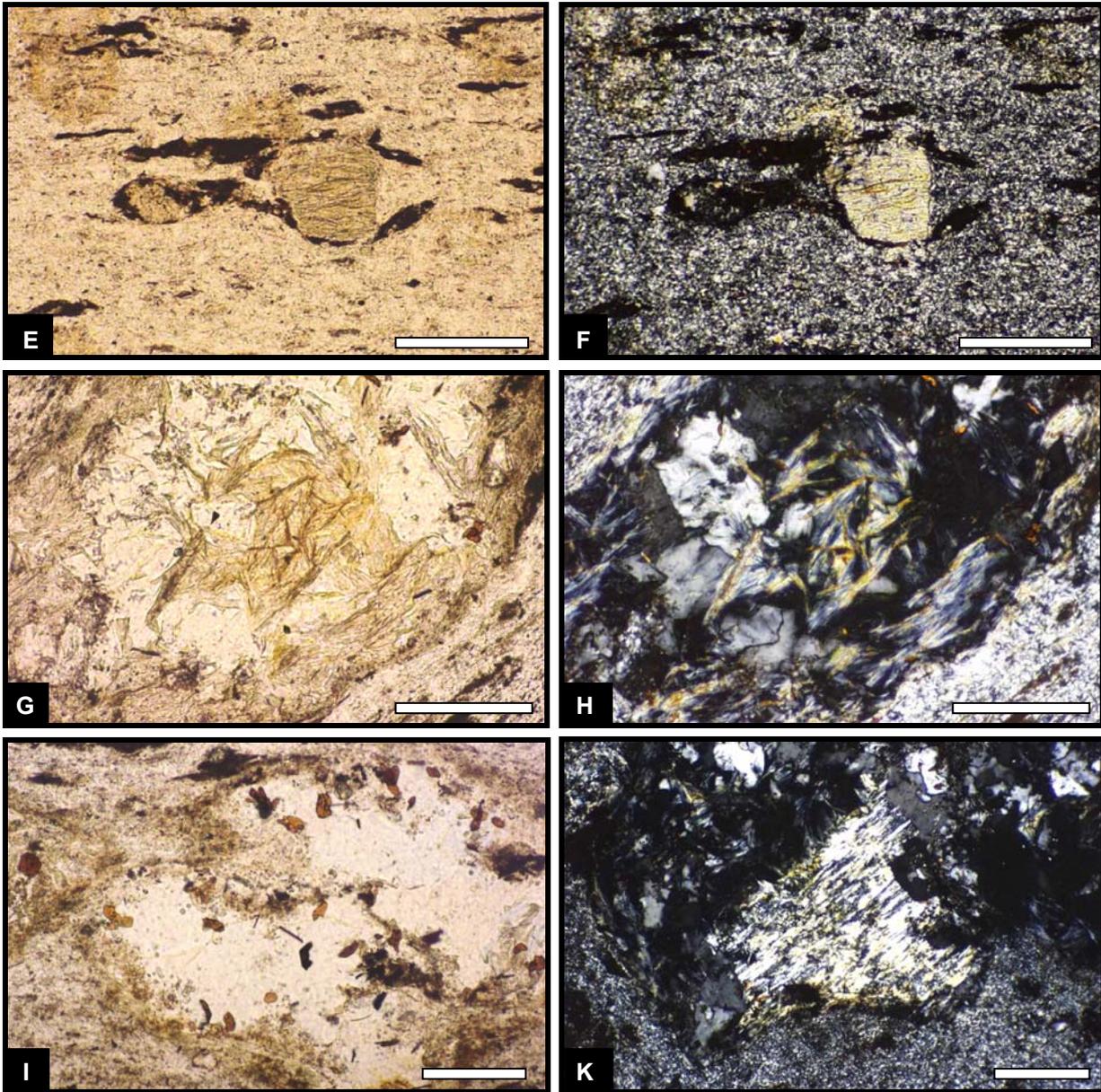
Fig. 3.13: Polished slab and thin section photographs of tuff OG-12 (cont.): **(E) & (F)** Big juvenile clast or crystal (altered and expanded biotite stack?) sandwiched between fiamme-like clasts. Plane-polarized light left, crossed polars right. Scale bars 200 µm **(G) & (H)** Vesicle filled with quartz and greenish-yellowish phyllosilicates. The lighter coloured parts of this phyllosilicate (e.g. lower right corner of vesicle) display under crossed polars (image (H) to the right) anomalous bluish-grey interference colours typical of chlorite, whereas the darker, more brownish coloured crystal bundels (e.g. centre of vesicle) display yellowish to orange interference colours hinting at alteration (oxidation) of chlorite. Scale bars 200 µm. **(I)** In stronger altered parts of the tuff tiny, orange-brown hematite-goethite platelets are interspersed in vesicles. Plane-polarized light. Scale bar 100 µm. **(K)** In some vesicles also crystals, which most probably represent completely pinitized, multiple lamellar twinned cordierite, have been observed. Crossed polars. Scale bar 200 µm.

The Itzawisis Tuffs

In the vicinity of the small village of Itzawisis, c. 40 km north of Keetmanshoop and c. 40 km south of Tses, there are a number of road cuts along the highway B1, in which whitish, intensively weathered layers, interbedded in greenish shales of the Prince Albert Formation, crop out. A closer inspection of these conspicuous layers revealed that these white layers represent altered, bentonitic ash-fall tuff layers. Two different tuff levels can be distinguished. In the three southern outcrops (ITZ-0, ITZ-1 and ITZ-2) a doublet of two thin tuff layers is exposed, in which the tuff layers are separated about 25 cm from each other. This tuff doublet is called TUBA. In the northernmost outcrop (ITZ-3) a relatively thick, single tuff layer is exposed, which is called DIBA (see Fig. 3.14 for outcrop localities).
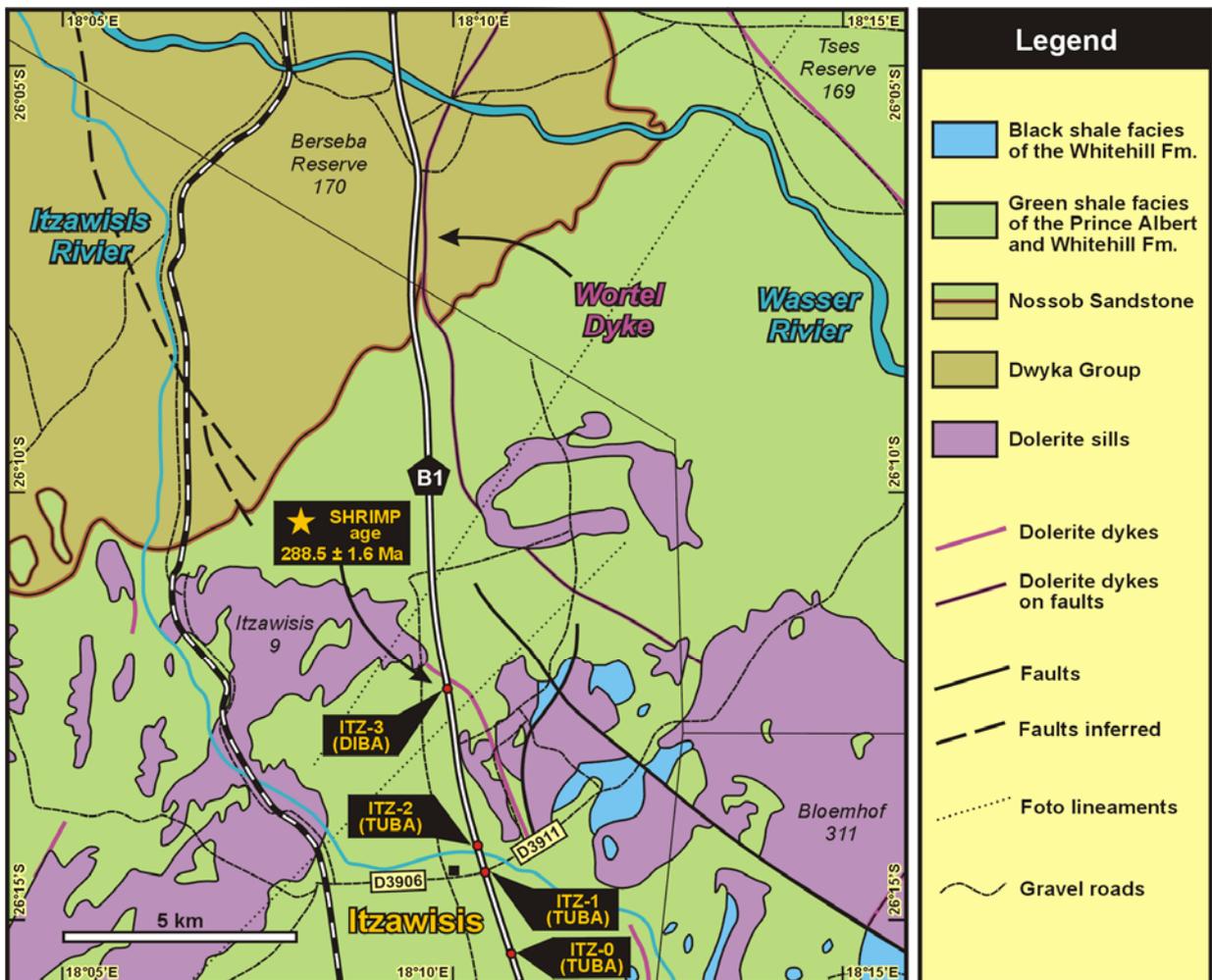
Fig. 3.14: Geological map of the area in the vicinity of Itzawisis showing the outcrop localities of the Itzawisis Tuffs. The map is mainly adopted from the Genis (1982).

Outcrop ITZ-0 is located about 1.8 km south of the road junction between the B1 highway and the gravel roads D3906 and D3911. Exposed is the doublet of the TUBA Tuffs. The lower, thinner tuff layer shows a variable thickness of 1 to 2 cm, whereas the upper, thicker tuff layer is about 2 cm thick. However, due to the strong alteration and weathering of the tuff layers, the true thickness, e.g. encountered in drill cores, might be considerably lower. The enclosing rocks are olive-green to bluish-grey, micaceous and silty shales of the Prince Albert Formation. These shales appear quite massive and chert-like in outcrops, probably due to diagenetic induration or thermal overprinting by dolerite intrusions. In places the shales contain streaks of very fine sand and some bedding surfaces are sprinkled with small, black coal flakes besides abundant light coloured mica flakes. In addition, the shales also contain rare intercalations of cm-sized, medium-grained, arcosic sand lenses. Flat, bedding-parallel bioturbation features are also observed quite frequently. Outcrop ITZ-1 is directly located at the intersection of the B1 with the D3906/3911. Here, a tuff doublet is again separated by a ~25 cm thick shale interval and it is suggested that it is the same tuff horizon as exposed in outcrop ITZ-0 (TUBA Tuffs). However, probably due to enhanced alteration and swelling of the bentonite, the lower tuff layer shows a thickness of ~3 cm, the upper one a thickness of ~7.5 cm, on the western side of the road cut. The road cuts at locality ITZ-1 also show that the sedimentary succession is slightly warped and cut by several fractures and faults, which also displace the TUBA Tuffs (Fig. 3.15). Another outcrop (ITZ-2) with an exposure of the TUBA tuff doublet lies about 200 m north of the bridge where the highway B1 crosses the Itzawisis Rivier. The TUBA Tuffs consist of crumbly pieces of a highly altered bluish-grey bentonite, embedded at surface outcrops in powdery white calcite.
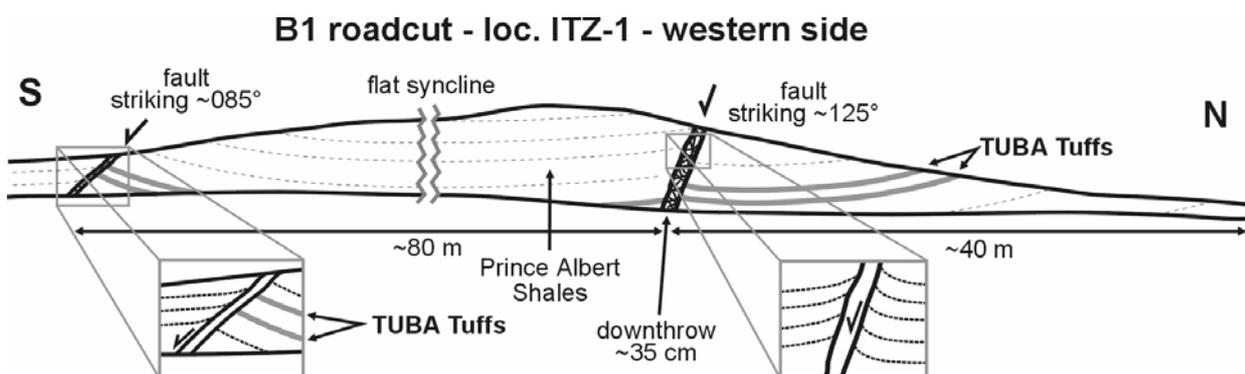
Fig. 3.15: Fieldbook sketch of outcrop ITZ-1 with the TUBA tuff doublet displaced by faults. Vertical scale is exaggerated and not to scale.

About 4 km north of the B1-D3906/3911 intersection (ITZ-3: S 26° 12.323' E 18° 09.823') a very prominent and relatively thick, whitish weathered bentonite layer crops out along the road cuts (Fig. 3.16). There is also a rest area at the western side, where a car can be parked safely next to the road. This is the type locality of the so-called DIBA Tuff. The lower contact to the olive-green, silty and somewhat cherty shales of the Prince Albert Formation is very sharp, whereas the contact to the overlying shale is gradational (Fig. 3.17). The basal part of the tuff is strongly weathered and the exposure surface is largely covered with a white, powdery substance that turned out to be, according to XRD analysis, almost pure calcite. However, digging a little bit deeper into the outcrop yields very soft and crumbly pieces of a clayey bentonite from the base of the layer (Fig. 3.18). In the lowermost, coarser grained part the altered tuff displays a dark greenish-grey colour, whereas in the following finer grained part the tuff samples show more light bluish-grey colours. The basal layer is overlain in places gradually by a zone of reddish, crumbly, tuffaceous material. On these tuff-rich zones follow greenish, still crumbly and fissile shales that become progressively firmer in upward direction until they grade again into olive-green, very hard, chert-like silty shales of the Prince Albert Formation (Fig. 3.17). The light coloured bentonite is about 10 to 15 cm thick, depending on weathering intensity, plus a ~20 cm thick overlying reddish to greenish tuffaceous zone. This tuff layer must have formed by a sudden, massive aeolian input of volcanic ash into the waterbody of the Ecca Inland Sea producing a sharp basal contact to the underlying shales. The aeolian input and suspension settling of the volcanic ash then decreased with time, while the silty-muddy background sedimentation continued, until the latter dominated the sedimentation again. Similar to outcrop ITZ-1 the sedimentary succession is cut by several faults and flexures causing warping, bending, displacement and brecciation (Fig. 3.19). At the northern part of the outcrop a dolerite dyke intruded into the shales.

Until now the precise stratigraphic position of the Itzawisis Tuffs has not been very well constrained, however, there is no doubt that they are enclosed in shales of the Prince Albert Formation. No really detailed mapping of the area exists and the most accurate geological map that is available for this part of the country is Sheet 2618 Keetmanshoop with a scale of 1:250000 (Genis, 1982). The only lithological marker horizons, which could help to determine the stratigraphic position of the Itzawisis Tuffs more accurately, are the Nossob Sandstone below and the zone with tuffs and dolomitic limestones (Goris Limestone Beds) within the Whitehill Formation above them (Fig. 3.2). The Auob Sandstone pinches out already north of Tses. Unfortunately, the Nossob Sandstone is also not very well developed in the area around Itzawisis. Between Tses (c. 40 km north of Itzawisis) and the Gellap Plateau (c. 30 km southwest of Itzawisis) the Nossob Sandstone looses its distinctive lithological and escarpment-forming character.

Fig. 3.16: The whitish weathered DIBA Tuff, exposed at the eastern road cut of the B1 highway, c. 4 km north of the B1-D3906/3911 intersection in the vicinity of Itzawisis (ITZ-3).

Fig. 3.17: (A/l.) The DIBA Tuff exposed at outcrop ITZ-3. Note in the left picture the sharp base and the gradational upper contact to the olive-green shales of the Prince Albert Formation. **(B/r.)** The right picture shows a reddish tuffaceous zone (not developed everywhere) between the light coloured bentonite and the greenish overlying shales. Scale in both pictures is 10 cm.

Since the Nossob Sandstone is used as the basal mapping unit of the Ecca Group in central southern Namibia (Mariental-Keetmanshoop area), the boundary between the Dwyka Group and the Prince Albert Formation, as drawn in the Geological Map Sheet Keetmanshoop, should approximately indicate the outcrop trace of the Nossob Sandstone. About 8.5-9 km north of ITZ-3 (DIBA outcrop) indeed dark brown, fine- to medium-grained, in places also coarse-grained and pebbly, wave-rippled and convolute-bedded, intensively carbonate cemented sandstones crop out east of the B1 highway along the western flank of the Wortel Dyke, which forms a prominent ridge running parallel to the tar road (Fig. 3.14). These outcrops of the Nossob Sandstone lie at a height of about 1000 m asl., whereas the DIBA Tuff outcrop is at a height of about 1065 m asl. From some outcrops close to the former boundary of farm Bloemhof and Itzawisis to the Berseba and Tses community areas the base of the Whitehill Formation can be estimated to be not higher than 1100 m asl. in the

region c. 5 km ESE of the DIBA Tuff outcrop. These topographic data would imply a position of the Itzawisis Tuffs in the middle to upper part of the Prince Albert Formation but faults and intrusions of dolerite dykes and sills complicate the geological situation to such an extent that using topographic information for the construction of stratigraphic positions appears not reliable enough for this area. Nevertheless, the Itzawisis Tuffs represent very conspicuous marker layers within the Prince Albert Formation, which should be traceable in the field by detailed future mapping projects, especially the relatively thick DIBA tuff bed, which was chosen for radiometric age dating. From the radiometric age of the DIBA Tuff (288.5 ± 1.6 Ma; Sakmarian after Gradstein et al., 2005) a position in the lower half of the Prince Albert Formation is now preliminary supposed (Fig. 3.2) until future mapping projects can state this more precisely. The sandy streaks and arkosic lenses at outcrop ITZ-0 (TUBA Tuffs) might represent a very distal expression of the Auob Sandstone (Fig. 3.2), which forms the top of the Prince Albert Formation between Mariental and the Mukorob area, but is hardly recognizable south of Tses. Also the Khabus Tuff, which lies approximately in the middle of the Whitehill Formation, crops out in a road cut 5.9 km south of locality ITZ-0. Therefore, a position in the upper half of the Prince Albert Formation is suggested for the TUBA Tuffs (see Fig. 3.2), which is also in accordance with the observation, that there is a general younging trend of the exposed strata along the B1 highway from Tses in a southward direction towards Keetmanshoop.

Fig. 3.18: Whitish to light bluish-grey weathered pieces of bentonite from the DIBA Tuff. Scale is 5 cm in length.
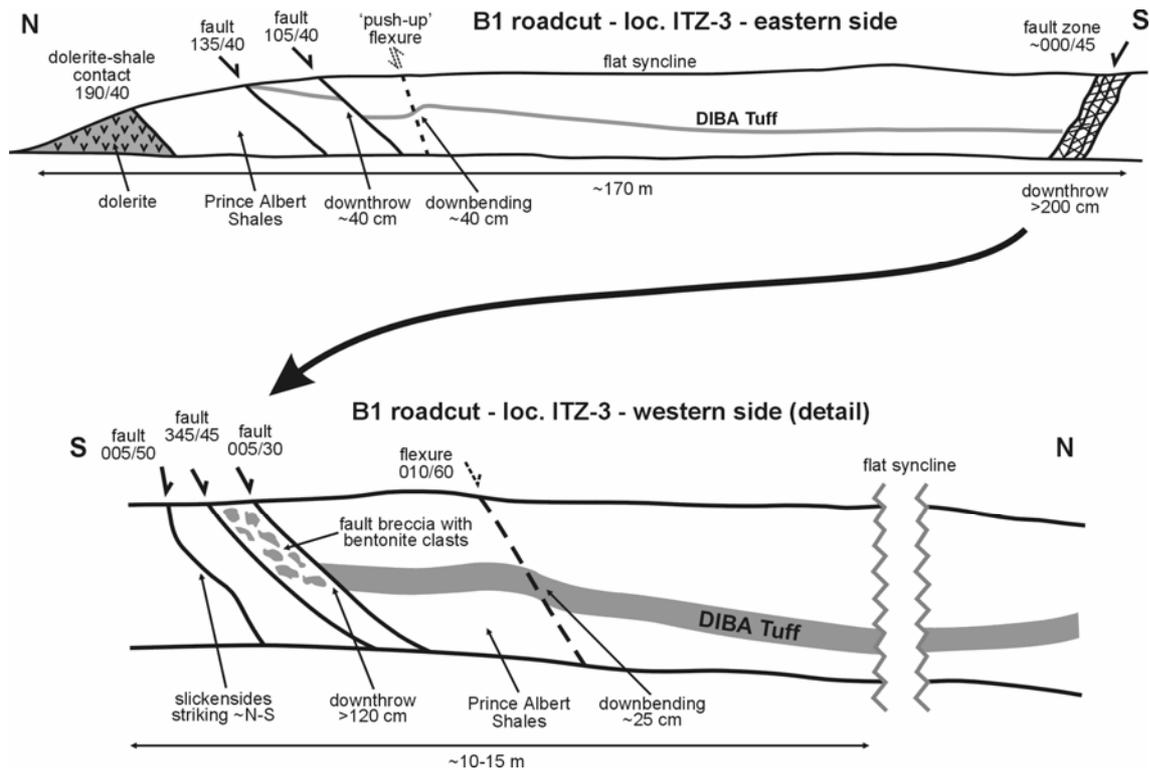
Fig. 3.19: Fieldbook sketch of outcrop ITZ-3 with the DIBA Tuff displaced by faults. Vertical scale is exaggerated and not to scale. Correlation of the two opposite road cuts by the thick arrow.

The Itzawisis Tuffs (DIBA & TUBA) are petrographically very similar and are therefore here described together. They show light bluish-grey to darker greenish-grey colours in outcrops and have a very crumbly, intensively weathered appearance with only a very weakly developed fissility. Upon moistening they readily swell and disintegrate indicating the presence of smectite and explaining their soapy feeling. The basal parts are micaceous and very rich in crystal fragments generating a clast- to matrix-supported fabric (Fig. 3.20-A). The mean grain size lies within that of coarse ash tuffs. In some thin sections it can be seen that coarser grained layers grade into and alternate with finer grained parts (Fig. 3.20-B), what may indicate several eruption and sedimentation cycles. The coarse ash tuffs grade upward into fine ash tuffs and tuffaceous siltstones. In thin sections the coarser portions of the tuffs appear quite poorly sorted, with quartz, biotite, and feldspar crystals dispersed in a fine-grained, claymineral-rich matrix, which is intensively stained by iron oxides and oxyhydrates. In addition, also large clay mineral booklets and vermicules with bright interference colours (illite pseudomorphs after kaolinite) are interspersed in the tuffs. These mineralogical characteristics, together with the softness of the rock, makes these tuffs very similar to the Ganigobis and Zwartbas Tuffs. Zircon, apatite, rutile, tourmaline, garnet, and possibly titanite occur as accessory crystal components. This diverse heavy mineral suite hints at a conside-rable admixture of xenocrystic material to the juvenile components of the tuffs indicated by

the heterogeneous population of zircons separated from the DIBA Tuff, of which some of them yielded Meso- and Palaeo-Proterozoic ages (see Chapter 5 Geochronology).

Quartz represents the most abundant crystal component in the tuffs and occurs mainly as very angular, almost equidimensional, and monocrystalline grains with straight extinction. The mean grain size lies between 50-150 µm, whereas the observed maximum grain size reaches about 300 µm. Only few quartz grains are polycrystalline or show undulose extinction. Also triangular- or thorn-shaped splinter quartzes (Fig. 3.20-C) with a typical size of c. 100-150 µm are relatively rare (<5% of the whole quartz fraction). Some quartz grains contain several ovoid to tubular inclusions or vacuoles and a few beta-quartz paramorph crystals, showing hexagonal outlines and containing dark glass inclusions, have been identified, too (Fig. 3.20-D). Feldspar is present only in minor quantities (~5% of the crystal fragments) and its mean and maximum grain size is similar to that of quartz. The majority of feldspar is apparently represented by plagioclase (polysynthetic twinning) but also some potassium feldspar crystals with Carlsbad twinning may be present. Almost all feldspar grains are angular. A wide range of feldspar alteration is seen in thin sections. Many appear very fresh without signs of alteration, most have a somewhat dusty appearance, and others are severely altered to clay minerals. Biotite is approximately as abundant as quartz in the Itzawisis Tuffs and is already visible in hand specimen as small mica flakes. Under the microscope biotite forms mainly dark orange-brown to light yellow-brown, pleochroitic, sub- to anhedral crystal flakes and platelets (Fig. 3.20-E/F), which are, in places, aligned roughly subparallel giving the tuffs a faint subplanar to wavy bedding and a weakly developed fissility. Some biotites also form book-like crystal stacks (Fig. 3.20-G/H). The majority of the biotite flakes has a grain size between 100 and 400 µm, the maximum observed length is 720 µm. Alteration processes have affected biotite in various ways. Some biotite stacks seem to be expanded and some show inclusions of a regular network of acicular crystals most probably representing rutile needles (sagenite) (Fig. 3.20-I). Others appear oxidised and pigmented by iron oxides or oxyhydrates causing a dark brown to near-opaque colour. Only few of the biotites are partly or entirely altered to greenish chlorite (Fig. 3.20-K). The most frequently observed alteration process is bleaching of biotite to various degrees, resulting in pale brown to greenish-yellowish colours and pointing towards a transformation to hydrobiotite or/and vermiculite. About one fourth of the biotite flakes in the tuffs are degraded to completely colourless crystals, which show no apparent change in thickness or microstructure and strongly resemble muscovite (Fig. 3.20-E/F). The same observation was also described by Bohor & Triplehorn (1993) and Huff et al. (1997a) when biotite alters to kaolinite. However, the flakes, which are colourless under plane-polarized light, display under crossed polars bright interference colours. Therefore, they cannot consist of kaolinite, which has a birefringence of 0.007, causing only first order shades of grey under crossed polars.

The bright interference colours point to a higher birefringent mineral, most probable illite, with a birefringence of 0.030-0.035. It is suggested that biotite was first early diagentically altered to kaolinite (cf. Bohor & Triplehorn, 1993) and then transformed to illite during a later diagenetic phase. The same suggestion applies also for another macro-crystal component of the tuffs. In addition to bleached biotite, the tuffs contain numerous colourless (under plane-polarized light), large crystal booklets and elongate, sometimes curved, vermicular crystal stacks, forming a very conspicuous crystal component in thin sections (Fig. 3.20-L to Q). Their size and length ranges from about 50 to 280 μm. The morphologies of these crystal aggregates are practically identical with those of kaolinite booklets and vermicules shown in the literature (e.g. Bohor & Triplehorn, 1993). However, like the above mentioned colourless mica flakes, they show under crossed polars bright interference colours, contradictory to the optical properties of kaolinite. Therefore, it is supposed that these crystal aggregates also represent illite pseudomorphs after kaolinite. Such a pseudomorphous transition of kaolinite to illite has been described for example by Bobos & Ghergari (1999) and by Knight et al. (2000). In their studies illitization is either related to hydrothermal processes or to tectonism. In the case of the Itzawisis Tuffs the thermal overprinting by Jurassic dolerite intrusions might have played a crucial role in the transformation of kaolinite (and also smectite) to illite. The same explanation most probably also applies to the secondary crystal booklets and vermicules of the Ganigobis and Zwartbas Tuffs. The origin of the vermicules and booklets is not fully understood. Commonly they form early diagenetically and a pre-compactional growth is inferred for the majority of the booklets and vermicules of the Itzawisis Tuffs. It can be shown that some of them were deformed during compaction of the tuffs, indicated by the displacement of individual crystal stack segments (Fig. 3.20-P/Q). Some of the booklets and vermicules may have pseudomorphically replaced biotite stacks, others, however, might have chemically precipitated, i.e. they might represent crystals without a biotite precursor, which have completely newly grown within the tuff matrix after deposition of the tuff (cf. Bohor & Triplehorn, 1993).

In the Itzawisis Tuffs euhedral to subhedral zircons show predominantly stubby, squat and semi-equidimensional forms (Fig. 3.20-R/S), whereas acicular crystals are less common. Some rounded, slightly metamictic zircons show a brownish colour (Fig. 3.20-S). Their size varies from <20 μm to 120 μm. Apatite forms euhedral to subhedral crystals with lengths between 30 and 100 μm and contain in some cases dark brown tubular inclusions. Rutile occurs as subhedral, dark brown crystals, which range in size between 60 and 210 μm. Euhedral to anhedral tourmaline (50-100 μm) can be observed quite frequently in thin sections of the Itzawisis Tuffs. The majority displays a dirty bluish-green colour, some are zoned with a dark bluish-green core surrounded by a yellow-greenish margin (Fig. 3.20-T/U), and more rarely blue varieties have been observed, too. A few garnets are present as small

(40-60 µm), colourless, rounded or angular grains. Some colourless to yellowish-brown, suhedral and angular crystal fragments (60-100 µm) may represent titanite.

Within the matrix irregular-shaped patches (~100 µm in diameter) are composed entirely of a mosaic of tiny (~10 µm in diameter), blocky crystal stacks, probably replacing feldspar grains (Fig. 3.20-V). Sometimes, also vermicular crystals are distributed in the fine-grained matrix of mosaic-textured clay mineral stacks (Fig. 3.20-W). Under crossed polars the blocky crystals and vermicules show grey to yellowish to bright blue interference colours, again indicating illitization. The matrix of the Itzawisis Tuffs consists mainly of clay minerals, probably inter-grown with microcrystalline quartz, and is intensively stained by iron oxides/oxyhydrates. XRD analyses show that the Itzwaisis Tuffs are strongly illite-dominated. Small peaks around 6° 2θ hint at the presence of minor amounts of smectite, vermiculite and/or hydrobiotite. A broad peak between 7.5 and 9° 2θ might reflect smectite interlayering with illite and/or biotite alteration. Peaks at 12.5° 2θ are either missing, very low, or appear as rather inconspicuous, broad bulges indicating that no substantial amounts of kaolinite and/or chlorite are present.
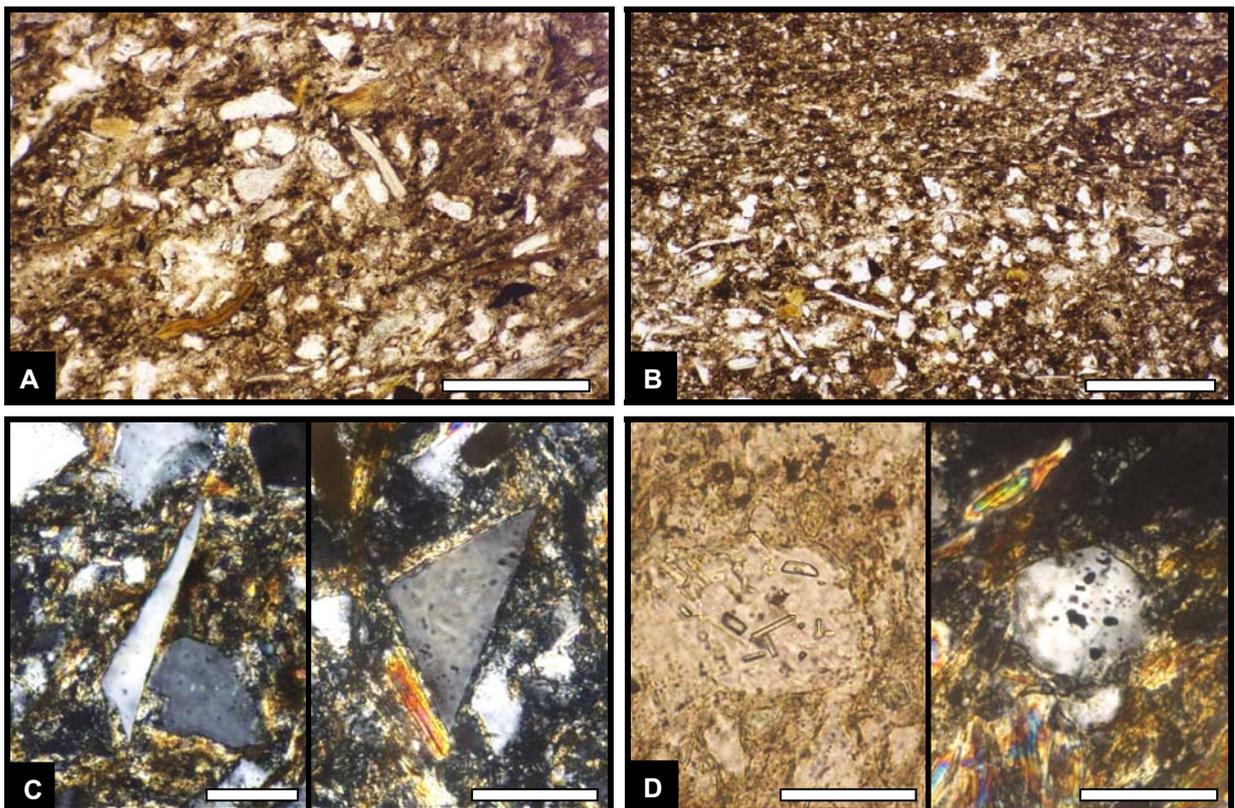
Fig. 3.20: Thin section photographs of the Itzawisis Tuffs: **(A)** Poorly sorted, coarse-grained basal part of the DIBA Tuff consisting mainly of quartz and biotite crystals set in a fine-grained matrix intensively stained by iron oxides/oxyhydrates (DIBA Tuff). Plane-polarized light. Scale bar 250 µm. **(B)** Coarser grained layers alternate with finer grained parts (DIBA Tuff). Plane-polarized light. Scale bar 500 µm. **(C)** Thorn- and triangular-shaped splinter quartz crystals (both DIBA Tuff). Crossed polars. Scale bars 50 µm. **(D)** Quartz crystals with inclusions. Left crystal contains light coloured vacuoles. Plane polarized light. Scale bar 100 µm. The right image shows a euhedral, hexagonal beta-form quartz paramorph crystal, slightly abraded in the lower right corner, containing dark (in plane-polarized light) glass inclusions (both DIBA Tuff). Crossed polars. Scale bar 50 µm.
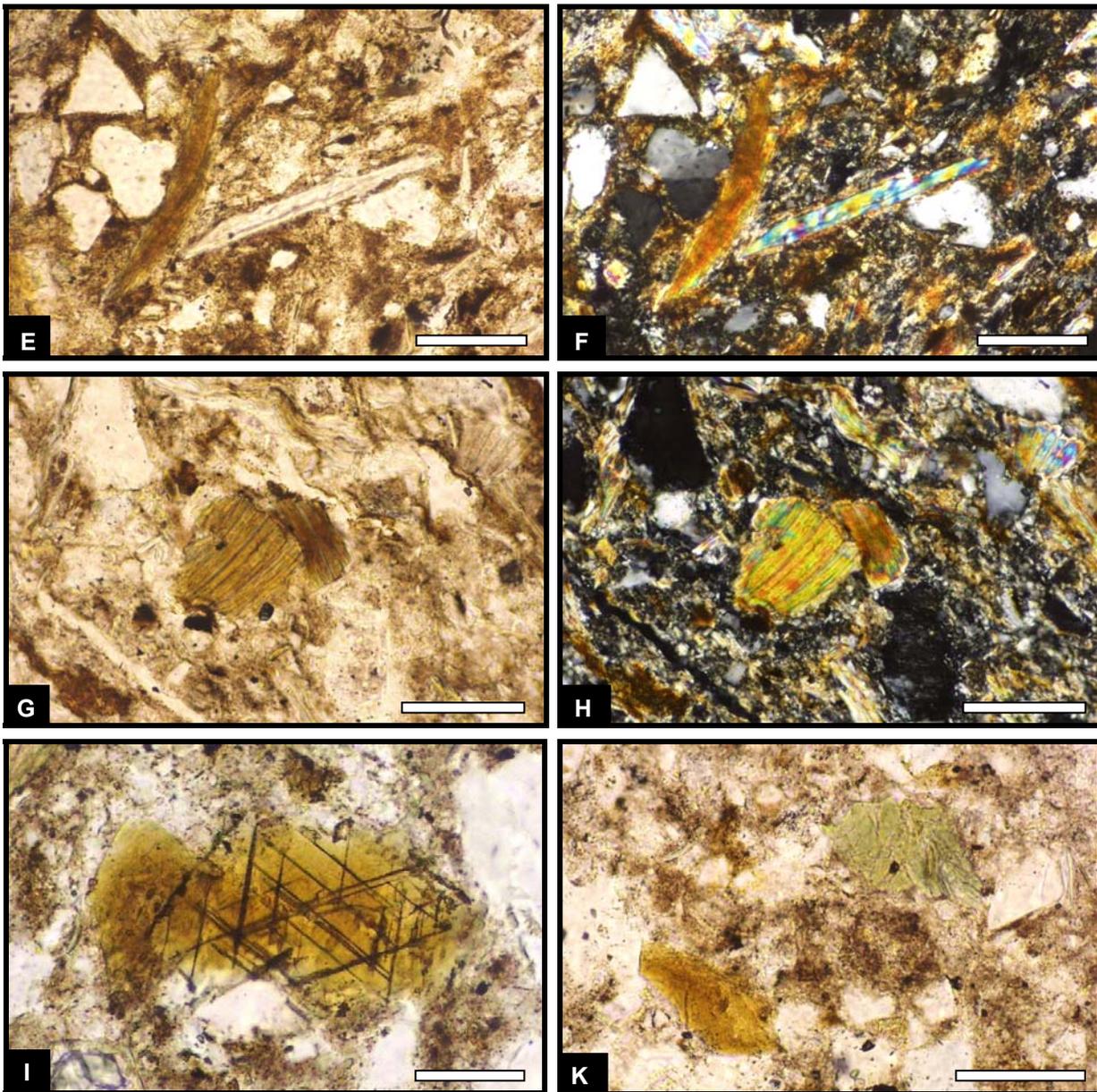
Fig. 3.20: Thin section photographs of the Itzawisis Tuffs (DIBA & TUBA) (cont.): **(E) & (F)** Dark brown, less degraded biotite (left crystal flake) can be observed together with colourless, bleached mica-like crystals (right crystal flake) (DIBA Tuff). The colourless flakes most probably represent kaolinite pseudomorphs after biotite, which were transformed at a later stage to illite, indicated by the bright interference colours. Plane-polarized light (left) and crossed polars (right). Scale bar 250 µm. **(G) & (H)** Book-like biotite stack (DIBA Tuff). Plane-polarized light (left) and crossed polars (right). Scale bars 100 µm. **(I)** Regular network of acicular alteration products (rutile needles; so-called sagenite) in biotite (TUBA Tuff). Plane-polarized light. Scale bar 50 µm. **(K)** Greenish, chloritized biotite flake next to a yellowish-brown biotite flake. Plane-polarized light. Scale bar 100 µm.
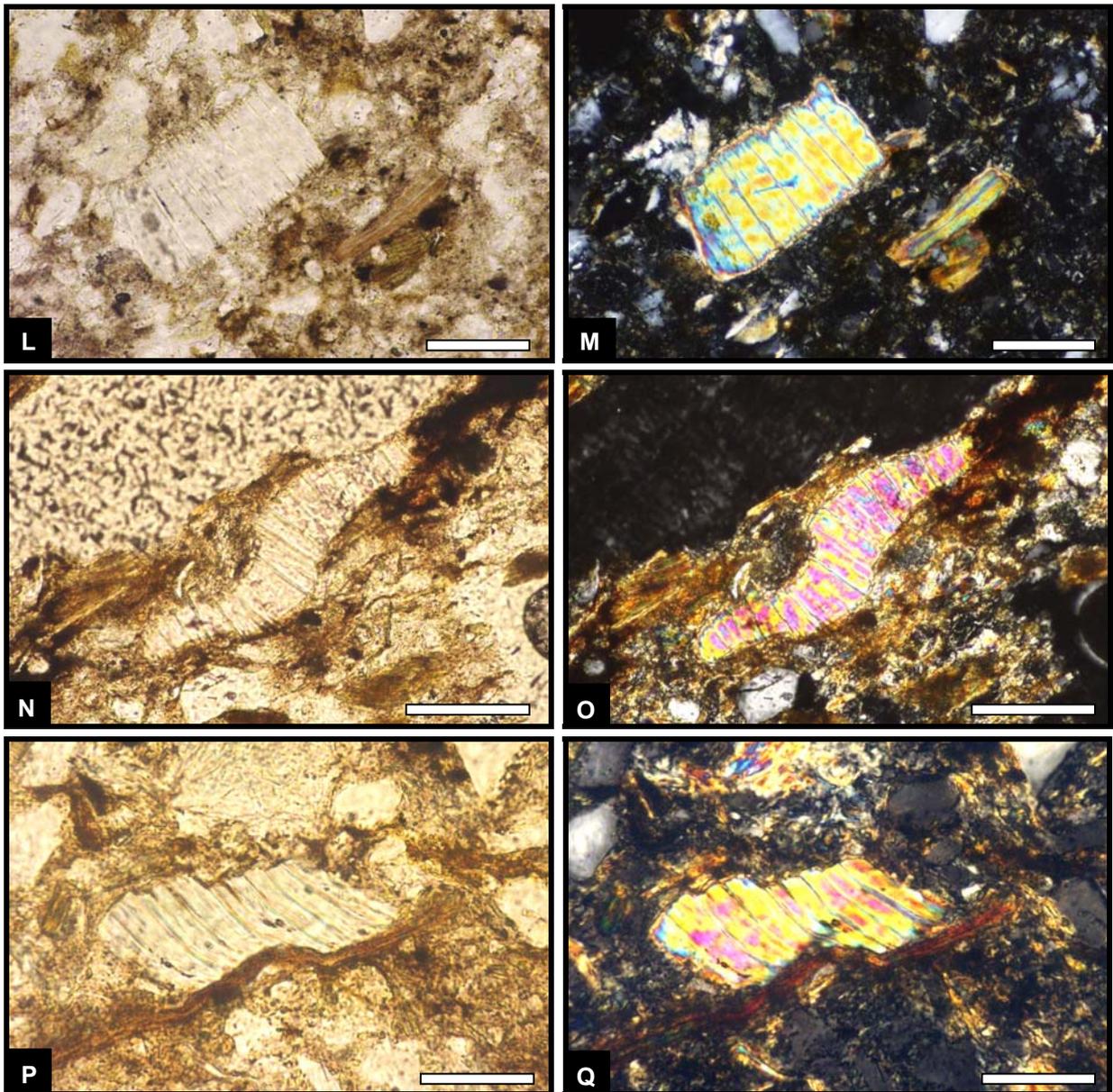
Fig. 3.20: Thin section photographs of the Itzawisis Tuffs (DIBA & TUBA) (cont.): **(L) & (M)** Large crystal booklet representing an illite pseudomorph after kaolinite indicated by the bright interference colours (TUBA Tuff). Plane-polarized light (left) and crossed polars (right). Scale bars 100 μm. **(N) & (O)** Large, curved vermicule representing an illite pseudomorph after kaolinite indicated by the bright interference colours (DIBA Tuff). Plane-polarized light (left) and crossed polars (right). Scale bars 100 μm. **(P) & (Q)** Deformed crystal booklet (illite pseudomorph after kaolinite) and biotite flake indicating a pre-compactional growth of the kaolinite booklets and vermicules (DIBA Tuff). Plane-polarized light (left) and crossed polars (right). Scale bars 50 μm.
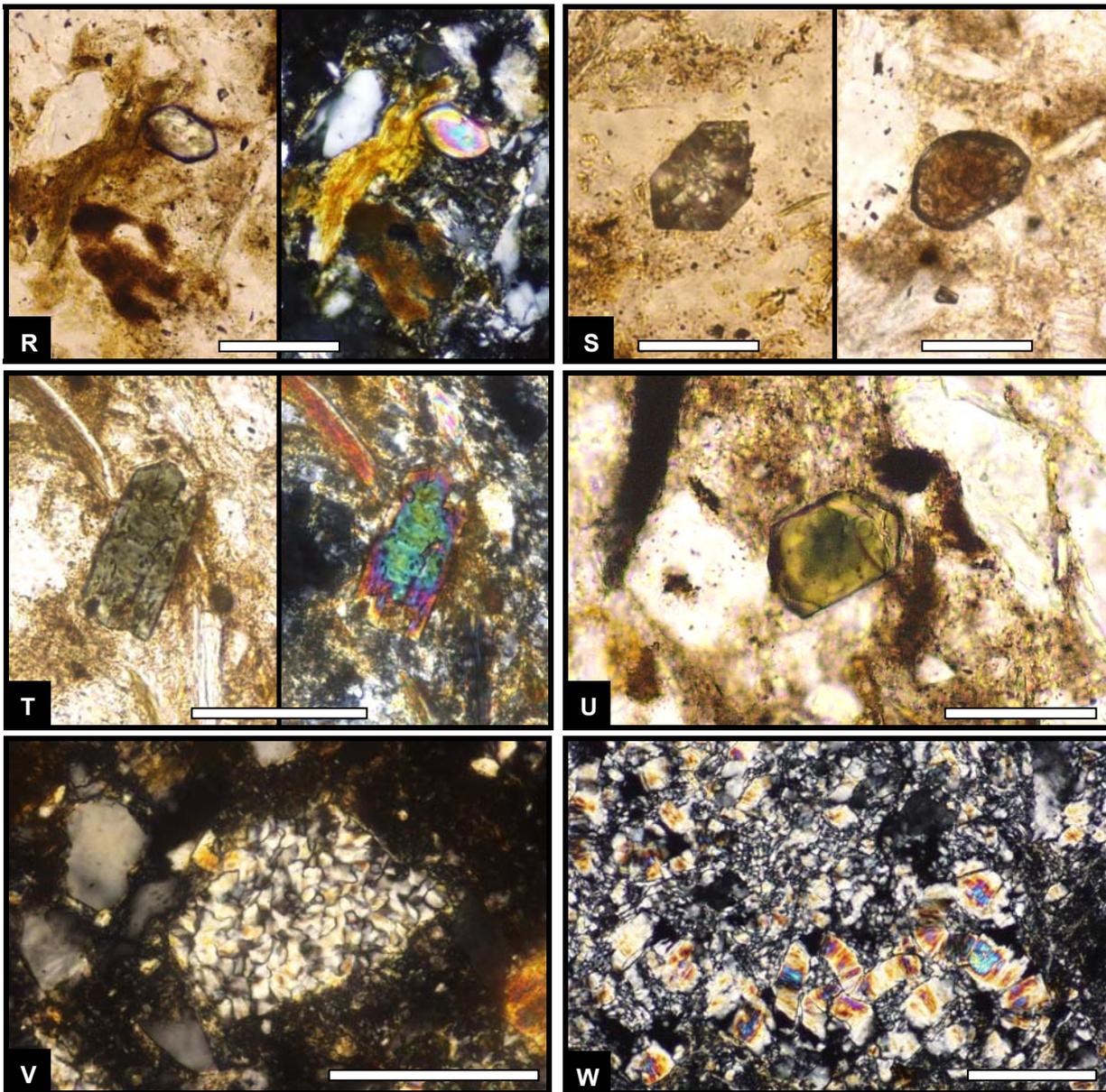
Fig. 3.20: Thin section photographs of the Itzawisis Tuffs (DIBA & TUBA) (cont.): **(R)** Euhedral, stubby zircon crystal, representing the dominant zircon morphology in the Itzawisis Tuffs (TUBA Tuff). Plane-polarized light (left) and crossed polars (right). Scale bar 100 μm. **(S)** Euhedral, stubby zircon crystal (left) and a rounded, brownish-metamictic zircon crystal (right) (both TUBA Tuff). Plane-polarized light. Scale bars 50 μm. **(T)** Sub- to euhedral tourmaline, forming the most abundant heavy mineral phase in the Itzawisis Tuffs (DIBA Tuff). Plane-polarized light (left) and crossed polars (right). Scale bar 100 μm. **(U)** Euhedral tourmaline crystal showing a well developed zoning with a darker core surrounded by a lighter margin (DIBA Tuff). Plane-polarized light. Scale bar 50 μm. **(V)** Mosaic-textured kaolinite (largely transformed to illite) probably replacing pseudomorphically a feldspar grain (TUBA Tuff). Crossed polars. Scale bar 100 μm. **(W)** Vermicular crystals distributed in a fine-grained matrix of mosaic-textured clay mineral stacks. Both the matrix and the vermicules most probably consisted originally of kaolinite but are now largely replaced by illite indicated by the bright interference colours (DIBA Tuff). Crossed polars. Scale bar 100 μm.

The Korabib Tuffs

About 30 km northeast of Noordoewer 21 light-weathered ash-fall tuff layers, interbedded in dark weathered shales of the Prince Albert Formation, are exposed in a road cut on the western side of the B1 highway (S 28° 32.673' E 17° 49.944') (Fig. 3.21). This outcrop, which lies within the area of farm Korabib, is named here KORA-1.
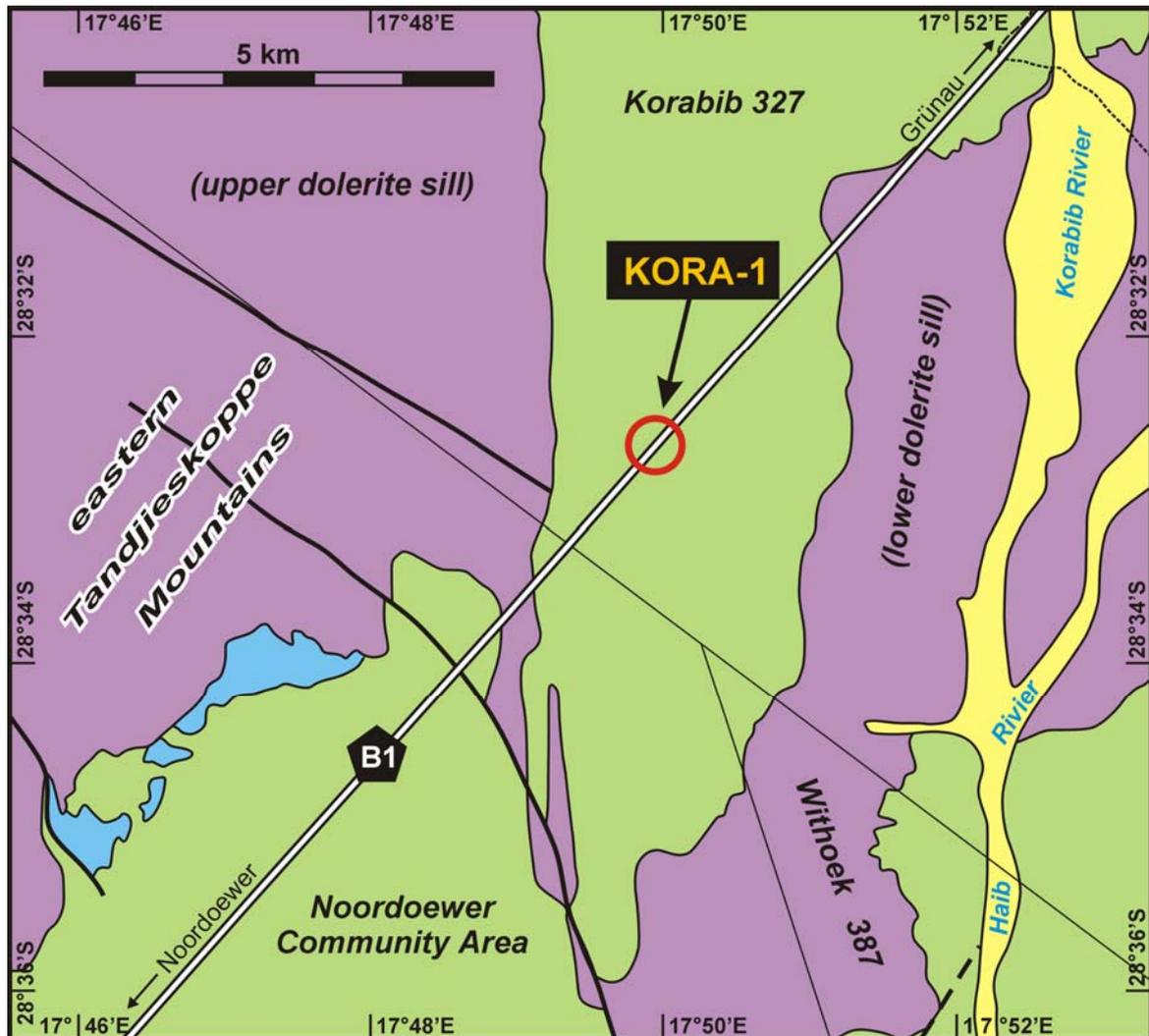
Fig. 3.21: Geological map of the vicinity of the Korabib Tuffs outcrop locality, mainly adopted from hand draft geological maps in the scale of 1:50000 drawn by C.P. Schreuder, G. Genis and G.J. Beukes (maps are stored in the map collection of the Geological Survey of Namibia). Jurassic dolerite sills are coloured in purple, shales of the Dwyka Group and the Prince Albert Formation are coloured in green, and larger outcrops of the white weathering black shales of the Whitehill Formation are coloured in blue. Smaller outcrops of the Whitehill Formation can be found along the lower and upper contacts of the upper dolerite sill, which intruded into the Whitehill Formation. During the time of geological mapping (1970-1973) the boundary between the glacigenic Dwyka Shales (with drop-stones) and the post-glacial Prince Albert Shales was not mapped. However, from own investigations it is known that the lower dolerite sill intruded approximately into the stratigraphic level of the Dwyka-Prince Albert boundary, which is marked in this area by the white weathering Owl Gorge Member. The upper and lower dolerite sills are connected in this area by a complex dyke-fault zone c. 2.5 km southeast of the KORA-1 locality.

The whole outcrop can be subdivided into three sections consisting of continuous shale-tuff successions, which have been logged in detail (Fig. 3.22). In the northernmost section (1) the beds are lying approximately horizontal, whereas in outcrop sections 2 and 3 the beds are tilted (Fig. 3.23). A NW-SE trending fault zone, which probably represents a reverse fault, separates outcrop sections 2 and 3. A light-weathering, intensively altered, relatively soft cataclastic rock, which is bordered by fracture zones formes the centre of the fault. Such compressional tectonic features, like thrusts and folds, have been observed at several localities in southern Namibia, where dolerite sills intruded into shales. The stratigraphic position of the Korabib Tuffs within the Prince Albert Shales is not exactly known. The Prince Albert Shales are sandwiched between an upper dolerite sill, which intruded into black, fissile shales of the Whitehill Formation, and a lower dolerite sill, which intruded close to the stratigraphic level of the Owl Gorge Member at the Dwyka-Ecca boundary (Fig. 3.21). According to this, the Korabib Tuffs seem to be positioned somewhere in the upper third of the Prince Albert Formation, however, faulting and tilting as well as interfering

Fig. 3.22: Detailed logs of the three outcrop sections exposed at the Korabib Tuffs locality (KORA-1). Numbers next to the logs denote the thickness of individual tuff layers (in cm).

small- and large-scale folding of the strata complicates the geological situation. Therefore, without detailed mapping of the area the stratigraphic positioning of the Korabib Tuffs should be considered as a preliminary suggestion. Due to the present stratigraphic uncertainties the Korabib Tuffs were not chosen as primary samples for radiometric age determination study but future radiometric age dating of these tuffs would definitely be useful if detailed mapping around the area could enable a more precise determination of their stratigraphic position.

outcrop section 3	fault zone	outcrop section 2
bedding:	orientation:	bedding:
205/08, 205/13, 215/10	050/30	195/05, 230/05, 295/05

Fig. 3.23: Photo interpretation of the geological situation at the KORA-1 outcrop. The tuff-bearing outcrop sections 2 and 3 are separated by a NW-SE trending fault, which probably represents a reverse fault. The centre of the fault is formed by a soft, light-weathering, and intensively altered cataclastic rock. Hammershaft is c. 30 cm long.

If the supposed stratigraphic position is correct, the Korabib Tuffs might correlate with the higher Itzawisis Tuffs (TUBA Tuffs), although their macroscopically appearance is very different. In contrast to the Itzawisis Tuffs the Korabib Tuffs form relatively firm rocks with a light grey to creamish or pale reddish colour. The well sorted tuffs are often intensively spotted with tiny (150-500 µm), brownish spots giving the rock a densely peppered appearance (Fig. 3.25). Most of the tuffs look massive, only in a few samples very faint horizontal bedding with beds of a thickness of about 0.5-1.5 cm becomes apparent due to alteration. Structures resembling low angle cross-bedding may indicate reworking by currents (Fig. 3.25). The majority of the tuffs shows a blocky to slightly nodular weathering (Fig. 3.24). The thickness of the tuff layers ranges from <0.5 cm up to about 9 cm (Fig. 3.22). The upper and lower contacts are mostly sharp, only in a few cases the upper contact appears slightly gradational (Fig. 3.24-B). The enclosing rocks are dark greenish, silty shales of the Prince Albert Formation, which are coated in outcrops by dark brown to black desert varnish.

Fig. 3.24: Korabib Tuffs: **(A/l.)** Blocky to nodular weathering tuff layer (sample KORA 1-1 T3a-c) between greenish shales of the Prince Albert Formation. **(B/r.)** Tuff layer showing a slightly gradational upper contact.

Fig. 3.25: Polished slab of tuff layer KORA 1-3 T11 of the Korabib Tuffs. In the lower third of the tuff inclined surfaces may represent cross-bedding possibly indicating reworking by currents. A not very pronounced horizontal bedding is visible in the upper two thirds of the tuff probably indicating several eruptive pulses. The tuff is densely speckled with tiny (150-500 µm) dots composed mainly of hematite and/or goethite, but probably originally representing cordierite porphyroblasts.

Under the microscope the Korabib Tuffs appear as very well sorted, relatively crystal-poor, and fine-grained ash tuffs. Despite the impression of faint horizontal and low angle cross-bedding structures within some of the tuffs (Fig. 3.25), no pronounced grain size variation or grading is visible in thin sections. Only concentrations of horizontally aligned biotite flakes form ill-defined, thin layers (50-100 µm) within the tuff. The Korabib Tuffs consist mainly of a fine-grained, clay mineral-rich matrix, whereas larger-sized crystals or crystal fragments (quartz, feldspar, biotite, and illitized kaolinite booklets) are not very abundant. According to whole-rock XRD analyses illite and quartz represent the only major mineral phases of the tuffs. Plagioclase is also present and forms a minor phase, whereas chlorite occurs only in traces. The speckling of the tuff with brownish spots (Fig. 3.26-A) might be caused by completely altered cordierite porphyroblasts due to Jurassic dolerite intrusions.

Quartz, forming the most abundant crystal component, occurs mainly as angular, more or less equidimensional crystal fragments, whose grain size ranges from <20-120 µm. Almost all quartz grains are monocrystalline showing straight extinction. Some thorn- or triangular-shaped splinter quartzes have been observed. Plagioclase crystals are much less abundant and occur as irregular-shaped, angular fragments with a grain size mainly ranging from 50-170 µm. Most of the plagioclase crystals appear very fresh or only slighlty altered (dusty). Also biotites are not present in great amounts compared to the Owl Gorge and Itzawisis Tuffs. The grain size of thin flakes lies mainly within 150 and 250 µm, apart from some exceptional large flakes reaching lenghts over 400 µm. Most of the biotite flakes are totally altered to dark brown iron oxides (Fig. 3.26-B). Probably also the majority of the colourless

booklet- and mica flake-shaped clay mineral crystals (Fig. 3.26-C/D), now composed of illite, represent pseudomorphs after biotite. It is suggested that, similar to the Itzawisis Tuffs, some of the biotite altered early diagentically to kaolinite, which was later transformed under pro-grade conditions to illite. In one observed case a large biotite flake, still showing pleochroism, is only partly replaced by illite (Fig. 3.26-E/F). The size of the illitized kaolinite booklets ranges between <20 and 100 µm, whereas the elongate, mica-like crystals reach up to 300 µm in length. In addition, zircon, apatite and tourmaline have been detected as accessories. The zircon population is, similar to the Itzawisis Tuffs, very heterogeneous. Present are (1) small rounded crystals (20-30 µm), (2) angular crystal fragments (up to 50 µm), and (3) euhedral, squat to equidimensional crystals (up to 50 µm). Some of the euhedral zircon crystals contain an inherited, anhedral crystal core (Fig. 3.26-G). Apatite forms sub- to euhedral crystals with a length of up to 60 µm and shows etched crystal surfaces (Fig. 3.26-H). Few dirty greenish-blue to yellowish-brown, angular tourmaline crystals (30-50 µm) have been observed, too. The latter, together with the heterogeneous zircon population and the presence of illitized kaolinite booklets, emphasizes the similarity with the Itzwisis Tuffs, i.e. they seem to belong to the same eruptive phase, although grain-size and abundance of crystal components is remarkable lower in the Korabib Tuffs. In addition, the Korabib Tuffs also apparently underwent a higher-grade thermal overprint than the Itzawisis Tuffs, resulting in a much harder rock, which shows a greatly reduced tendency towards swelling and disintegartion upon moistening. This thermal overprinting (contact-metamorphism) was most probably caused by nearby Jurassic dolerite intrusions. Also the intensive spotting of the tuffs (altered cordierite porphyroblasts) is suggested to be related to this thermal overprint. Such spots are also characteristic for the nearby Owl Gorge Tuffs, in which they are smaller (50-100 µm) than in the Korabib Tuffs (150-500 µm). The fine-grained matrix of the Korabib Tuffs appears recrystallized and consists mainly of tiny interlocking clay mineral crystallites with minor amounts of microscrystalline quartz (Fig. 3.26-C/D).
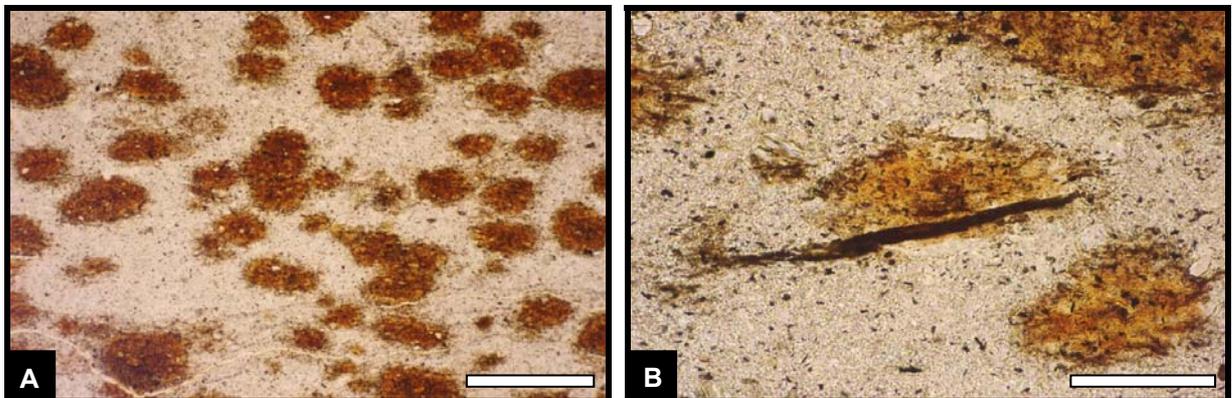
Fig. 3.26: Thin section photographs of the Korabib Tuffs: **(A)** The fine-grained, crystal-poor tuffs are intensively spotted with subspherical to ovoid, contact-metamorphically grown porphyroblasts, now mainly altered to hematite/goethite, but originally possibly composed of poikiloblastic cordierite. Plane-polarized light. Scale bar 500 µm. **(B)** Most biotite flakes, like in this picture, are altered within the Korabib Tuffs completely to hematite/goethite. Plane-polarized light. Scale bar 100 µm.
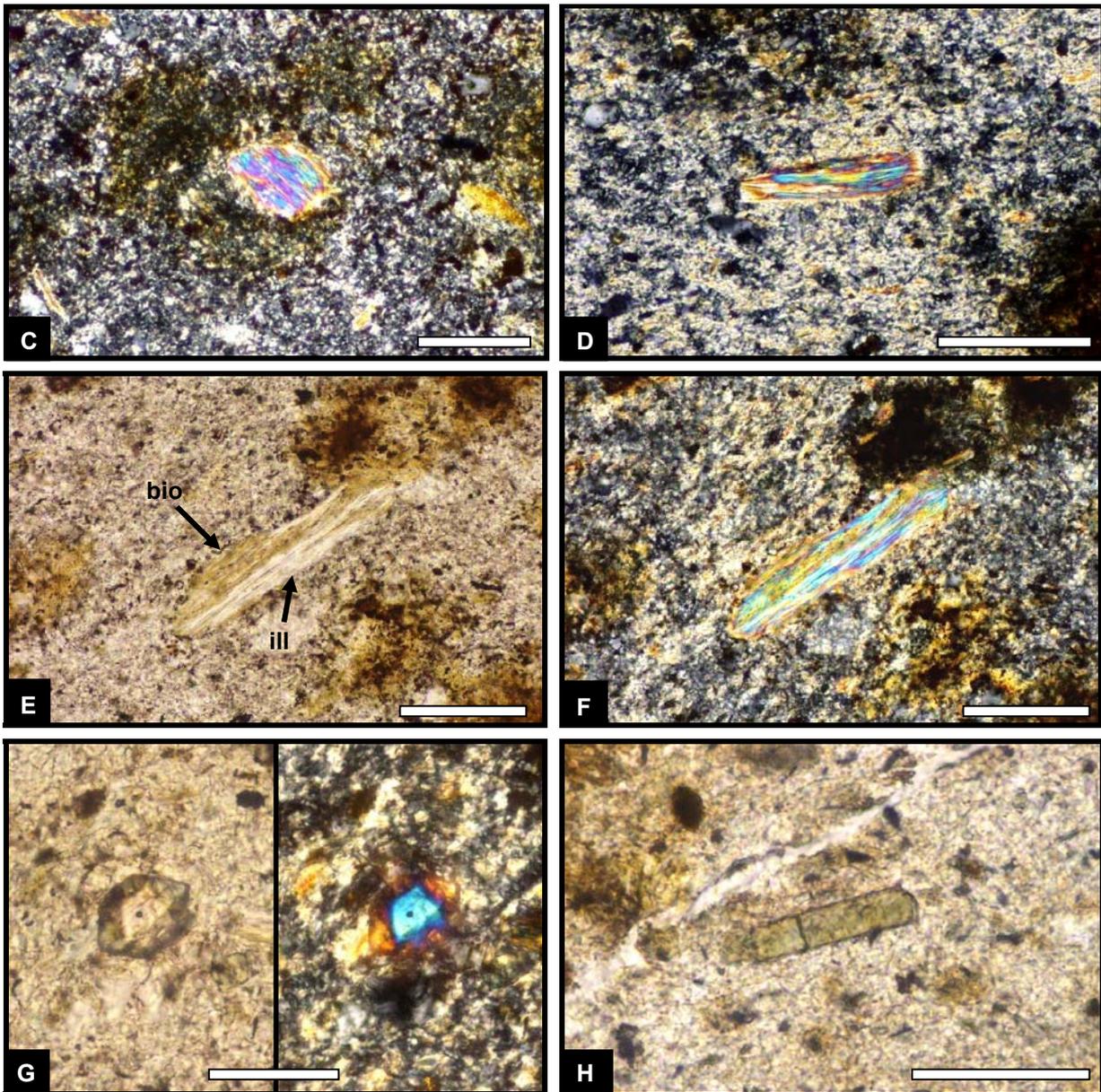
Fig. 3.26: Thin section photographs of the Korabib Tuffs (cont.): **(C) & (D)** Crystal booklet and flake composed of illite (bright interference colours) probably replacing kaolinite pseudomorphs after biotite. Note the recrystallized matrix. Crossed polars. Scale bars 100 µm (left) and 50 µm (right). **(E) & (F)** This image shows the rare case, in which a biotite flake is only partly altered to illite. Illite may have replaced earlier formed kaolinite. Note also the vertical expansion of the flake, contrasting to the thin altered biotite flake in Fig. 3.26-B. Plane-polarized light (left) and crossed polars (right). Scale bars 100 µm. **(G)** Euhedral, squat zircon crystal with inherited anhedral crystal core. Plane-polarized light (left) and crossed polars (right). Scale bar 50 µm. **(H)** Subhedral apatite crystal showing slight etching on crystal surfaces. Plane-polarized light. Scale bar 50 µm.

The Uhabis River Tuff

The outcrop, where the so-called Uhabis River Tuff was first discovered (its type locality), is situated at the southwestern margin of the eastern Tandjieskoppe Mountains, c. 2 km east of the Uhabis Rivier and c. 1.1 km east of the gravel road, which leads in upstream direction along the Uhabis River to the ruins of the former Uhabis farm houses and police station (Fig. 3.27). This gravel road leaves the tar road of the B1 highway c. 4.5 km northeast of Noordoewer leading in a northwesterly direction into a valley, which was cut by the Uhabis Rivier into a thick dolerite sill (lower dolerite sill). At the southern margin of the western Tandjieskoppe Mountains, c. 7 km west of the Uhabis Rivier and c. 3.3 km northwest of Duifiefontein, the Uhabis River Tuff was detected in another outcrop above the Duifie se Vlakte (Fig. 3.27). This outcrop can be reached via the Owl Gorge jeep track (see Fig. 3.6).
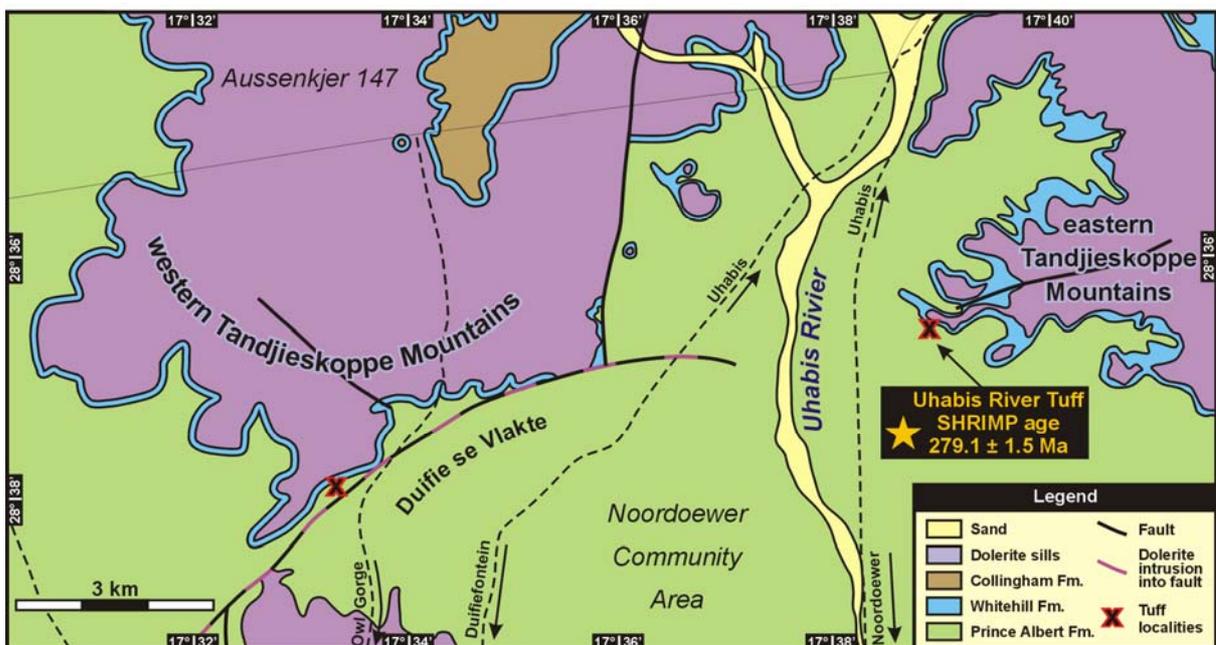
Fig. 3.27: Geological map of the area, where outcrops of the Uhabis River Tuff were found. The map is mainly adopted from hand draft geological maps in the scale of 1:50000 drawn by C.P. Schreuder, G. Genis and G.J. Beukes (1970-1973) (maps are stored in the map collection of the Geological Survey of Namibia).

Due to the excellent outcrop conditions at the type locality east of the Uhabis Rivier (S 28° 36.649' E 17° 38.861') it was possible to determine the stratigraphic position of the Uhabis River Tuff within the sediments of the lower Ecca Group quite precisely by using a Jacob staff. The Uhabis River Tuff lies c. 11 m below the boundary between the Prince Albert and the Whitehill Formation. This boundary is represented by a conformable contact surface. Morphologically the Uhabis River Tuff can be found near the base of the coarsening-upward succession at the top of the Prince Albert Formation, which is characterized in the Aussenkjer-Noordoewer area by a cliff-forming succession of brownish and slabby

weathering, greenish-grey, chert-like, silty shales (Uhabis Member). These shales are underlain by fissile, bluish- to greenish-grey shales of the Prince Albert Formation and overlain by fissile to papery, white weathering, black shales of the Whitehill Formation (Fig. 3.28). The latter are overlain by a thick dolerite sill (upper dolerite sill), which is responsible for the rugged terrain of the Tandjieskoppe Mountains. The stratigraphic position of the Uhabis River Tuff is quite comparable to the stratigraphic position of the Vreda Tuffs, which will be described in the following sub-chapter. Both tuff horizons are lying close to the base of the coarsening-upward succession, which forms the uppermost part of the Prince Albert Formation (see Fig. 3.2). The only difference is that in the Aussenkjer-Noordoewer Karoo outcrop area this coarsening-upward succession is formed by silty, chert-like shales, whereas in the northern part of the Martiental-Keetmanshoop Karoo outcrop area it is formed by the deltaic Auob Sandstone Member. In the Vreda borehole, close to the Namibian-Botswanan border (see Fig. 3.1), several tuff layers (here called Vreda Tuffs) were detected near the base of the Auob Sandstone (Grill, 1997).

Fig. 3.28: Outcrops of the upper part of the Prince Albert Formation (brownish colours) and the overlying Whitehill Formation (greyish colours) along the Uhabis Rivier. The Uhabis River Tuff lies near the top of the Prince Albert Formation, within the cliff-forming coarsening-upward succession of silty shales. View towards west.

The Uhabis River Tuff represents a single ash-fall tuff layer, which has a thickness of 1.5 cm at its type locality. In natural outcrops the Uhabis River Tuff is not easily recognizable because both the altered tuff and the enclosing shales show a similar yellowish to greenish-ochreous weathering colour and are both coated with dark brown to black desert varnish. Since the Uhabis River Tuff is a little bit softer than the enclosing shales, it forms a slightly back-weathering layer with slightly rugged weathering surfaces (Fig. 3.29). Because the stratigraphic position of the Uhabis River Tuff could be determined very precisely it was chosen for radiometric dating (see Fig. 3.29 and Chapter 5 Geochronology). Single zircon U-Pb SHRIMP dating yielded an age of 279.1 ± 1.5 Ma (Artinskian after Gradstein et al., 2005).

Fig. 3.29: Uhabis River Tuff : **(A/l.)** Typical outcrop of the Uhabis River Tuff (base and top indicated by arrows) at its type locality east of the Uhabis River. **(B/r.)** Excavation and sampling of the Uhabis River Tuff at the type locality for radiometric age determination.

In polished rock specimens the Uhabis River Tuff contrasts markedly with the enclosing shale (Fig. 3.30). The altered tuff layer has a yellowish-ochreous colour and is intensively spotted with larger sized (0.4-2 mm), dark olive green porphyroblasts and speckled with smaller sized (0.1-0.25 mm), light olive green dots. Also the enclosing shales are densely speckled with countless tiny (0.1-0.2 mm) dots. All these spots and dots are most probably the result of severe thermal overprinting of the rocks due to Jurassic dolerite intrusions and consist of completely pinitized cordierite. The thermal overprinting is also reflected by abundant, sericitized andalusite porphyroblasts within black shales of the overlying Whitehill Formation (Fig. 3.31). The size and distribution of spots gives the tuff layer macroscopically a normally graded appearance, although they do not represent a detrital component. However, thin sections show that the tuff is indeed normally graded according to the marked decrease of the grain size of crystal components from base to top. Both the lower and upper contact of the tuff to the enclosing shale is very sharp. In places, the overlying shale slightly incises into the very fine-grained lamina at the top of the tuff (Fig. 3.30), which is similar to the observations made on tuff OG-9 (Owl Gorge). A very conspicuous feature of the Uhabis River Tuff is the diagenetic phosphate impregnation forming a dark grey to black layer at the

top of the tuff (Fig. 3.30). The intensity of the phosphate impregnation is somewhat fluctuating as indicated by colour changes from black to light grey. This pristine phosphate impregnation consists of francolite, a carbonate hydroxyl fluorapatite.

2 cm
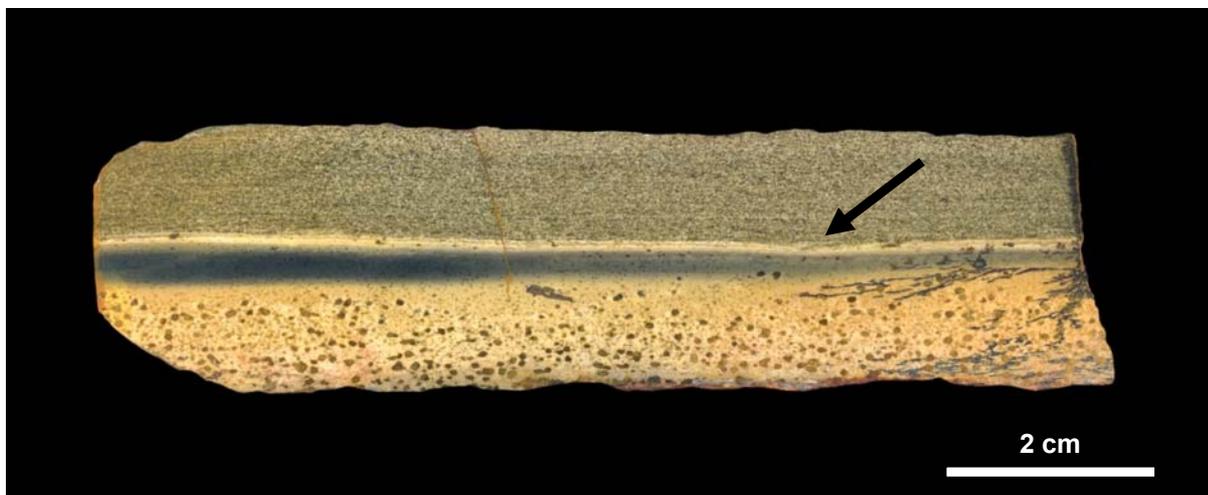
Fig. 3.30: Polished rock specimen showing the Uhabis River Tuff and the enclosing shale of the Prince Albert Formation, which, in places, slightly incises into the fine-grained lamina at the top of the tuff (arrow). A characteristic feature of this tuff is the early-diagenetic phosphate impregnation forming the black, lens-like layer near the top of the tuff. Due to the thermal overprinting by Jurassic dolerite intrusions the tuff is speckled with relatively large, dark spots, most probably representing completely pinitized cordierite porphyroblasts. In addition, both the tuff and the enclosing shales are intensively speckled with smaller porphyroblastic dots as a result of thermal overprinting.
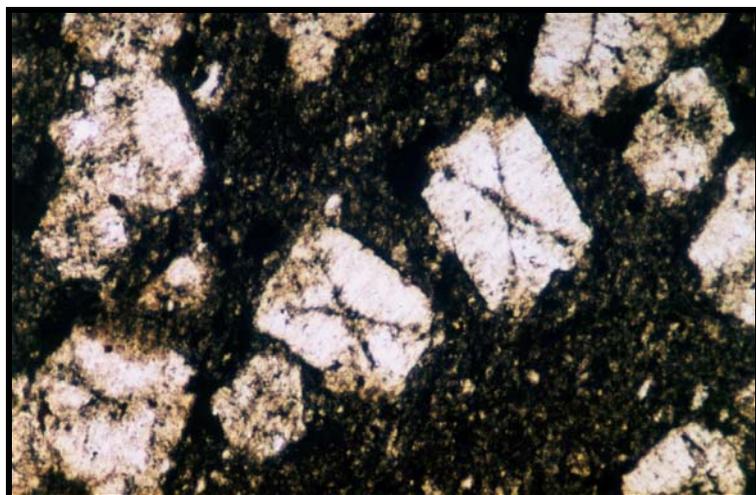
Fig. 3.31: Andalusite (variety chiastolite) porphyroblasts in black shales of the Whitehill Formation at he type locality of the Uhabis River Tuff, which is embedded in the underlying shales of the uppermost Prince Albert Formation. Due to retrograde hydrothermal alteration andalusite is degraded to illite. The black cross within the chiastolite crystals is formed by graphite inclusions sourced from the carbonized organic content of the black shales.

Thin sections show that the Uhabis River Tuff consists of a poorly sorted, very crystal-rich, matrix- to clast-supported coarse ash tuff in its lower portion (Fig. 3.32-A), which grades upwards into a successively finer grained, crystal-poorer, matrix-supported fine ash tuff. The crystal fraction comprises quartz, feldpar (mainly plagioclase), and biotite. Almost all crystals are highly angular and both quartz and feldspar can be present as splintery crystal fragments (Fig. 3.32-B). Compared to the other described tuffs, the Uhabis River Tuff appears relatively rich in juvenile zircon and exceptionally rich in juvenile apatite crystals. No vitroclastic

components (relics of pumice lumps, fiamme, or glass shards) have been detected. A very strong thermal overprinting of the tuff is indicated by numerous, large and small porphyroblasts and by the distinct recrystallization of the matrix, composed of interlocking clay mineral crystallites (mainly illite) as well as crystallites of quartz and possibly albite.

Quartz and feldspar form in most thin sections >90% of the crystal fraction, whereas biotite seems to be much less abundant. Both quartz and feldspar are present as very angular to splintery crystal fragments (Fig. 3.32-B). No crystals or crystal fragments of euhedral, hexagonal beta-quartz paramorphs have been detected. Elongate, splintery crystal fragments are often aligned parallel to the bedding of the tuff. The average size of quartz and feldspar crystals lies in the lower half of the tuff between 50 and 150 µm. The upper half of the tuff is, compared to other tuffs, still relatively rich in crystal fragments (Fig. 3.32-B), showing a mean grain size of 20-40 µm. Quartz shows generally straight extinction and is present as monocrystalline crystal fragments. According to the abundance of polysynthetic twinning observed in thin sections the feldspar crystal fraction seems to be strongly dominated by plagioclase (Fig. 3.32-C). Most plagioclase appears relatively fresh with only minor signs of alteration, and only few crystals show a pronounced sericitization. The majority of the strongly altered, sericitized feldspar crystals are untwinned and it is suggested that most of them represent potassium feldspar (Fig. 3.32-D). Replacement of feldspar by mosaic-textured kaolinite/illite (cf. Itzawisis Tuffs) has not been observed in the Uhabis River Tuff. Biotite is much less abundant than quartz and plagioclase. In places, somewhat larger concentrations of biotite flakes can be observed; the overall distribution within the tuff is quite irregularily. The basal part of the tuff contains thin, non-expanded flakes with a size of 100-200 µm (Fig. 3.32-E), whereas in the upper part smaller (~50 µm) but thicker, expanded flakes are present (Fig. 3.32-F). All biotites are strongly degraded to dark brown hematite or goethite, only some of the expanded flakes contain relics of yellowish-brown clay mineral alteration products (vermiculite and/or chlorite?). Neither bleaching of biotite to colourless phyllosilicates (kaolinite/illite) nor the presence of crystal booklets or vermicules, what is so common in the Ganigobis, Zwartbas, Itzawisis, and Korabib Tuffs, have been observed in the Uhabis River Tuff. From this point of view, the Uhabis River Tuff shows strong similarities with the Owl Gorge Tuffs. Zircon is fairly abundant in thin sections of the Uhabis River Tuff. The zircons, which were observed in thin sections, are mainly euhedral to subhedral and display dominantly stubby, shortened to almost equidimensional forms with square to roundish outlines (Fig. 3.32-G). Their size ranges from <10 µm up to 60 µm. Brownish melt inclusions were identified in one or two cases. Some of the zircons show some rounding and they might represent, together with some angular zircon crystal fragments, a detrital, xenocrystic component. The Uhabis River Tuff is exceptional rich in apatites and it is the first tuff in the

stratigraphic succession of the Ecca Group that contains conspicuous smokey-grey and internally zoned apatites (Fig. 3.32-H). Most of these apatites are euhedral to subhedral and frequently hexagonal-shaped basal sections can be observed. Their size ranges from <10-120 µm. Longitudinal sections reveal that most apatites show shortprismatic to squat rather than acicular forms. Often some slight etching phenomena can be seen along crystal surfaces. Some of the apatites contain colourless to yellowish-brown inclusions or multi-inclusion trails. In addition to zircon and apatite, some angular, greenish-blue to orange-brown, zoned tourmaline crystals (40-50 µm) and rounded, dark brown rutile crystals (40-70 µm) have been observed. The matrix of the altered tuff is markedly recrystallized and composed of interlocking clay mineral (illite) crystallites (Fig. 3.32-C/D). According to XRD analyses on the matrices of other Karoo tuffs (Viljoen, 1995; Bangert, 2000; Geiger, 2000), microcrystalline quartz and albite may also be present.
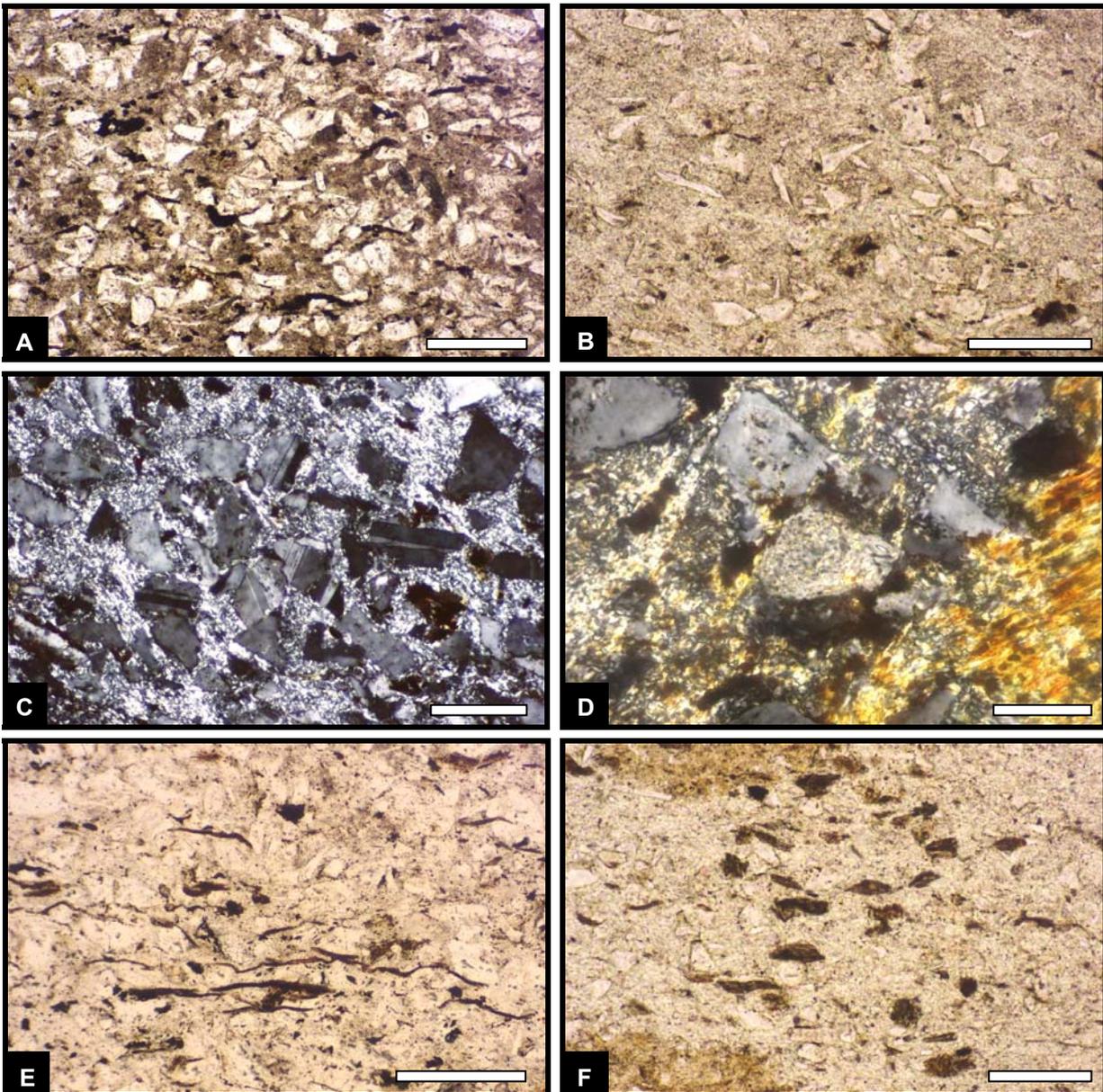
Fig. 3.32 (previous page): Thin section photographs of the Uhabis River Tuff – primary crystal components: **(A)** Crystal-rich (mainly quartz and feldspar), matrix- to clast-supported lower part of the tuff. Plane-polarized light. Scale bar 250 µm. **(B)** Crystal-poorer, matrix-supported upper part of the tuff with abundant splintery quartz and feldspar crystals. Plane-polarized light. Scale bar 100 µm. **(C)** Concentration of angular plagioclase crystal fragments (centre of image) in the lower half of the tuff. Note also the strongly recrystallized matrix, which is composed mainly of intelocking clay mineral crystallites. Crossed polars. Scale bar 100 µm. **(D)** Strongly altered (sericitized), untwinned feldspar fragment (centre of image) probably representing potassium feldspar. Note again the strongly recrystallized matrix. Crossed polars. Scale bar 50 µm. **(E)** Flat, large biotite crystals in the lower part of the tuff almost entirely altered to hematite and goethite. Plane-polarized light. Scale bar 200 µm. **(F)** Concentration of smaller biotite flakes in the upper part of the tuff showing vertical expansion. Plane-polarized light. Scale bar 100 µm.
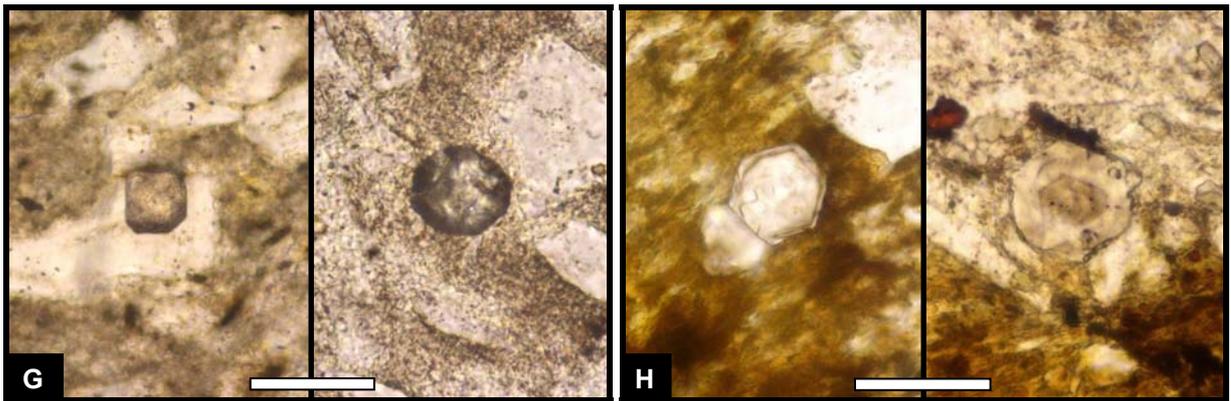
Fig. 3.32: Thin section photographs of the Uhabis River Tuff – primary crystal components (cont.): **(G)** Euhedral, equidimensional, juvenile zircon crystals showing square and roundish, octagonal outlines. Plane-polarized light. Scale bar 50 µm. **(H)** Basal sections of euhedral to subhedral, juvenile apatite crystals with pronounced internal zonation. Plane-polarized light. Scale bar 50 µm.

As a consequence of severe thermal overprinting due to Jurassic dolerite intrusions the Uhabis River Tuff is intensively interspersed with smaller and larger, porphyroblastic dots and spots. The smaller, light yellowish to olive-green ones have a size of 100-250 µm, are subspherical to ovoid, and do not show any internal structures. They behave pseudoisotropic under crossed polars and are most probably completely composed of crypto- to micro-crystalline pinite, a complex mixture of mainly sericite and chlorite, formed by alteration of cordierite (Tröger, 1969; Ogiermann, 2002). Within the tuff they occur mainly isolated, however, in the enclosing shales they are often so densely spaced that individual dots coalesce to form larger, irregular shaped areas (Fig. 3.33-A). Some medium-sized porphyroblasts contain a lamellar-structured core, which is surrounded by a structureless margin (Fig. 3.33-B). These porphyroblasts represent transitional types to the large, lamellar-structured ones. The bigger porphyroblasts, which are largely confined to the lower part of the tuff (Fig. 3.30), have a darker yellowish-brown to olive-green colour and a size of 0.4-2 mm. Their shape is mainly subspherical, ovoid to elongate (Fig. 3.33-C/D). However, some larger, more irregular-shaped ones also show partly polygonal outlines (Fig. 3.33-E/F), most probably reflecting relics of prismatic crystal surfaces of the original mineral (cordierite), of which the

porphyroblasts were composed of. These large porphyroblasts display a very conspicuous, strongly oriented, multi-lamellar internal structure, which is most probably inherited from multiple lamellar twinned cordierite (Fig. 3.33-B to I). In some of the porphyroblasts the growth orientation of these lamellae can be different in various parts of the porphyroblast indicating that they were composed of two or more individual crystals (composite porphyroblasts) (Fig. 3.33-E/F). Within the tuff the lamellar growth orientation of the porphyroblasts is random, which is very common for contact-metamorphic growth under no or very low strain conditions. The individual lamellae, which have a typical width of about 5-10 µm, are mainly composed of greenish-yellowish-brown, very fine-grained phyllosilicates, which are most probably composed of pinite, a sericite- and chlorite-dominated alteration product of cordierite (Fig. 3.33-G). Under crossed polars the lamellae show straight extinction, with light yellow to orange-brown interference colours dominating (Fig. 3.33-H). The straight extinction indicates that the crystal growth orientation of the main pinite-forming mineral phases, sericite and chlorite (both showing almost straight extinction), must be parallel to the orientation of the lamellae. Some of the lamellae are also partly replaced by microcrystalline quartz. Oxidation processes are indicated by dark brownish rims of hematite or goethite platelets fringing many of the porphyroblasts (Fig. 3.33-I). However, such hematite and goethite platelets are not only observed around but also within the porphyro-blasts, sometimes looking like small blood droplets (Fig. 3.33-K). In addition to ironoxides, conspicuous but very tiny, euhedral, short-prismatic, yellowish-brown crystals with an extremely high relief, i.e. with an extremely high refractive index, are frequently observed within porphyroblasts (Fig. 3.33-L/M). The extremely high relief, the relatively broad black total reflection rims, the straight extinction, the presence of heart-shaped crystal twins (Fig. 3.33-M), the lack of colour change under crossed polars due to extremely high birefringence, all these properties are characteristic for rutile. The rather light, yellowish colour of these rutiles indicates a low iron content. Since this type of rutile is not found outside the porphyroblasts, these rutiles must have formed during the thermal overprinting of the tuff as a result of the downbreak of a titanium-bearing mineral (or minerals), the redistribution of titanium, and its precipitation as oxide mineral. The most potential titanium source might be biotite, which shows in less intensively overprinted tuff samples well developed sagenite (acicular rutile) networks (see Fig. 3.11-H & 3.20-I; Owl Gorge & Itzawisis Tuffs). Also alteration of magnetite and ilmenite could provide titanium, however, their presence was not noticed.

Larger porphyroblasts, especially coalescing and intergrowing ones, sometimes show a rim (up to 200 µm in width), which appears under crossed polars slightly darker grey and coarser grained than the matrix of the tuff (Fig. 3.33-N). These rims form strongly recrystallized halos around the porphyroblasts and consist mainly of coarse-grained quartz crystals with a size of

20-50 µm (Fig. 3.33-O). Even larger quartz megacrysts, with inclusions of euhedral apatite and zircon, have been observed within porphyroblasts (Fig. 3.33-Q/R). Large, untwinned feldspar megacrysts occur in areas between coalescing porphyroblasts (Fig. 3.33-S/T). Spherulitic chalcedony is present within a few porphyroblasts as a late, low temperature formation (Fig. 3.33-P). Larger, radially, sheaf- and tuft-like grown, greenish crystals and crystal aggregates are also mainly observed within the marginal parts of porphyroblasts (Fig. 3.33-U to X). In plane-polarized light these phyllosilicate crystals show mainly pale yellowish-green to brownish-green colours and a slight pleochroism is visible. Darker brownish colours develop with progressive oxidation. Under crossed polars normal light yellowish to orange-brown low order interference colours dominate, however, in some cases also bright yellow, green, blue and purple colours are visible (Fig. 3.33-X). These bright colours are often associated with stronger oxidized parts of the crystal aggregates. In very few cases anomalous bluish-greenish-grey interference colours prevail and are associated with non- or less oxidized areas. These phyllosilicate crystals are representing with great certainty chlorites, probably with somewhat varying compositions and maybe intergrown with other phyllosilicates. These chlorites show mainly straight extinction under crossed polars and their sign of elongation is positive, i.e. they are length slow (the same is also valid for the pinitic lamellae!). In the case of the chlorite group length slow varieties are always optical negative and vice versa. This consequently means that the optical character of these chlorites is negative (Tröger, 1969). Within some porphyroblasts also radially grown aggregates of colourless phyllosilicates have been observed (Fig. 3.33-Y/Z). These show under crossed polars bright interference colours and might represent mainly sericite/illite. In one thin section of the Uhabis River Tuff elongate, lath-shaped to acicular, euhedral tourmaline was discovered as inclusions in large quartz megacrysts (Fig. 3.33-AA to AD), probably representing a late stage vug filling within a complex and composite porphyroblast area. These tourmalines exhibit dirty greenish-brown colours in plane-polarized light and contain a large amount of small, opaque particles as inclusions. The boron source for the tourmalines is probably rather located in the shales of the Karoo Supergroup than in the basaltic melt of the dolerites.
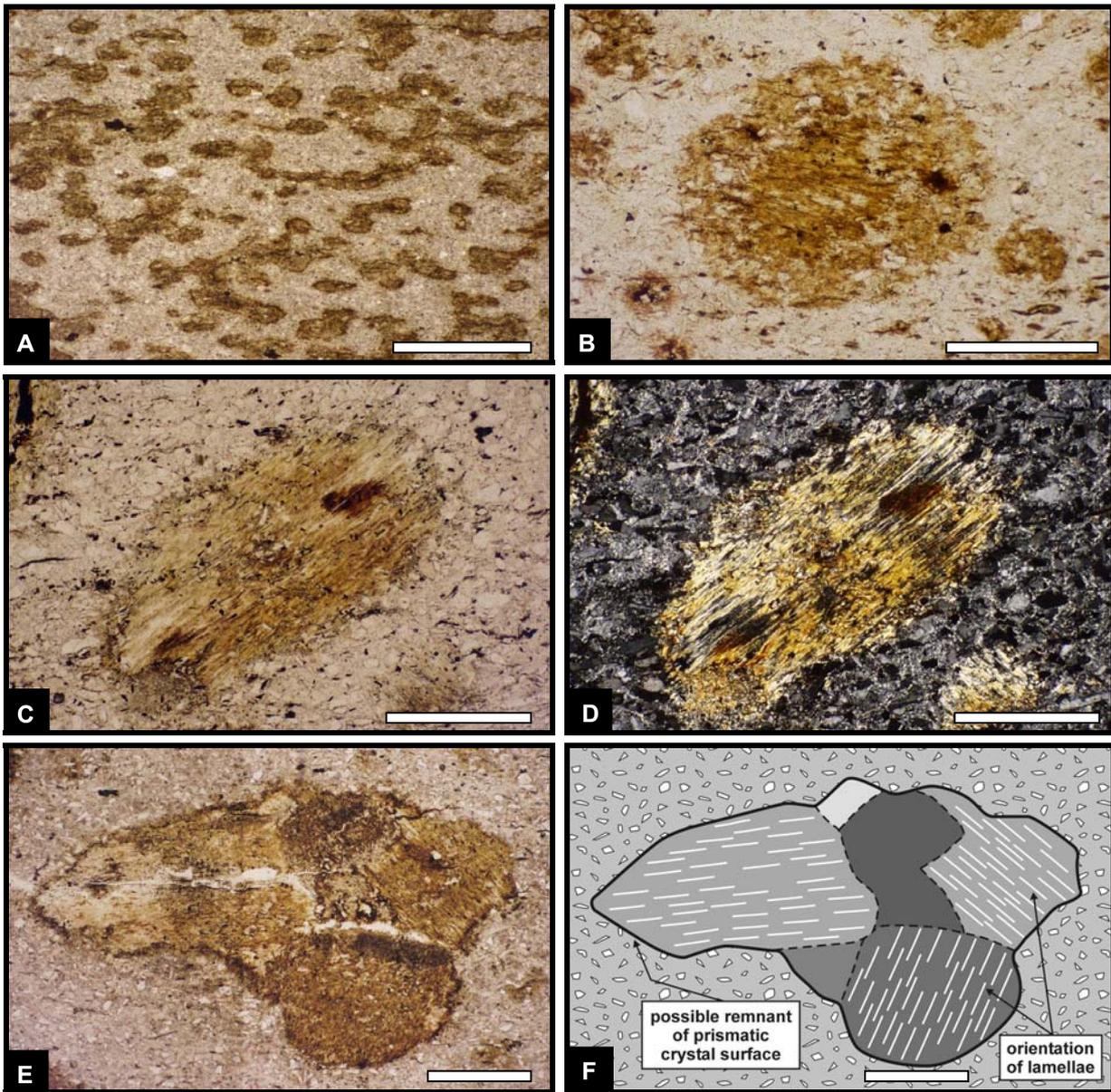
Fig. 3.33: Thin section photographs of the Uhabis River Tuff – secondary components: **(A)** Small, subspherical to ovoid porphyroblasts with no internal structure probably composed of pinite after poikiloblastic cordierite. Plane-polarized light. Scale bar 500 µm. **(B)** Medium-sized, spherical porphyroblast with lamellar-structured core and structureless margin. Plane-polarized light. Scale bar 250 µm. **(C) & (D)** Large, ellipsoidal porphyroblast showing a lamellar internal structure. It is probably mainly composed of pinite, a sericite- and chlorite-rich alteration product of cordierite, which formed contact-metamorphically due to Jurassic dolerite intrusions. The lamellar structure is most probably inherited from multiple lamellar twinning of cordierite. Plane-polarized light (left) and crossed polars (right). Scale bars 500 µm. **(E)** Large, irregular-shaped porphyroblast, which is composed of several individual crystals (composite porphyroblast), indicated by the different orientation of the internal lamellae. The V-shaped area at the left margin of the porphyroblast may represent the relics of prismatic crystal surfaces of cordierite. Plane-polarized light. Scale bar 500 µm. **(F)** Photointerpretation of (E).
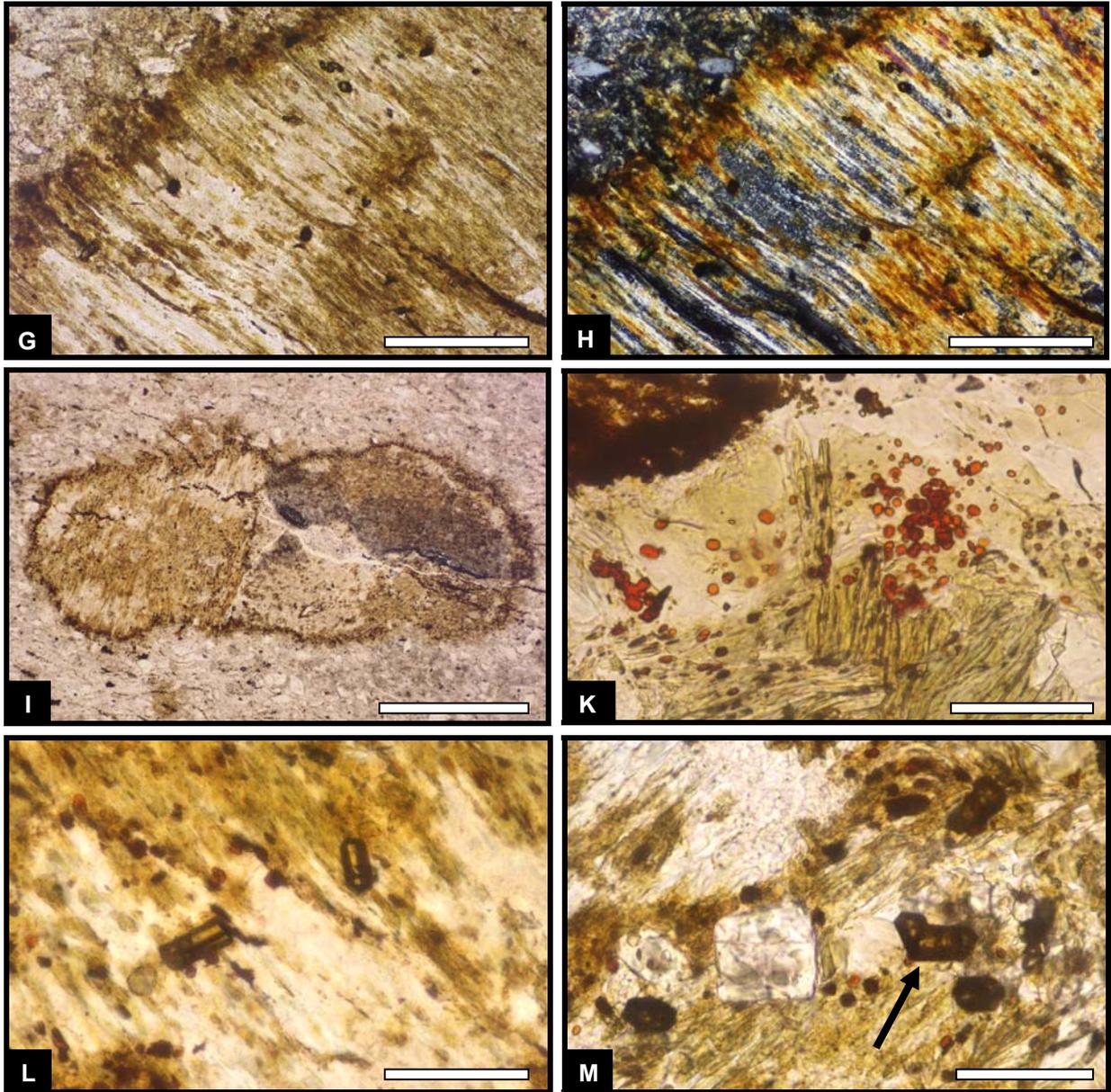
Fig. 3.33: Thin section photographs of the Uhabis River Tuff – secondary components (cont.): **(G) & (H)** Enlarged view on the internal lamellar structure of the large porphyroblasts, which are mainly composed of pinite, a sericite- and chlorite-rich alteration product of cordierite. The individual lamellae have a typical width of about 5-10 µm and are most probably inherited from multiple lamellar twinned cordierite. Plane-polarized light (left) and crossed polars (right). Scale bars 150 µm. **(I)** Large, elongate, composite porphyroblast showing a pronounced dark rim, composed of tiny hematite and/or goethite platelets, formed due to oxidation processes. Plane-polarized light. Scale bar 500 µm. **(K)** Tiny, droplet-like hematite crystals intergrown with a yellowish-greenish phyllosilicate (chlorite) within a large, pinitized cordierite porphyroblast. Plane-polarized light. Scale bar 50 µm. **(L)** Small, euhedral rutile crystals interspersed in the lamellar-structured part of a large porphyroblast. The relatively light yellowish colour of the secondary grown rutiles hints at a low iron content, in contrast to detrital rutiles, which display dark orange-brown colours. Plane-polarized light. Scale bar 50 µm. **(M)** Heart-shaped rutile crystal twin (arrow) next to apatite crystals (to the left) within a porphyroblast. Plane-polarized light. Scale bar 50 µm.

Coarse-grained quartz crystals (Fig. 3.33-O)

Lamellar internal structure of porphyroblast (Fig. 3.33-G/H)

Radially grown, greenish phyllo-silicate (chlorite) (Fig. 3.33-U/V)

Recrystallized, coarse-grained rim

Feldspar megacryst (Fig. 3.33-S)

Quartz (+ap & zr) megacryst (Fig. 3.33-Q/R)

Spherulitic chalcedony (Fig. 3.33-P)

Feldspar megacrysts (Fig. 3.33-T)
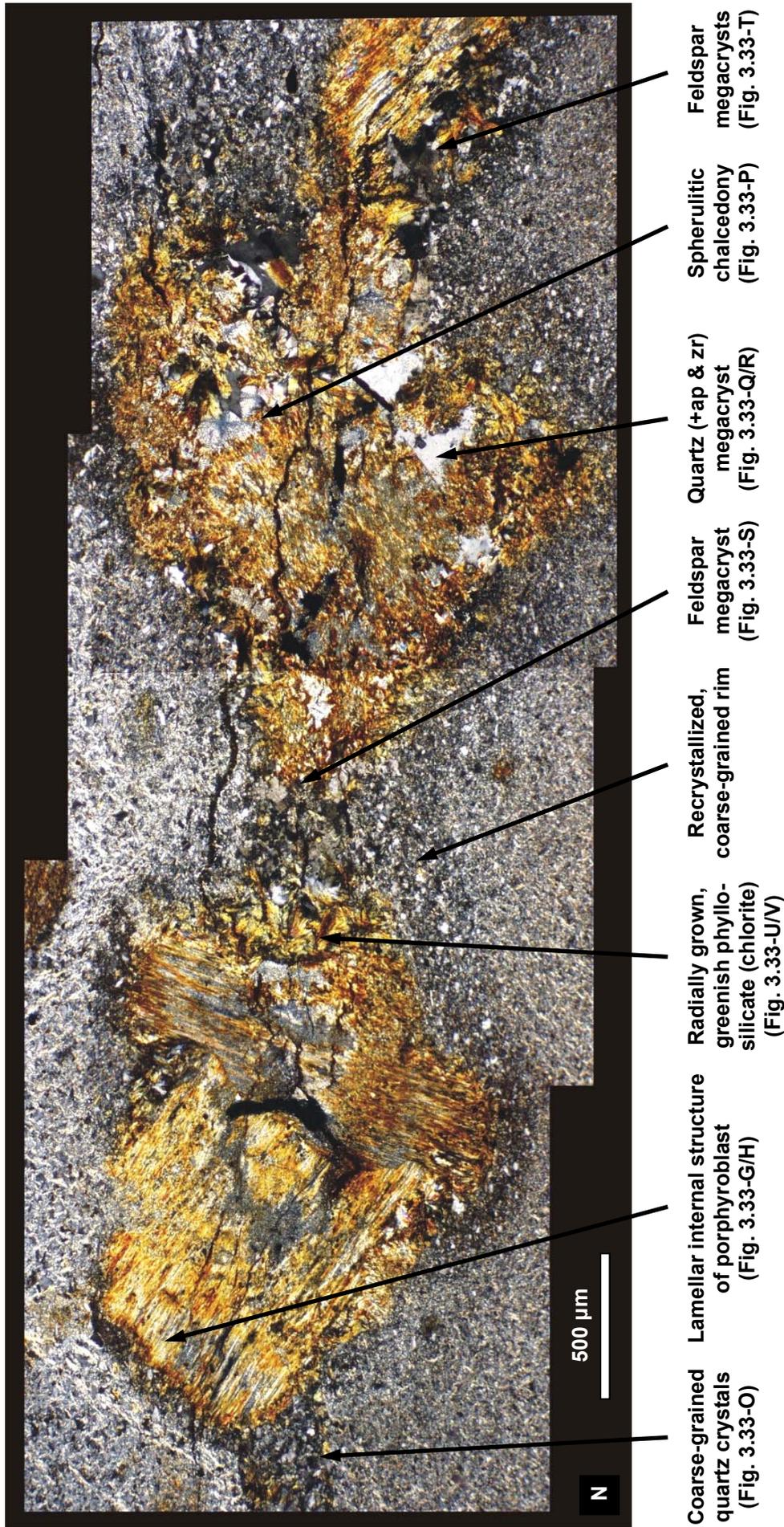
Fig. 3.33 (N): Large, coalescing, composite porphyroblasts, interpreted as completely pinitized cordierite porphyroblasts, surrounded by a coarse-grained recrystallization rim. Within and between the porphyroblasts also megacrysts of quartz and feldspar as well as larger areas of radially grown phyllosilicates (chlorite) and spherulitic chalcedony can be observed. Crossed polars. Scale bar 500 µm.
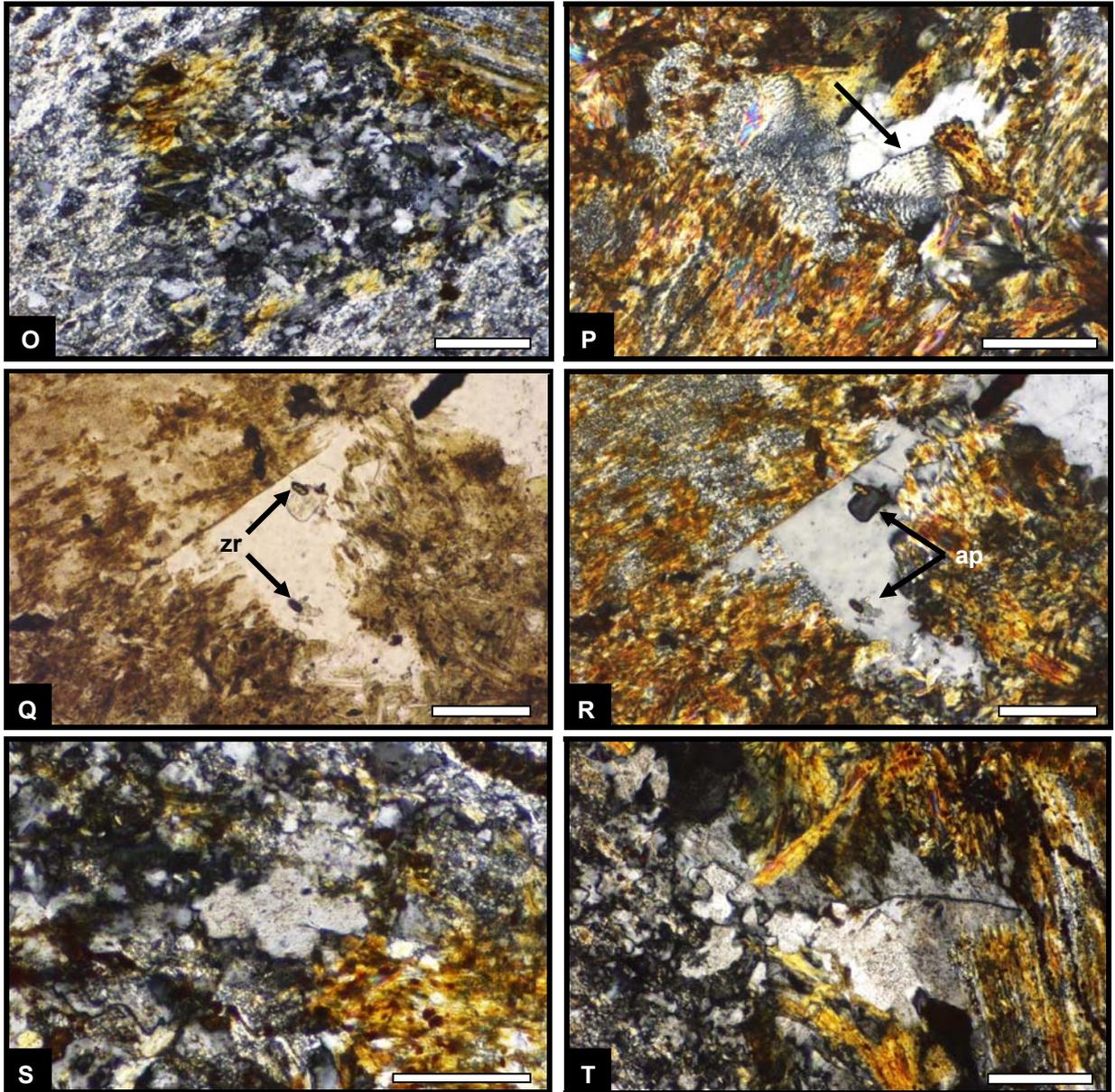
Fig. 3.33: Thin section photographs of the Uhabis River Tuff – secondary components (cont.): **(O)** Recrystallized area, consisting mainly of coarse-grained quartz, at the margin of a pinitized cordierite porphyroblast. Crossed polars. Scale bar 100 µm. **(P)** Spherulitic chalcedony with Brewster cross (arrow) within porphyroblast. Crossed polars. Scale bar 100 µm. **(Q) & (R)** Large quartz megacryst within porphyroblast showing inclusions of euhedral apatite (ap) and zircon (zr). Plane-polarized light (left) and crossed polars (right). Scale bars 100 µm. **(S) & (T)** Large feldspar megacrysts observed in the area between coalescing porphyroblasts. Crossed polars. Scale bars 100 µm.
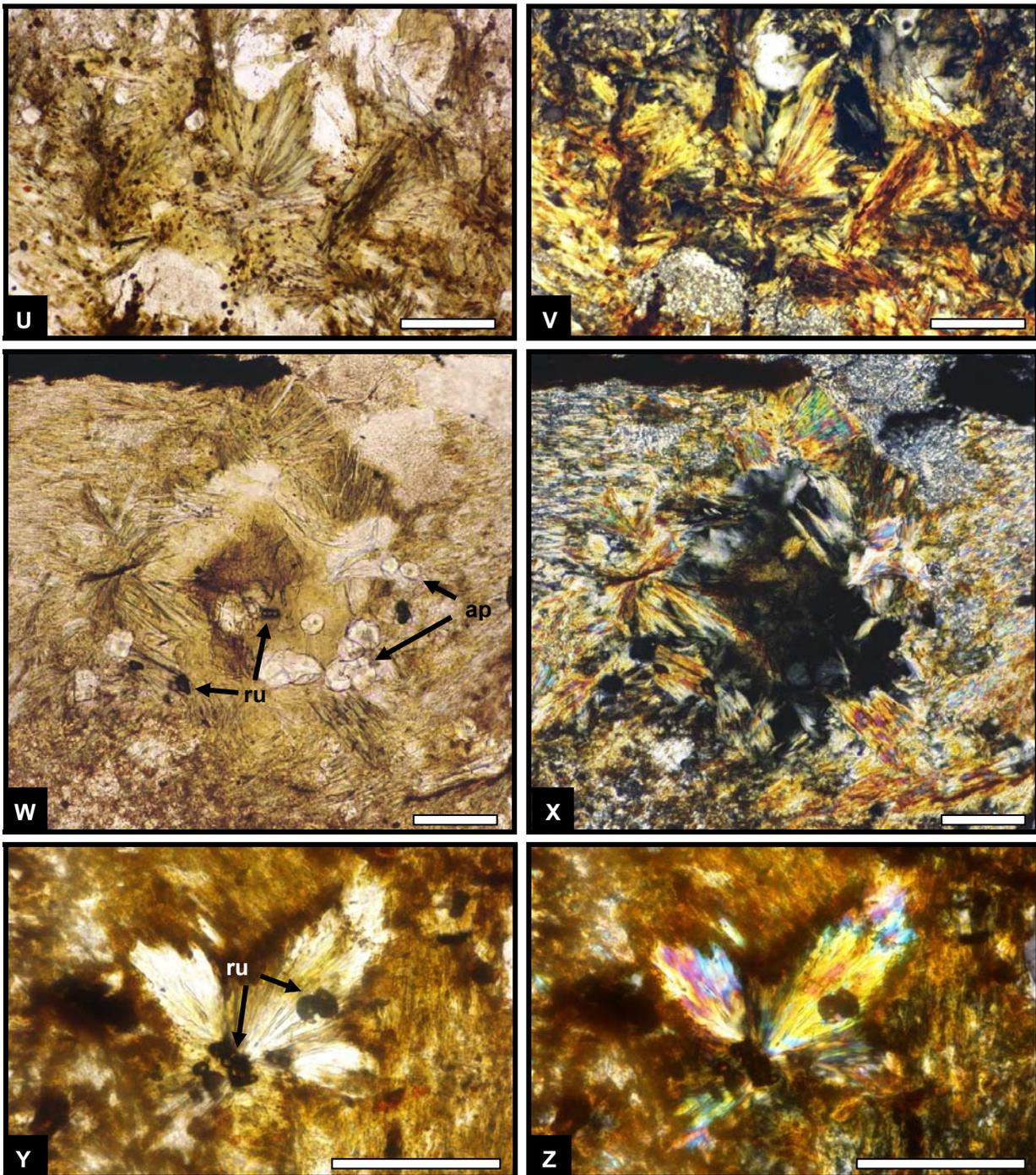
Fig. 3.33: Thin section photographs of the Uhabis River Tuff – secondary components (cont.): **(U) & (V)** Radially grown, greenish chlorite within the marginal part of a pinitized cordierite porphyroblast. Plane-polarized light (left) and crossed polars (right). Scale bars 100 μm. **(W) & (X)** Crystal aggregate of greenish chlorite within porphyroblast. Darker, greenish-brown parts (oxidized chlorite?) show bright interference colours under crossed polars (upper and lower right corner of right image). In the centre of the image chlorite is cut approximately perpendicular to the c-axis causing dark colours under crossed polars. Note the inclusions of rutile (ru) and apatite (ap). Plane-polarized light (left) and crossed polars (right). Scale bars 100 μm. **(Y) & (Z)** Radial aggregate of a colourless (in plane-polarized light) phyllosilicate. The bright interference colours under crossed polars hint at sericite or illite. Note the inclusions of rutile (ru). Plane-polarized light (left) and crossed polars (right). Scale bars 100 μm.
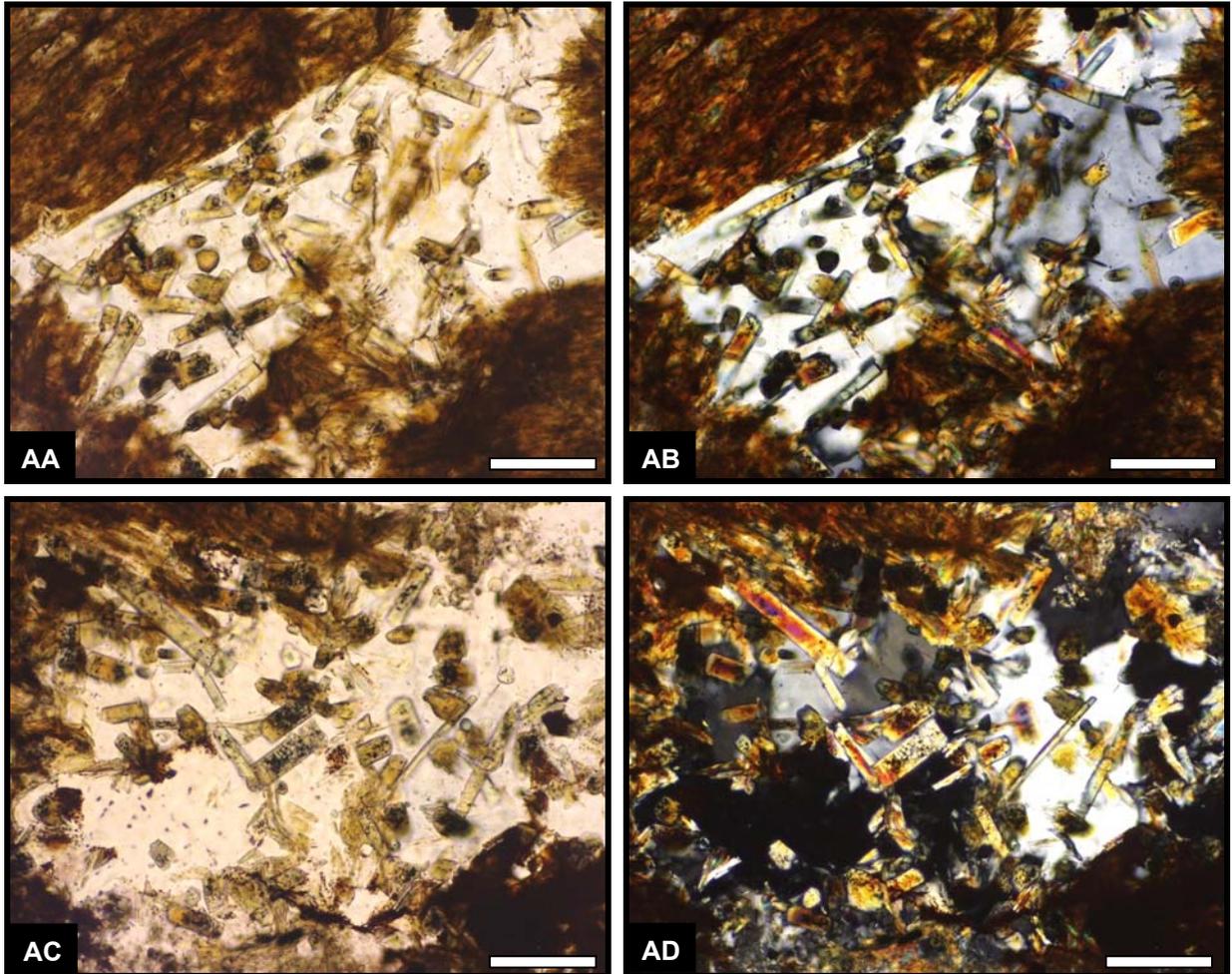
Fig. 3.33: Thin section photographs of the Uhabis River Tuff – secondary components (cont.): **(AA) to (AD)** Euhedral tourmaline inclusions in large quartz megacrysts within large, complex and composite porphyroblastic area. Note that tourmaline is crowded with inclusions composed of tiny, opaque particles of unknown origin. Plane-polarized light (left) and crossed polars (right). Scale bars 100 μm.

The Vreda Tuffs

A few tuff layers were discovered by H. Stollhofen and H. Grill in the cores of the Vreda well and are named here accordingly Vreda Tuffs. The tuff layers, which were found near the base of the Dwyka Group in the Vreda core, have already been shortly mentioned earlier in this study in the chapter on tuff layers in the Dwyka Group and are also indicated in Fig. 3.2. In a higher, lower Ecca Group stratigraphic position some more tuff layers occur in the Vreda well. These tuff layes were placed by Grill (1997) and Stollhofen et al. (2000a) within the uppermost part of the Mukorob Shale Member, just below the base of the Auob Sandstone Member (Fig. 3.34), which forms the top of the Prince Albert Formation in the northern part of the Mariental-Keetmanshoop Karoo outcrop area. However, in the case of the Vreda core, the stratigraphic subdivision of the sedimentary succession between the top of the Dwyka Group and the base of the Kalahari Group (latest Cretaceous-Cenozoic) is controversal (cf. Wilson, 1964; McDaid, 1985 (in Hegenberger, 1992); Grill, 1997; Stollhofen et al., 2000a). But taking all available data into account, a stratigraphic position of these tuffs in the upper

part of the Prince Albert Formation can be confirmed. Therefore, they might represent correlatives of the upper Itzawisis Tuffs (TUBA), the Korabib Tuffs and/or the Uhabis River Tuff. Petrographic descriptions of the Vreda tuffs are very scarce. Only Grill (1997) reported of the possible presence of relicts of completely recrystallized pumice fragments. Own investigations on some thin sections of the Vreda Tuffs have shown that they are very similar in their microscopic appearance to the majority of the Ganigobis Tuffs, i.e. they contain numerous illitized kaolinite book-lets, which are interspersed in a clay-rich and crystal-poor matrix.
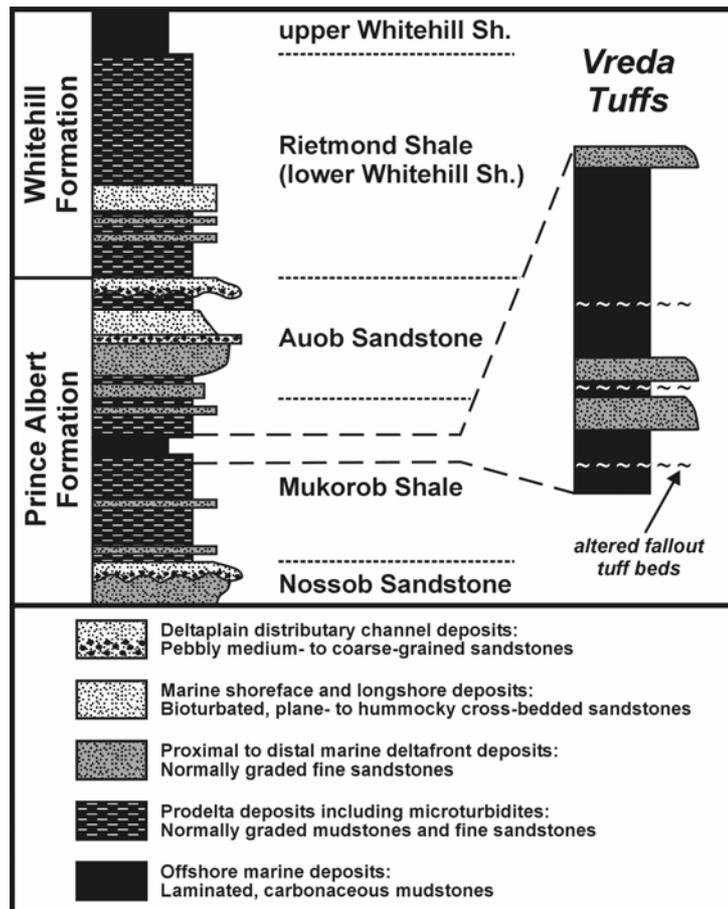
Fig. 3.34: Stratigraphic and sedimentological interpretation of the lower Ecca Group in southern Namibia and detailed position of the Vreda Tuffs within the Mukorob Shale Member (redrawn and modified after Stollhofen et al., 2000a).

3.4.2.2 Whitehill Formation

The Khabus, Panorama & Eisenstein Tuffs

A tuffaceous zone occurs within the Whitehill Formation a few metres below the stratigraphic interval, which contains several dolomitic limestones. This limestone interval forms a mapable unit in all outcrops of the Whitehill Formation in central southern Namibia, i.e. the Mariental-Keetmanshoop Karoo outcrop area. These sedimentary limestone layers are here informally named the Goris Limestone Beds, after Farm Goris, where they were first discovered. Tuff layers have been detected at three localities, which are situated in the northern, northeastern and eastern vicinity of Keetmanshoop (Fig. 3.35). The thickness and facies of these limestones as well as the facies of the shaly host rocks, in which the calcareous and tuffaceous layers are interbedded, however, can vary distinctly from place to place. Due to detailed stratigraphic logging at least five main Whitehill facies successions have been differentiated in southern Namibia (Werner et al., 2002). In the vicinity of Keetmanshoop the tuffaceous zone of the Whitehill Formation occurs both in the so-called Panorama facies succession (Khabus and Panorama Tuffs) and in the so-called Goris facies succession (Eisenstein Tuffs). In the Goris facies succession the Whitehill Formation is strongly dominated by light-weathering, bioturbation-free, laminated black shales, whereas in the Panorama facies succession greenish-bluish-grey, bioturbated shales dominate. Within the Panorama facies succession light-weathering, bioturbation-free, laminated, carbonaceous black shales occur only in the uppermost part of the Whitehill Formation. The sediments of the Goris facies succession are therefore interpreted as deeper water and lower energetic deposits, with fully anoxic conditions at the sea bottom, preventing any benthic life form. In contrast, the sediments of the Panorama facies succession are interpreted as shallower water and higher energetic deposits, with at most dysoxic conditions at the sea bottom, enabling some benthic activity, recorded in the relatively abundant bioturbation features in many parts of the shale succession. Anoxic conditions appear in the Panorama facies succession only in its uppermost part. Since the Whitehill Formation was originally defined (and differentiated from over- and underlying formations) as a white weathering, black carbonaceous shale unit (Cole & Basson, 1991), the greenish shales of the Panorama Whitehill facies succession were formerly incorporated in the underlying Prince Albert Formation resulting in markedly reduced outcrop areas on geological maps and markedly reduced thickness reportings for the Whitehill Formation (Genis, 1982; Genis & Schalk, 1984). Therefore, the Khabus and Panorama tuff localities are situated in the Geological Map of Keetmanshoop (scale 1:250000; Genis, 1982) within the outcrop areas of the Prince Albert Formation, however, as multi-stratigraphic correlations have shown, the tuffaceous zone belongs undoubtly to the Whitehill Formation (Werner et al., 2002). And, although the macro- and microscopic appearances as well as the enclosing rocks of the Khabus-Panorama and

Eisenstein Tuffs are different, all these tuff layers are positioned in a stratigraphically equivalent zone within the Whitehill Formation.
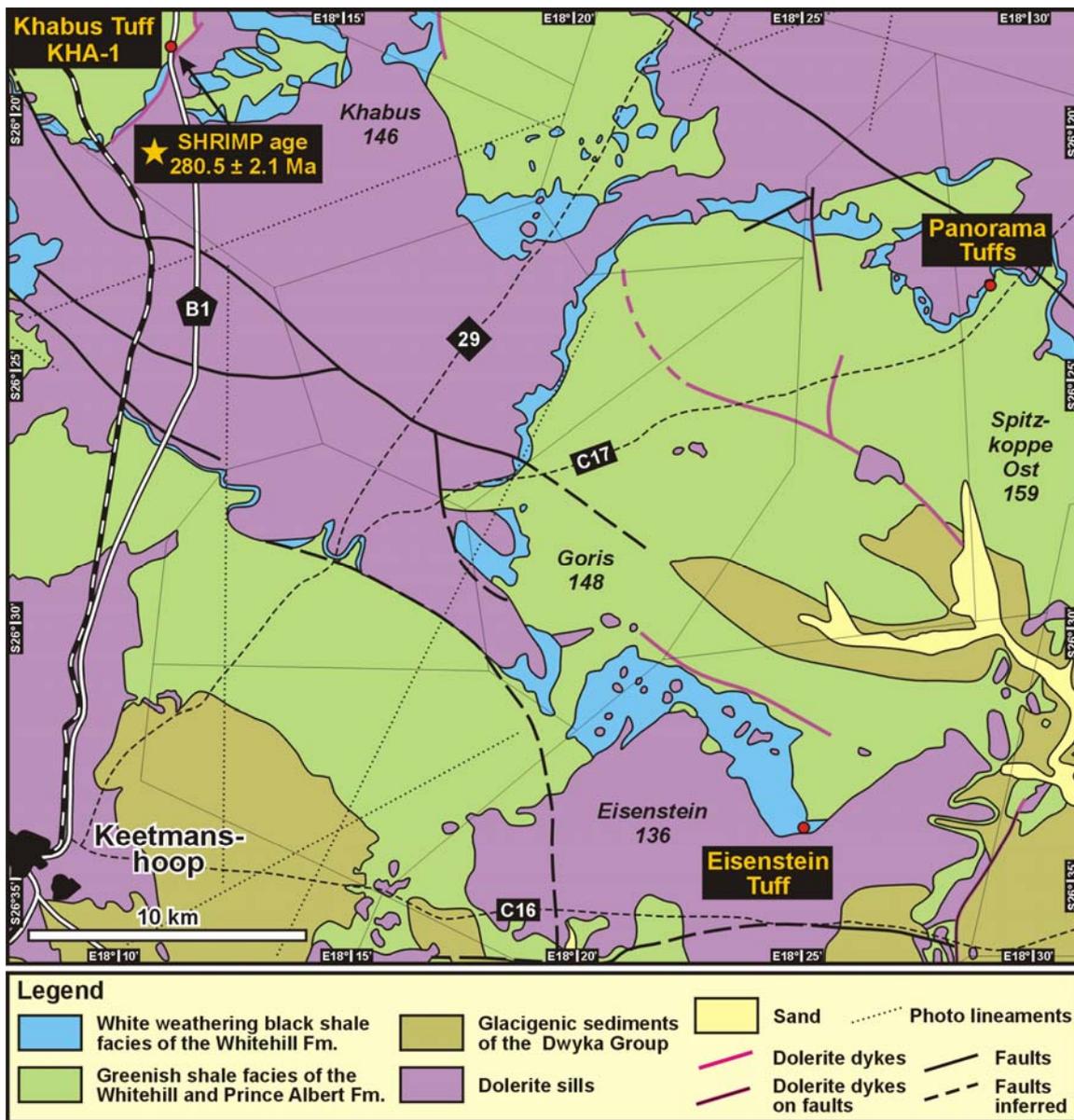
Fig. 3.35: Geological map of the northwestern vicinity of Keetmanshoop showing the outcrop localities of tuff layers within the Whitehill Formation. The map is adopted from Genis (1982).

At the Khabus Tuff locality KHA-1 (Fig. 3.35), which is situated 32.5 km north of Keetmanshoop (S 26° 18.932' E 18° 11.091'), there are small roadcuts on both sides of the B1 highway. Within these roadcuts a thin but conspicuous, whitish weathering, chert-like layer is exposed, which is interbedded in intensively peppered and bioturbated, bluish-greenish-grey shales (Fig. 3.36). Under the microscope this light coloured, chert-like layer was identified as a tuffaceous mudrock and named Khabus Tuff. However, during time of discovery, its stratigraphic position within the Whitehill Formation was not realized. Although the vertical and lateral extension of the Khabus outcrop is quite limited, it was possible to correlate the small

exposed succession precisely with the vertically and laterally more extensive succession at the Panorama locality. At the Khabus locality a bright, pale purple-bluish-grey shale marker horizon forms the top of the roadcut on the western side of the road, c. 1.3 m above the cherty tuffaceous layer. Exactly the same succession was also found within the outcrops at the Panorama locality, where, however, the vertical extent of outcropping strata is much larger (Fig. 3.39 & 3.40). Accordingly, the so-called Khabus Tuff and the Panorama Tuff 1 are identical layers. Since at the Panorama locality also the Goris Limestone Beds are exposed few metres above the tuffaceous zone, the latter must be positioned within the Whitehill Formation. These tuffs therefore represent the first discovery of volcanogenic material in the Whitehill Formation of southern Namibia.

Both the Khabus and the Panorama localities are situated within the so-called Panorama facies succession of the Whitehill Formation. In contrast, the so-called Eisenstein Tuffs, named after Farm Eisenstein, are situated in the so-called Goris facies succession. At the Eisenstein locality again two tuff layers were discovered a few metres below the dolomitic limestones of the Whitehill Formation, however, interbedded in darker, laminated, carbonaceous shales. In addition to the different facies of the host rocks, also the facies of this tuff layer is different. The Khabus-Panorama Tuffs are best described as relatively ill-defined (no sharp boundaries) tuffaceous horizons within silty (higher energetic), massive mudrocks, whereas the Eisenstein Tuffs form very well-defined (sharp-bounded) tuff layers within very fine-grained (lower energetic), laminated mudrocks.

At the Khabus locality the 1.5-2 cm thick, very hard, chert-like layer (Fig. 3.36) is interbedded in slightly softer, greenish-bluish-grey shales, which are intensively speckled (pinitized cordierite porphyroblasts) due to thermal overprinting by dolerite intrusions. However, thin sections show that there is hardly any difference between the chert-like rock and the enclosing greenish shales concerning the primary macro-crystal components and that there are no obvious sedimentary contact surfaces. The only readily visible difference in thin sections is the greenish colouration (chlorite) of the enclosing shales. Thin section, XRD and XRF analyses revealed that the chert-like rock represents a stongly albitized horizon developed along a tuffaceous zone within the Whitehill shales, containing splintery crystal fragments of quartz and feldspar, biotite flakes as well as euhedral zircons and apatites as volcanogenic crystal components. Therefore, the chert-like rock is not a tuff layer sensu stricto, but a secondary halo around a tuffaceous shale bed. Interestingly, some samples of the chert-like, tuffaceous rock have a geochemical composition that matches amazingly that of pure albite. Other samples of the cherty rock are additionally silicified with SiO_2 values >70 wt% and accordingly slightly reduced Al and Na values. XRD analyses of the chert-like layer showed only albite and quartz as the main mineral phases with traces of illite-muscovite. To obtain a radiometric age for the Whitehill Formation about 15 kg of the Khabus Tuff (sensu

lato) were sampled and processed (see Chapter 5 Geochronolgy). From the separated juvenile zircons a single zircon SHRIMP U-Pb age of 280.5 ± 2.1 Ma was calculated (Middle Artinskian after Gradstein et al., 2005).
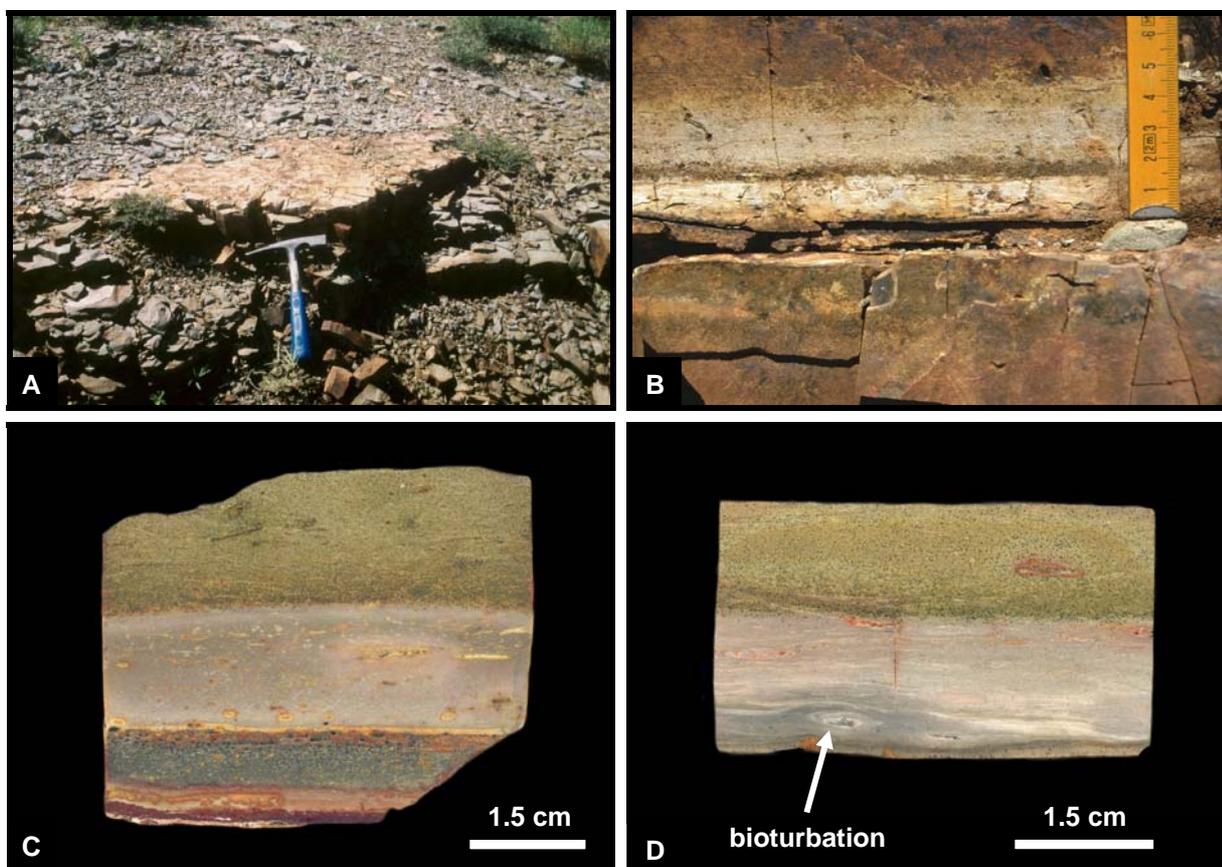
Fig. 3.36: Khabus Tuff: **(A) & (B)** Outcrops of the light-weathering, albitized tuffaceous layer forming a very hard, chert-like bed interbedded in greenish-bluish-grey, peppered shales of the Whitehill Formation (Panorama facies succession). **(C) & (D)** Polished sections of the tuffaceous zone. The upper and lower contacts do not represent primary, sedimentary contacts but secondary, e.g. diagenetic, boundaries. The light coloured, chert-like layer consists almost entirely of microcrystalline albite with minor amounts of quartz and illite-muscovite. As volcanogenic components occur splinter quartzes, feldspar crystal fragments and biotite flakes as well as euhedral zircon and apatite crystals. Both the albitized layer and the enclosing greenish shales show bioturbation features. The greenish peppering of the shale is due to thermal overprinting by Jurassic dolerite intrusions and is mainly formed by tiny, spherical, chlorite-rich aggregates, most probably representing completely pinitized cordierite porphyroblasts.

At the Panorama locality (S 26° 23.375' E 18° 29.037'), about 40 km northeast of Keetmanshoop (Fig. 3.35), on the farm area Spitzkoppe Ost, the same albitized, tuffaceous layer as at Khabus is exposed again. The Panorama outcrop comprises a much larger stratigraphic interval than the Khabus outcrop and especially the presence of the Goris Limestone Beds is very important for the assignment of the exposed strata to the Whitehill Formation (and not the Prince Albert Formation!). Fig. 3.39 shows a detailed measured section of the Panorama outcrop and indicated is also the part of the succession, which is exposed at the Khabus locality. The basal part of the Panorama outcrop contains several tuffaceous layers, of which the chert-like, albitized and sometimes silicified Panorama Tuff 1 is the most

prominent one (equivalent to the so-called Khabus Tuff) (Fig. 3.37 & 3.40). Above and below the Panorama Tuff 1 occur several other tuffaceous layers, which form less conspicuous, thin (<5 mm), ill-defined, yellowish, soft and back-weathering, often discontinuous beds within bluish-greenish-grey shales (Fig. 3.40). The induration of the Panorama Tuff 1 by albite and quartz is at this locality not so regular and laterally continuous as at the Khabus locality. In places, the chert-like Panorama Tuff 1 grades laterally for a short distance also into a yellowish, soft and back-weathering layer, showing that the albitization and silicification is a secondary phenomenon along this horizon. On this basal tuffaceous interval follows a conspicuous bright, pale purple-bluish-grey shale marker band, which allows a precise correlation with the Khabus locality. Above this light-weathering marker band follows another conspicuous, yellowish, soft, friable, and back-weathering, lateral continuous, 1.2 cm thick tuffaceous layer, which is called here Panorama Tuff 2 (Fig. 3.38 & 3.41). Due to its friable nature and its moderate richness in potassium (~5 wt%) the Panorama Tuff 2 shows similarities with the Ganigobis, Zwartbas, Itzawisis and Korabib Tuffs. About 1.5-2 m above the Panorama Tuff 2 several cm-thick dolomitic limestone layers (Goris Limestone Beds) are interbedded in the basal parts of thinly bedded, platy shales forming a coarsening upward succession (upper part of the lower retrogradation-progradation cycle of the Whitehill Formation) (Fig. 3.40).
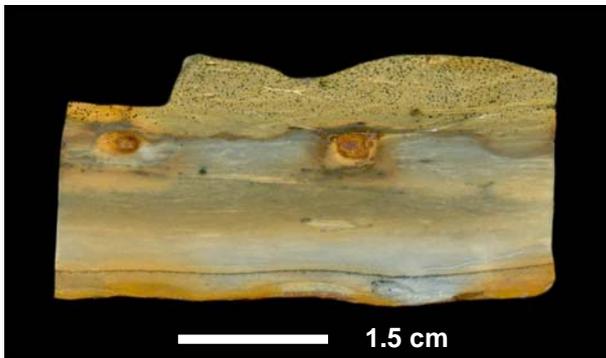
Fig. 3.37: Panorama Tuff 1: Polished section of the light weathering, chert-like, albitized and silicified zone along a tuffaceous horizon within bluish-greenish-grey, peppered shales of the Whitehill Fm. (Panorama facies succession). The brownish spots at the top of the layer most probably represent hematite-goethite pseudomorphs after pyrite. This layer is equivalent to that of the Khabus locality (see Fig. 3.36 & 3.39).

Fig. 3.38: Panorama Tuff 2: Polished chips of the yellowish weathering, soft and clay mineral-rich, bentonitic layer within dark bluish-greenish-grey shales of the Whitehill Fm. (Panorama facies succession). Both the tuff and the surrounding shales appear intensively peppered with tiny, spherical, chlorite-rich aggregates due to thermal overprinting by Jurassic dolerite intrusions. These spots represent completely pinitized cordierite porphyroblasts (see also Fig. 3.47 for thin section images).
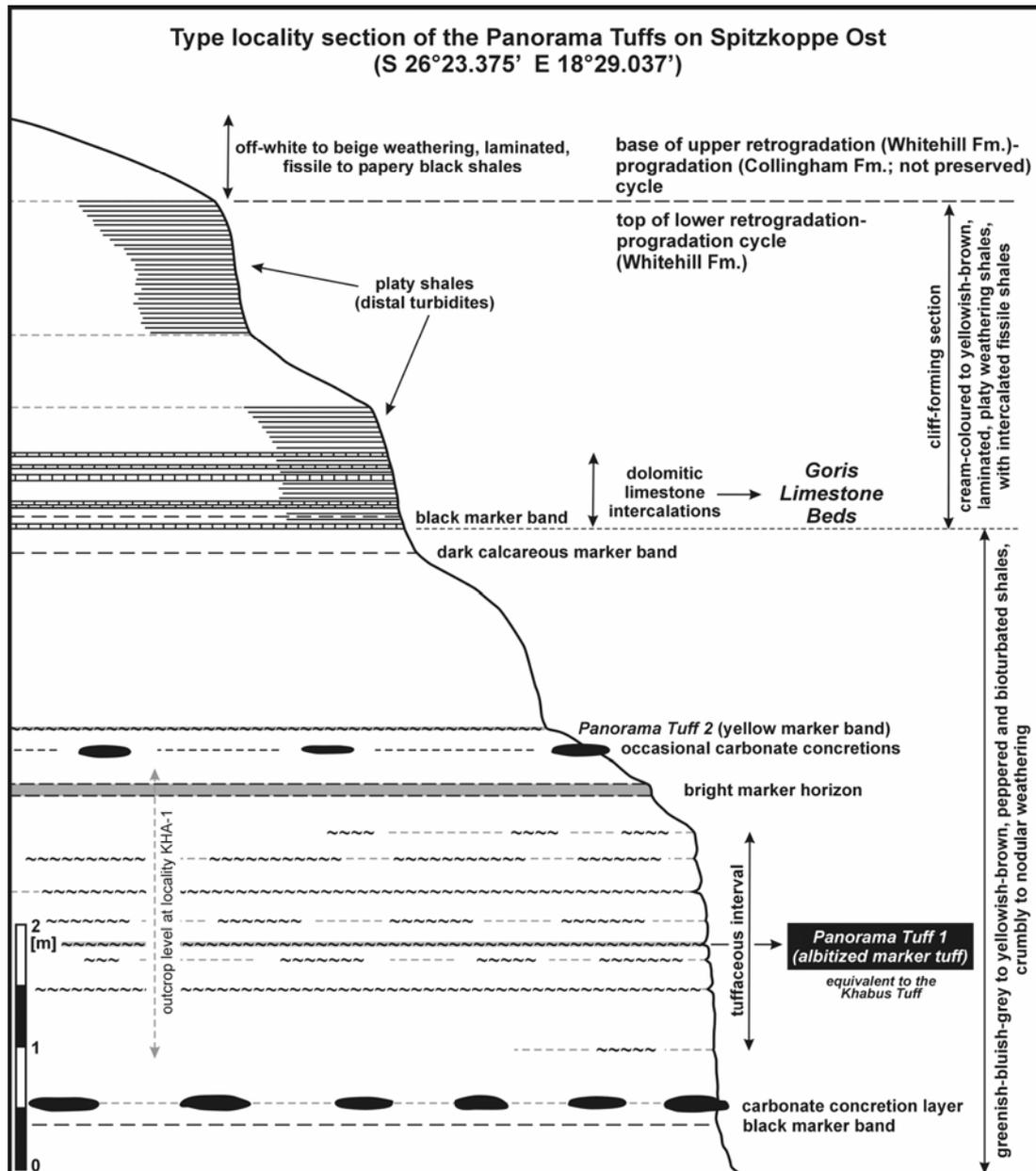
Fig. 3.39: Detailed measured section of the tuffaceous zone and the overlying limestone-bearing interval (Goris Limestone Beds) within the Whitehill Formation (Panorama facies succession) exposed at the Panorama locality on farm area Spitzkoppe Ost (Fig. 3.35). In this figure there is also indicated the stratigraphic interval, which crops out at the Khabus locality 30 km to the west. Since the so-called Panorama Tuff 1 and the Khabus Tuff are identical layers, the single zircon SHRIMP U-Pb age of 280.5 ± 2.1 Ma for the Khabus Tuff applies also to the Panorama Tuff 1.

Fig. 3.40 (next page): Outcrops of the Panorama locality, at which tuffaceous layers are exposed within the so-called Panorama facies succession of the Whitehill Formation: **(A)** Overview showing the succession, which is also illustrated in Fig. 3.39, from the base of the tuffaceous interval to the top of the coarsening-upward succession. **(B)** Photo of outcrop, in which the light-weathering, pale purple-bluish-grey shale marker horizon is well exposed, which allows a precise correlation with the Khabus locality. The inset shows a zoom-in on a dolomitic limestone bed of the here informally called Goris Limestone Beds of the Whitehill Formation). **(C) & (D)** Detailed view on the tuffaceous interval. The chert-like, albitized layer of the Panorama Tuff 1 forms the most conspicuous and lateral continuous tuffaceous layer, whereas other, tuffaceous, soft, bentonitic layers (indicated by white arrows) form less pronounced and often discontinuous, slightly back-weathering intercalations within greenish-bluish-grey shales.

A (level of dolomitic limestones (Goris Lmst. Beds); Panorama Tuff 2; Panorama Tuff 1; tuffaceous interval)

B (dolomitic limestone (Goris Lmst. Beds); Panorama Tuff 2; bright shale marker horizon; Panorama Tuff 1; tuffaceous interval)

C (Panorama Tuff 1)
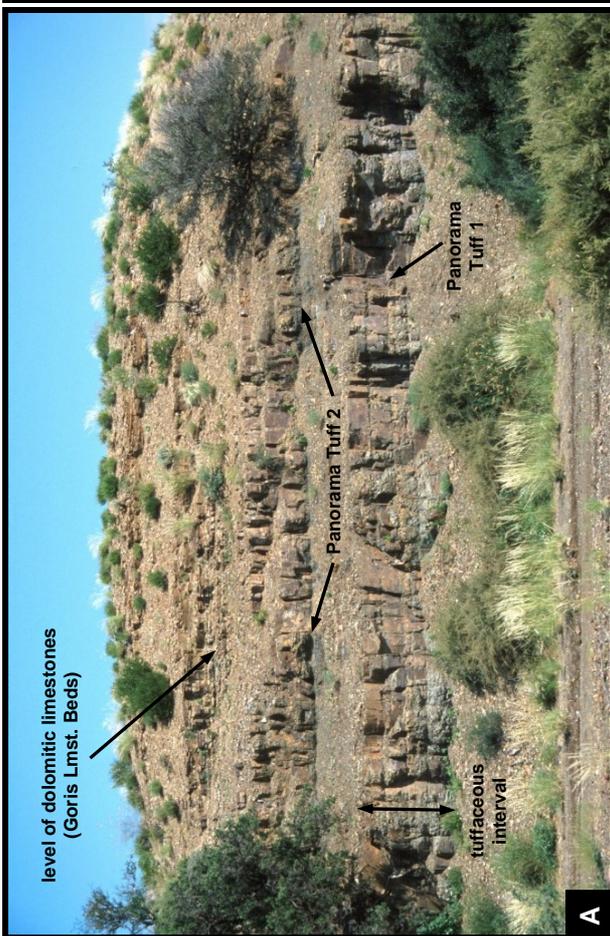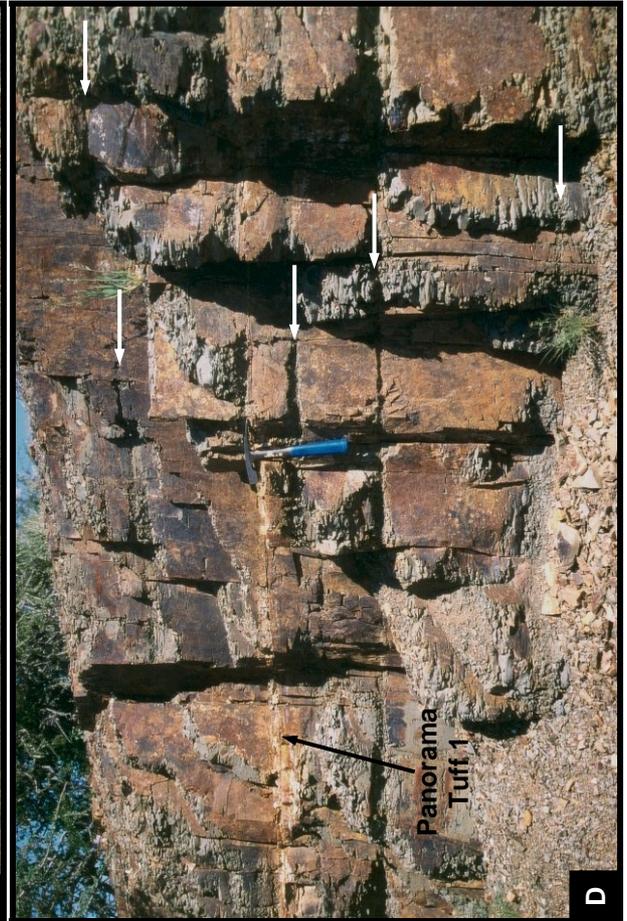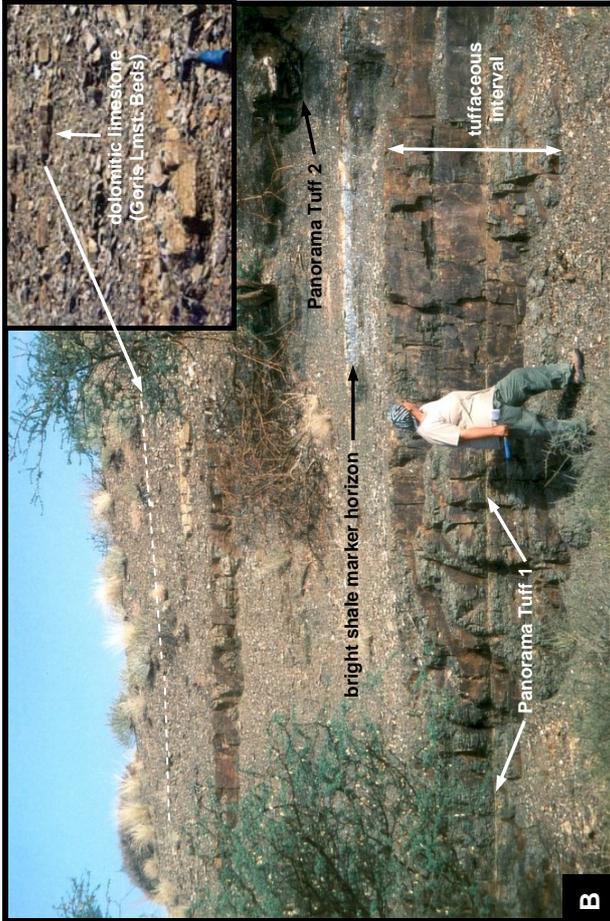
D (Panorama Tuff 1)

Fig. 3.41: Close-up photo of the yellowish, soft, bentonitic, back-weathering layer of the Panorama Tuff 2 (see also Fig. 3.39 for its stratigraphic position, Fig. 3.40-A/B for an outcrop overview, and Fig. 3.38 for polished chips of this tuff). The pencil length is about 15 cm and the thickness of the tuff layer is about 1.2 cm.

The Eisenstein locality (S 26° 34.417' E 18° 24.742'), c. 30 km east of Keetmanshoop (Fig. 3.35), represents the third locality, where pyroclastic material was found within the Whitehill Formation in southern Namibia. Two well-defined tuff layers with sharp upper and lower contacts have been discovered at an outcrop c. 2 km northeast of the Eisenstein Farm houses, a few metres below the dolomitic limestone interval (Goris Limestone Beds) of the Whitehill Formation. The outcrops on Farm Eisenstein are situated in the so-called Goris Whitehill facies succession, which is dominated by black, carbonaceous shales. Due to differential weathering colours of the shales, the Whitehill Formation can be subdivided there into several subzones (Fig. 3.42). The dolomitic limestones (Fig. 3.43) and the tuff layers (here called Eisenstein Tuffs) lie within the upper light-weathering zone, which is, apart from limestones and tuffs, characterized, in its upper part, by a slightly coarsening-upward, cliff-forming succession of shales, in which also the first occurrences of *Mesosaurus* remains can be found. The Eisenstein Tuffs form light-weathering, in fresh cuts dark coloured layers with a thickness of 0.9-1.0 and 0.2 cm. In weathered and polished section the thicker layer often shows a conspicuous speckling (Fig. 3.44 & 3.45) maybe caused by contact-metamorphic growth of white weathering porphyroblasts. These porphyroblasts weather out as tiny, mm-sized knots due to their greater hardness in comparison to that of the matrix. Macro-scopically, the overall appearance of the tuffs is massive. However, on some weathered surfaces, oriented perpendicular to bedding, very subtle features are visible in places, which are reminiscent of micro cross-lamination (Fig. 3.45). Since nothing of them is visible in thin sections their true nature is unclear. As mentioned earlier, both the upper and lower contacts

are very sharp, some specimen show a slightly wavy lower boundary (Fig. 3.44). The enclosing shales show a very pronounced lamination (Fig. 3.44). Both the tuff layers and the directly enclosing shales form very hard, chert-like rocks due to feldspathization. However, in comparison with the Khabus-Panorama Tuff 1 the Eisenstein Tuffs show only a moderate sodium content (~5 wt% Na_2O) but markedly increased contents of calcium (~7.5 wt% CaO) and aluminium (~25.5 wt% Al_2O_3) as well as a markedly decreased silica content (~53.5 wt% SiO_2). This might be hinting either at a more intermediate composition of the matrix-plagioclase (andesine-labradorite, resp. ~$Ab_{50}An_{50}$) or the presence of a mixed, partly albitized and plartly clay mineral-rich matrix. Calcite and apatite, two common Ca-bearing mineral phases in some of the other described tuff layers, have not been identified and are also not indicated by XRF analyses (low LOI and phospate values).
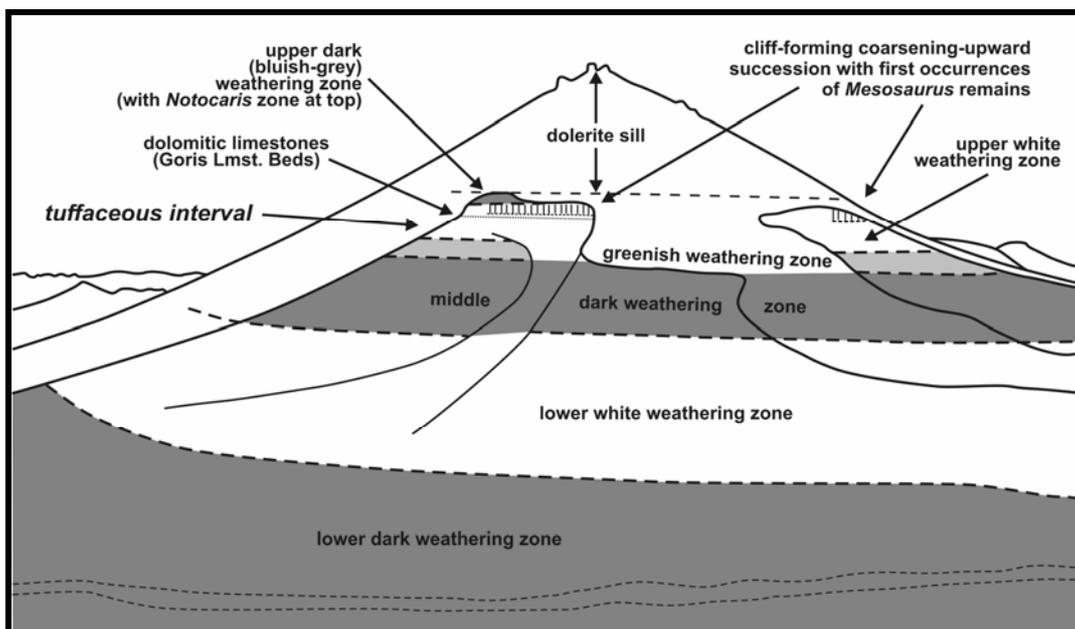
Fig. 3.42 (prev. page): Outcrop of the Whitehill Formation (Goris facies succession) at the eastern boundary of farm Goris, close to the Eisenstein farm area. Within the outcrop area of the Goris facies succession the Whitehill Formation can be subdivided into several sub-zones on the basis of different weathering colours. The tuffaceous interval is projected into this outcrop due to correlation with the Eisenstein Tuffs locality. Like in the Panorama facies succession, the tuffaceous zone lies a few metres below the interval with dolomitic limestones (Goris Limestone Beds), the latter again forming approximately the base of a cliff-forming coarsening-upward succession (cf. Fig. 3.40). At the shown outcrop the Eisenstein tuff layers were not detected due to unfavorable outcrop conditions.

Fig. 3.43: Black, carbonaceous, dolomitic limestone layer of the so-called Goris Limestone Beds in the upper part of the Whitehill Formation at the Eisenstein locality.
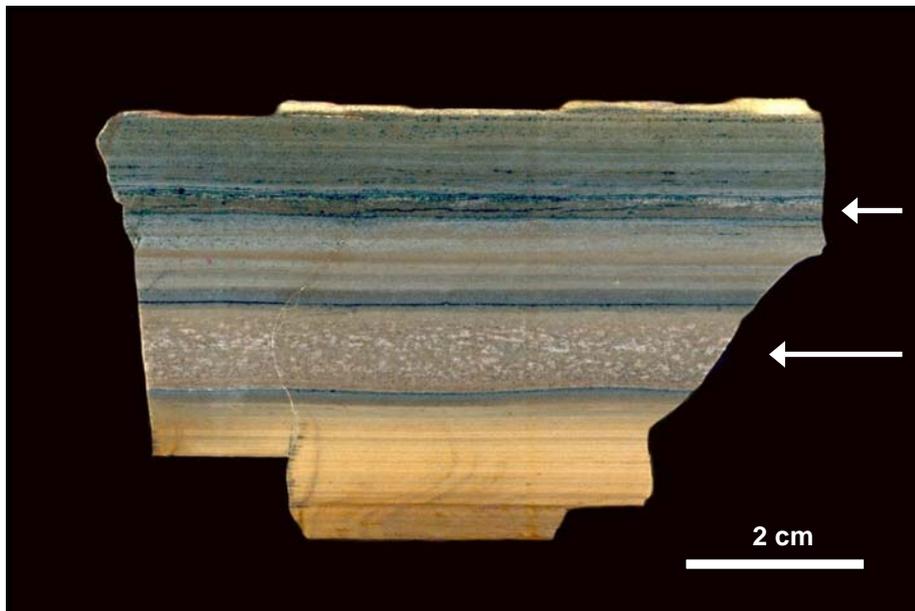
Fig. 3.44: Polished specimen of the Eisenstein Tuffs (arrows) embedded in dark, laminated shales of the Whitehill Formation. The light coloured spots within the thicker tuff layer possibly represent contact-metamorphic porphyroblasts. Due to digital brightness and contrast en-hancement the rock sample appears in this photo brighter than in nature.
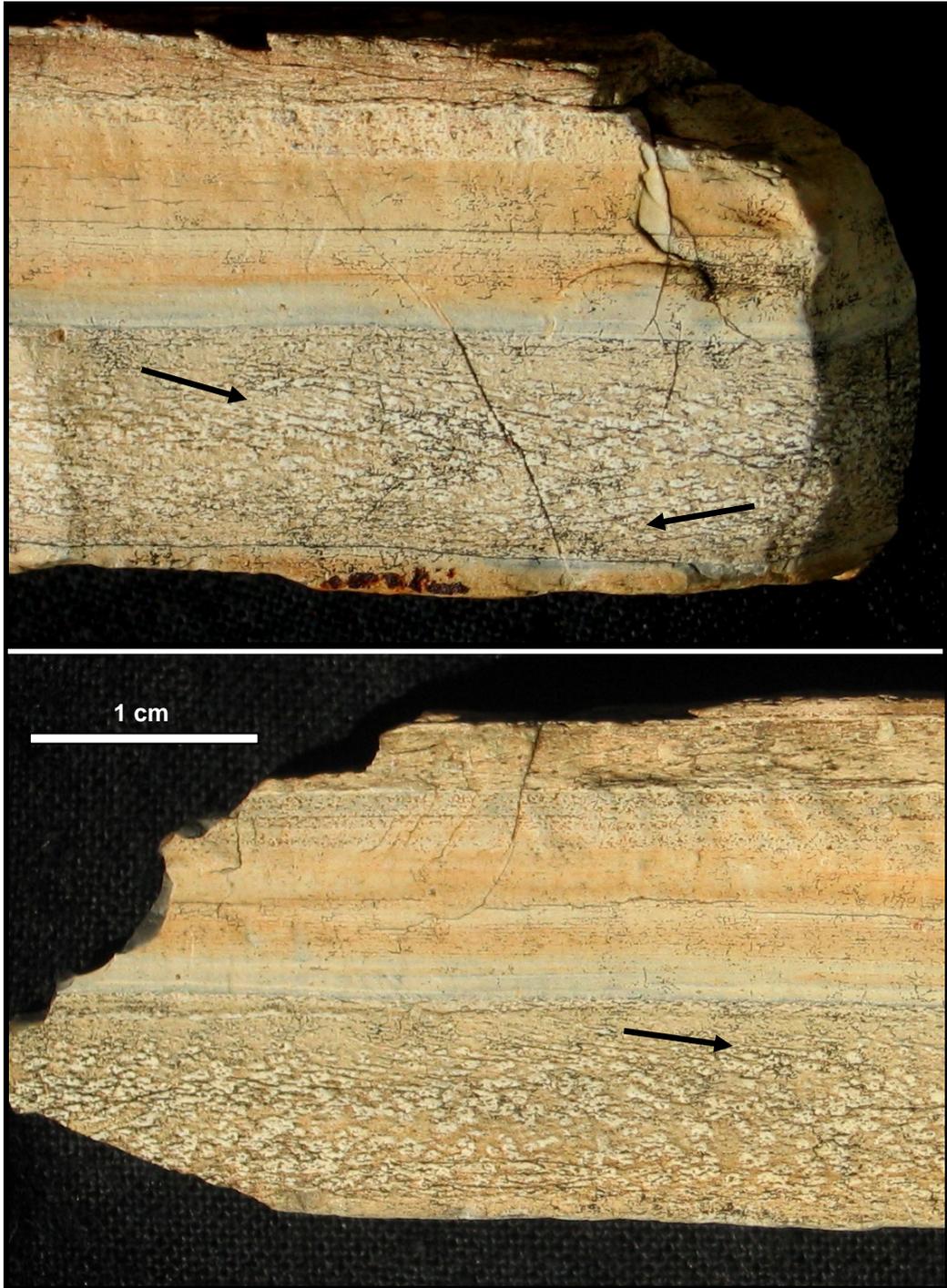
Fig. 3.45: Weathered samples of the Eisenstein Tuffs. Light coloured knots weather out of the feldspathic matrix of the tuff due to their greater hardness. They possibly represent contact-metamorphic porphyroblasts, however, their mineralogical nature is still unclear (feldspathic-siliceous?). Due to weathering also faint, inclined surfaces are visible, the origin of which is not clear. The dip direction is indicated on the photos by arrows. These structures are reminiscent of sedimentary micro cross-lamination. Surprisingly, nothing of these inclined surfaces is visible in thin sections and it is possible that they also could have a non-sedimentary origin.

In the following section descriptions of thin section of the three different types of tuffs and tuffaceous layers, found in the Whitehill Formation of southern Namibia, are given:

(1) the chert-like, albitic Khabus-Panorama Tuff 1,

(2) the bentonitic, illitic Panorama Tuff 2, and

(3) the chert-like, partly knotty weathering, feldspathic Eisenstein Tuffs.

The Khabus-Panorama Tuff 1 is a moderately crystal-rich, relatively fine-grained and moderately sorted tuffaceous rock of mixed epi- and pyroclastic origin. Within the Khabus-Panorama Tuff 1 no grading of primary macro-crystal components is visible. The upper contact is marked by a relatively sharp colour change from light grey to green (Fig. 3.36 & 3.37), which represents the boundary between the strongly albitized zone and the overlying zone, which is intensively speckled with greenish, chlorite-rich porphyroblasts (pinitized cordierite). However, there is no obvious change in size, abundance or composition of the detrital and volcanogenic components. Therefore, this boundary must be of secondary and not of primary, respectively sedimentary origin. Also the lower contact is formed in many samples by a quite sharp colour change from grey to bluish-green (Fig. 3.36). The underlying bluish-green shale, however, does not show the same greenish porphyroblasts as the over-lying shale but contains abundant platy chlorite aggregates aligned parallel to the bedding (chloritized biotite flakes or clay minerals?). In some samples the transition from the grey, albitic zone to the underlying greenish, chloritic zone can be very gradational. Again, no sharp sedimentary break can be observed at the lower contact, which has a secondary origin, too. In the albitized zone of the Khabus-Panorama Tuff 1 quartz, feldspar and biotite as well as zircon and apatite were observed as the main crystal components, which are interspersed in a fine-grained matrix. According to XRD & XRF analyses this matrix is mainly composed of albite but also flaky clay mineral aggregates (illite) aligned parallel to the bedding are abundant as observed in thin sections. Quartz occurs mainly as angular, monocrystalline crystal fragments, which show commonly straight extinction, and their mean grain size ranges between 30-60 μm. Also present are thorn- and splinter-shaped crystal fragments, which show average lengths of about 50-120 μm. No beta-quartz paramorphs have been observed. Two different types of feldspars are visible in thin sections. Most feldspar crystal fragments are angular to splintery, strongly altered and untwinned, whereas moderately altered, polysynthetically twinned plagioclase fragments are relatively scarce. The majority of the feldspar crystal fragments are almost invisible in plane-polarized light because of the poor contrast with the albitic matrix. However, most feldspar fragments show a faint dusty-brownish tint due to alteration (Fig. 3.46-A/B). Under crossed polars they often exhibit irregular, ragged grain boundaries and a fine-grained internal structure (due to secondary albitization?) (Fig. 3.46-C/D). The mean grain size of most feldspar fragments is

comparable to that of quartz, however, in some thin sections a fair number of 'oversized' feldspar grains with sizes of 150-210 μm have been observed, too. Biotite flakes form also an important and abundant crystal component within the albitized layer. The degree of biotite alteration is highly variable but there is a rough trend visible that in the basal and lower parts of the tuffaceous horizon biotite is strongly altered, whereas towards the top biotites with a relatively fresh appearance dominate. In the upper part the majority of biotites show a strong pleochroism with dark reddish-brown to pale yellowish colours (Fig. 3.46-E). Many biotites exhibit a somewhat grainy internal texture due to alteration, oxidation and pigmentation by iron oxides but only few show bleached margins. It seems that the biotites within the albitized zone, especially in its upper part, are somehow protected from alteration. In the lower half of the albitic zone and in the underlying transitional albitic-chloritic zone all biotites are strongly altered. Some platy chlorite pseudomorphs after biotite are present (Fig. 3.46-F) but most of the former biotites appear distinctly expanded, forming large, elongate booklet-like crystals. It seems that these biotites were early diagentically altered to hydrobiotite, vermiculite or kaolinite booklets but later largely replaced by chlorite within the greenish transitional zone (Fig. 3.46-G/H). Some booklets also contain larger illite lamellae. In upward direction, towards the lower part of the albitized zone, these chloritized booklets consist also partly of feldspar (± quartz) (Fig. 3.46-I/K), and within the albitized zone they are finally completely replaced by a mosaic of irregular blocky to lamellar feldspar (albite) (Fig. 3.46-L/M). The grain size of the less altered biotite flakes ranges mainly between 70 and 200 μm and that of the expanded, booklet-like pseudomorphs between 150 and 470 μm. The euhedral to sub-hedral zircons observed in thin sections show various forms from long-prismatic and acicular crystals to short-prismatic, stubby and equidimensional ones (Fig. 3.46-N to Q). The observed crystal size ranges in thin sections from <20 to over 100 μm but within the zircon concentrate, made for radiometric dating, the length of acicular crystals reaches even up to 280 μm. Some zircons show a well developed oscillatory zoning (Fig. 3.46-O). Tubular to vermiform melt inclusion are very abundant in the more elongate crystals. In addition, some rounded and partly brownish-metamict, xenocrystic zircons have been observed, too. Juvenile, euhedral to subhedral apatites occur either as smokey-grey and zoned or as colourless crystals with a size of <20 up to 125 μm (Fig. 3.46-R). Few apatites also contain brownish, tubular melt inclusions. In two cases hexagonal-shaped basal sections display a large brownish core and a radial microfracture system (Fig. 3.46-S) probably resulting from metamictization due to radiation damage. Furthermore, the albitized zone is interspersed with abundant opaque, irregular shaped particles, which are composed of minute (<1 μm) hematite/goethite (and titanium oxide?) crystallites. Interestingly, these opaque crystallite aggregates show a normally graded size distribution within the albitized zone, decreasing in size from base (20-50 μm) to top (<2 μm). Since they do not represent a primary component,

their size distribution most probably reflects the alteration intensity of biotite within the albitized zone, which is strongest at the base and least at the top. Therefore, these opaque crystallite aggregates are interpreted mainly as alteration products of biotite. As already mentioned, the matrix of the chert-like, tuffaceous rock consists predominantly of microcrystalline albite, however, XRD and XRF analyses indicate also a certain degree of silicification of some samples, which is most probably caused by the presence of microcrystalline quartz in the matrix. In addition, abundant platy clay mineral particles (illite), which are aligned parallel to bedding, are interspersed in the matrix. Under crossed polars they cause a marked brightening of the matrix (white to slightly yellowish colours) when thin sections are viewed under the microscope at a 45° angle against bedding (Fig. 3.46-U). It is supposed that the majority of these clay mineral aggregates have a primary sedimentary origin. Outside the albitized zone the abundance of such platy clay mineral aggregates is distinctly higher but there they consist predominantly of greenish chlorite. The shale above the albitized zone is speckled with greenish, subspherical to ovoid, porphyroblasts (poikilo-blastic) with a mean diameter of 100-150 µm (Fig. 3.46-T). In accordance with the speckling of other tuffs and shales these spots are again interpreted as pinitized cordierites, which grew due to thermal overprinting by Jurassic dolerite intrusions. In plane-polarized light the albitized zone looks at first sight apparently free of such secondary, poikiloblastic spots, however, under crossed polars subspherical to ovoid domains with ill-defined boundaries become visible, which appear darker than the surrounding matrix (only first order shades of grey interference colours) when thin sections are viewed at a 45° angle against bedding (Fig. 3.46-U). The darker colour results from the lack of clay mineral inclusions producing bright white to slightly yellowish interference colours, however, from a textural point of view these darker areas have the same poikiloblastic appearance as the pinitized cordierite porphyro-blasts. In plane-polarized light most of these spots are colourless and invisible within the albitc matrix, however, some of them are pigmented by brownish iron oxides. The diameter of these spots ranges approximately between 200 and 500 µm and thus is larger than that of the ones in the overlying greenish zone. The mineralogical composition of these spots within the albitized zone, however, was not identified with certainty. They possibly could either represent silicified areas within the albitic matrix or they could also represent albitized cordierite porphyroblasts. For example, hydrothermal albitization of cordierite porphyroblasts following pinitization have been reported by Tröger (1969). The whole issue raises the question if the albitization of the tuffaceous matrix occurred before, during or after the thermal imprint, which caused growth of cordierite porphyroblasts. If the spots within the albitic matrix indeed represent albitized cordierite porphyroblasts following pinitization, then the albitization must have occurred after the cordierite growth. The different size of the poikiloblastic spots within the greenish-chloritic and the greyish-albitic zones does not argue

against a different origin because cordierite porphyroblasts show often larger sizes in tuffs than in the enclosing shales (see for example Fig. 3.30 of the Uhabis River Tuff). On the other side, the relatively fresh appearance of biotites within the upper part of the albitized zone implies that the albitization had a somewhat protective effect, protecting biotite against alteration to expanded clay mineral booklets, which commonly form early diagenetically within tuffs. Therefore, an early diagenetic origin of the albitized zone appears also possible. However, it seems unlikely that albite formed early diagentically but it perhaps might have had an early diagenetic precursor mineral phase (like illite that forms in bentonitic tuffs at the expense of earlier smectite and/or kaolinite under prograde conditions). In the case of albite this could have been sodium-rich zeolites or analcime. Iijima (1988), for example, observed that with increasing temperature and burial depth alteration of volcanic glass can lead to the formation of clinoptilolite and mordenite (besides smectite and opal/chalcedony). Under prograde conditions these alkalic zeolites then transform to analcime, which in the highest grade zone changes to albite at temperatures around 120°C. In the Paraná Basin area Ecca-equivalent ash-fall tuff layers contain frequently glass shard relicts composed of analcime (Coutinho et al., 1991). In the NW-Namibian Huab area, volcanic ash, deposited in saline-alkaline lakes of the Late Permian Gai-As Formation, is altered to analcime- and potassium feldspar-rich layers but most probably developed from zeolite-rich precursors (Horsthemke, 1992). Is the occurrence of an albitized tuffaceous layer in the Whitehill Formation possibly also connected with evaporitic-saline depositional conditions and therefore early diagenetic in origin? There is indeed evidence of temporary saline conditions at the sea bottom during deposition of the Whitehill Formation. For example, at the Panorama locality solution casts of unidentified evaporite minerals have been found in the lower part of the Whitehill Formation and, further north at Daberas, calcite pseudomorphs after gypsum occur within limestones of the Whitehill Formation. Furthermore, within the South African Whitehill Formation, syngenetic gypsum crystals occur in dolomitic limestone lenses and halite imprints are known from the basal part of the formation (McLachlan & Anderson, 1977; Van der Westhuizen et al., 1981). In addition, anhydrite occurs locally at the base of the Whitehill-equivalent Irati Formation in Brazil (de Castro, 1994; Hachiro, 2000; Milani & Filho, 2000). The formation of albite from potential zeolitic precursors might have been associated with dolerite intrusions. However, neither an early diagenetic origin (alkaline/saline depositional conditions) nor a formation after the growth of cordierite porphyroblasts (under retrograde hydrothermal conditions following peak thermal metamorphism?) does explain the highly selective albitization of the Khabus-Panorama Tuff 1 layer, which is over- and underlain by several clay mineral-rich, bentonitic layers, not experiencing albitization. A similar explana-tion problem exists also for the Matjiesfontein Chert in the Collingham Formation of South Africa. The Matjiesfontein Chert is a mixed epi- and pyroclastic layer with a strongly albitized

matrix, which is surrounded by illitic, bentonitic tuff layers (Knütter, 1994; Viljoen, 1994). So far, a conclusive explanation for the highly selective albitization can neither be presented for the Matjiesfontein Chert in South Africa, nor for the Khabus-Panorama Tuff 1 in Namibia.
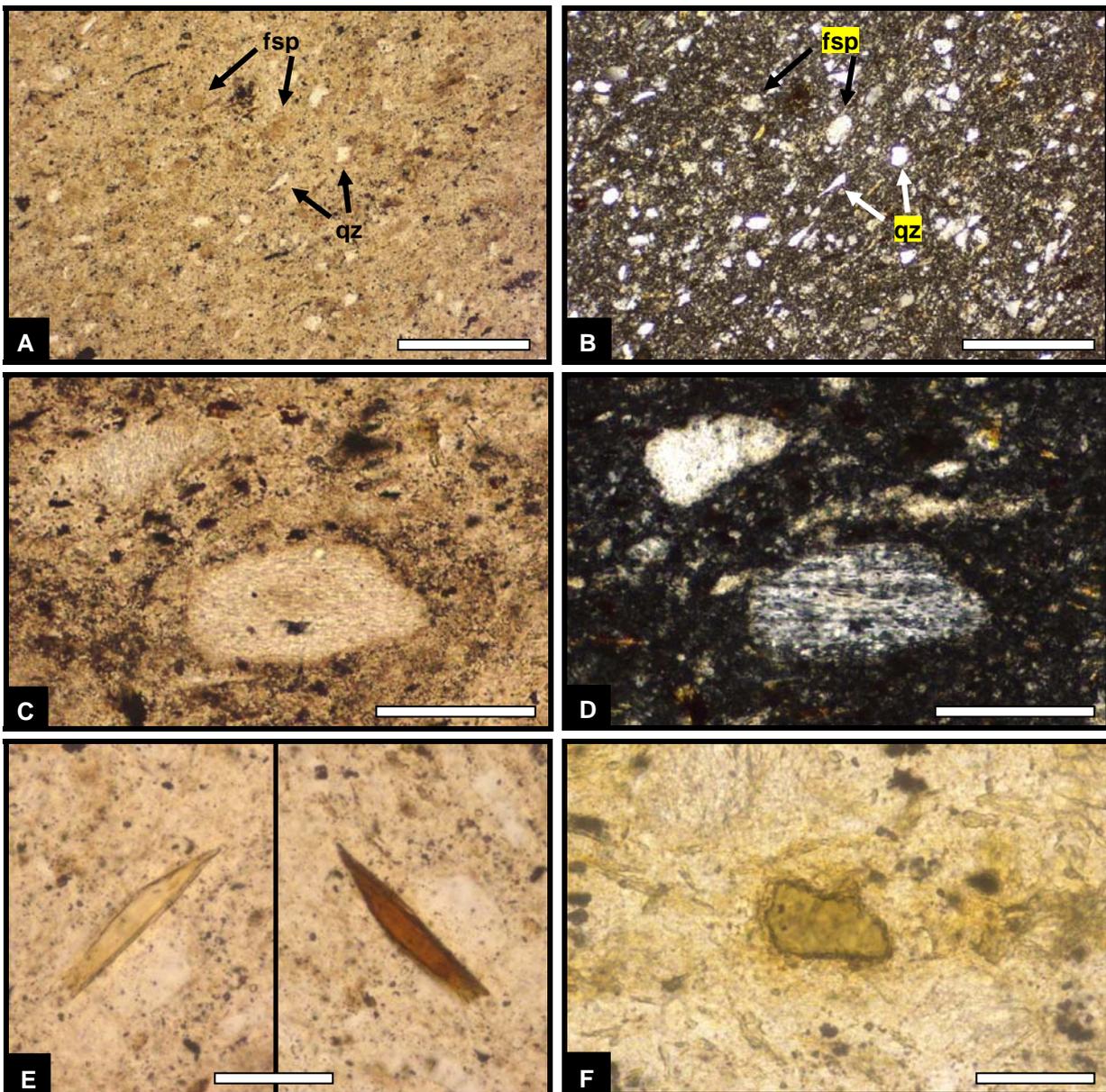
Fig. 3.46: Thin section photographs of the Khabus-Panorama Tuff 1: **(A) & (B)** Overview photo showing quartz and feldspar as the main crystal components. Feldspar fragments are almost invisible in plane-polarized light because of the lacking contrast against the albitic matrix. However, they often display a slightly brownish tint due to alteration. Under crossed polars bright, colourless quartz is easier to distinguish from slightly cream-coloured, altered feldspar. Plane-polarized light (left) and crossed polars (right). Scale bars 250 µm. **(C) & (D)** Two highly altered feldspar grains. Note the ragged grain boundaries of the untwinned feldspar in the upper left corner. The large feldspar grain in the lower half of the picture exhibits a conspicuous grainy internal texture and ghosts of former polysynthetic twinning (faint subhorizontal lines) are still visible. This feldspar grain probably represents albitized plagioclase. Plane-polarized light (left) and crossed polars (right). Scale bars 100 µm. **(E) & (F)** Biotite appears especially in the upper half of the albitized zone relatively fresh showing clear crystals with pronounced pleochroism. Towards the base and in the underlying greenish transitional zone most biotites are completely altered to chlorite, some forming platy chlorite pseudomorphs after biotite like in this picture. Both pictures in plane-polarized light. Scale bars 50 µm.
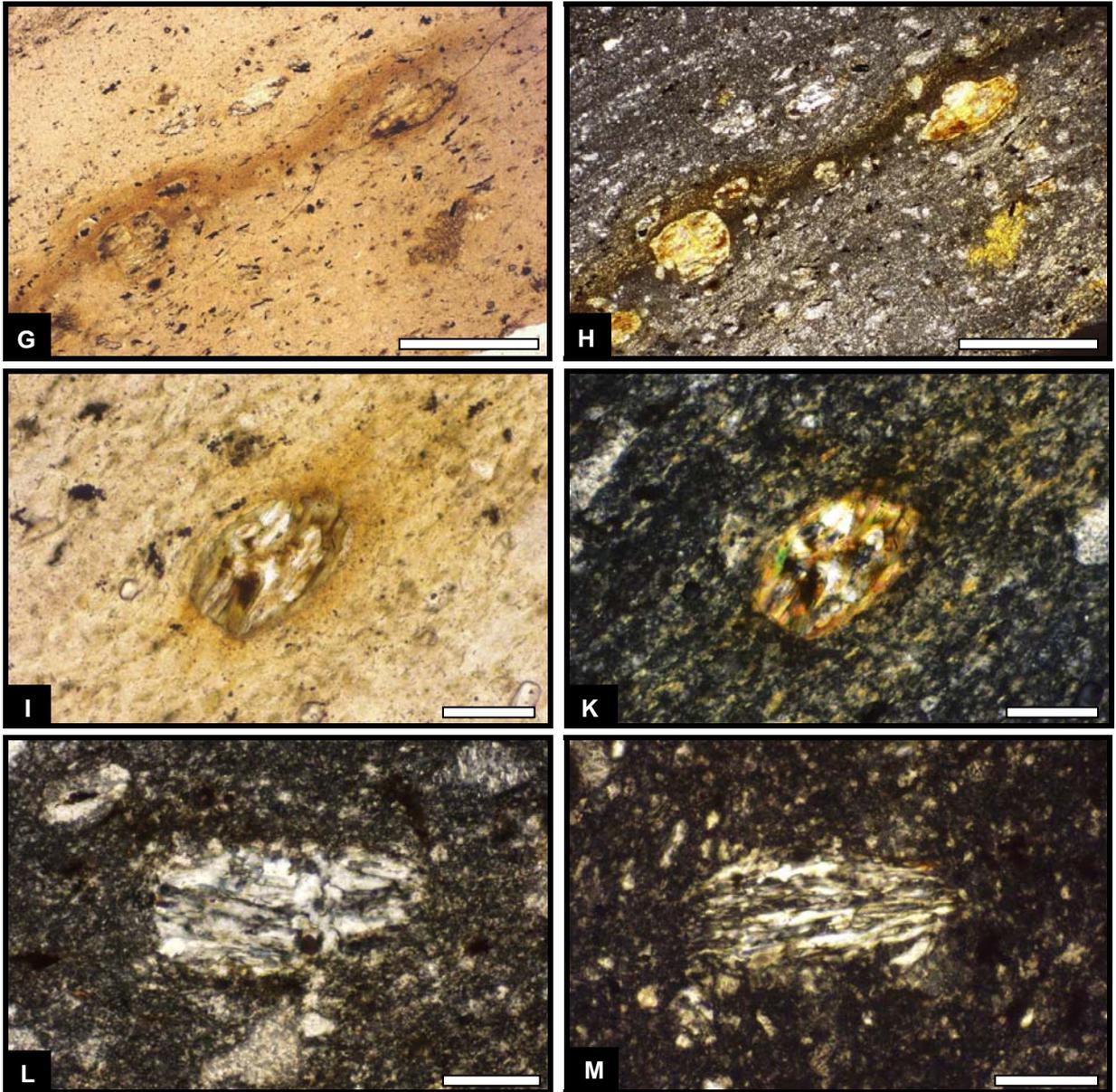
Fig. 3.46: Thin section photographs of the Khabus-Panorama Tuff 1 (cont.): **(G) & (H)** In the greenish, transitional zone below the albitized zone occur large, elliptical to elongate crystal booklets composed of chlorite. They probably originated as vermiculite or kaolinite pseudomorphs after biotite. Thin section is rotated ~45° against bedding. Plane-polarized light (left) and crossed polars (right). Scale bars 500 μm. **(I) & (K)** Closer to the albitized zone these crystal booklets are composed of chlorite and feldspar (± quartz). Thin section is rotated ~45° against bedding. Plane-polarized light (left) and crossed polars (right). Scale bars 100 μm. **(L) & (M)** Within the albitized zone crystal booklets (former clay mineral pseudomorphs after biotite) are completely replaced by a mosaic of irregular blocky to lamellar feldspar (albite). Both pictures crossed polars. Scale bars 100 μm.
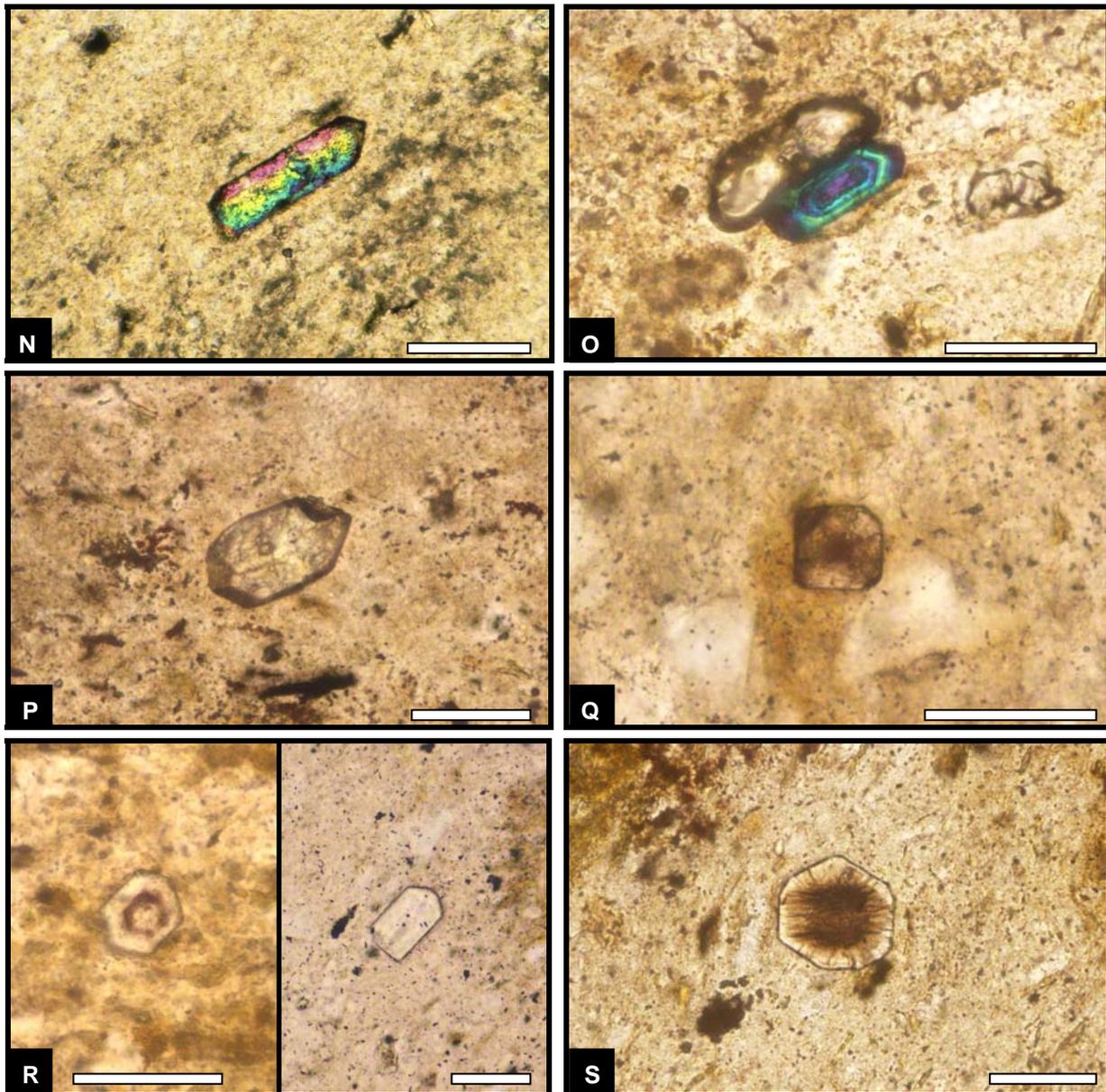
Fig. 3.46: Thin section photographs of the Khabus-Panorama Tuff 1 (cont.): **(N) to (Q)** Euhedral, juvenile zircons showing a high diversity of forms from elongate and long-prismatic to stubby to almost equidimensional. Within some a conspicuous oscillatory zoning is visible (O). Semi-crossed polars (N & O) and plane-polarized light (P & Q). Scale bar is 100 µm for (N) and 50 µm for (O to Q). **(R)** Euhedral, juvenile apatites are present either as zoned (left) and smokey-grey crystals or as clear and colourless (right) crystals. Plane-polarized light. Scale bars 50 µm. **(S)** Basal section of a euhedral apatite with a brownish core and a radial micro-fracture system (metamictization due to radiation damage?). Plane-polarized light. Scale bar 50 µm.
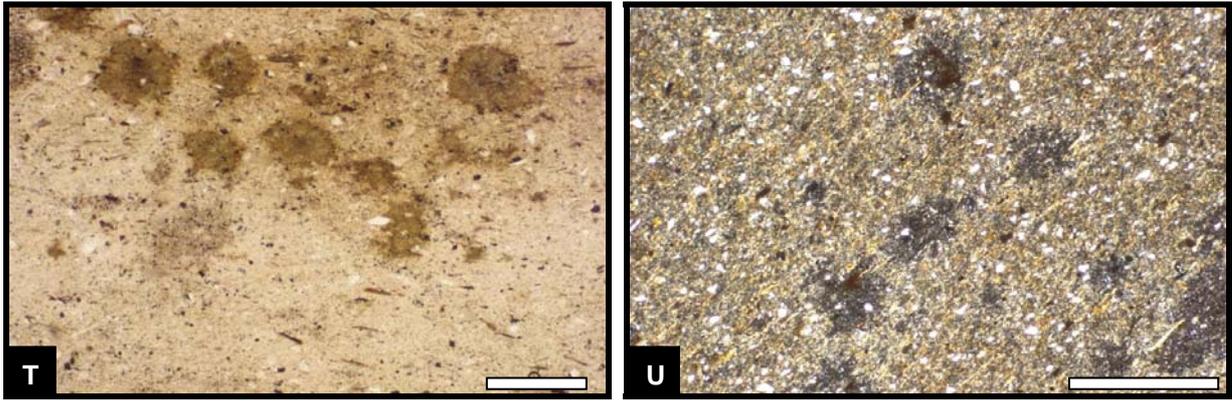
Fig. 3.46: Thin section photographs of the Khabus-Panorama Tuff 1 (cont.): **(T)** Approximately in the middle of the picture runs the boundary between the albitized zone (lower part) and the overlying zone with greenish, chlorite-rich porphyroblasts (pinitized, poikiloblastic cordierite) (upper part). Plane-polarized light. Scale bar 250 µm. **(U)** Subspherical, poikiloblastic domains within the albitized zone. Note the lack of clay minerals producing bright pale yellowish interference colours within the spots. Thin section is rotated ~45° against horizontal bedding causing maximum brightness of oriented clay mineral aggregates interspersed in the albitic matrix. Crossed polars. Scale bar 500 µm.

The Panorama Tuff 2 appears in thin sections as a poorly sorted, normally graded, matrix-supported, bentonitic ash-fall tuff, which is crystal-rich at the base (Fig. 3.47-A/B) and crystal-poor at the top. Quartz, strongly altered feldspar and biotite, as well as zircon and apatite, form the main crystal components. The tuff is intensively speckled with completely pinitized cordierite porphyroblasts due to thermal overprinting by dolerite intrusions. Crystal fragments of quartz are very angular, monocrystalline and show straight extinction. Their mean grain size lies between 50 and 100 µm. Feldspar fragments are also mainly angular but some of the larger grains have a slightly rounded appearance. Apart from few moderately altered, polysynthetically twinned plagioclase fragments, untwinned feldspar crystals are intensively or completely sericitized (Fig. 3.47-C/D). Most feldspar grains show sizes between 50 and 130 µm. Fresh or only moderately altered biotite is absent within this tuff. However, ghost structures of expanded, booklet-like mica stacks with sizes between 50 and 200 µm are present throughout the tuff. They are only visible in plane-polarized light as stacked, near-opaque iron oxide lamellae (Fig. 3.47-E/F). The space between these lamellae is occupied by clay minerals, which do not contrast with the matrix of the tuff. In this respect they are different to alteration products of biotite from other tuff layers, e.g. the Ganigobis or Itzawisis Tuffs, which contain discrete and well-developed, partly or completely illitized kaolinite pseudomorphs after biotite. Zircon and apatite form the only observed accessory crystal components. Zircons are relatively rare and appear mainly as juvenile, euhedral to sub-hedral, acicular to stubby crystals with sizes of 20-70 µm. In contrast, juvenile, euhedral to subhedral apatite crystals are fairly abundant. Most of them belong to the smokey-grey, zoned type and have sizes between 20 and 110 µm. Of all described tuff layers the apatites of the Panorama Tuff 2 show the strongest etching and corrosion phenomena (Fig. 3.47-

G/H), in accordance with the strong alteration of feldspars and biotites. This is also reflected in the large number of opaque Fe-Ti-oxide particles interspersed in this tuff. The clayey matrix of the bentonite is strongly dominated by illite, according to XRD analyses, which show quartz, albite and illite-muscovite as the major phases. Minor amounts of chlorite can be related to the pinitized cordierite porphyroblasts. In polished and thin sections they show subspherical, ovoid, barrel-shaped and hexagonal (Fig. 3.47-I) outlines and often exhibit relict structures of radial sector zoning (so-called cross triplets). Most of them have diameters between 200 and 400 µm. In thin sections it can be seen that they are often composed of a spotty, yellowish-brown internal part, which is surrounded by a lighter coloured outer margin. Faint remnants of the internal structures of the altered porphyroblasts are best viewed under crossed polars with an inserted gypsum plate. Fig. 3.47-K, for example, shows a sector-zoned porphyroblast, which is surrounded by a thin outer margin. The pseudohexagonal shape and the radial sector zoning (shown in Fig. 3.47-L to O) are very characteristic for cordierite (Tröger, 1969; Shelley, 1975).
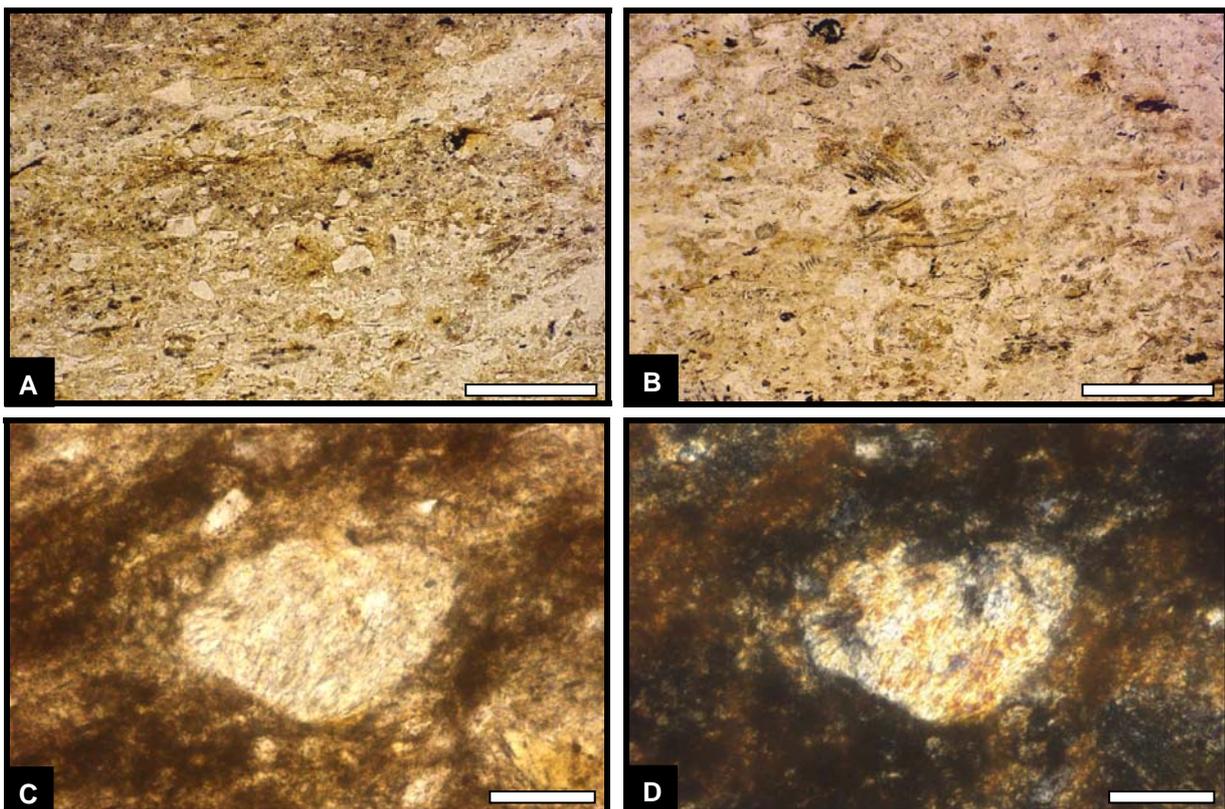
Fig. 3.47: Thin section photographs of the Panorama Tuff 2: **(A)** Poorly sorted, crystal-rich, basal part of the tuff with abundant angular crystal fragments of quartz floating in a clay mineral-rich, illite-dominated matrix. Plane-polarized light. Scale bar 250 µm. **(B)** Crystal-rich, basal part of the tuff showing relicts of large, altered and expanded biotite booklets (centre of picture). Plane-polarized light. Scale bar 250 µm. **(C) & (D)** Feldspar grain, which is completely altered to fine-grained, felty clay mineral crystallites (sericite). Plane-polarized light (left) and crossed polars (right). Scale bars 50 µm.
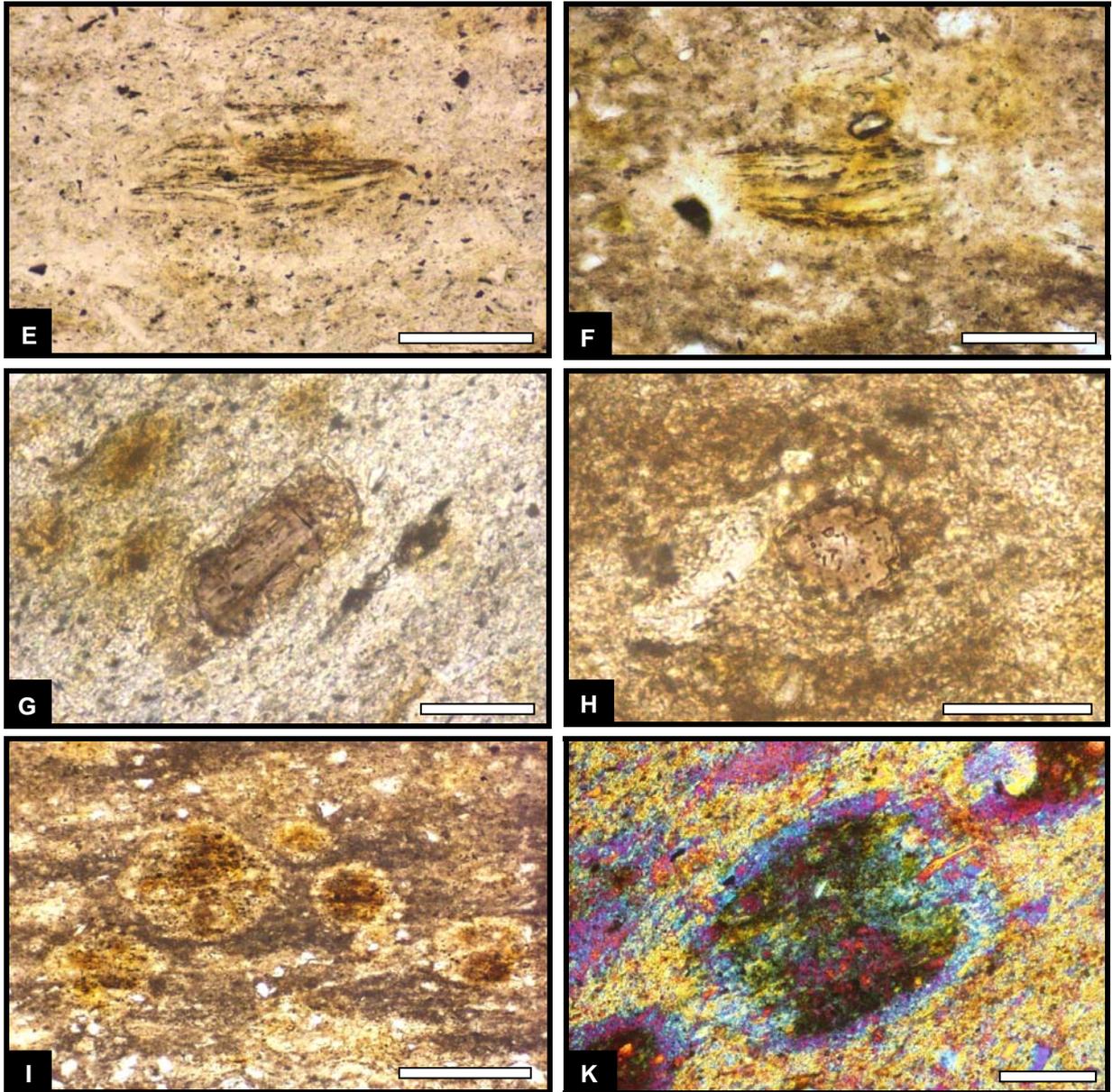
Fig. 3.47: Thin section photographs of the Panorama Tuff 2 (cont.): **(E) & (F)** Relict structures of extremely altered, expanded biotite crystal stacks. Both pictures in plane-polarized light. Scale bars 100 μm. **(G) & (H)** Very strongly corroded, formerly euhedral to subhedral, smokey-grey apatite crystals. Both pictures in plane-polarized light. Scale bars 50 μm. **(I)** Pseudohexagonal (upper left corner) and ovoid cordierite porphyroblasts completely altered to pinite. Plane-polarized light. Scale bar 250 μm. **(K)** Barrel-shaped, completely pinitized porphyroblast consisting of a large, radially sector-zoned core, which is surrounded by a thin, structureless (pseudoisotropic) rim. Crossed polars plus gypsum plate. Scale bar 100 μm.
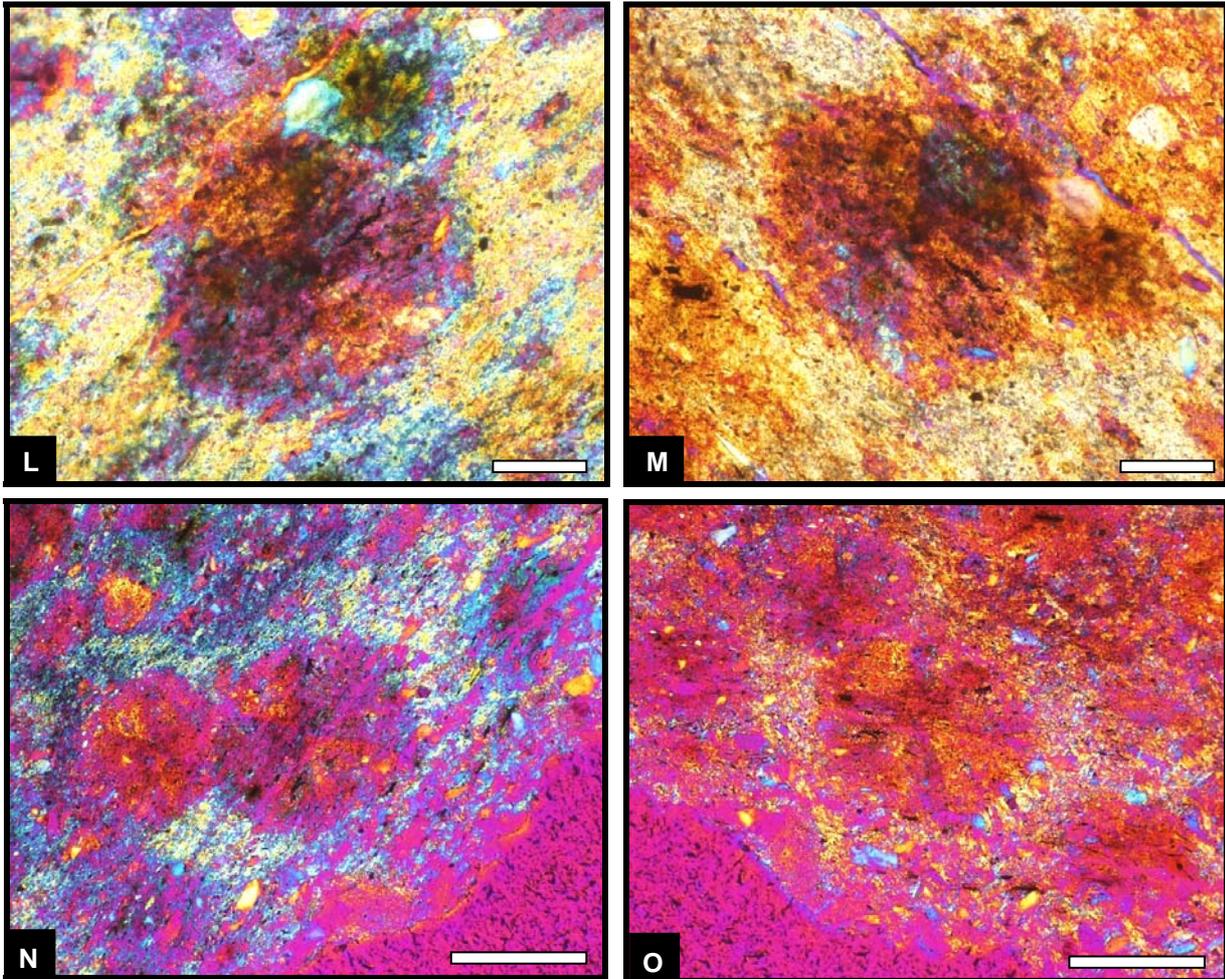
Fig. 3.47: Thin section photographs of the Panorama Tuff 2 (cont.): **(L) to (O)** Subspherical to ovoid, completely pinitized cordierite porphyroblasts showing relicts of radial sector zoning (so-called crosstriplets). Each row shows the same porphyroblast, but the thin section rotated about 90°. All photos are inclined about 45° against the horizontal bedding of the tuff. Crossed polars plus gypsum plate. Scale bars 100 µm (upper row) and 250 µm (lower row).

The Eisenstein Tuffs contrast markedly in thin sections with the Khabus-Panorama Tuff 1 and the Panorama Tuff 2 because they are virtually free of quartz crystal fragments and also altered feldspar grains form only a very minor crystal component. Very abundant, however, are altered biotite flakes and large, booklet-like crystals, which may well represent pseudomorphs after biotite, and classify the Eisenstein Tuffs as crystal-rich pyroclastic layers. As usual, also the Eisenstein Tuffs contain a fair amount of euhedral to subhedral zircon and apatite crystals as accessories. The thinner tuff forms a uniform single layer, whereas the thicker tuff bed is clearly composed of three distinctive subunits. Within the thicker tuff bed the central 0.7-0.8 cm thick layer, which is among other properties characterized by its knotty weathering (see Fig. 3.44-45), is underlain by a c. 250-350 µm thick basal and overlain by a c. 800-1000 µm thick top layer. The basal layer is characterized by the high abundance of brownish biotite flakes, which are aligned parallel to the bedding of the tuff. The top layer is

characterized by the high abundance of fragmented biotite flakes floating randomly in the tuff matrix and by large roundish areas, which have the appearance of cotton pads or cumulus clouds and are filled with vermicular clay mineral aggregates. Within the central layer no grain size grading is visible. The overall appearance of the tuff is poorly sorted and matrix-supported. In places this central layer exhibits in some specimen under low magnification a quite conspicuous honeycomb-like texture (Fig. 3.48-A), which is caused by the already mentioned knots and knobs that might have a contact-metamorphic, porphyroblastic origin. In thin sections these knots form largely ovoid domains within the tuff, which are lighter coloured than the surrounding, somewhat darker, brownish matrix (Fig. 3.48-A to C). From a textural point of view both the ovoid areas and the matrix exhibit a fine-grained, recrystallized texture and are most probably mainly composed of small feldspar (plagioclase) crystallites (Fig. 3.48-D, F, H, K, M, O). In addition, the darker matrix contains a large amount of inter-spersed clay mineral crystallites, which show slightly yellowish-brown interference colours under crossed polars (Fig. 3.48-D/Q). The latter are not present in the ovoid areas, which show only first order shades of grey interference colours under crossed polars. In this respect they resemble very much the porphyroblast-like spots within the matrix of the albitic Khabus-Panorama Tuff 1 (see Fig. 3.46-U). The mineralogical nature of these possible porphyroblasts is not clear but since they weather out positively from the matrix (Fig. 3.45) they may represent silicified areas within the matrix. The light brownish colour of the surrounding matrix might also be caused by finely dissiminated iron oxide pigment. The size of individual ovoid areas ranges approximately between 500 and 900 μm, however, they can also intergrow to form larger, irregular-shaped areas (>1 mm) (Fig. 3.48-B). An interesting observation is that the appearance of biotites and crystal booklets enclosed within the lighter coloured ovoid areas differs markedly from those enclosed within the darker coloured matrix. Within the ovoid areas both orange-brown biotite flakes and greenish-yellowish, chloritic crystal booklets can be observed, whereas in the surrounding, brownish matrix no biotite is present and the crystal booklets are mainly composed of a colourless mineral phase (Fig. 3.48-A to Q). The biotite flakes show still a pronounced pleochroism and seem to be only moderately altered to hydrobiotite or vermiculite. The large, greenish-yellowish crystal booklets often contain orange-brown relictic areas composed of pleochroitic biotite and can therefore certainly be interpreted as pseudomorphs after biotite (Fig. 3.48-G to K). Under crossed polars these booklets mainly show very conspicuous, anomalous blue interference colours (Fig. 3.48-D, F, H, K, M, O) indicating chlorite. According to their positive sign of elongation these chlorites possess a negative optical character. The intensity of the bluish interference colours of these chlorites from the Eisenstein Tuffs is much higher than that of the chlorites from other tuffs described in this study, which generally show only a slightly bluish hue among the dominating blackish-grey to yellowish interference colours. However, a

closer look at the crystal booklets reveal that only the lighter coloured greenish-yellowish parts (under plane-polarized light) display the intensive blue interference colour under crossed polars, whereas slightly darker, brownish-yellowish lamellae, bands or stringers (in plane-polarized light) show under crossed polars white to slightly yellowish interference colours (Fig. 3.48-L to O). These somewhat darker areas within the chloritic crystal booklets could either represent intermediate alteration products of biotite (to chlorite) or partly oxidized chloritic parts. As already mentioned above, outside the ovoid, porphyroblast-like areas, i.e. within the darker matrix area, no brownish biotite is present and the large crystal booklets appear mainly colourless under plane-polarized light (Fig. 3.48-B/C). In some cases these colourless booklets contain thin laminae or stringers of greensih-yellowish chlorite (Fig. 3.48-P/Q). Under crossed polars all mineral phases, of which these mainly colourless crystal booklets are composed of, display only frist order shades of grey (Fig. 3.48-P/Q). No anomalous bluish or bright interference colours are visible. In one case a booklet-like biotite pseudomorph at the base of the thinner tuff layer shows relict lamellae of biotite at the margin and chlorite in the centre, the latter surrounded by a rim of blocky quartz or zeolite crystals (Fig. 3.48-R/S). The size of biotite flakes and booklet-like crystals lies mainly within 50 and 250 µm, with the largest crystal reaching 400 µm. Summarizing the observations on biotite and its different alteration products it appears that biotite was preferentially preserved within the light coloured, ovoid areas as moderately altered crystals, whereas in the surrounding, darker coloured matrix biotite seems to be largely unstable and completely replaced. Similarily to the albitic Khabus-Panorama Tuff 1 also in the case of the Eisenstein Tuffs one step in the alteration history obviously had a partly protective effect on certain areas, leading to differential alteration of biotite.

The Eisenstein Tuffs are almost free of quartz crystals and also feldspar plays only a minor role within the crystal components, what is somewhat surprising, especially under the aspect, that the tuff layers are fairly rich in biotite and its alteration products (crystal booklets). Supposed feldspar remains are best visible under crossed polars as angular, brightening grains with ragged margins (Fig. 3.48-M). These grains are composed of a fine-grained mosaic of alteration products (sericite?) or recrystallized feldspar (plagioclase?). The few observed quartz crystal fragments are generelly smaller (40-70 µm) than the altered feldspar grains (60-150 µm).

Euhedral to subhedral zircon crystals are mainly short-prismatic to stubby, some are almost equidimensional, often with octagonal outlines in cross-section (soccer ball zircons) (Fig. 3.48-T). A fair amount of zircons also have a slightly abraded, rounded or fragmented appearance. Some elongate to acicular zircon crystals have been observed, too (Fig. 3.48-U). The observed crystal size ranges between 25 and 80 µm. The extraordinary richness of the Eisenstein Tuffs in apatites is also reflected in slightly increased whole rock phosphate

values (0.22 wt% P_2O_5). Almost all apatites are euhedral to subhedral and belong to the smokey grey-zoned type (Fig. 3.48-V). Many contain tubular inclusions, partly filled with a dark substance possibly composed of volcanic glass (Fig. 3.48-W). Etching phenomena are in these tuffs not very pronounced. The size of apatite crystals can reach up to 150 µm.

Furthermore, the Eisenstein Tuffs are interspersed with numerous, dark coloured mineral aggregates, which appear in thin sections almost opaque (visible in all thin section photographs of Fig. 3.48 taken under plane-polarized light). These aggregates are composed of generally submicron-sized crystallites, which under high magnification prove to be colourless and translucent. Their opaque appearance is caused by their minute crystal size and their high refractive index. Their relatively even distribution throughout the tuffs (and also the surrounding shale) indicates a secondary origin. According to the observed optical properties these aggregates might be composed of a carbonate mineral, epidote or possibly light coloured titanite. The latter could be the subsequent precipitation product of the mobilized and redistributed titanium content of altered biotites, whereas epidote and calcite could be alteration products of the matrix plagioclase of inferred intermediate composition.

Both the thin layer at the base and at the top of the thicker Eisenstein Tuff is characterized by the relatively high abundance of orange-brown, pleochroitic, apparently only moderately altered biotite flakes and the lower abundance of colourless crystal booklets. In the basal layer the biotite flakes are aligned parallel to the bedding of the tuff (Fig. 3.48-X), whereas in the upper layer the biotite flakes have a rather fragmented appearance floating randomly in the tuff matrix. In addition, the upper layer also contains light coloured, roundish, 300-600 µm large objects, the form of which is somewhat reminescent of cotton pads or cumulus clouds (Fig. 3.48-Y to AA). In one case the matrix of the tuff is clearly bent around this object indicating a precompactional origin (Fig. 3.48-Y). Under higher magnification it can be seen, that these objects are filled with vermicular clay mineral aggregates (Fig. 3.48-AB, AC). Under crossed polars these clay mineral crystallites exhibit largely first order shades of grey, however, in places there seems to be a slightly bluish tint noticeable. In the centre of some of these objects also slightly yellowish to orange interference colours are visible. The vermicular clay mineral aggregates are possibly composed of chlorite. The origin of these objects, however, remains enigmatic.

In one thin section of the Eisenstein Tuffs a cavity within the thicker tuff layer is filled with coarse-grained calcite and quartz. The coarse-grained quartz contains inclusions of several euhedral to subhedral, short-prismatic, largely colourless crystals with a high relief against quartz. Under crossed polars these crystals display partly first order pale white-yellow-orange interference colours, partly bright green and blue interference colours (Fig. 3.48-AD/AE). These crystals might represent epidote inclusions.
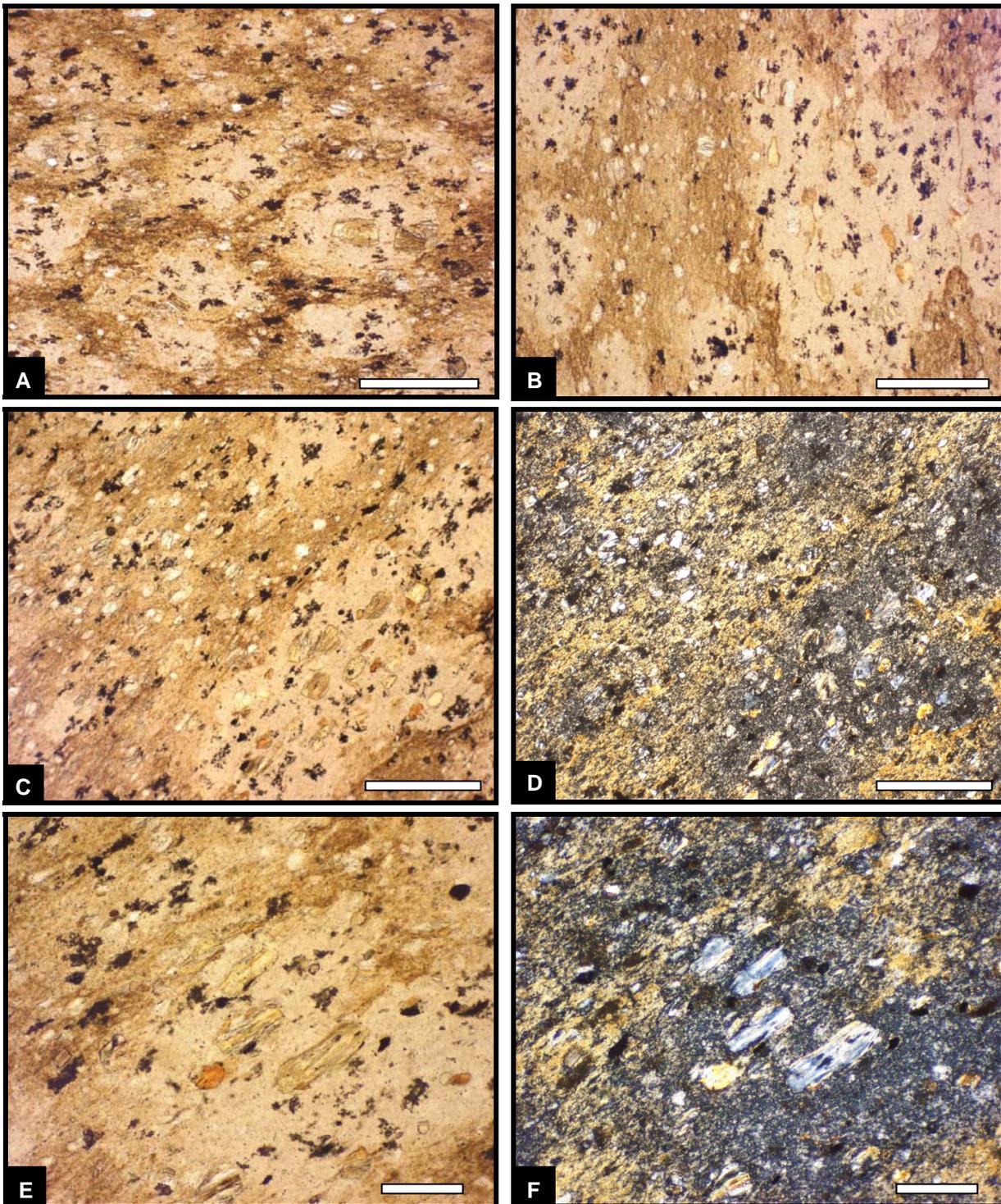
Fig. 3.48: Thin section photographs of the Eisenstein Tuffs: **(A)** Light coloured, ovoid, porphyroblast-like areas surrounded by a darker coloured, clay-rich tuff matrix resulting in a honey comb-like texture. Plane-polarized light. Scale bar 500 µm. **(B)** Light coloured, porphyroblast-like area (right), containing orange-brown biotite flakes and greenish-yellowish crystal booklets, contrasts with darker, clay-rich area (left), containig colourless crystal booklets. Top to the left. Plane-polarized light. Scale bar 500 µm. **(C) & (D)** Under crossed polars the matrix of the porphyroblast-like areas show first order shades of grey, whereas the darker tuff matrix contains abundant clay mineral crystallites showing yellowish interference colours. Plane-polarized light (left) and crossed polars (right). Scale bars 500 µm. **(E) & (F)** The light coloured, ovoid areas contain orange-brown biotite flakes and greenish-yellowish crystal booklets, the latter showing under crossed polars conspicuous anomalous blue interference colours indicating a mainly chloritic composition. Plane-polarized light (left) and crossed polars (right). Scale bars 100 µm. (B) rotated 90° and (C)-(F) rotated 45° against bedding of the tuff.
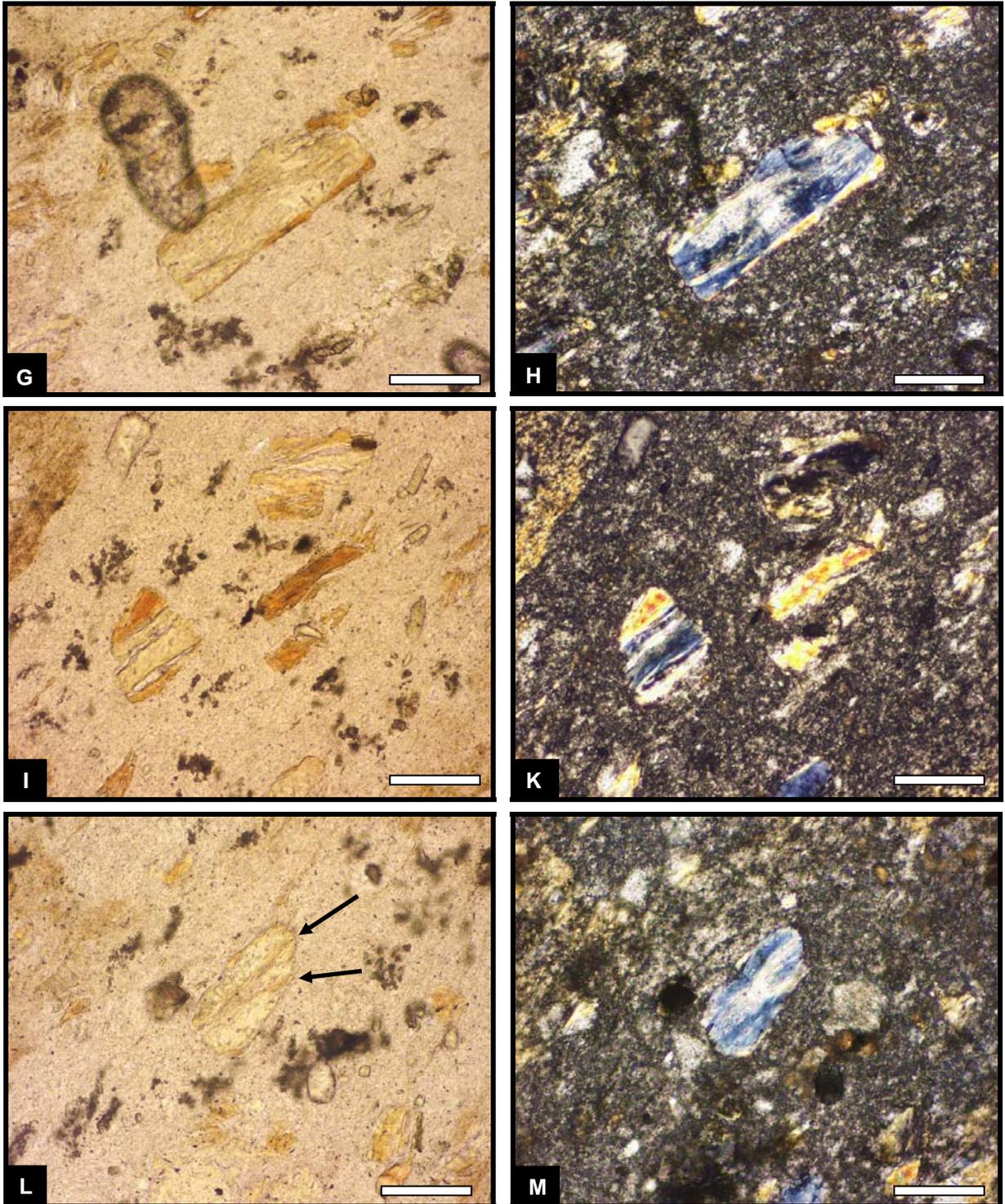
Fig. 3.48: Thin section photographs of the Eisenstein Tuffs (cont.): **(G) & (H)** Elongate, greenish-yellowish crystal booklet showing a relict lamella of orange-brown biotite (lower right margin) indicating that the crystal booklets represent pseudomorphs after biotite. Under crossed polars the crystal booklets show mainly anomalous blue interference colours typical of chlorite. Plane-polarized light (left) and crossed polars (right). Scale bars 100 µm. **(I) & (K)** Orange-brown biotite partly altering to greenish-yellowish, chloritic crystal booklets within the light coloured ovoid areas. Plane-polarized light (left) and crossed polars (right). Scale bars 100 µm. **(L) & (M)** The greenish-yellowish crystal booklets often contain, apart from chlorite (blue interference colours), also slightly darker lamellae or strings (arrows), which show under crossed polars a white colour. The dirty, light coloured, angular grain to the right of the chloritic crystal booklet in (M) might represent an altered feldspar crystal fragment. Plane-polarized light (left) and crossed polars (right). Scale bars 100 µm.
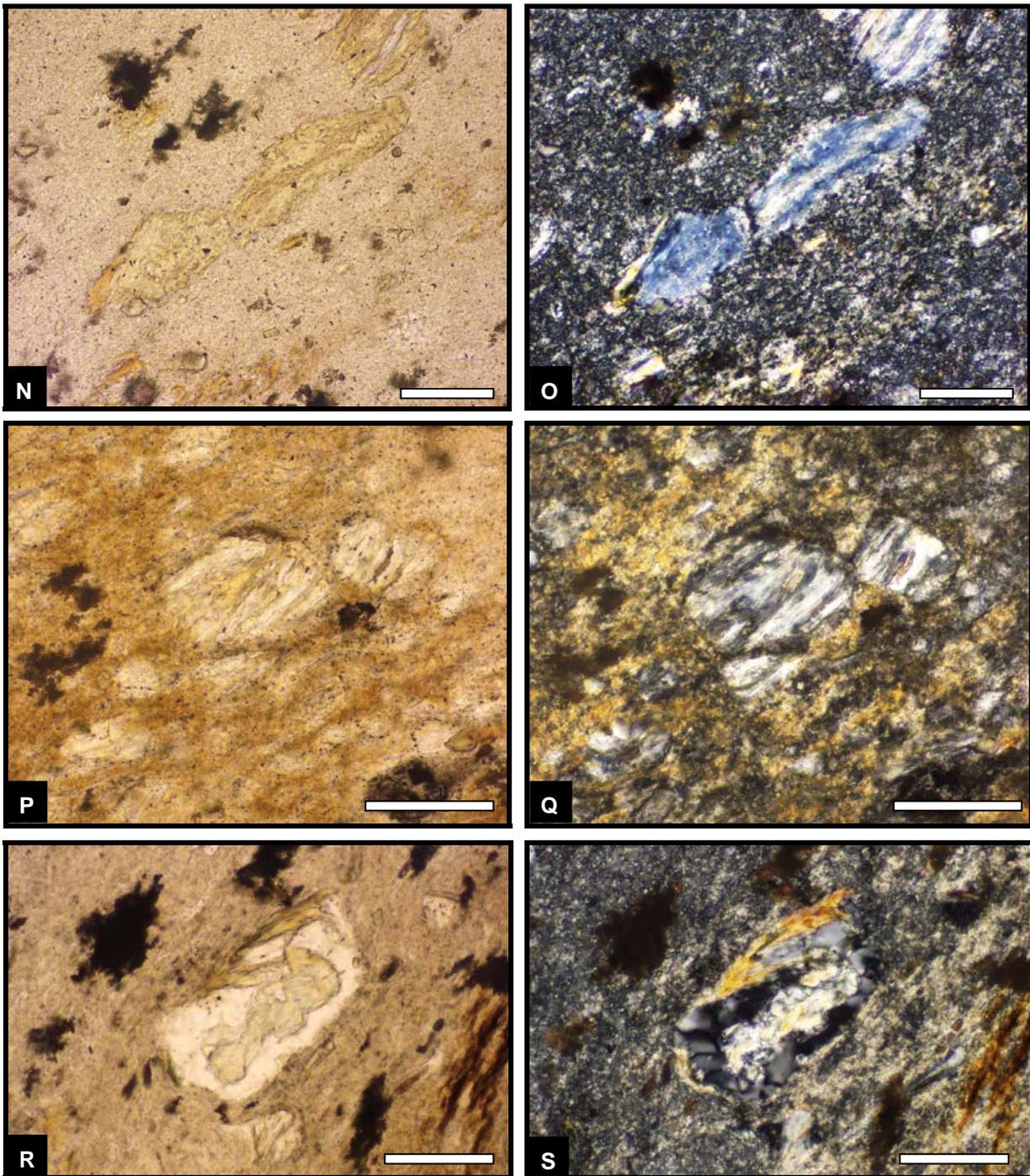
Fig. 3.48: Thin section photographs of the Eisenstein Tuffs (cont.): **(N) & (O)** Biotite pseudomorph containing biotite relict (lower left margin). The crystal is mainly composed of greenish-yellowish chlorite showing anomalous blue interference colours under crossed polars. Slightly darker stringers (central right area of crystal) appear white under crossed polars. Plane-polarized light (left) and crossed polars (right). Scale bars 100 µm. **(P) & (Q)** Within the darker coloured, clay-rich tuff matrix the crystal booklets are mainly composed of a colourless mineral phase (phyllosilicate or feldspar?) but in places they contain thin greenish-yellowish chlorite lamellae. The surrounding, feldspathic matrix is also rich in clay mineral crystallites showing yellowish interference colours. Plane-polarized light (left) and crossed polars (right). Scale bars 100 µm. **(R) & (S)** Biotite pseudomorph near the base of the thinner Eisenstein Tuff layer with relictic biotite in the upper left corner and chlorite in the centre, surrounded by a rim of blocky quartz or zeolite. Plane-polarized light (left) and crossed polars (right). Scale bars 50 µm.
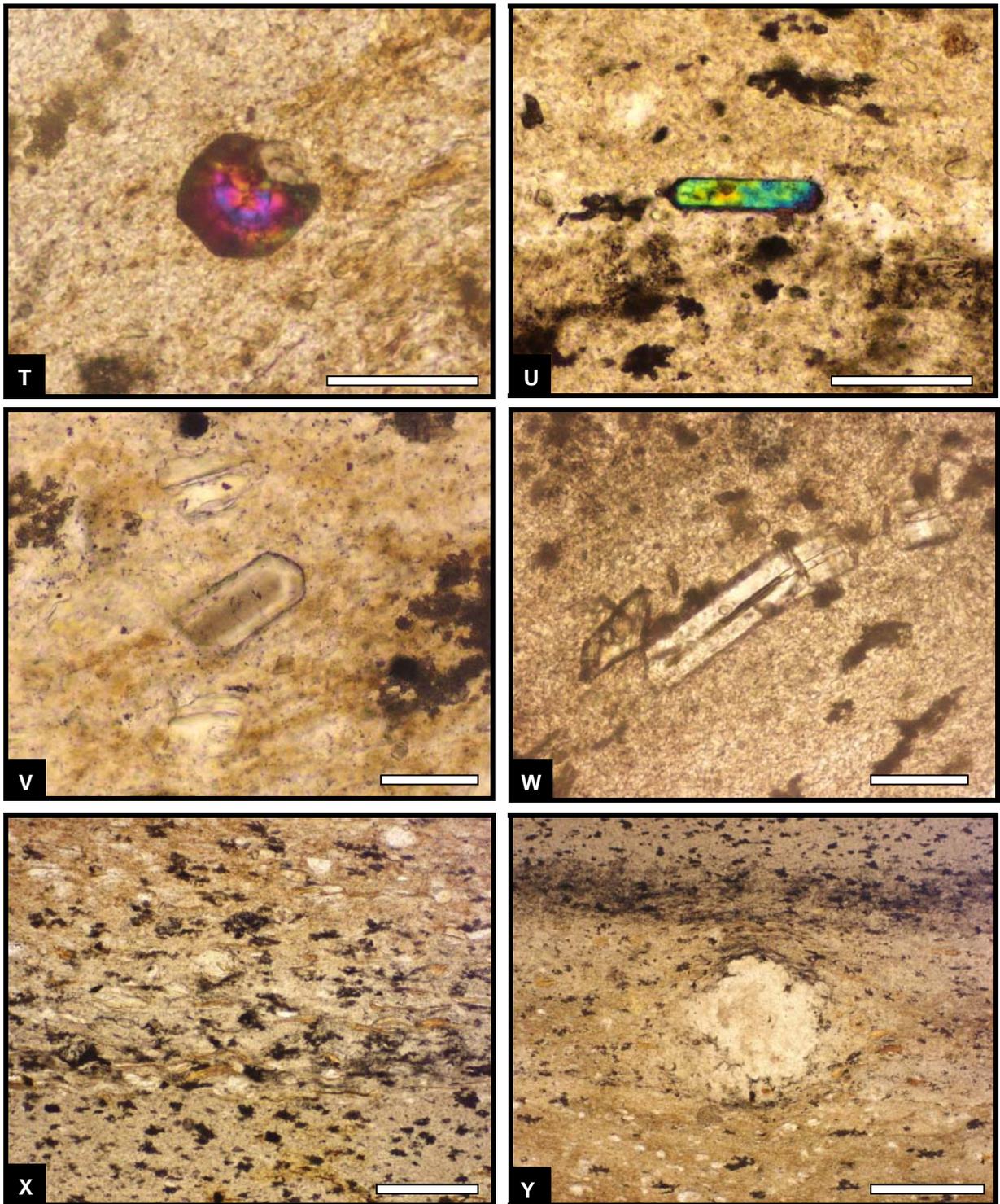
Fig. 3.48: Thin section photographs of the Eisenstein Tuffs (cont.): **(T)** Euhedral, juvenile zircon crystal showing an octagonal cross section (soccer ball zircon). Semi-crossed polars. Scale bar 50 μm. **(U)** Acicular zircon directly at the base of the thinner Eisenstein Tuff layer. Semi-crossed polars. Scale bar 100 μm. **(V)** Euhedral, zoned, partly smokey-grey juvenile apatite crystal. Plane-polarized light. Scale bar 50 μm. **(W)** Subhedral, acicular and fragmented juvenile apatite crystal containing a central tubular inclusion, which is partly filled with a dark coloured substance possibly representing volcanic glass. Plane-polarized light. Scale bar 50 μm. **(X)** ~350 μm thick basal layer (middle third of the picture) of the thicker Eisenstein Tuff containing abundant orange-brown biotite flakes, which are aligned parallel to the bedding of the tuff. Plane-polarized light. Scale bar 250 μm. **(Y)** ~1000 μm thick top layer (middle part of picture) of the thicker Eisenstein Tuff containing abundant orange-brown biotite flakes with a fragmented appearance. Laminae within the matrix are bent around a light coloured object, having a cotton pad- or cumulus cloud-like appearnace. Plane-polarized light. Scale bar 500 μm.
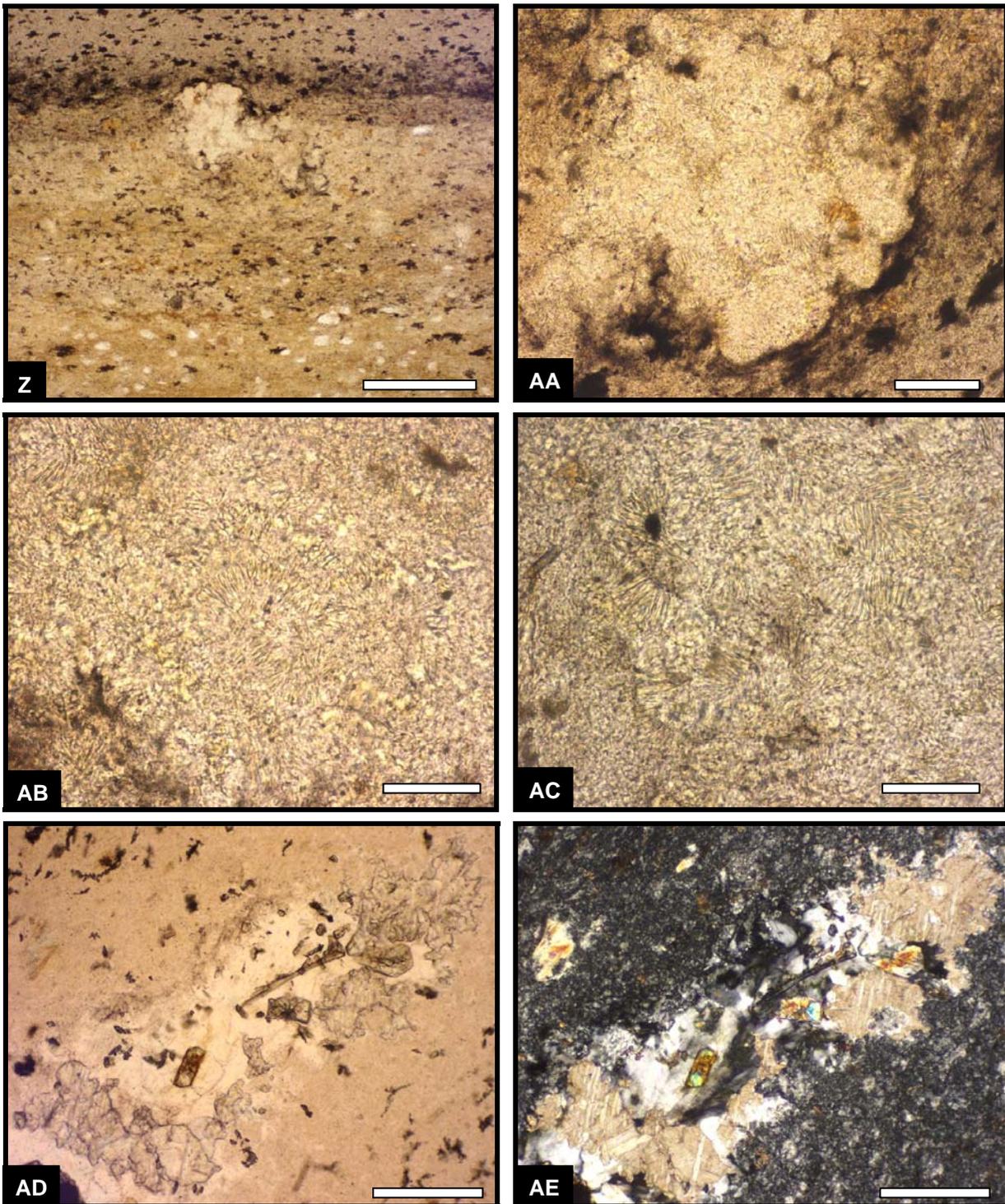
Fig. 3.48: Thin section photographs of the Eisenstein Tuffs (cont.): **(Z)** Another image of the cotton pad- or cumulus cloud-like objects at the top of the c. 1000 µm thick top layer (middle part of picture) of the thicker Eisenstein Tuff. Plane-polarized light. Scale bar 500 µm. **(AA)** One of the cotton pad- or cumulus cloud-like objects under higher magnification showing faint internal structures. Plane-polarized light. Scale bars 100 µm. **(AB) & (AC)** The cotton pad- or cumulus cloud objects are filled with vermicular stacks of platy phyllosilicate crystals (chlorite?). Both pictures in plane-polarized light. Scale bars 50 µm. **(AD) & (AE)** Cavity filled with calcite and quartz, the latter containing several euhedral to subhedral crystal inclusions showing bright interference colours and possibly representing epidote. Plane-polarized light (left) and crossed polars (right). Scale bars 250 µm.

3.4.2.3 Collingham and Aussenkjer Formation

The Ufo Valleys-Rhyofontein Tuffs

In the Mariental-Keetmanshoop Karoo outcrop area the Whitehill Formation represents the youngest preserved stratigraphic unit of the Ecca Group, whereas in the Aussenkjer-Noordoewer area also higher stratigraphic units of the Ecca Group are preserved and crop out. On the Whitehill Formation there follows conformably a succession of fine-grained, shaly mudrocks several hundred metres thick. For this succession the term Aussenkjer Formation was suggested (SACS, 1980). Fieldwork within the scope of this study has shown, however, that the basal c. 75 m of the Aussenkjer Formation can undoubtedly be correlated with the Collingham Formation (see Chapter 2.3.3 Collingham Formation), which crops out in the southern Cape Province of South Africa. Therefore it seems justified to transfer the term Collingham Formation to the southern Namibian outcrops and it is suggested to restrict the term Aussenkjer Formation to the argillaceous deposits, which overly conformably the Collingham-equivalent part of the Ecca succession in the Aussenkjer-Noordoewer area. The most conspicuous character of the Collingham Formation in South Africa is its extraordinary richness in bentonitic tuff layers (Viljoen, 1992a, 1994) and the same is also valid for the southern Namibian part, where of all formations of the Ecca Group the Collingham Formation contains the highest number of tuff layers and records a time of highly frequent volcanic ash falls. For the Late Palaeozoic part of the Karoo Supergroup the high abundance of tuff layers in the Collingham Formation can only be compared to the high abundance of tuff layers in the lower to middle parts of the Dwyka Group in southern Namibia. These two stratigraphic intervals can certainly be considered as periods of peak input of volcanish ash into the SW-African part of the Late Palaeozoic SW-Gondwanan Mesosaurus Inland Sea.

For the investigation of the bentonitic tuff layers within the Namibian Collingham Formation fieldwork was focused on an area west of the Amibberg. There, numerous small valleys are deeply incised into hard rocks comprising the stratigraphic interval from the Polisiewater Chert at the top of the Collingham Formation in the east to the Whitehill Formation in the west, which is intruded by thick dolerite sheets (Fig. 3.49). During fieldwork these small valleys have been informally named the 'Ufo Valleys'. In the eastern parts of these small valleys the sediments of the Collingham Formation are quite well exposed in cut walls several tens of metres high. At two localities the succession of bentonitic tuff layers within the Collingham Formation was logged in detail. From the southern locality (Ufo Valley) also one thick tuff layer was sampled for radiometric dating (sample UFO-43, see also Chapter 5 Geochronology). The northern locality was informally called 'Rhyofontein' because there a vegetated spring emerges a few metres above the Inaub Rivier where the boundary between the base of the Collingham Formation and a thick, underlying dolerite sill is intersected by a

felsic dyke (so-called 'rioliet-gang' after Schreuder & Genis, 1975) and an associated fracture zone (Fig. 3.49). As shown in Fig. 3.50 the highest concentration of thicker (>1 cm) tuff layers can be found approximately in the middle of the formation. A surprising outcome of the detailed logging was that the sum of the thickness of all tuff layers >0.1 cm, expressed as the minimum total thickness of tuff layers, is almost the same for both localities. For natural outcrops the almost identical measured minimum total thickness of tuff layers in the c. 75 m thick Collingham Formation from two localities is quite astonishing, considering that both outcrops contain also parts, in which conditions are not so favourable for detailed logging at cm-scale. At both localities the cumulative tuff thickness ranges between 77.0 to 87.5 cm, which corresponds to somewhat more than 1% of the total thickness of the Collingham Formation. This is in marked contrast to the situation in the southern Cape region of South Africa, where tuff beds constitute between 5 and 30% of the Collingham
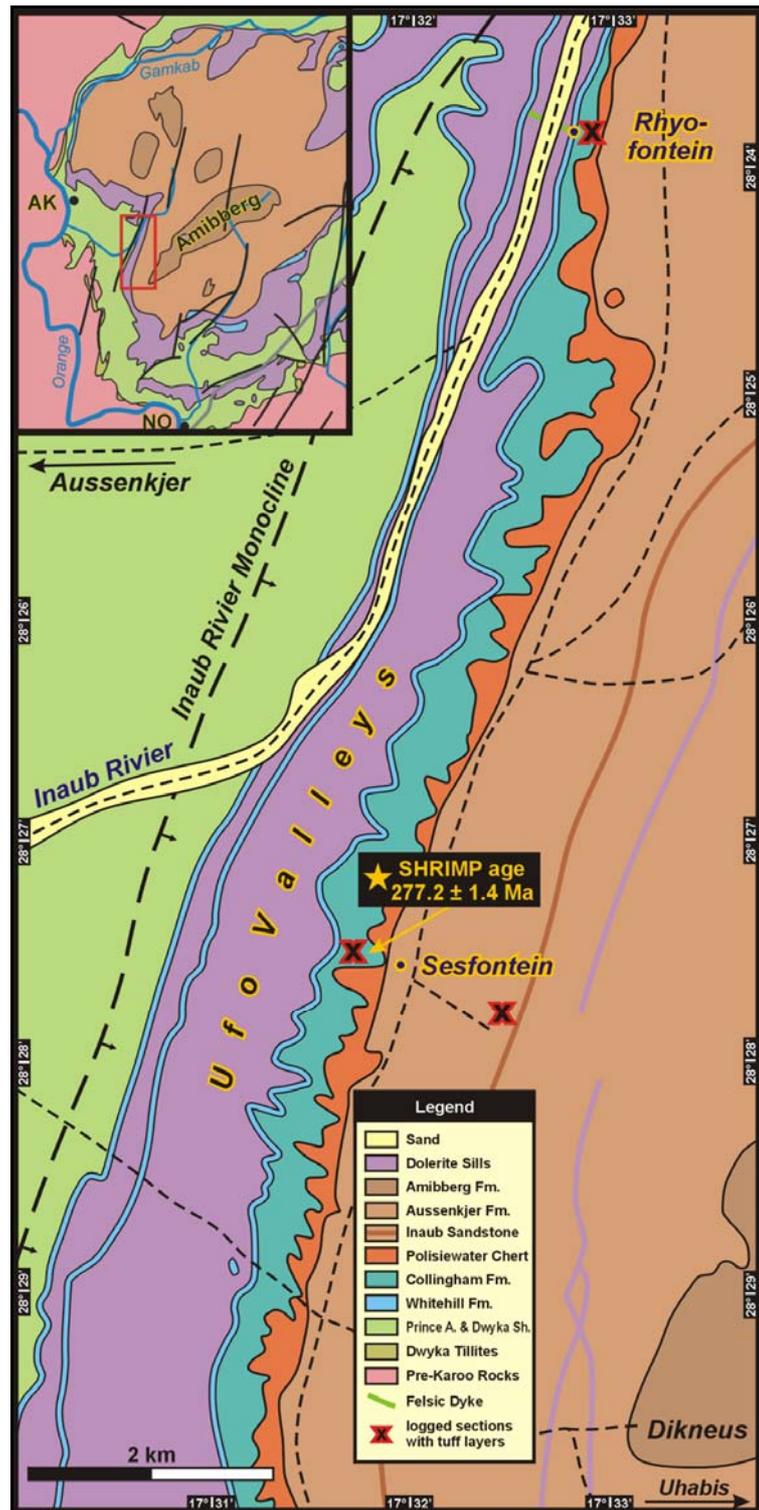
Fig. 3.49: Geological map of the 'Ufo Valleys' area east of the Inaub Rivier/Inaub Rivier Monocline and west of the Amibberg, with the Dickneus peak at its southern tip. Shown are the two localities (Ufo Valleys & Rhyofontein), where detailed sections of the tuffaceous Collingham Fm. were logged. Also the Sesfontein Tuff outcrop position within the Aussenkjer Fm. is indicated. The map is mainly adopted and modified from hand draft geological maps in the scale of 1:50000 drawn by C.P. Schreuder, G. Genis and G.J. Beukes between 1970 and 1973 (Geological Survey of Namibia).

Formation thickness (Viljoen, 1992a, 1994). In this respect the Collingham Formation in southern Namibia contains a distinctly smaller amount of pyroclastic material than the Collingham Formation in southern South Africa. Nevertheless, the abundance of tuff layers in the Collingham Formation is also in Namibia unparalled within the whole Ecca Group.
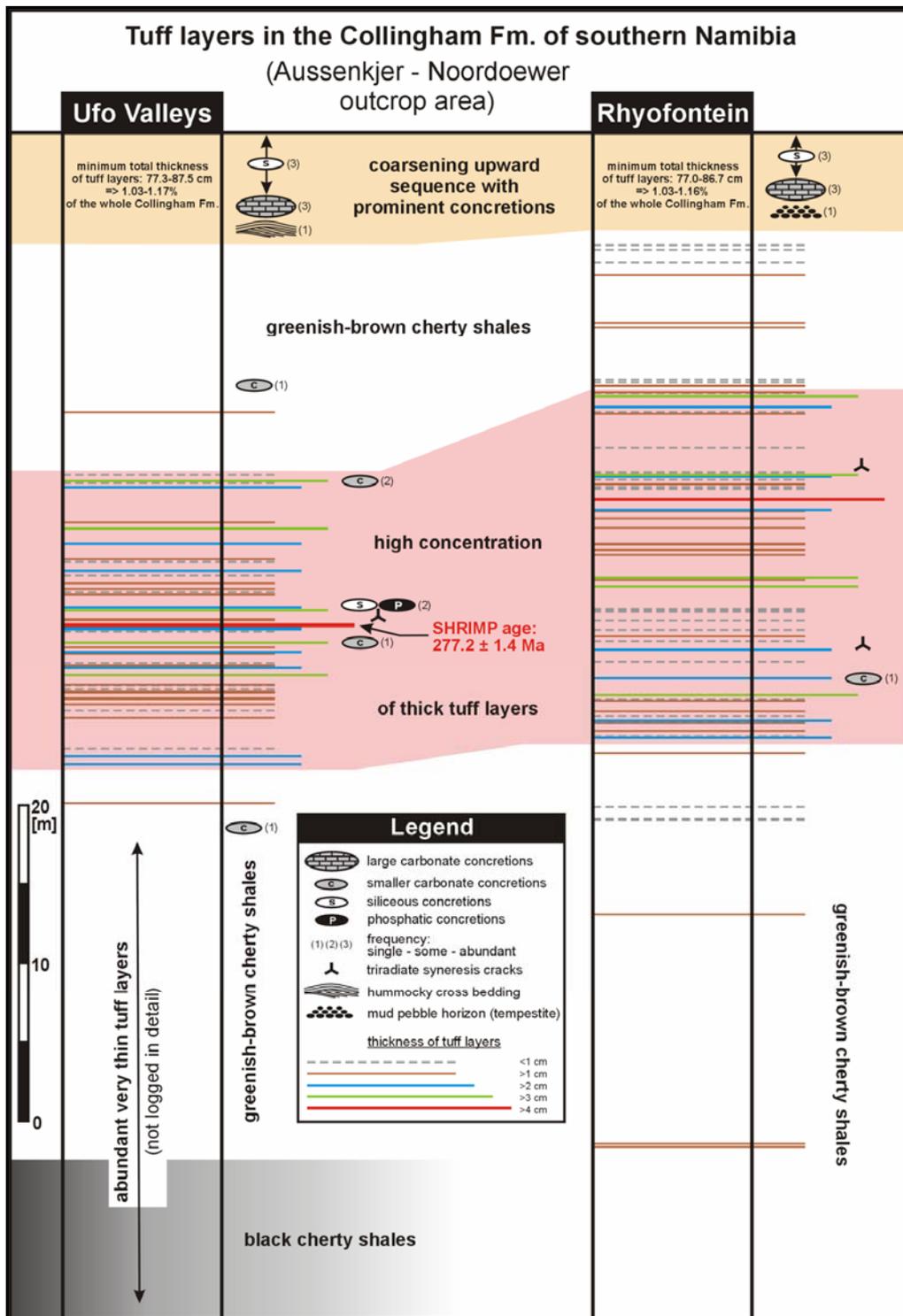
Fig. 3.50: Two detailed sections of the complete Collingham Formation showing the position and frequency of tuff layers. Indicated is also the position of the SHRIMP-dated sample. See Fig. 3.49 for the position of the Ufo Valleys and the Rhyofontein locality.

At the two investigated outcrop areas the lower ~30 m of the Collingham Formation contains a lot of tuff layers, which, however, are often very thin (around 0.1 cm and thinner) and normally not so easy to recognize in vertical outcrop sections. In the river beds, however, there are in places step-like outcrops in which the thin tuff laminae weather out as conspicuous, light coloured bands between the darker, olive-green to brownish shales (Fig. 3.51-A). Higher up in the section the bentonitic tuffs form very conspicuous, light coloured, slightly back-weathering layers within the brownish weathering, cherty shales of the Collingham Formation (Fig. 3.51-B to D).
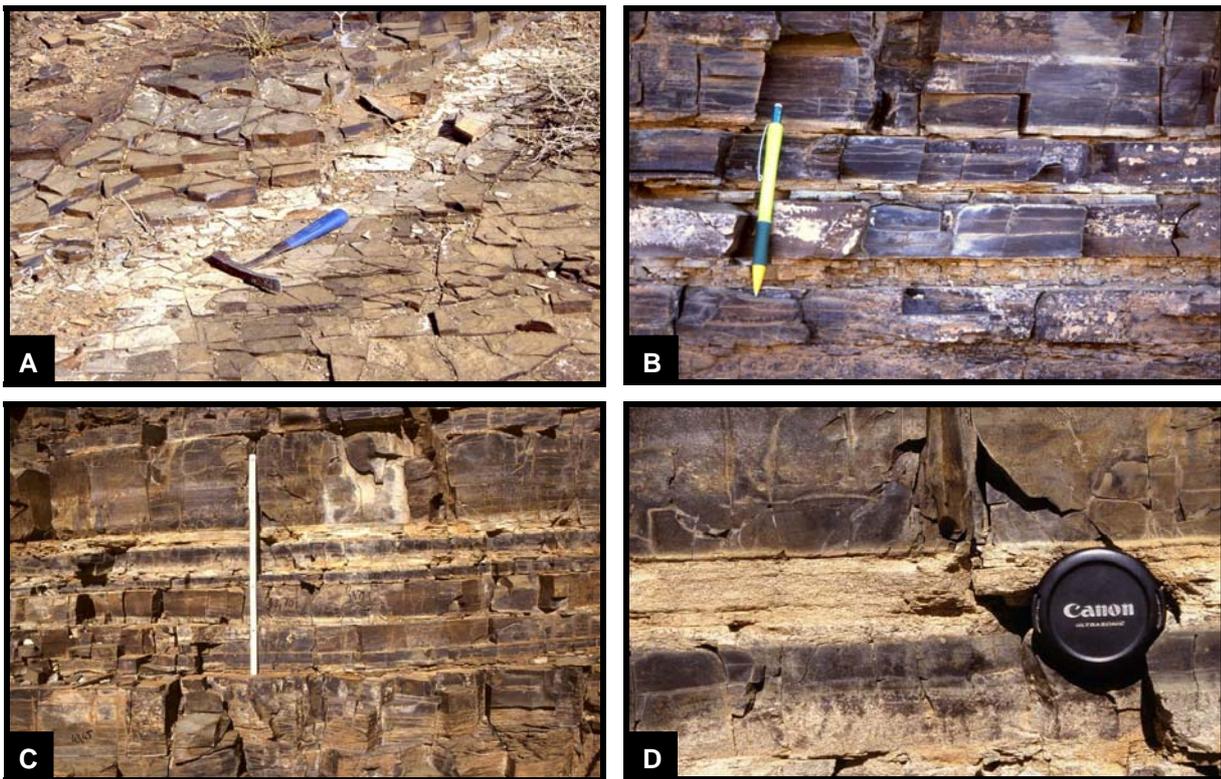
Fig. 3.51: (A) Light coloured, thin tuff lamina (~1 mm) within the basal part of the Collingham Formation. **(B) & (C)** Thicker, bentonitic tuff layers interbedded in cherty shales of the middle part of the Collingham Formation. Scale in (B) is 14.5 cm and in (C) 50 cm long. **(D)** Close-up of tuff UFO-43 (43.89 m above the base of the Collingham Formation), which was sampled for SHRIMP dating. In the picture the tuff layer has a thickness of 4 cm, but can thicken laterally up to 6 cm.

An equivalent to the Matjiesfontein Chert Member, a prominent, 15-60 cm thick, albitized layer of mixed epi- and pyroclastic origin (Viljoen, 1992a, 1994; Knütter, 1994), cropping out in the southern Cape region of South Africa, was not discovered in the southern part of the Aussenkjer-Noordoewer Karoo outcrop area in Namibia. However, Haughton & Frommurze (1927, 1936) reported of 'a band of massive white chert' at the base of the succession overlying the Whitehill Formation near Gaibes (a farm area at the northern margin of the Aussenkjer-Noordoewer outcrop area), but this observation could not be checked since no entry permission could be obtained for the Gaibes farm area. Schreuder & Genis (1975) stated that the Matjiesfontein Chert is absent in the Aussenkjer-Noordoewer area.

What can frequently be observed on the upper surfaces of tuff layers in the Namibian Collingham Formation are bioturbation features. These can range from single traces to intensive, high-density bioturbation (Fig. 3.52-A to D). Observed trace fossils belong among others to the *Undichna* ichnogenus, to the *Helminthopsis-Helminthoidichnites* group and possibly to the *Scalarituba-Neonereites* group. In polished hand specimen it can be seen that the Namibian Collingham tuffs are composed of a white to creamish or sometimes greyish matrix, which is intensively speckled with greenish porphyroblasts (completely pinitized cordierite) (Fig. 3.53 A to C). The shales of the Collingham Formation mainly display a greenish-grey colour, however, the basal 10-15 m can also be dominated in places by dark grey to black, carbonaceous, cherty shales. In the upper portion mainly light brown to greenish-brown shales occur and the top of the Collingham Formation is characterized by whitish-grey, intensively silicified, chert-like rocks (Polisiewater Chert), which show in places a reddish to orange-brown weathering colour. The highest frequency of tuff layers with a thickness >1 cm is found within the middle part of the formation, whereas in the upper third tuff layers become relatively scarce. The distribution of tuff layers within the middle part does apparently not follow a systematic pattern and no obvious grouping of tuff layers has been detected (Fig. 3.50). The bentonitic tuff layers are slightly softer than the surrounding shales but they show no swelling upon moistening. Most of the tuff layers appear massive, only within few tuff layers a very faint, ill-developed fissility can be observed. Some of the tuffs appear normally graded, however, polished hand specimen show that this grading is caused by the size distribution of porphyroblastic spots (Fig. 3.53-A to C), which cause an intensive speckling of both the tuffs and the shales. However, the porphyroblastic spots are generally larger in the tuffs than in the shales. The thickness of discrete tuff layers ranges from <0.1 cm up to 6 cm, some thicker units consist of two or more individual beds (Fig. 3.53-C/D). The boundaries between such subunits are in some cases not horizontal but oblique and sometimes step-like erosional features can be observed (Fig. 5.53-C/D). In outcrops both the upper and lower contacts of the tuff layers appear quite sharp (Fig. 3.51-B to D), but a closer look reveals that many of the tuff layers have a slightly gradational contact to the overlying shale (Fig. 3.53-A/B). Diagenetic nodules or concretions have only been observed in one tuff layer at the Ufo Valleys outcrop. A tuff layer c. 45 metres above the base of the Collingham Formation contains small (~1cm), black phosphate nodules and large (up to 6 cm), septarian concretions (Fig. 3.54 & 3.55). They might have been originally mainly calcareous but due to the contact-metamorphic effects of the dolerite intrusions these nodules are now charac-terized by a mineral paragenesis consisting of calcite, replaced dolomite(?), prehnite, zeolites (laumontite and heulandite?), grandite-group garnet, chlorite, and probably titanite as well as vesuvianite. Many of both the shale beds and the tuff layers do not form exactly tabular units but show some slightly undulating bounding surfaces what is expressed in an inconspicuous

lateral thickening or thinning of individual beds. This undulation is of a very low amplitude (<1 cm to few centimetres) and high wavelength (generelly several metres) nature. Probably the fine-grained muds and volcanish ashes were not exclusively deposited by pure suspension settling. Maybe they were to a certain degree also resuspended, transported and redeposited by weak turbidity, tempestite and/or contourite currents to form low-density nepheloid clouds. In this context it also worth mentioning that within the two outcrops at one or two stratigraphic levels quite conspicuous stellate and triradiate syneresis cracks (cf. Leeder, 1982; Viljoen, 1994) have been discovered (Fig. 3.50). The occurrence of such syneresis cracks within the Ecca Group is restricted to the Collingham Formation (Viljoen, 1994; and this study) and therefore the Collingham Formation represents a period in which the salinity of the basin waters of the Inland Sea sporadically, but finally gradually, changed from normal to brackish. It is believed that these salinity changes were caused by inflows of freshwater plumes or currents into the basin (cf. Viljoen, 1994).
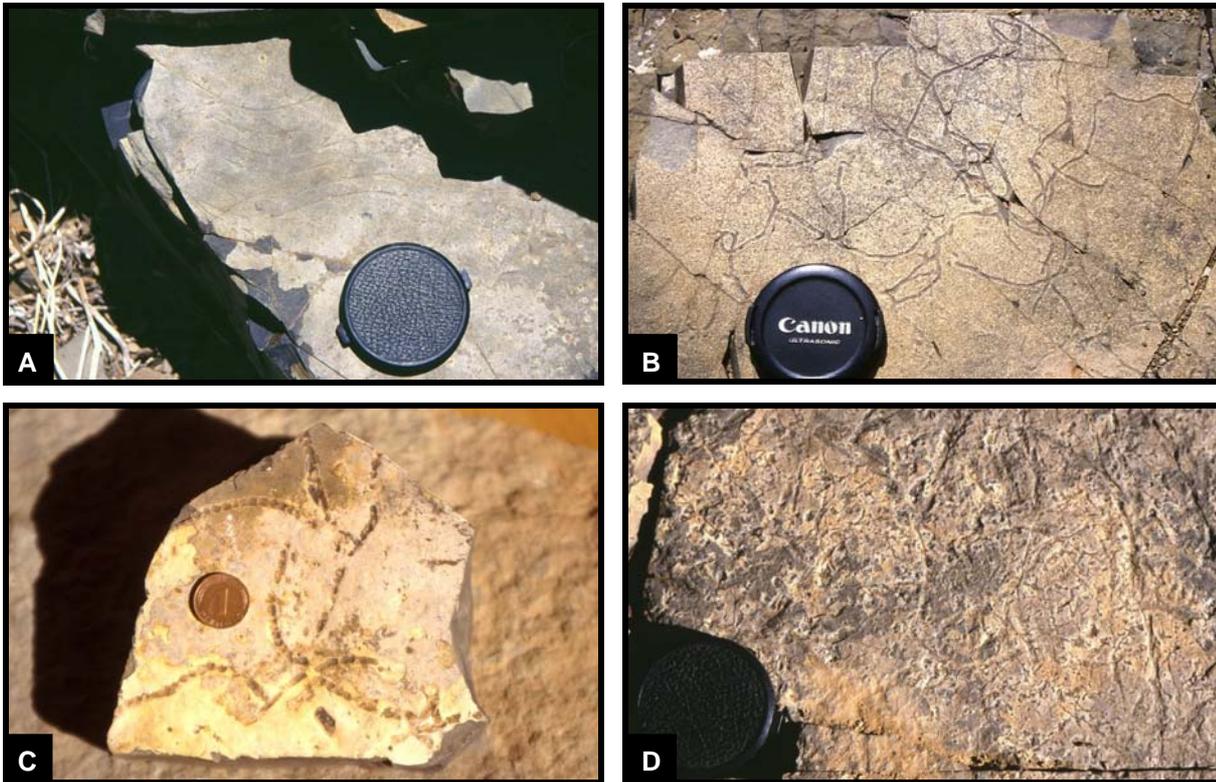
Fig. 3.52: Trace fossils on top surfaces of Collingham tuff layers: **(A)** Six parallel, in-phase sinusoidal, epichnial grooves in a tuff lamina within black, cherty and carbonaceous shales of the basal Collingham Formation. The traces are characteristic for the ichnogenus *Undichna*, interpreted as fin marks of fishes swimming close to a cohesive muddy substrate (Trewin, 2000). **(B)** Broad, shallow, winding and occasionally looped trails, preserved as epichnial grooves in a tuff layer (middle part of Collingham Formation). The trace possibly belongs to the *Helminthopsis-Helminthoidichnites* group. **(C)** Segmented trace showing characteristics of the *Scalarituba-Neonereites* group (lower part of the Collingham Formation). **(D)** Densely bioturbated top surface of a tuff layer from the middle part of the Collingham Formation. The lens caps have a diameter of 6 cm, the coin a diameter of 16.5 mm.
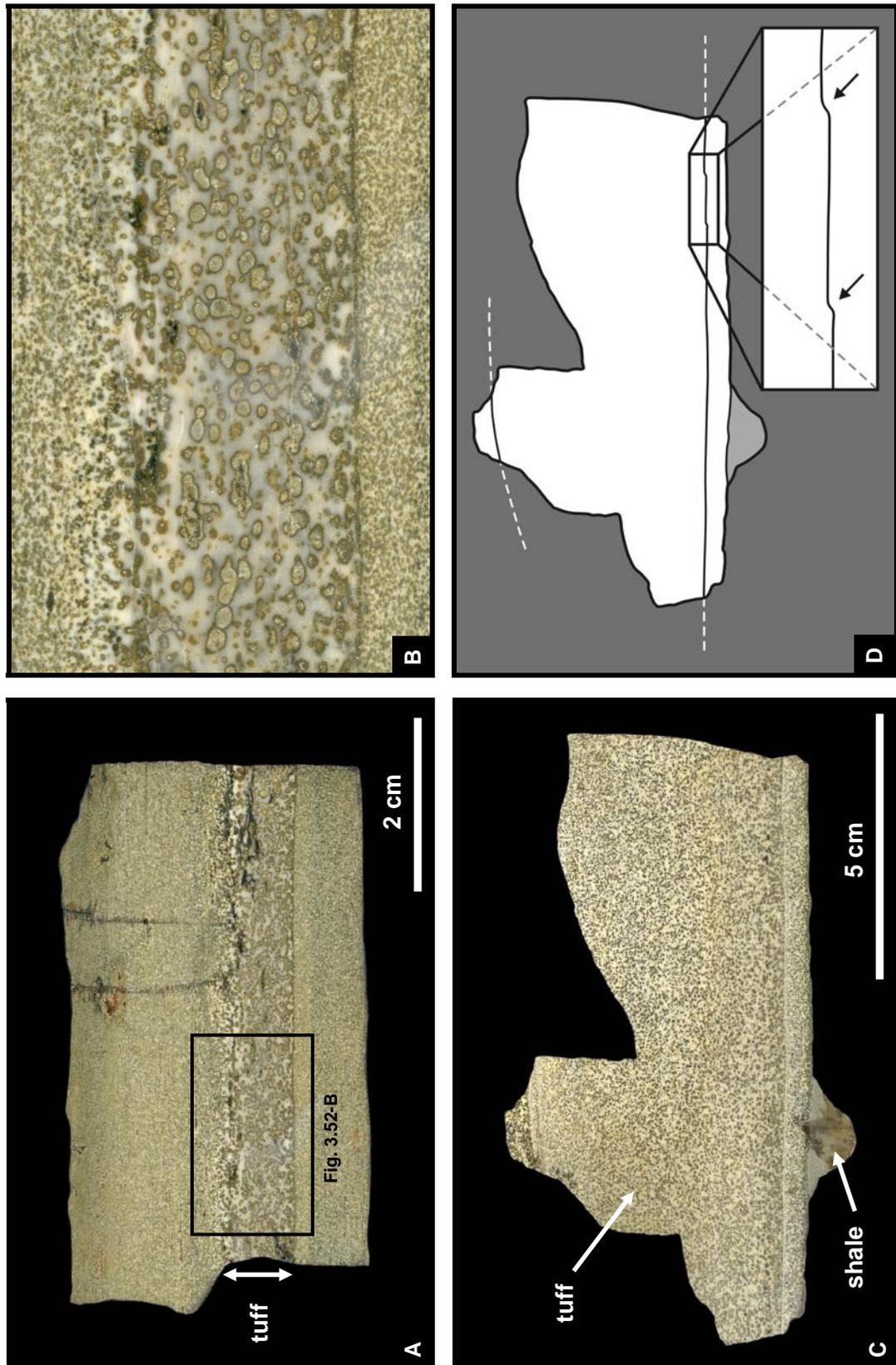
Fig. 3.53: **(A) & (B)** Polished hand specimen of one of the Ufo Valleys-Rhyofontein Tuffs showing a sharp basal and a slightly gradational upper contact. Both the tuff and the enclosing shales are intensively speckled due to contact-metamorphic growth of porphyroblasts (completely pinitized cordierite), however, the size of porphyroblasts is within the tuffs distinctly bigger than in the shales. The size distribution of these porphyroblasts gives the tuffs a normally graded appearance. **(C)** Polished hand specimen of tuff UFO-43 (SHRIMP geochronology sample) composed of three sharp-bounded subunits. The upper bounding surface is somewhat inclined and the lower bounding surface shows step-like erosion features indicated by arrows in the photo interpretation **(D)**.

Fig. 3.54: Nodular concretions within the upper part of a tuff layer 45 m above the base of the Collingham Formation. The shown tuff layer is the only one in the Namibian Collingham Formation, in which such concretions have been observed.
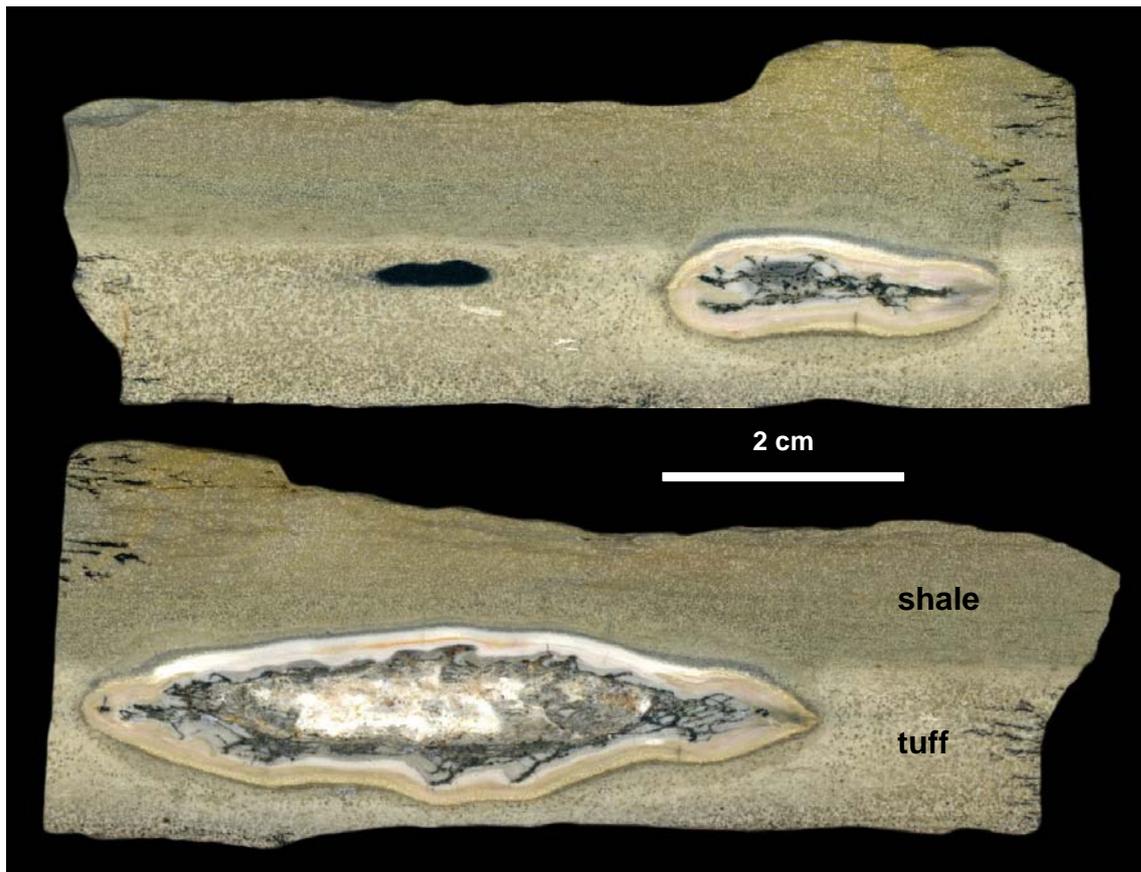
Fig. 3.55: Two polished hand specimen of the Collingham tuff with nodular concretions. The small, black nodule in the upper image consists of carbonate hydroxyl fluorapatite (francolite). The larger concretion exhibits a complex internal structure and due to contact-metamorphism shows an interesting mineral paragenesis consisting of calcite, replaced dolomite(?), prehnite, zeolites (laumontite and heulandite?), grandite-group garnet, chlorite, and probably titanite as well as vesuvianite.

In thin sections the Ufo Valleys Tuffs of the Collingham Formation classify as poorly sorted, moderately crystal-rich and normally graded pyroclastic rocks. As crystal components occur quartz, altered feldspar, relicts of possible former biotite, as well as zircon and apatite. The fine-grained, clay mineral-dominated matrix is distinctly recrystallized due to severe thermal overprinting and is composed of a mosaic of interlocking crystallites (Fig. 3.56-B) mainly composed of illite but quartz and feldspar may also be present. Contact-metamorphism also led to abundant growth of cordierite porphyroblasts, which are now completely pinitized and cause the conspicuous greenish speckling of the tuffs (and the shales).

Crystal fragments of quartz are not very abundant in the Ufo Valleys Tuffs. Most show a typical highly angular to splintery form, which is so characteristic for many tuff layers (Fig. 3.56-A/B). All observed quartz crystals (mainly 50-100 µm) are monocrystalline and show straight extinction. Feldspar crystal fragments seem to have formed a very abundant, major crystal component in the Ufo Valleys Tuffs (Fig. 3.56-C/D) but all supposed feldspar crystals are severely altered. Most of them appear almost completely altered to clay minerals, however, in some cases a mixture of clay mineral flakes (illite/sericite and chlorite) seems to be intergrown in an irregular blocky crystal mosaic of what could be fine-grained replacement feldspar (albitized feldspar?) (cf. Martini, 1974) (Fig. 3.56-E/F). In some cases some faint relict structures of former polysynthetic twinning are visible and it can be speculated that plagioclase was probably also in these tuffs the dominant feldspar type present as juvenile crystal fragments. Many of these altered feldspar crystals are angular to even splintery, others have a more rectangular, lath-shaped form. Their size ranges mainly between 70 and 150 µm, some can also reach a size of up to 300 µm. Often black laminae (completely altered biotite flakes?) are bent around feldspar crystal corners (Fig. 3.56-G/H). No fresh or relictic biotite has been observed in any thin section of the Ufo Valleys Tuffs and also no pseudomorphs of undoubted biotite origin have been detected. However, in thin sections the tuffs appear highly interspersed with countless thin, black streaks and laminae, which give many of the Ufo Valleys Tuffs or parts of individual tuff beds a somewhat wavy and discontinuous but quite distinct horizontal lamination to flaser-like bedding (Fig. 3.56-I). Often these laminae are draped over and bent around other crystal fragments (Fig. 3.56-K). They show typical lengths of about 100-300 µm, some are also continuous for almost 1000 µm. It can be speculated that many of these black laminae might represent completely altered, former biotite flakes. If this is true, this shows that expansion of biotite flakes during alteration, often seen in other tuffs, did not play a dominant role in the case of the Ufo Valleys Tuffs. However, a few crystal booklets, composed of fine-grained sericite/illite, which actually do look similar to expanded and replaced biotite stacks (Fig. 3.56-L/M), are present but they form only a very minor component in the Ufo Valleys Tuffs. A single occurrence of another type of crystal booklets, which look very similar to illitized kaolinite booklets, has been

observed, too (Fig. 3.56-N/O). However, it is not clear if really all the black laminae represent altered biotite flakes, which would actually imply a relatively unusual high biotite content, or if these streaks and laminae could be also derived partially from a former vitric component.

Zircons (20-80 µm) are present in thin sections in fair amounts but many of them appear to be rounded and of xenocrystic origin. Only a lesser amount is present as fragments of euhedral, juvenile crystals of usually squat form (Fig. 3.56-P). Apatites (20-150 µm) are not rare in the Ufo Valleys Tuffs but their abundance is distinctly lower than that of the Eisenstein or Uhabis River Tuff. Almost all the observed apatite crystals are clear and only one apatite crystal of the smokey-grey, zoned type has been observed. Most of the apatite crystals are quite fragmented or etched and euhedral forms are relatively scarce (Fig. 3.56-Q).
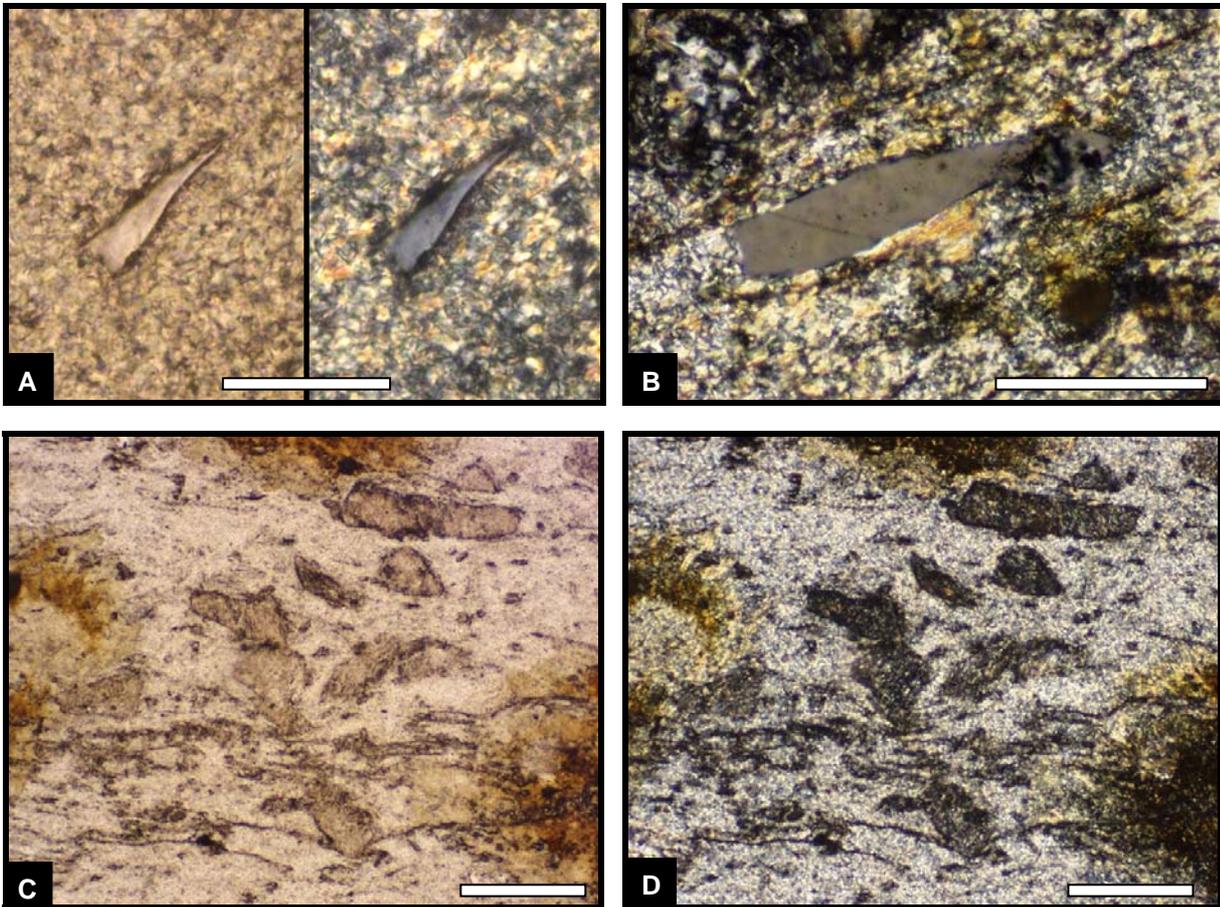
Fig. 3.56: Thin section photographs of the Ufo Valleys Tuffs: **(A) & (B)** Quartz crystals occur within the tuffs mainly as splinter- or thorn-shaped crystal fragments of various sizes. (A) plane-polarized light (left) and crossed polars (right), (B) crossed polars. Scale bar in (A) is 50 µm, in (B) 100 µm. **(C) & (D)** Angular feldspar crystal fragments are very abundant in the tuffs. Due to their strong alteration they often show a slighter darker brown colour compared to the argillaceous matrix and are often surrounded by a black rim. Plane-polarized light (left) and crossed polars (right). Scale bars 100 µm.
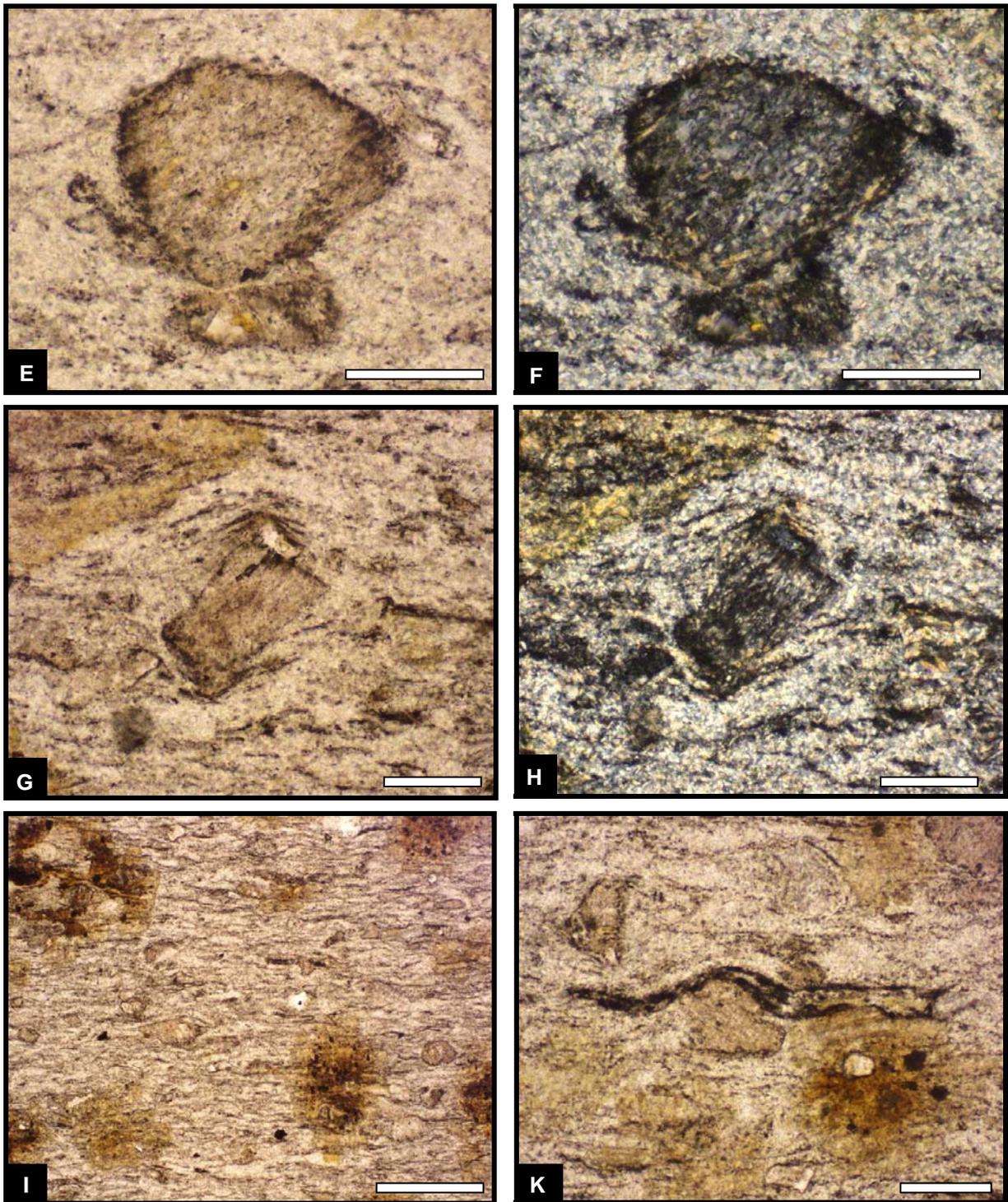
Fig. 3.56: Thin section photographs of the Ufo Valleys Tuffs (cont.): **(E) & (F)** Large feldspar crystal, which is strongly altered to phyllosilicates (illite/sericite and chlorite). These phyllosilicates seem to be enclosed in a mosaic of blocky, fine-grained crystals possibly representing replacement feldspar (albitized plagioclase?). Plane-polarized light (left) and crossed polars (right). Scale bars 100 µm. **(G) & (H)** Black laminae (altered biotite flakes?) are bent around the crystal corners of an altered feldspar grain. Plane-polarized light (left) and crossed polars (right). Scale bars 100 µm. **(I)** Abundant horizontal aligned black streaks and laminae give many tuff layers a wavy, discontinuous lamination or flaser-like bedding. Plane-polarized light. Scale bar 500 µm. **(K)** Black lamina, which certainly represents an altered but not expanded biotite flake. The flake is draped over an altered feldspar crystal due to compaction of the tuff. Plane-polarized light. Scale bar 100 µm.
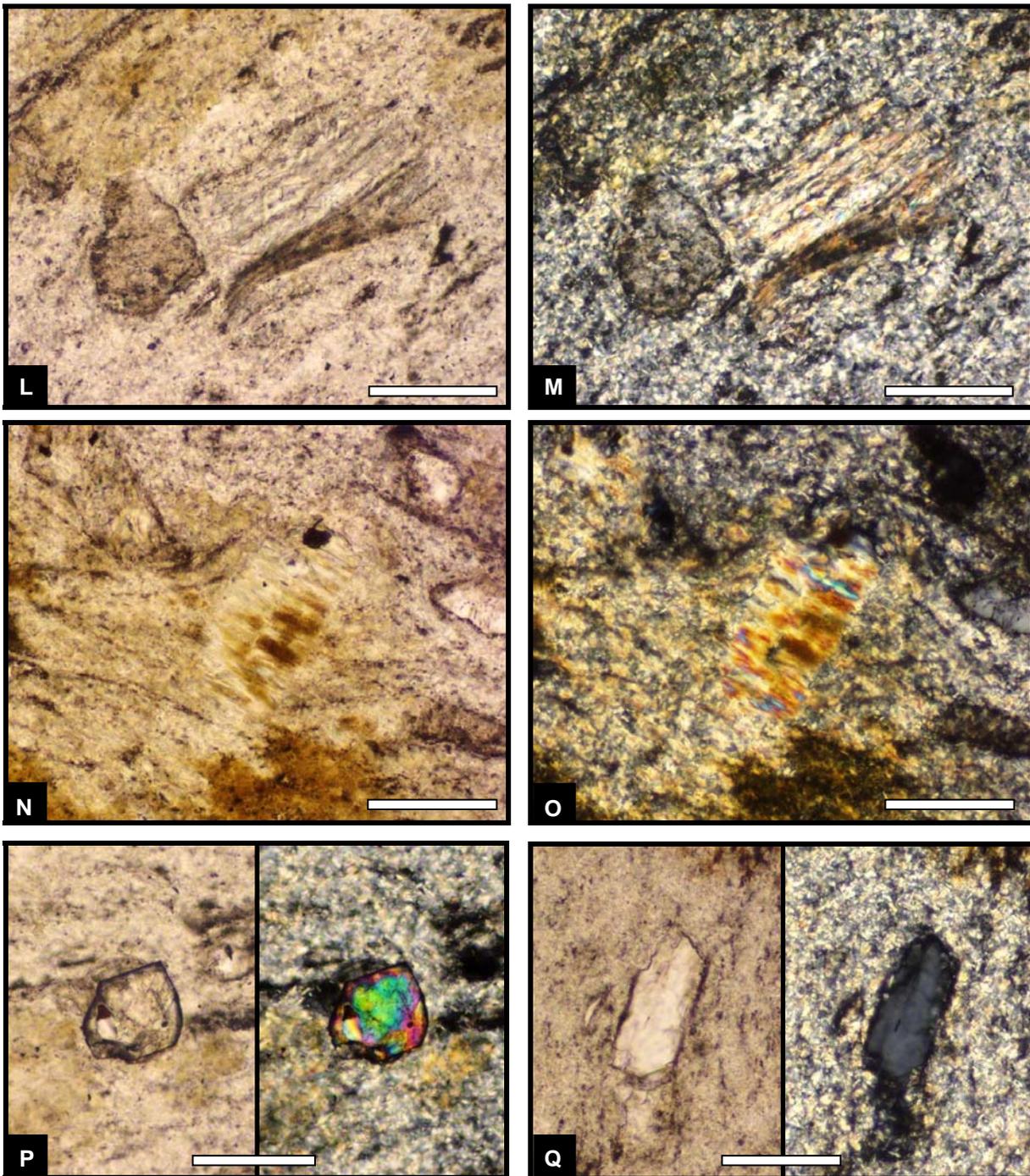
Fig. 3.56: Thin section photographs of the Ufo Valleys Tuffs (cont.): **(L) & (M)** Crystal booklet, which is composed of bright illite crystallites enclosed between dark iron oxide laminae. This type of crystal booklets represents altered and expanded biotite stacks (cf. Fig. 3.47-E/F Panorama Tuff 2 and Fig. 3.26-C/D Korabib Tuffs). Plane-polarized light (left) and crossed polars (right). Scale bars 100 µm. **(N) & (O)** Another type of crystal booklet with a more euhedral appearance but also mainly composed of illite/sericite (bright blue and red interference colours). Such booklets could represent illitized kaolinite booklets, which possibly grew diagenetically as new crystals within the altered tuff matrix without replacement of a precursor biotite (cf. Fig. 3.20-L/M Itzawisis Tuffs). Plane-polarized light (left) and crossed polars (right). Scale bars 100 µm. **(P)** Fragment of a large, euhedral zircon crystal. Plane-polarized light (left) and crossed polars (right). Scale bars 100 µm. **(Q)** Longitudinal section of a fragmented and/or etched apatite crystal. Plane-polarized light (left) and crossed polars (right). Scale bars 100 µm.

Within the Ufo Valleys Tuffs the porphyroblasts show dominantly spherical to ellipsoidal and ovoid forms, however, a few exhibit partly a hexagonal outline hinting at their cordierite origin (Fig. 3.57-A). Originally these porphyroblasts consisted of cordierite, which grew during thermal overprinting of the rocks by widespread Jurassic dolerite intrusions, but in the course of retrograde cooling these cordierites were completely altered to pinite, a fine-grained chlorite- and illite-dominated mixture. The size of the porphyroblasts ranges in the Ufo Valleys Tuff mainly between 300 and 600 µm. Similar to pinitized cordierite porphyroblasts in other investigated tuffs they often consist also in the Ufo Valleys Tuffs of a large, darker coloured, yellowish-brown central part, which is surrounded by a narrow, lighter coloured, greenish-yellowish margin (Fig. 3.57-A). In some cases this boundary is marked by a dark brown rim or by a circle of dark brown iron oxide inclusions (Fig. 3.57-B & E). The marginal parts always appear micro- to cryptocrystalline, whereas the inner parts appear either very fine-grained or show a strongly parallel oriented lamellar structure (Fig. 3.57-C/D & L/M). These lamellae most probably represent the relicts of polysynthetically twinned cordierite and they are also very characteristic for the porphyroblasts of the Uhabis River Tuff. The lamellar areas of the pinitized porphyroblasts are partly composed of iron oxide stained chloritic parts and partly of light coloured illitic/sericitic parts, the latter being characterized by bright blue, green and red interference colours (Fig. 3.57-M). A few porphyroblasts contain within their micro- to cryptocrystalline central area also a conspicuous, irregular formed aggregate of coarser grained chlorite crystals displaying yellowish-brown to bluish-grey interference colours (Fig. 3.57-E/F). Almost all porphyroblasts contain inclusions of dark brown, almost opaque aggregates (50-120 µm) of minute crystallites or particles, which form mainly roundish to irregular and in rare cases haxagonal objects (Fig. 3.57-G/H). The hexagonal outline of some of these aggregates implies that they might be dominantly composed of hematite but also titanium minerals like titanite or rutile could be constituents of these aggregates. In one case a fragment of a euhedral titanite crystal was observed enclosed within a porphyroblast, however, this seems to be a primary juvenile or xenocrystic component of the tuff. (Fig. 3.57-I). Also only one porphyroblast was observed, which contains a trail of tiny rutile crystals of supposedly contactmetamorphic origin (Fig. 3.57-L/M). Such newly formed rutile crystals within pinitized cordierite porphyroblasts are for example very common in the Uhabis River Tuffs. Quite frequently bright yellowish-brown pleochroitic halos were detected within the porphyroblasts of the Ufo Valleys Tuffs. These halos develop around greyish crystals (10-20 µm), which have a strongly altered appearance. These crystals often display a roughly spherical (cubic?) outline and are mounted by tiny, dark brown knobs (Fig. 3.57-K). The nature of these obviously radioactive minerals is not revealed. At least the majority of juvenile zircon inclusions do not cause visible radiation damage within the pinitic matrix of the porphyroblasts.
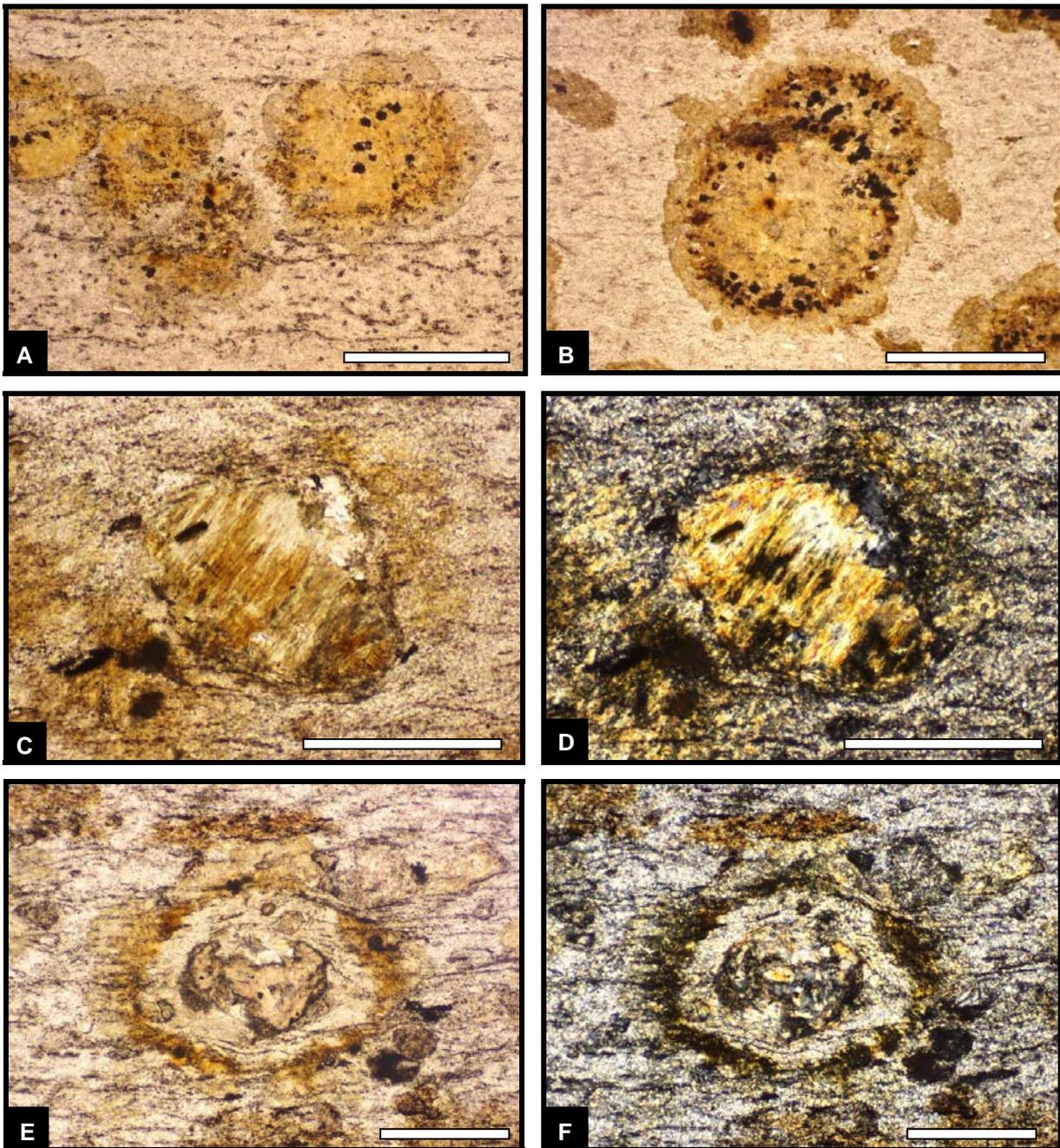
Fig. 3.57: Thin section photographs of pinitized cordierite porphyroblasts in the Ufo Valleys Tuffs: **(A)** Few of the porphyroblasts show a partly hexagonal outline (right margin of right porphyroblast) hinting at cordierite as the original, contact-metamorphically grown mineral. Most specimens consist of a darker coloured central part, which is surrounded by a lighter coloured margin. Plane-polarized light. Scale bar 500 µm. **(B)** Porphyroblast with a circular inclusion of brownish iron oxide particles along the core-margin contact. Plane-polarized light. Scale bar 500 µm. **(C) & (D)** Porphyroblast with a lamellar internal structure most probably inherited from multilamellar twinning of the original cordierite. Plane-polarized light (left) and crossed polars (right). Scale bars 500 µm. **(E) & (F)** Some of the porphyroblasts contain in their central part an irregular shaped area consisting of coarse-grained chlorite aggregates, whereas the remaining part is composed of crypto- to microcrystalline pinite (mainly chlorite-illite mixture). Plane-polarized light (left) and crossed polars (right). Scale bars 250 µm.
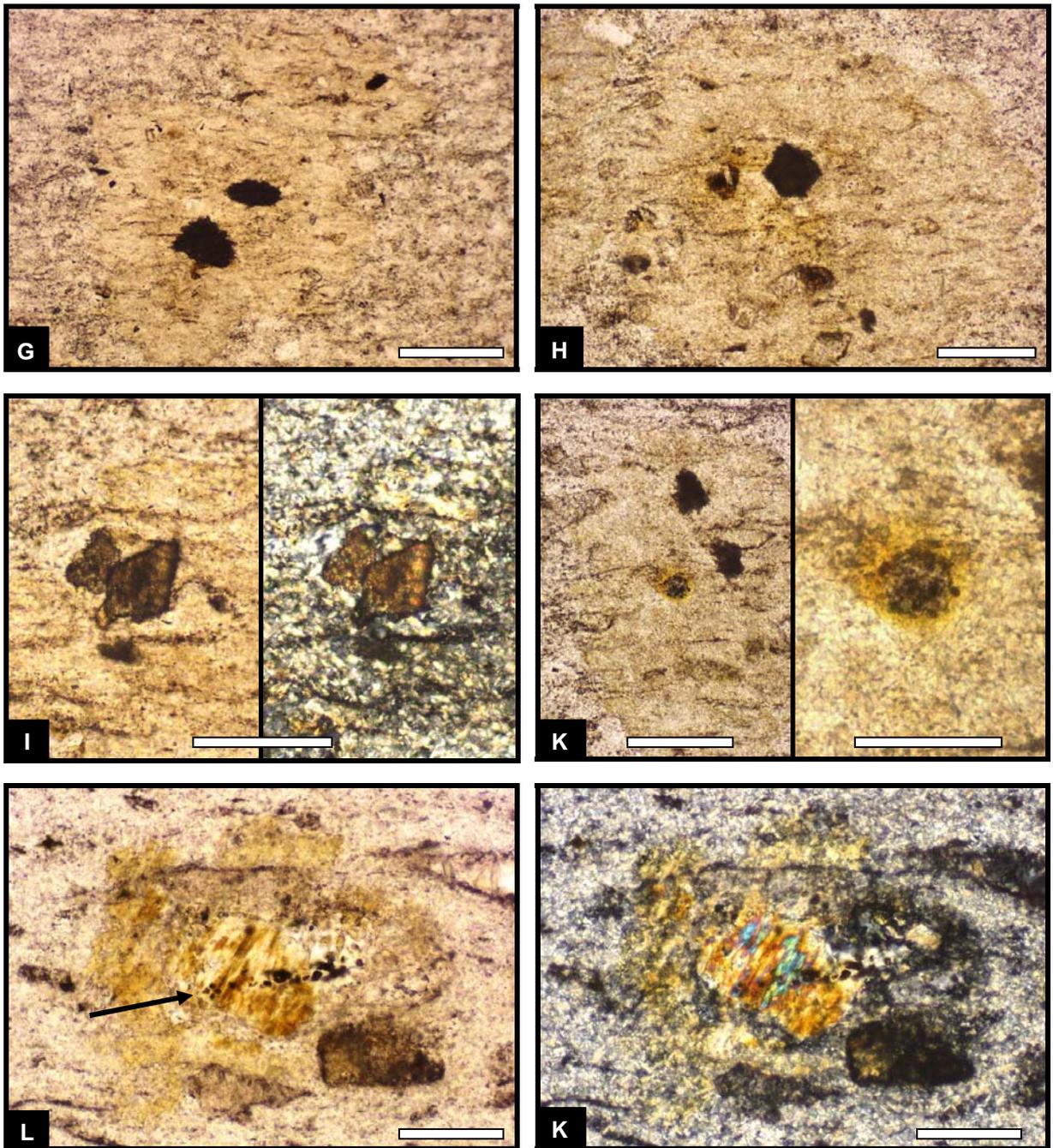
Fig. 3.57: Thin section photographs of pinitized cordierite porphyroblasts in the Ufo Valleys Tuffs (cont.): **(G) & (H)** Almost all porphyroblasts contain inclusions of dark brown to near opaque aggregates composed of minute crystallites or particles. Some of these aggregates display a hexgonal outline (G). These aggregates are possibly mainly composed of iron oxides and oxyhydrates but also titanium-bearing minerals like rutile or titanite may be present. Both pictures in plane-polarized light. Scale bars 100 μm. **(I)** Fragment of an euhedral titanite crystal enclosed by a porphyroblast and probably representing a primary juvenile or xenocrystic component of the tuff. Plane-polarized light (left) and crossed polars (right). Scale bar 100 μm. **(K)** Pleochroitic halo within a porphyroblast developed around a roughly spherical, greyish mineral of unknown origin. Under higher magnification this mineral has a rather altered appearance and is mounted with tiny dark brown knobs. Plane-polarized light. Scale bars 50 (left) and 25 (right) μm. **(L) & (M)** Porphyroblast with a lamellar internal structure containing a trail of small rutile crystals (arrow). This type of secondary rutile within porphyroblastic areas has been rarely observed in the Ufo Valleys Tuffs but is a very common feature in the Uhabis River Tuffs (cf. Fig. 3.33-L/M). Plane-polarized light (left) and crossed polars (right). Scale bars 100 μm.

The larger, lighter coloured concretions at the tuff-shale boundary c. 45 m above the base of the Collingham Formation (Fig. 3.54 & 3.55) reveal in thin sections a diverse and interesting mineralogical composition. These nodules consist of a marginal area, which is built up by several skin-like layers, however, due to their microcrystalline nature their mineralogical composition is unknown. These outer layers surround the larger inner part of the concretions, whose mineralogical composition can be studied very well in thin sections due to their macro-crystalline nature. The most conspicuous constituent is prehnite because of its bright second order interference colours under crossed polars (Fig. 3.58-A/B). Prehnite covers large areas and is present as columnar masses often forming fan-shaped crystal arrangements. Also very typical for prehnite is that individual crystals are frequently assembled in a parquet-like fashion to form a large composite crystal (Fig. 3.58-C). Calcite is another important mineral phase within the concretions. It often shows characteristic sets of deformation twins (Fig. 3.58-D) and not seldom calcite contains inclusions of the zeolite laumontite (Fig. 3.58-B).

Zeolites form essential constituents of the concretions but exact determination of individual zeolite minerals by optical mineralogy is in many cases somewhat ambiguous due to their similar optical properties and often requires support by XRD techniques. However, in this case, the identification of at least two zeolites appears not too speculative. The presence of zeolites in the concretions was primarily recognized by their extreme low (negative) relief due to their very low refractive indices (<1.55). One of the zeolites shows two characteristics, which strongly indicate laumontite as the present mineral. Firstly, this zeolite shows pale yellowish-grey to stramineous interference colours (Fig. 3.58-E/F) assigning it to the higher birefringent (>0.010) group of zeolites. Secondly, it shows several sets of perfect to good cleavages, two of them intersecting at angles of somewhat more than 50° (and ~130°), resembling those of amphiboles (Fig. 3.58-F). The sign of elongation is positive (length slow) and extinction is inclined. Fig. 3.58-E shows that this zeolite forms relatively large single crystals, which enclose other minerals in a manner similar to poikilotopic calcite. The aforementioned properties are characterisitc for laumontite and only phillipsite has very similar properties but according to its slightly lower birefringence it seems more probably that the mineral in question represents laumontite. The other zeolite shows greyish-black to light grey interference colours indicating its relatively low birefringence (~0.005) (Fig. 3.58-H to K). It occurs within the concretions mainly in two forms. Most form granular, pavement-like mosaics of anhedral crystals (e.g. Fig. 3.58-L) but very characteristic for this zeolite is also its occurrence as individual, euhedral, rhomb-shaped crystals (Fig. 3.58-H to M). Many of these rhomb-shaped crystals show either a concentric zonation (Fig. 3.58-H/I) or a sector zonation with sectors of variable extinction and the most distinctive sector boundary parallel to the long diagonal of the rhomb (Fig. 3.58-K to M). At first sight these crystals resemble zoned chabasite rhombohedrons (see for example Pichler & Riegraf (1993), Fig. 88), however,

chabasite rhombohedrons have generally a near-cubic form and show symmetric extinction, whereas the mineral in question shows inclined extinction. Of the zeolites showing pseudorhombic crystal forms heulandite appears to be the most compatible zeolite mineral with the aforementioned optical properties.

Another major component of the concretions is formed by dark coloured areas, which are composed of a mosaic of relatively coarse-grained crystals. The coarse-grained granular texture of these areas is best visible under crossed polars with an inserted gypsum plate (Fig. 3.58-N to P). The dark colouration is caused by an intensive staining of these crystals with a blackish-grey pigment giving the crystals a dusty appearance. Individual crystals display in several cases rhombohedral outlines (Fig. 3.58-Q to S). It can be speculated that these crystals originally represented dolomite but were replaced during contactmetamorphic-hydrothermal overprinting by another mineral or minerals. The blackish pigment might hint at an originally ferroan and/or manganesian dolomite. The dark, pigmented crystals are now composed predominantly of a (silicate) mineral, which shows low order interference colours, mainly first order shades of grey but in some cases also displaying very pale yellowish hues (zeolite?, quartz?) (Fig. 3.58-O). Many of these crystals are also composed of a very low birefringent mineral with blackish-grey interference colours similar to those of heulandite. In rare cases these rhombohedral crystals behave isotropic (replaced by garnet?). A common feature of these possibly replaced dolomite crystals is that the replacement crystals are strongly corroded at their margins and these corroded areas are again replaced by prehnite (Fig. 3.58-Q/S).

A further major component is represented by a colourless mineral (in thin sections in plane-polarized light) with an extremely high relief, even against calcite, in which it occurs as inclusions (but not exclusively). Therefore this mineral must have an extremely high refractive index (>1.7). Since this mineral appears mainly black under crossed polars, i.e. behaves isotropic, this mineral can only be garnet. This garnet forms in the concretions mainly very irregular-shaped, often elongate crystals, which have a strongly poikiloblastic to even skeletal appearance and often exhibit highly ragged grain margins (Fig. 3.58-T/U). Another peculiar feature of these garnet crystals is their partly anomalously birefringent, anisotropic behaviour, which is expressed by the clear brightening of crystal subregions (Fig. 3.58-U) or even the whole crystal under crossed polars. This anomalously birefringent behaviour is quite characteristic for grossular and andradite (grandite group garnets), which typically occur in metamorphosed carbonate-bearing rocks (Nesse, 2000). Often these garnets show in thin sections alteration rims, the optical properties of which strongly deviate from the central part of the garnet (Fig. 3.58-V/W).

Chlorite is found in larger quantities especially towards the more marginal parts of the concretions and is clearly associated with zeolite-rich areas. It often forms conspicuous,

spherical, radially grown crystal aggregates of a greenish-yellowish to light brownish colour (Fig. 3.58-X/Y) but smaller crystal flakes are also abundantly interspersed in the marginal zeolitic areas (Fig. 3.58-AA/AC). Under crossed polars these chlorites exhibit both bluish-grey and yellowish interference colours (Fig. 3.58-F, H & Y), the sign of elongation is positive (length slow) and therefore the optical character of these chlorites is negative.

A common accessory mineral, which has been observed in thin sections of the concretions, forms small, up to 100 µm long, euhedral to subhedral, colourless to dirty brownish crystals. Their forms vary from wedge-shaped or blade-like, pointed rhombs to slender bipyramids (Fig. 3.58-Z to AB). They are further characterized by their very high positive relief. Under crossed polars these crystals display higher order interference colours, which are paler than those of zircon but still relatively bright and distinguishable from the high order near-white of carbonates (Fig. 3.58-Z to AB). Most of these crystals show near-parallel extinction, some appear to have a slightly inclined extinction. The form of the crystals and their optical properties indicate titanite as the mineral in question. Furthermore, titanite is not an uncommon mineral phase in calcareous, respectively calc-silicate rocks. The relatively bright interference colours are not typical for titanite but might be caused by the smallness of the crystals.

Finally, a very rare accessory is represented by a mineral, the most characteristic property of which is its anomalous blue interference colour. In one case this mineral has been observed as a small, c. 40 µm long, euhedral, short-prismatic crystal with well-developed pyramidal tips (Fig. 5-58-AC). It has only been found intergrown in zeolites against which it shows a strong positive relief. However, this just indicates that this mineral must have at least a moderately high refractive index. Extinction is parallel however it appears incomplete with a moderately deep grey as the darkest interference colour in N-S and E-W orientation. If the mineral is oriented NW-SE or NE-SW under crossed polars it displays a conspicuous, anomalous deep blue glowing-like colour. The sign of elongation is negative. According to the crystal form and the optical properties this mineral could well represent vesuvianite (ditetragonal-bipyramidal), which is also commonly found in metamorphosed calcareous rocks.
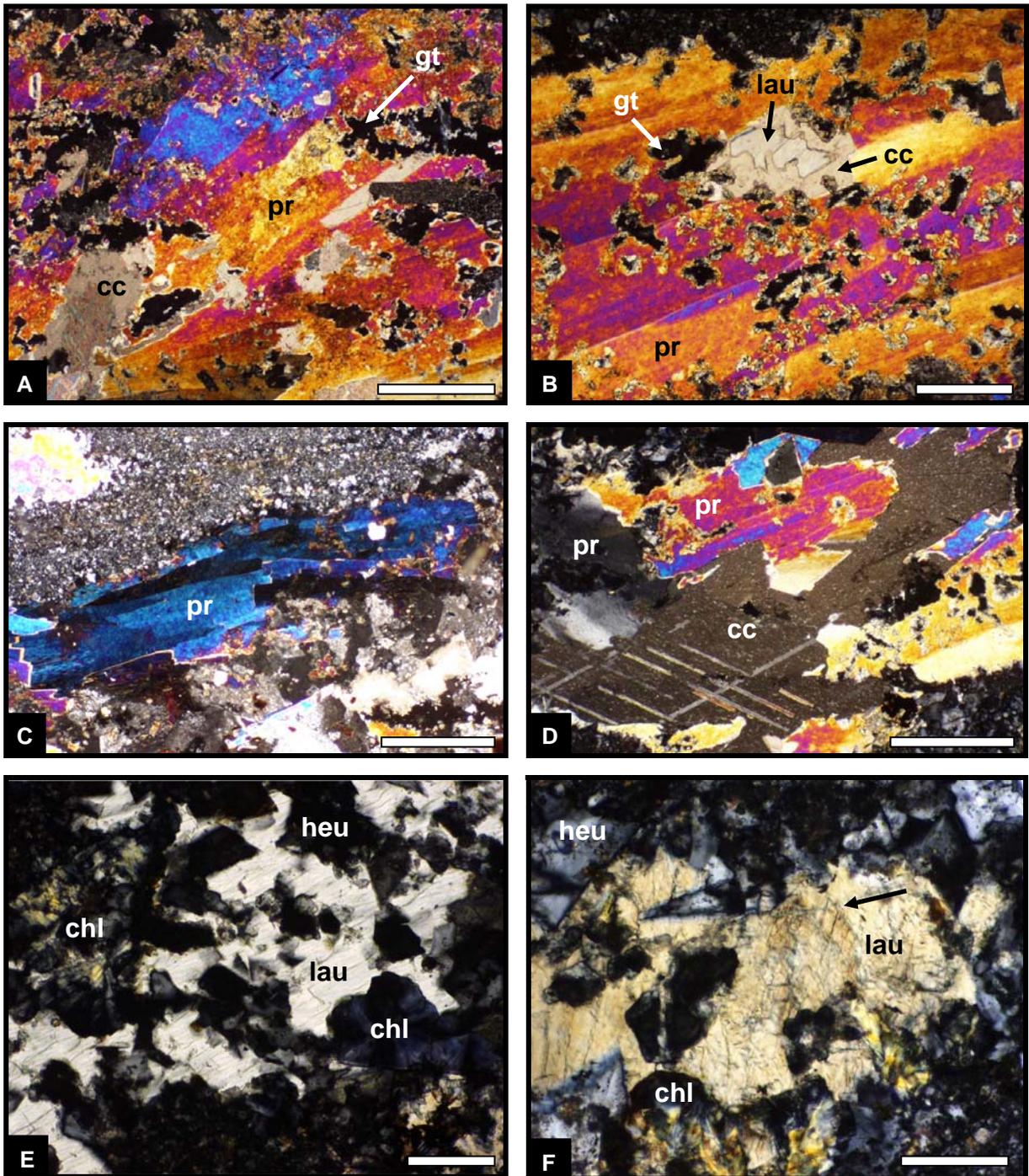
Fig. 3.58: Thin section photographs of a diagenetic concretion in a tuff of the Namibian Collingham Formation: **(A)** Prehnite (pr) crystals arranged in a fan-shaped fashion and showing bright second order interference colours. It is intergrown with calcite (cc) and garnet (gt). Crossed polars. Scale bar 500 µm. **(B)** Prehnite surrounding an inclusion of calcite, which itself contains laumontite (lau) as an inclusion. Numerous inclusions of garnet are present within prehnite. Crossed polars. Scale bar 250 µm. **(C)** Individual prehnite crystals are intergrown in a typical parquet-like fashion forming a large composite crystal. Crossed polars. Scale bar 500 µm. **(D)** Prehnite intergrown with calcite showing two sets of deformation twins. Crossed polars. Scale bar 500 µm. **(E)** A large, single laumontite crystal encloses numerous smaller heulandite (heu) crystals and chlorite (chl) crystal aggregates in a poikilotopic fashion. Crossed polars. Scale bar 100 µm. **(F)** Laumontite showing two sets of perfect cleavages intersecting at an angle slightly more than 50°. Note the yellowish-brown, stramineous interference colours. Heulandite in the upper part of the image displays first order blackish-grey interference colours, chlorite in the lower part displays bluish-grey and yellowish interference colours. Crossed polars. Scale bar 100 µm.
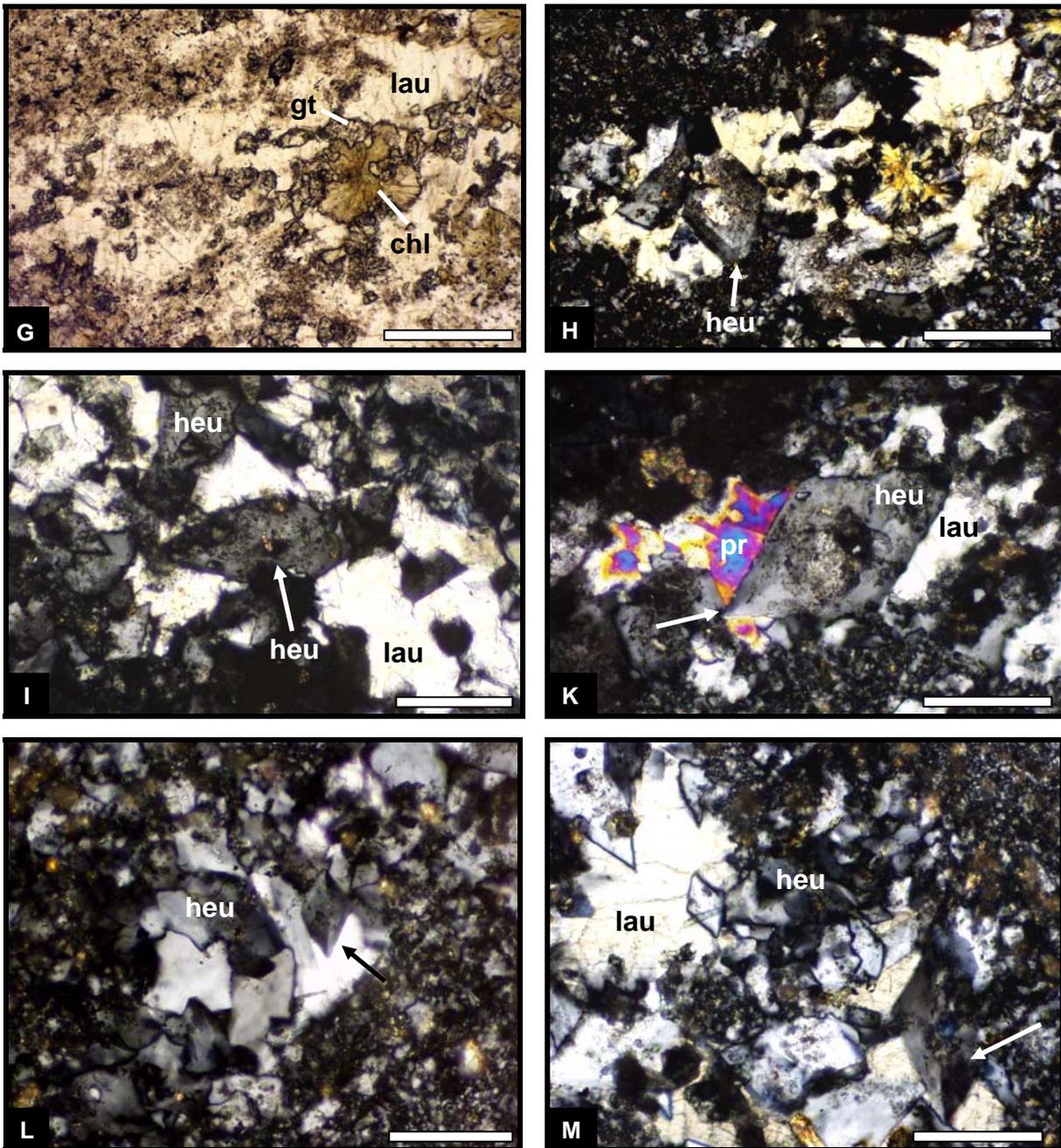
Fig. 3.58: Thin section photographs of a diagenetic concretion in a tuff of the Namibian Collingham Formation (cont.): **(G) & (H)** Rhomb-shaped heulandite crystal showing a concentric zonation (arrow). Note the missing relief against laumontite in (G) due to similar, low (zeolitic) refractive indices. Plane-polarized light (left) and crossed polars (right). Scale bars 250 µm. **(I)** Rhomb-shaped, concentrically zoned heulandite crystal (arrow) intergrown with laumontite. Crossed polars. Scale bar 100 µm. **(K) & (L) & (M)** Rhomb-shaped heulandite crystals showing sector zoning (arrows). A sharp sector boundary is developed along the long diagonal of the rhomb, whereas the perpendicular sector boundary (short diagonal) is developed quite diffusely. Apart from rhomb-shaped single crystals heulandite forms mainly granular, pavement-like mosaics of anhedral crystals. All images under crossed polars. Scale bars 100 µm.
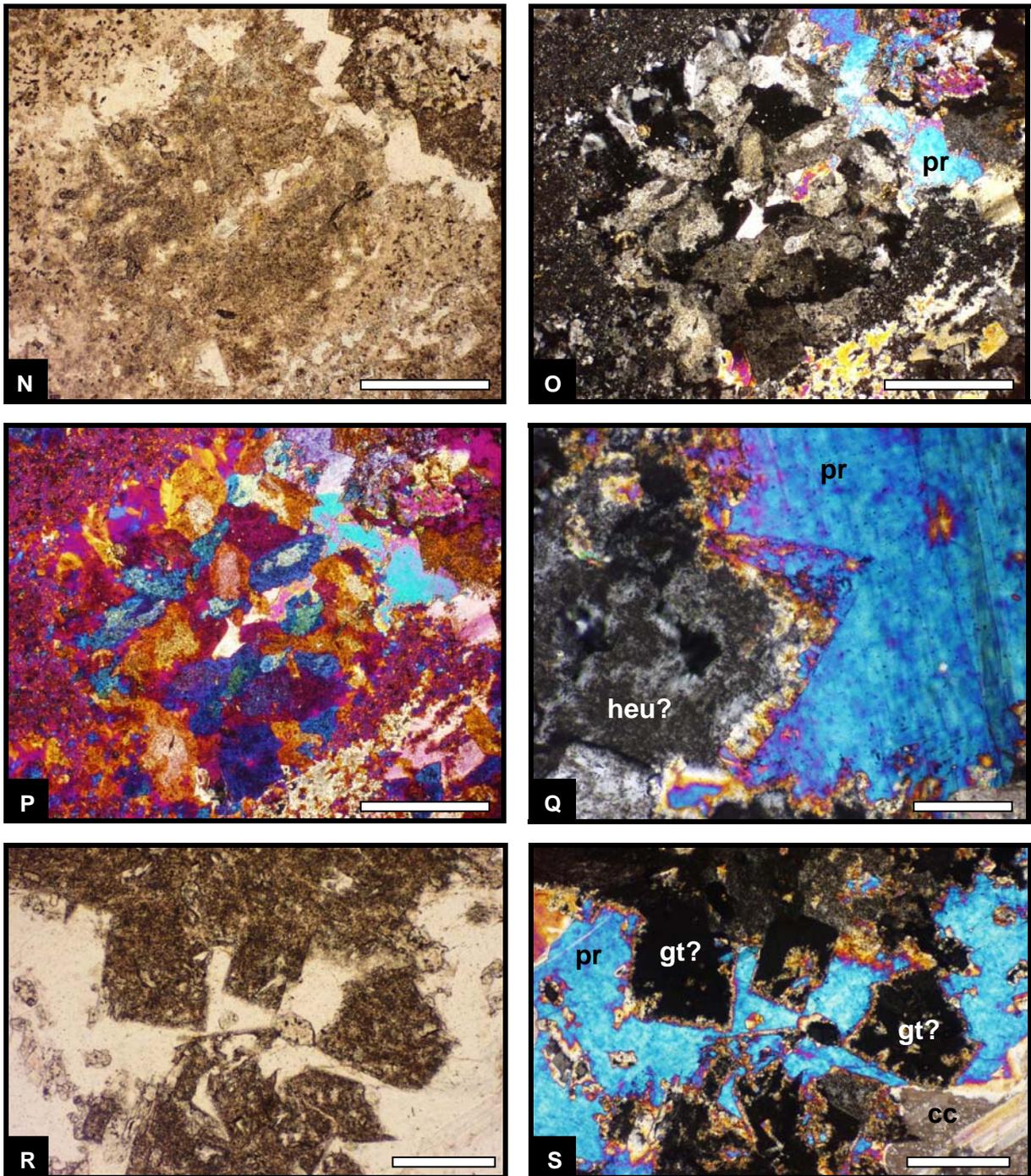
Fig. 3.58: Thin section photographs of a diagenetic concretion in a tuff of the Namibian Collingham Formation (cont.): **(N) & (O) & (P)** Large, dark coloured area consisting of a coarse-grained crystal mosaic in which the crystals are intensively stained with a blackish-grey pigment. Originally these crystals might have been composed of dolomite but are now replaced by other mineral phases (zeolites?, quartz?, garnet?). Plane-polarized light (N), crossed polars (O) and crossed polars with inserted gypsum plate (P). Scale bars 500 μm. **(Q)** Rhomb-shaped crystal outline of possibly originally dolomite now replaced by heulandite(?). The marginal area of the replaced crystal is strongly corroded and is replaced again by prehnite. Crossed polars. Scale bar 100 μm. **(R) & (S)** Several rhomb-shaped crystals of probable former dolomite. Due to the intensive staining with a blackish-grey pigment the original dolomite was possibly iron- and/or manganese-rich. In this case the crytals are replaced by an isotropic mineral (garnet?) but show also the strong marginal corrosion and replacement by prehnite. Plane-polarized light (left) and crossed polars (right). Scale bars 250 μm.
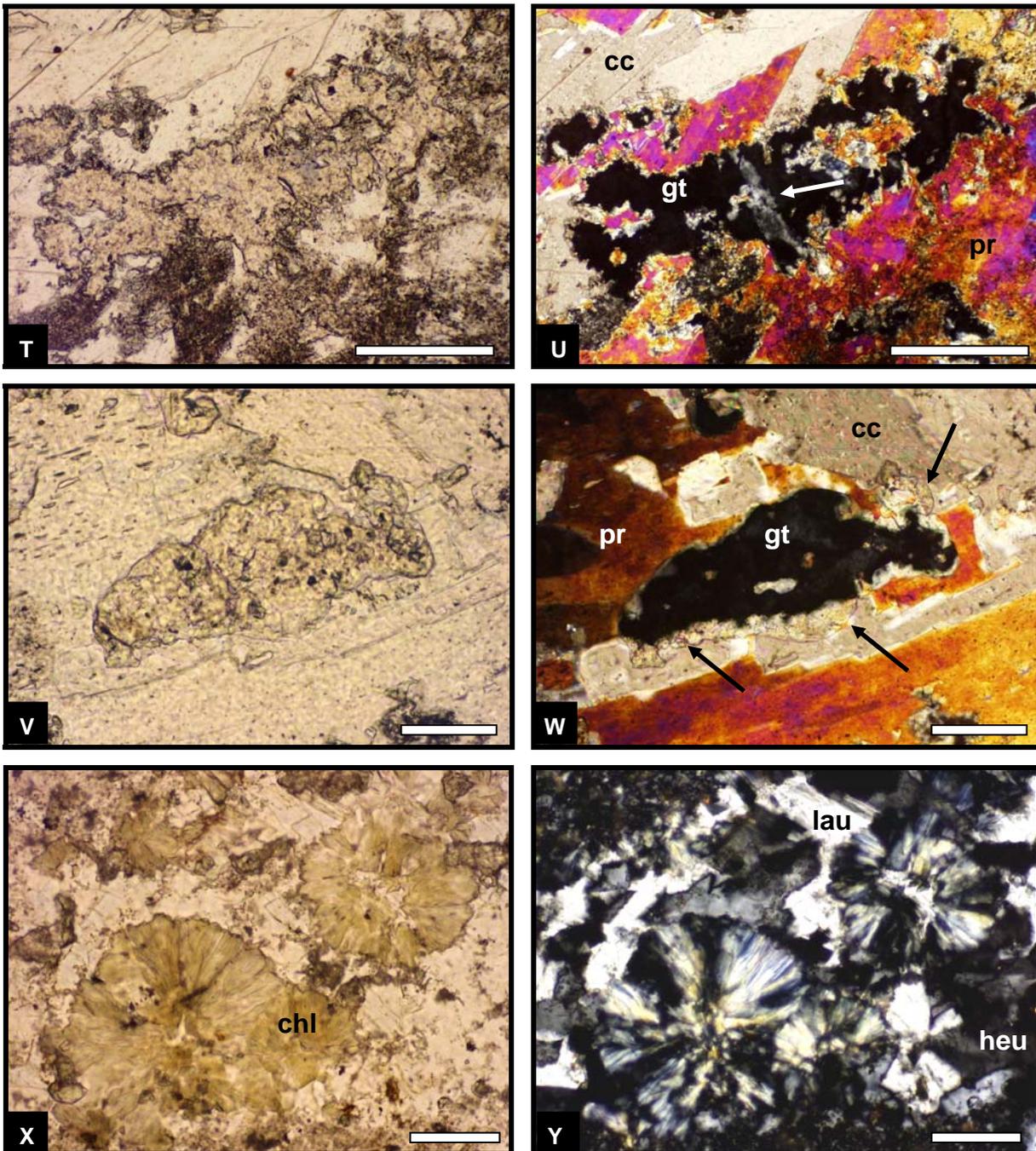
Fig. 3.58: Thin section photographs of a diagenetic concretion in a tuff of the Namibian Collingham Formation (cont.): **(T) & (U)** Elongate, irregular-shaped garnet crystal(s) with highly ragged crystal margins and a skeletal appearance. These garnet crystals behave partly anomalously birefringent expressed by the clear brightening of crystal subregions (arrow). This is a common observation in grandite-group garnets. Plane-polarized light (left) and crossed polars (right). Scale bars 250 µm. **(V) & (W)** Elongate, anhedral garnet crystal, which shows strong corrosion and alteration phenomena at its margin (arrows). The optical behaviour of parts of the rim strongly deviates from those of the central, isotropic part. Plane-polarized light (left) and crossed polars (right). Scale bars 100 µm. **(X) & (Y)** Spherical chlorite aggregates of radially grown crystals surrounded by zeolites. Plane-polarized light (left) and crossed polars (right). Scale bars 100 µm.
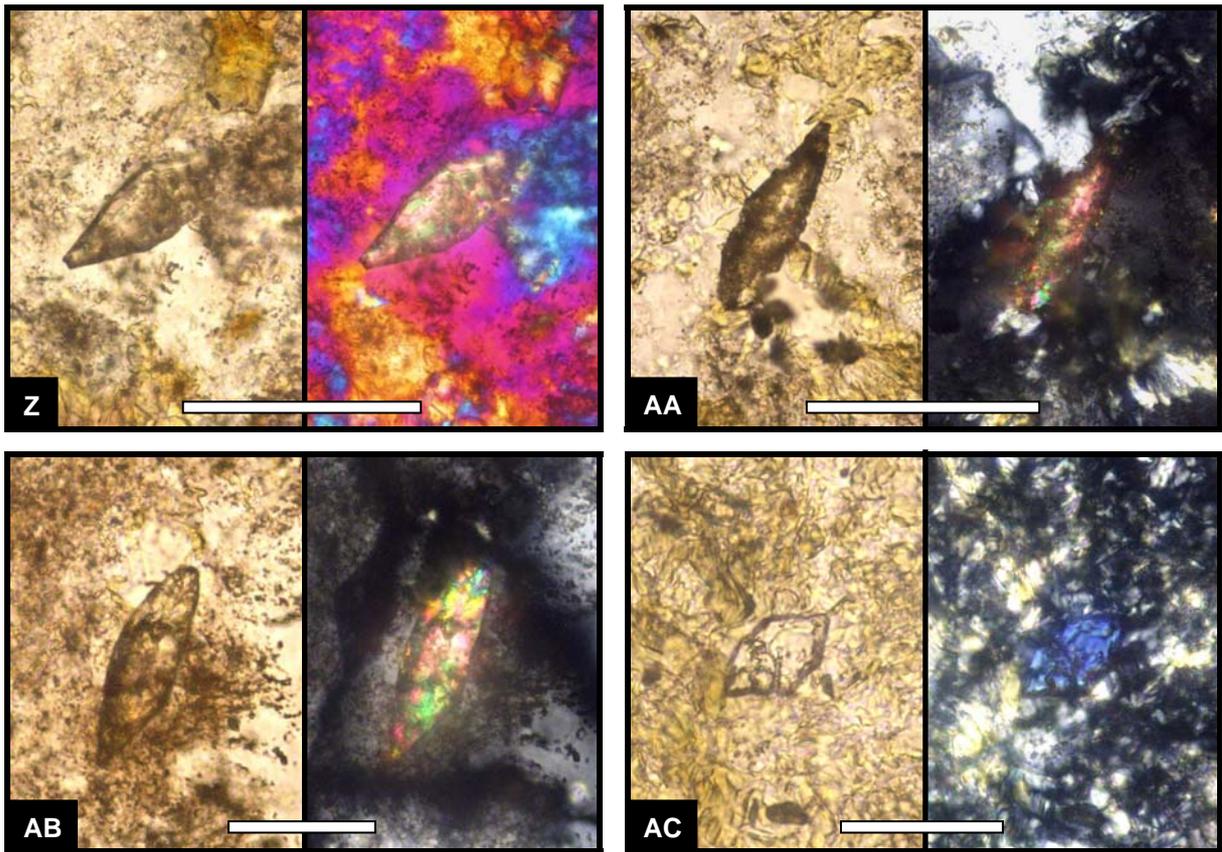
Fig. 3.58: Thin section photographs of a diagenetic concretion in a tuff of the Namibian Collingham Formation (cont.): **(Z) & (AA) & (AB)** Euhedral to subhedral crystals of an accessory mineral, which most probably represents titanite. Each photo in plane-polarized light (left) and under crossed polars (right). Scale bars 100 µm for (Z) & (AA) and 50 µm for (AB). **(AC)** Euhedral crystal of a rare, accessory mineral, which shows under crossed polars in NW-SE and NE-SW orientation a conspicuous, anomalous deep blue glowing-like interference colour. According to the crystal form and the optical properties this mineral could well represent ditetragonal-bipyramidal vesuvianite. Plane-polarized light (left) and crossed polars (right). Scale bar 100 µm.

Contact-metamorphism affecting carbonate nodules were also described by Hanekom (1962). Near Insizwa (Eastern Cape Province) a c. 1000 m thick dolerite sill intruded the basal shales of the Beaufort Group converting them at the contact into a hornfels, which is composed of quartz, orthoclase, biotite and plagioclase. Due to the contact-metamorphic effects the former calcareous nodules display concentric shells of a spectacular and rich variety of minerals. Minerals occuring are grandite-group garnet, wollastonite, quartz, hyalite, calcite, prehnite, titanite, diopsidic clinopyroxene, apophyllite, fluorite, apatite, vesuvianite, anorthite, epidote-group minerals, zeolites, wavellite, chlorite, actinolite, magnetite, hematite, chalcopyrite, and sphalerite. According to the reaction of quartz and calcite to wollastonite and CO_2, which is dependant on pressure and temperature as well as X_{CO_2}, the temperature at the shale-dolerite contact was estimated to be in the order of about 800°C. Prehnite, grossularite and calcite have also been reported by Barrett (1969) in hornfelses of the Upper Permian Buckley Formation in the Beardmore Glacier area of Antarctica.

The Sesfontein Tuff

This tuff layer, which was discovered in southern Namibia in the highest stratigraphic level, is positioned within argillaceous sediments of the Aussenkjer Formation, stratigraphically c. 110 m above the top of the Collingham Formation (Fig. 3.59). Only one outcrop has been found and this outcrop lies in the lower parts of the smooth and low to moderate gradient pediment surfaces (forming the outcrops of the Aussenkjer Formation) east of the steep-sided Amibberg sandstone massif (Amibberg Formation) and west of the rugged and incised terrane of the Ufo Valleys (comprising the outcrop successions of the Whitehill and Collingham Formations as well as interlayerd dolerite sheets). This outcrop can be reached via a jeep track that runs approximately in a NNE-SSW direction just above the head areas of the Ufo Valleys (Fig. 3.49). Leave this jeep track in the vicinity of a small vegetated spot, called Sesfontein, and head eastward in uphill direction towards a small but conspicuous hill, which is topped by a silicified, very localized sandstone above a laterally much more continuous, tempestitic mud pebble layer (Fig. 3.59). The outcrop of the Sesfontein Tuff can be found a few tens of metres north of the sandstone-topped hill and is characterized by a conspicuous greyish-white outcrop surface, formed by a thin tuff lamina, within dark olive-grey to brownish shales. Due to the small thickness of this layer (~1 mm) no thin sections were made and the pyroclastic nature of this rock is not definetly proven, however, since it looks exactly like the tuff laminae in the lower part of the underlying Collingham Formation there is little doubt about its volcanogenic origin. The tuff layer is also intensively traversed by trace fossils and mainly two types have been detected. One type represents arthropod trackways of the *Umfolozia sinuosa* ichnospecies (Savage, 1971; Anderson, 1981) (Fig. 3.60-A), the other type forms arcuate to spiral, epichnial grooves (Fig. 3.60-B), which are very similar to traces described from the Vryheid Formation (Ecca Group) of KwaZulu-Natal (South Africa) by Mason et al. (1983). These authors assigned these spiral traces to the ichnogenus *Spirodesmos*. However, the South African as well as the Namibian spiral traces differ from the type specimen *Spirodesmos archimedeus* (Hückreide, 1952) in having fewer coils in each spiral (max. two). In this context it is pointed out that just a few decimetres below the Sesfontein Tuff a shale layer with very conspicuous, helminthoid traces occurs. The overall form of this helminthoid (narrow, closely spaced meanders) trace is that of a mushroom with a closed head (Fig. 3.60-C/D). The meandering trails are formed by a chain of closely spaced, spherical pellets of possibly fecal origin and can therefore also be associated with *Neonereites*. The same trace fossil was also illustrated in Wickens (1996), who discovered them in the southern part of the South African Karoo Basin in a stratigraphic interval of the Ecca Group, which is equivalent to the Namibian Aussenkjer Formation. However, this trace fossil was definitly misinterpreted as *Lophoctenium*. This trace fossil is certainly an unnamed and not yet described ichnospecies.
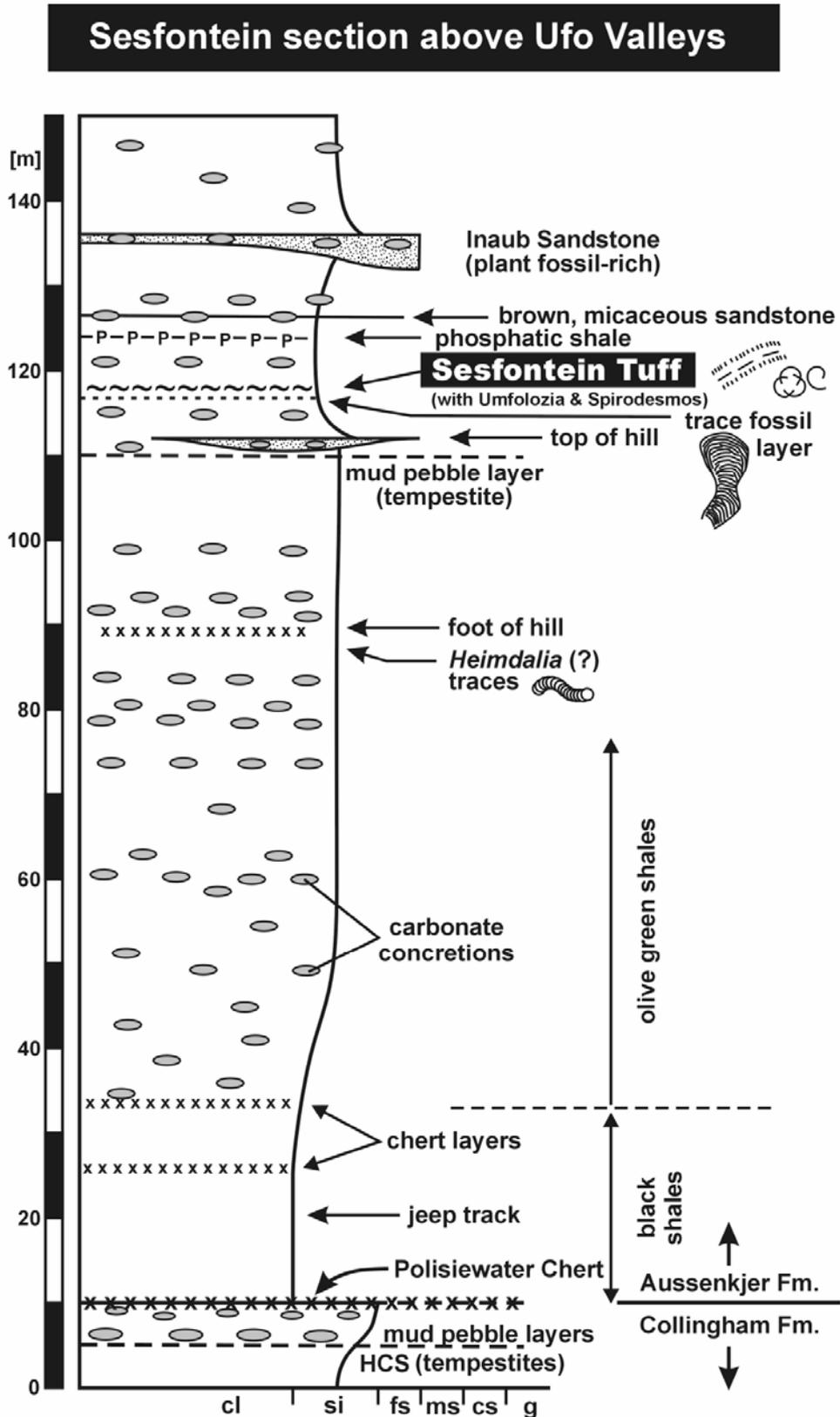
Fig. 3.59: Detailed section logged in the vicinity of Sesfontein above the Ufo Valleys (see Fig. 3.49) showing the stratigraphic position of the Sesfontein Tuff. The section comprises the basal ~130 m of the Aussenkjer Formation, which overlies conformably the Collingham Formation.

Fig. 3.60: (A) *Umfolozia sinuosa* trackways on the upper surface of the Sesfontein Tuff. **(B)** Arcuate and spiral traces of possibly *Spirodesmos archimedeum* on the upper surface of the Sesfontein Tuff. **(C) & (D)** Helminthoid, meandering traces formed by a chain of closely spaced, spherical pellets of possibly fecal origin. The overall shape of this trace fossil is that of a mushroom with a closed head. This so far unnamed and undescribed trace fossil is somewhat related to *Helminthoida* and *Neonereites*. The lens caps have a diameter of c. 6 cm.

Other tuff recordings from the Ecca Group and equivalent deposits

Apart from the study area in southern Namibia Early Permian postglacial sediments are also exposed in NW-Namibia in the Huab area. There, the argillaceous and coal-bearing Verbrandeberg Formation and the arenaceous Tsarabis Formation are considered as correlatives of the Prince Albert Formation. However, so far no bentonites or tonsteins have been described from the Verbrandeberg Formation but it contains one of the few known in-situ occurrences of Permian volcanites in southern Africa. Within the Verbrandeberg Formation an up to 2 m thick, scoriacious and vesicular lava is interlayered in carbonaceous shales (Horsthemke, 1992; Holzförster, 2002). The lava probably had originally a basaltic composition but was completely altered, probably already early diagentically in a swampy environment, to a hematite-rich rock. The fine-grained, carbonaceous sediments of the Verbrandeberg Formation actually have a good preservation potential for ash-fall tuff layers and it can be expected that they would be almost certainly altered to kaolinitic tonsteins. These layers could be very inconspicuous and probably only be detected after a deliberate search. Therefore, for future projects it is recommended to keep one's eyes open for such horizons in the Verbrandeberg Formation, which also could provide further radiometric ages. Due to the pronounced arenaceous character of the Tsarabis Formation the preservation potential of thin ash-fall tuff layers has to be considered as fairly low. Another occurrence of intra-Ecca Group volcanites is known from western central Botswana. In the borehole CKP 8A a volcanic breccia, possibly representing reworked volcanic muds and agglomerates, has been discovered at the Kweneng-Boritse Formation contact (Meixner & Peart, 1983, 1984; Smith, 1984).

Bentonites, similar to those described in this study from the Prince Albert Formation in Namibia, are also known from the South African part of this formation. They have been detected both in the southern part and in the north-western part of the South African Karoo Basin. Viljoen (1990) first recognized the widely distributed volcanogenic material in this formation. McLachlan & Jonker (1990) mentioned discrete tuff layers within the Prince Albert Formation from cores drilled in the north-western part of the Karoo Basin and provided detailed petrographic descriptions as well as geochemical data. Visser (1992) pointed out that in the south-western Cape Province the tuffaceous beds are intercalated within a dark-grey shale-phosphorite facies forming the top of the Prince Albert Formation. Additional geochemical data of Prince Albert tuffs, cropping out in the southern Cape Province, can be found in Knütter (1994) and Viljoen (1995). Bangert et al. (1999) and Bangert (2000) studied some tuff layers from the basal part of the Prince Albert Formation in the south-western Cape Province (Klaarstroom-Laingsburg area) and from two of them single zircon U-Pb SHRIMP ages were obtained (see also Chapter 5 Geochronology).

Towards the north-eastern part of the South African Karoo Basin the Prince Albert Formation loses its character but can broadly be correlated with the Pietermaritzburg Formation and the lower parts of the Vryheid Formation (Visser, 1992; Johnson, 1997). In both formations layers of supposed volcanic origin occur. McLachlan & Jonker (1990) described cherty, siliceous and partly kaolinite-rich laminae and lenticular beds from cores of the basal part of the Vryheid Formation in the Virginia area (Orange Free State). Further to the north-east Schmidt (1976) described montmorillonite deposits in the basal part of the Pietermaritzburg Formation in the Koppies area, 30 km north of Vredefort. These montmorillonite beds are light yellowish-grey in colour and contain nodules of barite 100-400 mm in diameter. Schmidt (1976) regarded the presence of cristobalite, as indicated by XRD analysis, to be a clear indication that these deposits formed by in-situ alteration of volcanic ash. Probably also the bentonite from the base of the Ecca Group in the nearby Parys areas (Coetzee & Hanekom, 1966) belongs to the same group of the aforementioned smectitic beds in the Pietermaritzburg Formation.

Altered tuff layers are also known from correlatives of the Prince Albert Formation in the Brazilian Paraná Basin area, which formed in the Late Palaeozoic the northern and western part of the Mesosaurus Inland Sea. The most well-known and best described tuff layers from Brazil are the tonsteins from the Candiota Coalfield in the Rio Grande do Sul state, positioned at the south-eastern margin of the Paraná Basin. These tonsteins are thin (1-10 cm), altered ash-fall tuff layers interbedded in coal seams and are composed of nearly pure kaolinite (c. 90%). Their geochemistry indicates an acidic origin (Formoso et al., 1997) and conventional U-Pb dating of zircon crystal fractions yielded an intercept age of c. 267 Ma (Matos et al., 2001). Further occurrences of tuffaceous material (mainly glass shards replaced by analcime) in sediments of the Rio Bonito Formation are reported by Coutinho et al. (1991) from several wells along the eastern margin of the Paraná Basin in Brazil and from the north-eastern margin within sediments of the Rio Bonito-equivalent Tatui Formation. Coutinho et al. (1991) further reported pyroclastic material from the Palermo Formation, which is a correlative of the upper part of the Prince Albert Formation (Holzförster et al., 2000). Thin-bedded tuffaceous beds were also detected in the Texaco Mallorquín #1 well as intercalations in deltaic sandstones and mudstones of the Rio Bonito age-equivalent San Miguel Formation along the western flank of the Paraná Basin in Paraguay (López-Gamundí et al., 1995; López-Gamundí, 1996).

Bentonitic layers within the Whitehill Formation were the first ones of those for which a volcanogenic origin was realized. In a report of the Robertson Research Co. (1967) a sample from the Whitehill Formation (well OL 1/69, western Cape Province/RSA), submitted for examination by Southern Oil Exploration Corporation (Pty) Limited of South Africa (SOEKOR), was interpreted as an altered vitric tuff in which the original glass had been

converted to clay minerals. McLachlan & Anderson (1977) then discovered that devitrified volcanic shards form a minor component of nearly all the dolomitic limestones of the Whitehill Formation. Within this study no hydrochloric acid-insoluble residues of the Whitehill dolomites were investigated but the tuffaceous interval, which was discovered by this author in southern Namibia, lies just a few metres below this calcareous interval (here informally called Goris Limestone Beds) (see Fig. 3.39). A first detailed description of altered tuff layers within the Whitehill Formation from boreholes in the northern part of the South African Karoo Basin as well as first geochemical data were provided by McLachlan & Jonker (1990). Visser (1992) showed the position of the tuff-bearing zone in several stratigraphic sections from the northern and southern margins of the Karoo Basin, in which he placed it at the base of a grey silty shale interval approximately in the middle of the Whitehill Formation. A comparison with the Whitehill tuffs in Namibia suggests that their actual position should be just below this silty shale interval. In Viljoen (1995) a few more geochemical data from Whitehill tuffs can be found and Veevers et al. (1994) provided some additional petrographic data as well as a good overview of the distribution of Prince Albert and Whitehill tuffs in the South African Karoo Basin (Veevers et al., 1994; Fig. 12-A). In Brazil tuffs occur also in the Whitehill-equivalent Irati Formation. Multiple smectite-rich bentonite beds with a thickness of 1-2 cm, as exposed in the Petrobras Corporation's SIX Quarry near São Mateus in south-eastern Brasil, were investigated geochemically by Maynard et al. (1996).

Due to the extremely high frequency of bentonitic layers within the Collingham Formation these tuff beds represent the most frequently mentioned and most extensively studied tuff beds of the whole Karoo Supergroup. Venter (1969), Elliot & Watts (1974), and Rowsell & de Swardt (1976) first recognized the soft yellowish mudstones as altered volcanic ash beds. Elliot & Watts (1974) reported of a green mudstone bed from the basal part of the Collingham Formation, which contains numerous devitrified glass shards that have been replaced by quartzfeldspathic intergrowths. Lock & Wilson (1975) then stated that 30-40% of the whole Collingham Formation actually consists of yellowish mudstones (bentonites) and revealed their mineralogical composition based on XRD analyses (quartz: 30-40%, K-feldspar: 10-25%, plagioclase: 15-20%, illite: 5-20%, traces of montmorillonite; note that neither Wickens (1984, 1996) nor Viljoen (1995) have identified substantial amounts of K-feldspar in their investigations on the Collingham tuffs). Further reports and studies followed by Johnson & Keyser (1979) and Wickens (1984). Due to their strongly illitic character Viljoen (1987) and Verwoerd et al. (1990) described them as K-bentonites. Extensive logging of the Collingham Formation in the southern Cape Province and a detailed mineralogical and geochemical study of the Collingham tuffs were performed by Viljoen (1987, 1990, 1992a, 1994, 1995). Additional petrographic data were provided by Veevers et al. (1994) and further geochemical data were produced by Knütter (1994) as well as Knütter et al. (1995). Wickens (1984, 1996)

published some more results about the mineralogical composition of the Collingham tuffs. Geochronological data for South African Collingham tuffs can be found in Viljoen (1995) and in Trouw & de Wit (1999) (see also Chapter 5 Geochronology). Within the Collingham Formation the Matjiesfontein Chert Member forms a very prominent marker band of 15-60 cm thickness. It is interpreted to be of mixed epi- and pyroclastic origin (Viljoen, 1992a, 1994; Knütter, 1994) and was probably formed by deposition of reworked and resuspended volcanic ash. Similarly to the Khabus-Panorama Tuff 1 of the Namibian Whitehill Formation the Matjiesfontein Chert represents an essentially albitized tuffaceous layer.

As the Collingham Formation loses its distinctive character towards the north in the South African Karoo Basin, due to a marked decrease in volcanogenic material and the northward wedging-out of the Matjiesfontein Chert Member at about 32°45'S, it gradually merges with the basal part of the Tierberg Formation. However, the age equivalence of these two stratigraphic intervals is indicated by the numerous yellowish tuff layers in the basal part of the Tierberg Formation found in outcrops (Wickens, 1984, 1996) and cores (Anglo American, 1986; McLachlan & Jonker, 1990) from the north-western part of the Karoo Basin. Further-more, the tuff layers in the lower part of the Volksrust Formation in Natal (eastern part of the South African Karoo Basin) (Viljoen, 1990) and the kaolinitic carbo-tonsteins in the Grootegeluk Formation of the Waterberg Coalfield (Ellisras Basin) (Spears et al., 1988; Faure et al., 1996a/b) are all correlated with the Collingham Formation (Viljoen, 1992a). So far it is not known if the suspected tonsteins within the Serowe Formation in the Makoro Karoo Trough (Smith, 1984), c. 150 km north of the Ellisras Basin, could also be considered as of Collingham age due to their close position to the Waterberg tonsteins. In Brazil, the Collingham Formation can broadly be correlated in the Paraná Basin area with the Serra Alta Formation, which also contains altered volcanic ash layers (Coutinho et al., 1991). And even on the Falkland/Malvinas Islands more than seventy yellowish weathering greenish K-bentonites have been detected in the Shepherds Brook Member (Port Sussex Formation), which appears to be essentially similar to the Collingham Formation (Trewin et al., 2002). This correlation is also confirmed by the fact that the tuffaceous Shepards Brook Member is underlain by the Black Rock Member, which is mainly composed of carbonaceous black shales, similar to the Whitehill Formation underlying the Collingham Formation.

In the following (post-Collingham Formation) middle Ecca sediments, which comprise argillaceous basin floor and arenaceous deep-water turbidite fan deposits, volcanic ash layers do occur but are distinctly less abundant than in the Collingham Formation. From the southern part of the South African Karoo Basin bentonitic tuff layers in the argillaceous Vischkuil Formation have been mentioned by Elliot & Watts (1974), described by Viljoen & Wickens (1992), and geochemically studied by Knütter (1994) and Viljoen (1995). These tuff layers are in a comparable stratigraphic position to the Sesfontein Tuff described here within

the Namibian Aussenkjer Formation. On top of the Vischkuil Formation follows the turbiditic sandstone-dominated Laingsburg Formation and towards the west the laterally equivalent Schoorsteenberg Formation, from which tuff layers were mentioned and described by Viljoen (1992b), Knütter (1994), Viljoen (1998) and Johnson et al. (2001). Towards the east, a correlative of the Vischkuil and Laingsburg Formations is represented by the Ripon Formation, from which tuff layers are also known (Viljoen, 1995, 1998). Higher up in the middle/upper Ecca succession further tuff layers have been reported from the argillaceous Fort Brown Formation (Veevers et al., 1994; Viljoen, 1998). The so-called Geelhoutboom Tuff within the Fort Brown Formation of the southern Cape Province was described by Lock & Johnson (1974) in greater detail, since it has a quite unique appearance. In contrast to the generally fine-grained, clay-rich bentonitic tuff layers, the Geelhoutboom Tuff is composed of several bands, each between one and two centimetre thick, consisting almost entirely of crystals of plagioclase (>90%) and quartz (<10%), with the crystal grain size around one millimetre. This tuff was probably emplaced in the form of a subaqueous semi-plastic slump or flow, whereas the great majority of the lower/middle Ecca tuffs in southern Africa are deposited as ash-fall tuffs. Finally, tuffs were also mentioned from the upper Ecca Waterford Formation (Viljoen, 1998), which is composed predominantly of shoreface and deltaic sandstones. In addition to discrete tuff layers in the middle/upper Ecca sediments, volcano-genic material in the form of lithic fragments within sandstones were also described by Elliot & Watts (1974), Martini (1974) and Johnson (1991). Again, a good overview of the distribution of middle and upper Ecca tuffs and other volcanogenic material in the South African Karoo Basin is given by Veevers et al. (1994; Fig. 12-B).

The middle/upper Ecca succession has its correllative in the Brazilian part of the Paraná Basin in form of the Teresina Formation, from which also several tuff layers were reported by Coutinho et al. (1991). Further to the south, in central eastern Argentina, sediments of comparable age to the Ecca Group in southern Africa are exposed in the Sierras Australes north of Bahía Blanca. The depositional centre of the Late Palaeozoic sediments is referred to as the Sauce Grande Basin, which was connected towards the west with the northerly lying Chaco-Paraná and Paraná basins, and to the east with the South African Karoo Basin (López-Gamundí & Rosello, 1998) (see Fig. 6.1). Within the Sauce Grande Basin the Early Permian sediments of the Tunas Formation are probably broadly age-equivalent to the middle/upper Ecca sediments. Similar to the latter, the Tunas Formation contains thin tuffaceous beds as well as smectite-rich claystones (Iñíguez et al., 1998), and sandstones of the Tunas Formation contain volcanic lithic fragments comprising grains of rhyolites, rhyodacites, andesites and scarce fragments of vitric tuffs (Andreis & Cladera, 1992; López-Gamundí et al., 1995). Early Permian pyroclastic rocks are further known from the NW

Argentinian Paganzo and Calingasta-Uspallata basins (López-Gamundí et al., 1990, 1994; and references therein).

East of the African Karoo basins volcanic and pyroclastic material have been discovered in the Early Permian postglacial Polarstar Formation, which crops out in the Ellsworth Mountains of Antarctica. The lithic fragment population of sandstones within this formation is typically dominated by felsic volcanic rock fragments, which consist of a microcrystalline mosaic of anhedral quartz and feldspar. In addition, in the upper part of the formation vitric and crystal tuffs were discovered, in which former glass shards were replaced by calcite (Collinson et al., 1992).

3.4.3 Tuff beds in the Beaufort Group

The Gai-As/Doros Tuffs of north-western Namibia (Huab area)

In southern Namibia no deposits of the continental, fluvio-lacustrine Beaufort Group (see Fig. 1.7 & 3.18) are preserved, which follow on the entirely subaqueously deposited sediments of the inland sea phase represented by the Ecca Group. The most continuous succession of Permo-Triassic Beaufort Group sediments is known from South Africa, but age-equivalent (only the basal Upper Permian part) fluvio-lacustrine deposits are also known from the Brazilian Paraná Basin (Rio do Rasto Formation). In north-western Namibia Beaufort-equivalent deposits occur in the Waterberg and Huab-Brandberg areas (Upper Permian Gai-As and Doros Formations as well as the Triassic Omingonde Formation). Thin horizons in the Gai-As Formation and the basal Doros Formation, rich in remains of the bivalve *Terraia altissima*, can be correlated biostratigraphically with the *Terraia altissima*-biozone in the Paraná Basin (Ledendecker, 1992; Rohn, 1994), which is restricted to the Serrinha Member, forming the lower part of the Rio do Rasto Formation. In addition, vertebrate occurrences (*Endothiodon*) in the overlying Morro Pelado Member, forming the upper part of the Rio do Rasto Formation, can be correlated with the *Cistecephalus*-biozone of the lower Beaufort Group in South Africa (Barbarena at al., 1991). Zircon ages from tuffs within the top part of the Namibian Gai-As Formation (~265 Ma; Wanke, 2000) and from tuffs within the *Ciste-cephalus*-biozone of the South African Teekloof Formation (~261 Ma; Bowring, pers. comm., 1998; cited in Stollhofen, 1999) reveal that the lower part of the Beaufort Group and its equivalents in Brazil and north-western Namibia are of Upper Permian age.

In north-western Namibia Late Palaeozoic tuff layers have been discovered so far only in the Gai-As and Doros Formations in the Huab Karoo outcrop area. They were first described by Horsthemke et al. (1990) and Horsthemke (1992), and subsequently studied by Holzförster (2000, 2002) and Wanke (2000). In 1999 the author of this study conducted field work with Ansgar Wanke in the Huab area and sampled the Gai-As Tuffs. Since these samples show some characteristics, which were not mentioned in the earlier descriptions of the Gai-As/Doros Tuffs, they are shortly reviewed here and new, additional observations are supplemented.

The Gai-As/Doros Tuffs form conspicuous snow-white, porcelain-like, thin (2-15 cm), usually very fine-grained layers, which contain laminated as well as massive parts. They are usually relatively well-sorted and often a poorly developed normal grading is visible in thin sections. The Gai-As/Doros Tuffs appear apparently in three stratigraphic levels and their mineralogical composition seems to be dependant on their position within the succession. The lowermost tuff level lies approximately in the middle part of the Gai-As Formation (tuff beds I-III: Holzförster, 2000; Wanke, 2000) and these layers are mainly composed of analcime (10 to >60%) plus minor amounts of quartz, calcite, dolomite and ankerite

(Horsthemke, 1992). These tuffs can contain sandy intercalations, which are rich in biotite flakes and contain also euhedral zircon and apatite crystals as accessories. The matrix of the altered tuffs behaves optically isotropic.

The second tuff level is positioned approximately at the transition zone between the upper part of the Gai-As Formation and the lower part of the Doros Formation (tuff beds IV and V: Holzförster, 2000; Wanke, 2000). In comparison to the analcime-rich tuffs of the lower tuff zone these tuffs are mainly composed of cryptocrystalline K-feldspar, which forms the matrix of the tuffs and also behaves optically isotropic. Calcite forms conspicuous reddish coloured spherical concretions up to 6 mm in diameter and in places quartz- and biotite-rich layers and lenses occur. Other minor phases are illite, dolomite, ankerite and analcime.

A third tuff level was reported by Wanke (2002) in the middle to upper part of the Doros Formation (tuff beds VI and VII), however, their mineralogical composition was not determined.

The presence of analcime respectively K-feldspar was interpreted by Horsthemke (1992) as an alteration product of volcanic ash, deposited in an alkaline lacustrine environment, and dolomitic stromatolites associated with halite pseudomorphs document for the upper part of the Gai-As Formation indeed temporary hypersaline conditions.

Two samples of the Gai-As/Doros Tuffs were SHRIMP-dated by Wanke (2000), which revealed their Upper Permian age (see also Chapter 5 Geochronology for details).

The tuff layers, which were sampled and investigated by the author of this study originate from the second tuff level at the top of the Gai-As Formation. The locality lies c. 13 km SSW of Mount Awahab in the central southern Huab area (S 20° 44.50' E 14° 08.40') (Fig. 3.61). There, two white, porcelain-like tuff beds (tuff beds IV and V) are intercalated in reddish-brown to purple to bluish-grey shales (Fig. 3.62). The thickness of these two tuff layers is about 2.7 and 4.5 cm, however, thickness can vary slightly. The upper and lower contacts are sharp and near-plane to somewhat wavy. Polished hand specimens mainly show a white colour but greenish and reddish laminae and schlieren do also occur (Fig. 3.63). The lower part of the tuffs is characterized by conspicuous reddish-brown carbonate (mainly calcite) concretions of diagenetic origin. Most of them have a near-spherical form and reach sizes of up to 2 mm in diameter. These lower parts of the tuffs appear always massive. One tuff shows in its middle part a somewhat wavy and discontinuous but distinct lamination. Due to the lamination, the lateral consistency of the tuff layers and the very fine-grained nature of the tuffs it is suggested that they have been deposited mainly as ash-fall tuffs, however some minor reworking and disturbance during deposition has taken place as indicated by coarser grained layers and lenses within the tuffs. The upper part of the tuffs appears either massive again or shows an in-situ brecciated texture (Fig. 3.63). The brecciated nature of the upper part is most probably caused by pedogenetic processes. For example, especially in the

eastern Huab area the sediments of the Gai-As and Doros Formations are strongly modified by pedogenetic processes characterized by in-situ brecciation and a network of calcareous and siliceous concretions (Stollhofen, 1999).
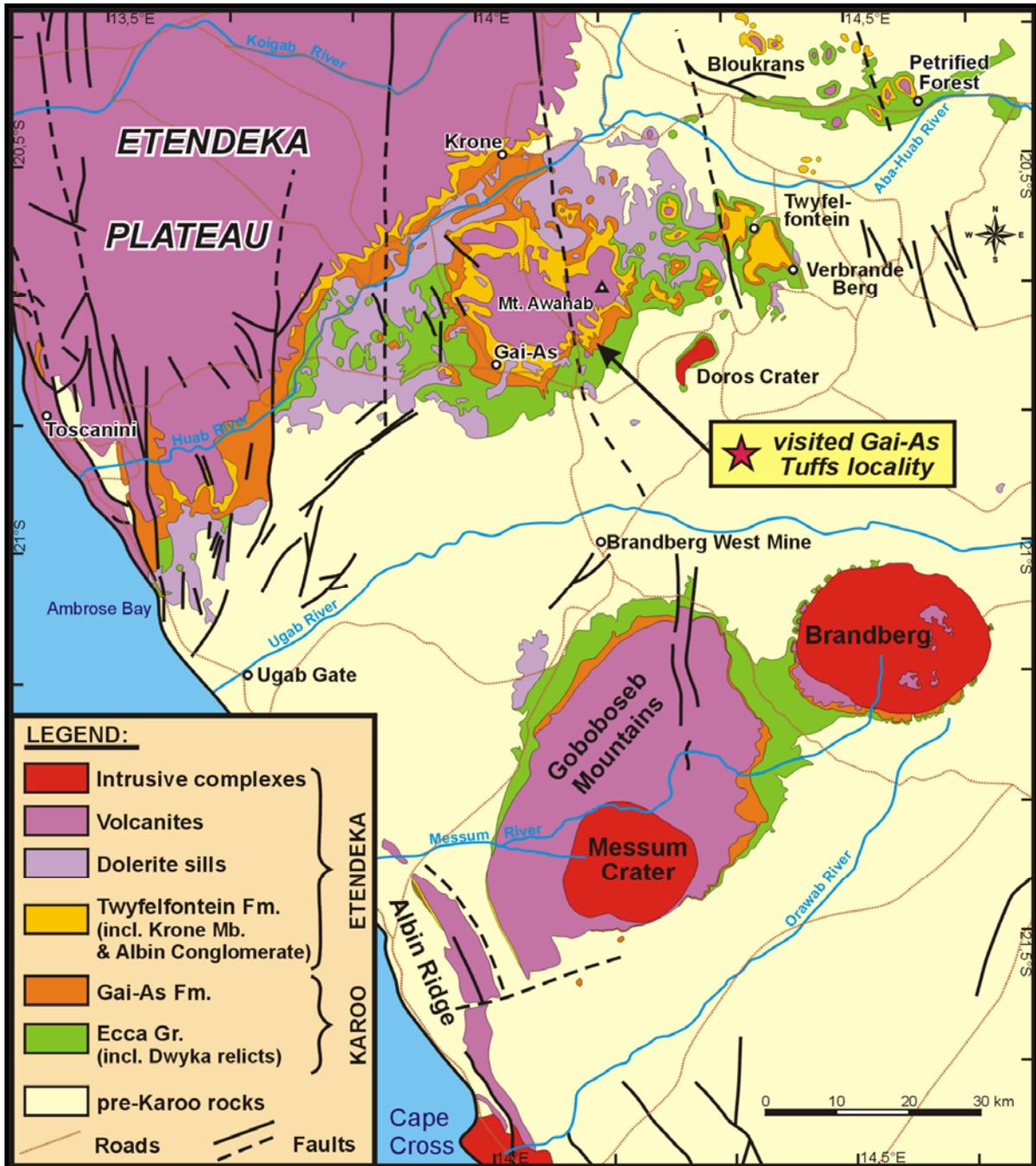
Fig. 3.61: Geological overview map of the Huab River and Goboboseb Mountains-Brandberg area. Indicated is the locality, where samples of the Gai-As/Doros Tuffs were collected. Note, that remnants of the glacigenic Dwyka Group are not shown seperately due to their small size. Also the occurrences of the Triassic Omingonde Formation in the Goboboseb Mountains-Brandberg area, identified by Holzförster (2002), are not indicated in this map. The map is compiled from Miller & Schalk (1980), Miller (1988), Milner (1997), Wanke (2000), Junker (2001), and Holzförster (2002).

Fig. 3.62: Outcrop of two white, K-feldspar-rich, altered tuff layers interbedded in purple to bluish-grey lacustrine shales of the uppermost part of the Upper Permian Gai-As Formation. The light brownish sandstone blocks, which partly cover the outcrop, represent the unconformably overlying aeolianites of the Cretaceous Etendeka Group. See Fig. 3.61 for the location of the outcrop locality (southern-central Huab area, c. 13 km SSW of Mount Awahab: S 20° 44.50' E 14° 08.40').

XRD analyses of the collected samples of the Gai-As Tuffs show as major components K-feldspar, calcite and barite as well as minor amounts of quartz. Barite has so far not been reported as a major mineral phase of the Gai-As Tuffs. K-feldspar forms the main component of the tuffs and is present in form of the cryptocrystalline matrix, which behaves optically iso-tropic. Calcite is the main constituent of the spherical to ovoid concretions. In plane-polarized light these concretions often show a colourless core, which is surrounded by a darker, pigment-stained outer rim indicating a certain iron or manganese content in the carbonate grains (Fig. 3.64-A/B). The minor amounts of quartz can be related to numerous angular, silt-sized (50-80 µm) quartz crystal fragments, which form together with plagioclase fragments and biotite flakes (some altered to chlorite) as well as accessory, euhedral, juvenile zircons (Fig. 3.64-C) and apatites the crystal components of the tuffs. The distribution of these crystals produces a weakly developed normal grading of the tuffs. Generally, the tuffs are crystal-poor. In some thin sections rounded grains (~200 µm in diameter), consisting of phyllosilicates (partly altered biotite) interspersed in a very fine-grained groundmass, could represent felsic volcanic rock fragments (Fig. 3.64-D). Especially in the lower half of the tuffs

large concentrations of beautifully preserved, former glass shards are patchily distributed throughout the matrix (Fig. 3.64-E to O).
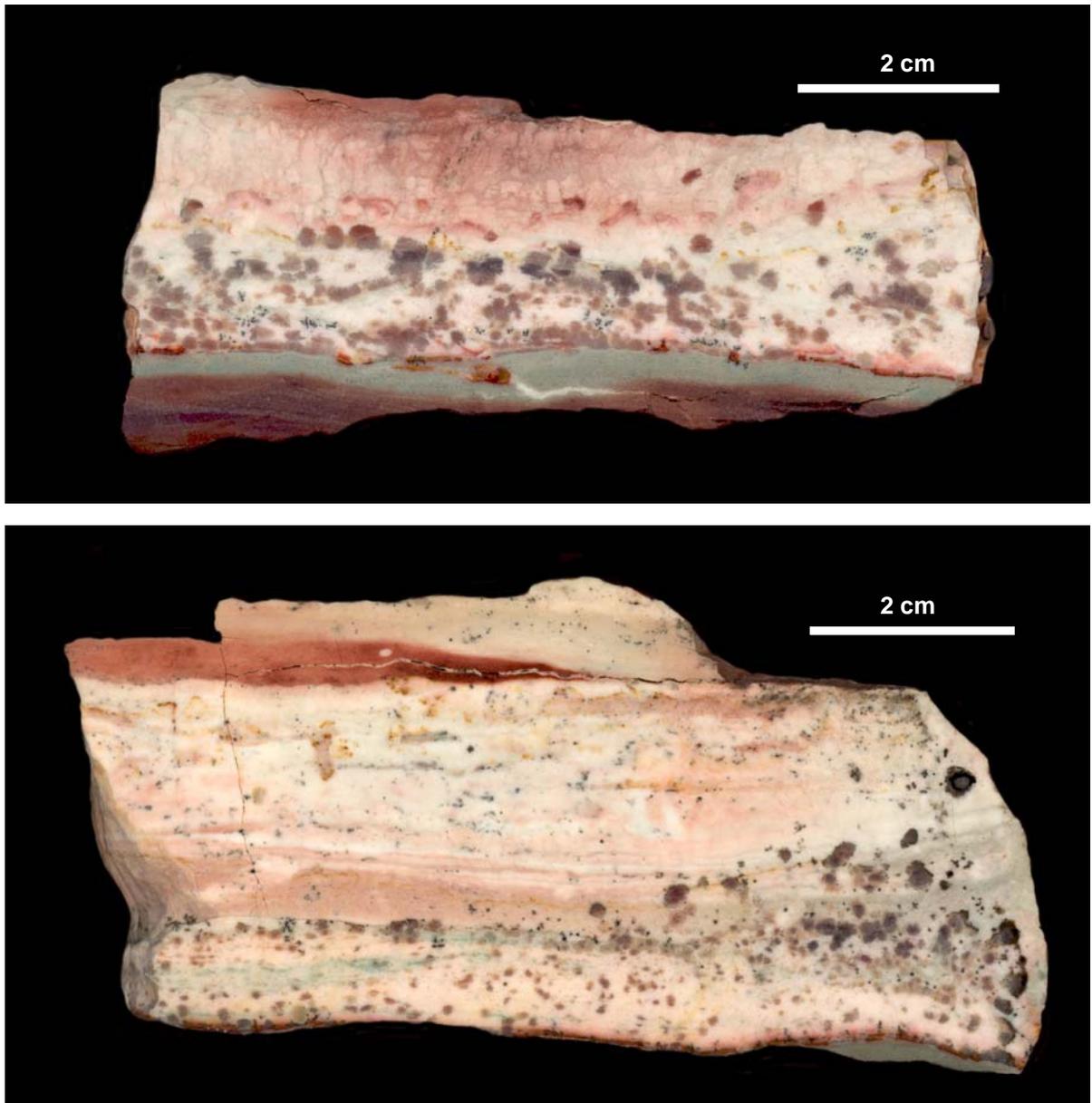
Fig. 3.63: Two polished hand specimens of the Gai-As Tuffs. Both contain reddish carbonate (mainly calcite) concretions in their lower parts. Directly at the lower contact the underlying shales, normally reddish-brown, show a greenish reduction colour. In the lower image a vaguely horizontally laminated middle part can be seen, whereas in the upper image the upper part is characterized by pedogenetic in-situ brecciation. See Fig. 3.61 for the position of the visited locality and Fig. 3.62 for an outcrop photo.

They show mainly platy and arcuate forms but also tricuspate and Y-shaped shards are not uncommen (Fig. 3.64-G to K). Their size lies mainly in the range of 50 to 150 μm. These former glass shards are now replaced by a mineral, which is colourless under plane-polarized light and displays greyish to pale yellowish interference colours under crossed

polars (Fig. 3.64-F). This indicates that this mineral has a birefringence probably between 0.010 and 0.015. In plane-polarized light one can see that the replaced glass shards show a moderatly but distinct positive relief, indicating that the replacing mineral must have a higher refractive index than the matrix K-feldspar. With the additional support of the XRD data the replacing mineral can now almost certainly be identified as barite, which is in accordance with the observed optical properties. However, it must be pointed out that not only the barite-rich domains or patches originally contained glass shards, because faint ghost structures of glass shards adjacent to the baritic areas indicate that the whole tuff was originally almost entirely composed of such glass shards (Fig. 3.64-L/M). Most of them are now replaced by K-feldspar, a considerable amount is replaced by barite and in a few cases shards are replaced by calcite (Fig. 3.64-N/O).
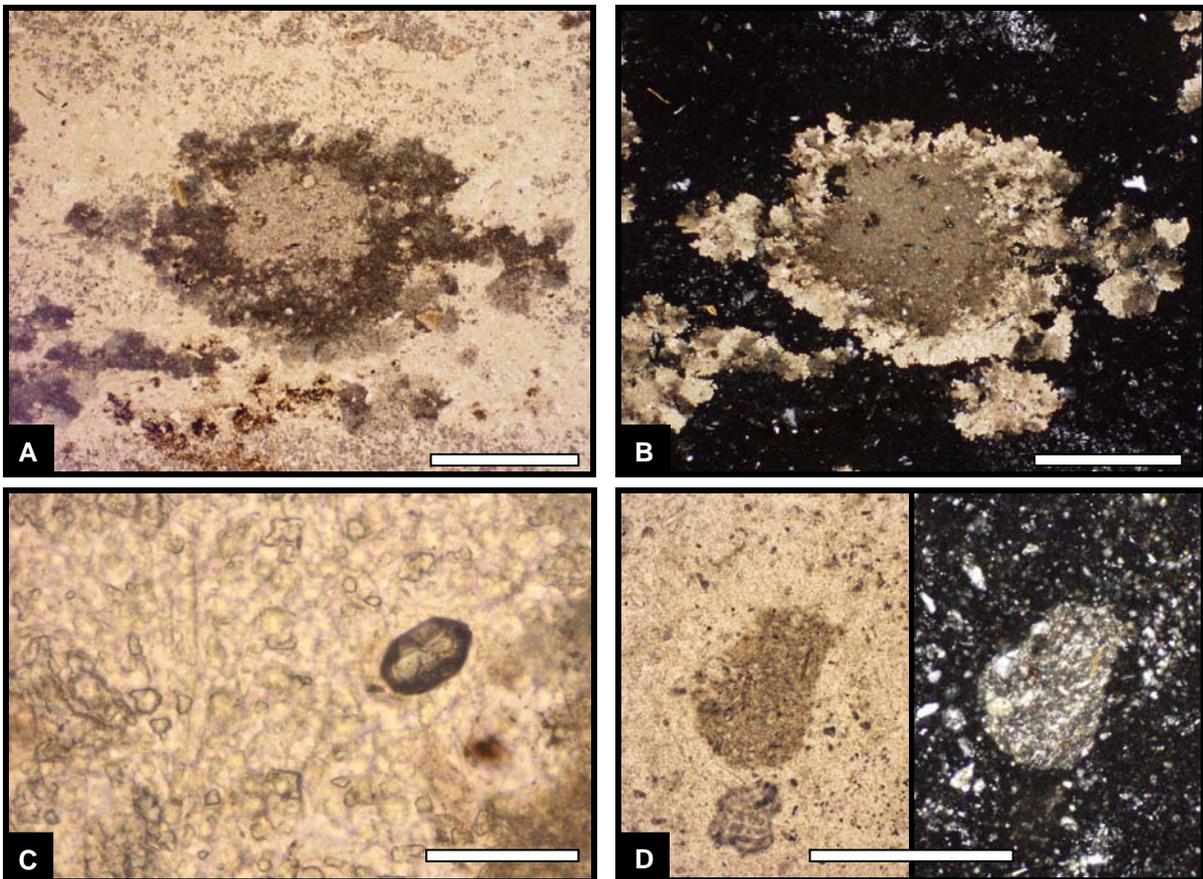
Fig. 3.64: Thin section photographs of the Gai-As Tuffs: **(A) & (B)** Roughly ovoid carbonate concretion, consisting mainly of calcite, surrounded by the cryptocrystalline, pseudoisotropic K-feldspathic matrix of the tuff. These concretions are often composed of a lighter coloured core, which is surrounded by a darker coloured, pigment-stained margin indicating a certain iron or manganese content. Plane-polarized light (left) and crossed polars (right). Scale bars 250 µm. **(C)** Euhedral, juvenile zircon crystal showing a stubby form. Plane-polarized light. Scale bar 50 µm. **(D)** Rounded grains consisting of small phyllosilicate crystals interspersed in a very fine-grained matrix. These grains may represent volcanic rock fragments. Plane-polarized light (left) and crossed polars (right). Scale bar 250 µm.
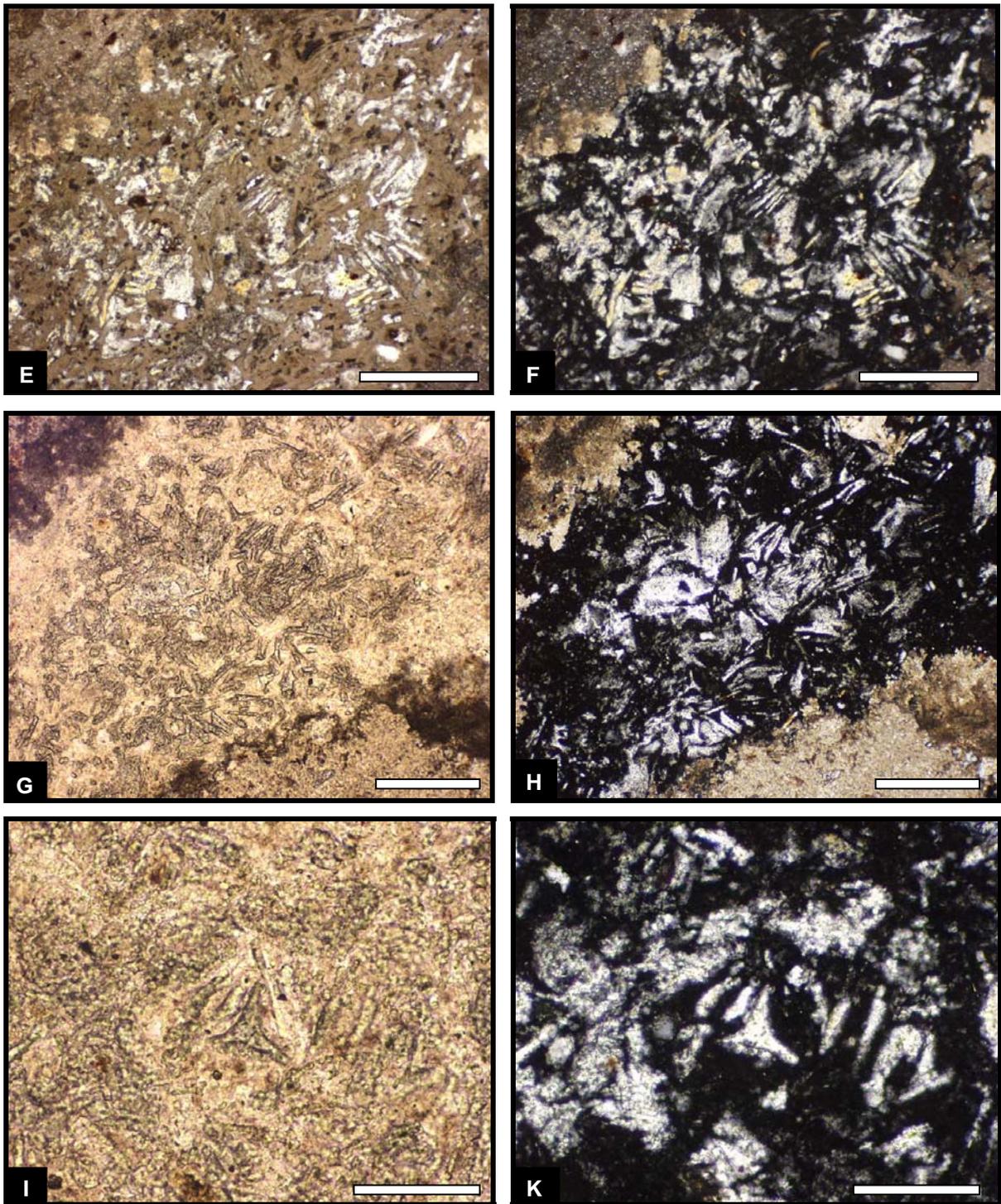
Fig. 3.64: Thin section photographs of the Gai-As Tuffs (cont.): **(E) & (F)** Platy, arcuate and cuspate former volcanic glass shards now replaced by barite (note the partly yellowish interference colours). The pseudoisotropic matrix (black areas in the right images) is composed of cryptocrystalline K-feldspar. In the upper left corner and at the right margin of the image calcite is seen. Semi-crossed polars (left) and crossed polars (right). Scale bars 250 μm. **(G) & (H)** Former volcanic glass shards replaced by barite. Note the distinct positive relief of the shards against the feldspathic matrix in the left image. Plane-polarized light (left) and crossed polars (right). Scale bars 250 μm. **(I) & (K)** Tricuspate (centre of image) and Y-shaped (lower right area of image) forms of former volcanic glass shards replaced by barite. Plane-polarized light (left) and crossed polars (right). Scale bars 100 μm.
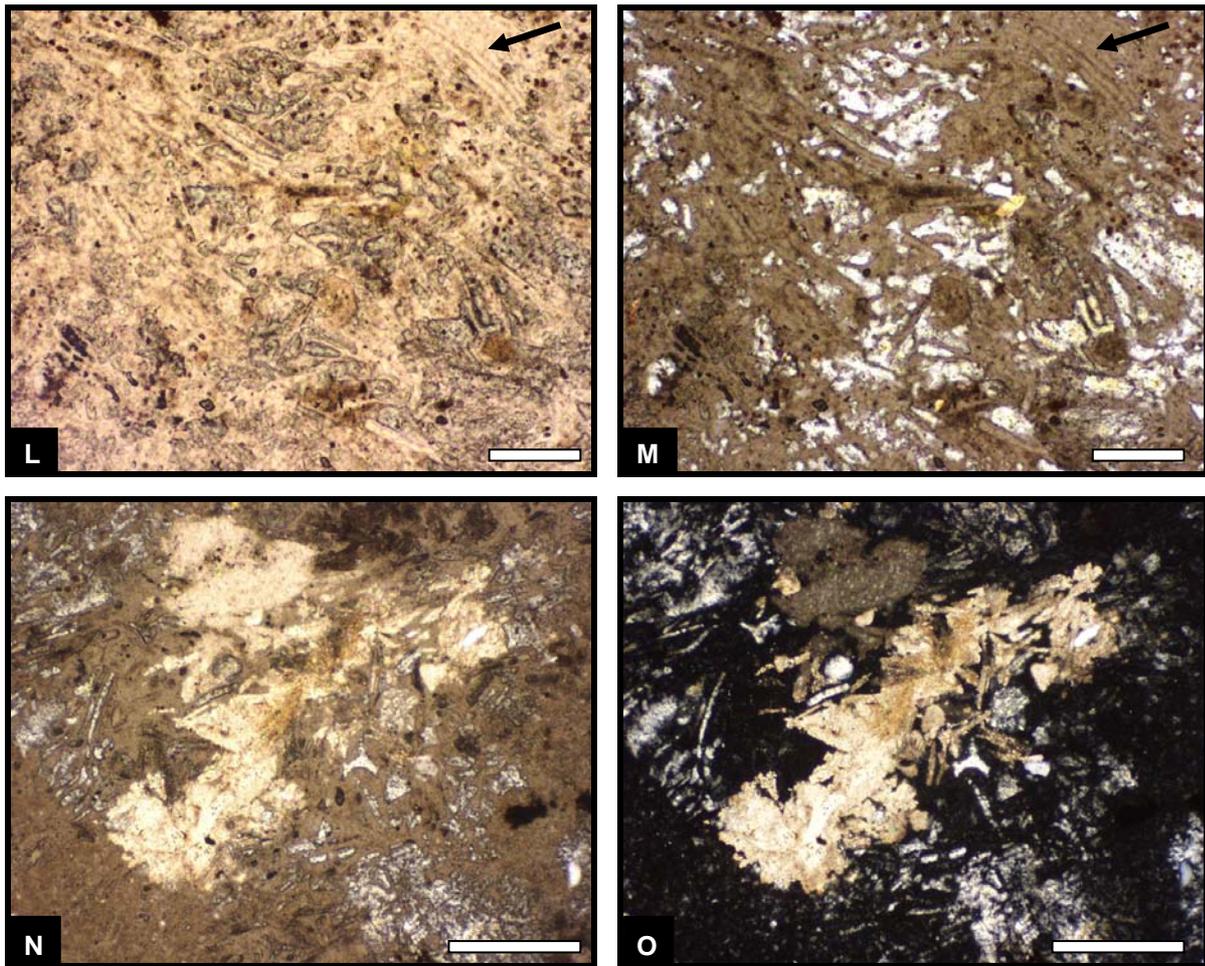
Fig. 3.64: Thin section photographs of the Gai-As Tuffs (cont.): **(L) & (M)** Former volcanic glass shards, which are replaced by barite, appear in plane-polarized light (L) darker and show a positive relief, under crossed polars (M) they appear white. Shards, which are replaced by K-feldspar, are visible as faint, lamellar, slightly brownish ghost structures in these images (e.g. in upper right corner; see arrow). Plane-polarized light (left) and semi-crossed polars (right). Scale bars 100 μm. **(N) & (O)** These images show the rarer case, in which former volcanic glass shards are partly replaced by calcite (bright creamish white area in the images). In the upper left and lower right corners shards replaced by barite can be seen. Semi-crossed polars (left) and crossed polars (right). Scale bars 100 μm.

Other tuff recordings from the Beaufort Group and equivalent deposits

In the South African Main Karoo Basin altered volcanish ash layers occur also within Upper Permian to Lower Triassic continental sediments of the Beaufort Group, mainly as horizons of chert-like rocks. These cherty layers within the Beaufort Group were discovered already very early in the course of mapping projects and were mentioned in several explanations to geological maps (Blignaut et al., 1948; Rossouw & de Villiers, 1953; Rossouw et al., 1964) as well as in reports about the petroleum potential of Karoo rocks (Haughton et al., 1953). However, at this time their volcanic nature was not recognized. Blignaut et al. (1948), for example, interpreted the 'cherts' as siliceous precipitates within a swampy environment. The volcanic origin of these chert beds was probably first suggested by Martini (1974), who described them in some detail. He recognized that the matrix of some of these altered volcanic ash layers from the basal part of the Beaufort Group is either mainly composed of silica or of prehnite. A probable volcanogenic origin of the chert layers was also suggested by Karpeta (1977) as well as by Johnson & Keyser (1979). The latter described such chert beds from the basal two formations of the Beaufort Group (Abrahamskraal and Teekloof Formation) from the southern central Cape Province. In the Abrahamskraal Formation grey or greenish cherty beds range in thickness from 10 cm to 2 m and they are laterally traceable over a distance of a few hundred metres to a few kilometres. Martini (1974) concluded from the descriptions of Blignaut et al. (1948), Rossouw & de Villiers (1953) as well as Rossouw et al. (1964) that the most prominent of these chert layers, the so-called 'Green Chert', appears to be traceable even over a distance of 250 km. It has been suggested that these cherty beds were originally ash-fall tuffs, however, micro-cross-lamination in some of them indicate some sort of reworking and transportation by water. In the Teekloof Formation a number of pink layers, 10-30 cm thick, consist almost entirely of laumontite and are also interpreted as altered volcanic ash deposits. Ho-Tun (1979) reported the presence of volcanic glass shards and trachytic rock fragments in rocks of the lower Beaufort Group. Further information about occurrences of volcanic glass shards in the lower Beaufort Group is provided by Le Roux (1985). The first really detailed petrographic, mineralogical and geochemical study on tuff layers from the Beaufort Group was undertaken by Keyser & Zawada (1988), who investigated tuffs in the northern part of the Orange Free State, about 100-140 km south of Johannesburg. In contrast to the fine-grained ash-fall tuffs of the Ecca Group, these two tuff occurrences (Oranje and Blydschap Tuff) in the lowermost Beaufort Group represent coarse-grained ash-flow tuffs. The Oranje Tuff has a thickness of around one metre, whereas the Blydschap Tuff is about 85 cm thick, but is overlain by an additional 1.7 metres of tuffaceous sediment. The juvenile crystal components of the tuffs comprise plagioclase crystals, biotite flakes and chlorite pseudomorphs after pyroxene or amphibole. The xenocrystic components are formed by quartz and feldspar grains. Secondary minerals are microlitic, spherulitic, and

acicular plagioclase, chlorite, interstitial quartz, calcite and analcime. Devitrified glass shards, occasionally draped over mineral grains, can be observed within the tuffs, too. Numerous glass shards and pumice lapilli occur also in the overlying tuffaceous sediment. Furthermore, the tuffs contain lapilli-sized (2-30 mm) lava and pumice clasts. Amygdales are distributed throughout the tuffs and are filled with quartz, calcite, chlorite and/or analcime. Trace element analyses indicate a rhyodacitic-dacitic composition of the tuffs, whereas a lava fragment from one of the tuffs shows an andesitic composition. Apart from tuffs in the Ecca Group, Knütter (1994) and Knütter et al. (1995) investigated tuffs within the Abrahamskraal Formation from the southern Cape Province. South of Laingsburg two tuff layers were found c. 25 m above the Ecca-Beaufort contact. In contrast to the illite-dominated tuffs of the Ecca Group and the albitic Matjiesfontein Chert, the investigated tuffs show a siliceous, quartz-rich matrix and the SiO_2 contents of the tuffs range from about 70 to over 90 wt%. Another distinguishing feature are the relatively large quartz grains (up to 1 mm) within the tuffs of the Abrahamskraal Formation, whereas the quartz grains in the investigated Ecca tuffs are generally smaller than 350 µm. Another detailed petrographic, mineralogical and geochemical study on lower Beaufort tuffs, the so-called Rietfontein-Wolwekop Tuffs, was done by Karpeta (1996). Vitric tuffs of probable ash-flow and secondary hydro-eruption surge origin occur in the Oudeberg Sandstone Member of the Teekloof Formation in the central southern Cape Province. The Oudeberg Member consists of braided fluvial sandstones as well as floodplain and interchannel mudrocks. Coarse-grained, poorly sorted, massive tuffs were emplaced by hot pyroclastic flows, and where these flows encountered pools of standing water, the latter were flashed to steam resulting in hydro-eruptions, which produced localized cool, wet base surges and deposited lenticular, laminated tuffs. The latter contain in places accretionary lapilli up to 5 mm in diameter. Fine ash, elutriated by air ingested at the pyroclastic flow head, formed ash-cloud surges depositing fine-grained, graded tuffs on top of massive tuffs. Diagenetic alteration of the tuffs resulted in the conversion of volcanic glass to zeolites (heulandite, clinoptilolite, laumontite) and the precipitation of silica in open visicles and pipes. In addition to the tuffs, the Oudeberg Sandstone contains also fragments of altered acid volcanic rocks comprising feldspar phenocrysts in a microcrystalline, flow banded matrix. Mineralogically, the Rietfontein-Wolwekop Tuffs consist of scattered anhedral muscovite, quartz, biotite, and epidote crystals up to 1 mm long in a groundmass of anhedral laumontite crystals up to 300 µm across. Relict glass shards, averaging 200 µm across, have also been commonly observed. Recently, a 0.75 cm thick tuff layer of yellowish-grey colour intercalated in siltstones and very fine-grained sandstones of the Beaufort-aged Estcourt Formation has been described from the Wagendrift Quarry near Estcourt/KwaZulu-Natal by Selover & Gastaldo (2005). At its base this microcrystalline tuff bed is dominated by angular, elongate, fine sand-sized quartz grains. Apart from quartz also scattered and isolated

elongate isotropic grains occur in this ash bed. In addition to discrete tuff layers volcanic rock fragments and volcanoclastic material in Beaufort sandstones have also been reported by Fuller (1970), Martini (1974), Ho-Tun (1979), Simmonds (1982, 1984), and Johnson (1991). Furthermore, pebbles of magmatic origin (e.g. granitc rocks and hornblende-bearing intrusives) occur in the Katberg Formation (Mountain, 1939; Elliot & Johnson, 1972; Elliot & Watts, 1974). A good overview of the distribution of volcanogenic material in the Beaufort Group of South Africa is provided by Veever et al. (1994; Fig. 13).

In this context it should be noted that for the Jwaneng kimberlite cluster in Botswana also an Upper Permian age was suggested based on Rb-Sr dating of macrocrystic phlogopite, which yielded an isochron age of 250 ± 17 Ma. Subsequent SHRIMP-dating of macrocrystic zircons from one kimberlite pipe of the Jwaneng cluster resulted in a Middle Triassic (Anisian-Ladinian) $^{206}Pb/^{238}U$ weighted mean age of 235 ± 4 Ma (Kinny & Compston, 1989).

As already mentioned in the description of the NW Namibian Gai-As Tuffs, Beaufort Group-equivalent rocks are also known from the Paraná Basin in Brazil. There, the Serrinha and the Morro Pelado members of the Rio do Rasto Formation can be correlated on biostrigraphic grounds with the lower parts of the Beaufort Group (Abrahamskraal and Teekloof Formations). Bentonitic tuff beds have been described from the Rio do Rasto Formation in the south-eastern part of the Paraná Basin in the Aceguá area, Brazil (Pintaude & Formoso, 1972) and from the age-equivalent and correlative Yaguari Formation in the Melo area, Uruguay (Bossi et al, 1975; Andreis et al., 1991; López-Gamundí & Rosello, 1998). These bentonites have recently been studied mineralogically and geochemically by Calarge et al. (2003a, b). At both localities these altered tuff beds are composed of a nearly pure smectite mineral that is dominantly a montmorillonite and trace elements indicate a rhyodacitic composition. Further to the south, in the Sauce Grande Basin, tuff layers occur in the upper part of the Tunas Formation, which might be age-equivalent with the lower part of the Beaufort Group (Abrahamskraal and Teekloof Formations) (López-Gamundí & Rosello, 1998). Pyroclastic and volcaniclastic deposits of Upper Permian age are further known from the South American Late Palaeozoic 'Pacific basins', namely the Paganzo, Calingasta-Uspallata, and San Rafael basins (López-Gamundi et al., 1990, 1992, 1994; and references therein).

Also pyroclastic rocks and volcaniclastic material from Beacon rocks in Antarctica could be age-equivalent to tuffs in the Beaufort Group. Volcanic detritus in Beacon strata was first recognized by Minshew (1967) in Permian strata of the eastern Queen Maud Mountains, and later by Barret (1969) in the nearby Beardmore Glacier region (Elliot & Watts, 1974). In the Beardmore area, the lowest occurrence of volcanic detritus is in the middle part of the Upper Permian Buckley Formation.

3.5 Summary of petrography

3.5.1 Field and macroscopical observations

Almost all the mentioned and described altered tuff layers crop out in southern Namibia, only the Gai-As Tuffs originate from northwestern Namibia. The studied tuff layers have been found at the following localities: Ganigobis, Zwartbas, Owl Gorge, Itzawisis, Korabib, Vreda, Uhabis River, Khabus, Panorama, Eisenstein, Ufo Valleys, Rhyofontein, Sesfontein, and Gai-As. The Ganigobis and Zwartbas tuffs are interbedded in marine, glacigenic, dark carbonaceous, occasionally dropstone-bearing shales of the Dwyka Group, whereas almost all the other tuff layers originate from the Ecca Group, in which they are mainly interbedded in marine to brackish, greenish shales, with the exception of the Eisenstein Tuffs, which are interlayerd in dark carbonaceous shales. The Beaufort Group-equivalent Gai-As Tuffs are found within saline, lacustrine, purple to bluish-grey shales.

The number of individual tuff layers varies considerable from locality to locality, respectively from one stratigraphic interval to the other. The Ganigobis, Zwartbas, Korabib and Collingham tuffs comprise a large number of individual tuff beds, which is in the range of about 20 to 65. At the other localities either single tuff layers (e.g. Uhabis River Tuff) or several tuff layers up to about eight (Panorama Tuffs) are exposed. The Ganigobis and Zwartbas Tuffs are commonly grouped into bundles, which are designated as tuff sets. Stollhofen et al. (2000a) reported that in the case of the Ganigobis Tuffs often the uppermost tuff layer within a set shows the greatest thickness. Furthermore, they pointed out that the amount of volcanic material decreases within the Ganigobis Shale Member upwards and interpreted this as waning volcanic activity with time. For the Ufo Valleys-Rhyofontein Tuffs within the Collingham Formation a more symmetrical picture is apparent, with numerous thin tuff laminae in the lower part of the Collingham Formation, a zone with the highest frequency and thicknesses of tuff layers in the middle part, and decreasing thickness and abundance in the upper part (Fig. 3.50).

The colour of the altered tuff layers is mainly dependant on the mineralogical composition of the fine-grained matrix and ranges from yellowish-ochreous to reddish to bluish-grey and creamish, dirty greyish or bright white. Contact-metamorphic porphyroblasts of pinitized (chloritic) cordierite induce a greenish or brownish (oxidized) colouration, whereas the basal parts of the Gai-As Tuffs appear often reddish due to the presence of hematite-pigmented calcite concretions. Also the hardness of the tuff layers is matrix dependant. Bentonitic tuff layers, which contain small amounts of smectite or illite-smectite mixed layer clay minerals are relatively soft, have a waxy or soapy feeling and show a weakly to moderately well developed fissility. These tuffs (e.g. Ganigobis, Zwartbas, and Itzawisis tuffs) often contain also significant amounts of kaolinite booklets and vermicules or illite pseudomorphs after them, making them very similar to tonsteins. Furthermore, these soft tuffs show a swelling

ability upon moistening and disintegrate more or less easily in water. In contrast, highly illitic tuff layers, so-called K-bentonites, represent usually relatively hard, indurated and massive rocks (e.g. Owl Gorge and Ufo Valleys tuffs). Tuff layers with a dominantly feldspathic or partly siliceous matrix even appear as porcellanite-like (Gai-As Tuffs) or chert-like (Khabus-Panorama Tuff 1) rocks. The thickness of the tuff layers is generally relatively small and in the field they occur mainly as thin laminae around 1 mm or less up to 2 cm thick layers. Relatively few layers reach a thickness of up to 5 cm and tuff layers up to 10 cm or even more are very rare. The original thickness of the tuff layers is reduced due to compaction. However, the present day thickness is not only dependant on the original deposited thickness but also on its clay mineral content, which is in turn largely controlled by diagenetic or other secondary processes. Tuff layers, which contain smectite or illite-smectite mixed layer clay minerals are expandable and their thickness can vary considerably within an outcrop area. Also surface weathering can cause local expansion due to calcite, gypsum or barite growth. However, the indurated, illitic tuff layers normally show laterally a quite constant thickness, only in the case of the Ufo Valley Tuffs in the Collingham Formation a slight swelling and thinning of individual layers can be observed along strike and is most probably of sedimentary origin. None of the tuff layers seems to lens out completely over a shorter distance. The lower contacts of the tuff layers to the underlying shales are almost always plane and sharp, only in few cases (e.g. Eisenstein Tuffs) this lower contact is somewhat wavy. The upper contacts can be either very sharp or slightly gradational. In some cases it can be seen that the sharp-bounded and very fine-grained top of a tuff layer obviously attained a certain cohesiveness before a subsequent muddy turbidite ripped small pieces out of this lamina (cf. Owl Gorge Tuff OG-9). At the other end of the spectrum the DIBA Tuff of the Itzawisis Tuffs shows a highly gradational transition to the overlying shales by an up to 20 cm thick tuffitic zone, however, this case is quite exceptional, since in all other cases the gradational contact is only represented by a thin (0.1-1 cm) transition zone. Concerning contact relationships to the enclosing host rock the Khabus-Panorama Tuff 1 represents an exception in that it has neither a sharp lower nor a sharp upper contact. In thin sections the boundaries to the surrounding shales are very ill-defined and so this tuff is actually best described as a tuffaceous or tuffitic horizon within the shales. The fact that this tuff forms nevertheless a quite conspicuous light coloured horizon within the greenish shales is attributed to secondary albitization and silicification along this tuffitic horizon. All investigated tuff layers represent fine-grained pyroclastic rocks. The diagenetically modified matrix is mainly crypto- to microcrystalline and the crystal components range from fine to coarse ash size. No lapilli-sized components have been observed. The tuff layers are generally relatively well sorted, but this depends also on the crystal components. Crystal-rich basal parts of the tuffs often have a quite poorly sorted appearance in thin section, whereas

the upper parts are always very well sorted. A normal grain size grading is visible in many tuff layers due to the distribution of crystal components. Preserved sedimentary structures can rarely be seen in the altered tuff layers and most of them appear macroscopically at first sight more or less massive and structureless. Polished hand specimens, however, revealed that some tuff layers are composed of several sharp-bounded subunits (multiple layers), some even showing erosion phenomena (e.g. Ufo Valleys Tuffs; Fig. 3.53-C/D). Some tuff layers show in polished hand specimens, or even better in thin secions, a weakly developed, discontinuos, wavy lamination due to platy minerals or former vitric components aligned parallel to the bedding of the tuff. Load casts at the base of some Ganigobis Tuffs were reported by Stollhofen et al. (2000a). The structures, which can be seen on polished surfaces of the Korabib Tuffs and on weathered surfaces of the Eisenstein Tuffs resemble micro cross-lamination (Fig. 3.25 & 3.45). However, their origin is not fully understood but these structures might represent reworking. Bioturbation is quite common within the Khabus-Panorama Tuff 1 (Fig. 3.36-D) and the upper surfaces of the Ufo Valleys-Rhyofontein Tuffs as well as the Sesfontein Tuff are intensively traversed by tracks and trail (Fig. 3.52 and 3.60). The observed properties support an ash-fall origin of the investigated tuff layers, but some minor reworking, resuspension and redeposition might have taken place, too.

3.5.2 Microscopical observations

The coarser fraction of the investigated, altered tuff layers is composed of macrocrystal components as well as vitric, respectively former vitric components. Lithic components seem to be largely absent and only in the Gai-As Tuffs some rounded clasts could possibly represent volcanic rock fragments. The fine-grained matrix of the tuff layers is most probably mainly composed of altered, former vitric volcanic ash particles. Biogenic components are very rare. Other rare components are filled vesicles(?) as well as diagenetic nodules and concretions. Most of the studied tuff layers are quite intensively speckled by contact-metamorphically grown porphyroblasts due to the proximity of Jurassic dolerite intrusions (dykes and sills).

3.5.2.1 Macrocrystic components of pyroclastic and epiclastic origin

Both pyroclastic and epiclastic as well as diagenetic or other secondary crystal components can be observed within the tuffs. The pyroclastic crystal components can have a juvenile, a cognate or a xenocrystic origin. Quartz, plagioclase and biotite are the most common crystal components, however, the latter two are often severely altered. Zircon and apatite are the most common accessories and have been found in every tuff layer. Epiclastic components play in most of the investigated tuffs most probably no important role. However, the Khabus-Panorama Tuffs, which can be best described as tuffaceous horizons within the Whitehill

Shales, represent certainly a mixture of sediment and pyroclastic material. Also the DIBA Tuff of the Itzawisis Tuffs is separated from the overlying shale by a relatively thick transitional zone, composed of a shale-tuff mixture.

Crystal fragments of quartz represent the most abundant crystal component in most tuffs. The size of these fragments ranges mainly between 50 and 100 µm but some fragments can reach sizes of up to about 400 µm. The fragments are mostly very angular and often show characteristic thorn- or splinter-shaped forms. These forms testify the quite violent and explosive nature of the eruptions, e.g. plinian or phreato-plinian eruptions. Since almost all quartz fragments are monocrystalline and show straight extinction it can be suspected that the majority is of volcanic origin, either juvenile or at least cognate. Very rare occurrences of hexagonal-shaped quartz crystals can be interpreted as beta-quartz paramorphs, which are highly indicative for a volcanic origin. Fluid or solid (melt) inclusions within quartz crystals are also not uncommon.

Feldspar is in many tuffs a very common and abundant phase. Many feldspar grains show polysynthetic twinning and therefore plagioclase appears to be the dominant species. Potassium feldspar was seldomly identified with certainty but may be present in minor amounts. The feldspar crystal fragments are generally angular and even splintery forms have been observed. Only few lath-shaped, subhedral feldspar grains have been found. Most of the plagioclase crystal fragments are considered as juvenile or cognate. With a dominant grain size between 50 and 150 µm the feldspar size is comparable with that of quartz, however, with a tendency towards a slightly higher mean grain size. Some 'oversized' feldspar grains can reach sizes of up to 300 µm. Alteration of feldspar is extremely variable. Some grains are virtually free of alteration signs, whereas others are almost completely altered. Interestingly, all transitions from fresh to dusty-dirty to partly or entirely replaced grains are sometimes visible in one thin section. Sericitization seems to be the most common alteration process, however, in some cases also chloritization is involved. In some tuffs feldspar grains are composed of a fine-grained, irregular blocky crystal mosaic of what could be replacement feldspar (albitized feldspar?), e.g. in the albitized Khabus-Panorama Tuff 1, but also in some Ufo Valleys Tuffs. Replacement of feldspar by mosaic-textured, blocky kaolinite stacks, partly transformed into illite, has been observed, too (Itzawisis Tuffs).

Biotite is the third important, sometimes dominant, crystal component in the investigated tuffs and is also considered being largely a juvenile or cognate component. The mean grain size of biotite flakes ranges from 100-250 µm, but also grain sizes up to 500 µm are not rare and the maximum observed size is in the order of 1000 µm. Most of the biotite flakes are aligned parallel to the bedding of the tuff and in thin sections, cut parallel to the bedding, biotite displays mainly anhedral to subhedral crystal forms. However, also euhedral, hexagonal crystal shapes have been observed. Biotite shows an extremely broad spectrum of alteration

types. Fresh biotite normally exhibits a pleochroism with light brown to dark reddish brown colours. Biotite, which is affected by oxidation processes, first develops a chagrin-like, grainy internal texture, which is commonly associated with a darkening of its colour. This oxidation leads ultimately to dark brown to almost opaque hematite- or goethite-rich alteration products. Within a few biotite grains a network of acicular alteration products, so-called sagenite (mainly rutile needles), has been observed, too. On the other side, a very common alteration phenomenon is the gradual bleaching of biotite during which it initially turns to light brown to greenish-yellowish crystal flakes. During this bleaching biotite probably changed mineralogically to hydrobiotite and/or vermiculite. Ultimately, biotite is transformed into silvery or completely colourless and water clear crystals, which strongly resemble muscovite, but most probably represent kaolinite (cf. Bohor & Triplehorn, 1993), which was later transformed to illite. According to own observations (see Itzawisis Tuffs), this process can surprisingly take place without any apparent change of thickness or microstructure of the original biotite flake, a phenomenon also described (but not explained) by Bohor & Triplehorn (1993) and Huff et al. (1997a) when biotite alters to kaolinite. Also puzzling is the observation in thin sections that apparently fresh biotite is coexisting with completely bleached biotite, similar to the appearance of fresh plagioclase together with completely sericitized feldspar in one thin section. Furthermore, biotite has been observed to partly or completely transform to chlorite, however, this process is much less common. Again, chlorite pseudomorphs after biotite can coexist with fresh and completely bleached biotite in one and the same tuff. All these mentioned alterations to secondary minerals (hydrobiotite, vermiculite, kaolinite, and chlorite) can also happen under strong expansion and disruption of the individual platelets of biotite flakes, producing large, rectangular, booklet-like crystals.

In addition to quartz, feldspar and biotite, pseudomorphs after an unknown precursor mineral have been observed in the Owl Gorge Tuff OG-9. The size of these pseudomorphs lies within the range of quartz and feldspar. These pseudomorphs are filled with interlocking flakes of a greenish-yellowish, slightly pleochroitic phyllosilicate (chlorite?) intergrown with quartz. Often a dark, iron oxide-rich margin is developed around the pseudomorphs, which indicates a certain iron content in the original mineral. The precursor mineral was mainly subhedral and obviously had a short-prismatic habitus. From relictic crystal outlines it is suggested that at least some of these pseudomorphs represent former pyroxenes. Very similar pseudomorphs were described by McLachlan & Jonker (1990) from a deformed bed of an altered air-fall tuff from the northwestern part of the South African Karoo Basin. The occurrence of pyroxene, together with plagioclase, quartz and biotite as the dominant crystal fragments, testifies an intermediate, rhyodacitic-dacitic composition of the igneous source rocks.

Although euhedral zircons are an accessory phase in the tuffs, they have been detected in thin sections of every investigated tuff in greater or lesser abundance. Observed grain sizes mainly range from 20-100 μm. However, in heavy mineral separates zircons up to 280 μm length have been observed. Their crystal morphologies can vary considerably from long-prismatic, acicular forms to short-prismatic, squat and stubby forms. Also more or less equi-dimensional crystals occur, with square or octagonal outlines in thin sections. The octagonal ones probably represent so-called 'soccer ball' zircons, which have also been observed in fair amounts in the zircon concentrate of the Khabus Tuff. Especially the acicular zircons often contain tubular to vermiform inclusions, which are often filled with a brownish substance, almost certainly representing glass inclusions. Cathodoluminescence images revealed that many of the zircon crystals possess inherited cores. The SHRIMP analyses showed that most of the euhedral zircons are juvenile, however, some can be slightly older (<10 Ma) than the juvenile zircons and therefore they can be classified as 'young-xenocrystic'. In two cases euhedral zircons proved to be considerably older (Ordovician) than the juvenile fraction (Permian), and therefore they are clearly of 'old-xenocrystic' origin. Two zircons even yielded Proterozoic ages despite their euhedral and magmatic appearance.

Apatite is the second accessory phase that has been observed in every tuff. Their pre-dominantly euhedral to subhedral shape also suggests a mainly juvenile or cognate origin. Most apatites detected in thin sections have sizes or lengths from about 20 to 150 μm. Similar to zircons, apatites within heavy mineral concentrates reach lengths up to 280 μm. Two principle types of apatites have been distinguished in this study. One type is clear and colourless, whereas the other type displays in thin sections a smokey-grey colour and is often concentrically zoned. The latter type is restricted to the younger tuffs with the first occurrence noticed in the Uhabis River Tuff close to the top of the Prince Albert Formation. This certainly reflects changes in the source area(s). Also apatites contain quite frequently inclusions of spherical to tubular shape, which are often filled with brownish glass. Apatites are quite susceptible to alteration and often show more or less distinct etching or corrosion phenomena.

Tourmaline occurs in several tuff layers as euhedral crystals or angular crystal fragments. Since tourmaline is not considered as a volcanic phase it origin is most probably xenocrystic. Other, but much rarer xenocrysts are rounded rutiles and garnets. Bangert (2000) also observed in heavy mineral concentrates monazite and titanite crystals, which could be of volcanic (juvenile or cognate) origin.

3.5.2.2 Macro-components of diagenetic and metamorphic-hydrothermal origin

Diagenetic and metamorphic macrocrystic mineral formations play also an important role in the mineralogical composition of the tuffs. These non-primary and non-pyro-/epiclastic macrocrystal components can be divided into two groups. Within a first group fall all minerals that have pseudomorphically replaced former existing, primary mineral grains. The second group comprises these phases, which occur as newly grown, neoformed macrocrysts within the tuffs after their deposition, e.g. without replacing a precursor mineral. However, the latter phases can in turn be replaced pseudomorphically by later stage minerals. This means that these non-primary (secondary) mineral phases can have an early or late diagenetic or metamorphic origin.

The most conspicuous diagenetic macrocrystic components are crystal booklets of relatively large size with most of them 100-200 µm in diameter and with maximum sizes of up to almost 500 µm. These crystal booklets are mainly composed of phyllosilicates, respectively clay minerals, with either illite or chlorite as the dominant phase. Relicts of biotite within some of these booklets indicate that most of them represent altered and expanded biotites stacks. In some of the least thermally overprinted tuffs, e.g. the Ganigobis Tuffs, in rare cases these booklets appear to be composed, at least partly, of kaolinite. Due to their characteristic form they have been interpreted by Bangert (2000) and Geiger (2000) as kaolinite booklets, which are very characteristic for tonsteins, but also occur in bentonites within organic-rich sediments (Bohor & Triplehorn, 1993). However, the author of this study has recognized that most of these so-called 'kaolinite' booklets actually show bright interference colours under crossed polars and therefore realized that they are now composed of illite. However, it is suggested that most of these crystal booklets initially indeed represented early diagenetically formed kaolinite pseudomorphs after biotite, but were at a later stage replaced under prograde conditions either by illite (e.g. Itzawisis Tuffs) or by chlorite (e.g. Eisenstein and Khabus-Panorama 1 tuffs). In one case (Khabus Tuff) the phyllosilicates of such booklets seem to be finally replaced by blocky to lamellar, mosaic-textured feldspar (± quartz?) during albitization of the tuff. In several tuff layers crystal booklets of perfectly euhedral, rectangular or columnar to vermicular shape occur (see for example Fig. 3.20-L to Q of the Itzawisis Tuffs), which are either completely colourless or are stained by yellowish-brownish iron oxides. In some cases a median line oriented parallel to the long axis of these columnar crystals divides the crystals in two nearly equal parts. The individual clay mineral lamellae (illite platelets) are oriented in these crystals perpendicular to this median line (Fig. 3.56-N & O of the Ufo Valleys Tuffs). No biotite relicts have been observed in these crystals. These columnar crystal booklets and vermicules appear to be chemically precipitated, without any obvious biotite precursor (cf. Bohor & Triplehorn, 1993). Again it is suggested that they originally represented newly grown kaolinite booklets and vermicules, which were later

replaced by illite. The illitization of kaolinite is most probably related to thermal overprinting of most of the investigated tuff layers in the course of widespread Jurassic dolerite intrusions. Other secondary minerals replacing pseudomorphically primary phases are sericite (±chlorite) or feldspar (albite?) after feldspar (plagioclase) and chlorite (± illite/sericite) after biotite and possibly also after pyroxene. Further newly grown minerals are brownish aggregates of minute crystallites, which may be composed of iron and titanium minerals and probably formed due to the alteration of biotite.

Concretions and nodules of diagenetic origin have been very rarely observed within the studied tuff layers, but are quite common in the surrounding shales. Reddish carbonate (mainly calcite) concretions with a diameter up to 6 mm can be found in the basal parts of some feldspathic horizons of the Gai-As Tuffs, and within one tuff layer of the Ufo Valleys Tuffs small (~1 cm), black, ellipsoidal phosphate concretions and larger (up to 6 cm length), light coloured, septarian concretions of calcareous origin have been observed. These former carbonate concretions are transformed due to contact-metamorphism into calc-silicate rocks. Contact metamorphism and hydrothermal overprinting due to widespread dolerite intrusions of Jurassic age is also responsible for the growth of countless greenish to brownish porphyroblasts within the tuffs and the shales. These dolerite intrusions, which are extremely widespread in southern Africa, extend alone in the Keetmanshoop area for about 18000 km^2, where they consist of two major superimposed sills, each more than 120 m in thickness (Gerschütz, 1996). Comparable dolerite sills are also known in the Noordoewer-Karasburg area, e.g. the Tandijeskoppe Sill. The greenish porphyroblasts have mainly spherical, ellipsoidal or ovoid forms but also irregular, and in rare cases, hexagonal forms occur. The size of single porphyroblasts ranges mainly between 50 and 500 μm but can reach sizes of up to 2000 μm. If several porphyroblasts intergrow or merge up to a centimetre large porphyroblastic areas can be formed. The size of the porphyroblasts is generally larger within the tuffs than within the shales. The internal structure of the porphyroblasts is mostly massive, but larger ones also display a multilamellar structure. Furthermore, in some cases faint ghost structures of sector zoning, so-called cross triplets, have been discovered (Panorama Tuff 2). From these observations it can be deduced that these porphyroblasts originally were composed of cordierite, but have been altered under retrograde conditions to pinite, a chlorite- and illite-rich clay mineral mixture. The chloritic composition gives the porphyroblasts their greenish colour, which can turn into brownish colours due to oxidation processes. Other minerals, which are related to cordierite growth and breakdown are rutile, titanite, quartz, chalcedony, feldspar, zeolite?, tourmaline, chlorite, illite, hematite, and goethite. The nature of euhedral apatite and zircon inclusions within large porphyroblastic areas is not fully understood. They might simply represent inclusions of juvenile, primary crystals, but the possibility that they formed during contact-metamorphism cannot be ruled

out. Furthermore, a radioactive mineral of unknown nature causes yellowish pleochroitic halos within the porphyroblasts of the Ufo Valleys Tuffs. Interestingly, andalusite (variety chiastolite) porphyroblasts seem to be restricted to carbonaceous shales.

3.5.2.3 Vitric, respectively former vitric macro-components

Vitric or former vitric macro-components like glass shards, pumice fragments or accretionary lapilli seem not to form a very abundant or obvious component in most of the investigated tuffs but their identification might be quite difficult due to alteration. Few relictic shard and pumice relicts have been reported by Bangert (2000) from the Ganigobis Tuffs. However, tuff OG-9 of the Owl Gorge Tuffs contains numerous pyroclasts of a dirty, dark greenish-yellowish colour showing roundish-elliptical to flattened, lens-like outlines and some contain inclusions of angular quartz or feldspar grains. Under crossed polars they behave more or less isotropic and they might represent altered remnants of originally vitric, volcanic pyroclasts. Similarily, dark schlieren-like clasts form a very conspicuous component within tuff OG-12. These almost black, elongate, lens-like, flattened clasts are often warped, draped over or bent around crystals or contain mineral inclusions and their appearance has a striking similarity to so-called 'fiamme' in welded ignimbrites, representing flattened pumice. A vitric origin seems also highly likely for these schlieren-like clasts, their flattening, however, might have occurred during compaction of the tuff and has certainly nothing to do with welding of hot volcanic ash, which usually produces fiamme-textured ignimbrites. Pumice clasts, which were flattened by compaction and not welding, are also known from ignimbrites in the late Variscan Saar-Nahe Basin (Minning & Lorenz, 1983; Lorenz & Haneke, 2004). Furthermore, in thin sections the Ufo Valleys Tuffs appear highly interspersed with countless thin, black streaks and laminae, which give some tuff beds a wavy and discontinuous but quite distinct horizontal lamination to flaser-like bedding. Often these laminae are draped over and bent around other crystal fragments. It is not clear if these streaks and laminae represent predominantly altered biotite flakes or if they could also represent a former vitric component. Bubble wall glass shards have not been identified with certainty in one single investigated tuff from southern Namibia. This might have been caused by the strong alteration of former glassy components to clay minerals. However, it must be admitted that it cannot be ruled out that the one or the other supposed quartz splinter actually represents a glass shard, which is replaced by silica or zeolite. On the other side, the sampled Gai-As Tuffs of NW-Namibia contain large concentrations of beautifully preserved former glass shards. They show mainly platy and arcuate forms but also tricuspate and Y-shaped shards are quite commen. Their sizes lie mainly in the range of 50 to 150 μm. Many of these former glass shards are now replaced by barite, which make them very obvious in thin sections due to their strong relief against the feldspathic matrix. Furthermore, it has been observed that not only the barite-rich

domains or patches originally contained glass shards, because faint ghost structures of glass shards adjacent to the baritic areas indicate that the whole tuff was originally almost entirely composed of such glass shards. Most of them are now replaced by K-feldspar, a considerable amount is replaced by barite and in a few cases shards are replaced by calcite. True accretionary lapilli or accretionary ash grains have not been discovered yet, but Geiger (2000) mentioned a few spherical, internal structureless ash aggregates, 60-100 µm in diameter, within thin sections of the Zwartbas Tuffs.

3.5.2.4 Lithic components

Lithic components seem to be largely absent in the Late Palaeozoic tuffs of southern Namibia. Only in some thin sections of the NW Namibian Gai-As Tuffs rounded grains (~200 µm in diameter), which consist of phyllosilicates (partly altered biotite) interspersed in a very fine-grained groundmass, could represent felsic volcanic rock fragments.

3.5.2.5 Biogenic components

In a few thin sections of the Owl Gorge Tuffs small, dark-rimmed, perfectly round micro-spherules with a size of 20-40 µm have been observed. They are either filled with quartz or behave isotropically under crossed polars. Such micro-spherules have also been described by several authors from the underlying shales of the Dwyka Group (e.g. Bangert, 2000; Geiger, 2000) and have also been observed in phosphatic shales of the lower Ecca Group by the author. The question about their origin is not fully resolved but the most probable explanation is that they represent radiolarian remains. Beautifully preserved siliceous radiolarian skeletons, for example, have been isolated by Ian McLachlan from Dwyka rocks of the lower Orange River area (illustrated in MacRae, 1999).

3.5.2.6 The nature of the fine-grained matrix

Principally two types have been recognized, which form the fine-grained matrices of the investigated tuffs. One matrix type is dominantly composed of clay minerals, the other type is mainly formed by feldspar. Depending on the dominating clay or feldspar mineral, these types can be further subdivided.

XRD analyses have revealed that the fine-grained matrix of most of the investigated altered tuff layers is strongly dominated by illite and this is why they are often referred to as K-bentonites. Bangert (2000) also identified within the Ganigobis Tuffs the presence of illite-smectite mixed layer clay minerals (ISML) with a smectite content varying between 20-30%. The smectitic portion of the clay minerals gives the tuffs a somewhat soapy feeling and causes its swelling when moistened. Also traces of kaolinite were identified in some tuff layers (Bangert, 2000). Chlorite is present in minor amounts in most tuff layers, the major

part been represented by pinitized cordierite porphyroblasts. Furthermore, XRD analyses indicate that the often distinctly recrystallized matrix also contains certain amounts of microcrystalline quartz and albite. In some cases, e.g. the Owl Gorge and Uhabis River tuffs, black, layer-like phosphate impregnations composed of carbonate hydroxyl fluorapatite (francolite) appear in the upper part of the tuff layers.

In summary it can be concluded that the fine-grained clay mineral-rich matrix represents the alteration product of former vitric volcanic ash. The volcanic ash particles most probably altered early diagenetically mainly to smectite, or kaolinite if deposited within C_{org}-rich sediments (causing also the growth of large kaolinite booklets and vermicules). Within some tuff layers phosphate was precipitated forming black bands in the upper portion of the tuffs. Possibly already during burial diagenesis, but definitely during thermal overprinting by dolerite intrusions, most of the smectite and kaolinte was transformed to illite and chlorite. Some kaolinite could also have (re)formed subrecently due to weathering of pyrite-rich carbonaceous shales (e.g. Ganigobis Tuffs).

Altered tuffaceous beds with a feldspathic matrix are rare within the Ecca Group of Southern Africa. One example is the Khabus-Panorama Tuff 1 within the Whitehill Formation of southern Namibia. The matrix of this tuffaceous horizon is dominantly composed of albite, with some samples also showing an enrichment in silica. The matrix of the Eisenstein Tuffs (also within the Whitehill Formation) is feldspathic, too, but it seems to be mainly composed of plagioclase of intermediate sodic-calcic composition. Since temporary evaporitic-hyper-saline conditions existed during deposition of the Whitehill Formation, an early diagenetic origin of the feldspathization appears reasonable at first sight. However, thin section observations and the fact, that the feldspathic layers are under- and overlain by clay-rich bentonitic tuff layers, raise serious doubts about an early diagenetic origin of the feldspathization. But even a late diagenetic origin does not explain the highly selective feldspathization of individual tuffaceous layers. A similar explanation dilemma exists also for the albitic Matjiesfontein Chert of mixed pyroclastic and epiclastic origin, which is interbedded together with bentonitic layers in shales of the Collingham Formation of South Africa.

Other examples of tuffs with a feldspathic matrix are known from the NW Namibian Gai-As Formation. Some of these tuffs are mainly composed of K-feldspar, others are composed of zeolites (mainly analcime). Because these tuff layers were most probably deposited in an alkaline lake environment, zeolitization of the volcanic ash is very likely to be of early diagenetic origin, whereas feldspathization could be of early or late diagenetic or metamorphic-hydrothermal origin.

3.5.2.7 Other miscellaneous components

The Owl Gorge Tuffs contain large (200-2500 μm), dark coloured, spherical to ellipsoidal to irregular-shaped structures, which are mainly filled with a mosaic of coarse-grained quartz and radial or sheaf-like crystal aggregates of chlorite. Since these structures do not contain or enclose matrix minerals like the pinitized cordierite porphyroblasts, these minerals obviously filled an empty space. They are interpreted as the filling of vesicles, which might represent former trapped air bubbles or biogenically or chemically generated gas bubbles. Their partly irregular shapes could be explained by the mushy or pulpy consistence of the volcanic ash in which they were trapped during or after deposition, preventing the formation of perfectly spherical gas bubbles.

Chapter 4 – Geochemistry of volcanic ash-fall tuff layers

For this study the geochemical composition of all investigated tuff samples, occuring within sediments of the Ecca Group in southern Namibia, was determined. Whole rock samples were analysed for major and trace element contents by XRF at the Institute of Mineralogy, University Würzburg/Germany, whereas rare earth element and some selected trace element abundances were determined by ICP-MS at Actlabs Ltd., Ancaster/Canada. All geochemical data are listed in the appendix. Furthermore, also the U-Th mineral chemistry of zircon, determined during SHRIMP analysis, is discussed in this chapter.

4.1 Introduction

The obtained geochemical data are important to understand the present day mineralogical composition of the tuffs and the data can also be used to classify the altered pyroclastic rocks. In addition, trace element data can provide information about the nature of the source magma and its tectonic setting.

The present day mineralogical and geochemical composition of the altered tuff layers represents the result of a complex history of events and processes, which modified the original composition of the volcanic material. During eruption, transport, deposition, diagenesis, metamorphism, tectonism, exhumation, etc. various components were physically or chemically removed or added, various minerals and vitric particles were transformed into newly formed phases, and various elements were to different degrees depleted, removed, redistributed, reintroduced, enriched, or behaved more or less immobile.

Contamination with non-juvenile material may have taken place already during the eruption by the admixture of wall rock fragments, which can comprise older sedimentary, meta-morphic or igneous rocks, or by the admixture of 'young-xenolithic/-crystic' to cognate magmatic or pyroclastic material, which might be only slightly older, mineralogically and chemically similar or different, but is related to the same igneous phase and system. Especially in the case of highly explosive eruptions this admixture of wall rock fragments can be quite substantial.

Eruption columns can carry volcanic ash into the stratosphere, in which it can be transported hundreds to thousands of kilometres before being deposited. During this transport the composition of the ash may change due to aeolian fractionation. During settling in water fractionation due to different densities and grain sizes of tephra clasts can also affect the ash composition markedly. During settling and after deposition volcanic ash can also be mixed with epiclastic material. However, in the case of the investigated tuff layers, the pyroclastic material was deposited in a low energy marine to freshwater environment, where background sedimentation rates were in most cases distinctly lower than the ash imput and settling rates.

Nevertheless, in some cases reworking, resuspension and redistribution of volcanic ash during or shortly after deposition might have led to admixture of some epiclastic material and during waning ash-fall intensity fine-grained background sediments mixed to some extent with the settling ash.

Originally, the deposited pyroclastic material was most probably composed mainly of glass-rich volcanic ash, which is, however, very susceptible to alteration. Devitrification of volcanic ash commonly leads during diagenesis to the formation of clay minerals or zeolites, dependant on the nature of the depositional environment. Furthermore, in the saline to freshwater depositional environments of the Dwyka and Ecca shales and tuffs in southern Namibia early diagenetic precipitation of carbonate and phosphate lead also to the formation of calcareous concretions and band-like phosphatic impregnations. These diagenetic nodules and bands are one of the most obvious witnesses of element mobility. Furthermore, bleached biotite, sericitized feldspar as well as booklets and vermicules of supposed kaolinite origin within the altered tuff layers testify the intensity of leaching processes, during which mainly alkalies but also other elements were removed or redistributed (see also the summary at the end of Chapter 3). Early diagenetic devitrification of volcanic ash and its transformation into clay minerals or zeolites was followed by burial diagenesis. Under prograde conditions dewatering or dehydration and compaction of the shales and tuffs took place. Also commonly associated with burial diagenesis is the progressive transformation of early diagenetically formed smectite and kaolinite to illite via mixed layer clay minerals if sufficient amounts of potassium are available in fluids. A similar process represents the transformation of zeolites to analcime or feldspar. Numerous and widespread Jurassic dolerite intrusions (sills and dykes) have affected the tuffs to varying degrees. These intrusions caused a severe thermal overprinting of many of the investigated tuffs. Contact-metamorphic imprint is best documented in the intensive speckling of many tuffs caused by the growth of cordierite porphyroblasts. Associated hydrothermal activity later caused the downbreak of cordierite under retrograde conditions to greenish, chlorite-rich pinite pseudomorphs. Finally, sub-recent surface weathering during exhumation of the rocks again altered and modified the composition of the rocks (e.g. due to oxidation and renewed leaching).

4.2 Major elements and the mineralogical composition of altered tuff layers

The studied tuff layers are generally quite fine-grained and the overall abundance of macro-components (crystals, lithic fragments, etc.) is relatively low. Therefore, the major element composition of the altered tuffs mainly reflects the present day mineralogical composition of the fine-grained matrix, whereas crystal fragments influence the geochemical composition of the tuffs only to a minor degree. As explained in the introductionary paragraph of this chapter, the present-day mineralogical and geochemical composition is not very indicative of

the original composition of the volcanic source material due to a great number of modifying processes from eruption via deposition and burial to exhumation. Nevertheless, the major element composition of the tuffs is very helpful in classifying the altered tuffs and it is also indicative of the diagenetic maturity of the tuffs, e.g. how far illitization of smectite or kaolinite of the fine-grained matrix has progressed. In the case of this study these geochemical data are especially very helpful since no advanced XRD analyses were carried out on the tuff layers. Only bulk rock powder samples, but neither clay fraction separates nor glycol or heat treated samples were measured and therefore clay mineral identification and quantification has to be considered merely as a first approach. Illite seems to form in most tuff samples a substantial if not the dominant component of the tuffs. The peak interferences of kaolinite, chlorite and smectite-vermiculite, however, cannot be sufficiently resolved. Secondary quartz and albite may also be present as micro-crystals in the often distinctly recrystallized matrix. In the case of the feldspathic tuffs the geochemical data provide useful hints about the matrix feldspar compositions or the presence of variably mixed feldspar-quartz-clay mineral matrices.

The major element composition of the investigated tuffs is shown in six diagrams (Fig. 4.1 and Fig. 4.2-A to F). The geochemical data of the Ecca Group tuffs are supplemented with data of the Ganigobis Tuffs (Grill, 1997; Bangert, 2000) and of the Zwartbas Tuffs (Geiger, 2000) of the Dwyka Group. In addition to the tuff data also the element contents of some selected minerals are plotted within the diagrams for a better understanding of the relationship between mineralogical and geochemical composition of the investigated tuffs. For the calculation of individual element contents (in wt%) of selected mineral phases the following formulas have been used:

Muscovite:	$KAl_2[(OH)_2/Si_3AlO_{10}]$
Illite:	$K_{0.8}Al_2[(OH)_2/Si_{3.2}Al_{0.8}O_{10}]$
Kaolinite:	$Al_2[(OH)_4/Si_2O_5]$
Chlorite:	$Mg_{2.5}Fe_{2.5}Al[(OH)_8/Si_3AlO_{10}]$
Smectite:	$Ca_{0.23}K_{0.01}Mg_{0.53}Fe_{0.08}Al_{1.43}Ti_{0.01}[(OH)_2/Si_{3.87}Al_{0.13}O_{10}]$
Albite Ab_{100}:	$NaAlSi_3O_8$
Plagioclase $Ab_{50}An_{50}$:	$Na_{0.5}Ca_{0.5}Al_{1.5}Si_{2.5}O_8$

The muscovite, kaolinite and albite formulas represent ideal end-member compositions, whereas the plagioclase and chlorite formulas represent intermediate compositions between end-members (regarding Na-Ca, Mg-Fe, and Si-Al). The illite formula reflects a hypothetical alteration product of muscovite (Nesse, 2000), which is depleted in K and enriched in Si. However, natural illite shows a wide range of compositions and especially contains also

interstitial water which was not regarded here. The same is also valid for smectite. The smectite formula was calculated from an almost monomineralic, montmorillonitic bentonite layer, which was interpreted as an altered volcanic ash layer and is intercalated in sediments of the Upper Permian Rio do Rasto Formation of Brazil (Calarge et al., 2003b).

The geochemical difference between the two principle types of altered tuff layers found in southern Namibia, i.e. bentonitic, clay mineral-rich tuffs and chert-like, feldspathic (albitized) tuffs, is best shown in an element plot K_2O vs Na_2O, in which the K-dominated bentonites can be clearly distinguished from the Na-dominated, plagioclase-rich tuffs (Fig. 4.2-A). Within the group of bentonitic tuffs the Na_2O contents vary mainly around 1 wt%, whereas the K_2O contents vary considerably between ~2 wt% and ~10 wt%. However, most tuff groups plot as individual clusters showing a relatively narrow range of potassium and sodium values (e.g. Itzawisis, Korabib, Zwartbas, Owl Gorge, and Ufo Valleys Tuffs). An exception form the Ganigobis Tuffs with a quite large range of potassium and sodium contents, reflecting the sampling from a multitude of tuff layers from different stratigraphic levels and different localities (Bangert, 2000). Among the bentonitic tuff layers the softness or hardness of the rocks is strongly related to the potassium content. For example, the very soft and crumbly Itzawisis Tuffs show the lowest potassium contents with K_2O values between 2 and 4 wt%. Also the Korabib Tuffs with ~4 wt% K_2O represent relatively soft rocks. In contrast, the very hard and indurated Owl Gorge and Ufo Valleys Tuffs show K_2O contents of 6-7 wt% and 8-10 wt%, respectively, and their matrices are strongly recrystallized. The degree of induration and recrystallization seems to be related to the proximity of dolerite sill intrusions and their associated contact aureoles and hydrothermal cells. Therefore, it can be concluded that strong thermal overprinting is associated with increased potassium contents. The increased potassium content is supposed to be related to progressive illitization of smectite and/or kaolinite clay mineral components and the progressive dehydration of illite towards muscovitic compositions. The potassium contents of the altered bentonitic tuffs are cleary reflecting diagenetic and/or hydrothermal-metasomatic processes and can therefore be used as a proxy for thermal alteration intensity. In this respect the Ufo Valleys Tuffs represent the strongest and the Itzawisis Tuffs the least overprinted rocks. The majority of the Ganigobis Tuffs plot in an intermediate position with ~5-6 wt% K_2O. Interestingly, the Zwartbas Tuffs are quite comparable to the Owl Gorge Tuffs with respect to their potassium and sodium contents, despite their softer and crumblier appearance, which is more similar to the Ganigobis Tuffs. The two Collingham Tuff samples from the Rhyofontein locality are distinctly K-poorer and Na-richer than the samples from the Ufo Valleys locality. This is most probably related to enhanced hydrothermal fluid activity at the Rhyofontein locality, which lies at the eastern edge of a felsic dyke and its associated fracture and alteration zone (Fig. 3.49). The Uhabis River and some of the Ganigobis Tuffs show a similar trend with even lower

potassium and higher sodium contents. This trend most probably reflects increased albitization and/or silicification of the matrix of the tuffs, or this could also have been caused by zeolite growth.

The element plot K_2O vs SiO_2 of Fig. 4.2-B shows that the progressive illitization is connected with a progressive decrease in the silica contents from around 65 wt% (Itzawisis and some of the Ganigobis Tuffs) to about 50 wt% (Ufo Valleys, Zwartbas, and the majority of the Ganigobis Tuffs). In the strongly phosphatic samples of the Uhabis River and Owl Gorge Tuffs the silica content is further depressed due to strong impregnation with francolite (carbonate hydroxyl fluorapatite). Conversely to decreasing silica contents, the alumina contents are increasing from around 15-20 wt% Al_2O_3 for the Itzawisis and some of the Ganigobis Tuffs up to almost 30 wt% Al_2O_3 for the Ufo Valleys, Itzawisis and Owl Gorge Tuffs with increasing K_2O contents, respectively with prograde illitization (Fig. 4.2-C). The K_2O vs SiO_2 and vs Al_2O_3 diagrams also show that despite the presence of illite pseudomorphs after supposed kaolinite the diagenetic-metamorphic alteration path reflects a development from smectite-rich to illitic rocks rather than from kaolinitic compositions. This means that the early diagenetic composition of the studied tuffs was certainly more of a bentonitic rather than of a tonstein-like nature.

Fig. 4.2-D & E show that the potassium content of the bentonitic tuff layers neither correlates with their magnesium nor with their iron content. The MgO values range from around 0.5 to almost 3 wt% and the Fe_2O_3 values from around 1.5 to 10 wt%. However, what becomes apparent if the two diagrams are compared to each other is that within individual tuff groups similar trends for magnesium and iron can be observed, e.g. within the Itzawisis, the Korabib, the Uhabis River, the Zwartbas, and also the Ufo Valleys-Rhyofontein Tuffs. This means that magnesium and iron must be positively correlated within individual tuff groups, which reflects the presence of more or less amounts of a magnesium- and iron-bearing mineral phase. The mineral phase in question is certainly chlorite, which is widely present as an alteration product of biotite flakes, as an alteration product of cordierite porphyroblasts, and possibly also in the fine-grained matrix (either as individual crystallites or as a component of mixed layer clay minerals). It is speculated that most of the chlorite might form a part of the pinitic alteration products of cordierite. Variable Mg-Fe ratios for individual tuff groups may indicate variable chlorite compositions or the presence/absence of other magnesium- or iron-bearing phases (biotite, smectite). The relatively high iron content of some samples of the Ganigobis Tuffs is probably related to intensive limonite staining, which in turn might be largely caused by the downbreak of biotite, magnetite or ilmenite, since some of these samples are also quite rich in titanium.

Other important major elements are calcium and phosphorus, the contents of which are displayed in Fig. 4.2-F. Within the bentonitic tuffs the highest calcium and phosphorus

contents are found in the diagenetically phosphate-impregnated samples (Uhabis River, Owl Gorge, and Ufo Valleys Tuffs), which are shown in the small inset of Fig. 4.2-F. Their CaO-P_2O_5 ratio ranges from ~1.4, which is quite comparable to igneous apatite (~1.3), to ~1.75. In the tuff samples with P_2O_5 values lower than 0.50 wt% much higher CaO-P_2O_5 ratios are found. In these samples the phosphorus content is probaly dependant on the abundance of both igneous (juvenile) and diagenetic apatite, but also other calcium-bearing phases must be present to explain the strongly deviating CaO-P_2O_5 ratios. In the least thermally overprinted Itzawisis Tuffs as well as in some of the less affected Ganigobis Tuffs the calcium contents may be mainly controlled by the presence of smectite and, especially for the Ganigobis Tuffs, by the presence of calcite, explaining the very high CaO-P_2O_5 ratios ranging from ~10 to ~25. Intermediate ratios (~3.5-5.5) are found for the Ufo Valleys, Korabib and Panorama 2 Tuffs. The two samples of the Rhyofontein Tuffs have a somewhat isolated position within this diagram. Their phosphorus values are too high to be explained by juvenile, igneous apatite and are therefore surely slightly enriched with diagenetic francolite. However, their calcium values are also too high to be explained by smectite, and since they are not calcareous another mineral phase must be present. As mentioned above, this sample locality is in the vicinity of a felsic dyke with an associated fracture zone. The latter is intensively mineralized with prehnite and it can be speculated that also the Rhyofontein Tuffs have been affected by fluids which may have introduced calc-silicate mineral phases.

Among the chert-like, feldspathic tuff layers of the Whitehill Formation of southern Namibia three geochemical subtypes can be distinguished (Tab. 4.1). Firstly, two samples of the Khabus Tuffs show a composition, which matches quite well that of pure albite. The matrix of these two samples seems therefore to be largely composed of albite, which is also supported by XRD analyses. Secondly, sample KHA-1BT of the Khabus Tuffs and the Panorama Tuff 1 sample appear also strongly albitized. However, increased SiO_2 values indicate also a certain degree of silicification, causing a suppression of the other element contents. Thirdly, the composition of the Eisenstein Tuff sample is geochemically quite distinct from the other feldspathic tuff samples. Its geochemical composition either indicates a more intermediate composition of the matrix plagioclase (closer to the composition of $Ab_{50}An_{50}$) or it is the result of a mixed albite- and clay mineral-rich matrix. The inhomogeneous, honey-comb-like texture of this tuff (see Fig. 3.48-A) might support the latter explanation, however, the relatively high CaO content (see also Fig. 4.2-F) cannot be explained with the presence of Ca-smectite, but must be related to the presence of another calcium-bearing mineral. Since no calcite or apatite/francolite is present, a calcium-bearing plagioclase might be a possible explanation, or there is another undetected calcium mineral phase present (e.g. epidote-group mineral?). Possibly electron microprobe analyses of matrix domains could shed some more light onto this problem. The Fig. 4.2-A to C also show the position of the individual feldspathic tuff

samples in relation to pure albite and an intermediate plagioclase ($Ab_{50}An_{50}$) composition. Quite enigmatic is the relatively high magnesium content of the Eisenstein Tuff sample. From thin section analyses it is know that this tuff contains a large amount of chlorite, however, the distinct bluish interference colours of these chlorites are more indicative for the presence of an iron-rich rather than a magnesium-rich chlorite variety, but the iron content of the Eisenstein sample is actually much lower than the magnesium content (Fig. 4.2-D & E).

[wt%]	Plagioclase Ab_{100}	Khabus KHA-1AT	Khabus KHA-1CT	Khabus KHA-1BT	Panorama Tuff 1	Plagioclase $Ab_{50}An_{50}$	Eisenstein Tuff
SiO_2	68.74	64.54	67.44	73.03	72.76	55.59	53.48
Al_2O_3	19.44	19.50	18.45	14.34	15.05	28.30	25.59
Na_2O	11.82	9.76	10.07	7.28	5.15	5.73	4.86
CaO	0	0.70	0.30	0.49	0.55	10.38	7.52

Tab. 4.1: In this table the geochemical compositions of the chert-like, feldspathic tuffs of the Whitehill Formation of southern Namibia are shown in comparison to element contents of pure albite (Ab_{100}) and an intermediate plagioclase ($Ab_{50}An_{50}$).

Fig. 4.1: Legend for the following element plots within this Geochemistry Chapter for various altered tuff samples from southern Namibia. The geochemical data for the Ganigobis Tuffs are from Grill (1997) and from Bangert (2000), the data for the Zwartbas Tuffs are from Geiger (2000).

The manganese contents of the studied tuffs are generally very low (<0.1 wt%) and this element rather represents a trace element. Manganese enrichment has been observed in phosphatic and calcareous samples.

Titanium is conventionally listed among the major elements, however, here it is considered as a trace element and therefore discussed in the following subchapter together with other elements, which also tend to show a very low mobility behaviour.
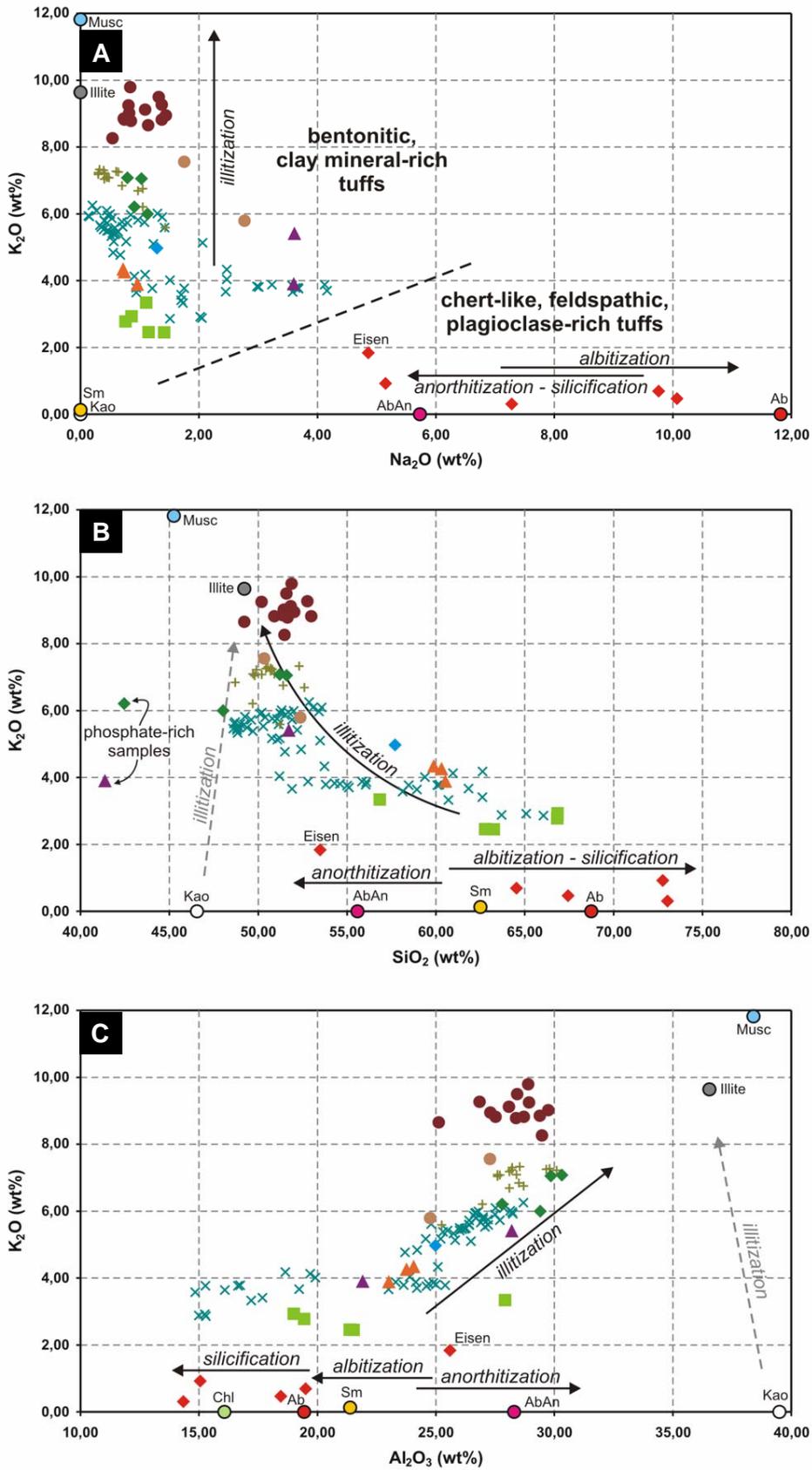
Fig. 4.2-A to C: Diagrams showing the potassium, sodium, silica and alumina contents of altered tuff layers from the Dwyka and Ecca Groups of southern Namibia.
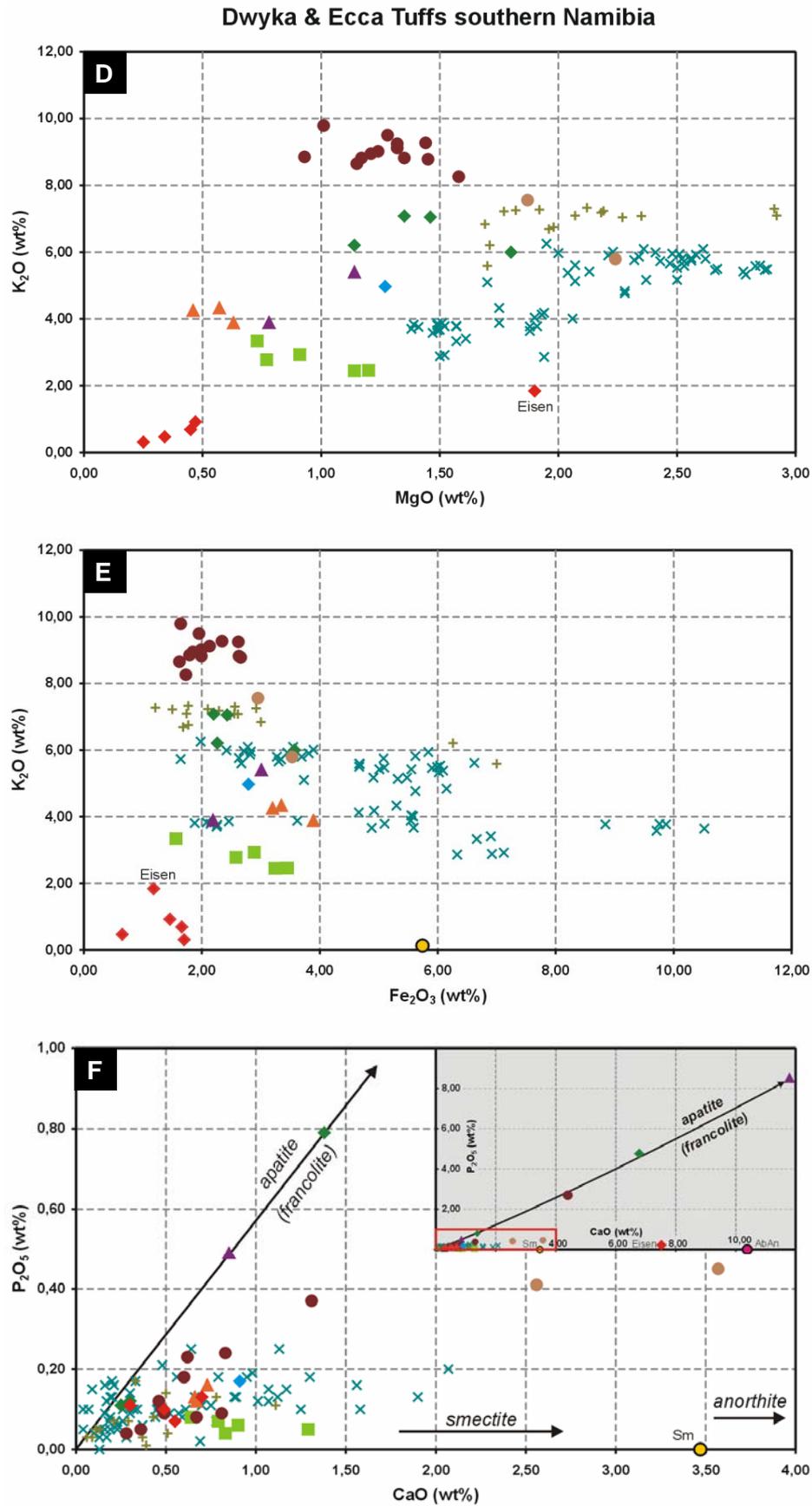
Fig. 4.2-D to F: Diagrams showing the magnesium, iron, calcium, and phosphorus contents of altered tuff layers from the Dwyka and Ecca Groups of southern Namibia.

4.3 Trace elements and the supposed nature of source magmas

Only some selected trace elements, which tend to show a more or less immobile character, are considered here. To determine the nature of the source magma of bentonites and tonsteins traditionally the Zr/TiO_2 vs Nb/Y diagram after Winchester & Floyd (1977) is used. Recently, Batchelor et al. (2003) and Batchelor (2005) attempted to improve this approach by developing a diagram, in which the Ti/Th ratio is plotted against the Zr/Nb ratio avoiding the use of yttrium, which can behave mobile under certain circumstances. To gain some information about the possible geotectonic environment of the volcanic source region often various diagrams of Pearce et al. (1984), originally developed for granitic rocks, are applied. However, the use of rubidium, e.g. in the Rb vs Y+Nb diagram, is considered as inappropriate for the altered Dwyka and Ecca tuffs of southern Namibia because it can be shown that the rubidium contents of the investigated tuffs are mainly controlled by secondary processes. Alternatively, the Nb vs Y as well as the Ta vs Yb diagram may provide more reliable informations about the geotectonic environment of the volcanic source region.

In the following the Rb, Ti, Nb, Zr, Y and Th contents of the investigated tuffs are shown in a number of K_2O vs trace element and trace element vs trace element plots (Fig. 4.3-A to M). Potassium is used as a reference element because it has been shown in the major elements chapter that this element can be considered as the most indicative proxy for alteration, especially the late-stage thermal overprinting leading to progressive illitization. Therefore, none of the trace elements, which are used in order to gain some information about the primary volcanic source material, should show any correlation with potassium.

The first diagram (Fig. 4.3-A), in which K_2O is plotted against Rb, clearly shows the strong positive correlation between these two elements and therefore proves that also the rubidium contents are largely controlled by secondary processes and cannot be used in diagrams discriminating between geotectonic environments of source magmas.

Fig. 4.3-B & C show that neither titanium nor niobium correlates with potassium. Due to comparable sizes of ionic radii, niobium can readily enter the structures of titanium minerals (Werner & Cook, 2001). Therefore, a positive correlation of niobium and titanium can be expected. The TiO_2 vs Nb diagram of Fig. 4.3-D indeed shows a discernable positive correlation, however with a rather low positive correlation coefficient.

Also no correlation exists between the zirconium and the potassium contents of the tuffs. Fig. 4.3-E shows a quite interesting feature concerning the zirconium contents of the investigated tuff layers. Among all Dwyka and Ecca tuffs of southern Namibia, the Ufo Valleys & Rhyofontein Tuffs within the Collingham Formation show the highest zirconium contents and a unique wide range of zirconium contents ranging from about 170 up to 520 ppm, whereas most of the other tuffs lie within the narrow range of 100-300 ppm zirconium.

The diagram K_2O vs Y of Fig. 4.3-F contains a small inset revealing that for tuff samples, which are markedly impregnated with diagenetic phosphate, there exists a strong negative correlation between yttrium and potassium. Yttrium is strongly enriched in apatite/francolite and therefore the phosphate-impregnated tuff samples contain the highest yttrium contents (Fig. 4.3-G). The potassium contents are markedly 'diluted' by the diagenetic phosphate impregnations explaining the negative correlation between potassium and yttrium for high-phosphate tuff samples, whereas for low-phosphate tuff samples (large diagram area of Fig. 4.3-F) no correlation can be observed between these two elements. Interestingly, low-phosphate tuff samples (<0.3 wt% P_2O_5) also do not show a positive correlation between phosphorus and yttrium (Fig. 4.3-H). An explanantion for this phenomenon provide the zirconium vs yttrium plots (Fig. 4.3-I & K). Strongly phosphate-impregnated, and therefore high-yttrium tuff samples show a rather negative correlation between zirconium and yttrium (Fig. 4.3-I), similar to the plot K_2O vs Y, whereas in low-phosphate samples yttrium strongly correlates positively with zirconium. This trend is also clearly visible in Fig. 4.3-K and is particularly expressed by the Zr-Y-data of the Ufo Valleys-Rhyofontein Tuffs. This leads to the important conclusion that the yttrium content of low-phosphate tuff samples is primarily strongly controlled by the zircon (mineral) content of the tuff samples (especially in the zircon-rich Ufo Valleys-Rhyofontein Tuffs) and only to a lower extent by the presence of phosphate minerals, e.g. diagenetic francolite and/or igneous apatite, monazite or xenotime (expressed by the other tuff groups, which show a slight shift towards higher yttrium contents; Fig. 4.3-K). This is in so far very important because it shows that in low-phosphate tuff samples the yttrium signal can largely be considered as a primary, volcanic signal rather than a secondary, diagenetic or metasomatic signal, what affects the validity of the Zr/TiO_2 vs Nb/Y diagram after Winchester & Floyd (1977) in a positive way for the investigated tuffs.

Finally, Fig. 4.3-L & M show the plots K_2O vs Th and Zr vs Th. Contrary to the other K_2O vs trace element diagrams there is a slight positive correlation between potassium and thorium discernable, however, a rather weak one. Interestingly, thorium shows no obvious correlation with zircon (Fig. 4.3-M) and the same is also valid for phosphorus. This implies that the thorium contents of the investigated tuffs are obviously not controlled by the presence of zircon and phosphate minerals (e.g. monazite), which are commonly the main host minerals for thorium. As thorium can be mobile in hydrothermal systems it can be speculated that thorium might to a large extent be adsorbed on clay mineral or limonite microparticles in the investigated tuffs, which might also explain the slightly positive correlation with potassium. Therefore it cannot be ruled out that the thorium contents of the investigated tuffs are possibly controlled by secondary processes, which means that the interpretations derived form the Ti/Th vs Zr/Nb diagrams after Batchelor et al. (2003) and Batchelor (2005) have to be handled with great caution.
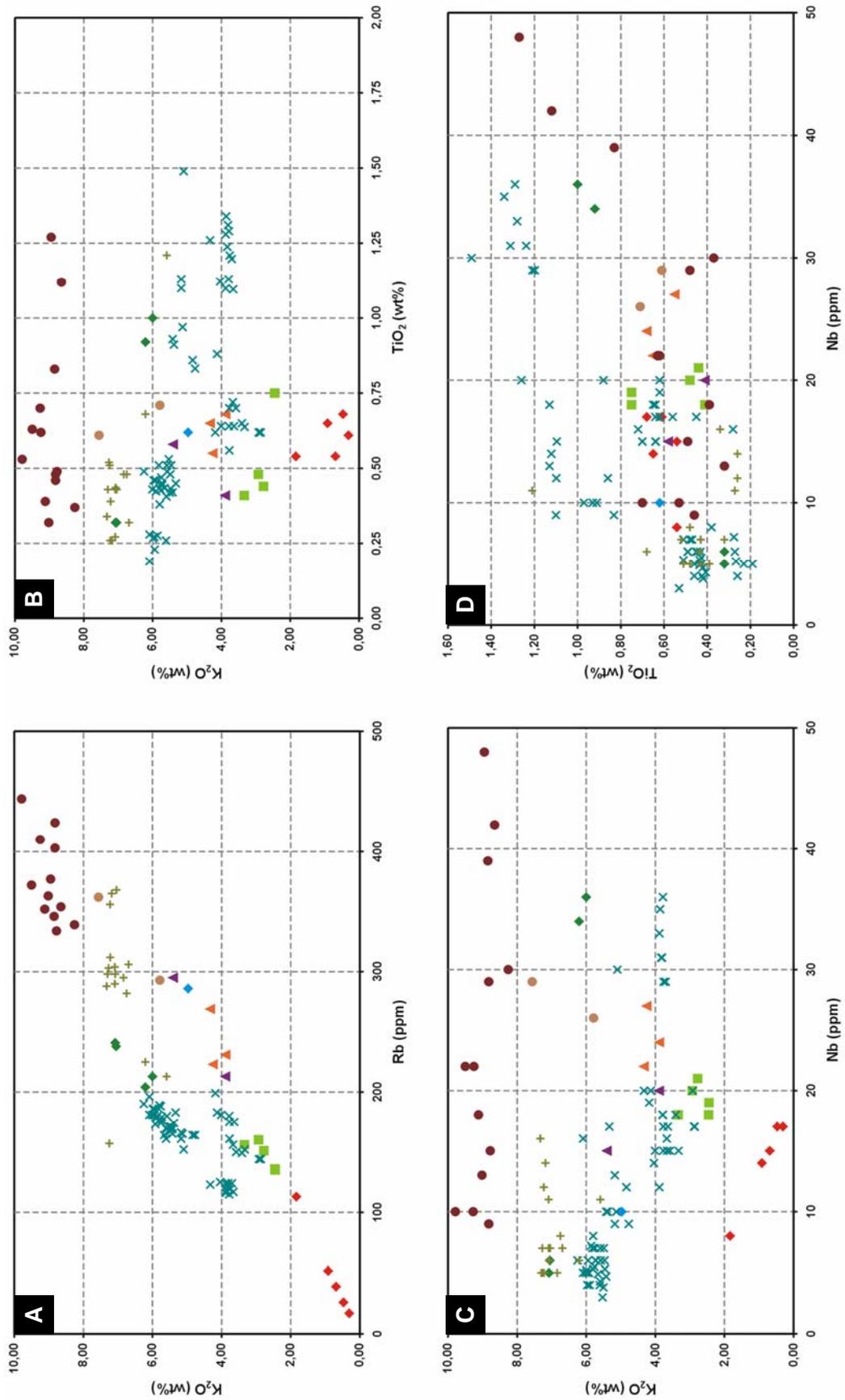
Fig. 4.3-A to D: K_2O vs Rb, TiO_2 and Nb as well as TiO_2 vs Nb diagrams for Dwyka and Ecca tuffs of southern Namibia. See text for explanations.
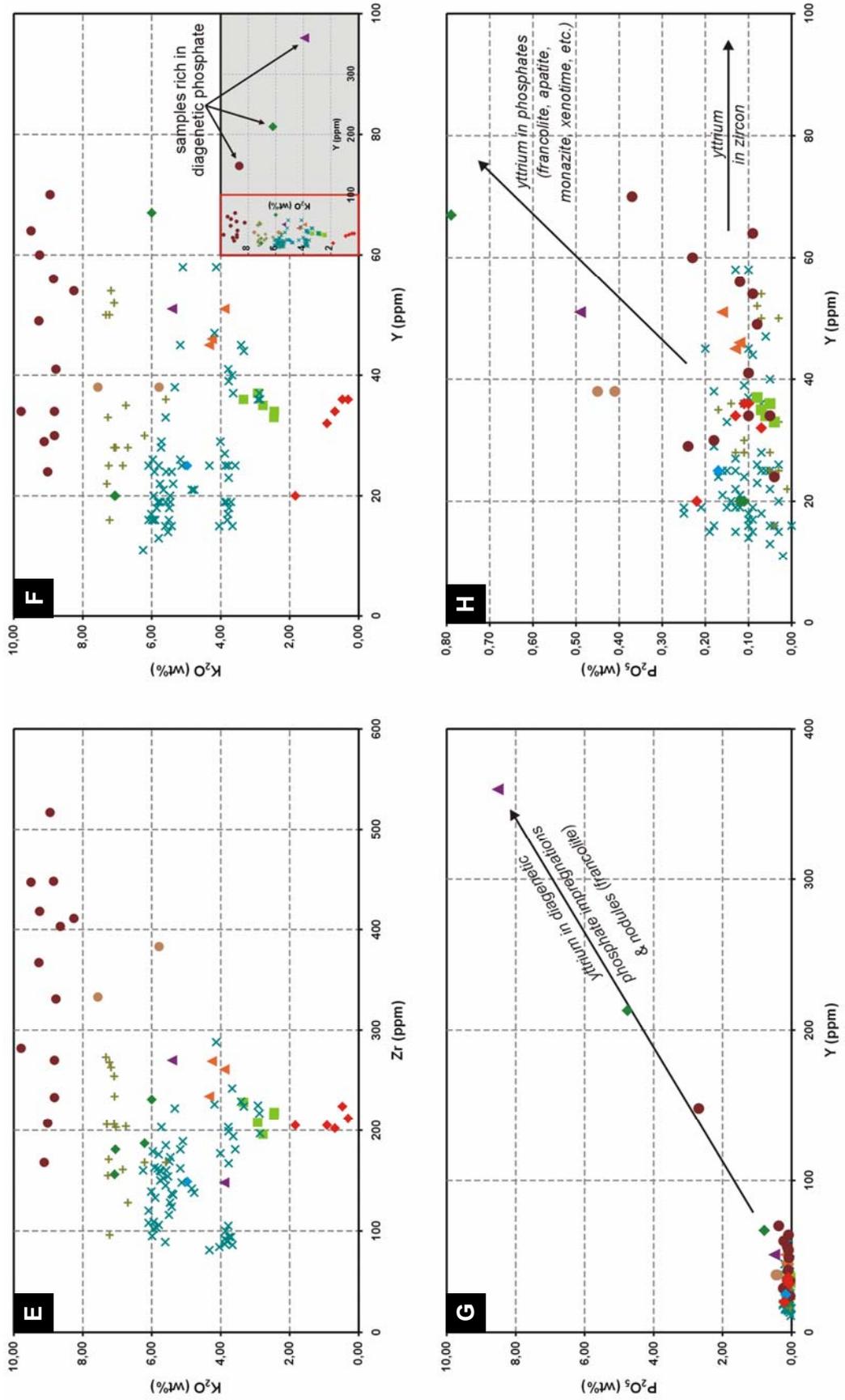
Fig. 4.3-E to H: K_2O vs Zr and Y as well as P_2O_5 vs Y diagrams for Dwyka and Ecca tuffs of southern Namibia. See text for explanations.
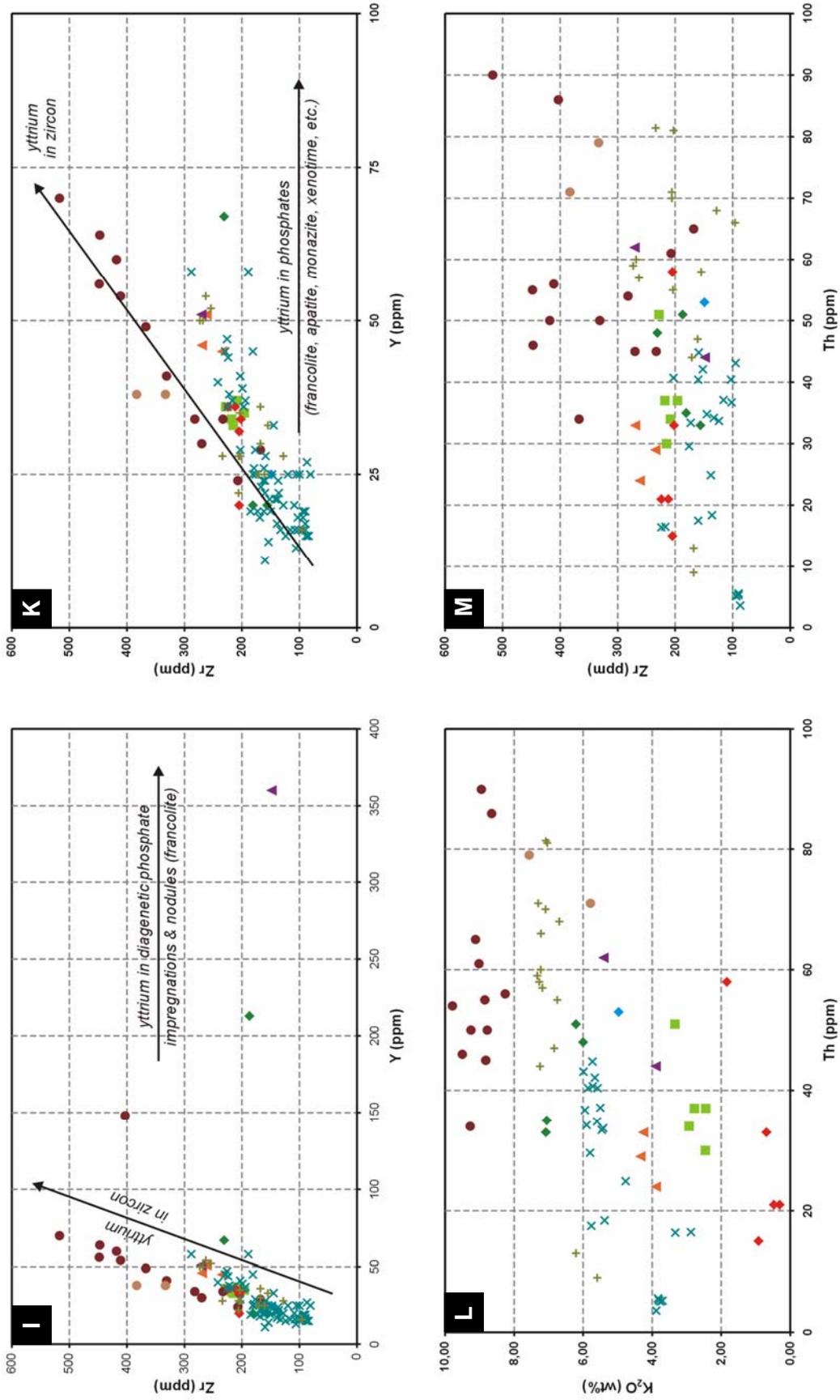
Fig. 4.3-I to M: Zr vs Y as well as K$_2$O and Zr vs Th diagrams for Dwyka and Ecca tuffs of southern Namibia. See text for explanations.

Zr/TiO$_2$ vs Nb/Y discrimination diagram after Winchester & Floyd (1977)

This variation diagram is used to distinguish common volcanic rock types. Both the Nb/Y ratio and the Zr/TiO$_2$ ratio are indices of alkalinity, but only the Zr/TiO$_2$ ratio represents a differentiation index. Winchester & Floyd (1977) therefore found that the plot of Nb/Y against Zr/TiO$_2$ discriminates between different volcanic magma series (alkaline and calc-alkaline) and rock types. Since Ti, Zr, Y and Nb are generally considered to remain largely inert during secondary alterationen processes this discrimination diagram has also widely been applied for bentonites and tonsteins. However, the present day contents of these elements in the studied tuffs may not be the same than in the original volcanic rock. For example, already during eruption, distribution and deposition contamination and fractionation can take place in the atmosphere and in water. But since all these elements are largely incorporated in heavy minerals the aeolian fractionation effect should affect them to a similar extent. This is also valid for other dilution or concentration processes and due to the ratio-ratio plot these effects are minimized. In the case of the Dwyka and Ecca tuffs of southern Namibia it can be shown that some of the involved elements are certainly not strictly immobile under the observed alteration conditions. For example, neoformed rutile crystals have been observed within pinitized porphyroblasts. However, it appears that titanium is not markedly introduced to or removed from but rather redistributed over short distances within the tuffs due to downbreak of titanium-bearing minerals and precipitation of neoformed titanium phases (rutile, anatase?, titanite?). Furthermore, titanium and niobium act geochemically in a very similar way during these alteration processes. Therefore it can be concluded that the relative amounts of titanium and niobium remain more or less constant but also the absolute contents are likely to be relatively close to the original volcanic source composition. Zirconium, more or less exclusively controlled by the zircon content of the tuffs, can be affected physically by aeolian fractionation in the same way as titanium- and niobium-bearing heavy minerals. Geochemically, zirconium can be considered as the most immobile element among the discussed elements due to the stability of zircon. Only zircons with high contents of radioactive elements like uranium and thorium can suffer radiation damage, which might affect the zirconium mobility to a certain extent. For the Zr/TiO$_2$ vs Nb/Y diagram after Winchester & Floyd (1977) yttrium is considered as a somewhat problematic element. Among the involved elements yttrium is probably the least immobile element (Hill et al., 2000; Batchelor et al., 2003; Batchelor, 2005). Therefore, a closer look has been taken at the distribution and behaviour of yttrium in the investigated tuffs (see also trace element discussion above). In summary it can be concluded that the yttrium content is controlled only in high-phosphate tuffs, which are impregnated with diagenetic phosphate, largely by secondary processes. In low-phosphate tuffs the majority of the yttrium content seems to be incorporated within the zircon structure and only to a minor extent in those of phosphate

minerals. Therefore, for this study it can be concluded that for most of the low-phosphate tuffs the yttrium content represents mainly a primary signal reflecting the the original content of the source rock. Phosphate-impregnated tuffs are diagenetically enriched in yttrium, which causes a shift of data points within the Zr/TiO_2 vs Nb/Y diagram towards the left (see for example the Nondweni Tuff sample in the Dwyka Group diagram as well the Uhabis River and OG-12 tuff samples in the Prince Albert Formation diagram; Fig. 4.4-B & C). The geochemical data for the investigated Dwyka and Ecca tuffs of southern Namibia are plotted into a series of Zr/TiO_2 vs Nb/Y diagrams representing various stratigraphic levels and for comparison also geochemical data from age-equivalent tuff layers from neighbouring areas (South Africa and Brazil) are plotted in separate diagrams (Fig. 4.4-A to K).
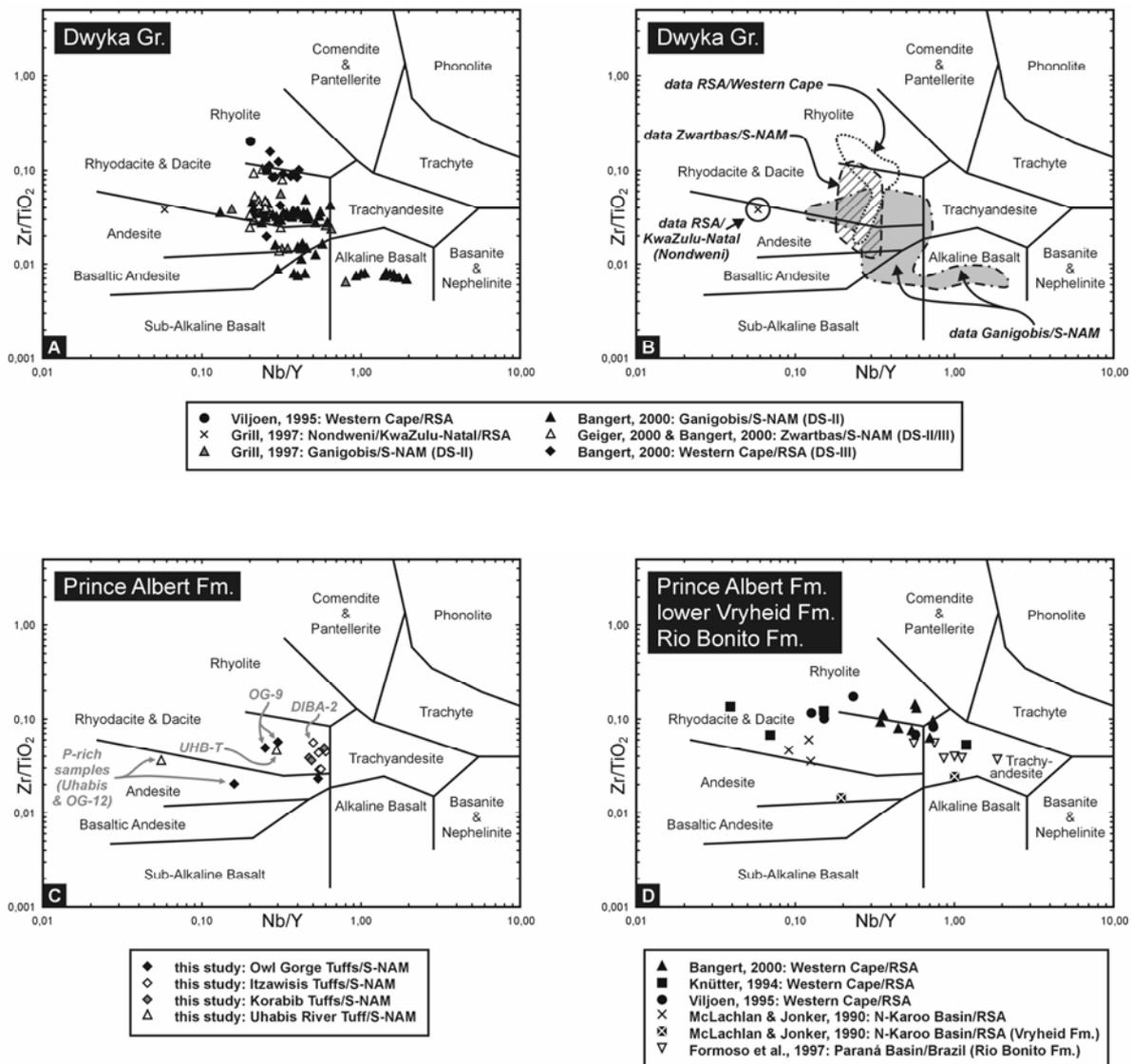
Fig. 4.4-A to D: Zr/TiO_2 vs Nb/Y discrimination diagrams after Winchester & Floyd (1977) for studied Dwyka and Ecca tuffs from southern Namibia and age-equivalent tuffs from neighbouring regions.
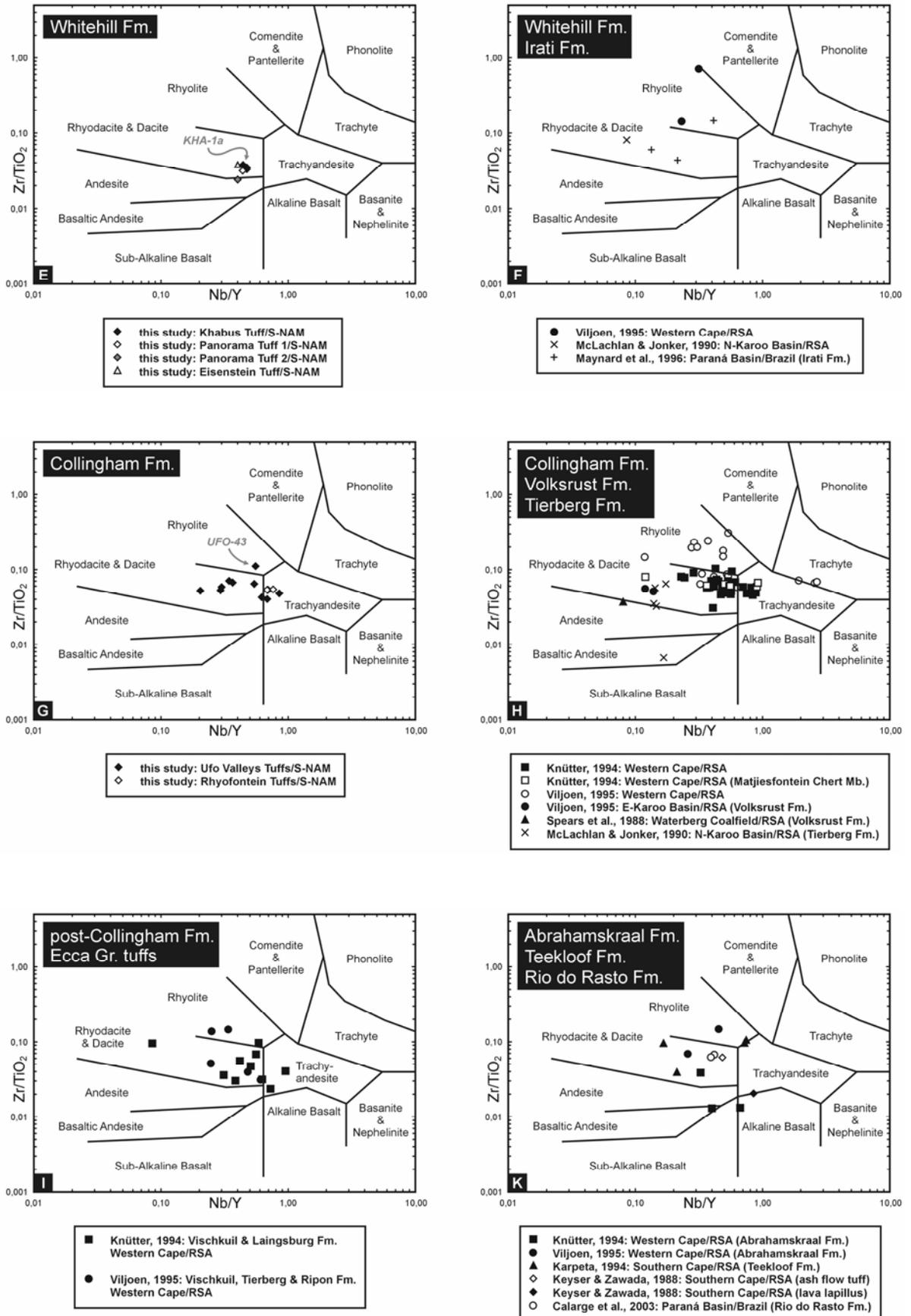
Fig. 4.4-E to K: Zr/TiO$_2$ vs Nb/Y discrimination diagrams after Winchester & Floyd (1977) for studied Ecca tuffs from southern Namibia and age-equivalent tuffs from neighbouring regions as well as slightly younger tuffs from middle/upper Ecca and lower Beaufort Group tuffs.

Fig. 4.4-A shows a wide range of compositions for the bentonitic tuffs within the Dwyka Group. In combination with Fig. 4.4-B, which shows only the data fields for the Ganigobis and the Zwartbas Tuffs as well as the South African Dwyka tuffs, a clearer picture evolves. The South African tuffs show mainly acid to intermediate compositions ranging from rhyolite to andesite, whereas the data field for the Zwartbas Tuffs is more restricted to intermediate to slightly basic compositions ranging from rhyodacite to andesite. The data points of the Ganigobis Tuffs form three more or less well-defined clusters. The first cluster lies close to the lower boundary of dacites, whereas a second cluster is positioned around the intersection point of the andesite, basaltic andesite and sub-alkaline basalt fields. In addition, most of the data points of the Ganigobis Tuff IVa plot within the alkaline basalt field forming a quite well-defined third cluster. Therefore, the Ganigobis Tuffs record the most basic compositions of all three areas (Ganigobis, Zwartbas, Western Cape/RSA). The shift from acid to intermediate compositions in the south (Western Cape) towards intermediate to basic compositions in the north (Ganigobis) might hint at the presence of at least two different volcanic source regions and this might also explain that tuffs in the Dwyka Group of Namibia are much more prominent and frequent than in the Dwyka Group of South Africa. The supposed different geochemical nature of the volcanic source rocks also indicate that the higher frequency of Dwyka tuffs in Namibia is probably not just reflecting a higher preservation potential due to different depositional environments and conditions. The trimodal composition of the Ganigobis Tuffs could either reflect the presence of several, different source areas or a bi/trimodal character of the volcanic material erupted within one source area or a combination of both. In summary, the data points and fields of tuffs from the Dwyka Group reveal that different regions show different geochemical signatures indicating different source areas. For the tuffs within the Ecca Group and equivalent strata such a differentiation cannot be observed due to large overlaps of data points.

The majority of tuffs from the Namibian Prince Albert Formation plot within the rhyodacite-dacite field (Fig. 4.4-C). The data points of the phosphate-impregnated Uhabis River and OG-12 tuff samples are shifted to the left due to a strong yttrium enrichment associated with diagenetic francolite precipitation (the same is also valid for the phosphate-rich sample of the Nondweni Tuff in the Dwyka Group diagram). The data points for tuffs within the Prince Albert Formation and equivalent strata outside Namibia are widely scattered over the rhyolite, rhyodacite-dacite and trachyandesite fields (Fig. 4.4-D). The data points of the feldspathic, mainly albitized tuff samples of the Namibian Whitehill Formation form a narrow cluster at the lower margin of the dacite field, whereas Whitehill/Irati tuff data from outside Namibia show rhyolitic to dacitic compositions (Fig. 4.4-E & F). Similarily to the Namibian tuffs in the Prince Albert and Whitehill Formations also the Namibian Collingham tuffs plot mainly within the rhyodacite-dacite field, however, they are more positioned in the upper half

of the field towards a more acidic character. Additionally, there is also a distinct overlap into the trachyandesite field recognizable (Fig. 4.4-G). This data spread is also clearly mirrored by the data points for the Collingham Formation tuffs of South Africa strongly indicating a common source of the Collingham Tuffs for both regions (Fig. 4.4-H). In addition, a number of samples from the South African Collingham tuffs plot within the rhyolite field, whereas only for the thickest tuff layer of the Namibian Ufo Valleys Tuffs (sample UFO-43) a rhyolitic composition can be deduced. Tuff layers within post-Collingham Ecca strata, which are not represented in southern Namibia (except the Sesfontein Tuff in the Aussenkjer Formation) also mainly plot within the rhyodacite-dacite field with some minor overlap into the rhyolite and the trachyandesite fields (Fig. 4.4-I). As a summary it can be concluded that the tuffs within the Ecca Group and equivalent strata show in all regions a predominantly inter-mediate, rhyodacitic-dacitic compositon and most probably have a common source. A few geochemical data are also available for the Upper Permian tuffs intercalated in sediments of the fluvio-lacustrine Beaufort Group and equivalent strata in Brazil. They also show predominantly intermediate compositions with some data points in the rhyolite field and some data points indicating more basic, andesitic-basaltic compositions (Fig. 4.4-K).

Ti/Th vs Zr/Nb discrimination diagrams after Batchelor et al. (2003) and Batchelor (2005)

Batchelor et al. (2003) argued that the traditional discrimination diagram of Winchester & Floyd (1977), which utilizes Zr/TiO_2 vs Nb/Y, is considered unsuitable for metabentonites, which have undergone a high degree of alteration. In particular, the use of yttrium is considered unreliable (Hill et al., 2000) due to its mobility under certain conditions and should be avoided. Instead, an adaption of traditional discrimination diagrams for volcanic rocks based on Zr/Nb vs Ti/Th seem to allow for certain highly altered tuffs a cautious classification of the source material to be made. Data for the rock fields of this diagram type were taken from Wilson (1989). So far two versions of the Zr/Nb vs Ti/Th diagram were published. The version of Batchelor et al. (2003) has linear scaled axes with Ti/Th ratios between 0 and 500 on the y-axis and Zr/Nb ratios between 0 and 30 on the x-axis (Fig. 4.5-A). The axes of the Batchelor (2005) version are in logarithmic scale with Ti/Th ratios between 100 and 10000 on the y-axis and Zr/Nb ratios between 1 and 100 on the x-axis (Fig. 4.5-B). The Batchelor diagrams look like an inverted version of the Winchester & Floyd diagram with the more primitive, basaltic compositions in the upper half and the more evolved, rhyolitic to phonolitic compositions in the lower half of the diagrams. The alkaline volcanic rocks plot in the left half, whereas the sub-/calc-alkaline volcanics plot in the right half of the diagrams.

For a comparison with the Zr/TiO_2 vs Nb/Y diagram after Winchester & Floyd (1977) the geochemical data of the investigated tuffs from southern Namibia are also plotted in the Ti/Th

vs Zr/Nb diagram (Fig. 4.6-A & B). In order to plot the geochemical data of the investigated tuffs from southern Namibia properly the Batchelor diagrams had to be modified slightly, i.e. the linear Zr/Nb-axis and the logarithmic Ti/Th-axis were extended somewhat. As already discussed above, the yttrium contents of the low-phosphate samples of the studied tuffs are considered to reflect a primary signal of the erupted source volcanics. Therefore, Batchelor's criticism regarding the use of yttrium seems not justified in the case of this study. Actually, the Th vs K_2O and Zr diagrams (Fig. 4.3-L & M) as well Th vs P_2O_5 (not shown above) rather indicate that the Th contents might not reflect essentially a primary signal but could be controlled also by secondary processes (see discussion above).
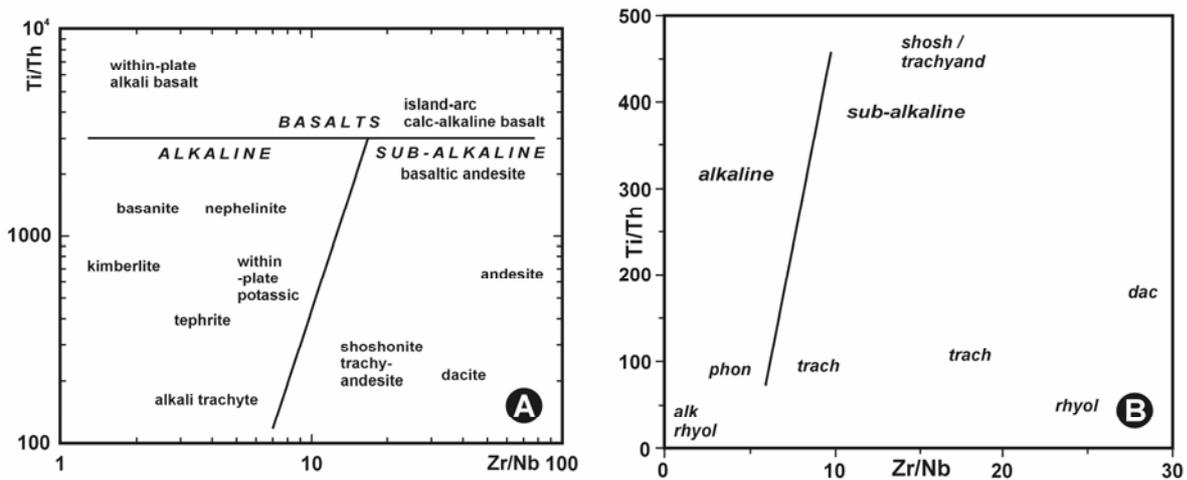
Fig. 4.5: The original Ti/Th vs Zr/Nb discrimination diagrams **(A)** after Batchelor (2005) (left diagram) and **(B)** after Batchelor et al. (2003) (right diagram).

In the logarithmical scaled version of the Batchelor diagram most geochemical data points of the southern Namibian tuffs are positioned within the sub-alkaline field clustering in the vicinity of the rhyolite area. Again the Ganigobis Tuffs show a wide range of compositions but most of the data points tend to plot towards more basic compositions compared to the other tuffs, a trend that is also visible in the Winchester & Floyd diagram. Furthermore, most of the samples of the Ganigobis IVa Tuff, which plot in the Winchester & Floyd diagram in the alkaline basalt field, form a distinctly separated cluster within the Batchelor diagram, also indicating an alkaline basaltic composition (basanite-nephelinite area) (Fig. 4.6-A). In this respect both diagram types seem to support the existence of more than one volcanic source area for the Ganigobis Tuffs. These volcanic source areas appear also to be different in terms of their geotectonic environments (alkaline vs calc-alkaline compositions). Fig. 4.6-B shows the Batchelor diagram version with linear scaled axes, representing a zoom-in into the logarithmical scaled version with more limited ratio values. Due to the linear scale of both axes two geochemical trends within the sub-/calc-alkaline composition group of the investigated tuffs are clearly discernable. One half of the tuffs forms a 'horizontal' trend with

compositions ranging from trachytic via rhyolitic towards dacitic, a trend reflected by the compositions of the Owl Gorge, Uhabis River, Panorama 2, Eisenstein, Zwartbas, Ufo Valleys-Rhyofontein, and some of the Ganigobis Tuffs. The other half of the data points forms a 'vertical' trend with compositions ranging from trachytic towards trachyandesitic, a trend reflected by the compositions of the Itzawisis, Korabib, Khabus-Panorama 1, and some of the Ganigobis Tuffs. Although none of the studied tuffs from southern Namibia plot in the Winchester and Floyd diagram within the trachyte field and only one within the rhyolite field, there are also striking similarities between the two discrimination diagram types. Firstly, one group of the tuffs ('vertical' trend) plot quite close to the alkaline-subalkaline boundary, a feature that is also seen in the Winchester & Floyd diagrams with lots of data points plotting close to the rhyodacite/dacite-trachyandesite boundary in the latter diagram type. Secondly, trends from rhyodacitic/dacitic compositions on the one hand towards rhyolitic compositions and on the other hand towards trachytic and trachyandesitic compositions are also visible in the Winchester & Floyd plots, for example for the combined dataset of Namibian and South African as well as Brazilian samples of the Prince Albert and Collingham tuffs. So far it is not clear what processes are responsible for the splitting of the data set of the Namibian Dwyka and Ecca tuffs into two compositional trends and what these trends mean in geochemical terms. Furthermore, the Batchelor plots raise the question if the two trends indicate also for the Ecca Group tuffs the existence of more than one volcanic source area. From the Winchester & Floyd plots rather a common source was supposed. Have these trends a primary origin or are they generated by secondary processes?

In summary it can be concluded that despite some differences between the Winchester & Floyd and the Batchelor diagrams, concerning the composition of the tuffs, there are also striking similarities concerning compositional trends. Furthermore, for the present data set it appears as if different composition groups of tuffs are better depicted in the Batchelor diagrams due to better resolution. However, it also appears that the position of composition fields within the Batchelor diagrams might need some correction or refinement. Nevertheless, for altered pyroclastic rocks the Batchelor diagrams represent certainly a suitable and interesting alternative or a valuable supplementary tool to the Winchester & Floyd diagram.
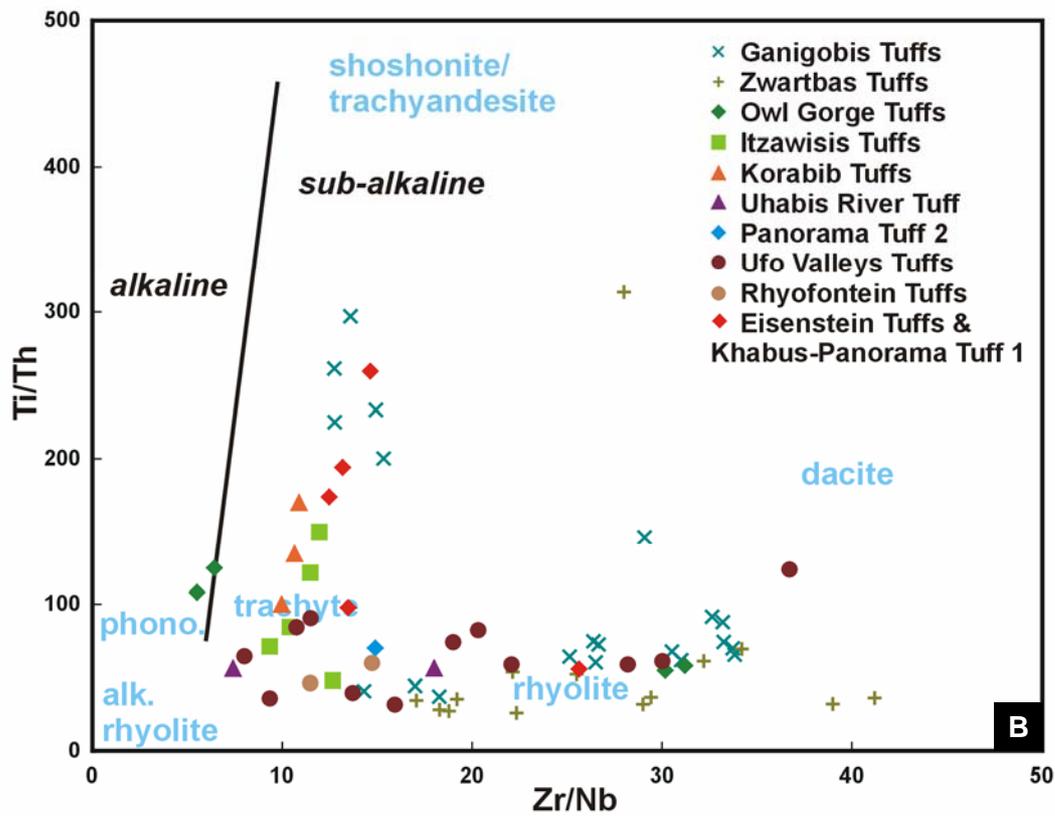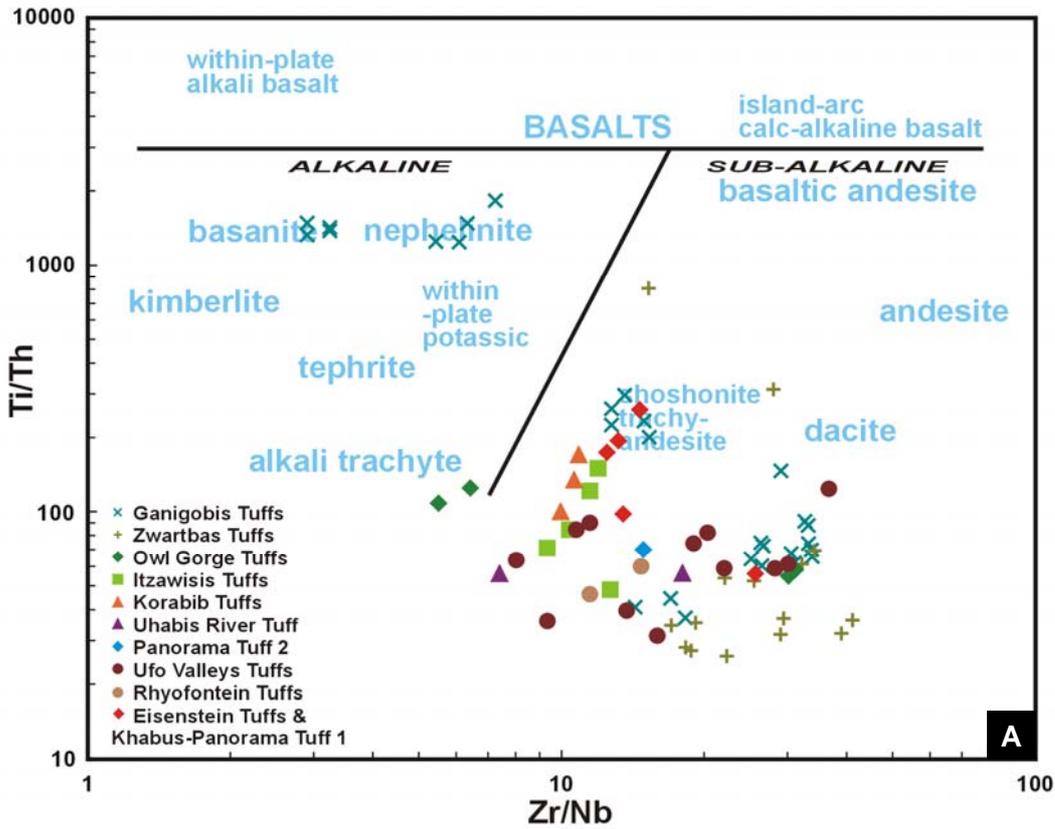
Fig. 4.6: Ti/Th vs Zr/Y discrimination diagrams after **(A)** Batchelor (2005) and **(B)** after Batchelor et al. (2003) for the studied Dwyka and Ecca tuffs of southern Namibia. Data for the Ganigobis Tuffs are taken from Bangert (2000), those of the Zwartbas Tuffs are taken from Geiger (2000).

Nb vs Y and Ta vs Yb discrimination diagrams after Pearce et al. (1984)

Originally developed for granitic rocks the Pearce diagrams have also been used in an attempt to gain some information about the geotectonic environment of the volcanic source area of bentonites and tonsteins. For these diagrams Pearce et al. (1984) subdivided granites into four main groups – ocean ridge granites (ORG), volcanic arc ganites (VAG), within plate granites (WPG), and collision granites (COLG).

They argued that Rb, Y (or Yb) and Nb (or Ta) are likely to be the most effective elements for the tectonic discrimination of granites. However, the diagenetic-metasomatic control of the rubidium contents of the investigated tuffs excludes the use of rubidium for this purpose. Therefore only the 'Rb-free' diagrams can be applied. The Nb vs Y and the Ta vs Yb diagrams are actually projections of three-dimensional diagrams (including rubidium) onto the Nb-Y or Ta-Yb space. Due to the projection of the data VAGs and COLGs cannot be distinguished in the Nb vs Y diagram but should plot in different fields in the Ta vs Yb diagram. In applying these diagrams one should keep in mind that in these diagrams absolut values of certain elements are plotted against each other. These values can, however be reduced ('diluted') in the investigated rocks by introduction of other elements or increased ('concentrated') by the removal of other elements. Such effects can only be avoided in ratio-ratio plots. Fig. 4.7-A & B show the results for the Dwyka and Ecca tuffs of southern Namibia.
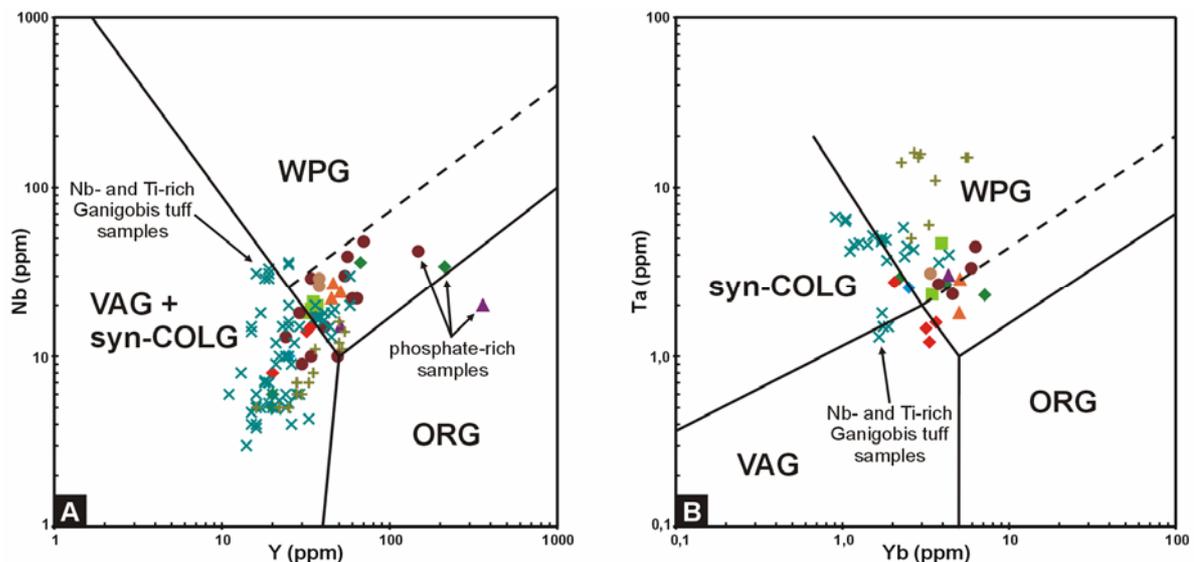
Fig. 4.7: Nb-Y (A) and Ta-Yb (B) dicriminant diagrams for syn-collision granites (syn-COLG), volcanic arc granites (VAG), within plate granites (WPG) and ocean ridge granites (ORG). The dashed line represents the upper compositional boundary for ORG from anomalous ridge segments. Note that post-collision granites can plot in all but the ORG fields, and that supra-subduction zone ocean ridge granites plot in the VAG field (see Pearce et al. (1984) for further explanantions). See Fig. 4.6 for symbols. Note that only for a limited number of tuffs Ta and Yb data are present. The data for the Ganigobis Tuffs are from Grill (1997) and Bangert (2000), and for the Zwartbas Tuffs from Geiger (2000).

The Nb-Y diagram reveals a positive correlation between these two elements for most of the tuff samples. The phosphate-rich samples are shifted to the right due to a marked yttrium enrichment in association with diagenetic phosphate precipitation. The tuff samples from the Namibian Ecca Group show a tendency towards higher niobium and yttrium contents compared to the abundances recorded for the Dwyka tuffs. About two third of the samples plot within the VAG/syn-COLG field, whereas about one third plot within the WPG field. The Nb- and Ti-rich samples of the Ganigobis Tuffs (mainly tuff IVa), for which a more alkaline character can be deduced from the Winchester & Floyd as well as the Batchelor diagrams (Fig. 4.4-A/B and Fig. 4.6-A), do actually not clearly plot within the WPG field as expected. In the Ta-Yb diagram most of the tuffs plot within the WPG field and only a minor amount of samples plot within the syn-COLG and VAG fields. In comparison with the Nb-Y diagram the Ecca tuffs are clearly shifted into the WPG field, due to generally higher ytterbium contents compared to Dwyka tuff samples. Most of the Zwartbas tuff samples form an isolated cluster, which is characterized by unusual high tantalum contents compared to other tuffs. Interestingly, the niobium- and titanium-rich samples of the Ganigobis Tuffs show very low tantalum values, what is surprising, because the geochemical behaviour of niobium and tantalum is quite comparable and a positive correlation between these elements can normally be expected. These tuff samples were actually expected to plot within the WPG field due to their alkaline character, however, their very low tantalum and ytterbium contents position them distinctly within the VAG and syn-COLG fields. In summary it becomes apparent that within the Ta-Yb diagram most of the tuffs are clearly shifted towards the WPG field compared to the Nb-Y diagram. However, for most of the tuffs within the Dwyka and Ecca Groups so far a volcanic arc origin was favored due to the active nature of the southern continental margin of Gondwana below which oceanic crust of the Panthalassan Ocean was subducted. Ironically, those samples of the Ganigobis Tuffs (mainly tuff IVa), for which a within plate origin appears to be likely due to their apparent alkaline character, plot in the Ta-Yb diagram among all tuff samples most distinctivly within the VAG and syn-COLG fields. Bangert (2000) already mentioned that the results of a study by Tischendorf et al. (1995), who tested the reliability of tectonomagmatic discrimination diagrams, showed that they should be used with great caution. Concerning the Pearce diagrams (and others), Tischendorf et al. (1995) for example pointed out that according to their study volcanic arc granites (VAG) show considerable overlap into the WPG field. Granites emplaced in the main volcanic arc plot neatly in the VAG area, but granites of the back-arc area tend to be located in the WPG field (see also Tischendorf et al. (1995) and Bangert (2000) for further discussion). Geochemical differences may also result from wether the source volcanoes are situated within an island arc or along an active continental plate margin.

4.4 Rare earth elements

The overall pattern of chondrite-normalized rare earth element (REE) diagrams for altered pyroclastic rocks is primarily controlled by the original composition of the source magma, reflecting the degree of partial melting and fractionation, but also secondary processes like diagenesis, hydrothermal activity and metasomatism can influence the REE abundances. For example, Uysal & Golding (2003) have shown that REE in illitic clay minerals can be mobile and fractionated during illitization. The REE are commonly subdivided into the light rare earth elements (LREE) from La to Eu and the heavy rare earth elements (HREE) from Gd to Lu. Most of the REE are trivalent under most geological conditions. Eu is both trivalent and divalent in igneous system with the Eu^{2+}/Eu^{3+} ratio dependant on the oxygen fugacity. Ce may be tetravalent under highly oxidizing conditions. Partition coefficients of REE between common minerals and melt in igneous systems are generally quite low and therefore they are considered as incompatible elements. However, the HREE are somewhat less incompatible than the LREE causing a stronger enrichment of the LREE in the residual melt of fractionated magmas. In most felsic, granitoid rocks the main host minerals of the LREE are apatite, titanite, monazite and allanite, whereas the HREE are more concentrated in clinopyroxene, zircon and especially garnet. Eu in the oxydation state +2 has an ionic radius similar to Sr and is strongly partitioned into plagioclase, resulting in strong neagtive Eu anomalies in plagioclase-fractionated melts. Since plagioclase is a quite common macrocrystal component within the tuffs and is most probably of juvenile origin, i.e. plagioclase crystalized within the magma before eruption, a primary negative Eu anomaly can be expected for most of the tuffs, as long as it is not erased by secondary processes. The generally higher incompatibility of the LREE compared to the HREE should result in primary negatively sloping curves, with steep slopes in the LREE region for highly fractionated melts.

The REE data of a number of altered tuff layers from southern Namibia are plotted in a series of chondrite-normalized diagrams. For normalization the recommended REE abundances in CI carbonaceous chondrites of McDonough & Sun (1995) were used. The value for the radioactive element promethium (Pm) was not measured but calculated from the values of the neighbouring elements Nd and Sm, producing a fairly smooth REE pattern for this area. To quantify Eu anomalies the Eu/Eu* ratio was calculated. The Eu* value was calculated as the square root of the product of the chondrite-normalized values for Sm and Gd. For comparison also the available REE data for the Ganigobis Tuffs (Bangert, 2000) and the Zwartbas Tuffs (Geiger, 2000) have been plotted in chondrite-normalized diagrams. The resulting REE patterns of the individual tuffs are shown in Fig. 4.8 and the various recognized types of REE patterns are illustrated in Fig. 4.9.
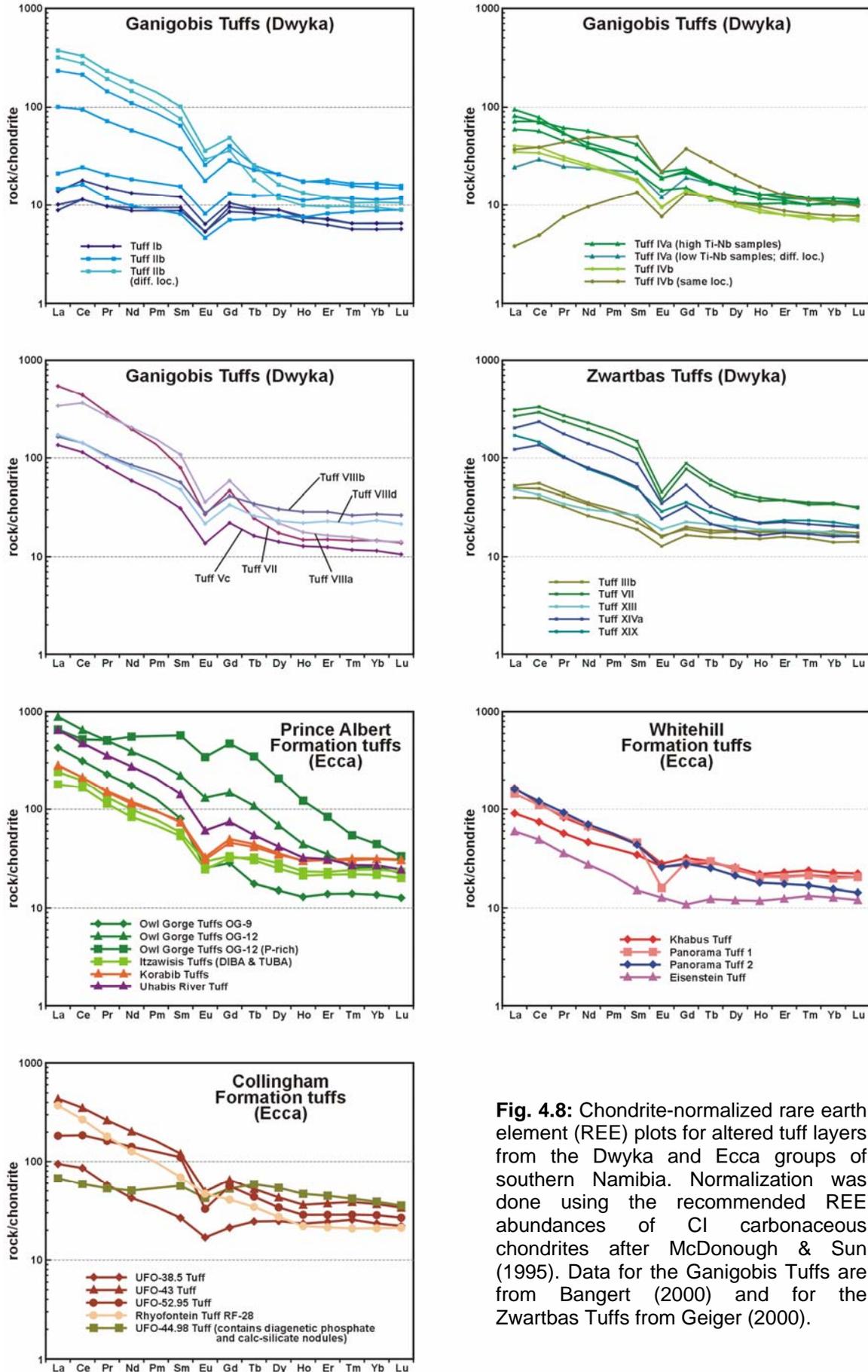
Fig. 4.8: Chondrite-normalized rare earth element (REE) plots for altered tuff layers from the Dwyka and Ecca groups of southern Namibia. Normalization was done using the recommended REE abundances of CI carbonaceous chondrites after McDonough & Sun (1995). Data for the Ganigobis Tuffs are from Bangert (2000) and for the Zwartbas Tuffs from Geiger (2000).
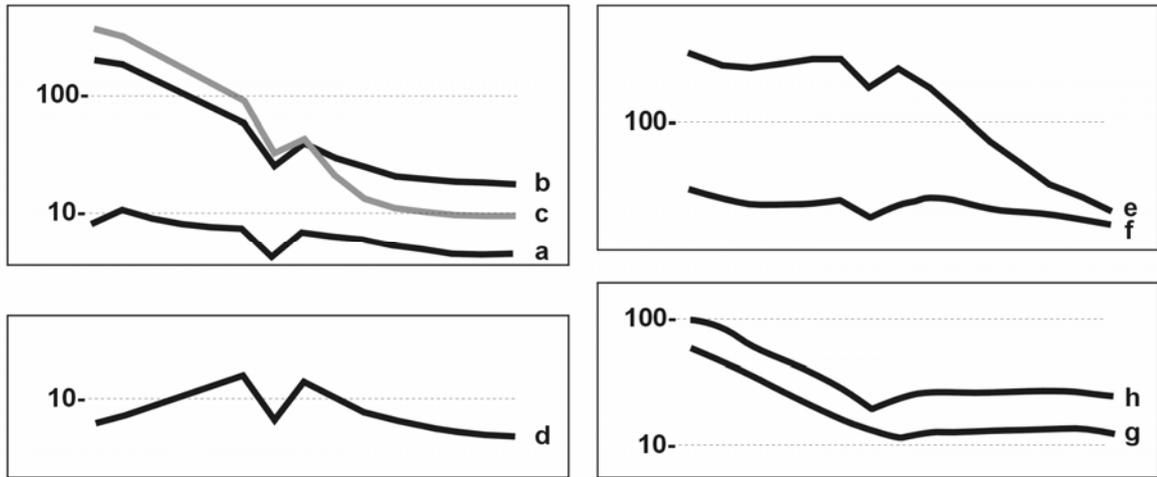
Fig. 4.9: Various recognized types of chondrite-normalized REE patterns for altered tuff layers from the Dwyka and Ecca Groups of southern Namibia.

A first quick overview shows that the REE abundances of most tuff samples produce gentle to steep negatively sloping curves with an overall enrichment of the LREE of 10-900 times chondritic, and of HREE a factor of mainly <10-50. Furthermore, most samples show a fairly pronounced Eu anomaly. These features are quite characteristic for calc-alkaline magmas erupted in subduction-related volcanic arc environments (Taylor & McLennan, 1988; Huff et al., 2000). The pronounced negative Eu anomalies also indicate derivation from a highly evolved magma in which plagioclase fractionation was significant (Huff et al., 1998).

The samples of the Ganigobis Tuffs Ib and IIb already show three different REE patterns, which are illustrated in Fig. 4.9 as pattern types (a), (b) and (c). Samples of Tuff Ib have generally very low REE contents and the curves are very gently sloping from La to Lu, representing pattern type (a). The low REE contents and the relatively flat pattern could reflect more basic and less evolved melts, however, plagioclase fractionation is evident through the negative Eu anomaly. With overall increasing REE contents the curves develop steeper slopes gradually approaching pattern type (b). Associated with the overall increase in REE is the stronger enrichment of the LREE in contrast to the HREE, which can be explained by the higher compatibility of the latter elements. The trend from pattern type (a) towards type (b) reflects the development from more primitive towards more evolved (fractionated) melts. Pattern type (c) seems to be a derivate of pattern type (b) because it looks like a rotated version of the latter. Type (c) shows an enhanced enrichment of the LREE but in comparison to type (b) the HREE appear to be depleted with very steep negative slopes in the region of the elements Gd to Ho. Since the REE pattern types (b) and (c) are derived from the same supposed tuff layer (Ganigobis Tuff IIb) but sampled from different localities, it seems likely that pattern type (c) is probably produced by secondary processes rather than reflecting a primary, igneous signal. However, the geochemical

mechanism, which is responsible to form this conspicuous REE pattern type (c) with the prominent 'hiccup' in the middle rare earth region, is not known. Most samples of the Ganigobis Tuffs IVa and IVb are similar to the stratigraphically lower tuffs and take an intermediate position between pattern type (a) and (b). This second REE plot of the Ganigobis Tuffs contains also those samples of tuff IVa, which have high Ti and Nb contents and plot in the Winchester & Floyd diagram within the field of alkaline basalts. Interestingly, their REE pattern does not deviate markedly from those of other Ganigobis Tuffs and the overall REE content of the Ti- and Nb-rich samples of tuff IVa is actually even slightly higher than that of the tuff sample with a low Ti-Nb content. However, their negative Eu anomaly is distincly weaker than those of the majority of the Ganigobis Tuffs. Although the overall REE contents of the samples with an alkaline basaltic composition are higher than that of the low-Ti-Nb sample, their distinctly higher Eu/Eu* ratios (0.67-0.77), i.e. their distinctly weaker negative Eu anomalies, in comparison to the average Eu/Eu* ratio for all Ganigobis Tuffs (0.57), reflects their more primitive and less evolved character. Therefore, the Eu data apparently support the implication drawn from the Winchester & Floyd as well as from the Batchelor diagrams that the Ti-Nb-rich samples of Ganigobis Tuff IVa are derived from a less fractionated and less evolved magmatic source. The REE patterns for samples of the Ganigobis Tuff IVb are quite puzzling. Although sampled from the same locality two very differing patterns appear. Two samples of this tuff layer show a pattern which can be assigned to REE pattern type (b). The two other tuff layers, however, show a very strange REE pattern, which is illustrated in Fig. 4.9 as type (d). This pattern type is in so far very different to the other pattern types in that it shows a positively sloping curve for the LREE, followed by a pronounced Eu anomaly, which is in turn followed by a 'normal', negatively and gently sloping curve for the HREE. According to Bangert (2000) these four samples originate from the same locality. Therefore it can be concluded that this strange pattern must have a secondary origin but again no explanation for the control mechanism can be provided. REE pattern for tuff groups V, VII and VIII of the Ganigobis Tuffs belong either to type (b) or to type (c).

The REE pattern for most samples of the Zwartbas Tuffs are similar to type (b) with some showing a slight component of type (c). The Zwartbas Tuffs display mildly to strongly pronounced Eu anomalies. What is worth mentioning is that with increasing total REE contents the Eu anomaly becomes more pronounced resulting in decreasing Eu/Eu* ratios ranging from 0.79 to 0.38. The average Eu/Eu* ratio for all Zwartbas Tuffs is 0.61, which is quite comparable to that of the Ganigobis Tuffs (0.57).

The tuff samples from the Prince Albert Formation in southern Namibia yield REE patterns, which are mainly quite similar to type (b). Only for tuff OG-9 the LREE appear relatively enriched against the relatively depleted HREE resulting in a sinuous curvature somewhat

reminscent of pattern type (c). The LREE show relative to the other REE plots overall elevated levels. All tuff patterns contain a fairly pronounced negative Eu anomaly with Eu/Eu* ratios ranging between 0.71 and 0.47 (average 0.58). One REE pattern is clearly different to all the other ones and characterizes pattern type (e). The pattern for tuff sample OG-12, which is strongly impregnated by diagenetic francolite (Fig. 3.12), shows a strong enrichment of most of the REE except La, Ce and Pr. This kind of enrichment produces a shallow saucer-shaped, elevated plateau for the LREE, whereas the HREE form a steep, negatively sloping line representing a continuous decrease in the HREE enrichment from Gd to Lu. The saucer-shaped course of the LREE can also be depicted from the REE plot of tuff UFO-44.98 of the Collingham Formation forming pattern type (f). This tuff layer contains phosphate and calc-silicate nodules (Fig. 3.55). Therefore, a saucer-shaped LREE pattern is suggested to reflect a diagenetic phosphate enrichment. REE pattern types (e) and (f) are closely related in terms of their LREE pattern, however, the strongly elevated REE contents of pattern type (e) are due to a highly phosphatic tuff sample (OG-12 with ~5 wt% P_2O_5), whereas pattern type (f) can be seen as a slightly phosphate-influenced (UFO-44.98 with ~0.4 wt% P_2O_5) derivate of pattern type (a).

The REE patterns for the altered tuff layers discovered within the Whitehill Formation of southern Namibia are in turn quite different to the patterns of the Prince Albert tuffs. Remember that the Khabus and Panorama Tuff 1 samples represent the same tuff layer but originate from different localities. The Khabus-Panorama Tuff 1 samples represent mainly albitized and partly silicified samples, the Eisenstein Tuff is also highly feldspathic but shows a composition closer to intermediate plagioclase (Tab. 4.1), whereas the Panorama Tuff 2 is a typical clay-rich, bentonitic layer. Compared to the Prince Albert tuffs they are only moderately enriched in REE, especially in the LREE, producing gently sloping curves, which show more similarities with some samples of the Ganigobis and Zwartbas tuffs. Most conspicuous, however, are their Eu signals. Three of the five measured samples show a fairly weak negative Eu anomly (Eu/Eu* 0.72-0.85), one does not show an Eu anomaly at all (Eu/Eu* 0.98), and one sample is characterized by a strong negative Eu anomaly (Eu/Eu* 0.43). The sample without an Eu anomaly, forming REE pattern type (g), represents the Eisenstein Tuff, which has a secondary matrix that is dominated by a Ca- and Na-rich plagioclase. Since Eu^{2+} is strongly partitioned into plagioclase, this secondary feldspathization has probably erased a primary negative Eu anomaly, or could have even turned it into a positive anomaly, unless redox conditions were not too strongly oxidizing. However, the non-feldspathized, clay-rich, bentonitic sample of the Panorama Tuff 2 also does only show a rather weak Eu anomaly. The picture is further complicated because the albitized and silicified sample of the Panorama Tuff 1 actually shows a very pronounced negative Eu anomaly, whereas the equivalents from another locality, the Khabus samples, also either

albitized or albitized plus silicified, are characterized by weak negative Eu anomalies, comparable to that of the Panorama Tuff 2 sample. It looks as if secondary feldspathization with a Na- and Ca-rich plagioclase indeed can erase neagtive Eu anomalies, whereas in the case of secondary albitization the behaviour of Eu, respectively its mobility during secondary processes (diagenesis, hydrothermal activity, metamorphism, etc.), might strongly depend on local conditions. In the case of the bentonitic Panorama Tuff 2 it is not really clear if the weak Eu anomaly indeed represents a primary signal.

Also the plotting of the REE data of tuff samples from the Namibian Collingham Formation resulted in a quite inhomogeneous picture. Two of the five measured tuff samples (UFO-43 and UFO-52.95) show a clear enrichment of the LREE and a pronounced negative Eu anomaly, a REE pattern that belongs to type (b), which is characteristic for evolved and fractionated magmas of subduction-related volcanic arc environments. The REE pattern of tuff UFO-44.98 was already mentioned above forming REE pattern type (f). This tuff layer contains diagenetic phosphate (francolite) concretions and calc-silicate nodules, the latter representing thermally metamorphosed calcareous concretions. This tuff is characterized by a flat, shallow saucer-shaped LREE pattern, which is most probably related to the precipitation of diagenetic francolite. The overall low LREE abundances, which appear relatively depleted compared to other tuffs, are probably also related to francolite precipitation. The LREE behaved apparently mobile during diagenesis or thermal meta-morphism and were concentrated in the phosphate nodules, resulting in a relative depletion in the surrounding altered tuff. The Rhyofontein tuff sample shows a REE pattern, which is similar to the REE pattern of the tuffs UFO-43 and UFO-52.98, but completely lacks an Eu anomaly. The reason for this lacking Eu anomaly is probably the proximity of the sample locality to a felsic dyke and an associated fracture and alteration zone, which is characterized by prehnite mineralization. Presumably also the Rhyofontein Tuffs were to some degree affected by this calc-silicate mineralization, which may have acted, similar to plagioclase, as an Eu collector, erasing a former existing neative Eu anomaly. Finally, the REE pattern of tuff UFO-38.5 represents another quite unique one, which is illustrated in Fig. 4.9 as pattern type (h). This pattern type is different to all other observed REE pattern in so far that is does not show a typical negative anomaly, which is restricted to Eu, but displays a V-shaped sink in the area of the middle rare earth elements from Sm to Dy. Especially the 'lighter' HREE elements Gd, Tb and Dy appear to be depleted relative to the majority of the other tuff REE patterns. The overall REE pattern of tuff UFO-38.5 could represent a derivate of pattern type (a) or (b), however containig an enigmatic middle rare earth element depletion. At the present state of the art no explanantion for this unusual REE behaviour can be given.

4.5 U-Th mineral chemistry of magmatic zircons

During SHRIMP analyses the Th and U contents of mainly juvenile zircons from tuff layers were measured. Many of the zircons exhibit oscillatory zoning, which also implies an inhomogeneous distribution of Th and U within a single zircon crystal reflected in Th- and U-richer and -poorer zones. Therefore, the absolute values for Th and U derived from spot analyses can vary dramatically even for genetically related zircons. However, the Th-U spot analysis data from a single zircon population, which crystallized in a more or less geochemically homogeneous melt environment under more or less equal physico-chemical conditions, should produce a linear Th/U ratio. Due to the high stability of crystalline zircon alteration processes should have no substantial impact on the Th and U chemistry of zircon. However, high level abundances of Th and U could cause radiation damage to the crystal lattice and even at low temperatures trace elements can be leached easily from such damaged (metamict or partly metamict) areas. The available Th-U data from twelve SHRIMP-dated tuff samples from Carboniferous-Permian Karoo strata of Namibia and South Africa have been plotted in order to reveal similarities or differences in their Th/U ratios. From this study Th-U zircon data are available for tuff layers from the lower Ecca Group (Prince Albert to Collingham Formation) of southern Namibia. These data are supplemented by data from Bangert (2000) and Geiger (2000) for tuff layers from the Dwyka and basal Ecca Group of southern Namibia and the Western Cape Province of South Africa as well as data from Wanke (2000) for a tuff from the Gai-As Formation of NW-Namibia. The juvenile or xeno-crystic origin of individual zircons is revealed by their U-(Th)-Pb isotope systematics resulting in radiometric ages for single crystals. The data for xenocrystic zircons have been omitted from the Th-U data set, except the Ordovician zircon population within the tuff bed from the basal Ecca Group cropping out south of Laingsburg/RSA. Fig. 4.10-A to C shows the results for tuff layers from three subsequent stratigraphic levels. The Th-U data for zircons from the Dwyka Group and the Dwyka-Ecca boundary are plotted in Fig. 4.10-A. Juvenile zircons from tuff layer IIb of the Ganigobis Tuffs, sampled from two localities (#23 & #45; see Bangert, 2000), and from tuff layer IIIb of the Zwartbas Tuffs show a mean Th/U ratio which is close to 1, however, the data for locality #45 are scattered over a quite wide data range. In contrast, juvenile zircons from a younger Dwyka tuff from the Klaarstroom area/RSA show a mean Th/U ratio which is close to 0.5. The data set of the Owl Gorge Tuff OG-9, positioned close to the Dwyka-Ecca boundary, reveales an admixture of genetically different zircons to the juvenile zircon population. Most data points plot within the field of Th/U ratios between 1 and 2, but several zircons show distinctly lower ratios. This mixture of zircon populations is also reflected in a clear bimodality of the age data for tuff OG-9 with an age difference of around 10 million years (see also Chapter 5 – Geochronology). The age of the younger zircons are interpreted to reflect more the time of eruption which produced this ash layer, whereas the

slightly older zircons originated most probably from older but genetically related volcanogenic material, which was incorporated into the younger, juvenile pyroclastics during an explosive eruption. The Th-U data of zircons from tuff layers within the Prince Albert Formation are plotted in Fig. 4.10-B. It can be seen that almost all data points are positioned below the line for a Th-U ratio of 1, which differentiates them from the Namibian Dwyka tuffs. The data for the Uhabis River and the Laingsburg tuffs are lying closer to a Th/U ratio of 1, whereas the data for the DIBA (Itzawisis) and Klaarstroom tuffs are closer to 0.5. The Ordovician zircons also plot around the line for a Th/U ratio of 0.5 but show a large data scatter. Similar to the zircons of tuffs from the Prince Albert Formation also the zircons of tuffs from the Whitehill (KHA-1a) and Collingham Formations (UFO-43) show mainly Th/U ratios between 0.25 and 1 (Fig. 4.10-C). In contrast, the majority of zircons of the Gai-As tuff have high Th/U ratios between 1 and 4, and show the strongest data scatter possibly indicating a mixed source. Two interesting phenomena can furthermore be depicted from these series of Th vs U diagrams. Firstly, the Th-U zircon data sets for the Itzawisis, Khabus and Ufo Valleys tuffs indicate that with increasing total Th and U contents also the Th/U ratio increases resulting in a curved data array, whereas the Th an U contents of zircons from other tuffs, e.g. from the Ganigobis, Owl Gorge or Uhabis River tuffs, show a more linear correlation. Secondly, all data arrays of Fig. 4.10-B & C originate more or less from the (0; 0)-coordinate of the Th-U diagram, whereas the regression lines of the data sets for the Owl Gorge, Ganigobis and Zwartbas tuffs (Fig. 4.10-A) originate approximately from the (0; 100)-coordinate. No explanations for these phenomena can be given at the present state of the art. Fig. 4.11 represents a crossplot of calculated average zircon Th and U contents for the individual tuffs. Firstly it becomes apparent that almost all tuffs plot in a well-defined field, which is bounded by the lines for Th/U ratios of 0.5 and 2 as well as the lines for total Th+U contents of 400 and 800 ppm. However, the Dwyka and Gai-As tuffs tend towards higher Th/U zircon ratios (1-2), in contrast to the Ecca tuffs (0.5-1). Neverless, these zircon data indicate that all these tuffs are genetically closely related and might originate maybe from different source areas but rather from a common geotectonic environment, i.e. a subduction-related magmatic arc. The DIBA tuff sample of the Itzawisis Tuffs is separated from the other tuffs in this diagram due to exceptional high average Th+U contents of its juvenile zircons. The position of the Ordovician zircon population from the Laingsburg tuff is not equally comparable to those of the Carboniferous-Permian zircons due to a limited data base.

Fig. 4.10 (next page): Th/U ratio plots for juvenile zircons of Carboniferous-Permian tuffs from the Dwyka and Ecca Groups of southern Namibia and the Western Cape Province of South Africa as well as Permian zircons from a Gai-As Formation tuff layer from NW-Namibia. In addition, also data from a xenocrystic zircon population of Ordovician age within one of the tuffs (Laingsburg) are plotted.
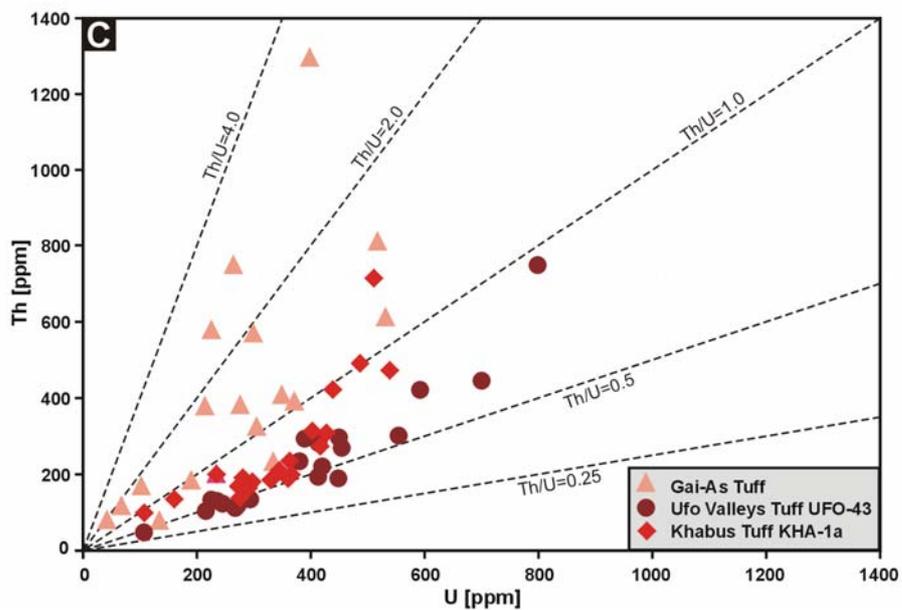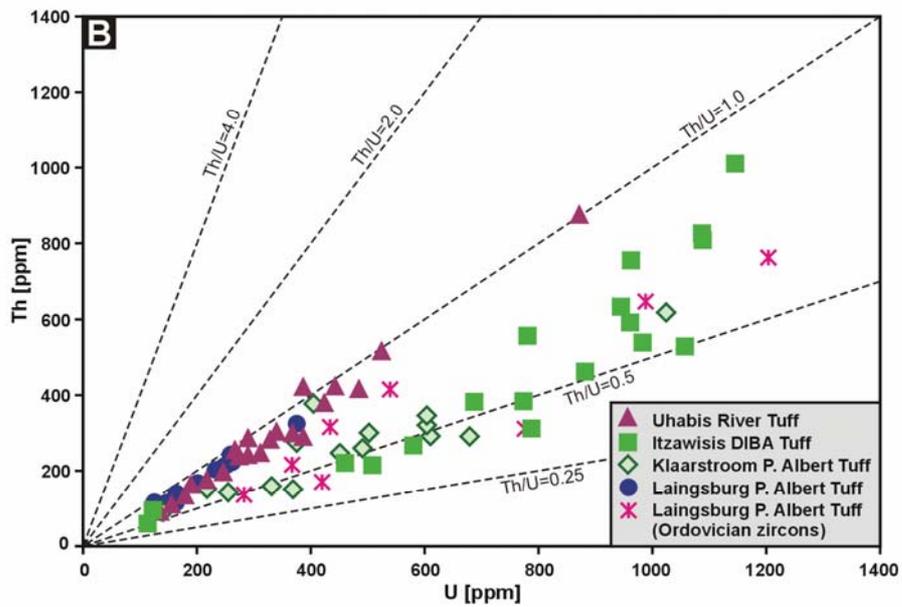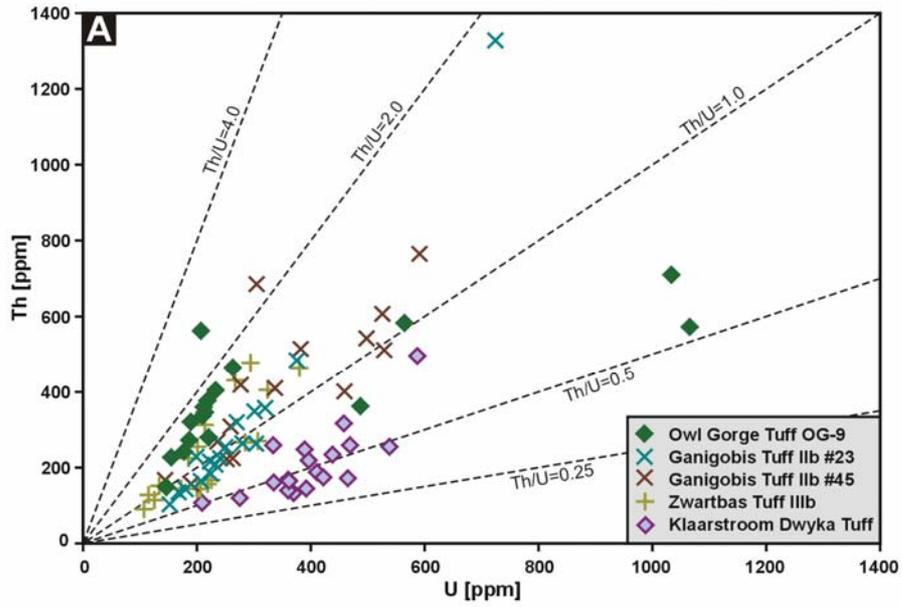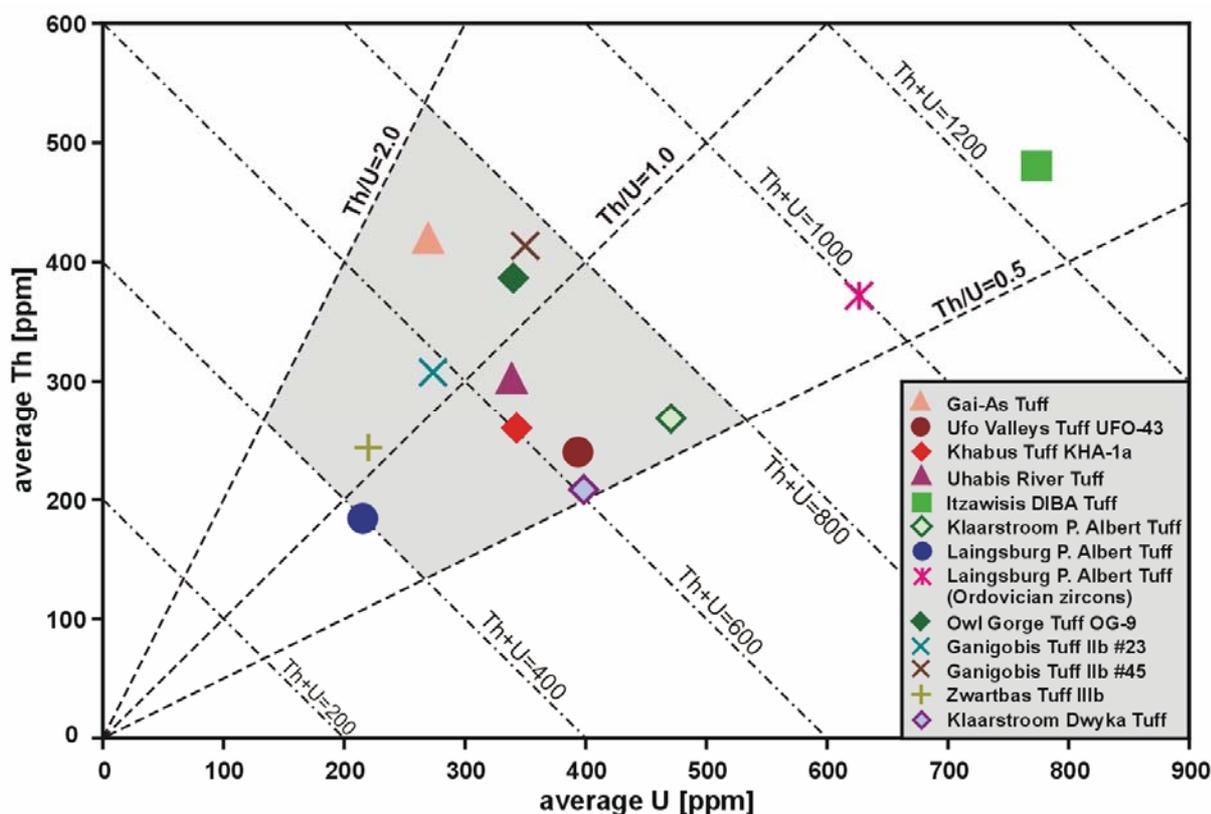
Fig. 4.11: Crossplot of average Th and U contents of SHRIMP-analysed zircons from various tuff layers within Carboniferous-Permian Karoo sediments of Namibia and South Africa.

4.6. Geochemistry summary

The major element compositions of the fine-grained altered tuffs reflect mainly the present-day mineralogical composition of the tuff matrices. They are only influenced to a minor degree by macrocrystic components, the abundances of which are commonly relatively low compared to matrix contents.

In a K_2O vs Na_2O plot the two principle types of tuffs present in the Namibian Dwyka and Ecca Groups can clearly be distinguished. The bentonitic, clay mineral-rich tuffs show relatively low sodium and highly variable potassium contents, whereas the chert-like, feldspathic (plagioclase-rich) tuffs show relatively low potassium and highly variable (but generally increased) sodium contents.

The potassium contents of the bentonitic tuffs can be used as a proxy for the intensity of their thermal alteration. Increased potassium contents are related to progressive illitization of the former smectitic/kaolinitic matrix of early diagenetic origin. This progressive illitization is regarded as the combined result of later stage burial diagenesis and hydrothermal-metasomatic overprinting during Jurassic dolerite sill intrusions. The progressive illitization is associated with decreasing silica and increasing alumina contents. Furthermore, the K_2O vs

SiO_2 and Al_2O_3 diagrams indicate an alteration path from smectitic to illitic (rather than kaolinitic to illitic) compositions for the bentonitic tuffs.

The P_2O_5 vs CaO diagram is also very insightful concerning the mineralogical composition of the bentonitic tuffs. Some highly Ca- and P-enriched samples are impregnated by early diagenetic francolite. Slightly increased Ca contents combined with low P values are controlled by the presence of smectite. Tuff samples from the Rhyofontein locality with distinctly elevated Ca contents (at only slightly elevated P contents) are probably mineralized with prehnite. The Fe and Mg contents of the bentonitic tuffs are mainly controlled by the abundances of biotite and chlorite, and probably to a minor degree by opaque phases.

Among the chert-like, feldspathic tuffs within the Whitehill Formation of southern Namibia three geochemically and mineralogically distinct subtypes can be distinguished. The first subtype shows a geochemical composition that matches very well that of albite. The second subtype appears also strongly albitic but increased silica contents associated with lowered alumina and sodium contents indicate additional silicification of the tuffs. The third subtype is characterized by a geochemical composition that matches well that of an intermediate plagioclase ($Ab_{50}An_{50}$).

In order to determine the geochemical nature and the geotectonic environment of the source magmas of the investigated tuffs a number of so-called immobile trace elements have been considered. In addition to the 'traditional' Zr/TiO_2 vs Nb/Y diagram after Winchester & Floyd (1977) also the more recently developed Ti/Th vs Zr/Nb diagrams of Batchelor et al. (2003) and Batchelor (2005) have been applied. The latter diagrams avoid the use of yttrium, which even under low grade conditions can show a considerable mobility. This is for example testified in the early diagenetically strongly phosphate-enriched tuff samples, which show corresponding high yttrium contents. However, it can also be shown that in the low-phosphatic tuff samples the yttrium contents strongly correlate positively with the zirconium contents and should therefore represent a primary signal. The thorium contents of the tuffs do not really show positive correlations with zirconium or phosphorus and it is suspected that thorium is largely adsorbed on clay mineral and iron oxide particles. Consequently, the primary nature of the thorium contents of the investigated tuffs is uncertain affecting also the validity of the Batchelor diagrams.

In the Winchester & Floyd diagrams the Dwyka tuffs show a wide range of compositions. The Zwartbas Tuffs are more restricted to intermediate compositions but the Ganigobis Tuffs range from intermediate (rhyodacite-dacite) to basic (alkaline basalt) compositions. This could indicate several different volcanic sources or a bimodal character of the erupted volcanic material. The lower Ecca Group tuffs from southern Namibia within the Prince Albert, Whitehill, and Collingham Formations show mainly intermediate, rhyodacitic-dacitic

compositions, which is in accordance with the data of other tuff samples in equivalent or comparable stratigraphic positions from a wide range of SW-Gondwanan localities (Namibia, South Africa, and Brazil).

In the logarithmical scaled version of the Batchelor diagrams most of the investigated tuffs plot in the lower right (sub-alkaline) corner below the trachyandesite and dacite fields indicating an intermediate to acidic composition of the source magmas. The samples of the Ganigobis Tuff that plot in the Winchester & Floyd diagram in the alkaline basalt field fall in the Batchelor diagram into the area of alkaline basanites and nephelinites (upper right corner). Both diagrams therefore apparently support an alkaline basic character of these tuff samples. In the linear scaled version of the Batchelor diagrams, representing a zoom-in into the logarithmical scaled version, two geochemical trends become apparent within the group of sub-alkaline tuff samples. About one half of the tuffs forms a 'horizontal' trend with compositions ranging from trachytic to rhyolitic to dacitic, whereas the other half forms a 'vertical' trend ranging from trachytic towards trachyandesitic compositions.

The predominantly intermediate, rhyodacitic-dacitic composition of the investigated tuffs is also in accordance with the spectrum of observed juvenile macrocrystals, comprising mainly quartz, biotite and plagioclase, with minor amounts of potassium feldspar, and in some cases pseudomorphs after hornblende or pyroxene. Also the relatively high abundances of accessory zircon and apatite are indicative of intermediate to acidic compositions of the source magmas. Those samples of the Ganigobis Tuffs, which plot either as alkaline basalts (Winchester & Floyd) or alkaline basanites-nephelinites (Batchelor) should not contain juvenile quartz crystals (Lorenz, pers. comm. 2005). Unfortunately, no specific petrographic data have been found in Bangert (2000) for these geochemically distinctly different tuff samples. It is strongly suggested that in future projects also the glass inclusions in juvenile apatites and zircons are analyzed to better constrain the compositions of the source magmas.

Discrimination diagrams of Pearce et al. (1984) have in the past also been used for altered tuffs to disclose the geotectonic environment of their source magmas. Since the rubidium contents in the investigated Dwyka and Ecca Group tuffs are strongly controlled by secondary processes only rubidium-free Pearce diagrams can be used. However, the applied Nb vs Y and Ta vs Yb gave no conclusive results.

Most tuff samples produce gentle to steep negatively sloping chondrite-normalized REE curves with an overall enrichment of the LREE of 10-900 times chondritic, and of HREE a factor of mainly <10-50. Furthermore, most samples show a fairly pronounced Eu anomaly.

These features are quite characteristic for calc-alkaline magmas of intermediate to acidic composition erupted in subduction-related volcanic arc environments. Most samples of the Ganigobis Tuffs show low REE contents and relatively flat REE patterns possibly reflecting more basic and less evolved source melts. Some REE patterns that are unusual of igneous rocks are interpreted as the result of secondary processes.

Thorium and uranium data of a number of juvenile and xenocrystic zircons are available from SHRIMP spot analyses. Zircons from the investigated Late Palaeozoic tuffs show a wide range of Th/U ratios from about 0.25 to 3.5. In a crossplot of calculated average zircon Th and U contents for individual tuffs or tuff groups almost all investigated tuffs cluster in a relatively narrow field implying that these tuffs are genetically closely related and might originate from a common geotectonic environment (i.e. subduction-related magmatic arc). However, the possibility of the presence of different source areas cannot be excluded.

Chapter 5 – Geochronology of volcanic ash-fall tuff layers

5.1 Introduction

Volcanic debris is often injected into the stratosphere by explosive eruptions and can be transported hundreds to thousands of kilometres before being deposited. Ash-fall tuffs are excellent time markers in the geological record and are very useful for dating sedimentary successions. Geochronological data obtained from such units can also be used to estimate rates of sediment accumulation and biological evolution, calibrate excursions recorded in chemostratigraphic proxies, calibrate molecular clocks, constrain the timing of tectonic events, and confirm or deny problematic lithostratigraphic correlations (Bowring & Schmitz, 2003) across local outcrop areas, basins and even transcontinental areas. In the same way problematic bio-, chemo-, tephro-, cyclo-, and sequence stratigraphic correlations could be verified or corrected. Juvenile zircon crystals are often present in fair amounts within tuff layers and are the prime target in most geochronological studies on altered pyroclastic rocks. The crystal structure of zircon can incorporate certain amounts of U and Th (typically in the range of tens- to thousands-of-ppm) among a number of other trace elements due to their somewhat compatible ionic and crystal radii (CR: [VIII]Zr^{4+} 0.98 Å, [VIII]U^{4+} 1.14 Å, [VIII]Th^{4+} 1.19 Å; values are crystal radii (CR), not ionic radii, because according to Hoskin & Black (2000) CR more accurately represent the radii of ions in crystals). However, non-radiogenic Pb (CR: [VIII]Pb^{2+} 1.43 Å), also known as common or initial Pb, is largely excluded from a crystallizing zircon (Watson et al., 1997), what is very important because Pb is also the stable endproduct of the U-Th decay series (so-called radiogenic Pb). Furthermore, zircon is stable in most geological environments (Watson, 1996) and makes it an excellent geochronometer as long as the zircon crystal remains crystalline and does not become metamict due to radiation damage. Zircon grains can even survive episodes of partial melting with little or no effect on their U-Pb system (Davis et al., 2003). Although zircon is very resistant to alteration, in a metamict state zircon could lose 50-85% of its radiogenic Pb even at ambient temperatures (Stern et al., 1966).

Two main techniques are currently applied to the U-Pb dating of zircons which both have their strengths and weaknesses. ID-TIMS (Isotope Dilution Thermal Ion Mass Spectrometry) requires dissolution of zircon, whereas with SIMS (Secondary Ion Mass Spectrometry) largely non-destructive in-situ measurements can be done on a mounted and polished zircon using a SHRIMP (Sensitive High-Resolution Ion Micro-Probe). The big advantage of a SHRIMP is its great spatial resolution with the target areas of the primary ion beam usually being 10-50 µm in diameter and a total sampling depth of typically less than 5 µm. Therefore, problems with mineral or melt inclusions, inherited older cores, complex overgrowths and

alteration domains within the zircon crystal can in most cases be avoided or resolved with the SHRIMP. Measuring such complex grains can pose a significant challenge to the ID-TIMS method but is a strength of the ion microprobe. The disadvantage of the SHRIMP is that it has difficulty achieving better than 1% accuracy in Pb-U measurements. The accuracy of SHRIMP microanalysis is achieved at the expense of precision, a consequence of the sampled number of ions available from the sampled mass, which is only a few nanograms. Age precisions from SHRIMP are normally 5 to 10 times worse per spot than they are from analyzing a whole grain by ID-TIMS (Davies et al., 2003). Therefore, SIMS analysis does not achieve the precision attainable by ID-TIMS but it remains unrivaled for its precision and accuracy in U-Th-Pb dating at an intracrystalline scale (Ireland & Williams, 2003).

The U-Pb zircon geochronology of tuffs is notoriously difficult, due to the fact that many tuffs have inheritance that is often extremely difficult to detect. There are several types of inheritance that cause problems in dating pyroclastic deposits. Very common is inheritance within a zircon crystal, composed of an older core that is overgown by younger magmatic zircon. In this study this type of inheritance was observed in one case already in thin section (Fig. 3.26-G) but is normally better revealed in cathodoluminescence images (see figures in Chapter 5.4.2 Results). Another common type of inheritance encountered in pyroclastic rocks is the physical admixture of older magmatic zircons to the juvenile zircons during explosive eruptions. Sometimes, these older zircons can be identical in their appearance to the indigenous, juvenile magmatic population. These older zircons can be clearly of xenocrystic origin, as revealed by large age differences, despite their juvenile appearance. For example, Bangert (2000) reported an Ordovician magmatic zircon population among a Permian population within a Permian Karoo tuff layer from South Africa. A similar type of inheritance is the mixture of young juvenile and only slightly older zircons from genetically related but earlier volcanogenic rocks during an explosive eruption. Zircons with very similar chemistry and form can be derived from the same magmatic source, but can be several million years different in age, due to long lasting volcanic activity in the source area, which is in the case of this study most probably a magmatic arc system at the southern, active margin of Gond-wana. The lifespan of large magmatic arcs can be on the order of tens of millions of years. The zircon ages of the Owl Gorge Tuff reflect such a type of inheritance (see Fig. 5.4 in Chapter 5.4.2 Results). SHRIMP dating has proven to be a successful tool to reveal and cope with such inheritance phenomena. Another frequently encountered problem in U-Pb dating of zircon is Pb-loss which may be subtle. Zircon analyses that are too young and/or exhibit discordance might be attributed to Pb-loss. Experimental measurements of Pb diffusivity in zircon indicate that Pb-loss is not likely dominated by volume diffusion through crystalline zircon (Lee at al., 1997; Cherniak & Watson, 2000) but rather related to loss from

radiation-damaged domains through crystal defects and fractures. This process was possibly one complicating factor in dating the zircons of the DIBA Tuff, which have overall high U and Th contents (see also Fig. 4.11 in Chapter 4.5 U-Th mineral chemistry of zircons). As a consequence of these difficulties the choice of the analyses that define the true magmatic age of a tuff layer can be difficult and very often biased.

5.2 Previous SHRIMP and conventional radiometric datings of Late Palaeozoic tuffs from southern Gondwana

Probably the earliest attempt to determine the age of a tuff layer from the Karoo Supergroup radiometrically was undertaken by Karpeta (1996), who sampled tuffs from the Teekloof Formation of the lower Beaufort Group in the Cape Province of South Africa. However, the chosen method, the whole-rock K-Ar method, proved to be inappropriate for altered tuffs, giving wrong ages of 10.4 ± 8.1 and 1962.3 ± 39.2 Ma (A. Fallick, Scottish University Research and Reactor Centre, 1993; cited in Karpeta, 1996). The first attempt to date a Karoo tuff applying the SHRIMP method was undertaken by Viljoen (1995), who sampled a tuff layer about one metre above the base of the Collingham Formation in the Western Cape (Laingsburg section) of South Africa. Juvenile zircons separated from this tuff layer were dated at the Research School of Earth Sciences (RSES) – ANU Canberra/Australia. From the SHRIMP analyses of the zircons a preliminary age of 262 ± 4 Ma was calculated. However, this early SHRIMP measurement was done with old standards and no cathodo-luminescence imaging was done prior to spot analyses at that time. Therefore, this age was considered as very preliminary work and not intended for publication (Armstrong, pers. comm., 2003). Later, an age of 270 ± 1 Ma for a tuff bed from the middle part of the Collingham Formation was quoted by Trouw & de Wit (1999) as a personal communication of S. Bowring (1998). A further zircon age, which was also only cited as a personal communication, was derived from a tuff layer within the *Cistecephalus* biozone of the Teekloof Formation (basal Beaufort Group), which was dated at about 261 Ma (Bowring, pers. comm., 1998; cited in Stollhofen, 1999).

Bangert et al. (1999) then published a number of SHRIMP zircon U-Pb ages from several tuff layers of the Dwyka and the basal Ecca Group in Namibia and South Africa. Juvenile zircons of supposedly the same tuff horizon (Ganigobis Tuff IIb), but from different localities in the vicinity of Ganigobis in southern Namibia, gave weighted mean $^{206}Pb/^{238}U$ ages of 302.0 ± 3.0 Ma and 299.5 ± 3.1 Ma (Bangert, 2000). The dated tuff horizon IIb lies about 5 m above the base of the Ganigobis Shale Member, which is considered to represent the upper part of deglaciation sequence two (DS II) (Bangert et al., 1999). From a comparable stratigraphic

level a tuff layer from the Dwyka outcrops at the Orange River near Zwartbas was sampled and dated. Zwartbas Tuff IIIb lies about 15 m above the base of the Dwyka deposits and yielded an age of 302.3 ± 2.1 Ma (Geiger, 2000; Bangert et al., 2000), which corresponds very well with the 302.0 ± 3.0 Ma age for tuff layer IIb at Ganigobis. From a sample of the Zwartbas Tuff XXXIV, positioned about 80 m above the base and about 55 m below the top of the Dwyka Group at this locality, unfortunately only two zircons could be separated. Two SHRIMP analyses on one zircon gave ages of 302.87 ± 4.31 Ma and 297.28 ± 4.74 Ma, from which a weighted mean age of 300.6 ± 6.3 Ma could be calculated. However, such an age, based only on data of two single zircons, cannot be regarded as very reliable for the age of the tuff layer because of possible inheritance effects. In order to determine a reliable age for the upper part of the Dwyka Group, Bangert (2000) sampled a tuff from a higher stratigraphic level of the Dwyka Group, exposed in the vicinity of Klaarstroom in South Africa. Juvenile, magmatic zircons were separated from an 8-9 cm thick tuffaceous zone, which is enclosed in a 3 m thick shale unit and probably represents the top of DS III. SHRIMP analysis revealed a weighted mean $^{206}Pb/^{238}U$ age of 297 ± 1.8 Ma (Bangert et al., 1999). To obtain a more extensive picture also the Dwyka-Ecca boundary, and therewith the top of DS IV, respectively the base of the Prince Albert Formation, was targeted for dating. Juvenile zircons from two tuff horizons of the basal part of the Prince Albert Formation, sampled north of Klaarstroom and south of Laingsburg in the south-western Cape Province, were dated at 288.0 ± 3.0 and 289.6 ± 3.4 Ma (Bangert et al., 1999; Bangert, 2000).

Around the same time Wanke (2000) and Holzförster (2000, 2002) sampled tuff layers from the Gai-As and Doros Formations in NW-Namibia. Both formations are correlatives of the lower part (Upper Permian) of the Beaufort Group in South Africa. Unfortunately the stratigraphic position of the two dated tuff layers is quite controversial. Whereas Wanke (2000) placed the dated tuff layers in the uppermost part of the Gai-As Formation and in the upper half of the overlying Doros Formation, Holzförster (2002) placed both close to the boundary between the Gai-As and the Doros Formation. Adding to the confusion, in Wanke et al. (2000) one dated tuff layer is reported to originate from the top of the middle part of the Gai-As Formation. Nevertheless, from the zircon analyses of one tuff bed (sample B18; Wanke, 2000) a weighted mean $^{206}Pb/^{238}U$ SHRIMP age of 265.5 ± 2.2 Ma was calculated. The second sample (sample 30/98; Wanke, 2000) yielded 25 zircon analyses with appreciable scatter due to Pb-loss and inheritance of older zircon xenocrysts. The calculated age of 272.7 ± 1.8 Ma is probably too old and may not represent the true age of the tuff layer. The 265.5 Ma age is similar to the 261 Ma age reported by Bowring (pers. comm., 1998; cited in Stollhofen, 1999) for a tuff bed from the lower Beaufort Group and therefore supports the above mentioned correlation.

Another radiometric age has been published recently from a tuff layer in the Rio Bonito Formation of the Paraná Basin in Brazil. The Rio Bonito Formation is a correlative of the Verbrandeberg Formation in northern Namibia and a correlative of the lower part of the Prince Albert Formation in southern Namibia (Holzförster et al., 2000). Within the Candiota Coalfield in southern Brazil the Rio Bonito Formation contains a set of tonsteins interbedded with coal seams. These tonsteins are mainly composed of kaolinite flakes and vermicules with zircon, apatite and beta-quartz paramorphs as accessory minerals. By conventional U-Pb dating of zircons from tonstein A an intercept age of 267.1 ± 3.4 Ma was determined (Matos et al., 2001). This age, however, strongly conflicts with the SHRIMP ages presented here. A potential correlative of the described tuffs from the Candiota Coalfield is the DIBA tuff bed of the Itzawisis Tuffs from southern Namibia, which was dated at 288.5 ± 1.6 Ma. From this point of view the proposed age for the Candiota tonstein appears much too young. A reason for this discrepancy possibly lies in the applied method. From the Candiota tonstein about 200 zircon crystals were separated and split into four fractions. Conventional U-Pb isotope analyses of these four different zircon fractions permitted to define a concordia with two intercepts, one at 267.1 ± 3.4 Ma, interpreted as the crystallization age of the zircons, and one at 867 ± 32 Ma, interpreted as the age of inherited cores. Nevertheless, the effects of lead loss and inheritance of older zircons are very difficult to control in mixed zircon fraction analyses and therefore the zircons from the Candiota tonstein should be re-examined by single zircon analysis.

Further datings of Late Palaeozoic tuffs are also known from the Sydney-Bowen Basin area in Australia, which was positioned near the southeastern active margin of Gondwana. Conventional U-Pb dating of zircons from tuff layers in this region first yielded ages of about 310-255 Ma (Gulson et al., 1990). Subsequent extensive single zircon SHRIMP datings of bentonites and tonsteins of the Sydney-Bowen Basin yielded ages ranging between ~294 to ~250 Ma (Roberts et al., 1996).

SHRIMP dating of zircon macrocrysts from the Botswanan Jwaneng kimberlite diatremes of supposedly Permian age revealed the presence of at least two distinct zircon populations (Kinny & Compston, 1989). The older zircons are of Precambrian age, whereas the younger zircons yielded a $^{206}Pb/^{238}U$ age of 235 ± 4 Ma (Lower to Middle Triassic).

5.3 New SHRIMP radiometric datings of Late Palaeozoic tuffs from southern Namibia

Altogether five newly discovered tuff layers were sampled for SHRIMP dating. They all originate from the lower part of the Ecca Group in southern Namibia and therefore represent a continuation of Bangert´s earlier geochronological investigations on the tuffs of the under-lying Dwyka Group. Sample OG-9 of the Owl Gorge Tuffs lies close to the Dwyka-Ecca boundary, sample DIBA-2 of the Itzawisis Tuffs originates from the lower part of the Prince Albert Formation, sample UHB-T of the Uhabis River Tuff from the uppermost part of the Prince Albert Formation, sample KHA-1a of the Khabus Tuff from the middle part of the Whitehill Formation, and sample UFO-43 of the Ufo Valley Tuffs from the middle part of the Collingham Formation.

5.3.1 Sample processing and analytical procedures

Sample KHA-1a was processed at the geochronology lab of the University of Giessen in Germany. First, the greenish-chloritic, shaly host rock and alteration products were removed from the raw rock samples (Fig. 5.1-A) of the albitized tuffaceous layer with a rock saw (Fig. 5.1-B). The albitized tuff concentrate was cleaned with water and air-dried. About 10 kg of rock pieces were then crushed in a steel jawbreaker. To remove the zircons from the albitic matrix the crushed tuff was carefully ground in a specially constructed rotating mill (Pulveri-sette - Fig. 5.1-C/D) to a fine-grained powder. A Wilfley Table (Fig. 5.1-E) was used to con-centrate the heavy mineral content. Only the first fraction was further processed.

For heavy liquid separation first bromoform was used (Fig. 5.1-F). After cleaning with acetone and air-drying the heavy mineral fraction (sink) underwent a magnetic separation. First ferromagnetic particles were removed with a hand magnet, and then the heavy mineral concentrate was divided by a Frantz magnetic separator (Fig. 5.1-G) into several magnetic fractions (0.4, 0.8, 1.2 and 1.6 A). The non-magnetic fraction at 1.6 A underwent a further heavy liquid separation with dijodmethane. The heavy mineral fraction, actually a zircon concentrate (Fig. 5.1-H), was again cleaned with acetone and air-dried.

The zircon concentrate was divided with a microsieve into a fraction >100 μm and a fraction <100 μm. By handpicking under a binocular microscope euhedral acicular to long-prismatic zircons and euhedral short-prismatic, squat and semi-equidimensional zircons were separated from the >100 μm concentrate.
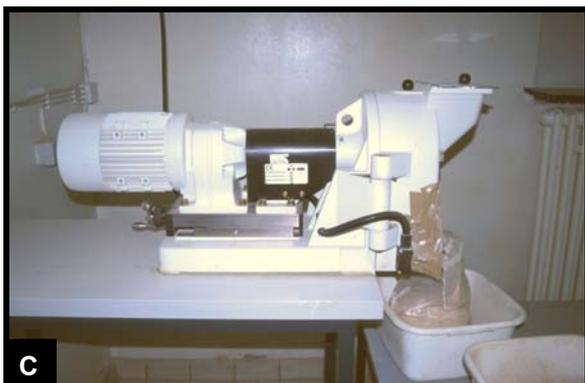
Fig. 5.1 (prev. page): Illustrated are successive steps of processing the KHA-1a tuff sample for zircon separation and concentration at the Giessen geochronology lab: **(A)** Raw rock samples of the Khabus Tuff. **(B)** Rock saw used to cut off altered and shaly portions. **(C) & (D)** Rotating mill (Pulverisette) in which pre-broken (steel jawbreaker) tuff chips were ground to a fine-grained powder. **(E)** Wilfley Table separation of the heavy mineral fraction. **(F)** Heavy liquid separation. **(G)** Frantz magnetic separator for extracting the diamagnetic fraction. **(H)** Zircon concentrate after processing.

The zircons from the four other whole-rock tuff samples (OG-9, DIBA-2, UHB-T and UFO-43) were separated at the Research School of Earth Sciences (RSES) – ANU Canberra/Australia using standard heavy liquid and magnetic procedures. All the separates (incl. several separates of sample KHA-1a) were handpicked under a binocular microscope at the RSES and mounted in epoxy, together with the RSES reference zircons AS3, FC1 and SL13. Photomicrographs in transmitted and reflected light were done on all zircons and these, together with SEM cathodoluminescence images, were used to decipher the internal structures of the sectioned grains and to target specific areas within the zircons for spot analysis.

U-Pb analyses were done using SHRIMP II at the RSES. The data have been reduced in a manner similar to that described by Williams (1998; and references therein), using the SQUID Excel Macro of Ludwig (2000). For the zircon calibration the Pb/U ratios have been normalised relative to a value of 0.1859 for the $^{206*}Pb/^{238}U$ ratio of the AS3 or FC1 reference zircons, equivalent to an age of 1099 Ma (Paces & Miller, 1993). U and Th concentrations were determined relative to the SL13 standard. Uncertainties given for individual analyses (ratios and ages) are at the 1σ level, however uncertainties in the calculated weighted mean ages are reported as 95% confidence limits and include the uncertainties in the standard calibrations. Concordia plots and weighted mean age calculations were carried out using Isoplot/Ex (Ludwig, 1999). Concordia ages (Ludwig, 1998) are calculated using the SQUID macro (Ludwig, 2000) with uncertainties from the standard calibration included in the final errors quoted.

Theoretically, the U-Pb method can exploit two independant chronometres (^{238}U-^{206}Pb and ^{235}U-^{207}Pb) that can be compared to evaluate open-system behaviour (loss of radigenic Pb and later incorporation of common Pb leading to discordance. A given U-Pb zircon dataset provides therfore a multiplicity of dates that can be used to calculate an age of crystallisation, including the weighted mean $^{206}Pb/^{238}U$, $^{207}Pb/^{235}U$, or $^{207}Pb/^{206}Pb$ dates, the Concordia age algorithm of Ludwig (1999) which combines all three chronometres, or the upper intercept age of an array of variably discordant data. With optimal data sets of concordant and equivalent zircons, these data converge and the Concordia age algorithm provides the best age estimation, including the appropriately minimized decay constant errors. However, in

Late Palaeozoic and younger rocks that have low U zircons, the lower abundances of ^{235}U and radiogenic ^{207}Pb result in a large uncertainty in the ^{207}Pb/^{235}U date due to measurement errors and increased sensitivity to common Pb corrections. Small biases in ^{207}Pb/^{235}U are correspondingly magnified in the ^{207}Pb/^{206}Pb date because of the relatively reduced ingrowth of ^{207}Pb over the past several hundred million years (reflected in the limited curvature of concordia). Because of these factors the ^{207}Pb/^{206}Pb date is generally not the preferred age for zircon SHRIMP datings of Late Palaeozoic and younger rocks (Claoué-Long et al., 1995). Instead, the U/Pb dates are more robust, and the weighted mean ^{206}Pb/^{238}U date is most often used to calculate the age of a rock because of its better precision and insensitivity to systematic error relative to the ^{207}Pb/^{235}U date (Bowring & Schmitz, 2003; and references therein). In the case of this study only for the high U zircons of the DIBA Tuff a concordia age was calculated, all other ages represent weighted mean ^{206}Pb/^{238}U ages (see Claoué-Long et al., 1995) concerning accuracy of zircon SHRIMP ^{206}Pb/^{238}U ages and the comparability with ID-TIMS zircon dating and ^{40}Ar-^{39}Ar dating of sanidines).

As for the new Geologic Time Scale 2004 radiometric ages with the U-Pb method on zircons have lately being accepted only from the ID-TIMS method, but generally not from high-resolution ion microprobes (SHRIMP) that uses the Sri Lanka SL13 standard (Gradstein & Ogg, 2004), it is considered necessary to comment here on the reference standards that were used for the SHRIMP measurements in this study.

Pb and U have different secondary ionization efficiencies which change during each SHRIMP analysis. The efficiencies are also matrix dependant, so Pb/U and Pb/Th are measured relative to concordant reference minerals. These reference standards must be dated inde-pendantly by ID-TIMS. Early zircon work in the ANU lab was referenced to a U-rich Sri Lankan zircon megacryst, SL3. As techniques improved, this metamict crystal was replaced by another megacryst with lower U and more uniform composition, SL13 (Williams et al., 1988; Claoué-Long et al., 1995). This also proved heterogeneous on the microscale, however (Compston, 1999), and has been abandoned except as a U and Th concentration reference. SHRIMP analysts at ANU have tried a succession of potential zircon standards, retaining SL13 as a concentration reference but searching for zircon more uniform in Pb/U for interelement calibrations. First choice was AS3, a zircon from a 1.1 Ga anorthositic syenite from the Duluth Complex, Minnesota, from which Paces & Miller (1993) obtained consistently concordant ID-TIMS analyses. AS3 also proved quite uniform in Pb/U when analyzed by SIMS, however, good quality zircon was scarce, with most grains being skeletal, finely fractured and stained by iron oxides (Ireland & Williams, 2003). Attempts to collect better material from the original sample site were unsuccessful, so a site at Forest Centre,

250 km NW of Duluth (FC1: Paces & Miller, 1993), was chosen from which abundant good quality zircon was obtained. FC1 is now widely used as a Pb/U standard in the ANU lab and other institutions.

It is therefore important to express that the SL13 standard is only used to measure U and Th concentrations but it is no longer used to measure ages. Nevertheless, replicate SIMS analyses of well-characterized reference materials suggest that with present Pb/U calibration techniques, the accuracy of SIMS determinations of $^{206}Pb/^{238}U$ and $^{208}Pb/^{232}Th$ appears limited to about 1%. For samples less than 100 Ma old this equates to an uncertainty of less than 1 Myr, an acceptable age resolution, but for early Palaeozoic samples the same uncertainty amounts to as much as 5 Myrs, of little value for defining the numerical time scale or dating rapid faunal changes (Ireland & Williams, 2003). However, SHRIMP ages of individual Karoo tuff layers are now confirmed by dates from equivalent or correlative stratigraphic intervals of neighbouring outcrop areas or basins and by correspondence with dates from under- and overlying tuff layers. This statistically substantiates these ages and strengthens their relevance.

At this point it should be noted that by dating zircons from volcanic ashes it is often tacitly assumed that the zircon age represents the age of the tuff layer, or more specifically the eruption age. However, it is not necessarily the case that zircon ages of volcanic rocks record crystallization during or after eruption but an earlier time when the magma became saturated in Zr, i.e. when it cooled to its zircon saturation temperature (Reid et al., 1997). However, the time difference between the crystallization of zircon and the eruption as well as the deposition of the ash is almost certainly within the error on the measured isotopic ages.

5.3.2 Results

The presented results of the SHRIMP U-Pb dating of the Namibian Karoo tuffs are based on a PRISE report written by R.A. Armstrong (ANU) (Armstrong, 2003) and are supplemented by own considerations. Only a representative portion of all measured zircons of each tuff sample is shown below in the cathodoluminescnce (CL) images. The complete set of CL images is included in the PRISE report. The summaries of the SHRIMP U-Pb zircon data for all tuffs are listed in the appendix (pages IX-XIII).

Sample OG-9 of the Owl Gorge Tuffs: Owl Gorge Member – base Prince Albert Formation

The Owl Gorge tuff sample produced abundant zircons, most of which are euhedral to subhedral but with a range of forms from acicular with sharp, well-developed pyramidal tips to more tabular and platy crystals. Many grains have cores of inherited zircon (Fig. 5.2). For the SHRIMP analysis spots were sited within the magmatically zoned tips to ensure there was no overlap onto inherited cores.
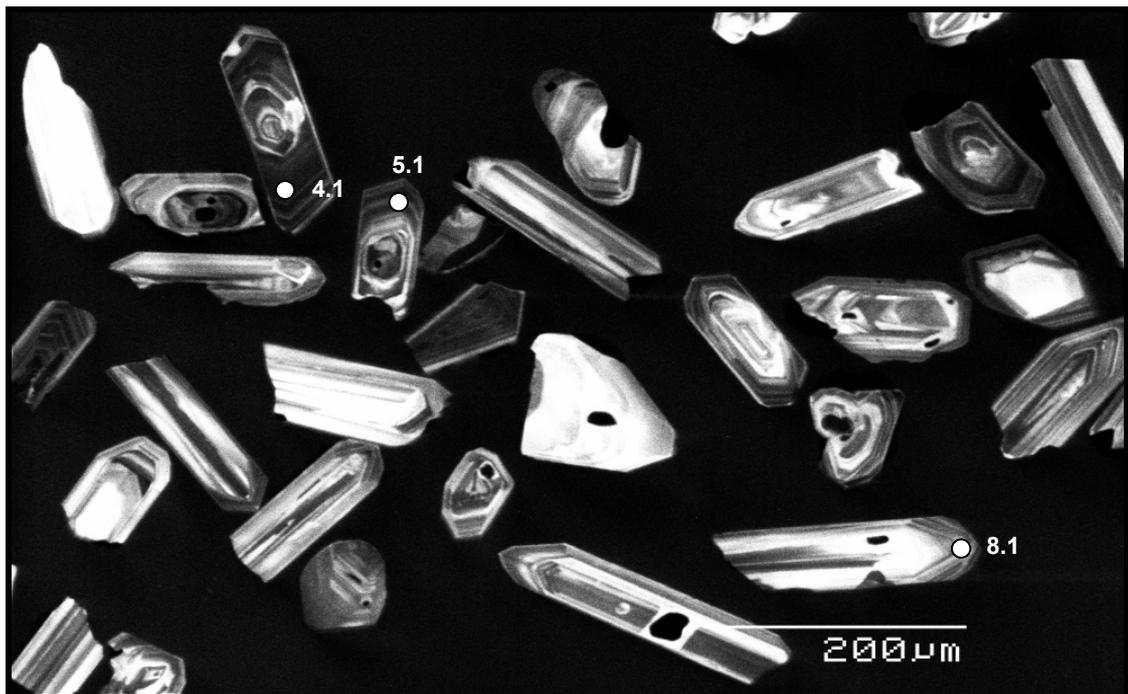
Fig. 5.2: Cathodoluminescence image of magmatic zircons from the Owl Gorge Tuff (sample OG-9). In the upper left corner some grains with suspected inherited cores can be seen. Analysed grain spots are indicated.

From the Tera-Wasserburg plot of the data (Fig. 5.3; Appendix Page IX) it is clear that there is some scatter of the data along the concordia. This could be due to Pb-loss from a single population, or it could reflect a heterogeneous population. An interesting view of the data is given by the histogram and cumulative probability plot shown in Fig. 5.4, which is an attempt to deconvolve the data into different age groups using the Mixture Modelling procedure of

Sambridge and Compston (1994). Apart from the analyses (2.1, 8.1 and 18.1), which have apparent U/Pb ages that are clearly too young (*i.e.* have suffered Pb-loss) it is possible to identify two distinct ages within this group of data. Weighted mean $^{206}Pb/^{238}U$ ages for these groups are 290.9 ± 1.7 Ma and 298.7 ± 2.0 Ma (95% conf. limits). It is not obvious that the two ages can be correlated with any particular zircon type or chemistry. Such a bimodality of data on tuffs has been noted also in other studies (Fanning et al., 2003).
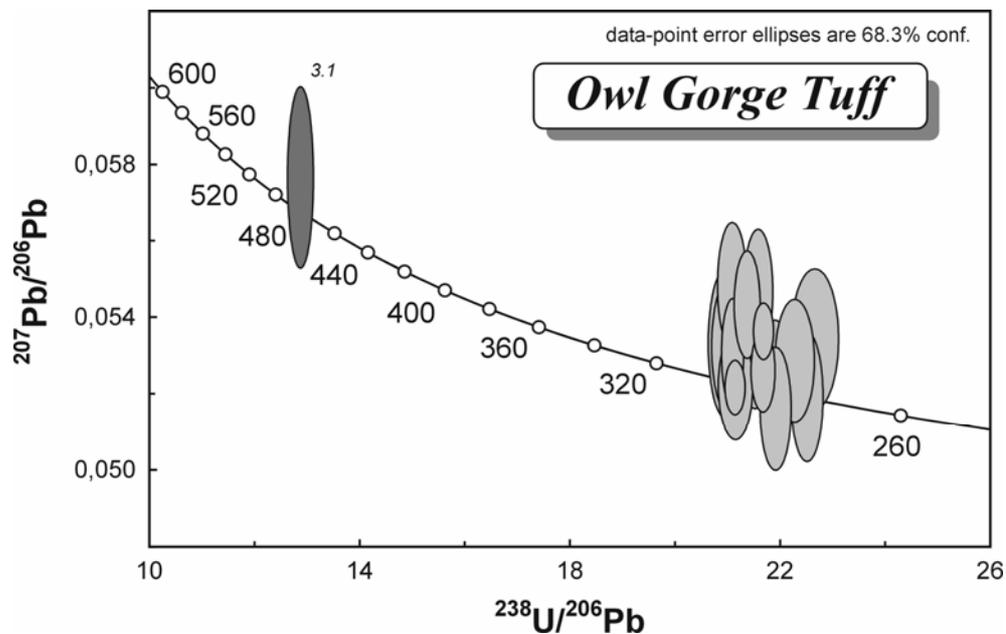
Fig. 5.3: SHRIMP U-Pb zircon data from the Owl Gorge Tuff (sample OG-9). The data are plotted uncorrected for common Pb.
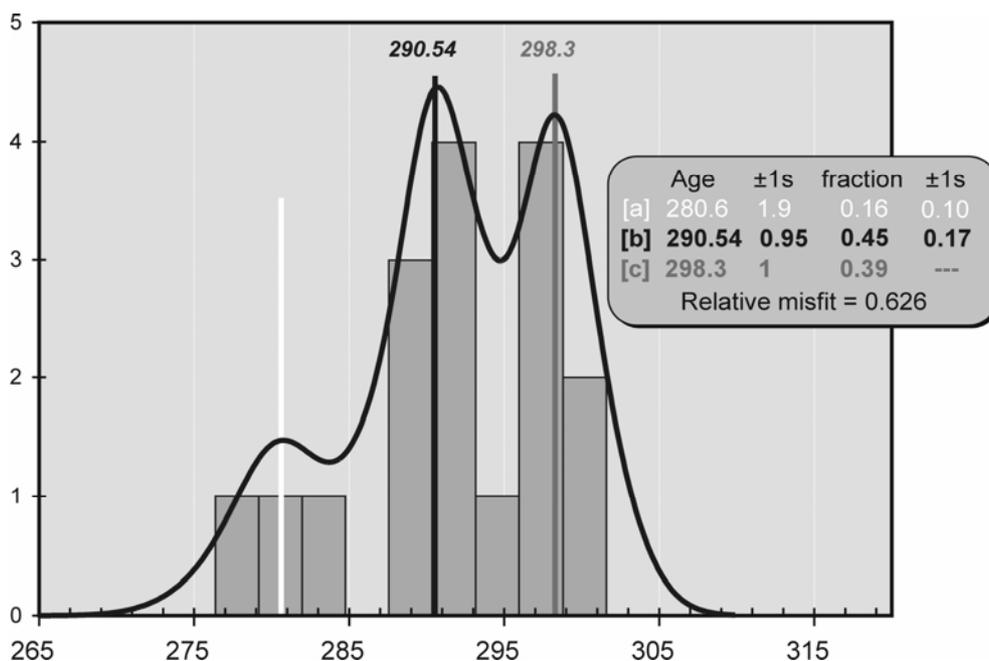
Fig. 5.4: A cumulative probability and histogram plot of the data of the Owl Gorge Tuff (OG-9) showing the bimodality of the magmatic zircons. The small peak showing an apparently younger age represents analyses, the respective zircons having suffered Pb-loss.

In the case of the Owl Gorge Tuff this bimodality most probably reflects not an artefact. The Owl Gorge Tuff is underlain by an approximately 150 m thick succession of glacigenic, dropstone-bearing mudrocks of the Dwyka Group, which contains abundant tuff layers, especially in the lower to middle part of the succession (Zwartbas Tuffs). Excellent outcrops of these tuff layers can be seen at the northern cut banks of the Orange River about 2 km south of the Owl Gorge tuff locality. These tuff layers were investigated in detail by Geiger (2000) and a tuff layer from the basal part of the succession yielded a SHRIMP U-Pb age of 302.3 ± 2.1 Ma (Bangert, 2000; Geiger, 2000). Therefore, it is most likely that the zircons in this case represent a mixed population. The younger age of 290.9 ± 1.7 Ma represents the age of the Owl Gorge Tuff, which is in accordance with the dating results of South African tuff layers from horizons close to the Dwyka-Ecca boundary yielding ages of 289.6 ± 3.8 and 288.0 ± 3.0 Ma (Bangert et al., 1999). The slightly older zircons with an age of 298.7 ± 2.0 Ma within the Owl Gorge Tuff most probably represent a 'young-xenocrystic' component, which was incorporated from a slightly older pyroclastic deposit during the slightly younger eruption event into the volcanic ash. In this context it is also interesting to note that one single zircon (analysis 3.1) from the Owl Gorge Tuff yielded an age of about 480 Ma (Early Ordovician). Ordovician zircons are also present in another tuff sample from the basal Prince Albert Formation 10 km south of Laingsburg/RSA. This tuff sample contained a number of older magmatic zircons that yielded an age of 464 ± 5 Ma, apart from the younger juvenile zircons yielding an age of 289.6 ± 3.4 Ma (Bangert, 2000). Therefore it seems compelling that in the source area of these Late Palaeozoic tuffs also Early-Middle Ordovician magmatic rocks must have been present, which were incorporated during explosive eruptions into the younger eruption column as a xenocrystic component. This association of Late Palaeozoic and Early-Middle Ordovician magmatic rocks is a very important aspect in the search for the possible volcanic source areas of the lower Karoo tuffs (see Chapter 6 – Source area considerations). In this respect it is also interesting to note that tuffaceous beds were reported from the lower part of the Ordovician Natal Group in KwaZulu-Natal, South Africa (Thomas et al., 1992; Marshall, 2002). So far, no source area was suggested for these tuff layers.

Sample DIBA-2 of the Itzawisis Tuffs: lower Prince Albert Formation

This sample produced a variable and heterogeneous population of zircons. Most are euhedral to subhedral and are clearly magmatic in origin. Shapes and forms range from squat and equidimensional to rare acicular forms (Fig. 5.5). Cathodoluminescence imaging shows zoning of variable intensity and many, if not most, zircons have cores or suspected cores. These were avoided during analysis where possible, but two much older xenocrysts were still found, illustrating yet again the difficulties inherent in doing geochronology in tuffs.
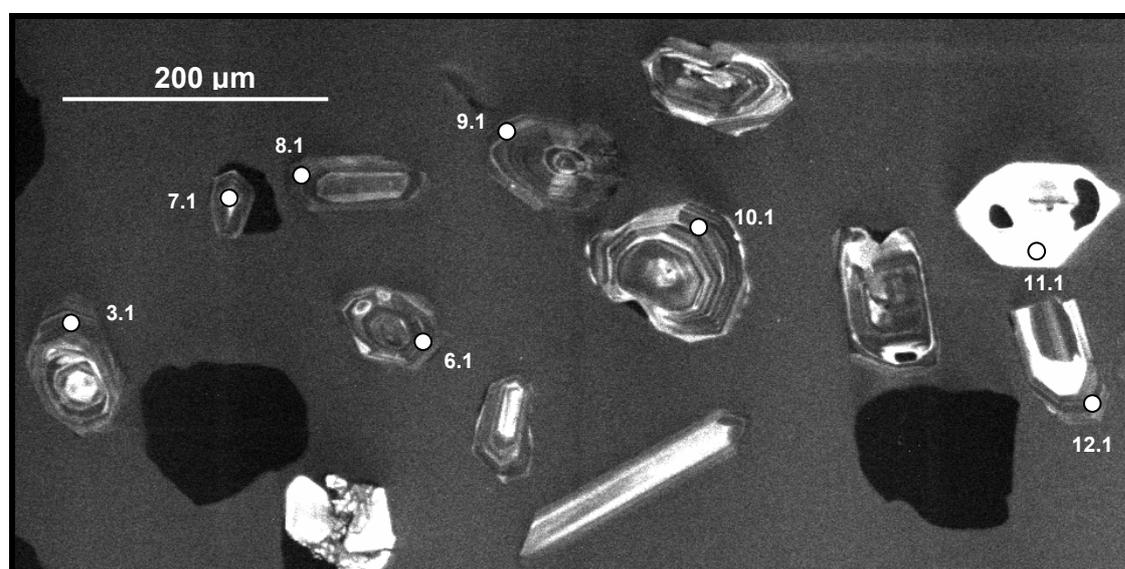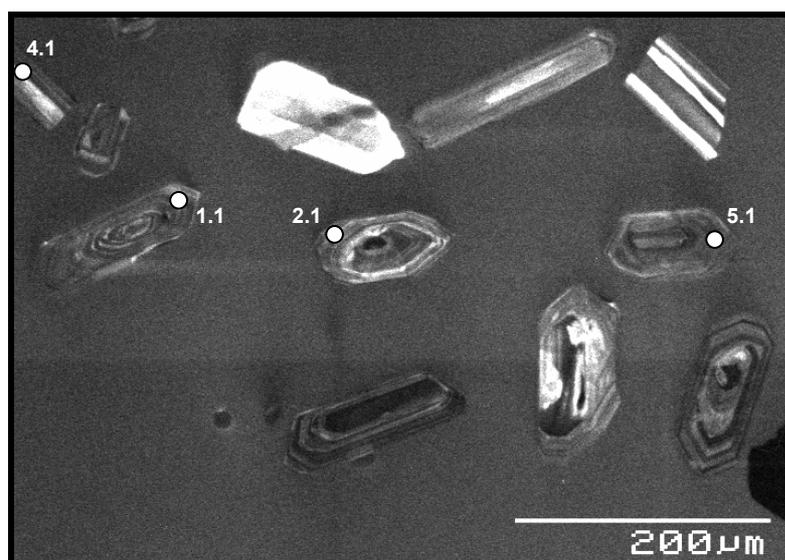
Fig. 5.5: Cathodoluminescence image of magmatic zircons from the Itzawisis Tuff (sample DIBA-2) showing highly variable forms. Analysed grain spots are indicated. Grain 10.1 represents a xenocryst having an age of about 2 Ga.

From the data plotted in Fig. 5.6 and 5.7 (and Appendix Page X) it is clear that the zircons from this sample include some xenocrysts with a large range of ages. In addition, the data set is further complicated by Pb-loss. Overall, these zircons have high U and Th contents (relative to the other tuffs analysed) and this might be a contributing factor towards Pb-loss. Picking the magmatic population is subjective, but in calculating an age the following criteria were followed:

1) Four analyses (3.1, 5.1, 7.1 and 17.1; marked in Fig. 5.7) have very high common Pb contents and were rejected;
2) Those analyses which have obviously lost Pb and give low apparent U/Pb ages were also rejected;
3) Sorting out of inherited grains: this can be obvious (e.g. for grains 10.1 and 18.1) where large age differences can be identified, but in some cases this can be very subtle when the spot was inadvertently overlapped onto an older core or where the age of a xenocryst is not much greater than the host rock.

Eight analyses were selected as defining a uniform, coherent age population and a Concordia Age of 288.5 ± 1.6 Ma (MSWD = 1.2) can be calculated from these data. This is considered to be the best estimate of the emplacement age of this tuff.
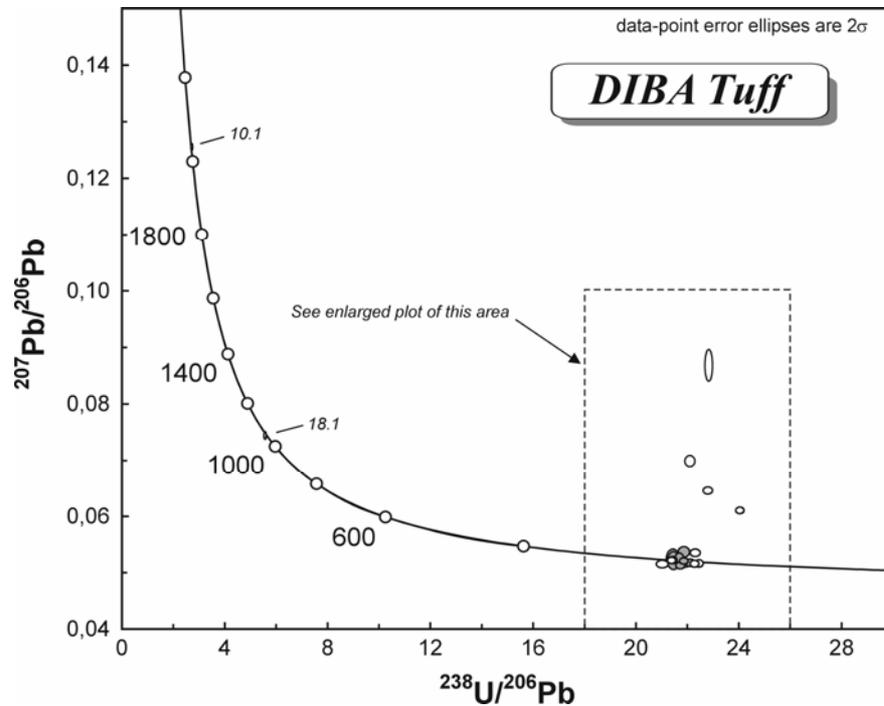
Fig. 5.6: U-Pb concordia plot of all SHRIMP data for zircons from the DIBA-Itzawisis Tuff (sample DIBA-2). See Fig. 5.7 for an enlarged view of the analyses used for the age calculation.
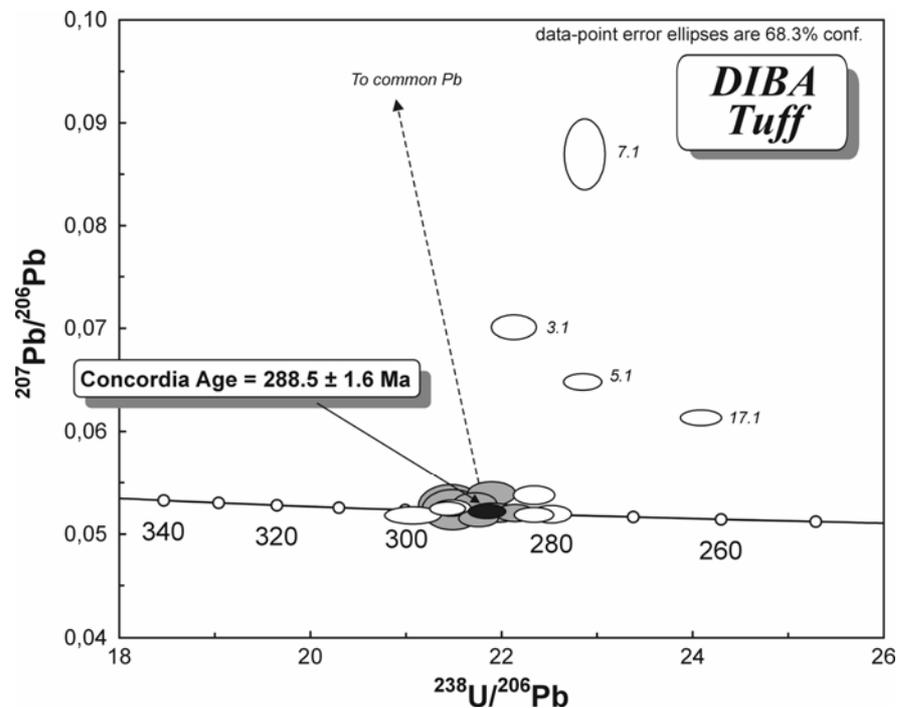
Fig. 5.7: Tera-Wasserburg plot of the Palaeozoic zircons analysed from the DIBA-Itzawisis Tuff (sample DIBA-2). The data are plotted uncorrected for common Pb and the error ellipses coloured grey represent those analyses used to calculate the Concordia Age (shown as a black error ellipse with 95% confidence limits.

Sample UHB-T of the Uhabis River Tuff: uppermost Prince Albert Formation

This sample yielded a good crop of euhedral to subhedral zircons. Most are clear, transparent and have a stubby, shortened form, although rare more acicular forms are also present (Fig. 5.8). Some grains have cores that appear to be of inherited zircon. All grains show good concentric oscillatory zoning and these were areas targeted in order to obtain a magmatic age for the zircons and the tuff

Fig. 5.8: Cathodoluminescence image of magmatic zircons from the Uhabis River Tuff (sample UHB-T) showing various morphologies. Most of the zircons display a well-developed concentric oscillatory zoning, some appear to have inherited cores. Analysed grain spots are indicated.

Twenty-one analyses were performed on twenty different grains, with the data plotted in Fig. 5.9 and listed in the Appendix Page XI. Generally the data plot as a well-defined group with very little common Pb. Several analyses are not part of this group with six analyses (shown in Fig. 5.9) having apparently lower $^{206}Pb/^{238}U$ ages, interpreted to be a consequence of radiogenic Pb-loss. One analysis (4.1) is apparently older and must be a xenocryst. The weighted mean $^{206}Pb/^{238}U$ age calculated for the remainder of the data is 279.1 ± 1.5 Ma (MSWD = 0.75; probability = 0.70).
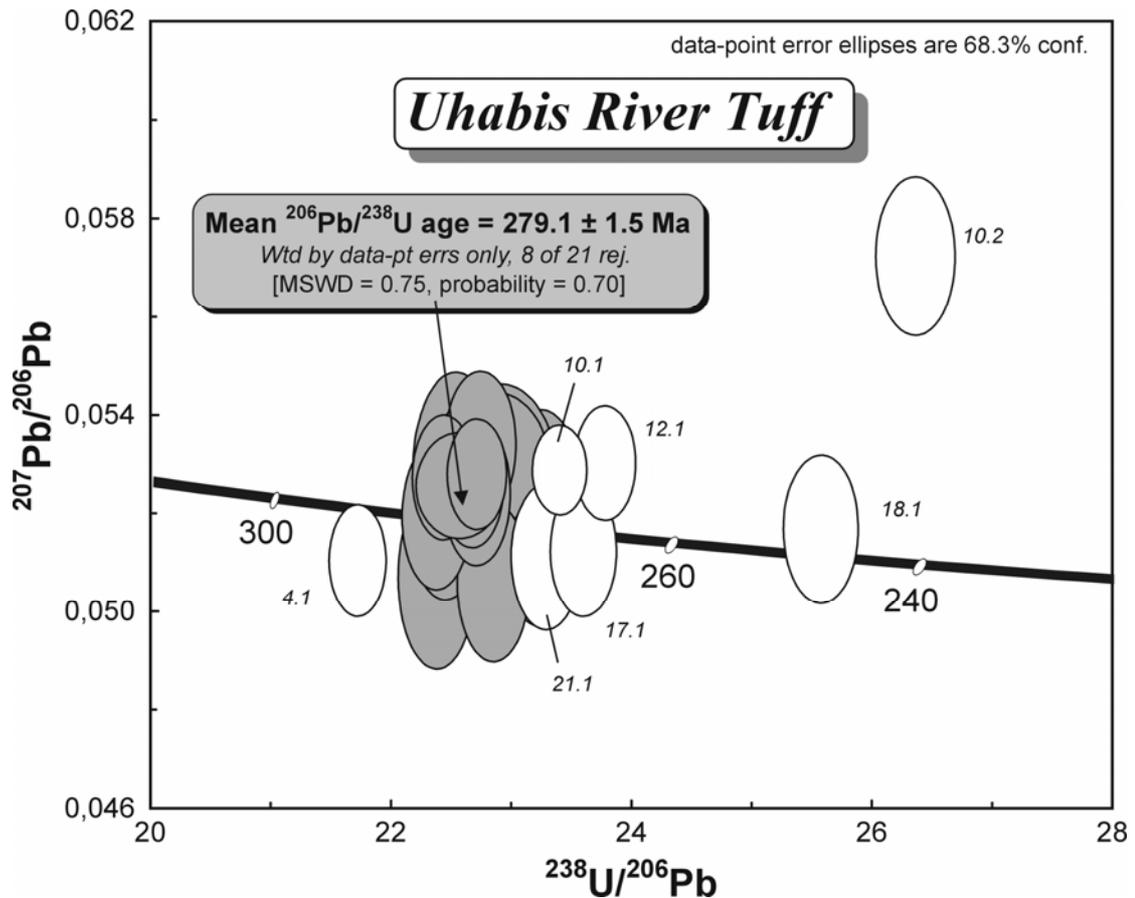
Fig. 5.9: A Tera-Wasserburg U-Pb plot of the SHRIMP data (uncorrected for common Pb) for zircons from the Uhabis River Tuff (sample UHB-T).

Sample KHA-1a of the Khabus Tuff: middle part of the Whitehill Formation

Most zircons of the albitized Khabus Tuff (sample KHA-1a) are clear, and only lightly coloured with various forms from very acicular grains up to 280 μm in length and length-breadth ratios of over 8:1 to shortened, semi-equidimensional grains. For sample KHA-1a the separated zircons were supplied as several fractions based on either size (<100 μm or >100 μm) or form ("long-prismatic" and "short-prismatic"). Representative grains from all these fractions were mounted and those from the "long-prismatic" and the ">100 μm" fractions were analysed. The zircons are generally euhedral to subhedral and show well-developed oscillatory composition zoning. Melt inclusions and mineral inclusions of varying composition (including sulphides) are common, as are elongate "worm-burrow" cavities in some of the more elongate grains (Fig. 5.10). Cathodoluminescence imaging shows some possible inherited cores but these were avoided, as the aim of the study was to establish a magmatic age for the zircons and the tuff.
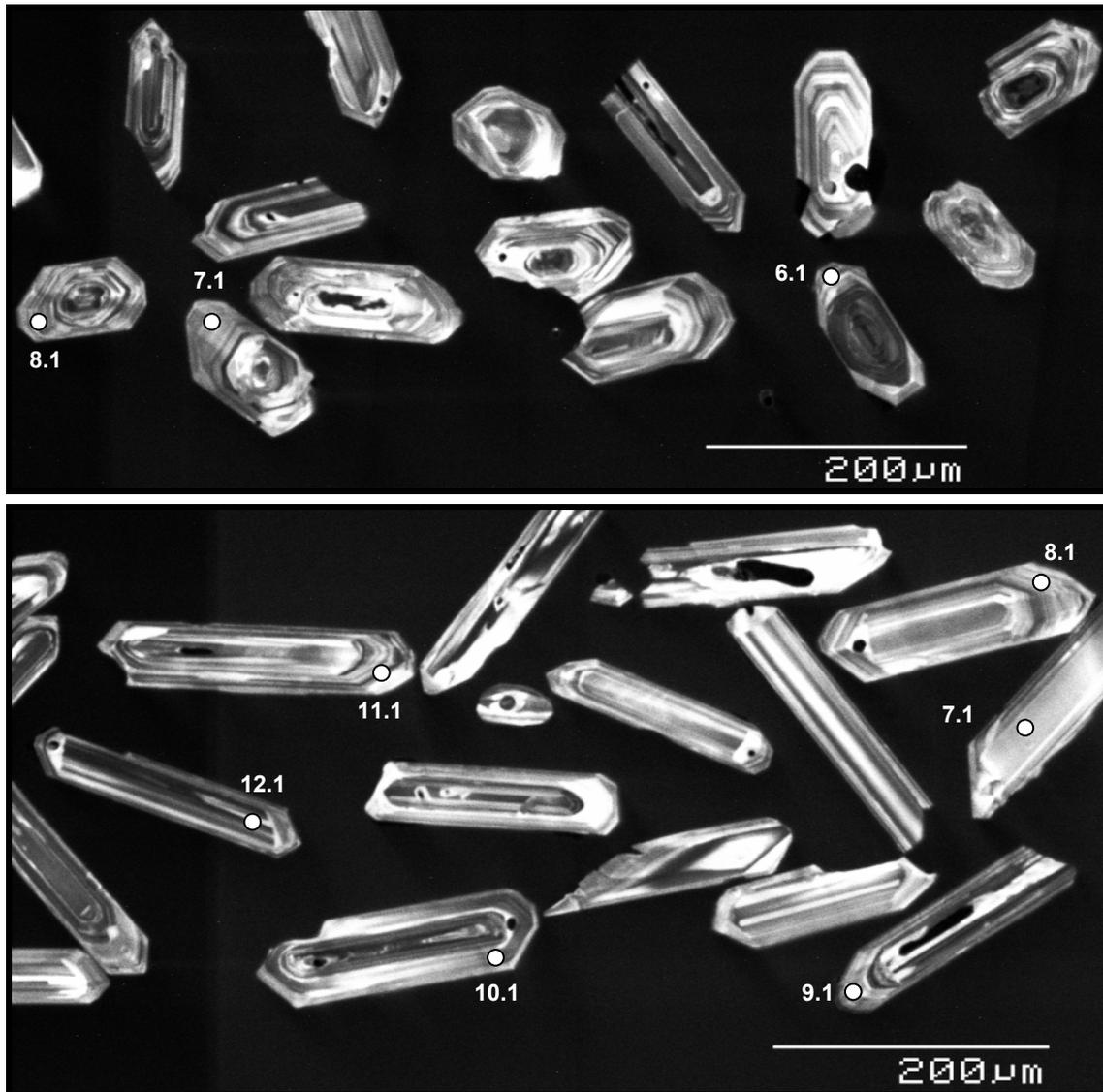
Fig. 5.10: Cathodoluminescence images of magmatic zircons of the Khabus Tuff (sample KHA-1a). Short, stubby forms with suspected inherited cores contrast with long, acicular forms, the latter often containing elongate melt inclusions. Analysed grain spots are indicated.

Nineteen analyses were done on zircons from the tuff sample KHA-1a. The data are listed in the Appendix Page XII and are plotted as measured ratios (i.e. uncorrected for common Pb) in the Tera-Wasserburg plot (Fig. 5.11). Apart from a few exceptions, the zircons have very low common Pb contents and plot as a cluster on or slightly above the concordia curve. With two analyses rejected it is possible to calculate a weighted mean $^{206}Pb/^{238}U$ age of 280.5 ± 2.1 Ma (MSWD = 1.2; probability-of-fit = 0.23) from the remaining 17 data points. One rejected analysis has high common Pb and the respective zircon appears to have suffered Pb loss resulting in a too young age. The other rejected analysis could represent an older, inherited zircon.
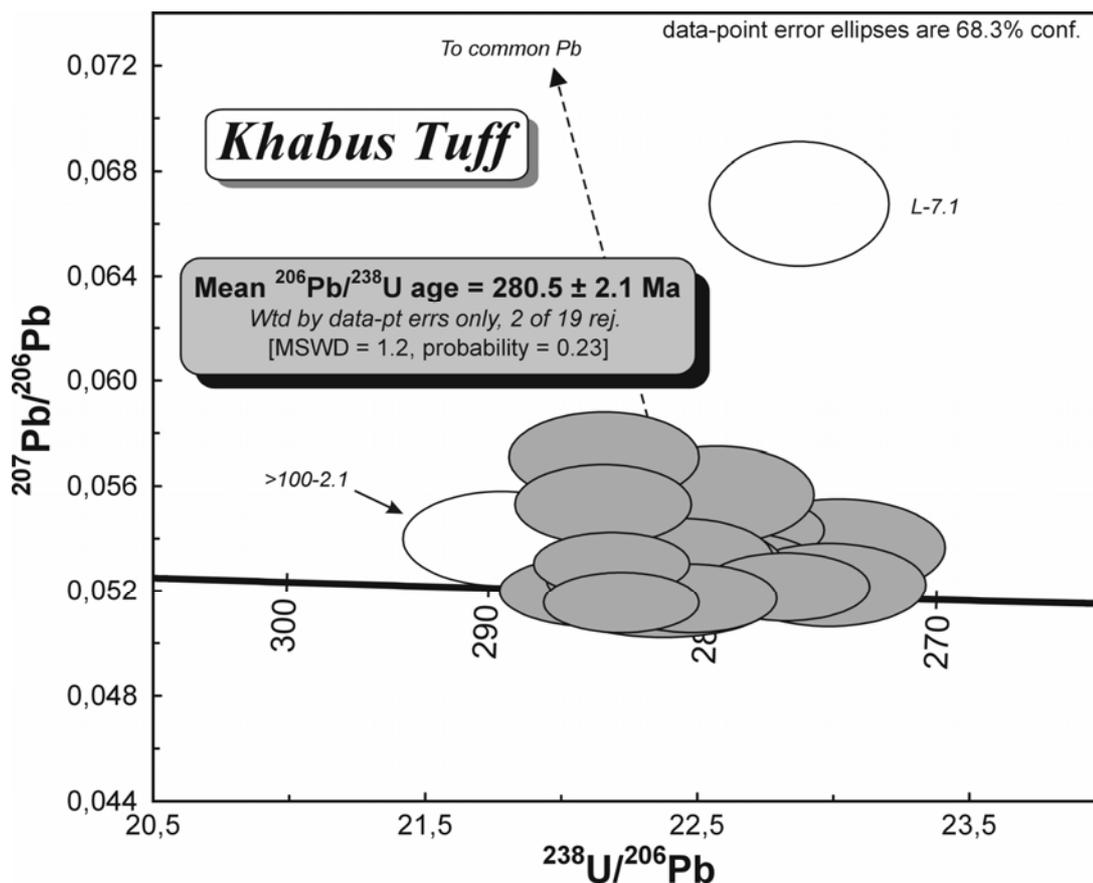
Fig. 5.11: U-Pb concordia plot of all SHRIMP data for zircons from the Khabus Tuff (sample KHA-1a). The data are plotted uncorrected for common Pb.

Sample UFO-43 of the Ufo Valleys Tuffs: middle part of the Collingham Formation

The zircons from this tuff are clear and light pink and generally euhedral with squat, almost equidimensional form (Fig. 5.12). A few more elongate or tabular crystals are also present and might be exotic. One rounded grain with obvious percussion marks was observed, indicating the presence of an inherited (detrital) component. Cathodoluminescence imaging shows an apparently uniform population characterised by concentric oscillatory zoning with brighter CL-zones towards the margins. Some grains have inherited cores.

Twenty analyses were performed on different grains (data listed in the Appendix Page XIII), which show some variability in U and Th contents (depending on where the spot was sited) but relatively uniform Th/U chemistry. The data are plotted on a Tera-Wasserburg plot (Fig. 5.13) as measured ratios. Fifteen of the analyses plot as a group with minimal or no common Pb, giving a weighted mean $^{206}Pb/^{238}U$ age of 277.2 ± 1.4 Ma (MSWD = 0.77; probability-of-fit = 0.70). The five analyses excluded from this group appear to have either lost Pb (giving apparently younger $^{206}Pb/^{238}U$ ages) or to be slightly too old. The latter spots might have been sited in inherited grains or overlapped onto older cores.
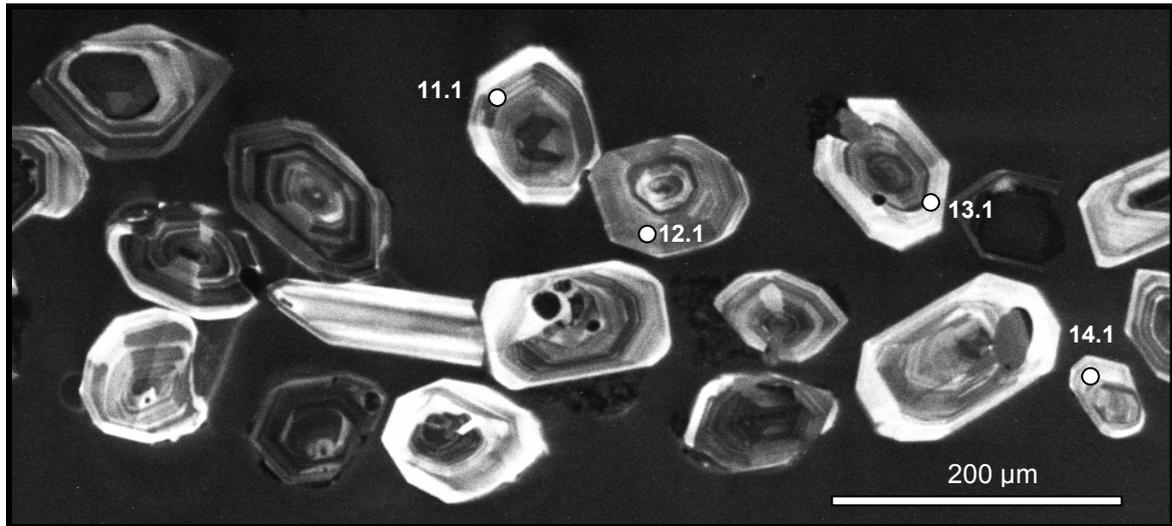
Fig. 5.12: Cathodoluminescence image of magmatic zircons from the Ufo Valleys Tuff (sample UFO-43). Squat to equidimensional forms prevail, some inherited cores may be present. Analysed grain spots are indicated.
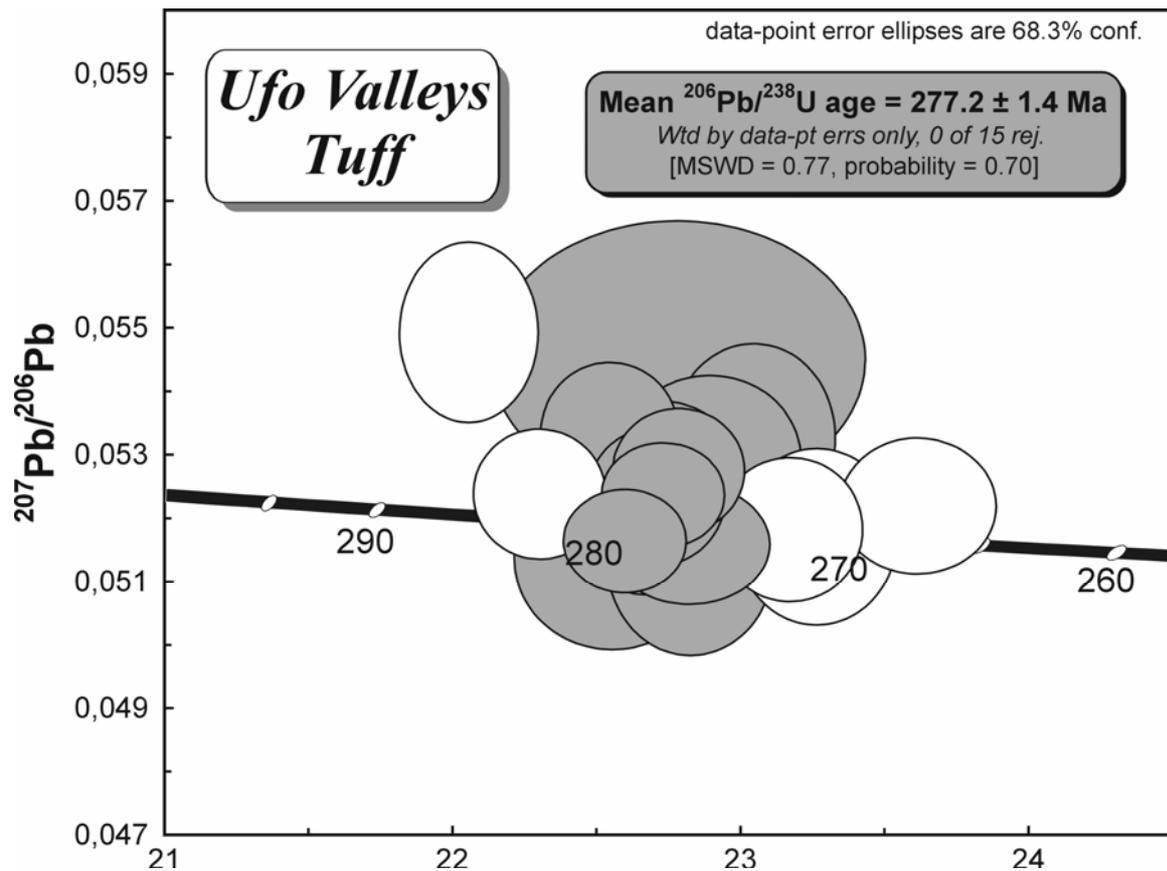
Fig. 5.13: Tera-Wasserburg U-Pb concordia plot of all SHRIMP data for zircons from the Ufo Valleys Tuff (sample Ufo-43), plotted uncorrected for common Pb. The white error ellipses represent those analyses that were excluded from the age calculation.

5.4 Summary, discussion and outlook

Fig. 5.14 shows a compilation of the new SHRIMP data of this study and the earlier SHRIMP data for tuff layers within the Dwyka, Ecca and Beaufort Groups in Namibia and South Africa. For the Dwyka Group SHRIMP ages from about 302 to 297 Ma have been recorded for deglaciation sequences DS II and III. The age of the Dwyka-Ecca boundary is now fairly well constrained by several SHRIMP ages clustering around 290 Ma (Fig. 5.14). There is a gap of age data between 297 and 290 Ma, which comprises mainly the time interval during deposition of the last deglaciation sequence (DS IV) of the Dwyka Group. Tuff layers within this stratigraphic interval have not been recorded yet. Also missing are radiometric age data for the basal part of the Dwyka Group (DS I), which is in Namibia not very well-developed and/or incompletely preserved. The available age data have been used to obtain improved estimates on the duration of Dwyka deglaciation sequences (Visser, 1997b; Bangert, 2000). Although the duration of individual cycles may vary somewhat, for DS II to IV they seem to be within the same order of magnitude. By extrapolation of the data it can be estimated that Dwyka deposition began at around 310 Ma and lasted approximately until 290 Ma resulting in a total duration of about 20 Ma for the Dwyka Group and an average duration of about 5 Ma for each deglaciation cycle. Since these data originate from tuff layers in southern Namibia and southern South Africa, it seems likely that final deglaciation was relatively synchronous throughout a large part of southwestern Africa. However, Visser (1982, 1996) suggested that the top of the Dwyka Group becomes somewhat younger towards the eastern part of the South African Karoo Basin due to small remaining ice caps in upland areas.

The single zircon U-Pb Shrimp age data for tuff layers from the basal part of the Prince Albert Formation in southern Namibia and South Africa (~290 Ma and slightly younger) are in marked conflict with the U-Pb age of a tonstein from the upper part of Rio Bonito Formation in Brazil (~267 Ma; Matos et al., 2001) and age estimates derived from palynological studies on the coal-bearing interval (Cazzulo-Klepzig et al., 2003). Litho-, bio- and sequence-strati-graphic considerations indicate that the Rio Bonito Formation is a correlative of the lower half of the Prince Albert Formation (Stollhofen, 1999; Holzförster et al., 2000; and this study) and therefore should have approximately an age between 290 and 285 Ma. So far it can only be speculated that the origin of the large age discrepancy lies within the applied dating methods. In contrast to the single zircon SHRIMP measurements for the Namibian and South African tuffs, the Brazilian tuff was dated by conventional ID-TIMS of several zircon fractions (four fractions comprising a total of about 200 zircon grains). With this procedure it might be quite difficult to control inheritance and Pb-loss phenomena commonly encountered in zircon dating of pyroclastic rocks. It is therefore strongly suggested to carry out single zircon age datings of the Rio Bonito tonsteins and overlying tuff layers (e.g. bentonites in the Whitehill-equivalent Irati Formation: Coutinho et al., 1991; Maynard et al., 1996).

Fig. 5.14: Compilation of available radiometric age data from tuff layers of the lower part of the Karoo Supergroup in Namibia and South Africa. Data without reference are the result of this study. Chronostratigraphic units after Gradstein et al. (2005).

The age data from tuffs of the uppermost Prince Albert Formation (Uhabis River Tuff) and the middle part of the Whitehill Formation (Khabus-Panorama-Eisenstein Tuffs) are almost identical and clearly show the limits of SHRIMP dating zircons from tuff layers. In this case the temporal resolution is not high enough to demonstrate the age difference between the two tuff horizons. Nevertheless, these data are very important inasmuch as they give a good age constraint for the boundary between the Prince Albert and the Whitehill Formation, representing a time when environmental conditions changed considerably within the inland sea of the Karoo-Paraná Basin area. These new data show that the widespread deposition of black shales and the first occurrence of a highly endemic fauna took place at around 280 Ma. This represents the time when connection to the Panthalassan Ocean was largely cut off leading to restricted circulation and anoxic conditions at the sea bottom. This time is also marked by a distinct positive excursion in the $\delta^{13}C_{org}$ record, reaching maximum values of up to -18‰ in the Whitehill Formation and equivalents, whereas under- and overlying deposits of the Dwyka and Ecca Groups are characterized by maximum values in the range of -24 to -20‰ (Faure & Cole, 1999; de Wit & Anderson, 2003; Scheffler et al., 2003). During this time the so-called Mesosaurus Inland Sea reached its maximum extent and the Whitehill Formation marks the turning point from a large-scale (2nd order) transgressive episode (Dwyka Group to Whitehill Formation) to a large-scale regressive episode (Whitehill Formation to the middle part of the Beaufort Group).

The enormous abundance and density of tuff layers as well as other sedimentological characteristics within the former basal part of the Aussenkjer Formation in southern Namibia strongly suggests equivalence with the South African Collingham Formation. Consequently, the supposed pinch-out of the South African Collingham Formation towards the northern and northeastern part of the South African Karoo Basin (Viljoen, 1992a, 1994), and therefore also towards the Aussenkjer-Noordoewer Karoo outcrop area in southern Namibia, appears to be largely a matter of poor outcrop conditions in the NW Cape Region. The dated tuff layer of the Collingham Formation in southern Namibia, which originates approximately from the middle part of the formation, yielded an age of about 277 Ma. This contrasts with the earlier radiometric ages of about 262 Ma (Viljoen, 1995) and about 270 Ma (pers. comm. de Wit, 1998; cited in Turner, 1999) for tuff samples derived from the South African part of the Collingham Formation. These ages, however, are not considered as very reliable because during these earlier SHRIMP datings old, inhomogenous standards were used (pers. comm. Armstrong, 2003). The probability or correctness of the 277 Ma age for the Collingham tuff layer can be tested by calculating durations of depositional sequences (3rd order trans-gressive-regressive cycles, or more correctly, progradational-retrogradational cycles) within the Ecca Group. The dated Collingham tuff layer lies in the upper third or fourth of deposi-tional sequence IV of the Ecca Group in southern Namibia (Fig. 5.15). Including all age data

errors (samples OG-9 and UFO-43) the resulting cycle duration lies between 2.8 and 4.5 Ma. Since for the top of the Ecca Group an age of around 260 Ma can be expected (Bowring (1998; cited in Stollhofen, 1999), the whole Ecca Group should span a time interval of about 30 Ma. As eight to ten depositional sequences can be determined for the Ecca Group in southern Namibia, each cycle should have lasted approximately 3-3.75 Ma. Based on this cycle duration the age of the top of the Collingham Formation can be calculated to be between 278 and 275 Ma, which is in good accordance with the 277 Ma age of tuff sample UFO-43 from the Namibian part of the Collingham Formation. Comparable cycle durations have been recorded

Fig. 5.15: Depositional sequences of the lower part of the Ecca Group in southern Namibia and U-Pb zircon SHRIMP ages from tuff layers within this stratigraphic interval.

by Catuneanu & Bowker (2001) and Catuneanu & Elango (2001) for the basal, entirely continental formations of the Beaufort Group (5 Ma for the Koonap-Middleton succession and 4 Ma for the overlying Balfour Formation). Since these cycles are interpreted by these authors to be mainly tectonically controlled (Cape Orogenesis), a tectonic component should also be considered for the control mechanisms of the Ecca Group cycles.

So far no radiometric age data for the middle and upper part of the Ecca Group (post-Collingham to Waterford Formation) are available, but the occurrence of tuff layers within this stratigraphic interval is well known for the South African part of the Karoo Basin (Viljoen, 1992b, 1995; Viljoen & Wickens, 1992; Knütter, 1994; Veevers et al., 1994; Wickens, 1996; Johnson et al., 2001). Therefore, it is very desirable that in future projects these tuff layers will be resampled and dated. A complicating factor concerning the Ecca-Beaufort boundary is that palaeontological finds indicate a diachronous contact. Vertebrate fossils show that the outcropping part of the Ecca-Beaufort boundary is oldest in the southwestern part of the

South African Karoo Basin and is younging towards the north-east, in direction of the basin centre (Rubidge, 1995; Rubidge et al., 2000; Hancox & Rubidge, 2001). This has to be kept in mind, since the Ecca-Beaufort boundary represents the gradual retreat of the Ecca Inland Sea. Consequently, the best approach to determine the Ecca-Beaufort boundary, in areas where the contact is conformable, is to map the shoreline deposits, which separate entirely subaquatically deposited inland sea sediments (offshore to upper shoreface) from continental fluvio-lacustrine deposits. Therefore, the basal terrestrial Beaufort deposits will be older in the more marginal parts of the inland sea and younger in the more central-distal parts. This also explains the relatively old age (~265 Ma) of a tuff layer from the Beaufort-equivalent Gai-As Formation in NW-Namibia because this area represents a region at the eastern margin of the Paraná Basin (Porada et al., 1996). In addition, the Ecca-Beaufort contact is marked in this region by a pronounced hiatus (Holzförster et al., 2000; Stollhofen et al., 2000b).

According to the currently available age data the inland sea (ice-covered and ice-free) which covered large parts of southwestern Gondwana during the Late Palaeozoic had a life-span of about 40-50 Ma (310/305 to 265/260 Ma), of which the first 20-25 Ma showed an at least temporary marine influence, whereas in the remaining 20-25 Ma mainly brackish to freshwater but also temporary evaporitic (during Whitehill-Irati time) conditions prevailed.

The above mentioned numerical age estimates, derived from the radiometric ages of dated tuff layers, can also be used to errect an updated chronostratigraphic chart for the Dwyka and Ecca Groups. In this study an excessive review of earlier chronostratigraphic age estimates is largely avoided due to the fact that valid chronostratigraphic units and their supposed numerical ages have changed for the Carboniferous-Permian period frequently. Since 1980 no less than ten time scales were suggested and applied for the Late Palaeozoic (Fig. 5.16) and therefore the individual chronostratigraphic age estimates within the large number of articles published on the Karoo are hardly comparable to each other. Often only the publication year of an article gives a hint on the time scale, which might have been used to assign chronostratigraphic terms to certain stratigraphic intervals. Major changes include the replacement of the Namurian to Stephanian with the Serpukhovian to Gzhelian age stages in the Upper Carboniferous and in a similar way the Upper Permian terminology was largely revised. Also the numerical age estimates as well as the duration of individual chrono-stratigraphic units have changed considerably with time. For example, the Carboniferous-Permian boundary shifted within an age interval of almost 10 Ma, the Artinskian-Kungurian boundary even up to 15 Ma. In this study the Geologic Time Scale (GTS) 2004 of Gradstein et al. (2005) was used to assign chronostratigraphic units to certain stratigraphic intervals based on the radiometric ages of tuff layers within the succession (see Fig. 5.14). Fig. 5.16 can be used to compare this newest time scale with earlier ones. Based on this latest available time scale (GTS 2004) deposition of the Dwyka Group began probably in the

Moscovian, corresponding to the Middle Westphalian, and lasted approximately until the Middle Sakmarian. The Whitehill Formation, which can be correlated with the Huab Formation in NW-Namibia (Holzförster et al., 2000), the Irati Formation in Brazil (Oelofsen, 1987) and the Black Rock Member of the Falkland Islands (Trewin et al., 2002), has, according to the GTS 2004, a Middle Artinskian age. Since all these formations are considered to represent a transcontinental isochronous unit (Oelofsen, 1987), the Middle Artinskian age, derived from radiometric dating in Namibia (~280 Ma), should be also transferable to the Paraná Basin area. However, the ~280 Ma age transfered from the Namibian Whitehill Formation to the Brazilian Irati Formation conflicts again with the ~267 Ma age of the stratigraphically lower Rio Bonito tonstein (see above). Although Faure & Cole (1999) pointed out that the Whitehill-Huab-Irati-Black Rock units may not necessarily be strictly isochronous, it seems very unlikely that the same endemic vertebrate (*Mesosaurus*) and arthropod (*Notocaris*) fauna appears in southern Africa 15-20 Ma earlier than in South America, especially under the aspect that the mesosaurids are believed to have evolved in the northern part of the Paraná Basin (Oelofsen, 1987). Most age estimates for the Whitehill and the Irati Formation are mainly based on palynomorph studies. However, no consensus has been reached and both Early and Late Permian ages have been suggested for the Whitehill Formation. Early Permian ages were promoted by McLachlan & Anderson (1973), Anderson (1977), Anderson (1981) (Upper Artinskian), and Oelofsen & Araújo (1987) (Late Sakmarian), whereas Late Permian ages were promoted by Visser (1990, 1992b) (Late Kungurian-Early Ufimian) and MacRae (1992) (Late Kazanian). Also for the partly Whitehill-equivalent Vryheid Formation Early Permian (Millsteed, 1994) and Late Permian ages (Kovács-Endrödy, 1991) were suggested. This uncertainty in the age of the Whitehill Formation (and other stratigraphic units or intervals) is for example reflected in two publications by O. Catuneanu. In Catuneanu et al. (1998) an Upper Kungurian age (~260 Ma) is shown for the Whitehill Formation, whereas in Catuneanu (2004b) an Upper Sakmarian age (~270 Ma) is suggested. Age estimates for the Irati Formation in Brazil, which are also mainly based on palynological studies, clearly favour a Late Permian age (Kungurian: Holz (2003); Ufimian: Holz (1999) and Kalkreuth et al. (1999); Kazanian: Milani & Filho (2000) and de Castro (1994); Tatarian: Maynard et al. (1996) and França et al. (1995); Wordian: Cazzulo-Klepzig et al. (2002)). As a way out of these problematic discrepancies in the supposed age estimates again single zircon SHRIMP datings of the South American Irati bentonites as well as under and overlying tuff layers in future projects are highly recommended. As an outcome of such a study not only the varying age estimates could be resolved but also the individual palynomorh zones and their suggested chronostratigraphic ages could be newly calibrated with radiometric age data derived from the regions for which they have been applied or/and errected.
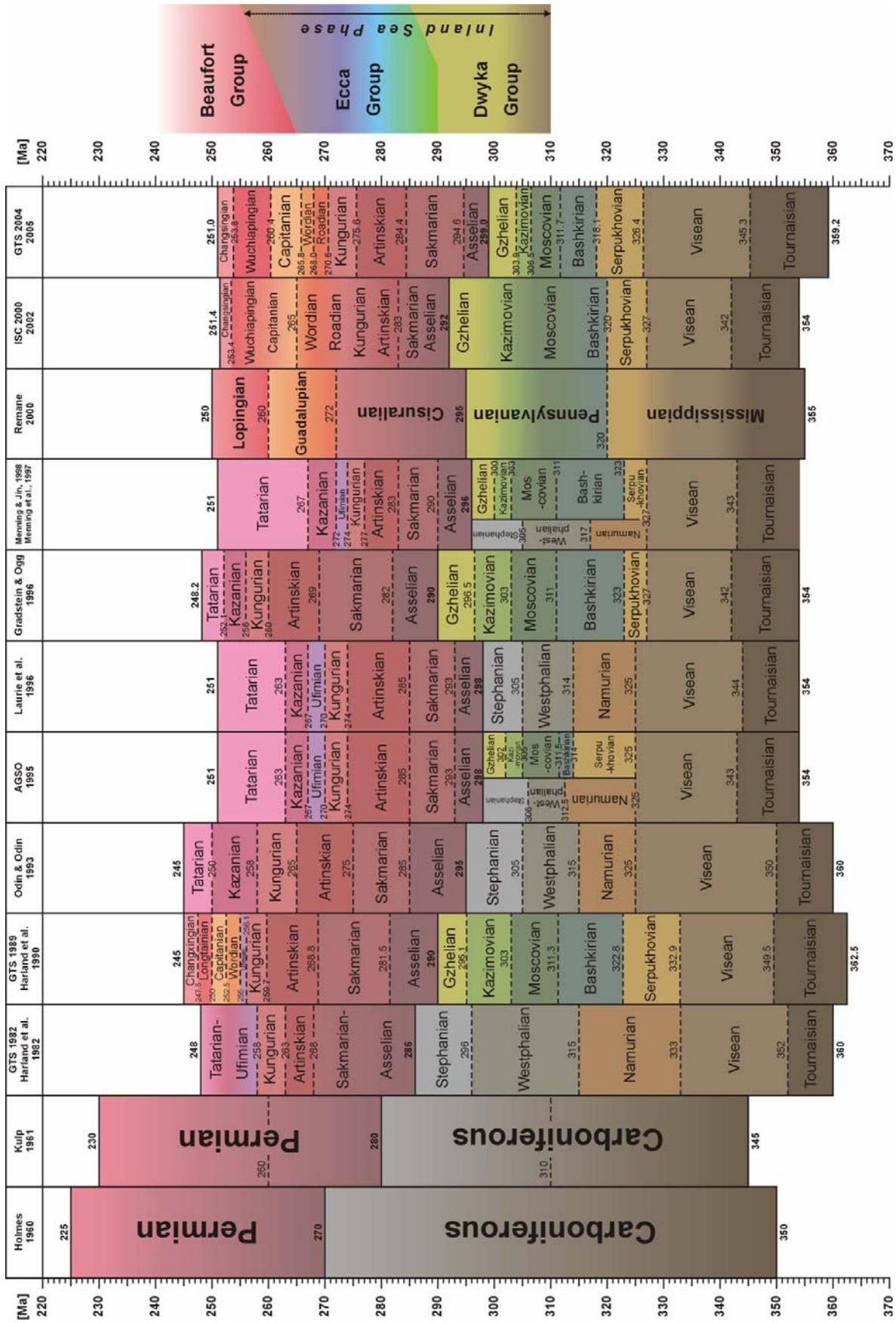
Fig. 5.16: Compilation of various time scales and (chrono-) stratigraphic charts published within the past 25 years. All data are sourced from the internet-based CHRONOS system portal (see Chapter 7 References for URL), except data from Menning et al. (1997) and Menning & Jin (1998).

Concerning palynomorph studies it is interesting to see that both in the Karoo Basin and in the Sydney-Bowen Basin (eastern Australia) palynology implies younger ages for the Late Palaeozoic glacial and post-glacial successions than U-Pb SHRIMP data do (see Stollhofen (1999) and Bangert (2000) as well as Roberts et al. (1996) for compilative age overviews).

Further single zircon SHRIMP datings of tuff layers could also improve, verify or deny other stratigraphic correlations and contribute to the question of syn- or diachroniety of correlated stratigraphic intervals.

Firstly, one future tuff dating project could shed some more light on the syn- or diachroneity of the transition from glacial to post-glacial deposional environments. In southern Africa this represents the Dwyka-Ecca boundary. However, so far no tuff layers have been reported for the glacial stratigraphic interval in the Paraná Basin and adjacent areas (Itararé Group), the Falkland Islands (Fitzroy Tillite/Lafonian Diamictite) and the Antarctic Gondwanan basins (Whiteout Conglomerate), although they surround the southern African Karoo basins, in which tuff layers in glacigenic deposits are not uncommon (S-Namibia, S-Cape Province, Natal). Since the preservation of volcanic ash as thin tuff layers requires low energy depositional environments, the search for new tuff layers should concentrate on the argillaceous parts of glacially influenced deposits. This largely excludes areas and intervals composed of coarse-grained terrestrial tillites and proximal, deltaic or turbiditic diamictites, but dropstone-bearing shales are known from almost all the above mentioned areas. Also from the directly subsequent post-glacial part tuff reportings are rather sparse, again despite the fact that they are known from Namibia and South Africa. An exception forms the Antarctic Ellsworth Mountains, where tuffs and abundant volcanic detritus begin to appear at the base of the post-glacial Polarstar Formation (Collinsen et al., 1992). Therefore, the post-glacial, fine-grained sediments, which are also known from the surrounding areas (Paraná, Falkland Islands, Antarctica), should be a promising target in the search for basal post-glacial ash-fall tuff layers.

Secondly, another tuff dating project could help to understand the puzzling and complex stratigraphic relationships between the depositional sequence of the Ecca Group in the western, basinal part and the Ecca Group in the eastern, marginal part of the South African Karoo Basin. Whereas in the western part the greater portion of the Ecca Group is characterized by hemipelagic, argillaceous (offshore muds) and turbiditic, arenaceous (deepwater fans) deposits, the eastern part is dominated by shallower water(?), argillaceous and fluvio-deltaic, arenaceous and coal-bearing successions. 'Traditionally', the carbonaceous Whitehill Formation is correlated with the coal-bearing Vryheid Formation, or at least with its upper, glauconite-bearing part (van Eeden, 1973; Cole & McLachlan, 1991, 1994) (Fig. 5.17 left diagram).

Fig. 5.17: Two alternative and conflicting correlations of the sedimentary formations of the Ecca Group in the western (first three columns) and the eastern-northeastern parts (grey-shaded fourth column) of Southern African Karoo basins. Black stars indicate highly tuffaceous stratigraphic intervals. In the left diagram the tuffaceous Collingham Formation is correlated with the tuff-bearing basal part of the Volksrust Formation in Natal and the kaolinitic carbotonstein-rich basal part of the Grootegeluk Formation in the Waterberg Coalfield. In the right diagram the correlation of the Vryheid Formation with the Ripon Formation is based on the concept of reciprocal stratigraphies. The stratigraphic units of the Ellisras Basin (Waterberg Coalfield) (Swartrand and Grootegeluk Formation) are after Faure et al. (1996a/b).

This correlation was corroborated by Viljoen (1994), who correlated the tuff-rich Collingham Formation with the tuff-rich basal part of the Volksrust Formation in Natal and the tuffaceous, kaolinitic carbotonstein-rich basal part of the Grootegeluk Formation in the Waterberg Coalfield (Fig. 5.17 left diagram). These earlier correlations were recently challanged by Catuneanu et al. (2002), who correlated the Ripon Formation with the Vryheid Formation, according to the concept of reciprocal stratigraphies in foreland basins (Fig. 5.17 right diagram).

For a potential future dating project, which could clarify the stratigraphic relationships between the Ecca Group formations in the western and the eastern parts of the South African Karoo Basin, it is suggested to date at least two more tuffs from the Whitehill and Collingham Formations, preferentially from South African localities, to verify and substantiate the Namibian age data from this stratigraphic interval. These data could then be compared with at least one dating of a tuff layer originating from the basal part of the Volksrust Formation in Natal and one dating of a sample from the basal, kaolinitic carbotonstein zone of the Grootegeluk Formation in the Waterberg Coalfield (Ellisras Basin). In such a study it would be also highly desireable to obtain a radiometric age for the Vryheid Formation. So far, no tuff layers have been described from this formation, except the chert layers of possibe tuffaceous origin recorded by McLachlan & Jonker (1990) from the basal part of Karoo Supergroup deposits in the Virginia area, which were assigned to the Vryheid Formation. However, an intensive search for a tonstein layer in the coal-bearing intervals of the Vryheid Formation might be rewarding. Furthermore, the montmorillonite beds described by Schmidt (1976) from the Pietermaritzburg Formation in the northern Orange Free State deserve further investigation in such a project.

Thirdly, extensive dating around the Ecca-Beaufort contact should lead to an enhanced understanding of the diachroniety of this boundary and the terminal phase of the gradually retreating Ecca Sea as mentioned above. In this context it would be highly desireable to obtain also a radiometric age of the lowermost tuff zone of the Gai-As Formation in NW-Namibia (see also Chapter 3.4.3 Tuff beds in the Beaufort Group), because the reddish lacustrine sediments, in which these tuff layers are intercalated, may have been deposited contemporaneously with upper Ecca inland sea sediments in southern Namibia and western South Africa. Tuff age dates within the Beaufort Group could also provide a better view about the temporal evolution of land vertebrates in the Upper Permian of Southern Africa.

In addition, dating of Beaufort Group tuff layers could also improve the understanding of the depositional responses to the tectonic deformation phases in the Cape Fold Belt, which were dated by Hälbich et al. (1983). $^{40}Ar/^{39}Ar$ step heating analysis of cleaved pelites from the Cape Fold Belt indicated four main episodes of intense folding and thrusting (S1-S4). Hälbich (1983) and Cole (1992) correlated the individual tectonic phases (paroxysms) with pulses of

high-energy sedimentation in the Karoo Basin of South Africa. Hälbich (1983) suggested that the first deformation phase S1 (Swartberg folding), dated at 277 ± 5 Ma, took place during deposition of the Ecca Group, whereas Cole (1992) believed that this deformation happened earlier, whilst the Dwyka Group was still deposited. Cole (1992) suggested that the second deformation phase S2 (Outeniqua folding), dated at 259 ± 5 Ma, triggered the deposition of middle Ecca sandy submarine fans (Collingham, Vischkuil, Laingsburg, Ripon, and Skoor-steenberg Formations), whereas Hälbich (1983) associated this phase with the deposition of the lower Beaufort Group. The new radiometric ages of this study now confirm that S1 (~277 Ma) must have occurred during deposition of the Ecca Group and strengthens Hälbich's interpretation (Fig. 5.18). This deformation phase in the Cape Fold Belt was apparently connected with the deposition of the deep sea fans in the southern Karoo Basin (Tanqua, Laingsburg and Southern subbasins). So far the sedimentological response to S2 appears to be not fully understood, however, it might be related to the unconformity at the base of the Balfour Formation in the lower Beaufort Group (cf. Catuneanu & Elango, 2001) (Fig. 5.18). Therefore, the dating of tuff layers and so-called 'chert' beds (Martini, 1974; Keyser & Zawada, 1988; Knütter, 1994; Viljoen, 1995; Karpeta, 1996) in the lower Beaufort Group could shed some more light onto this issue. Both Hälbich (1983) and Cole (1992) as well as Turner (1999) correlated the later deformation events S3 and S4, dated at 246 ± 2 and 229 ± 5 Ma, with pulses of sedimentation of coarse-grained, braided-fluvial sands in the middle Beaufort Group (Katberg Formation) and several pulses of prograding fluvial braidplain sands in the lower Stormberg Group (Molteno Formation) (Fig. 5.18). This correlation could be confirmed by dating of possible laumontitic tuff layers in the upper Beaufort Group (Fuller, 1970), by dating of granitc rocks and hornblende-bearing intrusives, which occur as pebbles in the Katberg Formation (Elliot & Johnson, 1972; Elliot & Watts, 1974), and by dating the tonsteins and bentonites of coal-bearing succession in the basal Molteno Formation (Turner, 1971; Heinemann & Bühmann, 1987).

Interestingly, López-Gamundí et al. (1994) registered also four metamorphic events in the Sierras Australes, which represent the western continuation of the Cape Fold Belt in central eastern Argentina. The deformation phases in the Sierras Australes are dated at: (1) ~278 Ma, (2) ~262 Ma, (3) ~250 Ma, and (4) ~230 Ma, and thus are almost identical with the afore-mentioned deformationen phases in the Cape Fold Belt.
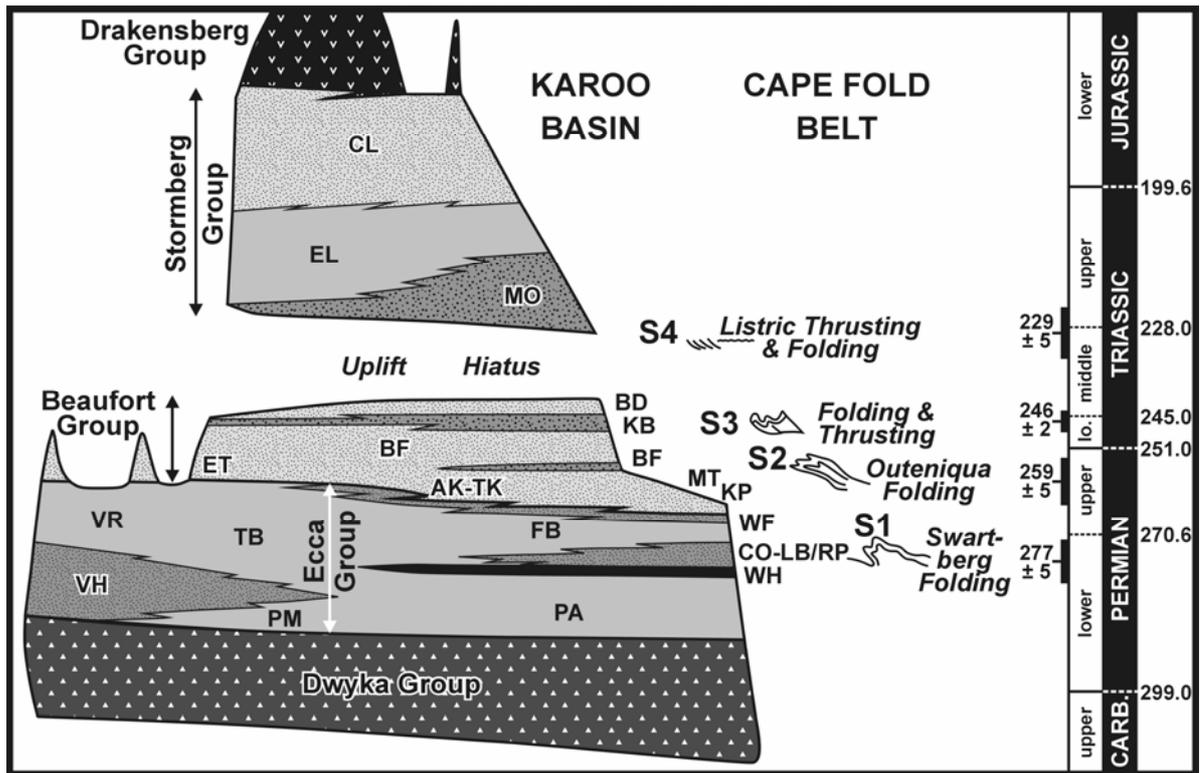
Fig. 3.18: Schematic illustration of the distribution of lithostratigraphic units in the Main Karoo Basin of South Africa and their relationship to tectonic deformation phases of the Cape Fold Belt. This graphic is an updated and modified version of the original one of Cole (1992), which was subsequently modified by Veevers et al. (1994) and Stollhofen (1999). The ages of the deformation phases are taken from Hälbich (1983) and the time scale (GTS 2004) is after Gradstein et al. (2005). Abbreviations for lithostratigraphic formations: PA – Prince Albert, PM – Pietermaritzburg, VH – Vryheid, WH – Whitehill, CO – Collingham, LB – Laingsburg, RP – Ripon, FB – Fort Brown, TB – Tierberg, VR – Volksrust, WF – Waterford, KP – Koonap, MT – Middleton, AK – Abrahamskraal, TK – Teekloof, ET – Estcourt, BF – Balfour, KB – Katberg, BD – Burgersdorp, MO – Molteno, EL – Elliot, CL – Clarens.

Chapter 6 – Provenance of Late Carboniferous-Early Permian tuff layers from SW-Gondwana

The provenance of tuff layers within Late Palaeozoic strata of the Karoo Supergroup in Namibia and South Africa as well as their equivalents and possible equivalents in Antarctica, the Falkland/Malvinas Islands, and southern South America has already been intensively discussed by previous researchers. Most authors favoured a distal source area (or areas) within a Late Palaeozoic magmatic arc that fringed the southern Panthalassan margin of Gondwana (Elliot & Watts, 1974; Martini, 1974; Johnson, 1991; Visser, 1992a; Viljoen, 1992a, 1994, 1995; Veevers et al., 1994; Bangert et al., 1999; Bangert, 2000), however, also more proximal (within plate) sources were brought into discussion (Keyser & Zawada, 1988; McLachlan & Jonker, 1990; Bangert, 2000; Stollhofen et al., 2000a). In the following paragraph discussion will be focussed on the studied tuff layers in the Late Carboniferous-Early Permian Dwyka and lower Ecca Groups of southern Namibia as well as on tuff layers from age-equivalent strata in South Africa and neighbouring areas. The provenance of Upper Ecca and Beaufort Group tuffs, which have not been studied in detail here (except the tuff layer from the Gai-As Formation), will not be discussed intensively.

In order to resolve the question about possible source areas a number of important indicative data can be used. These include frequency, thickness, grain size, spatial distribution, mineralogical and geochemical composition, as well as the age of the tuffs. The time frame, in which the tuffs from the Dwyka and lower Ecca Groups have been laid down, is now very well constrained due to a number of available U-Pb SHRIMP ages for the tuffs in question. Their deposition comprises approximately the time interval from about 305 Ma to about 275 Ma, i.e. latest Carboniferous to Early Permian. Petrography of the tuffs shows that the parental magma contained phenocrysts of quartz, feldspar (mainly plagioclase) and biotite as well as micro-phenocrysts of zircon and apatite pointing towards intermediate to acid magmas. Furthermore, also the trace element data indicate mainly calc-alkaline rhyodacitic to dacitic parental magmas, however, also show trends from such intermediate compositions towards rhyolitic and trachydacitic/andesitic but also to more basic and alkaline compositions. On the other hand, such trends could also have been caused by secondary processes and might not necessarily reflect the true original compositional range of source melts. Therefore, it is strongly suggested that in future projects melt inclusions in volcanic quartz, zircon and apatite should be investigated to improve the knowledge about the parental magma compositions. The REE data of the investigated tuffs yielded a relatively complex picture, but the majority of tuffs show a chondrite-normalized REE pattern, which is very characteristic for calc-alkaline, highly evolved felsic magmas (enriched LREE, negative

Eu anomaly, and fairly flat HREE abundances). Both trace and REE data seem to indicate that at least some of the Ganigobis Tuffs from the Dwyka Group of southern Namibia could be derived from more basic and less evolved magmas. Especially samples of one tuff layer (Ganigobis Tuff IVa) plot as a distinctly separate data group in the alkaline basalt field in different composition discrimination diagrams. Nevertheless, within discrimination diagrams after Pearce et al. (1984), indicating tectonic settings of granitic rocks, all studied tuffs plot as a single, elongate data cluster (except diagenetically phosphatized samples), which implies that all tuffs are derived from volcanoes positioned in a common tectonic setting. The majority of tuffs plot in the Nb vs Y diagram within the field of volcanic arc and syn-collision granites but there is also considerable overlap into the field for within plate granites. However, Tischendorf et al. (1995) already mentioned that their data base for volcanic arc granites also shows a considerable overlap into the within plate granite field and therefore it is supposed that the studied tuffs are most probably derived from a subduction-related volcanic arc environment. Also the samples of Ganigobis Tuff IVa with an apparent alkaline basalt trace element signature do not plot as an isolated group in the within plate granite field and their origin and significance remains rather enigmatic. In accordance with a volcanic arc environment is also that crystal fragments of quartz and partly also of feldspar show dominantly splinter- and thorn-shaped forms, which are indicative of highly explosive plinian or phreato-plinian volcanic eruptions. In summary, tuffs within the Dwyka and lower Ecca Groups were most probably derived from a subduction-related volcanic arc region but trace element data indicate that the tuffs could have originated from a variety of source magmas with different compositions, which is also supported by the variable Th-U mineral chemistry of juvenile zircons (SHRIMP data; see Fig. 4.10 & 4.11) and the presence of two different types of juvenile apatites (clear colour type and smokey-grey, colour-zoned type).

A magmatic arc, which was active in the Late Palaeozoic to Early Triassic, fringed the southern Panthalassan margin of Gondwana (largely equivalent to the so-called 'Samfrau Orogenic Zone' of du Toit, 1937) (Fig. 6.1). Although the picture concerning this Late Palaeozoic arc magmatism is highly complex and still not fully understood, it appears that two magmatic subcycles can be distinguished. The older subcycle, which includes the so-called Elqui Complex of the Chilean Frontal Cordillera (Mpodozis & Kay, 1992), is preserved as an incipient magmatic arc in the western region of southern South America and can be traced from northern Chile (Breitkreuz & Zeil, 1994) southward along the Andes on the Argentine-Chilean border to the Mendoza-Neuquén Province border area in central western Argentina (López-Gamundí et al., 1994) (Fig. 6.1). Immediately west of and parallel to this magmatic belt (and actually forming a part of it) lies also the Late Carboniferous-Early Permian calc-alkaline granitoid belt of Coastal Chile, which intruded accretionary prism

sediments (Fig. 6.1). Magmatic activity of this older subcycle probably lasted from the Early-Late Carboniferous to the late Early Permian (~330 to ~275 Ma). This magmatic episode is considered as a preliminary minor expression of the subsequent, very extensive arc volcanism of the younger subcycle. Magmatic rocks of the younger subcycle, which includes the Choiyoi Group magmatism and the Ingaguás Batholith Complex (Mpodozis & Kay, 1992), form a broad belt along and slightly shifted eastward parallel to the line of the older subcycle. Note that the Choiyoi Group can in certain regions in turn be subdivided into an andesitic-dacitic lower section and a dacitic-rhyolitic upper section (Llambías et al., 2003). At about 34°S the Late Palaeozoic magmatic arc apparently widens and swings southeastward (Fig. 6.1), deduced from the distribution of Choiyoi-equivalent volcanics in the northern Pata-gonian Massif. The younger cycle is considered to represents the climax of calc-alkaline arc volcanism and volcaniclastic sedimentation in southwestern South America during the Late Palaeozoic. Radiometric dates suggest the onset of this volcanism at about 275 Ma and that it lasted until the Late Permian to Early/Middle Triassic (until ~260 to ~230 Ma). In the Chilean Andes magmatic rocks of the older subcycle comprise calc-alkaline tonalites and granodiorites, whereas the younger magmatites represent mainly peraluminous granitoids and associated rhyolitic volcanics. Elsewhere in southern South America the younger sub-cycle is characterized by hypersilicic granites and consanguinous volcanics, showing evidence of increasing crustal melting with time. Coupled with this extensive crustal melting, leading to a progressive enrichment of crustal components in the melts, is also an eastward movement or expansion of the magmatic arc with time (see López-Gamundí et al. (1994) for a comprehensive overview). So far, the geodynamic and teconic processes, which caused intensifying and expansion of volcanic activity during transition from the older to the younger subcycle, are still poorly understood. Especially the subduction-related accretion processes at the southwestern margin of Gondwana (South America) in the Carboniferous-Permian period are not fully understood yet. Possible models include subduction and subsequent accretion of the Chilenia (and Equis?) Terrane to the Cuyania/Precordillera Terrane in the Late Carboniferous to Early Permian (Mpodozis & Kay, 1992; Ramos, 1994). This phase was subsequently followed by cessation of subduction and collapse of the subducted slab, the development of strike-slip tectonics subparallel to the continental margin, extension of previously thickened and weakened lithosphere, leading to decompressional mantle melting, underplating of basaltic melts, extensive crustal melting and generation of the volumetrically important Choiyoi magmatism (Mpodozis & Kay, 1992; Franzese & Spalletti, 2001). The origin and history of Patagonia (exotic terrane or par-autochthoneous crustal block?) in this context is also not fully understood (cf. Ramos, 1994; López-Gamundí & Breitkreuz, 1997).

Towards the east this Late Palaeozoic magmatic arc was probably continuos and can be connected with a Late Palaeozoic/Early Mesozoic subduction complex and an associated

magmatic arc stretching from the Antarctic Peninsula, Thurston Island and Marie Byrd Land to New Zealand and Eastern Australia (Smellie, 1981; Collinson et al, 1994). Although Veevers (2001) shows for the Late Carboniferous to Early Permian period a southeastern Panthalassan margin of Gondwana (Antarctica to Australia), which was affected by extension due to supposed nearby sea floor spreading, there is also sparse but widespread evidence for subduction-related calc-alkaline magmatism in the West-Antarctic region already in the Early/Late Carboniferous to Early Permian period. A banded gneiss from the Target Hill area of the Antarctic Peninsula indicates anatexis at around 330 Ma (Millar et al., 2002), for the calc-alkaline Morgan Inlet Orthogneiss a Rb-Sr isochron age of about 310 Ma was calculated, and dating of calc-alkaline grano-monzo-diorites and diorites from Marie Byrd Land yielded ages approximately between 320 and 275 Ma (Pankhurst et al., 1998; Mukasa & Dalziel, 2000). The younger ages are derived from the Kohler Range Intrusives (Fig. 6.1), which are interpreted to represent the source of the Permian volcanic detritus in the Ellsworth Mountains (e.g. in the Polarstar Formation; Collinson et al., 1992). From the late Early Permian onward the Late Palaeozoic magmatic arc can be followed further to the east up to eastern Australia, forming a large continuous magmatic arc along the entire southern Panthalassan margin of Gondwana.

The aforementioned data indicate that the tuffs within the Dwyka and lower Ecca Groups of southern Namibia and South Africa might be related to the arc volcanism of the older magmatic subcycle (~320-275 Ma) and not to the younger Choiyoi magmatism (<275 Ma). Aeolian deposits in the Paganzo Basin, lying directly east of the adjacent magmatic arc, indicate dominant wind directions from west to east for the SW-Gondwanan region in the Late Palaeozoic (Limarino & Spalletti, 1986). Using present day geographic directions, prevailing westerly to southwesterly winds for this region were also indicated by Kutzbach (1994). These wind directions are also in accordance with predominantly N-S trending wave ripples in Upper Ecca sandstones in southern Namibia (Amibberg Formation; own measure-ments) and South Africa (Carnarvon (=Waterford) Formation; Rust et al., 1991). From this perspective it appears highly likely that volcanic ashes erupted from volcanoes within the Late Palaeozoic magmatic arc in southern South America could have been transported by winds towards easterly directions and deposited in the Paraná and Karoo basin areas. Viljoen (1992a) could demonstrate that the thickness and number of tuff layers within the Collingham Formation of South Africa decreases north- and eastwards, which is in accordance with own observations from southern Namibia. In southern Namibia the cumulative thickness of tuff layers represents only about 1% of the whole Collingham Formation thickness, whereas in the Western Cape Province of South Africa the tuff beds constitute between 5 and 30% of the Collingham Formation thickness. These observations

indicate a source area to the southwest, which is in turn again in accordance with an origin of the volcanic ash in southern South America. Favouring a source area in southern South America for the studied tuffs, however, means that the volcanic ashes must have been transported over a distance of about 1000-2000 kilometres. Considering the grain sizes of juvenile quartz and plagioclase crystals within the studied tuffs, which are mainly in the range of 50-150 µm, but can also reach lengths of up to 300 or 400 µm, and those of heavy minerals like zircon, which often reach sizes between 100 and 200 µm within the tuffs, some researchers dispute such a distal source area. Stollhofen et al. (2000a), for example, supposed that volcanic material within some of the Dwyka and Ecca tuffs could have been derived from a more proximal source area. As a possible source they suggested volcanic vents located along a northwesterly trending intracontinental rift zone extending from southwestern Africa through the Brazilian interior of South America (Stollhofen, 1999; Stollhofen et al., 2000b). So far, proximal in-situ volcanism, which possibly could be associated with this rifting, is only known from one locality in NW Namibia. In the Huab area a thin scoriaceous basalt lava flow is intercalated in sediments of the Lower Permian Verbrandeberg Formation (Horsthemke, 1992) (Fig. 6.1). A second site with possible intra-Ecca Group volcanism might be present in central Botswana from where sedimentary-volcanic breccias at the Kweneng-Boritse Formation contact have been reported (Meixner & Peart, 1983, 1984; Smith, 1984). Carboniferous and Permian K-Ar whole rock ages from dolerite intrusions (Erlank et al., 1984; F.M. Consultants Ltd., 1969; the latter cited in Rowsell & de Swart (1976) and in McLachlan & Jonker, 1990), which have been mentioned in this context, have to be considered as highly questionable. Erlank et al. (1984) discarded Late Palaeozoic ages for the Albin Ridge lavas, the Horingbaai dolerites and a dolerite sill from the Huab area in their publication. The anomalously high K-Ar ages have been considered as suggestive of the presence of excess radiogenic argon, what was confirmed by ^{40}Ar/^{39}Ar step-heating technique. However, Stollhofen et al. (2000a) also argued that possible sources of this rift zone would probably be buried in the Namibian to Cape offshore areas. Nevertheless, these authors also agreed 'that the bulk of the volcanogenic material contained in the Dwyka and Ecca Group sediments was provided by various distant, essentially dacitic sources, most probably associated with a magmatic arc situated south of Gondwana'. Apart from the large grain sizes transported in the ash clouds, also the high number of tuff layers in the Dwyka sediments of southern Namibia, contrasting markedly with the paucity of Dwyka tuff layers in neighbouring South Africa, implies at first sight a more local volcanic source. However, this could also be an effect of depositional conditions. The Ganigobis Tuffs are intercalated in very dropstone-poor shales indicating a more or less ice-free sea during this depositional period. This is also valid for the Dwyka deposits in the Aussenkjer-Noordoewer area in southernmost Namibia, which host the Zwartbas Tuffs. In

contrast, the Dwkya Group in the adjacent northern and western Cape areas of South Africa seems to be dominated by subaqueously deposited diamictites, which could reflect generally more proximal and higher energetic depositional environments preventing the preservation of continuous thin ash layers. The stronger diamictic character of the Dwyka deposits in South Africa, however, could also be the result of a much stronger ice-covered sea. In comparison to the Dwyka sediments of southern Namibia those of South Africa were laid down in higher (southerly) palaeo-latitudes and the Dwyka Sea may have been more intensively covered in this region by drifting ice plates largely preventing the deposition of volcanic ash on the sea-bottom directly after fall out. Such a model of supposed different ice cover could explain the contrasting number of intercalated tuff layers within Dwyka sediments of southern Namibia and South Africa and requires no local volcanic source for the Namibian Dwyka tuffs.

Largely based on grain size observations also McLachlan & Jonker (1990) favoured a proximal source for lower Ecca Group tuffs within the Prince Albert, Whitehill, Tierberg, and Vryheid Formations from localities in the central northern and northeastern part of the South African Main Karoo Basin. However, the grain size of supposed juvenile crystals and devitrified glass shards in these tuffs is generally quite comparable to the size of those in the Namibian tuffs (up to a few hundereds of micrometre but not exceeding 500 µm). Only one deformed bed, the interpretation of which is ambiguous as the authors state by themselves, contains feldspar crystals, which reach lengths of 700-1680 µm. They are interpreted as original phenocrysts, but the authors also discuss and do not rule out a secondary origin for these large crystals.

In summary it can be said that all tuff layers from the Dwyka and lower Ecca Groups are relatively fine-grained and contain juvenile macrocrysts, which are normally not larger than 500 µm, with the possible exception of the size of some biotite flakes. This textural characteristic concerning grain size is definitely changing towards younger tuff occurrences. Grain sizes of juvenile volcanogenic components in some tuffs intercalated in Upper Ecca and Beaufort Group sediments are indeed distinctly larger than those in the older ones. For example the Geelhoutboom Tuff within the Fort Brown Formation, exposed in the southern Cape Province and described by Lock & Johnson (1974), is composed of several bands consisting almost entirely of crystals of plagioclase (>90%) and quartz (<10%), with the crystal grain size around one millimetre. Furthermore, metre-thick, coarse-grained ash-flow tuffs have been described by Keyser & Zawada (1988) from the lowermost Beaufort Group in the northern part of the Orange Free State. These tuffs contain lapilli-sized (2-30 mm) lava and pumice clasts. In addition, for the Rietfontein-Wolwekop Tuffs from the lower Beaufort Group in the central southern Cape Province, described by Karpeta (1996), accretionary

lapilli up to 5 mm in diameter are reported. A proximal volcanic source supposed for these younger (Upper Permian) tuffs is not disputed here, although also for these tuffs no potential, proximal volcanic vents are known. However, for the older Dwyka and Ecca tuffs of southern Africa a distal volcanic source probably located in South America is strongly suggested here.

There is another indication, which seems to support rather a distal magmatic arc provenance than a proximal within plate volcanic source. Among the dozen SHRIMP-dated Late Palaeozoic tuff layers from Namibia and South Africa two contained also xenocrystic but mainly euhedral Ordovician magmatic zircons, which appeared optically non-conspicuous among the juvenile zircon populations of Carboniferous-Permian age. Within the zircon concentrate of tuff sample OG-9 of the Owl Gorge Tuffs (southern Namibia) one fragment of an euhedral zircon crystal yielded an age of about 480 Ma (Early Ordovician). The zircon concentrate of a tuff layer from the basal portion of the Prince Albert Formation, cropping out c. 13 km south of Laingsburg in the Western Cape Province of South Africa, contained even a larger number of Ordovician zircons. Among the nineteen analysed zircons eight yielded an Ordovician age and from seven spot analyses a weighted mean $^{206}Pb/^{238}U$ age of 464 ± 5 Ma was calculated (close to the Middle-Upper Ordovician boundary; Gradstein et al., 2005). One of these Ordovician zircons is shown in Bangert (2000) within a CL-image (Fig. 147; p. 189) and appears as a euhedral, non-fragmented, oscillatory-zoned crystal, which is virtually undistinguishable from the younger zircon population. It is suggested that these Ordovician zircons were collected from the wall rocks of a Permian volcanic vent during an explosive eruption and incorporated into the eruption column. Due to the magmatic appearance of the Ordovician zircons the Permian volcanic vent(s) must have penetrated Ordovician magmatic or pyroclastic rocks. The nearest possible source where Ordovician volcanogenic material can be found represents the Natal Group of KwazuluNatal in South Africa. There, sericitized volcanic glass shards occur in red-bed mudstones (Eshowe Formation) within the lower part of the Natal Group (Thomas et al., 1992; Marshall, 2002). According to the results of $^{40}Ar/^{39}Ar$ spectrum analysis of micas from these mudstones Thomas et al. (1992) suggested that this part of the Natal Group was deposited at ~490 Ma (Late Cambrian-Early Ordovician). The preservation of delicate shard shapes indicates deposition by ash-fall and therefore evidence volcanic activity contemporaneous with deposition of the Natal Group (Marshall & von Brunn, 1999, 2000; Winter & Kingsley, 2000). Consequently, the volcanic detritus within the Eshowe Formation should have the same age as the deposition of the mudstones. However, within the outcrop area of the Natal Group no Late Palaeozoic volcanic activity is known, which could have picked up volcanic detritus deposited with the mudstones of the Eshowe Formation. Therefore, the Ordovician magmatic zircons found within the two tuff layers of the Early Permian Prince Albert Formation as well as the volcanogenic material present in the

Eshowe Formation of supposed Early Orodovician age must originate from a more distal source area. For the Permian tuffs Late Palaeozoic explosive volcanism must have penetrated Early-Mid Ordovician intrusives or volcanogenic deposits.

Within the region of southwestern Gondwana principally two sites of Ordovician magmatism are known, namely Antarctica and southern South America. In Antarctica Cambrian to Early Ordovician magmatism is related to the late phases of the Ross Orogenesis. However, geochronological studies on magmatogenic rocks from East Antarctica have shown that the younger recorded intrusion ages are in the range of 505-480 Ma (Pankhurst et al., 1998; Stump et al., 2002; Wysoczanski et al., 2003) and thus they are largely too old to represent the source for the Middle/Upper Ordovician zircons (464 ± 5 Ma) within the aforementioned Early Permian tuff cropping out south of Laingsburg/RSA. So far, the only area in the Antarctic region from where Middle Ordovician zircons are known lies in the Antarctic Peninsula. Euhedral zircons extracted from granitoid clasts of the View Point conglomerate (Permo-Triassic?) (Fig. 6.1), NE Graham Land, yielded a weighted mean $^{206}Pb/^{238}U$ SHRIMP age of 463 ± 5 Ma (Millar et al., 2002), which is almost identical to the 464 ± 5 Ma age for the South African zircons. Together with zircons from an orthogneiss from the Campbell Ridges (Antarctic Peninsula) (Fig. 6.1), containing a prominent 460 Ma component, this indicates the presence of a Middle Ordovician detritus source within the peninsula area. However, so far no magmatic activity is known from the Antarctic Peninsula for the Late Carboniferous to Early Permian period as the radiometric ages compilation of Millar et al. (2002) shows a gap of recorded magmatic activity between ~330 and 270 Ma. Nevertheless, Late Carboniferous to Early Permian magmatic activity is known from elsewhere in the West-Antarctic region (see above) and potentially could have picked up Middle Ordovician magmatic zircons, which have been detected in granitoid clasts that indicate a nearby but yet undetected in-situ occurrence of Middle Ordovician magmatites.

In southwestern South America Late Cambrian to Middle Ordovician magmatism is well-known from the so-called Famatinian Magmatic Arc of the Sierras Pampeanas, the Puna and the Eastern Cordillera of Argentina (Fig. 6.1). The Famatinian Magmatic Arc formed due to subduction of oceanic crust and subsequent collision and amalgamation of the Precordillera Terrane, which is also known as the Cuyania Terrane, to the proto-margin of western Gondwana (Rapela, 2000; Ramos, 2004). The Famatinian magmatism is dominated by I- and S-type granitic intrusions but also volcanic and volcaniclastic successions crop out in the northwestern sector of the Sierra de Famatina and the Puna (Fanning et al., 2004). Furthermore, in the Argentine Precordillera, constituting the major part of the Precordillera or Cuyania Terrane, a number of K-bentonite layers (Fig. 6.1), age-equivalent to the Famatinian

magmatism further east, are intercalated in Lower to Middle Ordovician (Arenigian to Llanvirnian) marine sediments (Huff et al., 1998). Geochemical and isotope data of Fanning et al. (2004) demonstrated the similarity between K-bentonites from the Precordillera and rhyolitic rocks from the Famatinian Arc, indicating that the Famatinian arc volcanoes provided the ash for the K-bentonite layers. U-Pb zircon ages of Famatinian magmatism in the Sierras Pampeanas range from 499 ± 5 Ma to 468 ± 3 Ma (Pankhurst et al., 2000), a SHRIMP-dated Famatinian rhyolite was dated at 468.3 ± 3.4 Ma (Fanning et al., 2004), and three K-bentonites from the Argentine Precordillera yielded ages of 464 ± 2 Ma (Huff et al., 1997b) as well as 469.5 ± 3.2 Ma and 470.1 ± 3.3 Ma (Fanning et al., 2004).

The Famatinian magmatic rocks, traceable from the Puna area in NW-Argentina southward up to about San Luis, and the genetically related K-bentonites, extending throughout the region between Guandacol (La Rioja Province) and San Juan (San Juan Province) in the Argentine Precordillera, form a N-S trending outcrop belt, which lies parallel to the westerly adjacent outcrop belt of the Late Palaeozoic-Early Mesozoic magmatic arc. Especially in the Argentine Precordillera area (San Juan-Callingasta region, western Paganzo Basin) Middle Ordovician, Famatinian arc-derived K-bentonites and Late Carboniferous-Permian intrusive and volcanic rocks are spatially closely associated (Fig. 6.1). Within this region it was probably very likely that Early Permian volcanism penetrated Ordovician, bentonite-bearing rocks, which contaminated the erupted volcanic detritus. Thus the Lower Permian, 289.6 ± 3.4 Ma old tuff layer from the Laingsburg area in South Africa, which contains Middle Ordovician, 464 ± 5 Ma old zircons, could well originate from the Precordillera area in western Argentina.

As a sythesis of this chapter it can be concluded that at least the two Early Permian tuff layers, which both contain magmatic, xenocrystic Middle Ordovician and juvenile Early Permian zircons, are derived from a distal volcanic source positioned within the Late Palaeozoic magmatic arc fringing the southwestern Panthalassan margin of Gondwana. According to the presented geochronological data the Argentine Precordillera region seems to be the most likely source area, however a volcanic source in the West-Antarctic region can also not completely be ruled out. Furthermore it is believed that the provenance of the other Late Carboniferous to Early Permian tuffs of southern Namibia and South Africa was also located within this magmatic arc. However, minor pyroclastic contribution from an unknown, proximal, within plate volcanic source can also not be disproved.
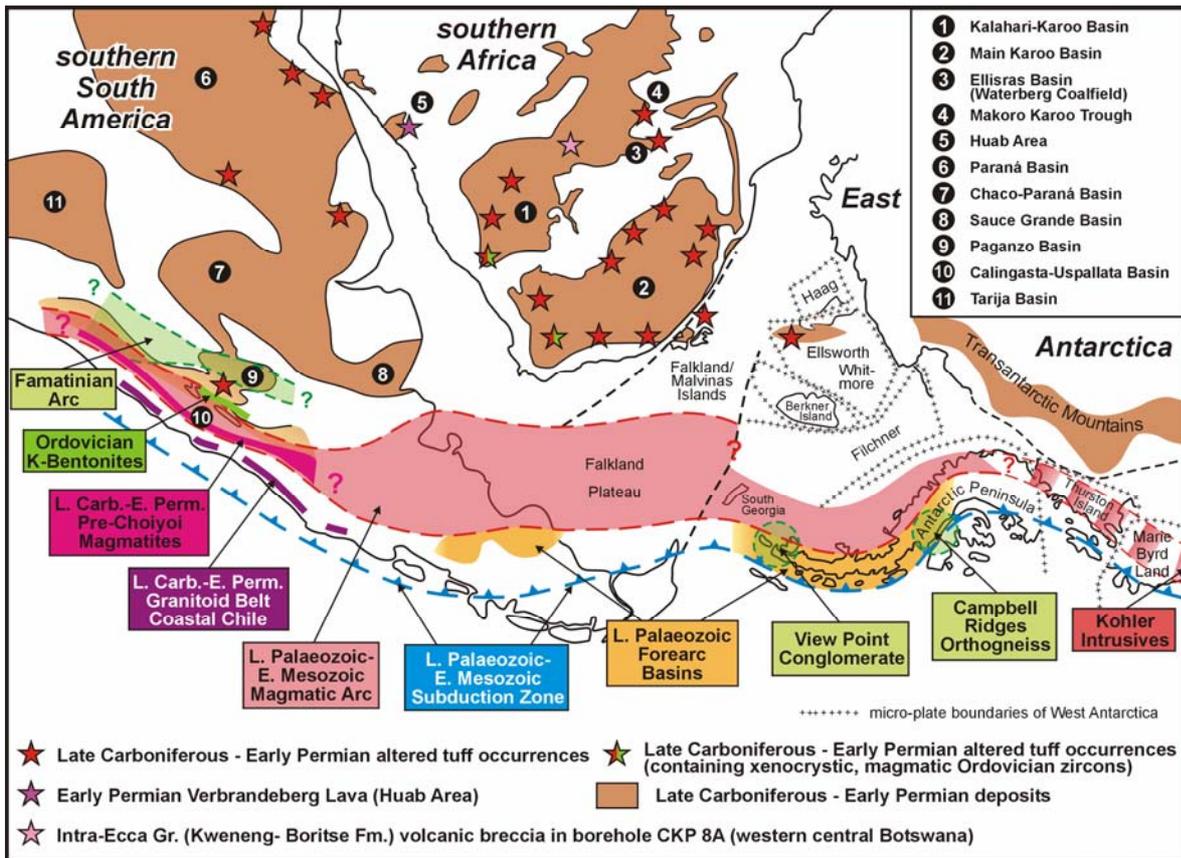
Fig. 6.1: Palaeogeographic reconstruction of southwestern Gondwana during the Late Carboniferous and Early Permian, showing the probable location of a subduction-related magmatic arc (red to purple), the distribution of Late Carboniferous-Early Permian sedimentary deposits (brown and yellow), the locations of intercalated horizons of altered tuffs (stars), the sites of Ordovician magmatic activity and pyroclastics in South America (green) as well as localities on the Antarctic Peninsula from where Middle Ordovician ages originate (green). Large parts of this map are adapted from Johnson et al. (1997), the course of Late Palaeozoic magmatic belts in Chile and Argentina is from López-Gamundí et al. (1994), the location of the Famatinian arc and genetically related K-bentonites is from Fanning et al. (2004), and the localities of Middle Ordovician zircons, respectively zircons with a Middle Ordovician age component on the Antarctic Peninsula are from Millar et al. (2002).

Chapter 7 – References

Anderson, A.M. (1974): Arthropod trackways and other trace fossils from the Early Permian lower Karroo beds of South Africa. Unpubl. Ph.D. thesis, Univ. Witwatersrand, Johannesburg, 322 pp.

Anderson, A.M. (1975): Turbidites and arthropod trackways in the Dwyka glacial deposits (Early Permian) of southern Africa. Trans. Geol. Soc. S. Afr., 78, 265-273.

Anderson, A.M. (1981): The *Umfolozia* arthropod trackways in the Permian Dwyka and Ecca Series of South Africa. J. Paleont., 55, 84-108.

Anderson, A.M. and McLachlan, I.R. (1979): The oil-shale potential of the Early Permian White Band Formation in southern Africa. In: Anderson, A.M. and van Biljon, W.J. (eds.) Some sedimentary basins and associated ore deposits of South Africa. Spec. Publ. Geol. Soc. S. Afr., 6, 83-89.

Anderson, J.M. (1977): The biostratigraphy of the Permian and Triassic. Part 3. A review of the Gondwana Permian palynology with particular reference to the northern Karoo Basin, South Africa. Mem. Bot. Surv. S. Afr., 41, 188 pp.

Anderson, J.M. (1981): World Permo-Triassic correlations: their biostratigraphic basis. In: Cresswell, M.M. and Vella, P. (eds) Proc. 5th Gondwana Symp., Wellington, New Zealand, 3-10.

Andreis, R.R. and Cladera, G. (1992): Las epiclastitas pérmicas de la cuenca Sauce Grande (Sierra Australes, Buenos Aires, Argentina). Parte I: composición y procedencia de detritos. Actas, IV Reunión Argentina de Sedimentología, La Plata, 127-134.

Andreis, R.R., Ferrando, L., and Herbst, R. (1991): Terrenos Carboníferos y Pérmicos de República Oriental del Uruguay. El sistema Pérmico en la República Argentina y en la República Oriental del Uruguay. Congreso Internacional de la Estratigrafía del Carbonífero y Pérmico, Academia Nacional de Ciencias de Córdoba, Argentina, 309-343.

Anglo American (1986): Report on Britstown drilling. Int. Versl., Anglo American Corporation (unpublished report).

Armstrong, R.A. (2003): SHRIMP U-Pb zircon dating of tuff samples from Namibia. Unpubl. report #A02-690, PRISE, Research School of Earth Sciences, Australian National University, Canberra, 13 pp.

Bangert, B. (2000): Tephrostratigraphy, petrography, geochemistry, age and fossil record of the Ganigobis Shale Member and associated glaciomarine deposits of the Dwyka Group, Late Carboniferous, southern Africa. Dr. rer. nat. thesis, Univ. Würzburg, 260 pp. [URL: http://opus.bibliothek.uni-wuerzburg.de/opus/volltexte/2002/223/]

Bangert, B. and von Brunn, V. (2001): Tuffaceous beds in glaciogenic argillites of the Late Palaeozoic Dwyka Group of KwaZulu-Natal, South Africa. J. Afr. Earth Sci., 32, 133-140.

Bangert, B., Stollhofen, H., Geiger, M., and Lorenz, V. (2000): Fossil record and high-resolution tephrostratigraphy of Carboniferous glaciomarine mudstones, Dwyka Group, southern Namibia. Communs. Geol. Surv. Namibia, 12, 235-245.

Bangert, B., Stollhofen, H., Lorenz V., and Armstrong, R., (1999): The geochronology and significance of ash-fall tuffs in the glaciogenic Carboniferous-Permian Dwyka Group of Namibia and South Africa. Journal of African Earth Science, 29, 33-49.

Barbarena, M.C., Araujo, D.C., Lavina, E.L., and Faccini, U.F. (1991): The evidence for close paleofaunitic affinity between South America and Africa, as indicated by Late Permian and Triassic tetrapods. Proc. 7th Int. Gondwana Symp., São Paulo 1988, 455-467.

Barnard, K.J. (1962): The Daberas alunite occurrence, Keetmanshoop district, S.W.A. Economic Geology Series, Geol. Surv. Nam., Open File Rep., EG 31, 5 pp.

Barret, P.J. (1969): Photomicrographs of some sedimentary and volcaniclastic Permian and Triassic Beacon rocks from the Beardmore Glacier area, Antarctica. Inst. Polar Studies, Ohio State University, Columbus, Ohio, 31, 30 pp.

Barton, J.M., Cairncross, B., and McLachlan, I. (2004): Rb-Sr isotopic and elemental studies of the origin of glauconite in the Permian northern Karoo Coal Fields, South Africa: evidence for a thermal Mid-Jurassic influence. S. Afr. J. Geol., 107, 499-504.

Batchelor, R.A. (2005): Tephra-fall deposits in the Sleat Group (Torridonian), Isle of Skye, Scotland. Geol. Mag., 142, 209-215.

Batchelor, R.A., Harper, D.A.T., and Anderson, T.B. (2003): Geochemistry and potential correlation of Silurian (Telychian) metabentonites from Ireland and SW Scotland. Geol. J., 38, 161-174.

Becker, T. and Schreiber, U.M. (1999): Provisional Geological Map Sheet 2816 Oranjemund: scale 1:250000. Geol. Surv. Namibia, Windhoek.

Bellanca, A., Masetti, D., Neri, R., and Venezia, F. (1999): Geochemical and sedimentological evidence of productivity cycles recorded in Toarcian black shales from the Belluno Basin, Southern Alps, northern Italy. J. Sed. Res., 69, 466-476.

Blignaut, J.J.G., Rossouw, P.J., de Villiers, J., and Russel, H.D. (1948): The geology of the Schoorsteenberg area, Cape Province. Explanation of sheet 166 (Schoorsteenberg), Geol. Surv. S. Afr., 40 pp.

Bobos, I. and Ghergari, L. (1999): Conversion of smectite to ammonium illite in the hydrothermal system of Harghita Bai, Romania: SEM and TEM investigations. Geologica Carpathica, 50, 379-387.

Bohor, B.F. and Triplehorn, D.M. (1993): Tonsteins: altered volcanic-ash layers in coal-bearing sequences. Geol. Soc. Am. Spec. Paper, 285, 44 pp.

Bossi, J., Ferrando, L.A., Fernandez, A.N., Elizalde, G., Morales, H., Ledesma, J.J., Carbelo, E., Medina, E., Ford, I., and Montana, J.R. (1975): Carta Geologica del Uruguay. Montevideo, Uruguay, p. 32.

Bourdon, M.M., Burollet, P.F., Combaz, A., Dufaure, Ph., Ferrero, J., and Sacal, V. (1966): Examens de laboratoire sur quelques échantillons recueillis par la mission C.F.P. en Afrique du Sud et au Sud-Ouest Africain. Companie Française des Petroles. Unpubl. report to Southern Oil Exploration Corporation (SOEKOR). Library ref. No SV 19, 53 pp.

Bowring, S.A. and Schmitz, M.D. (2003): High-precision U-Pb zircon geochronology and the stratigraphic record. In: Hanchar, J.M. and Hoskin, P.W.O. (eds.) Zircon, Revs. in Min. & Geochem., 53, 305-326.

Brandt, J.W., Martin, H., and Kirchner, J.G. (1961): Interim report of the Coal Commission of South West Africa. Economic Geology Series, Geol. Surv. Namibia, EG 035, 125 pp.

Breitkreuz, C. (1991): Fluvio-lacustrine sedimentation and volcanism in a Late Carboniferous tensional intra-arc basin, northern Chile. Sed. Geol., 74, 173-187.

Breitkreuz, C. and Zeil, W. (1994): The Late Carboniferous to Triassic volcanic belt in northern Chile. In: Reutter, K.-J., Scheuber, E., and Wigger, P.J. (eds.) Tectonics of the southern Central Andes, 277-292, Springer, Berlin.

Buatois, L.A., Mangano, M.G., Radek, M., and Maples, C.G. (1998): The ichnogenus *Curvolithus* revisited. J. Pal., 72, 758-769.

Buckman, J.O. (1996): *Heimdallia* from the Lower Carboniferous of Ireland: *H. mullaghmori*, a new ichnospecies, and re-evaluation of the three-dimensional format of the ichnogenus. Ichnos, 5, 43-51.

Cairncross, B., Beukes, N.J., Coetzee, L.L., and Rehfeld, U. (2005): The bivalve *Megadesmus* from the Permian Volksrust Shale Formation (Karoo Supergroup), northeastern Karoo Basin, South Africa: implications for Late Permian basin development. S. Afr. J. Geol., 108, 547-556.

Calarge, L.M., Lanson, B., Meunier, A., and Formoso, M.L. (2003a): The smectitic minerals in a bentonite deposit from Melo (Uruguay). Clay Minerals, 38, 25-34.

Calarge, L.M., Meunier, A., and Formoso, M.L.L. (2003b): A bentonite bed in the Aceguá (RS, Brazil) and Melo (Uruguay) areas: a highly crystallized montmorillonite. J. S. Am. Earth Sci., 16, 187-198.

Carey, J. (1978): Sedimentary environments and trace fossils of the Permian Snapper Point Formation, southern Sydney Basin. J. Geol. Soc. Aust., 25, 433-458.

de Castro, J.C. (1994): Field trip guide to Paraná Basin. 14th Int. Sed. Congr., Recife, 42 pp.

Catuneanu, O. (2004a): Basement control on flexural profiles and the distribution of foreland facies: the Dwyka Group of the Karoo Basin, South Africa. Geology, 32, 517-520.

Catuneanu, O. (2004b): Retroarc foreland systems: evolution through time. J. Afr. Earth Sci., 38, 225-242.

Catuneanu, O. and Bowker, D. (2001): Sequence stratigraphy of the Koonap and Middleton fluvial formations in the Karoo Foredeep, South Africa. J. Afr. Earth Sci., 33, 579-595.

Catuneanu, O. and Elango, H.N. (2001): Tectonic control on fluvial styles: the Balfour Formation of the Karoo Basin, South Africa. Sed. Geol., 140, 291-313.

Catuneanu, O., Hancox, P.J., Cairncross, B., and Rubidge, B.S. (2002): Foredeep submarine fans and forebulge deltas: orogenic off-loading in the underfilled Karoo Basin. J. Afr. Earth Sci., 35, 489-502.

Catuneanu, O., Hancox, P.J., and Rubidge, B.S. (1998): Reciprocal flexural behaviour and contrasting stratigraphies: a new basin development model for the Karoo retroarc foreland system, South Africa. Basin Res., 10, 417-439.

Catuneanu, O., Martins-Neto, M.A., and Eriksson, P.G. (2005): Precambrian sequence stratigraphy. Sed. Geol., 176, 67-95.

Catuneanu, O., Wopfner, H., Eriksson, P.G., Cairncross, B., Rubidge, B.S., Smith, R.M.H., Hancox, P.J. (2005): The Karoo basins of south-central Africa. J. Afr. Earth Sci., 43, 211-253.

Cazzulo-Klepzig, M., Guerra-Sommer, Formoso, N.L., and Calarge, L.M. (2002): Geo-chemical and palynological evidence for the age determination of Permian coals, southern Brazil. J. S. Am. Earth Sci., 15, 374-380.

Cherniak, D.J. and Watson, E.B. (2000): Pb diffusion in zircon. Chem. Geol., 172, 5-24.

Christidis, G.E. (1995): Mechanism of illitization of bentonites in the geothermal field of Milos Island Greece: evidence based on mineralogy, chemistry, particle thickness and morphology. Clays and Clay Minerals, 43, 569-585.

CHRONOS System Portal [URL: http://portal.chronos.org/gridsphere/gridsphere] *('Conduct Searches' – 'Time Scale' – 'Get Stratigraphic Subdivision Members')*

Claoué-Long, J.C., Compston, W., Robersts, J., and Fanning, C.M. (1995): Two Carboniferous ages: a comparison of SHRIMP zircon dating with conventional zircon ages and $^{40}Ar/^{39}Ar$ analysis. In: Berggren, W.A., Kent, D.V., Aubry, M.P. and Hardenbohl, J. (eds.) Geochronology, time scales and global stratigraphic correlation, Soc. Sediment. Geol. Spec. Publ., 54, 3-21.

Closs, D. (1967): Goniatiten mit Radula und Kieferapparat in der Itararé-Formation von Uruguay. Paläont. Z., 41, 19-37.

Closs, D. (1969): Intercalation of goniatites in the Gondwanic glacial beds of Uruguay. In: Amos, A.J. (ed.) Gondwana stratigraphy, Unesco, Paris, 197-212.

Coetzee, C.B. and Hanekom, H.J. (1966): Note on the bentonite in the Parys area. Unpubl. report, Geol. Surv. S. Afr., 1966-0009, 4 pp.

Cole, D.I. (1992): Evolution and development of the Karoo Basin. In: de Wit, M.J. and Ransome, I.G.D. (eds.) Inversion tectonics of the Cape Fold Belt, Karoo and Cretaceous basins of Southern Africa, 87-99, Balkema, Rotterdam.

Cole, D.I. and Basson, W.A. (1991): Whitehill Formation. In: Johnson, M.R. (ed.) Catalogue of South African lithostratigraphic units, 3, 51-52.

Cole, D.I. and McLachlan, I.R. (1991): Oil potential of the Permian Whitehill Shale Formation in the main Karoo Basin, South Africa. In: Ulbrich, H. and Rocha, A.C. (eds.) Gondwana Seven Proceedings, Insituto Geociencias, Universidade de São Paulo, 379-390.

Cole, D.I. and McLachlan, I.R. (1994): Oil shale potential and depositional environment of the Permian Whitehill Shale Formation in the main Karoo Basin. Open file report, Geol. Surv. S. Afr., 1994-0213, 1 & 2, 89 pp.

Collinson, J.W., Isbell, J.L., Elliot, D.H., Miller, M.F., Miller, J.M.G., and Veevers, J.J. (1994): Permian-Triassic Transantarctic Basin. In: Veevers, J.J. and Powell, C.McA. (eds.) Permian-Triassic Pangean basins and foldbelts along the Panthalassan margin of Gondwanaland, Geol. Soc. Am. Mem., 184, 173-222.

Collinson, J.W., Vavra, C.L., and Zawiskie, J.M. (1992): Sedimentology of the Polarstar Formation (Permian), Ellsworth Mountains, West Antarctica. In: Webers, G.F., Craddock, C. and Splettstoesser, J.F. (eds.) Geology and Palaeontology of the Ellsworth Mountains, West Antarctica, Geol. Soc. Am. Mem., 170, 63-79.

Compston, W. (1999): Geological age by intrumental analysis: the 29th Hallimond Lecture. Min. Mag., 63, 297-311.

Cooper, M.R. and Kensley, B. (1984): Endemic South American Permian bivalve molluscs from the Ecca of South Africa. J. Paleont., 58, 1360-1363.

Coutinho, J.M.V., Hachiro, J. Coimbra, A. M., and Santos, P. R. (1991): Ash-fall-derived vitro-clastic tuffaceous sediments in the Permian of the Paraná Basin and their provenance. Proc. 7th Int. Gondwana Symp., São Paulo, Brazil, 147-160.

Creech, M. (2002): Tuffaceous deposition in the Newcastle Coal Measures: challenging existing concepts of peat formation in the Sydney Basin, New South Wales, Australia. Int. J. Coal Geol., 51, 185-214.

Davies, D.W., Williams, I.S., and Krogh, T.E. (2003): Historical development of zircon geochronology. In: Hanchar, J.M. and Hoskin, P.W.O. (eds.) Zircon, Revs. in Min. & Geochem., 53, 146-181.

Dickins, J.M. (1961): *Eurydesma* and *Peruvispira* from the Dwyka beds of South Africa. Palaeontology, 4, 138-148.

Diessel, C.F.K. (1985): Tuffs and tonsteins in the coal measures of New South Wales, Australia. Congr. 10th Int. Strat. Geol. Carbonifere, Madrid, 1983, Comptes Rendus, 4, 197-210.

van Eeden, O.R. (1973): The correlation of the subdivisions of the Karroo System. Trans. Geol. Soc. S. Afr., 76, 201-206.

Elliot, D.H. and Johnson, M. (1972): The Gondwanide Orogeny: new data from South Africa and the problem of the Falkland Islands. Geol. Soc. Am. Abstr. with Progr., 4, 498-499.

Elliot, D.H. and Watts, D.R. (1974): The nature and origin of volcaniclastic material in some Karoo and Beacon rocks. Trans. Geol. Soc. S. Afr., 77, 109-111.

Erlank, A.J., Marsh, J.S., Duncan, A.R., Miller, R.McG., Hawkesworth, C.J., Betton, P.J., and Rex, D.C. (1984): Geochemistry and petrogenesis of the Etendeka volcanic rocks from SWA/Namibia. In: Erlank, A.J. (ed.) Petrogenesis of the volcanic rocks of the Karoo province, Spec. Publ. Geol. Soc. S. Afr., 13, 195-245.

Euro Namibian Investment Company (1992): Aranos Coal Project. Unpubl. report, 29 pp.

Fanning, C.M., Pankhurst, R.J., Rapela, C.W., Baldo, E.G., Casquet, C., and Galindo, C. (2004): K-bentonites in the Argentine Precordillera contemporaneous with rhyolite volcanism in the Famatinian Arc. J. Geol. Soc. London, 161, 747-756.

Fanning, C.M., Pankhurst, R.J., Rapela, C.W., and Herve, F. (2003): Unravelling complex SHRIMP U-Pb zircon ages for Palaeozoic and Mesozoic magmatic rocks: fact or artefact. South American symposium on isotope geology, IV short papers, Salvador, 549-552.

Faure, K., Armstrong, R.A., Harris, C., and Willis, J.P. (1996a): Provenance of mudstones in the Karoo Supergroup of the Ellisras Basin, South Africa: geochemical evidence. J. Afr. Earth Sci., 23, 189-204.

Faure, K. and Cole, D. (1999): Geochemical evidence for lacustrine microbial blooms in the vast Permian Main Karoo, Paraná, Falkland Islands and Huab Basins of southwestern Gondwana. Palaeogeogr. Palaeoclimatol. Palaeoecol., 152, 189-213.

Faure, K., Willis, J.P., and Dreyer, J.C. (1996b): The Grootegeluk Formation in the Waterberg Coalfield, South Africa: facies, palaeoenvironment and thermal history – evidence from organic and clastic matter. Int. J. Coal Geol., 29, 147-186.

Fisher, R.V. and Schmincke, H.U. (1984): Pyroclastic rocks. Springer, Berlin, 472 pp.

F.M. Consultants Ltd. (1969): Geochronological report on a core sample OL1/69 3100 ft. of a dolerite intruded into Ordovician Table Mountain Sandstone, South Africa. Unpubl. report FMK 722 for Soekor, Library ref. no. LABR.8-3A.

Formoso, M.L.L., Calarge, L.M., Garcia, A.J.V., Alves, D.B., Gomes, M.B., and Misusaki, A.M. (1997): Permian tonsteins from the Paraná Basin, Rio Grande do Sul, Brazil. Proc. Clay Conf., Ottawa, Canada, 613-621.

Frakes, L.A. and Crowell, J.C. (1970): Late Paleozoic glaciation: II, Africa exclusive of the Karroo Basin. Geol. Soc. Am. Bull., 81, 2261-2286.

França, A.B., Milani, E.J., Schneider, R.L., P. López, O., M. López, J., S. Suárez, R., Santa Ana, H., Wiens, F., Ferreiro, O., Rossello, E.A., Bianucci, H.A., Flores, R.F.A., Vistalli,

M.C., Fernandez-Seveso, F., Fuenzalida, R.P., and Muñoz, N. (1995): Phanerozoic correlation in southern South America. In: Tankard, A.J., Suárez, R. and Welsink, H.J. (eds.) Petroleum basins of South America, AAPG Mem., 62, 129-161.

Franzese, J.R. and Spalletti, L.A. (2001): Late Triassic-Early Jurassic continental extension in southwestern Gondwana: tectonic segmentation and pre-break-up rifting. J. S. Am. Earth Sci., 14, 257-270.

Fuller, A.O. (1970): The occurrence of laumontite in strata of the Karoo System, South Africa. Proc. Papers 2nd Gondwana Symp. Johannesburg, 455-456.

Geiger, M. (1999): An explanation of the Geological Map 1:10000 of the Namibian borderland along the Orange River at Zwartbas, Warmbad District, Karas Region, Namibia. Unpubl. Diplomkartierung, Univ. Würzburg, 80 pp.

Geiger, M. (2000): The geology of the southern Warmbad basin margin – tephrostratigraphy, age, fossil record and sedimentary environment of Carboniferous-Permian glacigenic deposits of the Dwyka Group, Zwartbas, southern Namibia. Unpubl. Diplom thesis, Univ. Würzburg, 79 pp.

Genis, G. (1982): Geological Map Sheet 2618 Keetmanshoop: scale 1:250000. Geol. Surv. S.W. Afr./Namibia.

Genis, G. and Schalk, K.E.L. (1984): The geology of area 2618: Keetmanshoop. Explanation of sheet 2618 scale 1:250000. Geol. Surv. S.W. Afr./Namibia, 12 pp.

Gerschütz, S. (1996): Geology, volcanology and petrogenesis of the Kalkrand Basalt Formation and the Keetmanshoop Dolerite Complex, southern Namibia. Unpubl. Dr. rer. nat. thesis, Univ. Würzburg, 186 pp.

Gradstein, F.M. and Ogg, J.G. (2004): Geologic Time Scale 2004 – Why, how, and where next! Internet article, 7 pp. [URL: http://www.stratigraphy.org/scale04.pdf]

Gradstein, F.M., Ogg, J.G., Smith, A.G., and with contributions of Agterberg, F.P., Bleeker, W., Cooper, R.A., Davydov, V., Gibbard, P., Hinnov, L., House, M.R., Lourens, L., Luterbacher, H-P., McArthur, J., Melchin, M.J., Robb, L.J., Shergold, J., Villeneuve, M., Wardlaw, B.R., Ali, J., Brinkhuis, H., Hilgen, F.J., Hooker, J., Howarth, R.J., Knoll, A.H., Laskar, J., Monechi, S., Powell, J., Plumb, K.A., Raffi, I., Röhl, U., Sanfilippo, A., Schmitz, B., Shackleton, N.J., Shields, G.A., Strauss, H., van Dam, J., Veizer, J., van Kolfschoten, Th., and Wilson, D. (2005): A Geologic Time Scale 2004. Cambridge University Press, 610 pp.

Grill, H. (1997): The Permo-Carboniferous glacial to marine Karoo record in southern Namibia: sedimentary facies and sequence stratigraphy. Beringeria, 19, 98 pp.

Grote, W. (1984): Voorlopige verslag oor die Group Ecca in gebiede 2518 A en C (Namaland). Geol. Surv. Nam. Open File report, RG 7, 18 pp.

Gulson, B.L., Diessel, C.F.K., Mason, D.R., and Krogh, T.E. (1990): High precision radiometric ages from the northern Sydney Basin and their implications for the Permian time interval and sedimentation rates. Aust. J. Earth Sci., 37, 459-469.

Gunthorpe, R. J. (1987): Final report, Samoa and Tevrede prospecting grants, Otjiwarongo District, South West Africa/Namibia. Unpubl. open file report, Tsumeb Corp. Ltd., grant M46/3/1240 and 1241, Geol. Surv. Namibia, 9 pp.

Hachiro, J. (2000): Occurrences of evaporites in the Irati Subgroup (Late Permian, Paraná Basin). An. Acad. Bras. Ciênc., 72 , 600-601.

Hälbich, I.W. (1983): A tectogenesis of the Cape Fold Belt. In: Söhnge, A.P.G. and Hälbich, I.W. (eds.) Geodynamics of the Cape Fold Belt, Spec. Publ. Geol. Soc. S. Afr., 12, 165-175.

Hälbich, I.W., Fitch, F.J., and Miller, J.A. (1983): Dating the Cape orogeny. In: Söhnge, A.P.G. and Hälbich, I.W. (eds.) Geodynamics of the Cape Fold Belt, Spec. Publ. Geol. Soc. S. Afr., 12, 149-164.

Hancox, P.J. and Rubidge, B.S. (2001): Breakthroughs in the biodiversity, biostratigraphy, and basin analysis of the Beaufort Group. J. Afr. Earth Sci., 33, 563-577.

Hanekom, H.J. (1962): The metamorphism of the nodular calcareous hornfels at Insizwa, Cape Province. Ann. Univ. Stellenbosch, Vol. 37, Ser. A, No. 6, 425-479.

Harrington, H.J. (1955): The Permian *Eurydesma* Fauna of Eastern Argentina. J. Paleont., 29, 112-128.

Haughton, S.H., Blignaut, J.J., Rossouw, P.J., Spies, J.J., and Zaght, S. (1953): Results of an investigation into the possible presence of oil in Karroo rocks in parts of the Union of South Africa. Mem. Geol. Surv. S. Afr., 45, 130 pp.

Haughton, S.H. and Frommurze, H.F. (1927): The Karroo beds of the Warmbad District, South-West Africa. Trans. Geol. Soc. S. Afr., 30, 133-142.

Haughton, S.H. and Frommurze, H.F. (1936): The geology of the Warmbad district, South West Africa. An explanation of geological sheets Amib (H-33-F), Umeis (H-34-A) and Nakop (H-34-B). SWA Department of Mines, Memoir, 2, 64 pp.

Heath, D.C. (1972): Die geologie van die Sisteem Karoo in die gebied Mariental-Asab, Suidwes-Afrika. Mem. Geol. Surv. S. Afr., 61, 36 pp.

Hegenberger, W. (1985): Some aspects of Nama and Karoo sedimentation from a borehole south-east of Gobabis. Communs Geol. Surv. S.W. Afr./Namibia, 1, 63-67.

Hegenberger, W. (1992): Coal. In: The mineral resources of Namibia, Geological Survey of Namibia, 7.2-1 – 7.2-29.

Hegenberger, W. and Seeger, K.G. (1980): The geology of the Gobabis area. Explanation of sheet 2218 scale 1:250000. Geol. Surv. S.W. Afr./Namibia, 11 pp.

Heinrich, H. (1988): Origin and consequences of cyclic ice rafting in the Northeast Atlantic Ocean during the past 130000 years. Quaternary Research, 29, 142-152.

Hill, I.G., Worden, R.H., and Meighan, I.G. (2000): Yttrium: the immobility-mobility transition during basaltic weathering. Geology, 28, 923-926.

Ho-Tun, E. (1979): Volcaniclastic material in lower Beaufort Group, Karoo rocks. Abstr. 18th Congr. Geol. Soc. S. Afr., 197-199.

Holz, M. (1999): Early Permian sequence stratigraphy and the palaeophysiographic evolution of the Paraná Basin in southernmost Brazil. J. Afr. Earth Sci., 29, 51-61.

Holz, M. (2003): Sequence stratigraphy of a lagoonal estuarine system: an example from the lower Permian Rio Bonito Formation, Paraná Basin, Brazil. Sed. Geol., 162, 305-331.

Holz, M., Kalkreuth, W., and Banerjee, I. (2002): Sequence stratigraphy of paralic coal-bearing strata: an overview. Int. J. Coal. Geol., 48, 147-179.

Holzförster, F. (2000): Sedimentology, stratigraphy and synsedimentary tectonics of the Karoo Supergroup in the Huab and Waterberg-Erongo areas, N-Namibia. Unpubl. Dr. rer. nat. thesis, 296 pp.

Holzförster, F. (2002): Sedimentology, stratigraphy and synsedimentary tectonics of the Karoo Supergroup in the Huab and Waterberg-Erongo areas, N-Namibia. Beringeria, 30, 144 pp.

Holzförster, F., Stollhofen, H., and Stanistreet, I.G. (2000): Lower Permian deposits of the Huab area, NW Namibia: a continental to marine transition. Communs Geol. Surv. Namibia, 12, 247-257.

Horsthemke, E. (1992): Fazies der Karoosedimente in der Huab-Region, Damaraland, NW-Namibia. Göttinger Arb. Geol. Paläont., 55, 102 pp.

Horsthemke, E., Ledendecker, S., and Porada, H. (1990): Depositional environments and stratigraphic correlation of the Karoo Sequence in northwestern Damaraland. Communs Geol. Surv. Namibia, 6, 63-73.

Hoskin, P.W.O. and Black, L.P. (2000): Metamorphic zircon formation by solid-state recrystallization of protolith igneous zircon. J. Metam. Geol., 18, 423-439.

Hückreide, R. (1952): Eine spiralförmige Lebensspur aus dem Kulmkieselschiefer von Biedenkopf an der Lahn (*Spirodesmos archimedeus* n. sp.). Paläontologische Zeitschrift, 26, 175-180.

Huff, W.D., Bergström, S.M., and Kolata, D.R. (2000): Silurian K-bentonites of the Dnestr Basin, Podolia, Ukraine. J. Geol. Soc. London, 157, 493-504.

Huff, W.D., Bergström, S.M., Kolata, D.R., Cingolani, C.A., and Astini, R.A. (1998): Ordovician K-bentonites in the Argentine Precordillera: relations to Gondwana margin evolution. In: Pankhurst, R.J. and Rapela, C.W. (eds.) The Proto-Andean margin of Gondwana. Geol. Soc. London Spec. Publ., 142, 107-126.

Huff, W.D., Bergström, S.M., Kolata, D.R., and Sun, H. (1997a): The Lower Silurian Osmundsberg K-bentonite, Part II: mineralogy, geochemistry, chemostratigraphy and tectonomagmatic significance. Geol. Mag., 135, 15-26.

Huff, W.D., Davis, D.W., Bergström, S.M., Krekeler, M.P.S., Kolata, D.R., and Cingolani, C. (1997b): A biostratigraphically well-constrained K-bentonite U-Pb zircon age of the lowermost Darriwilian Stage (Middle Ordovician) from the Argentine Precordillera. Episodes, 20, 29-33.

Iijima, A. (1988): Diagenetic transformation of minerals as exemplified by zeolites and silica minerals: a Japanese view. In: Chilingarian, G.V. and Wolf, K.H. (eds.) Diagenesis II, Developments in Sedimentology, 43, 147-211.

Iñíguez, A.M., Andreis, R.R., and Zalba, A.A. (1988): Eventos piroclásticos en la Formación Tunas (Pérmico), Sierras Australes, provincia de Buenos Aires, República Argentina. Actas, II Jornadas Geológicas Bonaerenses, Bahía Blanca, 383-395.

Ireland, T.R. and Williams, I.S. (2003): Considerations in zircon geochronology by SIMS. In: Hanchar, J.M. and Hoskin, P.W.O. (eds.) Zircon, Revs. in Min. & Geochem., 53, 215-241.

Johnson, M.R. (1991): Sandstone petrography, provenance and plate tectonic setting in Gondwana context of the southeastern Cape-Karoo Basin. S. Afr. J. Geol., 94, 137-154.

Johnson, M.R. and Keyser, A.W. (1979): The geology of the Beaufort West area. Explanation to sheet 3222, scale 1:250000. Geol. Surv. S. Afr., 14 pp.

Johnson, M.R., van Vuuren, C.J., Hegenberger, W.F., Key, R., and Shoko, U. (1996): Stratigraphy of the Karoo Supergroup in southern Africa. J. Afr. Earth Sci., 23, 3-15.

Johnson, M.R., van Vuuren, C.J., Visser, J.N.J., Cole, D.I., Wickens, H. de V., Christie, A.D.M., and Roberts, D.L. (1997): The foreland Karoo Basin, South Africa. In: Selley, R.C. (ed.) African Basins, Sedimentary basins of the world, 3, 269-317.

Johnson, S.D., Flint, S., Hinds, D., and Wickens, H. de V. (2001): Anatomy, geometry and sequence stratigraphy of basin floor to slope turbidite systems, Tanqua Karoo, South Africa. Sedimentology, 48, 987-1023.

Jones, J.G., Conaghan, P.J., and McDonnell, K.L. (1987): Coal measures of an orogenic recess: Late Permian Sydney Basin, Australia. Palaeogeogr. Palaeoclimatol. Palaeoecol., 58, 203-219.

Junker, R. (2001): Erläuterungen zur geologischen Karte des Albin Ridge, NW Namibia. Unpubl. Diplomkartierung, Univ. Würzburg, 63 pp.

Kalkreuth, W., Holz, M., Cazzulo-Klepzig, M., Marques-Toigo, M., Utting, J., and Semikiwa, P. (1999): A comparative study of the geology, petrology and palynology of Permian coals in Tanzania and southern Brazil. J. Afr. Earth Sci., 29, 91-104.

Karpeta, W.P. (1977): The geology of the Aberdeen-Murraysburg area, Cape Province. Unpubl. report Geol. Surv. S. Afr., 16 pp.

Karpeta, W.P. (1996): Tuffs from the Permian Teekloof Formation (Beaufort Group) from Murraysburg and Aberdeen, Cape Province: their origin and alteration. S. Afr. J. Geol., 99, 51-67.

Ketzer, J.M., Holz, M., Morad, S., and Al-Aasm, I.S. (2003): Sequence stratigraphic distribution of diagenetic alterations in coal-bearing, paralic sandstones: evidence from the Rio Bonito Formation (early Permian), southern Brazil. Sedimentology, 50, 855-877.

Keyser, N. and Zawada, P.K. (1988): Two occurrences of ash-flow tuff from the Lower Beaufort Group in the Heilbron-Frankfort area, northern Orange Free State. S. Afr. J. Geol., 91, 509-521.

Kingsley, C.S. (1981): A composite submarine fan-delta-fluvial model for the Ecca and Lower Beaufort Groups of Permian age in the eastern Cape Province, South Africa. Trans. Geol. Soc. S. Afr., 84, 27-40.

Kingsley, C.S. (1985): Sedimentological analysis of the Ecca Sequence in the Kalahari Basin, South West Africa/Namibia. Unpubl. report CDM Mineral Surveys, 39 pp.

Kingsley, C.S. (1990): Sedimentological model of the Permian Kalahari basin, Namibia. 13th Int. Sediment. Congr. Abstr., Nottingham-London, 274-275.

Kinney, P.D. and Compston, W. (1989): Archean mantle xenocrysts in a Permian kimberlite: two generations of kimberlitic zircon in Jwaneng. In: Ross, J., Jaques, A.L., Ferguson, J., Green, D.H., O'Reilly, S.Y., Danchin, R.V. and Janse, A.J.A. (eds.) Kimberlites and related rocks, Spec. Publ. Geol. Soc. Australia, 14, 833-842.

Kisch, H.J. (1966): Chlorite-illite tonstein in high-rank coals from Queensland, Australia: notes on regional epigenetic grade and coal rank. Am. J. Sci., 264, 389-397.

Knight, J.A., Burger, K., and Bieg, G. (2000): The pyroclastic tonsteins of the Sabero Coalfield, north-western Spain, and their relationship to the stratigraphy and structural geology. Int. J. Coal Geol., 44, 187-226.

Knütter, R.K.C. (1994): Geologische Kartierung in der Umgebung von Laingsburg (Westliche Kapprovinz/Südafrika) sowie geochemische Untersuchungen an vulkanischen Gesteinen der Prince Albert-, Whitehill-, Vischkuil und Laingsburg Fms. sowie der Abrahamskraal Fm. (Beaufort Group). Unpubl. Diplom thesis, Univ. Bonn, 93 pp.

Knütter, R.K.C., Hoernes, S., and Siehl, A. (1995): Geochemical and stable isotopic characteristics of tuffs and enclosing sedimentary rocks in the Cape Fold Belt – Karoo transition (Laingsburg area). Abstr. Geocongr. `95, Geol. Soc. S. Afr, 740-742.

Kovács-Endrödy, E. (1991): On the late Permian age of Ecca *Glossopteris* floras in the Transvaal Province with a key to and description of twenty five *Glossopteris* species. Mem. Geol. Surv. S. Afr., 77, 111 pp.

Kramer, W., Weatherall, G., and Offler, R. (2001): Origin and correlation of tuffs in the Permian Newcastle and Wollombi Coal Measures, New South Wales, Australia, using chemical fingerprinting. Int. J. Coal Geol., 47, 115-135.

Krenkel, E. (1939): Geologie der deutschen Kolonien in Afrika. Borntraeger, Berlin, 272 pp.

Kutzbach, J.E. (1994): Idealised Pangean climates: sensitivity to orbital change. In: Klein, G. (ed.) Pangea: palaeoclimate, tectonics and sedimentation during accretion, zenith, and breakup of a supercontinent, Geol. Soc. Am. Spec. Publ., 288, 41-55.

Lane, N.G. and Frakes, L.A. (1970): A Permian starfish from South West Africa. J. Paleont., 44, 1135-1136.

Le Roux, J.P. (1985): Palaeochannels and uranium mineralization on the main Karoo Basin of South Africa. Unpubl. Ph.D. thesis, Univ. Port Elizabeth, 250 pp.

Ledendecker, S. (1992): Stratigraphie der Karoosedimente der Huabregion (NW-Namibia) und deren Korrelation mit zeitäquivalenten Sedimenten des Paranàbeckens (Südamerika) unter besonderer Berücksichtigung der überregionalen geodynamischen und klimatischen Entwicklung Westgondwanas. Göttinger Arb. Geol. Paläont., 54, 87 pp.

Lee, J.K.W., Williams, I.S., and Ellis, D.J. (1997): Pb, U and Th diffusion in natural zircon. Nature, 390, 159-162.

Leeder, M.R. (1982): Sedimentology: process and product. Allen & Unwin, London-Boston, 344 pp.

Limarino, C.O. and Spalletti, L. (1986): Eolian Permian deposits in west and northwest Argentina. Sed. Geol., 49, 109-127.

Llambías, E.J., Quenardelle, S., and Montenegro, T. (2003): The Choiyoi Group from central Argentina: a subalkaline transitional to alkaline association in the craton adjacent to the active margin of the Gondwana continent. J. S. Am. Earth Sci., 16, 243-257.

Lock, B.E. and Johnson, M.R. (1974): A crystal tuff from the Ecca Group near Lake Mentz, Eastern Cape Province. Trans. Geol. Soc. S. Afr., 77, 173-174.

Lock, B.E. and Wilson, J.D. (1975): Discussion on "The nature and origin of volcaniclastic material in some Karroo and Beacon rocks". Trans. Geol. Soc. S. Afr., 78, 171.

López-Gamundí, O.R. (1996): Permian volcanic activity along the Proto-Pacific plate margin reflected in the basins of southern South America. In: Dimri, D.B. (ed.) Gondwana Nine – 9th Int. Gondwana Symp. 1994, Hyderabad, India, 2, 833-838.

López-Gamundí, O.R. and Breitkreuz, C. (1997): Carboniferous-to-Triassic evolution of the Panthalassan margin in southern South America. In: Dickins, J.M. (ed.) Late Palaeozoic and Early Mesozoic Circum-Pacific events and their global correlation, 8-19.

López-Gamundí, O.R., Conaghan, P.J., Rossello, E.A., and Cobbold, P.R. (1995): The Tunas Formation (Permian) in the Sierras Australes Foldbelt, east central Argentina:

evidence for syntectonic sedimentation in a foreland basin. J. S. Am. Earth Sci., 8, 129-142.

López-Gamundí, O.R., Espejo, I.S., and Alonso, M.S. (1990): Sandstone composition changes and paleocurrent reversal in the Upper Paleozoic and Triassic deposits of the Huaco area, western Paganzo Basin, west-central Argentina. Sed. Geol., 66, 99-111.

López-Gamundí, O.R., Espejo, I.S., Conaghan, P.J., Powell, C.McA., and Veevers, J.J. (1994): Southern South America. In: Veevers, J.J. and Powell, C.McA. (eds.) Permian-Triassic Pangean basins and foldbelts along the Panthalassan margin of Gondwanaland, Geol. Soc. Am. Mem., 184, 281-329.

López-Gamundí, O.R., Limarino, C.O., and Cesari, S.N. (1992): Late Paleozoic paleo-climatology of central west Argentina. Palaeogeogr. Palaeoclimatol. Palaeoecol., 91, 305-329.

López-Gamundí, O.R. and Rossello, E.A. (1998): Basin fill evolution and paleotectonic patterns along the Samfrau geosyncline: the Sauce Grande Basin – Ventana Foldbelt (Argentina) and Karoo Basin – Cape Fold Belt (South Africa) revisited. Geol. Rundsch., 86, 819-834.

Lorenz, V. and Haneke J. (2004): Relationship between diatremes, dykes, sills, laccoliths, intrusive-extrusive domes, lava flows, and tephra deposits with unconsolidated water-saturated sediments in the late Variscan intermontane Saar-Nahe Basin, SW Germany. In: Breitkreuz, C. and Petford, N. (eds.) Physical geology of high-level magmatic systems. Geol. Soc. London Spec. Publ., 234, 75-124.

Ludwig, K.R. (1998): On the treatment of concordant uranium-lead ages. Geochim. Cosmochim. Acta, 62, 665-676.

Ludwig, K.R. (1999): Isoplot/Ex version 2.00: A Geochronological Toolkit for Microsoft Excel. Berkeley Geochronology Center Spec. Publ., 1a, 46 pp.

Ludwig, K.R. (2000): SQUID 1.00: A User´s Manual. Berkeley Geochronology Center Spec. Publ., 2, 17 pp.

MacRae, C. (1992): Age of the Whitehill Formation in the Hopetown area, northeastern Cape Province. Abstr. 7th Conf. Palaeont. Soc. S. Afr., Johannesburg, p. 29.

MacRae, R. (1999): Life etched in stone – Fossils of South Africa. Geol. Soc. S. Afr., Johannesburg, 305 pp.

Marshall, C.G.A. (2002): The stratigraphy, sedimentology and basin evolution of the Natal Group. Mem. Council for Geoscience S. Afr., 91, 179 pp.

Marshall, C.G.A. and von Brunn, V. (1999): The stratigraphy and origin of the Natal Group. S. Afr. J. Geol., 102, 15-25.

Marshall, C.G.A. and von Brunn, V. (2000): Authors' reply to discussion on 'The stratigraphy and origin of the Natal Group' (S. Afr. J. Geol., 102, 15-25). S. Afr. J. Geol., 103, 100-103.

Martin, H. (1953): Notes on the Dwyka succession and on some pre-Dwyka valleys in South West Africa. Trans. Geol. Soc. S. Afr., 56, 37-41.

Martin, H. (1961): The hypothesis of continental drift in the light of recent advances of geological knowledge in Brazil and in South West Africa. Alex. L. du Toit Memorial Lectures No. 7, Annex. Trans. Geol. Soc. S. Afr., 64, 47 pp.

Martin, H. (1973): The Atlantic margin of Southern Africa between latitude 17° south and the Cape of Good Hope. In: Nairn, A.E.M. and Stehli, F.G. (eds.) The ocean basins and margins, the South Atlantic, 1, 277-300.

Martin, H. (1981a): The Late Palaeozoic Dwyka Group of the South Kalahari Basin in Namibia and Botswana and the subglacial valleys of the Kaokoveld in Namibia. In: Hambrey, M.J. and Harland, W.B. (eds.) Earth´s pre-Pleistocene glacial record, Cambridge University Press, New York, 61-66.

Martin, H. (1981b): The Late Palaeozoic Dwyka Group of the Karasburg Basin, Namibia. In: Hambrey, M.J. and Harland, W.B. (eds.) Earth´s pre-Pleistocene glacial record, Cambridge University Press, New York, 67-70.

Martin, H., Walliser, O.H., and Wilczewski, N. (1970): A goniatite from the glaciomarine Dwyka beds near Schlip, South West Africa. Proc. Pap. IUGS 2nd Gondwana Symp., South Africa, 621-625.

Martin, H. and Wilczewski, N. (1970): Palaeoecology, conditions of deposition and the palaeogeography of the marine Dwyka beds of South West Africa. Proc. Pap. IUGS 2nd Gondwana Symp., South Africa, 225-232.

Martini, J.E.J. (1974): On the presence of ash beds and volcanic fragments in the graywackes of the Karoo system in the southern Cape Province (South Africa). Trans. Geol. Soc. S. Afr., 77, 113-116.

Mason, T.R., Stanistreet, I.G., and Tavener-Smith, R. (1983): Spiral trace fossils from the Permian Ecca Group of Zululand. Lethaia, 16, 241-247.

Matos, S.L.F. de, Yamamoto, J.K., Hachiro, J., and Coimbra, A.M. (2000): Tonsteins da Formação Rio Bonito no depósito de carvão Candiota, RS. Rev. Bras. Geociênc., 30, 679-684.

Matos, S.L.F. de, Yamamoto, J.K., Riccomini, C., Hachiro, J., and Tassinari, C.C.G. (2001): Absolute dating of Permian ash-fall in the Rio Bonito Formation, Paraná Basin, Brazil. Gondwana Research, 4, 421-426.

Maynard, J.B., Chocyk-Jaminski, M., Gaines, R.R., Krekeler, M.P., Prokopenko, M., Summers, A.M., and Huff, W.D. (1996): Bentonites in the Late Permian (Tatarian) Irati Formation of Brazil: geochemistry and potential for stratigraphic correlation. Abstracts with Programs, Geol. Soc. Am., 28, p. 280.

McDaid, J.A. (1985): SWA coal project (Aranos Basin). CDM Mineral Surveys, Open file report, Geol. Surv. Namibia, EG 087, 18 pp.

McDonough, W.F. and Sun, S.-s. (1995): The composition of the Earth. Chem. Geol., 120, 223-253.

McLachlan, I.R. and Anderson, A.M. (1973): A review of the evidence for marine conditions in Southern Africa during Dwyka times. Palaeont. Afr., 15, 37-64.

McLachlan, I.R. and Anderson, A.M. (1977): Carbonates, "stromatolites" and tuffs in the lower Permian White Band Formation. S. Afr. J. Sci., 73, 92-94.

McLachlan, I. R. and Jonker, J. P. (1990): Tuff beds in the north-western part of the Karoo Basin. S. Afr. J. Geol., 93, 329-338.

McLachlan, I.R., Tsikos, H., and Cairncross, B. (2001): Glendonites (pseudomorphs after ikaite) in Late Carboniferous marine Dwyka beds in Southern Africa. S. Afr. J. Geol., 104, 265-272.

Meixner, H.M. and Peart, R.J. (1983): GS12 Project: the Kalahari Drilling Project. A report on the geophysical results of follow-up drilling of the Aeromagnetic Survey, 1979-1983.

Meixner, H.M. and Peart, R.J. (1984): The Kalahari Drilling Project. Geol. Surv. Botswana Bull., 27, 224 pp.

Mello, M.R., Koutsoukos, E.A.M., Santos Neto, E.V., and Silva Telles, A.C. Jr. (1993): Geochemical and micropaleontological characterization of lacustrine and marine hyper-saline environments from Brazilian sedimentary basins. In: Katz, B.J. and Pratt, L.M. (eds.) Source rocks in a sequence stratigraphic framework, AAPG studies in geology, 37, 17-34.

Menning, M. and Jin, Y.G. (1998): Comment on 'Permo-Triassic magnetostratigraphy in China: the type section near Taiyuan, Shanxi Province, North China' by B.J.J. Embleton, M.W. McElhinny, X. Ma, Z. Zhang, and Z.X. Li. Geophys. J. Int., 133, 213-216.

Menning, M., Weyer, D., Drozdzewski, G., and van Amerom, H.W.J. (1997): Carboniferous time scales revised. Carboniferous Newsletter, 15, 26-28.

Milani, E.J. and Filho, A.T. (2000): Sedimentary basins of South America. In: Codani, U.G., Milani, E.J., and Thomaz, F.A. (eds.) Tectonic evolution of South America, 389-449.

Milani, E.J. and Zalán, P.V. (1999): An outline of the geology and petroleum systems of the Paleozoic interior basins of South America. Episodes, 22, 199-205.

Millar, I.L., Pankhurst, R.J., and Fanning, C.M. (2002): Basement chronology of the Antarctic Peninsula: recurrent magmatism and anatexis in the Palaeozoic Gondwana margin. J. Geol. Soc. London, 159, 145-157.

Miller, M.F. and Collinson, J.W. (1994) : Late Palaeozoic post-glacial inland sea filled by fine-grained turbidites: Mackellar Formation, Central Transantarctic Mountains. In: Deynoux,

M., Miller, J.M.G., Domack, E.W., Eyles, N., Fairchild, I.J., and Young, G.M. (eds.) Earth´s Glacial Record, Cambridge University Press, 215-233.

Miller, R.McG. (1988): Geological map area 2013 Cape Cross: scale 1:250000. Geol. Surv. Namibia.

Miller, R.McG. (1992): Stratigraphy. In: The mineral resources of Namibia, Geological Survey of Namibia, 1.2-1 – 1.2-34.

Miller, R.McG. and Schalk, K.E.L. (1980): Geological Map of South West Africa/Namibia: scale 1 : 1 000 000. Geol. Surv. Namibia.

Millsteed, B.D. (1994): Palynological evidence for the age of the Permian Karoo coal deposits near Vereeniging, Northern Orange Free State, South Africa. S. Afr. J. Geol., 97, 15-20.

Milner, S.C. (1997): Geological map area 2114 Omaruru: scale 1:250000. Geol. Surv. Namibia.

Minning, M. and Lorenz, V. (1983): Rotliegend-Ignimbrite in der Prims-Mulde (Saar-Nahe-Senke/Südwestdeutschland). Mainzer Geowissenschaftliche Mitteilungen, 12, 261-290.

Minshew, V.H. (1967): Geology of the Scott Glacier and Wisconsin Range areas, central Transantarctic Mountains, Antarctica. Unpubl. Ph.D. thesis, Ohio State Univ., Columbus, 268 pp.

Mountain, E.D. (1939): Pebble beds in the lower Beaufort Series of the East London Division. S. Afr. J. Sci., 26, 164-169.

Mpodozis, C. and Kay, S. Mahlburg (1992): Late Paleozoic to Triassic evolution of the Gondwana margin: evidence from Chilean Frontal Cordilleran batholiths (28°S to 31°S). Geol. Soc. Am. Bull., 104, 999-1014.

Mukasa, S.B. and Dalziel, I.W.D. (2000): Marie Byrd Land, West Antarctica: evolution of Gondwana's Pacific margin constrained by zircon U-Pb geochronology and feldspar common-Pb isotopic compositions. Geol. Soc. Am. Bull., 112, 611-627.

Nesse, W.D. (2000): Introduction to mineralogy. Oxford University Press, Oxford-New York, 442 pp.

Net, L.I. (1999): Petrografía, diagénesis y procedencia de areniscas de la sección inferior del Grupo Paganzo (Carbonífero) en la cuenca homónima. Unpubl. Ph.D. thesis, Universidad de Buenos Aires, Argentina.

Net, L.I., Alonso, M.S. and Limarino, C.O. (2002): Source rock and environmental control on clay mineral associations, lower section of Paganzo Group (Carboniferous), northwest Argentina. Sed. Geol., 152, 183-199.

Oelofsen, B.W. (1987): The biostratigraphy and fossils of the Whitehill and Irati shale formations of the Karoo and Paraná Basins. Gondwana Six: Stratigraphy, sedimentology, and paleontology. Geophys. Monogr. AGU, 41, 131-138.

Oelofsen, B.W. and Araújo, D.C. (1983): Palaeoecological implications of the distribution of mesosaurid reptiles in the Permian Irati sea (Paraná Basin), South America. Rev. Bras. Geociêc., 13, 1-6.

Ogiermann, J.C. (2002): Cordierite and its retrograde breakdown products as monitors of fluid-rock interaction during retrograde path metamorphism: case studies in the Schwarzwald and the Bayerische Wald (Variscan belt, Germany). Dr. rer. nat. thesis, Univ. Heidelberg, 199 pp. [URL: http://www.ub.uni-heidelberg.de/archiv/3082]

Paces, J.B. and Miller, J.D. (1993): Precise U-Pb ages of Duluth Complex and related mafic intrusions, North-eastern Minnesota: Geochronological insights to physical, petrogenic, paleomagnetic and tectonomagmatic processes associated with the 1.1 Ga midcontinent rift system. J. Geophys. Res., 98B, 13997-14013.

Pankhurst, R.J., Rapela, C.W., and Fanning, C.M. (2000): Age and origin of coeval TTG, I- and S-type granites in the Famatinian belt of NW Argentina. Trans. Roy. Soc. Edinburgh, Earth Sci., 91, 151-168.

Pankhurst, R.J., Weaver, S.D., Bradshaw, J.D., Storey, B.C., and Ireland, T.R. (1998): Geochronology and geochemistry of pre-Jurassic superterranes in Marie Byrd Land, Antarctica. J. Geophys. Res., 103B, 2529-2547.

Pearce, J.A., Harris, N.B.W., and Tindle, A.G. (1984): Trace element discrimination diagrams for the tectonic interpretation of granitic rocks. J. Petrol., 25, 956-983.

Pichler, H. and Schmitt-Riegraf, C. (1993): Gesteinsbildende Minerale im Dünnschliff. 2. Auflage, Enke, Stuttgart, 233 pp.

Pintaude, D.A. and Formoso, M.L.L. (1972): Ocorrencia de Argila montmorilonitica em Aceguá-RS. Boletim Instituto Tecnologico do Rio Grande do Sul, 57, p. 40.

Porada, H., Löffler, T., Horsthemke, E., Ledendecker, S., and Martin, H. (1996): Facies and palaeo-environmental trends of northern Namibian Karoo sediments in relation to West Gondwanaland palaeogeography. In: Dimri, D.B. (ed.) 9th Int. Gondwana Symp. 1994, Hyderabad, India, 2, 1101-1114.

Pysklywec, R.N. and Mitrowica, J.X. (1999): The role of subduction-induced subsidence in the evolution of the Karoo Basin. J. Geol., 107, 155-164.

Ramos, V.A. (1994): Terranes of southern Gondwanaland and their control in the Andean structure (30°-33°S latitude). In: Reutter, K.-J., Scheuber, E., and Wigger, P.J. (eds.) Tectonics of the southern Central Andes, 249-261, Springer, Berlin.

Ramos, V.A. (2004): Cuyania, an exotic block to Gondwana: review of a historical success and the present prolems. In: Vujocich, G.I., Fernandes, L.A.D., and Ramos, V.A. (eds.) Cuyania, an exotic block to Gondwana, Gondwana Research, 7, 1009-1026.

Range, P. (1908): Dwykakonglomerat in Deutsch-Südwestafrika. Z. dt. geol. Ges., 60, 64-66.

Range, P. (1912): Geologie des deutschen Namalandes. Beiträge zur geol. Erforsch. Dt. Schutzgeb., 2, 1-104.

Range, P. (1920): Geologische Spezialaufnahmen in Südwestafrika. Beiträge zur geol. Erforsch. Dt. Schutzgeb., 18, 33-42.

Range, P. (1928): Die geologischen Verhältnisse der Karruformation Deutsch-Südwest-afrikas. Beiträge zur geol. Erforsch. Dt. Schutzgeb., 20, 1-16.

Rapela, C.W. (2000): The Sierras Pampeanas of Argentina. In: Codani, U.G., Milani, E.J., and Thomaz, F.A. (eds.) Tectonic evolution of South America, 381-387.

Reid, M.R., Coath, C.D., Harrison, T.M., and McKeegan, K.D. (1997): Prolonged residence times for the youngest rhyolites associated with Long Valley Caldera: ^{230}Th-^{238}U ion microprobe dating of young zircons. Earth Planet. Sci. Lett., 150, 27-39.

Roberts, J., Claoué-Long, J.C., and Foster, C.B. (1996): SHRIMP zircon dating of the Permian System of eastern Australia. Aus. J. Earth Sci., 43, 401-421.

Robertson Research Co. (1967): Data on altered vitric tuff in the White Band. Unpubl. report, 1967-0130, Council of Geoscience, Pretoria, 7 pp.

Robertson Research Co. (1968): Study of a sample from borehole OL1/69. Unpubl. internal SOEKOR report.

Rohn, R. (1994): Evolução ambiental da Bacia do Paraná durante o Neopermiano no leste de Santa Catarina e do Paraná. Unpubl. Ph.D. thesis, Instituto de Geociências, Universidade de São Paulo, 386 pp.

Ross, C.S. and Shannon, E.V. (1926): The minerals of bentonite and related clays and their physical properties. J. Am. Ceramic Soc., 9, 77-96.

Rossouw, P.J., Meyer, E.I., Mulder, M.P., and Stocken, C.P. (1964): Die geologie van die Swartberge, die Kangovallei en die omgewing van Prins Albert, K.P. Explanation to sheet 3321 B (Gampoort) and 3322 A (Prince Albert). Geol. Surv. S. Afr., 93 pp.

Rossouw, P.J. and de Villiers, J. (1953): The geology of the Merweville area, Cape Province. Explanation to sheet 198 (Merweville). Geol. Surv. S. Afr., 70 pp.

Rowsell, D.M. and de Swardt, A.M.J. (1976): Diagenesis in Cape and Karroo sediments, South Africa, and its bearing on their hydrocarbon potential. Trans. Geol. Soc. S. Afr., 79, 81-145.

Rubidge, B.S. (1995): Biostratigraphy of the Beaufort Group (Karoo Supergroup). South African Committee for Stratigraphy ("SACS"), Biostratigraphic Series, 1, 45 pp.

Rubidge, B.S. (2005): Re-uniting lost continents – fossil reptiles from the ancient Karoo and their wanderlust. S. Afr. J. Geol., 108, 135-172.

Rubidge, B.S., Hancox, P.J., and Catuneanu, O. (2000): Sequence analysis of the Ecca-Beaufort contact in the southern Karoo of South Africa. S. Afr. J. Geol., 103, 81-96.

Runnegar, B. and Newell, N.D. (1971): Caspian-like relict molluscan fauna in the South American Permian. Am. Mus. Natural History, 146, 1-66.

Rust, I.C., Shone, R.W., and Siebrits, L.B. (1991): Carnarvon Formasie: golf-oorheersde sedimentasie in ´n vlak Karoosee (Carnarvon Formation: wave mastered sediments in the flat Karroo Basin). S. Afr. J. Sci., 87, 198-202.

SACS (1980): South African Commitee for Stratigraphy: Stratigraphy of South Africa. Part 1 (Comp. Kent, L.E.) Lithostratigraphy of the Republic of South Africa, South West Africa/Namibia, and the Republics of Bophuthatswana, Transkei and Venda. Handb. Geol. Surv. S. Afr., 8, 690 pp.

Sambridge, M.S. and Compston, W. (1994): Mixture modelling of multi-component data sets with application to ion-probe zircon ages. Earth Planet. Sci. Lett., 128, 373-390.

Savage, N.M. (1971): A varvite ichnocoenosis from the Dwyka Series of Natal. Lethaia, 4, 217-233.

Schalk, K.E.L. and Germs, G.J.B. (1980): The geology of the Mariental area. Explanation of Sheet 2416 Scale 1:250000. Geological Survey South West Africa/Namibia, 7 pp.

Scheffler, K., Hoernes, S., and Schwark, L. (2003): Global changes during Carboniferous-Permian glaciation of Gondwana: linking polar and equatorial climate evolution by geochemical proxies. Geology, 31, 605-608.

Schlirf, M. and Werner, M. (2001): (Introduction to our ichnology research interests; with drawings of 'Pseudo-Plagiogmus' from the Ecca Group in southern Namibia). Contribution to the 23rd Ichnology Newsletter, 1 p.

Schmidt, E.R. (1976): Clay. In: Coetzee, C.B. (ed.) Mineral ressources of the Republic of South Africa, 5th edition, Handbk. Geol. Surv. S. Afr., 7, 467 pp.

Schobbenhaus, C., Campos, D.A., Derze, G.R., and Asmus, H.E. (1984): Geologia do Brasil. D.N.P.M., Brasília, 501 pp.

Schreuder, C.P. and Genis, G. (1975): Die Geologie van die Karasburgse Karookom. Ann. Geol. Surv. S. Afr., 10, 7-22.

Schreuder, C.P. and Genis, G. (1977): Explanatory notes to the Geological Map area 2718 Grünau: scale 1:250000. Geol. Surv. Namibia.

Schroeder, H. (1908): Marine Fossilien in Verbindung mit permischem Glazialkonglomerat in Deutsch-Südwestafrika. Jb. Preuss. Geol. Landesanst, Bergakad., 29, 694-697.

Schulze-Hulbe, A. (1979): Geological map area 2616 Bethanien: scale 1:250000. Geol. Surv. Namibia.

Seilacher, A. (1977): Pattern analysis of Paleodictyon and related trace fossils. In: Crimes, T.P. and Harper, J.C. (eds.) Trace fossils 2. Geol. J. Spec. Issue, 9, 289-334.

Selover, R.W. and Gastaldo, R.A. (2005): A reinterpretation of the Wagendrift Quarry, Estcourt, KwaZulu-Natal Province, and its implications for Karoo Basin paleogeography. S. Afr. J. Geol., 108, 429-438.

Shelley, D. (1975): Manual of optical mineralogy. 4th edition, Elsevier, Amsterdam, 240 pp.

Simmonds, A.L.E. (1982): Sedimentology of the Teekloof Formation to the east of Aberdeen (C.P.) with reference to uranium mineralization. Ext. Abstr. Sedimentology `82, Rand Afrikaans Univ., Johannesburg, 26-30.

Simmonds, A.L.E. (1984): The sedimentology of the Teekloof Formation east of Aberdeen (C.P.). Unpubl. M.Sc. thesis, Univ. Port Elizabeth, 115 pp.

Smellie, J.L. (1981): A complete arc-trench system recognized in Gondwana sequences of the Antarctic Peninsula region. Geol. Mag., 118, 139-159.

Smith, R.A. (1984): The lithostratigraphy of the Karoo Supergroup in Botswana. Geol. Surv. Botswana, Bulletin Series, 26, 239 pp.

Spears, D.A., Duff, P.McL.D., and Caine, P.M. (1988): The West Waterberg tonstein, South Africa. Int. J. Coal Geol., 9, 221-233.

Stanistreet, I. G., Le Blanc-Smith, G., and Cadle, A.B. (1980): Trace fossils as sedimentological and palaeoenvironmental indices in the Ecca Group (Lower Permian) of the Transvaal. Trans. Geol. Soc. S. Afr., 83, 333-344.

Stern, T.W., Goldich, S.S., and Newell, M.F. (1966): Effects of weathering on the U-Pb ages of zircon from the Morton gneiss, Minnesota. Earth Planet. Sci. Lett., 1, 369-371.

Stollhofen, H. (1999): Karoo Synrift-Sedimentation und ihre tektonische Kontrolle am entstehenden Kontinentalrand Namibias. Z. dt. geol. Ges., 149, 519-632.

Stollhofen, H., Stanistreet, I. G., Bangert, B., and Grill, H. (2000a): Tuffs, tectonism and glacially related sea-level changes, Carboniferous-Permian, southern Namibia. Palaeogeogr. Palaeoclimatol. Palaeoecol., 161, 127-150.

Stollhofen, H., Stanistreet, I.G., Rohn, R., Holzförster, F., and Wanke, A. (2000b): The Gai-As lake system, northern Namibia and Brazil. In: Gierlowski-Kordesch, E.H. and Kelts, K.R. (eds.) Lake basins through space and time, AAPG Studies in Geology, 46, 87-108.

Stratten, T. (1977): Conflicting directions of Dwyka ice flow in the Western Cape Province and southern South West Africa. Trans. Geol. Soc. S. Afr., 80, 79-86.

Stump, E., Foland, K.A., van Schmus, W.R., Brand, P.K., Dewane, T.J., Gootee, B.F., and Talarico, F. (2002): Geochronology of deformation, intrusion, and cooling during the Ross Orogeny, Byrd Glacier area, Antarctica. Geol. Soc. Am. Abstr. with Prog., 34, 560-561.

Taylor, S.R. and McLennan, S.M. (1988): The significance of the rare earths in geochemistry and cosmochemistry. In: Gschneider, K.A. and Eyring, L. (eds.) Handbook on the physics and chemistry of rare earths. Elsevier, New York, 485-578.

Theron, J.N. and Blignault, H.J. (1975): A model for the sedimentation of the Dwyka glacials in the southwestern Cape. In: Campbell, R.S.W. (ed.) Gondwana Geology, University Press, Canberra, 347-356.

Thomas, R.J., Marshall, C.G.A., Watkeys, M.K., Fitch, F.J., and Miller, J.A. (1992): K-Ar and ^{40}Ar/^{39}Ar dating of the Natal Group, southeast Africa – a post Pan-African molasse? J. Afr. Earth Sci., 15, 453-471.

Tischendorf, G., Förster, H.-J., and Trumbull, R.B. (1995): Evaluation of trace element tectonic discrimination diagrams for silicic igneous rocks. Terra Nostra, 7, 137-140.

du Toit, A.L. (1915): Discussion on Dr. P.A. Wagner's paper entitled "The Dwyka Series in South-West Africa" (within the "Monthly meeting, held in the Council Chamber, Chamber of Mines, Johannesburg, on Monday, 18th October, 1915, at 8.15 p.m., Mr. D. Wilkinson, in the Chair"). Proc. Geol. Soc. S. Afr., 18, xlii-xlvii.

du Toit, A.L. (1916): Notes on the Karoo System in the southern Kalahari. Trans. Geol. Soc. S. Afr., 19, 1-13.

du Toit, A.L. (1921): The Carboniferous glaciation of South Africa. Trans. Geol. Soc. S. Afr., 24, 188-227.

du Toit, A.L (1937): Our wandering continents. Oliver and Boyd, Edinburgh, 366 pp.

Trewin, N.H. (2000): The ichnogenus *Undichna*, with examples from the Permian of the Falkland Islands. Palaeontology, 43, 979-997.

Trewin, N.H., MacDonald, D.I.M., and Thomas, C.G.C. (2002): Stratigraphy and sedimentology of the Permian of the Falkland Islands: lithostratigraphic and palaeo-environmental links with South Africa. J. Geol. Soc. London, 159, 5-19.

Tröger, W.E. (1969): Optische Bestimmung der gesteinsbildenden Minerale. Textband Teil 2, Schweizerbart, Stuttgart, 822 pp.

Trouw, R.A.J. and de Wit, M.J. (1999): Relation between the Gondwanide Orogen and contemporaneous intracratonic deformation. J. Afr. Earth Sci., 28, 203-213.

Tucker, E.M. (2001): Sedimentary petrology. Blackwell Science, 3rd edition, 262 pp.

Turner, B.R. (1971): Coal Resources of the North-East Cape Province. Bull. Geol. Surv. S. Afr., 52, 74 pp.

Turner, B.R. (1999): Tectonostratigraphical development of the Upper Karoo foreland basin: orogenic unloading versus thermally-induced Gondwana rifting. J. Afr. Earth Sci., 28, 215-238.

Uysal, I.T. and Golding, S.D. (2003): Rare earth element fractionation in authigenic illite-smectite from Late Permian clastic rocks, Bowen Basin, Australia: implications for physico-chemical environments of fluids during illitization. Chem. Geol., 193, 167-179.

Veevers, J.J. (2000): Billion-year earth history of Australia and neighbours in Gondwanaland. Gemoc Press, Sydney, 388 pp.

Veevers, J.J. (2001): Atlas of billion-year earth history of Australia and neighbours in Gondwanaland. Gemoc Press, Sydney, 76 pp.

Veevers, J.J., Cole, D.I., and Cowan, E.J. (1994): Southern Africa: Karoo Basin and Cape Fold Belt. In: Veevers, J.J. and Powell, C.McA. (eds.) Permian-Triassic Pangean basins and foldbelts along the Panthalassan margin of Gondwanaland, Geol. Soc. Am. Mem., 184, 223-279.

Venter, J.J. (1969): Stratigraphy and correlation of the Cape and Karoo Supergroups in the Southern Cape Province. Internal report SOEKOR, 38 pp.

Versfeld, W. (1914): The geological structure of portions of German South-West Africa. S. Afr. J. Sci., 10, 187-238.

Verwoerd, W.J., Viljoen, J.H.A., and Viljoen, K.S. (1990): Olivine melilitites and associated intrusives of the southwestern Cape Province. Guidebook, Geocongress 1990, Geol. Soc. S. Afr., PR3, 60 pp.

Viljoen, J.H.A. (1987): Subaqueous fallout tuffs of the Ecca Group in the southern Cape Province. In: Brown, G. and Preston, V.A. (eds.) Workshop on pyroclastic volcanism and associated deposits, Univ. Natal, Pietermaritzburg, 45-48.

Viljoen, J.H.A. (1990): K-bentonites in the Ecca Group in the south and central Karoo Basin. Abstr. Geocongr. 1990 Geol. Soc. S. Afr., Johannesburg, 574-577.

Viljoen, J.H.A. (1992a): Lithostratigraphy of the Collingham Formation (Ecca Group), including the Zoute Kloof, Buffels River and Wilgehout River Members and the Matjiesfontein Chert Bed. South African Committee for Stratigraphy ("SACS"), Lithostratigraphic Series, 22, 10 pp.

Viljoen, J.H.A. (1992b): Lithostratigraphy of the Laingsburg Formation (Ecca Group). South African Committee for Stratigraphy ("SACS"), Lithostratigraphic Series, 20, 7 pp.

Viljoen, J.H.A. (1994): Sedimentology of the Collingham Formation, Karoo Supergroup. S. Afr. J. Geol. 94, 167-183.

Viljoen, J.H.A. (1995) : Piroklastiese afsettings van Perm-ouderdom in die Karookom met spesiale verwysing na die Collingham Formasie. Unpubl. Ph.D. thesis, Univ. Stellenbosch, 278 pp.

Viljoen, J.H.A. (1998): Distribution of altered volcanic ash beds in the Dwyka and Ecca Groups of the Main Karoo Basin, South Africa. J. Afr. Earth Sci., 27(1A), 204-206.

Viljoen, J.H.A. and Wickens, H. de V. (1992): Lithostratigraphy of the Vischkuil Formation (Ecca Group). South African Committee for Stratigraphy ("SACS"), Lithostratigraphic Series, 19, 7 pp.

de Villiers, J. and Söhnge, P.G. (1959): The geology of the Richtersveld. Mem. Geol Surv. S. Afr., 48, 295 pp.

Visser, J.N.J. (1982): Implications of a diachronous contact between the Dwyka Formation and Ecca Group in the Karoo Basin. S. Afr. J. Sci., 78, 249-251.

Visser, J.N.J. (1983a): An analysis of the Permo-Carboniferous glaciation in the marine Kalahari Basin, Southern Africa. Palaeogeogr., Palaeoclimatol., Palaeoecol., 44, 295-315.

Visser, J.N.J. (1983b): Glacial-marine sedimentation in the Late Paleozoic Karoo Basin, southern Africa. In: Molnia, B.F. (ed.) Glacial-marine sedimentation, Plenum Press, New York, 667-701.

Visser, J.N.J. (1987a): The influence of topography on the Permo-Carboniferous glaciation in the Karoo Basin and adjoining areas, southern Africa. Gonwana six: Stratigraphy, sedimentology, and paleontology. Geophys. Monogr. AGU, 41, 123-129.

Visser, J.N.J. (1987b): The palaeogeography of part of southwestern Gondwana during the Permo-Carboniferous glaciation. Palaeogeogr., Palaeoclimatol., Palaeoecol., 61, 205-219.

Visser, J.N.J. (1989): The Permo-Carboniferous Dwyka Formation of Southern Africa: deposition by a predominantly subpolar marine ice sheet. Palaeogeogr., Palaeoclimatol., Palaeoecol., 70, 377-391.

Visser, J.N.J. (1990): The age of the late Palaeozoic glacigene deposits in southern Africa. S. Afr. J. Geol., 93, 366-375.

Visser, J.N.J. (1991a): Self-destructive collapse of the Permo-Carboniferous marine ice sheet in the Karoo Basin: evidence from the southern Karoo. S. Afr. J. Geol., 94, 255-262.

Visser, J.N.J. (1991b): The paleoclimatic setting of the late Paleozoic marine ice sheet in the Karoo Basin of southern Africa. In: Anderson, J.B. & Ashley, G.M. (eds.) Glacial marine sedimentation: Paleoclimatic significance. Geol. Soc. Am. Spec. Paper, 261, 181-189.

Visser, J.N.J. (1992a): Basin tectonics in southwestern Gondwana during the Carboniferous and Permian. In: De Wit, M.J. & Ransome, I.G.D. (eds.) Inversion tectonics of the Cape Fold Belt, Karoo and Cretaceous Basins of Southern Africa, 109-116.

Visser, J.N.J. (1992b): Deposition of the Early to Late Permian Whitehill Formation during a sea-level highstand in a juvenile foreland basin. S. Afr. J. Geol., 95, 181-193.

Visser, J.N.J. (1993a): A reconstruction of the Late Palaeozoic ice sheet on southwestern Gondwana. In: Findlay, R.H., Unrug, R., Banks, M.R., and Veevers, J.J. (eds.) Gondwana Eight – assembly, evolution and dispersal. Proc. 8th Gondwana Symp. 1991, Hobart, Australia, 449-458.

Visser, J.N.J. (1993b): Sea-level changes in a back-arc-foreland transition: the Late Carboniferous-Permian Karoo Basin of South Africa. Sed. Geol., 83, 115-131.

Visser, J.N.J. (1994): A Permian argillaceous syn- to post-glacial foreland sequence in the Karoo Basin, South Africa. In: Deynoux, M., Miller, J.M.G., Domack, E.W., Eyles, N., Fairchild, I.J. & Young, G.M. (eds.) Earth´s glacial record, Cambridge University Press, Cambridge, 193-203.

Visser, J.N.J. (1995): Post-glacial Permian stratigraphy and geography of southern and central Africa: boundary conditions for climatic modelling. Palaeogeogr., Palaeoclimatol., Palaeoecol., 118, 213-243.

Visser, J.N.J. (1996): Controls on Early Permian shelf deglaciation in the Karoo Basin of South Africa. Palaeogeogr. Palaeoclimatol. Palaeoecol., 125, 129-139.

Visser, J.N.J. (1997a): A review of the Permo-Carboniferous glaciation in Africa. In: Martini, I.P. (ed.) Late glacial and postglacial environmental changes, 169-191.

Visser, J.N.J. (1997b): Deglaciation sequences in the Permo-Carboniferous Karoo and Kalahari Basins of southern Africa: a tool in the analysis of cyclic glaciomarine basin fills. Sedimentology, 44, 507-521.

Visser, J.N.J. and Praekelt, H.E. (1996): Subduction, mega-shear systems and late Palaeozoic basin development in the African segment of Gondwana. Geol. Rundsch., 85, 632-646.

Visser, J.N.J. & Praekelt, H.E. (1998): Late Palaeozoic crustal block rotations within the Gondwana sector of Pangea. Tectonophysics, 287, 201-212.

Wagner, P.A. (1915): The Dwyka Series in South-West Africa. Trans. Geol. Soc. S. Afr., 18, 102-117.

van Wagoner, J.C., Posamentier, H.W., Mitchum, R.M., Vail, P.R., Sarg, J.F., Loutit, T.S., and Hardenbol, J. (1988): An overview of the fundamentals of sequence stratigraphy and key definitions. In: Wilgus, C.K., Hastings, B.S., Kendall, C.G.St.C., Posamentier, H.W., Ross, C.A., and van Wagoner, J.C. (eds.) Sea-level changes: an integrated approach. SEPM Spec. Publ., 42, 39-45.

Wanke, A. (2000): Karoo-Etendeka unconformities in NW Namibia and their tectonic implications. Dr. rer. nat. thesis, Univ. Würzburg, 167 pp. [URL: http://opus.bibliothek.uni-wuerzburg.de/opus/volltexte/2002/323/]

Wanke, A., Stollhofen, H., Stanistreet, I.G., and Lorenz, V. (2000): Karoo unconformities in NW Namibia and their tectonic implications. Communs Geol. Surv. Namibia, 12, 259-268.

Wass, R.E. (1970): Bryozoa from the Dwyka Series and their palaeogeographic significance. Ann. Geol. Surv. S. Afr., 8, 95-97.

Wass, R.E. (1972): Permian bryozoa from South Africa. J. Paleont., 46, 871-873.

Watson, E.B. (1996): Dissolution, growth and survival of zircons during crustal fusion: kinetic principles, geologic models and implications for isotopic inheritance. Proc. Roy. Soc. Edinburgh, 8, 43-56.

Watson, E.B., Cherniak, D.J., Hanchar, J.M., Harrison, T.M., and Wark, D.A. (1997): The incorporation of Pb into zircon. Chem. Geol., 141, 19-31.

Werner, M. and Cook, N.J. (2001): Nb-rich brookite from Gross Brukkaros, Namibia: substitution mechanisms and Fe^{2+}/Fe^{3+} ratios. Mineral. Mag., 65, 431-434.

Werner, M., Stanistreet, I.G., and Stollhofen, H. (2002): Tracing the Whitehill Fm. (Karoo Supergroup) into Namibia: a combined lithostratigraphic, biostratigraphic, tephro-stratigraphic, and sequence-stratigraphic approach. Abstr. 16th Int. Sed. Congr. 2002, Johannesburg, South Africa, 399-400.

Werner, M. and Stollhofen, H. (2004): The Albin Ridge in NW-Namibia: a fragmental, multi-unconformity stratigraphic record due to deposition on an uplifted palaeo-rift shoulder. Schriftenreihe dt. geol. Ges., 33, p. 177.

van der Westhuizen, W.A., Loock, J.C., and Strydom, D. (1981): Halite imprints in the Whitehill Formation, Ecca Group, Carnarvon District. Ann. Geol. Surv. S. Afr., 15, 43-46.

Wickens, H. de V. (1984): Die Stratigrafie en Sedimentologie van die Groep Ecca wes van Sutherland. Unpubl. M.Sc. thesis, Univ. Port Elizabeth, 86 pp.

Wickens, H. de V. (1996): Die Stratigrafie en Sedimentologie van die Ecca Groep wes van Sutherland. Bull. Geol. Surv. S. Afr., 107, 49 pp.

Williams, I.S. (1998): U-Th-Pb geochronology by ion microprobe. In: McKibben, M.A., Shanks, W.C., and Ridley, W.I. (eds) Applications of microanalytical techniques to understanding mineralizing processes, Reviews in Economic Geology, 7, 1-35.

Williams, I.S., Compston, W., Foster, J.J., Page, R.W., and McColloch, M.T. (1988): The comparison of conventional and SHRIMP ion probe ages. Abstr. 1st Australian Conf. On Geochronology, Canberra, p. 1.

Williams, K.E. (1995): Tectonic subsidence analysis and Paleozoic paleogeography of Gondwana. In: Tankard, A.J., Suárez Soruco, R., and Welsink, H.J. (eds.) Petroleum basins of South America. AAPG Mem., 62, 79-100.

Wilson, E.J. (1964): Core description, Vreda 281, no.1. Unpubl. rep., Artnell Exploration Company, 18 pp.

Wilson, M. (1989): Igneous petrogenesis. Chapman & Hall, London, 466 pp.

Winchester, J.A. and Floyd, P.A. (1977): Geochemical discrimination of different magma series and their differentiation products using immobile elements. Chem. Geol., 20, 325-343.

Winter, H. de la R. and Kingsley, C.S. (2000): Discussion on 'The stratigraphy and origin of the Natal Group' (S. Afr. J. Geol., 102, 15-25). S. Afr. J. Geol., 103, 99-100.

Winter, M.F. (1990): Supplementary geological report, Grant M46/3/1761 (Vreda), Open file report, Geol. Surv. Namibia, 2 pp.

de Wit, M.J. and Anderson, J.M. (2003): Gondwana Alive corridors: extending Gondwana research to incorporate the sixth extinction. Gondwana Research, 6, 369-408.

Wopfner, H. (2002): Tectonic and climatic events controlling deposition in Tanzanian Karoo basins. J. Afr. Earth Sci., 34, 167-177.

Wysoczanski, R.J., Forsyth, P.J., and Woolfe, K.J. (2003): Zircon dating and provenance of rhyolitic clasts in Beacon Conglomerate, southern Victoria Land, Antarctica. Terra Antarctica, 10, 67-79.

Ziegler, A.M., Hulver, M.L., and Rowley, D.B. (1997): Permian world topography and climate. In: Martini, I.P. (ed.) Late glacial and postglacial environmental changes, Oxford Univ. Press, 111-146.

APPENDIX – GEOCHEMISTRY   PAGE I

Geochemistry of altered tuff layers from the Ecca Group of southern Namibia
Major and trace element data: XRD – Institute of Mineralogy, University of Würzburg/Germany

sample	OG-9-1	OG-9-2	OG-12l	OG-12d	DIBA-2	DIBA-3	DIBA-4	TUBA-lo
locality	Owl Gorge	Owl Gorge	Owl Gorge	Owl Gorge	Itzawisis	Itzawisis	Itzawisis	Itzawisis
outcrop area	AK-NO	AK-NO	AK-NO	AK-NO	MT-KH	MT-KH	MT-KH	MT-KH
stratigraphy	Prince Albert Fm.	Prince Albert Fm.	Prince Albert Fm.	Prince Albert Fm.	Prince Albert Fm.	Prince Albert Fm.	Prince Albert Fm.	Prince Albert Fm.
SiO_2	51,21	51,60	48,02	42,46	56,84	66,83	66,85	62,77
TiO_2	0,32	0,32	1,00	0,92	0,41	0,44	0,48	0,75
Al_2O_3	30,32	29,85	29,40	27,79	27,92	19,44	19,00	21,36
Fe_2O_3	2,20	2,43	3,57	2,26	1,56	2,58	2,89	3,45
MnO	0,06	0,05	0,14	0,20	0,01	0,01	0,01	0,03
MgO	1,35	1,46	1,80	1,14	0,73	0,77	0,91	1,20
CaO	0,30	0,25	1,38	6,78	1,29	0,79	0,64	0,83
Na_2O	0,79	1,03	1,13	0,91	1,11	0,76	0,86	1,15
K_2O	7,08	7,05	6,00	6,21	3,34	2,78	2,93	2,46
P_2O_5	0,12	0,11	0,79	4,76	0,05	0,07	0,08	0,04
S	<0,02	<0,02	<0,02	<0,02	<0,02	<0,02	<0,02	<0,02
F	nd	nd	nd	nd	nd	nd	nd	nd
CO_2	nd	nd	<0,1	0,1	nd	nd	nd	nd
sum	93,75	94,15	93,23	93,43	93,26	94,47	94,65	94,04
LOI	5,23	4,82	5,45	5,11	6,07	4,45	4,30	5,03
TOTAL	**98,98**	**98,97**	**98,68**	**98,54**	**99,33**	**98,92**	**98,95**	**99,07**
Cr	<10	<10	<10	10	<10	29	32	63
Co	<10	12	<10	<10	<10	<10	<10	20
Ni	10	6	11	7	<5	8	11	28
V	59	51	105	105	38	61	62	95
Mo	<5	<5	<5	<5	<5	<5	<5	<5
Sn	<15	<15	<15	<15	<15	<15	<15	<15
Zn	88	92	172	174	39	39	36	77
Pb	34	25	29	17	24	29	19	21
Ga	27	28	26	23	19	22	23	27
Rb	241	238	213	204	156	151	160	136
Sr	55	83	116	174	292	157	124	215
Ba	750	681	866	807	623	591	601	527
Zr	156	181	231	187	228	196	208	215
Nb	<5	6	36	34	18	21	20	18
Th	33	35	48	51	51	37	34	30
U	<5	<5	<5	<5	<5	<5	<5	<5
Sc	18	13	18	10	<10	<10	<10	14
Y	20	20	67	213	36	35	37	33

APPENDIX – GEOCHEMISTRY   PAGE II

Geochemistry of altered tuff layers from the Ecca Group of southern Namibia
Major and trace element data: XRD – Institute of Mineralogy, University of Würzburg/Germany

sample	TUBA-up	Kora1-1T3a	Kora1-1T3c	Kora1-3T11	UHB-T	UHB-TP	KHA-1AT	KHA-1BT
locality	Itzawisis	Korabib	Korabib	Korabib	Uhabis River	Uhabis River	Khabus	Khabus
outcrop area	MT-KH	AK-NO	AK-NO	AK-NO	AK-NO	AK-NO	MT-KH	MT-KH
stratigraphy	Prince Albert Fm.	Prince Albert Fm.	Prince Albert Fm.	Prince Albert Fm.	Prince Albert Fm.	Prince Albert Fm.	Whitehill Fm.	Whitehill Fm.
SiO_2	63,26	60,54	59,88	60,32	51,72	41,37	64,54	73,03
TiO_2	0,75	0,68	0,65	0,55	0,58	0,41	0,54	0,61
Al_2O_3	21,53	23,01	24,06	23,76	28,20	21,91	19,50	14,34
Fe_2O_3	3,24	3,89	3,35	3,20	3,01	2,19	1,66	1,70
MnO	0,05	0,06	0,02	0,02	0,02	0,03	0,03	0,02
MgO	1,14	0,63	0,57	0,46	1,14	0,78	0,45	0,25
CaO	0,90	0,73	0,66	0,67	0,85	11,79	0,70	0,49
Na_2O	1,41	0,96	0,72	0,74	3,61	3,60	9,76	7,28
K_2O	2,45	3,88	4,33	4,25	5,40	3,89	0,69	0,31
P_2O_5	0,06	0,16	0,13	0,12	0,49	8,51	0,13	0,10
S	<0,02	<0,02	<0,02	<0,02	<0,02	0,02	<0,02	<0,02
F	nd	nd	nd	nd	nd	0,80	nd	nd
CO_2	nd	nd	nd	nd	<0,1	0,1	nd	nd
sum	94,79	94,54	94,37	94,09	95,02	95,30	98,00	98,13
LOI	4,77	4,60	4,75	4,83	4,10	3,28	0,76	0,84
TOTAL	99,56	99,14	99,12	98,92	99,12	98,58	98,76	98,97
Cr	56	25	27	33	<10	<10	20	43
Co	26	<10	<10	<10	<10	<10	<10	12
Ni	29	9	9	<5	8	<5	8	15
V	89	84	85	79	56	57	55	55
Mo	<5	<5	<5	<5	<5	<5	<5	<5
Sn	<15	<15	<15	<15	18	<15	<15	<15
Zn	83	66	58	43	60	41	91	171
Pb	21	12	10	15	8	6	27	47
Ga	15	27	26	28	27	28	9	15
Rb	135	231	269	223	295	213	39	17
Sr	231	124	103	89	189	311	117	71
Ba	525	790	920	794	537	382	141	110
Zr	218	261	234	269	270	148	202	212
Nb	19	24	22	27	15	20	15	17
Th	37	24	29	33	62	44	33	21
U	<5	<5	<5	<5	<5	10	<5	<5
Sc	12	17	<10	15	18	12	<10	10
Y	34	51	45	46	51	360	34	36

APPENDIX – GEOCHEMISTRY   PAGE III

Geochemistry of altered tuff layers from the Ecca Group of southern Namibia
Major and trace element data: XRD – Institute of Mineralogy, University of Würzburg/Germany

sample	KHA-1CT	Pano1	Pano2	Eisen-99B	UFO-35T	UFO-38.4T	UFO-38.5T	UFO-40.65T
locality	Khabus	Panorama	Panorama	Eisenstein	Ufo Valleys	Ufo Valleys	Ufo Valleys	Ufo Valleys
outcrop area	MT-KH	MT-KH	MT-KH	MT-KH	AK-NO	AK-NO	AK-NO	AK-NO
stratigraphy	Whitehill Fm.	Whitehill Fm.	Whitehill Fm.	Whitehill Fm.	Collingham Fm.	Collingham Fm.	Collingham Fm.	Collingham Fm.
SiO_2	67,44	72,76	57,70	53,48	51,83	52,77	51,88	51,44
TiO_2	0,68	0,65	0,62	0,54	0,39	0,70	0,53	0,32
Al_2O_3	18,45	15,05	24,98	25,59	28,08	26,84	28,89	29,74
Fe_2O_3	0,65	1,46	2,79	1,18	2,13	2,34	1,64	1,99
MnO	0,02	0,02	0,02	0,05	0,04	0,03	0,07	0,04
MgO	0,34	0,47	1,27	1,90	1,32	1,44	1,01	1,24
CaO	0,30	0,55	0,91	7,52	0,83	0,67	0,36	0,28
Na_2O	10,07	5,15	1,29	4,86	1,09	1,37	0,84	0,82
K_2O	0,47	0,92	4,97	1,84	9,12	9,27	9,79	9,02
P_2O_5	0,11	0,07	0,17	0,22	0,24	0,08	0,05	0,04
S	<0,02	<0,02	<0,02	<0,02		<0,02	<0,02	<0,02
F	nd	nd	nd	nd	nd	nd	nd	nd
CO_2	nd	nd	nd	nd	nd	nd	nd	nd
sum	98,53	97,10	94,72	97,18	95,07	95,51	95,06	94,93
LOI	0,44	1,84	4,51	1,30	3,78	3,48	3,91	4,29
TOTAL	**98,97**	**98,94**	**99,23**	**98,48**	**98,85**	**98,99**	**98,97**	**99,22**
Cr	42	39	18	<10	<10	<10	<10	<10
Co	<10	<10	<10	<10	<10	10	<10	<10
Ni	<5	<5	10	<5	<5	21	<5	<5
V	71	68	81	47	40	98	91	33
Mo	<5	<5	<5	<5	<5	<5	<5	<5
Sn	<15	<15	<15	<15	21	<15	<15	17
Zn	33	61	55	70	55	57	69	71
Pb	<5	6	6	39	28	29	30	22
Ga	14	8	23	21	26	27	24	37
Rb	26	52	286	113	352	504	444	363
Sr	37	267	235	673	347	352	243	209
Ba	96	262	910	2369	1449	1370	1307	898
Zr	224	205	149	205	168	367	282	207
Nb	17	14	10	8	18	10	10	13
Th	21	15	53	58	65	34	54	61
U	<5	<5	<5	8	<5	<5	6	<5
Sc	12	14	<10	13	<10	19	19	12
Y	36	32	25	20	29	49	34	24

APPENDIX – GEOCHEMISTRY PAGE IV

Geochemistry of altered tuff layers from the Ecca Group of southern Namibia
Major and trace element data: XRD – Institute of Mineralogy, University of Würzburg/Germany

sample	UFO-41.1-3T	UFO-43T	UFO-44.98T	UFO-47.00T	UFO-47.27T	UFO-49.95T	UFO-52.95T	UFO-TP
locality	Ufo Valleys	Ufo Valleys	Ufo Valleys	Ufo Valleys	Ufo Valleys	Ufo Valleys	Ufo Valleys	Ufo Valleys
outcrop area	AK-NO	AK-NO	AK-NO	AK-NO	AK-NO	AK-NO	AK-NO	AK-NO
stratigraphy	Collingham Fm.	Collingham Fm.	Collingham Fm.	Collingham Fm.	Collingham Fm.	Collingham Fm.	Collingham Fm.	Collingham Fm.
SiO_2	52,99	51,48	52,03	50,19	51,59	50,91	51,65	49,21
TiO_2	0,46	0,37	1,27	0,62	0,63	0,48	0,49	1,12
Al_2O_3	27,52	29,48	27,30	28,93	28,43	28,71	28,38	25,12
Fe_2O_3	1,99	1,73	1,85	2,62	1,95	2,63	2,66	1,62
MnO	0,04	0,04	0,04	0,07	0,06	0,03	0,02	0,04
MgO	1,17	1,58	1,21	1,32	1,28	1,35	1,45	1,15
CaO	0,60	0,81	1,31	0,62	0,49	0,48	0,48	4,40
Na_2O	1,37	0,54	1,44	0,81	1,32	0,74	0,85	1,14
K_2O	8,82	8,26	8,95	9,25	9,50	8,82	8,78	8,65
P_2O_5	0,18	0,09	0,37	0,23	0,09	0,10	0,10	2,69
S	<0,02	<0,02	<0,02	<0,02	<0,02	<0,02	<0,02	<0,02
F	nd	nd	nd	nd	nd	nd	nd	nd
CO_2	nd	nd	nd	nd	nd	nd	nd	<0,1
sum	95,14	94,38	95,77	94,66	95,34	94,25	94,86	95,14
LOI	3,84	4,47	3,41	4,21	3,61	4,62	4,22	3,63
TOTAL	**98,98**	**98,85**	**99,18**	**98,87**	**98,95**	**98,87**	**99,08**	**98,77**
Cr	<10	<10	20	<10	<10	<10	<10	27
Co	<10	<10	10	36	10	11	<10	13
Ni	6	<5	13	14	6	<5	7	12
V	65	16	125	42	58	25	34	119
Mo	<5	<5	<5	<5	<5	<5	<5	<5
Sn	<15	<15	<15	25	<15	<15	<15	<15
Zn	65	75	84	90	67	99	54	80
Pb	45	34	64	55	44	32	36	55
Ga	32	33	29	37	27	30	27	25
Rb	403	339	377	410	372	424	334	354
Sr	381	276	372	232	290	279	248	380
Ba	1055	728	1290	1163	1382	847	817	1173
Zr	270	411	517	418	447	233	331	403
Nb	9	30	48	22	22	29	15	42
Th	45	56	90	50	46	45	50	86
U	<5	6	12	7	<5	<5	<5	15
Sc	13	<10	16	<10	17	10	11	20
Y	30	54	70	60	64	34	41	148

APPENDIX – GEOCHEMISTRY   PAGE V

Geochemistry of altered tuff layers from the Ecca Group of southern Namibia
Major and trace element data: XRD – Institute of Mineralogy, University of Würzburg/Germany

outcrop areas:
AK-NO: Aussenkjer-Noordoewer
MT-KH: Mariental-Keetmanshoop

nd: not determined

sample	INB-6T	Rf-28c	Rf-28f
locality	Ufo Valleys	Rhyofontein	Rhyofontein
outcrop area	AK-NO	AK-NO	AK-NO
stratigraphy	Collingham Fm.	Collingham Fm.	Collingham Fm.
SiO_2	51,37	52,36	50,34
TiO_2	0,83	0,71	0,61
Al_2O_3	29,39	24,75	27,28
Fe_2O_3	1,79	3,53	2,95
MnO	0,02	0,42	0,18
MgO	0,93	2,24	1,87
CaO	0,46	3,57	2,56
Na_2O	0,73	2,77	1,75
K_2O	8,85	5,79	7,56
P_2O_5	0,12	0,45	0,41
S	<0,02	<0,02	<0,02
F	nd	nd	nd
CO_2	nd	<0,1	nd
sum	94,49	96,59	95,51
LOI	4,68	2,84	3,57
TOTAL	**99,17**	**99,43**	**99,08**
Cr	<10	17	<10
Co	<10	<10	<10
Ni	<5	<5	<5
V	49	68	58
Mo	<5	<5	<5
Sn	<15	<15	<15
Zn	78	52	51
Pb	49	194	126
Ga	33	22	33
Rb	346	293	362
Sr	226	724	520
Ba	925	1320	1038
Zr	448	383	333
Nb	39	26	29
Th	55	71	79
U	<5	10	7
Sc	17	13	11
Y	56	38	38

APPENDIX – GEOCHEMISTRY   PAGE VI

Geochemistry of altered tuff layers from the Ecca Group of southern Namibia
Trace and rare earth element data: ICP-MS – Actlabs Ltd., Ancaster/Canada

sample	OG-9-1	OG-12l	OG-12d	DIBA-2	TUBA-up	Kora1-1T3a	Kora1-3T11	UHB-T
locality	Owl Gorge	Owl Gorge	Owl Gorge	Itzawisis	Itzawisis	Korabib	Korabib	Uhabis River
outcrop area	AK-NO	AK-NO	AK-NO	MT-KH	MT-KH	AK-NO	AK-NO	AK-NO
stratigraphy	Prince Albert Fm.	Prince Albert Fm.	Prince Albert Fm.	Prince Albert Fm.	Prince Albert Fm.	Prince Albert Fm.	Prince Albert Fm.	Prince Albert Fm.
V	53	108	89	31	92	66	63	44
Cr	<20	<20	<20	<20	65	29	30	<20
Co	5	4	4	6	23	4	2	2
Ni	<20	25	<20	<20	38	21	<20	<20
Cu	13	69	<10	<10	31	<10	<10	24
Zn	84	154	144	<30	74	56	49	58
Ga	30	32	29	22	26	25	28	31
Ge	1	2	<1	2	2	1	2	1
As	<5	<5	9	6	17	<5	8	6
Rb	266	252	234	184	166	237	243	330
Sr	83	120	178	293	236	114	86	193
Y	22	73	223	39	35	50	49	55
Zr	167	193	159	214	220	239	246	199
Nb	5	30	23	19	20	19	23	14
Mo	<2	<2	<2	<2	<2	<2	<2	<2
Ag	<0,5	<0,5	<0,5	<0,5	<0,5	<0,5	<0,5	<0,5
In	<0,2	<0,2	0,2	<0,2	<0,2	<0,2	<0,2	0,2
Sn	6	6	5	6	4	5	6	8
Sb	<0,5	<0,5	<0,5	<0,5	1,1	<0,5	0,8	0,5
Cs	5,4	4,8	4,7	17,2	14,8	10,2	9,2	14,0
Ba	736	991	900	680	587	841	886	608
La	102	211	156	42,8	57,2	67,4	66,7	154
Ce	192	401	321	103	121	130	131	290
Pr	21,2	47,0	47,7	10,6	12,4	14,3	14,0	32,9
Nd	80,1	180	255	38,3	45,6	54,8	52,2	125
Sm	11,9	32,9	85,1	7,9	8,6	10,8	11,2	21,1
Eu	1,43	7,40	19,4	1,38	1,65	1,73	1,84	3,37
Gd	5,7	29,4	94,3	6,4	6,6	9,1	9,9	14,8
Tb	0,6	3,9	12,6	1,2	1,1	1,5	1,6	2,0
Dy	3,7	16,9	51,1	6,9	6,2	8,5	8,8	10,3
Ho	0,7	2,4	6,7	1,3	1,2	1,6	1,6	1,8
Er	2,2	5,6	13,4	3,7	3,5	4,9	4,9	4,9
Tm	0,35	0,63	1,34	0,60	0,54	0,75	0,78	0,67
Yb	2,2	4,2	7,1	3,9	3,5	5,0	5,1	4,4
Lu	0,31	0,55	0,82	0,57	0,49	0,75	0,76	0,60
Hf	8,3	9,9	8,2	8,7	6,9	8,0	9,3	8,8
Ta	2,9	2,7	2,3	4,7	2,3	1,8	2,9	3,0
W	3	4	4	1	3	3	3	3
Tl	1,2	1,4	1,2	1,4	1,3	2,2	2,5	2,8
Pb	19	25	17	9	19	11	20	13
Bi	<0,4	0,6	0,7	<0,4	1,0	0,5	1,0	<0,4
Th	37,0	53,5	43,8	49,6	35,5	24,2	36,9	66,7
U	3,7	8,3	13,4	10,9	7,8	9,5	9,7	9,8

APPENDIX – GEOCHEMISTRY   PAGE VII

Geochemistry of altered tuff layers from the Ecca Group of southern Namibia
Trace and rare earth element data: ICP-MS – Actlabs Ltd., Ancaster/Canada

	UHB-T (rep) Uhabis River AK-NO Prince Albert Fm.	KHA-1BT Khabus MT-KH Whitehill Fm.	KHA-1CT Khabus MT-KH Whitehill Fm.	Pano1 Panorama MT-KH Whitehill Fm.	Pano2 Panorama MT-KH Whitehill Fm.	Eisen-99B Eisenstein MT-KH Whitehill Fm.	UFO-38.5T Ufo Valleys AK-NO Collingham Fm.	UFO-43T Ufo Valleys AK-NO Collingham Fm.
V	44	49	73	65	83	45	95	10
Cr	<20	45	56	52	27	<20	<20	<20
Co	2	10	3	1	2	2	6	<1
Ni	<20	23	<20	34	<20	<20	<20	<20
Cu	26	28	18	22	11	11	17	66
Zn	53	190	41	61	50	96	72	81
Ga	32	12	17	14	23	23	26	35
Ge	2	1	<1	2	2	1	2	1
As	<5	42	<5	<5	<5	6	12	<5
Rb	339	25	39	70	336	141	508	385
Sr	198	66	34	267	239	679	246	283
Y	56	36	37	34	29	20	36	60
Zr	216	219	229	208	130	170	183	317
Nb	15	15	16	15	11	8	10	27
Mo	<2	<2	<2	<2	<2	<2	<2	<2
Ag	<0,5	<0,5	<0,5	<0,5	<0,5	<0,5	<0,5	<0,5
In	0,2	<0,2	<0,2	<0,2	<0,2	<0,2	<0,2	<0,2
Sn	9	1	2	<1	6	1	5	6
Sb	<0,5	2,4	<0,5	<0,5	<0,5	1,4	1,0	1,0
Cs	14,4	4,1	3,7	5,8	9,5	8,7	13,5	14,8
Ba	628	105	105	281	1.020	2.620	1.380	805
La	156	39,1	21,6	34,2	38,1	14,2	22,5	104
Ce	297	70,5	45,6	67,7	74,1	30,2	52,8	217
Pr	33,6	7,67	5,28	8,06	8,61	3,33	5,40	24,5
Nd	127	30,1	21,2	31,0	32,1	12,5	19,4	93,1
Sm	21,2	6,5	5,1	6,8	6,5	2,2	4,0	17,9
Eu	3,47	1,57	1,47	0,90	1,46	0,72	0,95	2,78
Gd	15,0	6,3	5,4	5,8	5,6	2,2	4,2	13,0
Tb	2,0	1,1	1,0	1,1	0,9	0,4	0,9	1,9
Dy	10,2	6,0	6,3	6,1	5,2	2,9	6,1	10,6
Ho	1,8	1,1	1,2	1,1	1,0	0,6	1,3	2,0
Er	5,0	3,3	3,7	3,3	2,8	2,0	3,9	6,0
Tm	0,66	0,53	0,59	0,53	0,42	0,33	0,63	0,95
Yb	4,3	3,3	3,6	3,2	2,5	2,0	3,8	5,9
Lu	0,60	0,50	0,55	0,50	0,35	0,30	0,54	0,83
Hf	9,2	6,3	7,2	6,0	5,9	7,7	10,2	11,7
Ta	3,1	1,2	1,6	1,5	2,6	2,7	2,7	3,3
W	3	3	2	2	9	2	2	1
Tl	2,7	0,7	1,2	0,7	2,6	2,1	5,4	3,9
Pb	19	45	8	<5	6	32	32	31
Bi	<0,4	<0,4	<0,4	<0,4	<0,4	<0,4	0,9	<0,4
Th	70,3	16,5	23,7	17,7	50,1	59,8	57,1	59,2
U	10,0	6,4	6,5	7,6	5,3	10,4	7,8	12,3

APPENDIX – GEOCHEMISTRY   PAGE VIII

Geochemistry of altered tuff layers from the Ecca Group of southern Namibia
Trace and rare earth element data: ICP-MS – Actlabs Ltd., Ancaster/Canada

outcrop areas:
AK-NO: Aussenkjer-Noordoewer
MT-KH: Mariental-Keetmanshoop

sample	UFO-44.98T	UFO-44.98T (rep)	UFO-52.95T	Rf-28f
locality	Ufo Valleys	Ufo Valleys	Ufo Valleys	Rhyofontein
outcrop area	AK-NO	AK-NO	AK-NO	AK-NO
stratigraphy	Collingham Fm.	Collingham Fm.	Collingham Fm.	Collingham Fm.
V	140	137	28	53
Cr	34	28	<20	22
Co	10	10	6	3
Ni	27	30	<20	27
Cu	72	66	14	31
Zn	90	60	46	54
Ga	32	30	31	31
Ge	2	1	1	2
As	31	22	5	<5
Rb	465	437	384	439
Sr	395	393	254	541
Y	78	77	45	40
Zr	410	425	256	277
Nb	43	44	16	28
Mo	<2	<2	4	2
Ag	<0,5	<0,5	<0,5	<0,5
In	<0,2	<0,2	<0,2	<0,2
Sn	5	5	5	4
Sb	1,1	0,6	<0,5	0,6
Cs	12,9	11,9	10,5	13,0
Ba	1.420	1.430	877	1.160
La	16,1	15,9	43,6	88,8
Ce	36,5	35,8	114	165
Pr	4,98	4,91	15,1	16,81
Nd	23,6	22,7	65,0	58,2
Sm	8,5	8,3	16,5	10,3
Eu	2,41	2,37	1,86	2,64
Gd	10,6	10,5	11,2	8,2
Tb	2,2	2,1	1,6	1,2
Dy	13,3	13,2	8,4	6,7
Ho	2,6	2,5	1,6	1,2
Er	7,3	7,0	4,6	3,4
Tm	1,05	1,02	0,71	0,52
Yb	6,4	6,2	4,6	3,4
Lu	0,89	0,87	0,66	0,52
Hf	14,1	14,7	10,0	9,1
Ta	4,5	4,4	2,3	3,1
W	7	7	2	4
Tl	6,2	3,9	2,7	4,7
Pb	71	51	23	136
Bi	<0,4	<0,4	<0,4	0,5
Th	97,4	98,8	53,5	85,2
U	15,9	15,4	9,0	17,1

APPENDIX – GEOCHRONOLOGY   PAGE IX
Geochronology of altered tuff layers from the Ecca Group of southern Namibia
Single zircon SHRIMP analysis data: PRISE – ANU – Canberra/Australia

Summary of SHRIMP U-Pb zircon data for sample OG-9 of the Owl Gorge Tuffs

Grain Spot	% $^{206}Pb_c$	ppm U	ppm Th	$^{232}Th/^{238}U$	ppm $^{206}Pb^*$	(1) $^{206}Pb/^{238}U$ Age	±	(2) $^{206}Pb/^{238}U$ Age	±	(1) $^{207}Pb/^{206}Pb$ Age	±	% Dis-cor-dant	Total $^{238}U/^{206}Pb$	±%	(1) $^{207}Pb^*/^{206}Pb^*$	±%	Total $^{207}Pb/^{206}Pb$	±%	(1) $^{207}Pb^*/^{235}U$	±%	(1) $^{206}Pb^*/^{238}U$	±%	err corr
1,1	0,16	233	405	1,80	9.37	294.4	±2.3	294.2	±2.4	329	±43	11	21.36	0.81	0.0530	1.9	0.05430	1.7	0.3415	2.1	0.04673	0.81	,391
2,1	0,00	177	242	1,41	6.72	278.4	±3.6	277.9	±3.6	346	±51	20	22.66	1.3	0.0534	2.3	0.0534	2.3	0.3250	2.6	0.04414	1.3	,500
3,1	0,00	66	32	0,50	4.40	484.5	±5.9	484.0	±6.0	517	±60	6	12.81	1.3	0.0577	2.7	0.0577	2.7	0.621	3.0	0.07805	1.3	,417
4,1	0,00	1033	710	0,71	42.0	298.0	±1.8	298.1	±1.8	290	±21	-3	21.13	0.60	0.05212	0.91	0.05212	0.91	0.3400	1.1	0.04732	0.60	,551
5,1	0,00	487	362	0,77	19.3	290.8	±2.0	290.6	±2.0	310	±31	6	21.67	0.70	0.05256	1.4	0.05256	1.4	0.3344	1.5	0.04614	0.70	,455
6,1	0,00	187	273	1,51	7.64	300.1	±2.6	299.8	±2.7	337	±47	11	20.98	0.90	0.0532	2.1	0.0532	2.1	0.3495	2.3	0.04766	0.90	,400
7,1	0,00	146	149	1,05	5.85	292.8	±2.8	292.3	±2.9	349	±53	16	21.52	0.98	0.0535	2.4	0.0535	2.4	0.3425	2.6	0.04646	0.98	,383
8,1	0,00	218	377	1,78	8.41	283.1	±3.2	282.8	±3.2	321	±46	12	22.27	1.2	0.0528	2.0	0.0528	2.0	0.3270	2.3	0.04490	1.2	,498
9,1	0,18	210	337	1,66	8.35	291.6	±2.5	291.2	±2.5	336	±51	13	21.57	0.87	0.0532	2.2	0.0546	2.0	0.3392	2.4	0.04627	0.87	,364
10,1	0,18	207	562	2,81	8.44	298.4	±2.6	298.0	±2.6	344	±57	13	21.07	0.89	0.0534	2.5	0.0548	2.0	0.3486	2.7	0.04738	0.89	,334
11,1	0,06	564	583	1,07	23.0	298.5	±2.0	298.4	±2.0	311	±42	4	21.09	0.67	0.05259	1.8	0.05303	1.8	0.3436	2.0	0.04739	0.67	,344
12,1	0,00	214	347	1,67	8.40	287.8	±2.5	288.0	±2.5	265	±48	-9	21.90	0.88	0.0515	2.1	0.0515	2.1	0.3245	2.3	0.04565	0.88	,389
13,1	0,19	1066	572	0,55	42.2	290.2	±1.7	290.2	±1.7	290	±30	0	21.68	0.60	0.05210	1.3	0.05360	0.91	0.3308	1.5	0.04604	0.61	,414
14,1	0,15	220	280	1,31	8.78	291.8	±2.5	291.6	±2.5	312	±57	6	21.56	0.86	0.0526	2.5	0.0538	2.1	0.3360	2.6	0.04631	0.86	,327
15,1	0,00	263	464	1,82	10.7	298.1	±3.0	298.2	±3.0	292	±41	-2	21.13	1.0	0.05215	1.8	0.05215	1.8	0.3404	2.1	0.04734	1.0	,492
16,1	0,00	155	227	1,52	6.34	300.6	±3.0	300.2	±3.0	341	±55	12	20.95	1.0	0.0533	2.4	0.0533	2.4	0.3506	2.6	0.04773	1.0	,382
17,1	0,00	189	321	1,75	7.43	287.9	±2.6	287.9	±2.6	291	±51	1	21.89	0.91	0.0521	2.2	0.0521	2.2	0.3284	2.4	0.04568	0.91	,380
18,1	0,00	212	360	1,76	8.08	280.3	±2.4	280.3	±2.5	279	±50	0	22.50	0.89	0.0519	2.2	0.0519	2.2	0.3178	2.3	0.04444	0.89	,380

Errors are 1-sigma; Pb_c and Pb^* indicate the common and radiogenic portions, respectively.

Error in Standard calibration was 0.12% (not included in above errors but required when comparing data from different mounts).

(1) Common Pb corrected using measured ^{204}Pb.

(2) Common Pb corrected by assuming $^{206}Pb/^{238}U$–$^{207}Pb/^{235}U$ age-concordance

APPENDIX – GEOCHRONOLOGY   PAGE X
Geochronology of altered tuff layers from the Ecca Group of southern Namibia
Single zircon SHRIMP analysis data: PRISE – ANU – Canberra/Australia

Summary of SHRIMP U-Pb zircon data for sample DIBA-2 of the Itzawisis Tuffs

Grain Spot	% $^{206}Pb_c$	ppm U	ppm Th	$^{232}Th/^{238}U$	ppm $^{206}Pb^*$	(1) $^{206}Pb/^{238}U$ Age	±	(2) $^{206}Pb/^{238}U$ Age	±	(1) $^{207}Pb/^{206}Pb$ Age	±	% Dis-cordant	Total $^{238}U/^{206}Pb$	±%	Total $^{207}Pb/^{206}Pb$	±%	(1) $^{238}U/^{206}Pb^*$	±%	(1) $^{207}Pb^*/^{206}Pb^*$	±%	(1) $^{207}Pb^*/^{235}U$	±%	(1) $^{206}Pb^*/^{238}U$	±%	err corr
1,1	0,00	1057	528	0,52	42.4	294.0	±1.7	293.9	±1.7	309	±19	5	21.43	0.84	0.05253	0.84	21.43	0.59	0.05253	0.84	0.3380	1.0	0.04666	0.59	,572
2,1	0,00	580	267	0,48	22.7	287.1	±1.8	287.1	±1.8	290	±26	1	21.96	1.2	0.05210	1.2	21.96	0.65	0.05210	1.2	0.3272	1.3	0.04555	0.65	,488
3,1	1,56	1145	1011	0,91	44.5	280.6	±2.0	278.6	±2.1	521	±94	46	22.13	1.1	0.07021	1.1	22.48	0.72	0.0578	4.3	0.354	4.3	0.04449	0.72	,167
4,1	0,00	781	557	0,74	31.8	299.0	±2.7	299.2	±2.8	280	±24	-7	21.06	1.0	0.05188	1.0	21.06	0.94	0.05188	1.0	0.3396	1.4	0.04748	0.94	,668
5,1	1,47	961	592	0,64	36.1	272.1	±1.7	271.6	±1.7	335	±100	19	22.85	0.81	0.06491	0.81	23.19	0.63	0.0531	4.5	0.316	4.5	0.04312	0.63	,140
6,1	0,00	1088	809	0,77	42.7	287.9	±1.8	287.7	±1.8	303	±19	5	21.90	0.85	0.05240	0.85	21.90	0.65	0.05240	0.85	0.3300	1.1	0.04567	0.65	,606
7,1	4,07	962	756	0,81	36.1	264.9	±2.0	263.9	±2.3	395	±250	33	22.87	2.6	0.0871	2.6	23.84	0.61	0.0546	11	0.316	11	0.04195	0.77	,068
8,1	0,00	983	539	0,57	37.8	282.4	±1.7	282.3	±1.7	284	±21	1	22.33	0.92	0.05196	0.92	22.33	0.60	0.05196	0.92	0.3208	1.1	0.04477	0.60	,545
9,1	0,00	945	633	0,69	36.6	284.8	±1.7	284.7	±1.7	291	±25	2	22.14	1.1	0.05212	1.1	22.14	0.60	0.05212	1.1	0.3246	1.2	0.04517	0.60	,485
10,1	0,00	333	452	1,40	107	2,055	±11	2,058	±13	2,037.9	±6.5	-1	2.664	0.37	0.12564	0.37	2.664	0.64	0.12564	0.37	6.504	0.74	0.3754	0.64	,866
11,1	0,00	122	96	0,81	4.90	293.6	±3.0	293.3	±3.1	321	±59	9	21.46	2.6	0.0528	2.6	21.46	1.0	0.0528	2.6	0.3393	2.8	0.04659	1.0	,373
12,1	0,00	774	384	0,51	30.6	289.7	±1.7	289.9	±1.8	269	±23	-8	21.75	1.0	0.05162	1.0	21.75	0.62	0.05162	1.0	0.3272	1.2	0.04597	0.62	,518
13,1	0,00	788	312	0,41	30.1	280.1	±1.7	280.1	±1.7	285	±24	2	22.52	1.1	0.05199	1.1	22.52	0.62	0.05199	1.1	0.3184	1.2	0.04441	0.62	,505
14,1	0,10	687	382	0,57	26.4	282.0	±1.7	281.6	±1.8	330	±29	15	22.34	1.1	0.05386	1.1	22.36	0.63	0.05302	1.3	0.3269	1.4	0.04472	0.63	,448
15,1	0,00	460	221	0,50	18.2	290.2	±2.0	289.8	±2.0	329	±31	12	21.72	1.3	0.05301	1.3	21.72	0.69	0.05301	1.3	0.3365	1.5	0.04604	0.69	,458
16,1	0,00	114	60	0,55	4.54	293.3	±2.8	293.2	±2.9	306	±56	4	21.48	2.4	0.0525	2.4	21.48	0.99	0.0525	2.4	0.3367	2.6	0.04655	0.99	,376
17,1	1,17	1087	827	0,79	38.8	259.2	±1.6	259.0	±1.6	286	±89	9	24.09	0.83	0.06142	0.83	24.38	0.60	0.0520	3.9	0.294	3.9	0.04102	0.63	,159
18,1	0,00	263	86	0,34	41.0	1,072.6	±9.3	1,073.1	±9.8	1,062	±15	-1	5.524	0.76	0.07474	0.76	5.524	0.94	0.07474	0.76	1.866	1.2	0.1810	0.94	,779
19,1	0,12	882	462	0,54	35.3	293.1	±1.8	293.3	±1.8	270	±25	-9	21.47	0.98	0.05260	0.98	21.50	0.63	0.05164	1.1	0.3312	1.3	0.04652	0.63	,496
20,1	0,12	508	215	0,44	19.9	287.5	±2.1	287.2	±2.2	329	±36	13	21.90	1.4	0.05399	1.4	21.92	0.75	0.05301	1.6	0.3334	1.8	0.04561	0.75	,427

Errors are 1-sigma; Pb_c and Pb^* indicate the common and radiogenic portions, respectively.
Error in Standard calibration was 0.16% (not included in above errors but required when comparing data from different mounts).
(1) Common Pb corrected using measured ^{204}Pb.
(2) Common Pb corrected by assuming $^{206}Pb/^{238}U$–$^{207}Pb/^{235}U$ age-concordance

APPENDIX – GEOCHRONOLOGY   PAGE XI

Geochronology of altered tuff layers from the Ecca Group of southern Namibia
Single zircon SHRIMP analysis data: PRISE – ANU – Canberra/Australia

Summary of SHRIMP U-Pb zircon data for sample UHB-T from the Uhabis River Tuff

Grain Spot	% 206Pbc	ppm U	ppm Th	232Th /238U	ppm 206Pb*	(1) 206Pb /238U Age	±	(2) 206Pb /238U Age	±	(1) 207Pb /206Pb Age	±	% Dis-cor-dant	Total 238U /206Pb	±%	Total 207Pb /206Pb	±%	(1) 238U /206Pb	±%	(1) 207Pb* /206Pb*	±%	(1) 207Pb* /235U	±%	(1) 206Pb* /238U	±%	err corr
1,1	0,00	135	91	0,70	5.16	280.2	±2.9	279.9	±3.0	318	±61	12	22.51	1.1	0.0527	2.7	22.51	1.1	0.0527	2.7	0.3231	2.9	0.04443	1.1	,367
2,1	0,00	267	255	0,99	10.2	282.2	±2.3	282.2	±2.4	284	±44	1	22.34	0.84	0.05198	1.9	22.34	0.84	0.05198	1.9	0.3207	2.1	0.04475	0.84	,401
3,1	--	443	423	0,99	17.5	290.8	±2.1	290.8	±2.1	285	±41	-2	21.70	0.73	0.05106	1.5	21.67	0.73	0.05200	1.8	0.3308	2.0	0.04614	0.73	,374
4,1	0,00	155	111	0,74	5.75	271.8	±2.9	271.7	±2.9	282	±64	4	23.22	1.1	0.0519	2.8	23.22	1.1	0.0519	2.8	0.3083	3.0	0.04307	1.1	,357
5,1	0,00	484	416	0,89	18.5	279.8	±2.9	279.5	±2.9	311	±31	10	22.54	1.1	0.05259	1.4	22.54	1.1	0.05259	1.4	0.3217	1.7	0.04436	1.1	,614
6,1	0,01	368	299	0,84	13.9	278.5	±2.0	278.3	±2.1	305	±40	9	22.65	0.75	0.05257	1.6	22.65	0.75	0.05246	1.8	0.3193	1.9	0.04415	0.75	,392
7,1	0,00	246	196	0,82	9.26	276.4	±2.4	276.8	±2.4	223	±49	-24	22.83	0.87	0.0506	2.1	22.83	0.87	0.0506	2.1	0.3057	2.3	0.04381	0.87	,381
8,1	0,03	524	516	1,02	19.8	278.0	±1.9	277.7	±1.9	309	±39	10	22.69	0.70	0.05282	1.4	22.69	0.70	0.05255	1.7	0.3193	1.8	0.04407	0.70	,380
9,1	0,15	189	163	0,89	7.24	280.7	±2.5	281.1	±2.6	231	±61	-22	22.43	0.92	0.0520	2.3	22.47	0.93	0.0508	2.6	0.3117	2.8	0.04451	0.93	,333
10,1	0,12	871	876	1,04	32.0	269.7	±1.7	269.6	±1.7	283	±31	5	23.37	0.64	0.05290	1.1	23.40	0.64	0.05194	1.4	0.3061	1.5	0.04273	0.64	,426
10,2	0,59	311	247	0,82	10.2	238.8	±2.0	238.3	±2.0	310	±110	23	26.34	0.82	0.0573	1.9	26.50	0.86	0.0526	4.6	0.274	4.7	0.03774	0.86	,183
11,1	0,19	340	303	0,92	12.8	276.2	±1.8	276.3	±1.9	269	±48	-3	22.80	1.4	0.05316	1.7	22.84	1.4	0.0516	2.1	0.3116	2.5	0.04378	1.4	,554
12,1	0,00	424	379	0,92	15.3	265.7	±1.8	265.3	±1.9	331	±33	20	23.76	0.71	0.05304	1.5	23.76	0.71	0.05304	1.5	0.3078	1.6	0.04208	0.71	,438
13,1	0,00	290	286	1,02	11.0	277.7	±2.4	277.2	±2.4	347	±42	20	22.72	0.87	0.05342	1.8	22.72	0.87	0.05342	1.8	0.3243	2.0	0.04402	0.87	,427
14,1	0,00	386	422	1,13	14.8	281.4	±2.1	281.2	±2.1	318	±36	12	22.41	0.75	0.05275	1.6	22.41	0.75	0.05275	1.6	0.3246	1.8	0.04463	0.75	,424
15,1	0,17	387	290	0,77	14.6	277.6	±2.2	277.9	±2.2	243	±55	-14	22.68	0.80	0.05242	1.8	22.72	0.81	0.0510	2.4	0.3097	2.5	0.04401	0.81	,319
16,1	0,00	217	175	0,84	8.34	282.1	±2.6	282.5	±2.7	227	±56	-24	22.36	0.95	0.0507	2.4	22.36	0.95	0.0507	2.4	0.3127	2.6	0.04473	0.95	,366
17,1	0,00	328	282	0,89	12.0	267.7	±2.0	267.8	±2.1	252	±39	-6	23.58	0.77	0.05124	1.7	23.58	0.77	0.05124	1.7	0.2996	1.9	0.04241	0.77	,410
18,1	0,00	290	241	0,86	9.75	247.4	±2.0	247.3	±2.0	272	±44	9	25.55	0.82	0.05170	1.9	25.55	0.82	0.05170	1.9	0.2789	2.1	0.03913	0.82	,390
19,1	0,00	179	135	0,78	6.73	275.7	±3.8	275.4	±3.8	312	±59	12	22.89	1.4	0.0526	2.6	22.89	1.4	0.0526	2.6	0.3169	2.9	0.04369	1.4	,477
20,1	0,00	274	239	0,90	10.1	271.2	±2.2	271.4	±2.2	247	±44	-10	23.27	0.83	0.05114	1.9	23.27	0.83	0.05114	1.9	0.3030	2.1	0.04297	0.83	,394

Errors are 1-sigma; Pb_c and Pb^* indicate the common and radiogenic portions, respectively.

Error in Standard calibration was 0.12% (not included in above errors but required when comparing data from different mounts).

(1) Common Pb corrected using measured ^{204}Pb.

(2) Common Pb corrected by assuming $^{206}Pb/^{238}U$-$^{207}Pb/^{235}U$ age-concordance

APPENDIX – GEOCHRONOLOGY   PAGE XII

Geochronology of altered tuff layers from the Ecca Group of southern Namibia

Single zircon SHRIMP analysis data: PRISE – ANU – Canberra/Australia

Summary of SHRIMP U-Pb zircon data for sample KHA-1a of the Khabus Tuff

Grain Spot*	% $^{206}Pb_c$	ppm U	ppm Th	$^{232}Th/^{238}U$	ppm $^{206}Pb^*$	(1) $^{206}Pb/^{238}U$ Age	(2) $^{206}Pb/^{238}U$ Age	(1) $^{207}Pb/^{206}Pb$ Age	% Discordant	Total $^{238}U/^{206}Pb$	±%	Total $^{207}Pb/^{206}Pb$	±%	(1) $^{238}U/^{206}Pb^*$	±%	(1) $^{207}Pb^*/^{206}Pb^*$	±%	(1) $^{207}Pb^*/^{235}U$	±%	(1) $^{206}Pb^*/^{238}U$	±%	err corr
L-3.1	0,50	275	138	0,52	10.7	283.3 ±2.8	283.5 ±2.7	257 ±130	-10	22.15	0.97	0.0554	1.8	22.26	1.0	0.0514	5.6	0.318	5.7	0.04492	1.0	,181
L-4.1	0,00	281	191	0,70	10.7	280.7 ±2.8	280.3 ±2.9	328 ±45	14	22.47	1.0	0.0530	2.0	22.47	1.0	0.0530	2.0	0.3251	2.2	0.04450	1.0	,458
L-5.1	0,20	417	273	0,68	15.9	279.1 ±3.4	279.3 ±3.2	260 ±56	-7	22.55	1.2	0.05306	1.7	22.60	1.2	0.0514	2.4	0.3138	2.7	0.04425	1.2	,431
L-6.1	0,00	511	714	1,44	19.6	281.8 ±4.1	281.9 ±3.5	276 ±43	-2	22.38	1.2	0.05180	1.9	22.38	1.2	0.05180	1.9	0.3192	2.3	0.04469	1.2	,549
L-7.1	0,41	108	99	0,95	4.11	279.7 ±4.1	280.2 ±4.2	221 ±110	-27	22.46	1.5	0.0539	3.0	22.55	1.5	0.0506	4.6	0.309	4.8	0.04435	1.5	,314
L-8.1	0,00	360	189	0,54	13.8	280.6 ±2.5	280.6 ±2.5	276 ±38	-2	22.48	0.91	0.05179	1.7	22.48	0.91	0.05179	1.7	0.3177	1.9	0.04449	0.91	,481
L-9.1	0,00	363	235	0,67	13.9	282.1 ±3.1	281.8 ±3.2	324 ±40	13	22.35	1.1	0.05288	1.7	22.35	1.1	0.05288	1.7	0.3262	2.1	0.04474	1.1	,546
L-10.1	0,00	438	422	1,00	16.5	276.4 ±2.5	276.3 ±2.5	296 ±55	7	22.82	0.90	0.05224	1.6	22.82	0.91	0.0522	2.4	0.3155	2.6	0.04381	0.91	,354
L-11.1	0,00	366	199	0,56	14.2	284.7 ±3.2	284.6 ±3.2	288 ±40	1	22.15	1.1	0.05206	1.7	22.15	1.1	0.05206	1.7	0.3241	2.1	0.04515	1.1	,546
L-12.1	0,15	487	491	1,04	18.8	283.9 ±2.4	283.9 ±2.4	282 ±45	-1	22.18	0.86	0.05310	1.5	22.21	0.86	0.0519	2.0	0.3223	2.1	0.04502	0.86	,404
L-13.1	0,00	160	135	0,87	6.11	280.3 ±3.3	279.9 ±3.4	326 ±58	14	22.50	1.2	0.0529	2.5	22.50	1.2	0.0529	2.5	0.3244	2.8	0.04444	1.2	,432
L-14.1	1,90	403	314	0,81	15.1	270.7 ±2.8	270.8 ±2.7	266 ±200	-2	22.87	0.96	0.0668	2.3	23.31	1.1	0.0516	8.6	0.305	8.7	0.04289	1.1	,122
>100-1.1	0,29	297	181	0,63	11.4	280.3 ±2.8	280.6 ±2.8	240 ±73	-17	22.44	0.99	0.0533	1.9	22.50	1.0	0.0510	3.2	0.312	3.3	0.04444	1.0	,302
>100-2.1	0,31	235	200	0,88	9.25	288.6 ±3.2	288.8 ±3.2	269 ±96	-7	21.77	1.1	0.0541	2.2	21.84	1.1	0.0516	4.2	0.326	4.4	0.04579	1.1	,259
>100-3.1	0,36	272	169	0,64	10.2	273.2 ±3.1	273.5 ±3.1	235 ±90	-16	23.02	1.1	0.0537	2.3	23.10	1.1	0.0509	3.9	0.304	4.1	0.04329	1.1	,281
>100-4.1	0,19	344	210	0,63	13.1	279.1 ±3.3	278.8 ±3.3	322 ±54	13	22.56	1.2	0.05439	1.8	22.60	1.2	0.0528	2.4	0.3224	2.6	0.04425	1.2	,452
>100-5.1	0,00	539	473	0,91	20.8	283.8 ±2.4	283.9 ±2.4	269 ±34	-6	22.22	0.85	0.05162	1.5	22.22	0.85	0.05162	1.5	0.3204	1.7	0.04501	0.85	,499
>100-5.2	0,00	291	164	0,58	11.2	282.8 ±2.9	282.6 ±2.9	311 ±47	9	22.30	1.0	0.0526	2.1	22.30	1.0	0.0526	2.1	0.3252	2.3	0.04485	1.0	,454
>100-6.1	0,76	292	171	0,60	11.3	282.5 ±3.2	282.8 ±3.0	243 ±180	-16	22.15	1.1	0.0572	2.0	22.32	1.1	0.0511	7.6	0.315	7.7	0.04480	1.1	,148
>100-7.1	0,43	330	185	0,58	12.5	278.3 ±2.9	278.2 ±2.9	298 ±78	7	22.57	1.1	0.0557	2.2	22.67	1.1	0.0523	3.4	0.318	3.6	0.04412	1.1	,297
>100-8.1	0,00	428	309	0,75	16.0	274.5 ±2.8	274.4 ±2.8	299 ±46	8	22.98	1.0	0.0523	2.0	22.98	1.0	0.0523	2.0	0.3138	2.2	0.04351	1.0	,459

Errors are 1-sigma; Pb_c and Pb^* indicate the common and radiogenic portions, respectively.

Error in Standard calibration was 0.25% (not included in above errors but required when comparing data from different mounts).

(1) Common Pb corrected using measured ^{204}Pb.

(2) Common Pb corrected by assuming $^{206}Pb/^{238}U$-$^{207}Pb/^{235}U$ age-concordance

* Grains prefaced with L are from the "Long prismatic" fraction; those prefaced by >100 are from the ">100 mm" fraction.

APPENDIX – GEOCHRONOLOGY   PAGE XIII
Geochronology of altered tuff layers from the Ecca Group of southern Namibia
Single zircon SHRIMP analysis data: PRISE – ANU – Canberra/Australia

Summary of SHRIMP U-Pb zircon data for sample UFO-43 of the Ufo Valleys Tuffs

Grain Spot	% $^{206}Pb_c$	ppm U	ppm Th	$^{232}Th/^{238}U$	ppm $^{206}Pb^*$	(1) $^{206}Pb/^{238}U$ Age	±	(2) $^{206}Pb/^{238}U$ Age	±	(1) $^{207}Pb/^{206}Pb$ Age	±	% Discordant	Total $^{238}U/^{206}Pb$	±%	Total $^{207}Pb/^{206}Pb$	±%	(1) $^{238}U/^{206}Pb^*$	±%	(1) $^{207}Pb^*/^{206}Pb^*$	±%	(1) $^{207}Pb^*/^{235}U$	±%	(1) $^{206}Pb^*/^{238}U$	±%	err corr
1,1	--	215	104	0,50	8.11	277.6	±2.4	276.6	±2.3	395	±93	30	22.82	0.83	0.05127	1.9	22.73	0.87	0.0546	4.1	0.331	4.2	0.04400	0.87	,204
2,1	0,05	450	296	0,68	17.3	282.3	±1.9	282.7	±1.9	235	±40	-20	22.30	0.68	0.05236	1.3	22.34	0.68	0.05087	1.7	0.3140	1.9	0.04477	0.68	,365
3,1	0,06	700	446	0,66	26.5	277.1	±1.7	277.5	±1.7	228	±36	-22	22.72	0.62	0.05234	1.0	22.77	0.63	0.05071	1.6	0.3071	1.7	0.04392	0.63	,371
4,1	0,14	454	269	0,61	17.1	275.0	±2.5	275.3	±2.5	247	±45	-11	22.89	0.91	0.05291	1.6	22.94	0.91	0.05113	1.9	0.3073	2.1	0.04359	0.91	,427
5,1	0,07	448	189	0,44	16.3	267.0	±2.0	267.2	±2.0	240	±45	-11	23.61	0.77	0.05217	1.4	23.64	0.77	0.05097	2.0	0.2972	2.1	0.04229	0.77	,366
6,1	0,06	420	221	0,54	15.9	277.1	±2.0	277.7	±1.9	195	±94	-42	22.70	0.70	0.05232	1.4	22.77	0.74	0.0500	4.0	0.303	4.1	0.04392	0.74	,179
7,1	0,09	293	134	0,47	11.1	279.2	±2.9	278.4	±2.9	379	±59	26	22.64	1.1	0.05259	1.7	22.59	1.1	0.0542	2.6	0.3307	2.8	0.04427	1.1	,374
8,1	0,04	225	134	0,61	8.46	275.1	±2.3	276.1	±2.3	140	±76	-97	22.84	0.83	0.05208	1.9	22.94	0.84	0.0488	3.2	0.2936	3.3	0.04360	0.84	,253
9,1	0,34	107	48	0,46	4.03	277.0	±5.1	276.1	±5.1	391	±60	29	22.78	1.9	0.0545	2.7	22.78	1.9	0.0545	2.7	0.330	3.3	0.04391	1.9	,577
10,1	0,01	389	293	0,78	14.4	271.3	±2.0	272.4	±1.9	114	±95	-138	23.17	0.72	0.05180	1.5	23.27	0.75	0.0483	4.0	0.286	4.1	0.04298	0.75	,184
11,1	--	271	119	0,45	10.00	270.5	±2.1	271.4	±2.2	151	±63	-79	23.26	0.80	0.05168	1.8	23.33	0.81	0.0491	2.7	0.2899	2.8	0.04286	0.81	,286
12,1	0,19	245	123	0,52	9.14	272.6	±2.2	273.4	±2.2	160	±99	-70	23.04	0.81	0.05326	1.8	23.16	0.84	0.0493	4.2	0.293	4.3	0.04319	0.84	,196
13,1	0,37	380	234	0,64	14.8	284.6	±2.0	284.9	±2.1	246	±69	-16	22.05	0.72	0.05492	1.7	22.16	0.73	0.0511	3.0	0.3181	3.1	0.04513	0.73	,238
14,1	--	236	130	0,57	8.98	279.0	±2.7	279.9	±2.8	162	±70	-72	22.55	10	0.05135	1.9	22.61	1.0	0.0493	3.0	0.3007	3.2	0.04423	1.0	,318
15,1	0,09	414	282	0,71	15.6	276.4	±2.3	277.4	±2.3	140	±56	-97	22.72	0.83	0.05258	1.6	22.83	0.84	0.0488	2.4	0.2949	2.5	0.04381	0.84	,330
16,1	0,11	554	302	0,56	20.9	277.5	±1.8	276.7	±1.8	379	±47	27	22.78	0.67	0.05272	1.2	22.74	0.68	0.0542	2.1	0.3286	2.2	0.04398	0.68	,310
17,1	--	798	749	0,97	30.4	279.5	±1.7	279.3	±1.7	305	±24	8	22.59	0.62	0.05161	1.0	22.57	0.62	0.05246	1.1	0.3205	1.2	0.04431	0.62	,508
18,1	0,18	413	193	0,48	15.7	279.9	±2.0	279.4	±2.0	342	±32	18	22.54	0.71	0.05330	1.4	22.54	0.71	0.05330	1.4	0.3261	1.6	0.04437	0.71	,449
19,1	0,04	267	112	0,43	10.1	277.5	±2.2	278.2	±2.2	173	±63	-60	22.66	0.80	0.05216	1.8	22.74	0.81	0.0495	2.7	0.3004	2.8	0.04398	0.81	,286
20,1	--	592	421	0,74	22.3	276.4	±2.2	276.6	±2.2	253	±53	-9	22.82	0.80	0.05156	1.2	22.82	0.81	0.0513	2.3	0.3097	2.4	0.04381	0.81	,333

Errors are 1-sigma; Pb_c and Pb^* indicate the common and radiogenic portions, respectively.

Error in Standard calibration was 0.16% (not included in above errors but required when comparing data from different mounts).

(1) Common Pb corrected using measured ^{204}Pb.

(2) Common Pb corrected by assuming $^{206}Pb/^{238}U$–$^{207}Pb/^{235}U$ age-concordance

Curriculum vitae

Name:	Mario Werner
Date of birth:	25.06.1968
Place of birth:	Schweinfurt/Germany
Place of residence:	Adelaide/Australia

Work History:

Since 2006   Research Associate, Australian School of Petroleum, University of Adelaide

2005-2006   Technical Assistant, Australian School of Petroleum, University of Adelaide

2004-2005   Guest Researcher, Australian School of Petroleum, University of Adelaide

2003-2004   Lecturer, Geological Institute, Technical University Aachen

2003   Research Associate, Geological Institute, Technical University Aachen

Education:

1999-2003   Dr. rer. nat. Student, Graduate College 'Geoscience Research in Africa',

Karoo Research Group, Institute of Geology, University of Würzburg

1998   Diplom in Geology, Gross Brukkaros Research Group, University of Würzburg

1991-1998   Studies Geology-Palaeontology, University of Würzburg

1989-1991   Alternative Service, Red Cross Ambulance Team, Schweinfurt

1987-1989   Studies Chemistry, University of Würzburg

1978-1987   Alexander von Humboldt Gymnasium, Schweinfurt

Erklärung:

Hiermit erkläre ich, dass ich die vorliegende Dissertation in allen Teilen selbständig angefertigt habe und keine anderen als die genannten Quellen und Hilfsmittel verwendet habe.

Adelaide, den 10. 07. 2006

Mario Werner